

http://researchcommons.waikato.ac.nz/

Research Commons at the University of Waikato

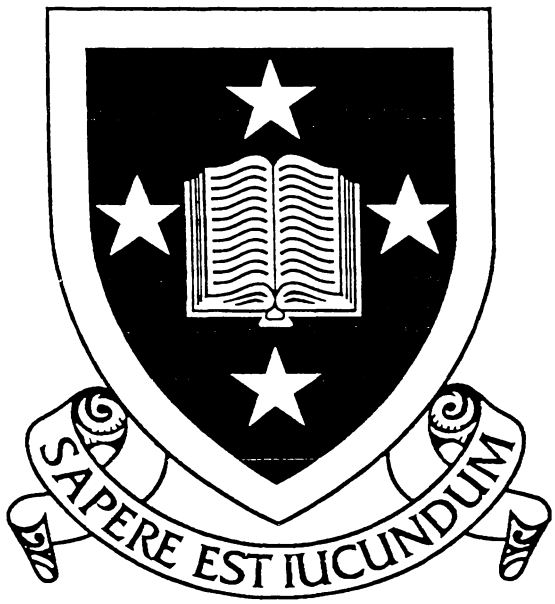
Copyright Statement:

The digital copy of this thesis is protected by the Copyright Act 1994 (New Zealand).

The thesis may be consulted by you, provided you comply with the provisions of the Act and the following conditions of use:

- Any use you make of these documents or images must be for research or private study purposes only, and you may not make them available to any other person.
- Authors control the copyright of their thesis. You will recognise the author's right to be identified as the author of the thesis, and due acknowledgement will be made to the author where appropriate.
- You will obtain the author's permission before publishing any material from the thesis.

Studies of the Structures and Redox Chemistries of Chromate Zeolites



A thesis submitted in partial fulfilment of the requirements for the degree of

Doctorate of Philosophy in Chemistry

by

Mark Langtry Brown

The University of Waikato

January, 1994

To Mum and Dad (and Winkles)

Abstract

Solid-state reactions of sodium chromate, sodium molybdate, and sodium tungstate and zeolites of the types A, X, Y, mordenite, and silicalite at temperatures between 465°C and 655°C resulted in substantial uptakes of the salts. The occluded oxyanions could not be removed by boiling water indicating either a strong interaction with the zeolite lattice or occlusion in β-cages. Factors found to influence the amount of oxyanion occluded were temperature, time, and zeolite to oxyanion mole ratio. Under certain conditions maximum loading was achieved within 24 hours in the absence of significant zeolite framework degradation. In the chromate system, solid-state reactions performed near 800°C resulted in collapse of the zeolite framework and crystallisation of chromate nosean. The kinetics of chromate uptake by 13X followed a $\sqrt{t}$ dependence over the initial stages of reaction indicating a diffusion controlled rate determining step. An apparent activation energy of 124 ± 10 kJ mol^{-1} was calculated. Occluded sodium chromate was removed from X and Y type zeolites upon heating in strong alkali or salt solutions. A salt-exchange mechanism for chromate removal is proposed.

The physiochemical nature of chromate loaded zeolites was examined using a variety of experimental techniques including PXRD, EPR, XRF, DTA, SEM, XPS, FTIR and Raman spectroscopies, and BET surface area determination. All results were consistent with the occlusion of chromate within the α-cages of X, Y, and A type zeolites. No evidence for β-cage occlusion was observed. Maximum chromate uptakes per unit cell were 13.6 for 13X, 13.4 for Y52, and 32.3 for 5A. These uptakes correlated with half the number of S6R facing α-cages of these zeolites suggesting coordination across two S6R. A model consisting of the oxyanion coordinated across its two sodium cations located near the S_{II} sites is proposed. Coordination across S5R

of mordenite and silicalite was proposed. The Si/Al ratio had no effect on the maximum chromate uptake.

Redox reactions of sodium chromate salt were investigated. Reduction by $H_{2(g)}$ formed $NaCrO_2$ and NaOH. Reoxidations were incomplete ceasing at an average oxidation state of Cr(+4.67) through the formation of Na_2CrO_4 and Na_2CrO_3 in a 1:2 ratio. The addition of NaOH to the partially oxidised product allowed full oxidation indicating a dependence of oxidation product on NaOH concentration. A mechanism consistent with the degree of reoxidation was deduced.

Chromate occluded in zeolites was reduced by $H_{2(g)}$ and reoxidised by $O_{2(g)}$. The degree of loading affected the product of reduction. Reductions of chromates in lowly-loaded zeolites ceased at Cr(IV), chromates in moderately-loaded zeolites (*MLZ*) were reduced to Cr(III), while chromates in highly-loaded zeolites (*HLZ*) were reduced to an average oxidation state of Cr(+3.5) containing equimolar amounts of Cr(III) and Cr(IV). The formation of occluded Cr(III)-Cr(IV) "dimers" was postulated.

Chromates in chromate nosean reacted with $H_{2(g)}$ to give a reduction product similar to that of *HLZ*, i.e. with an average oxidation state of Cr(+3.5). A unit cell edge contraction from 9.107(2) Å for chromate nosean to 8.916(6) Å upon reduction was shown to be consistent with the formation of $[Na_4.CrO_2]^{3+}$, $[Na_4.CrO_3]^{2+}$, $[Na_4.OH]^{3+}$, and $[Na_4]^{4+}$ clusters per two unit cells. Changes to the X-ray pattern upon reduction to an average oxidation state of Cr(+3.5) indicated transformation of chromate noselite to a reduced chromate sodalite. The movement of the reduced chromate species off the anion site and coordination to the lattice was envisaged. Reaction with $O_{2(g)}$ at 600°C formed chromate sodalite. Retention of the sodalite framework was attributed to the anion lying off the anion site. Heating the chromate sodalite in air at 1000°C for 2 hours reformed chromate noselite through movement of the chromate oxyanions back to anion sites.

The effect of temperature, zeolite type, and degree of loading on the kinetics of redox reactions were investigated. Unlike the reactions in nosean, transport control was not a feature of the reactions and zeolite structure had no significant effect on the redox kinetics. Reductions generally followed second-order kinetics and were highly activated processes with apparent activation energies between 86 ± 2 kJ mol^{-1} and 97 ± 10 kJ mol^{-1}. In contrast, reoxidations were usually described by chemisorption kinetics.

Preliminary investigations indicated a lack of activity of chromate zeolites in ethylene polymerisation and oxidation of methanol reactions. Chromate zeolites were also unable to oxidise $CO_{(g)}$ and $CH_{4(g)}$.

Acknowledgments

Thanks to my supervisor, Dr Alan Langdon, for assisting in the production of this thesis. My co-supervisor, Dr Tony Cartner, also deserves immense credit for blindly signing my progress reports.

Sincere thanks to Dave H. whose door, if not fridge, was always open- "Story".

Praise must go to people the likes of Les A., Johannes Z., Terry S., and Janine C., who have contributed to the raising of the average D.Phil. registration time almost to the extent that my time fell to within 2σ of the mean. A fart must of course be blown in the general direction of those people who have, will, or even plan to finish on time.

To my $9.95 pizza-fest buddies, Greg O., Bill H., Murph (when she's not hyper), Les A. (when he can keep it down), Soggy, and others, live long and prosper (excuse the philosophy but it is New Year).

Thanks to Terry S. and Chris S. for brightening up the place by leaving. Thanks would go to Lucy but she came back.

Thanks to Brett for pushing me to the Chemistry Department high score for Packman of 67,690. Remember play hard and don't let the RSI get you.

Thanks to the likes of Shane B., Ian G., Bruce R., Warren G., and Snowy whose company, although not always pleasant, meant I never had to drink my beer alone.

Lastly, thanks to Baldrick for making my drives look long and my short game look good.

Table of Contents

Abstract	(ii)
Acknowledgments	(v)
Table of Contents	(vi)
Abbreviations	(xi)
List of Tables	(xii)
List of Figures	(xiv)
List of Schemes	(xviii)
List of Plates	(xx)

Chapter One Introduction

1.1 Introduction	1
1.2 Aluminosilicate Structures	2
1.2.1 The Tetrahedron	2
1.2.2 Framework Structures	3
1.3 Adsorption by Zeolites	8
1.3.1 Ion-Exchange via Solid-State Reactions	9
1.3.2 Salt Occlusion or Imbibation	10
1.4 Intracage Reactions of Feldspathoids	12
1.5 Catalytic Activity of Supported Chromium Species	12
1.6 Previous Zeolite Studies at The University of Waikato	13
1.7 Scope of this Investigation	14

Chapter Two Methods and Materials

2.1 Introduction 22
2.2 Materials 22
2.3 Solid-State Reactions 23
2.4 Loaded Samples and Sample Notation 23
2.5 Powder X-Ray Diffraction (PXRD) 24
2.6 Electron Paramagnetic Resonance (EPR) 27
2.7 X-Ray Fluorescence (XRF) 30
2.8 Laser Raman Spectroscopy 31
2.9 Differential Thermal Analysis (DTA) 32
2.10 BET Surface Area 32
2.11 X-Ray Photoelectron Spectroscopy (XPS) 33
2.12 Scanning Electron Microscopy (SEM) 33
2.13 Fourier Transform Infrared (FTIR) 33
2.14 Reactivity Studies 34

Chapter Three Solid-State Reactions Between Zeolites and Group (VI) Oxyanions

3.1 Introduction 37

3.2 Methods and Materials 37

3.3 Results and Interpretation 38
3.3.1 Hydrothermal Uptake from Strong Salt Solution 38
3.3.2 Reaction of 13X and Sodium Chromate at 800°C 38
3.3.3 DTA Analysis of the Chromate-Zeolite Interaction 39
3.3.4 Occlusion of Chromate, Molybdate, and Tungstate 41
3.3.5 Kinetics of Sodium Chromate Uptake by 13X 48

3.4 Discussion 53
3.4.1 Hydrothermal Reactions of 13X and Salts 53
3.4.2 Devised Strategy for Oxyanion Occlusion 54
3.4.3 Possibility of Chromate Occlusion Within β-Cages 55

Chapter Four Structural Elucidation of Chromate Zeolites

4.1 Introduction 58
4.2 Methods and Materials 58
4.3 Possible Means of Occlusion 59
4.3.1 Reaction with Surface Hydroxyls 59
4.3.2 Formation of Chromyl Cations and Solid-State Reaction with the Protons of Structural Hydroxyls 60
4.3.3 Formation of Chromyl Cations and Solid-State Reaction with Zeolite Cations 61
4.3.4 Occlusion of Microcrystalline Sodium Chromate Phases within Supercages or Channels 62
4.3.5 Replacement of Framework Atoms 62
4.3.6 Encapsulation within Sodalite Cages 63
4.3.7 Coordination to the Lattice through Cations 64
4.3.8 Formation of Crystalline Phases on Crystal Surfaces 64
4.3.9 Formation of a New Oxyanion Containing Aluminosilicate Phases 64
4.4 Results and Interpretation 65
4.4.1 Chromate Leaching By NaOH, NaCl, and Na_2SO_4 65
4.4.2 SEM Analysis of Zeolite Morphologies 66
4.4.3 PXRD Analysis of Chromate Zeolites 78
4.4.4 Laser Raman Spectroscopic Analysis of Loaded Zeolites 82
4.4.5 FTIR Analysis of Loaded Zeolites 97
4.4.6 DTA Analysis of X-Type Zeolites 99
4.4.7 EPR Analysis of Chromate Zeolites 100
4.4.8 Analysis of Sodium Uptakes 103
4.4.9 BET Surface Area Analyses 104
4.4.10 XPS Analysis of Chromate Zeolites 105
4.4.11 Analysis of Maximum Chromate Uptakes 108
4.4.12 Summary of the Experimental Results 111
4.5 Discussion 112
4.5.1 Framework Stability 112
4.5.2 Modes of Occlusion that can be Eliminated 112
4.5.3 Proposed Mode of Chromate Occlusion 115
4.5.4 Proposed Mechanism of Chromate Removal 124
4.5.5 Usefulness of Raman for the Differentiation Between Chromates in α- and β-cages of Zeolites 125

Chapter Five Intracage Reactions of Chromate Nosean and Chromate Zeolites

5.1 Introduction 130

5.2 Methods and Materials 130

5.3 Results 131
- 5.3.1 Redox Reactions of Sodium Chromate Salt 131
- 5.3.2 Redox Reactions of 13.6CrX 138
- 5.3.3 Redox Reaction of 2.1CrX and 5.8CrX 142
- 5.3.4 Redox Reactions of 13.4CrY and 2.8CrY 144
- 5.3.5 Redox Reactions of 4.8Cr5A and 32.3Cr5A 145
- 5.3.6 Redox Reactions of Chromate Nosean 148
- 5.3.7 Redox Reactions of Na_2MoO_4 and Na_2WO_4 Loaded Zeolites 154

5.4 Discussion 155
- 5.4.1 Redox Reactions of Sodium Chromate 155
- 5.4.2 Redox Reactions of 13.6CrX 161
- 5.4.3 Redox Reactions of 4.8Cr5A and 32.3Cr5A 162
- 5.4.4 Redox Reactions of 2.1CrX and 5.8CrX 165
- 5.4.5 Effect of Encapsulation on Maximum Hydrogen Uptakes 165
- 5.4.6 Comparison of the Redox Behaviours of Chromate Zeolites 166
- 5.4.7 Reason for the Differences in Reduction Chemistries 167
- 5.4.8 Model Structure of the "Dimer" 170
- 5.4.9 Stability of the "Dimer" 173
- 5.4.10 Reason for the Differences in Reoxidation Chemistries 173
- 5.4.11 Proposed Structures of the Occluded Chromate Species 173
- 5.4.12 Redox Reactions of Chromate Nosean 175
  - 5.4.12.1 Space Group and Cluster Considerations 175
  - 5.4.12.2 Correlation between IR Band Frequencies and Unit Cell Edge 180
  - 5.4.12.3 Interpretation of a_0 Contraction upon Chromate Reduction 180
  - 5.4.12.4 Reduction to Cr(+4.5) 189
  - 5.4.12.5 Conversion of Chromate Nosean to Reduced Chromate Sodalite 191
  - 5.4.12.6 Conversion of Reduced Chromate Sodalite to Chromate Sodalite 194
  - 5.4.12.7 Conversion of Chromate Sodalite to Chromate Noselite 196
  - 5.4.12.8 Proposed Scheme for the Redox Reactions of Chromate Nosean 198
  - 5.4.12.9 Differences Between the High and Low Temperature Reductions 199
- 5.4.13 Comparison of the Redox Chemistries of Occluded Chromates and Chromium Ions in Zeolites 199
- 5.4.14 Comparison of the Redox Reactions of Occluded Chromate, Molybdate, and Tungstate 203

Chapter Six Kinetics of the Reactions of Chromate Zeolites

6.1 Introduction 206

6.2 Methods and Materials 206

6.3 Heterogeneous Reaction Kinetics 207
- 6.3.1 The Consecutive Steps 207
- 6.3.2 Diffusion of Reactant Molecules to the Surface 207
- 6.3.3 Diffusion of Gas Molecules into the Crystals 207
- 6.3.4 Chemisorption Processes 209
- 6.3.5 Chemical Reaction 211
- 6.3.6 Complexities of Gas-Solid Reactions 212

6.4 The Activation Energy 212

6.5 Results 213
- 6.5.1 Rate Dependence on Gas Pressure 213
- 6.5.2 Reactivity of Chromate Zeolite 5.8CrX 214
- 6.5.3 Reactivity of Chromate Zeolite 2.1CrX 219
- 6.5.4 Reactivity of Chromate Zeolite 2.8CrY 222
- 6.5.5 Reactivity of Chromate Zeolite 13.4CrY 226
- 6.5.6 Reactivity of 4.8Cr5A 231
- 6.5.6 Reactions Between Chromate Zeolites and Other Gases 236

6.6 Discussion 236
- 6.6.1 Reductions of 4.8Cr5A 236
- 6.6.2 Second-Order Dependence of the Reductions 237
- 6.6.3 Kinetics of Reoxidations 237
- 6.6.4 Effect of Degree of Loading on Reoxidation Kinetics 241
- 6.6.5 Discussion of Reaction Kinetics 242
- 6.6.6 Comparison with the Chemistry of Intrazeolitic Chromate Complexes 243

Chapter Seven Summary of Conclusions 246

Appendices 256

List of Abbreviations

A	Surface Area
BE	Binding Energy
BET	Brunauer, Emmett, and Teller
EPR	Electron Paramagnetic Resonance
Cr^{nos}	Chromate Nosean
Cr^{salt}	Sodium Chromate Salt
Cr^{sol}	Chromate Solution
D	Diffusion Coefficient
DTA	Differential Thermal Analysis
E_a	Apparent Activation Energy
EXAFS	Extended X-ray Absorption Fine Structure Spectroscopy
FTIR	Fourier Transform Infrared
HLZ	Highly-Loaded Zeolites
ICC	Intrazeolitic Chromate Complex
k_n	n^{th}-Order Rate Constant
LLZ	Lowly-Loaded Zeolites
MAS NMR	Magic Angle Spinning Nuclear Magnetic Resonance
PDF	Powder Diffraction File
PXRD	Powder X-Ray Diffraction
R	Gas Constant
r_a	Anion Radius (Thermochemical)
RDS	Rate Determining Step
r_o	Crystal Radius
r^2	Correlation Coefficient
SEM	Scanning Electron Microscopy
SBU	Secondary Building Unit
T	Temperature
t	Time
uc	Unit Cell
V	Volume
XPS	X-Ray Photoelectron Spectroscopy
XRF	X-Ray Fluorescence
θ	Extent of Reaction

List of Tables

Table 1.1 Solid-state reactions between various anions and zeolite Y 11

Table 2.1 Sources and grades of the various reagents used. 22
Table 2.2 Details of the syntheses of the loaded zeolites. 24
Table 2.3 Settings generally used for the recording of PXRD patterns. 25
Table 2.4 Data for the estimation of random errors in the determination of unit cell edge (a_o) from PXRD peaks. 26
Table 2.5 Settings generally used for the recording of EPR spectra. 27
Table 2.6 Results of the experiment to determine the errors in the recording of EPR signal intensities. 28
Table 2.7 Results of the EPR signal quantification. 29
Table 2.8 Settings used for the recording of FTIR spectra. 34

Table 3.1 Reaction of faujasite type zeolites and sodium chromate. 42
Table 3.2 Reaction of A and mordenite type zeolites and sodium chromate. 43
Table 3.3 Reaction of faujasite type and mordenite zeolites and sodium molybdate. 44
Table 3.4 Reaction of faujasite type and mordenite zeolites and sodium tungstate. 45
Table 3.5 Reaction mixtures and maximum chromate uptakes. 46
Table 3.6 Diffusion coefficient data obtained from the $\sqrt{t}$ plot for the uptake of sodium chromate by zeolite 13X. 51
Table 3.7 Activation energies (Ea) for the elution of chloride and fluoride compounds from zeolite A. 53

Table 4.1 Non-zeolite peaks in the PXRD pattern of 10.3CrY72. 78
Table 4.2 Positions of the chromate Raman bands for the various chromate-loaded zeolites. 83
Table 4.3 Positions of the Raman bands of sodium chromate salt and their assignments to the various vibrational modes. 83
Table 4.4 Structural data of dichromate. 91
Table 4.5 Structures and derived structural data of the possible configurations of anchored dichromates. 92
Table 4.6 Distances between Si atoms in the rings of various sizes. 92

Table 4.7 Ratio of the dichromate and chromate Raman band intensities and the structural data of the various ring sizes. 95
Table 4.8 DTA data of various X-type zeolites. 99
Table 4.9 Sodium uptakes during solid-state reactions of various zeolites with sodium chromate. 104
Table 4.10 Surface areas of various zeolites. 105
Table 4.11 XPS data of 13X. 105
Table 4.12 XPS data of 5.8CrX. 106
Table 4.13 XPS data of 13.6CrX. 106
Table 4.14 XPS data of 2.1CrX. 106
Table 4.15 Maximum chromate uptakes of various zeolites. 108
Table 4.16 Relationship between the numbers of the various structural features and the maximum chromate uptake 110
Table 4.17 Summary of the experimental results. 111
Table 4.18 Sodium deficiencies and maximum chromate uptakes of the zeolites examined. 114

Table 5.1 Data obtained from the PXRD patterns of Na_2CrO_4(R) and Na_2CrO_4(R,O). 133
Table 5.2 Intensities of the Na_2CrO_4 peaks in the PXRD patterns of samples Na_2CrO_4(R,O) and Na_2CrO_4(0.4). 134
Table 5.3 Binding energies and atomic concentrations of species in the surface layers of sodium chromate alt and its redox products. 135
Table 5.4 Products obtained from various redox treatments on Cr^{nos}. 148
Table 5.5 a_os and position of the framework IR bands for Cr^{nos} and the products obtained after various redox treatments. 148
Table 5.6 Summary of the redox chemistries of chromate zeolites and sodium chromate. 167
Table 5.7 Possible cage clusters in the cages of the redox products of Cr^{nos} 177
Table 5.8 Differences between the frameworks of sodalite and noselite. 178
Table 5.9 Thermochemical radii of various anions (r_a) and the unit cell edges (a_o) of the corresponding sodalite or nosean. 183
Table 5.10 Thermochemical radii of various anions relevant to this work. 185
Table 5.11 Average unit cell edge (a_o) expected for various cluster formations in reduced chromate nosean. 186

Table 6.1 Kinetic analysis of the reduction of 5.8CrX by hydrogen gas. 215
Table 6.2 Kinetic analysis of the reduction of chromate zeolite 2.1CrX by hydrogen gas. 221
Table 6.3 Kinetic analysis of the reduction of chromate zeolite 2.8CrY by hydrogen gas. 224
Table 6.4 Kinetic analysis of the reduction of chromate zeolite 13.4CrY by hydrogen gas. 228
Table 6.5 Apparent activation energies of the reduction of various chromate-loaded zeolites by hydrogen gas. 243

List of Figures

Figure 1.1 Various ways of representing the tetrahedral coordination of oxygen ions with aluminium and silicon. 2
Figure 1.2 The secondary building units (SBU) in zeolite structures according to Meier. 3
Figure 1.3 Three ways of depicting the truncated octahedron (or sodalite unit or β-cage) in aluminosilicate frameworks. 4
Figure 1.4 Stereodiagram of the framework of sodalite. 4
Figure 1.5 Stereodiagram of the framework of zeolite A. 6
Figure 1.6 Stereodiagram of the framework of faujasite. 7
Figure 1.7 The framework structure of mordenite 8

Figure 2.1 Diagram of the modified BET line used for surface area determinations and reactivity studies. 35

Figure 3.1 DTA patterns of sodium chromate salt, 13X and a reaction mixture of 13X and sodium chromate salt 40
Figure 3.2 Uptakes of sodium chromate by zeolite 13X via the solid-state reaction between sodium chromate and zeolite 13X at various temperatures. 48
Figure 3.3 $\sqrt{t}$ dependency of sodium chromate uptake by zeolite 13X at various temperatures. 49
Figure 3.4 Arrhenius plot for the uptake of sodium chromate by 13X. 50

Figure 3.5 Comparison of the effects of temperature on the coefficients of self-diffusion for sodium cations in zeolite Y and the diffusion coefficients of sodium chromate into zeolite 13X. 52

Figure 4.1 PXRD patterns of (a) 13X, (b) 13.6CrX, and (c) 2.1CrX. 80
Figure 4.2 PXRD patterns of (a) LZ-Y72 and (b) 10.3CrY72. 81
Figure 4.3 Raman spectra of (a) anhydrous chromate salt, (b) chromate solution, (c) chromate nosean. 84
Figure 4.4 Raman spectra of (a) 13.6CrX, (b) 2.1CrX, and (c) 13.4CrY. 85
Figure 4.5 Raman spectra of (a) 3.3Cr4A, (b) 2.3Cr3A, and (c) 32.3Cr5A. 86
Figure 4.6 Raman spectra of (a) 0.94CrS115 and (b) 0.87CrM5. 87
Figure 4.7 FTIR spectra of (a) sodium chromate salt, (b) 13X, (c) 13.6CrX, and (d) chromate nosean. 98
Figure 4.8 EPR spectra of (a) LZ-Y72, (b) 10.3CrY72. 101
Figure 4.9 Effect of various redox treatments on the EPR spectrum of the zeolite 13.6CrX. 102
Figure 4.10 Anchoring site for hexacarbonylmetal(0) complex in alkali metal zeolite Y. 116
Figure 4.11 Photoxidaton products of matrix isolated rhenium(I) and molybdenum(0). 116
Figure 4.12 Structural illustration of (a) 8{$W(CO)_6$}-$Na_{56}Y$ and (b) 16(WO_3)-$Na_{56}Y$. 117
Figure 4.13 Structures proposed by Özkar of (a) dehydrated $Na_{56}Y$, (b) 16{$Mo(CO)_6$}-$Na_{56}Y$, (c) 16(MoO_3)-$Na_{56}Y$, (d) 16(MoO_2)-$Na_{56}Y$. 118
Figure 4.14 Model proposed by Özkar for the "zeolate" ligation bonding in the *fac*-trioxomolybdenum(VI) unit of (MoO_3)-$Na_{56}Y$ (I). 119
Figure 4.15 Two possible configurations of occluded chromates. 120

Figure 5.1 PXRD patterns of the products of the redox reactions of sodium chromate salt 132
Figure 5.2 Average chromium oxidation state as a function of cyclic redox reactions on sodium chromate salt. 137
Figure 5.3 Effect of various redox treatments on the PXRD pattern of the zeolite 13.6CrX. 138
Figure 5.4 Effect of various redox treatments on the IR spectrum of the zeolite 13.6CrX. 139
Figure 5.5 Effect of various redox treatments on the EPR spectrum of the zeolite 13.6CrX. 140

Figure 5.6 Average chromium oxidation state as functions of successive redox reactions for zeolite 2.1CrX. 142
Figure 5.7 Average chromium oxidation state as functions of successive redox reactions for zeolite 5.8CrX. 143
Figure 5.8 Effect of cyclic redox reactions on the average chromium oxidation state of chromates occluded in 13.4CrY. 144
Figure 5.9 Effect of various redox treatments on the EPR spectrum of 4.8Cr5A. 146
Figure 5.10 Chromium oxidation state as a function of successive redox reactions on zeolite 4.8Cr5A. 147
Figure 5.11 PXRD patterns of chromate nosean and products of various redox treatments. 149
Figure 5.12 Infrared spectra of chromate nosean and products of various redox treatments. 150
Figure 5.13 Raman spectra of chromate nosean and products of various redox treatments. 151
Figure 5.14 Average oxidation state of Mo upon cyclic redox reactions on 2.3MoX. 154
Figure 5.15 Structures of the model Cr(III) and Cr(IV) compounds. 171
Figure 5.16 Model used to calculate interatomic distance between the oxygen atom of CrO_3^{2-} and the Cr atom of CrO_2^- in the Na_3CrO_5 "dimer" occluded in the α-cage of X zeolite. 172
Figure 5.17 Proposed structures of occluded chromates and the various reduced species. 174
Figure 5.18 Possible reaction routes for the transformation of chromate noselite to reduced chromate sodalite. 179
Figure 5.19 Relationship between the frequencies of the IR bands of the framework and the a_o of Cr^{nos}. 181
Figure 5.20 Plot showing the linear relationship between the a_o of Na sodalites and the radius of the occluded anion. 182
Figure 5.21 Proposed structure of the "dimer" in the sodalite. 193
Figure 5.22 Model proposed by Beuhrer *et al.* of the jump rotation of the $(Na_4.OH)^{3+}$ complex cation. 197
Figure 5.23 Proposed species involved in the redox chemistry of chromium cations in zeolites. 201
Figure 5.24 Oxidation state free energy diagram for chromium, molybdenum, and tungsten. 204

Figure 6.1 Hydrogen uptakes by 5.8CrX as functions of time at various temperatures. 215
Figure 6.2 Second-order reaction kinetics plot for reductions of 5.8CrX at various temperatures. 216
Figure 6.3 Arrhenius plot for the reduction of zeolites 2.1CrX and 5.8CrX by hydrogen gas. 216
Figure 6.4 Oxygen uptakes by reduced 5.8CrX as functions of time at various temperatures. 217
Figure 6.5 Plots of $1/(1-\theta)^n$ for reoxidation of reduced 5.8CrX by oxygen gas at 350°C. 218
Figure 6.6 Plot of θ against ln$t$ for reoxidations of reduced 5.8CrX. 219
Figure 6.7 Hydrogen uptakes by 2.1CrX as functions of time at various temperatures. 220
Figure 6.8 Second-order reaction kinetics plot for reductions of 2.1CrX at various temperatures. 221
Figure 6.9 Kinetics of the reoxidation of reduced 2.1CrX by oxygen gas at various temperatures. 222
Figure 6.10 Hydrogen uptakes by 2.8CrY as functions of time at various temperatures. 223
Figure 6.11 Second-order kinetics plots for the reductions of 2.8CrY. 224
Figure 6.12 Arrhenius plot for the reduction of 2.8CrY by hydrogen gas. 225
Figure 6.13 Uptakes of oxygen gas by reduced 2.8CrY at 300°C. 226
Figure 6.14 Plots of extent of reaction against time for the reductions of 13.4CrY by hydrogen gas at various temperatures. 227
Figure 6.15 Second-order reaction kinetics plot for reductions of 13.4CrY at various temperatures. 228
Figure 6.16 Arrhenius plot for the reduction of 13.4CrY by hydrogen gas. 229
Figure 6.17 Plots of extent of reaction against time for reoxidations of reduced 13.4CrY by oxygen gas. 230
Figure 6.18 Third-order kinetics plots for the reoxidations of reduced 13.4CrY by oxygen gas at various temperatures. 231
Figure 6.19 Uptake of hydrogen gas as functions of time by 4.8Cr5A at various temperatures. 232
Figure 6.20 Plots of chromium oxidation state and $1/(1-\theta)$ as functions of time for the primary reduction of 4.8Cr5A by hydrogen gas at 400°C. 233

Figure 6.21 Oxygen uptakes as functions of time by reduced 4.8Cr5A at various temperatures. 234
Figure 6.22 Oxygen uptakes as functions of √t by reduced 4.8Cr5A at various temperatures. 234
Figure 6.23 Plots of θ against √t for the reoxidations of two sample weights of 4.8Cr5A at 400°C. 235
Figure 6.24 Plots of θ against ln$t$ and ln(t + 1.1) for reoxidation of reduced 5.8CrX by oxygen gas at 300°C. 239
Figure 6.25 Plot of θ against ln$t$ for a reoxidation of reduced 5.8CrX by oxygen gas at 350°C. 240

List of Schemes

Scheme 4.1 Reaction of sodium chromate with zeolitic surface hydroxyls. 60
Scheme 4.2 Solid-state reaction between chromium trioxide and hydrogen zeolites involving the replacement of the protons of structural hydroxyls by chromyl cations 60
Scheme 4.3 Possible reaction between the H^+ forms of zeolites and sodium chromate involving the replacement of the protons of structural hydroxyls by chromyl cations. 60
Scheme 4.4 Reaction between zeolites and sodium chromate involving the replacement of the protons of structural hydroxyls by sodium cations. 61
Scheme 4.5 Possible reaction of zeolitic sodium cations and sodium chromate involving the replacement of zeolite sodium cations by chromyl cations. 62
Scheme 4.6 Isomorphous replacement of aluminium by chromium during refluxing of zeolites X and Y with $CrCl_3$. 63
Scheme 4.7 Proposed mechanism for the removal of surface bound dichromates by NaOH solution. 96
Scheme 4.8 Proposed scheme for the reaction of sodium chromate with the acid sites of hydrogen zeolite LZ-Y72. 123
Scheme 4.9 Proposed mechanism for the removal of occluded chromates by salts such as NaOH. 125

Scheme 5.1 Stoichiometry consistent with reduction of sodium chromate by hydrogen gas to form $NaCrO_2$. 155
Scheme 5.2 Possible reactions between $NaCrO_2$, NaOH and oxygen gas. 159
Scheme 5.3 Mechanism consistent with the stoichiometry of the reoxidation of reduced sodium chromate salt. 159
Scheme 5.4 Overall stoichiometry of the reoxidation reduced sodium chromate salt to sodium chromate with an excess of NaOH. 160
Scheme 5.5 Proposed redox reactions of sodium chromate salt. 161
Scheme 5.6 Proposed reaction scheme for the reduction of 13.6CrX by hydrogen gas at 375°C. 162
Scheme 5.7 Proposed reaction scheme for the reoxidation of reduced 13.6CrX by oxygen gas. 162
Scheme 5.8 Proposed reaction between 4.8Cr5A and hydrogen gas. 163
Scheme 5.9 Proposed reaction mechanism for the reduction of 4.8Cr5A by hydrogen gas. 163
Scheme 5.10 Possible stoichiometry of the reactions of the reoxidation of $NaCrO_2$ within the pores of 4.8Cr5A by oxygen gas. 164
Scheme 5.11 Proposed reduction of the chromates in 2.1CrX by hydrogen gas to Cr(IV). 165
Scheme 5.12 Possible cluster formation during the reduction of Cr^{nos} to Cr(+3.5). 187
Scheme 5.13 Possible cage clusters and reaction sequence involved in the reduction of Cr^{nos} by hydrogen gas at 400°C. 188
Scheme 5.14 Reaction of Cr^{nos} to the average oxidation state of Cr(+4.5) through the formation of Cr(IV) and Cr(V) species. 190

Scheme 6.1 Proposed mechanism and overall stoichiometry for the primary reduction of 4.8Cr5A. 236
Scheme 6.2 Reaction of reduced 5.8CrX and oxygen gas consistent with the observation of chemisorption kinetics. 239

List of Plates

Plate 4.1 SEM photograph of zeolite 13X. Magnification = 8.0 k. 68

Plate 4.2 SEM photograph of zeolite 13X. Magnification = 18.0 k. 68

Plate 4.3 SEM photograph of zeolite 5.8CrX. Magnification = 8.0 k. 69

Plate 4.4 SEM photograph of zeolite 5.8CrX. Magnification = 18.0 k. 69

Plate 4.5 SEM photograph of zeolite 13.6CrX. Magnification = 6.0 k. 70

Plate 4.6 SEM photograph of zeolite 13.6CrX. Magnification = 25.0 k. 70

Plate 4.7 SEM photograph of zeolite 2.1CrX. Magnification = 8.0 k. 71

Plate 4.8 SEM photograph of zeolite 2.1CrX. Magnification = 20.0 k. 71

Plate 4.9 SEM photograph of zeolite 5A. Magnification = 1.8 k. 72

Plate 4.10 SEM photograph of zeolite 5A. Magnification = 6.0 k. 72

Plate 4.11 SEM photograph of zeolite 4.8Cr5A. Magnification = 6.6 k. 73

Plate 4.12 SEM photograph of zeolite 32.3Cr5A. Magnification = 4.5 k. 73

Plate 4.13 SEM photograph of zeolite Y52. Magnification = 8.0 k. 74

Plate 4.14 SEM photograph of zeolite Y52. Magnification = 18.0 k. 74

Plate 4.15 SEM photograph of zeolite 2.8CrY. Magnification = 8.0 k. 75

Plate 4.16 SEM photograph of zeolite 2.8CrY. Magnification = 18.0 k. 75

Plate 4.17 SEM photograph of zeolite LZ-Y72. Magnification = 15.0 k. 76

Plate 4.18 SEM photograph of zeolite 10.3CrY72. Magnification = 15.0 k. 76

Chapter One

Introduction

1.1 Introduction

The widespread application of zeolites as catalysts has attracted attention towards enhancing, extending or modifying catalytic activity through the introduction of catalytically active metal species. The dominant and most useful property of zeolites is their intracrystalline pore and cavity system which can occlude and release small molecules into and from the entire crystal. Work on salt inclusion in feldspathoid crystals by Barrer *et al.*[1,2,3] encouraged attempts to form irreversible zeolite-salt occlusion compounds. Rabo *et al.*[4] felt that salt occlusion into the sodalite cages of type X and Y zeolites would change several properties of these zeolites. The presence of guest salt or NaOH in sodalite minerals supported the simple concept that guest salts will reduce undesirable cation to cation interactions. The filling of empty cages of zeolites with properly arranged guest ions should increase the lattice energy and crystal stability. Tomisaka and Eugster[5] synthesised chromate, molybdate and tungstate noselites from nepheline under dry conditions. Their work led a focussing of attention on the characterisation of nosean systems[6,7,8,9] and the solid-state occlusion of chromate oxyanions by zeolites.[10] A principal aim of the present investigation was to gain a better understanding of the chemistry of these systems.

1.2 Aluminosilicate Structures

1.2.1 The Tetrahedron

Silicate and aluminosilicate chemistries are based on the tetrahedron. The fundamental unit is a tetrahedral complex consisting of a Si^{4+} or Al^{3+} cation coordinated to four oxygens (see Figure 1.1). The diverse nature and complexity of silicate structures arise from the large variety of ways tetrahedra can link to form polynuclear complexes, referred to as secondary building units (SBU), see Figure 1.2.

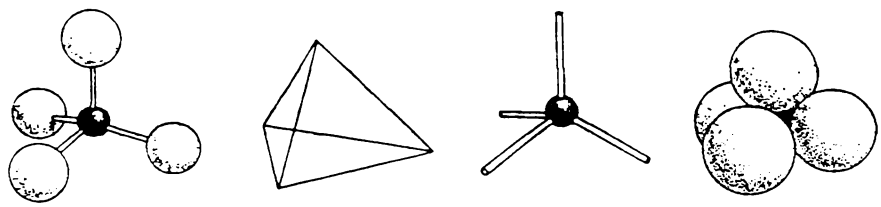


Figure 1.1 Various ways of representing the tetrahedral coordination of oxygen ions with aluminium and silicon. (a) ball and stick model, (b) solid tetrahedra, (c) skeletal tetrahedron, and (d) a space-filling model based on packed spheres.

Substitution of silicon by aluminium in silicate frameworks forms aluminosilicates. The nett negative charge resulting from Al^{3+} replacement of Si^{4+} is neutralised by the presence of cations, generally of the alkali metal or alkaline earth metal groups. Various aluminosilicate structures arise from different linking of tetrahedra, in one, two or three dimensions, and in the variety of incorporated framework cations.

Five main types of silicate and aluminosilicate structures exist. These are island structures, isolated group structures, chain structures, sheet structures, and framework structures. Breck[11] reviewed the structures of these types of compounds. Of interest within the scope of this work are the framework structures.

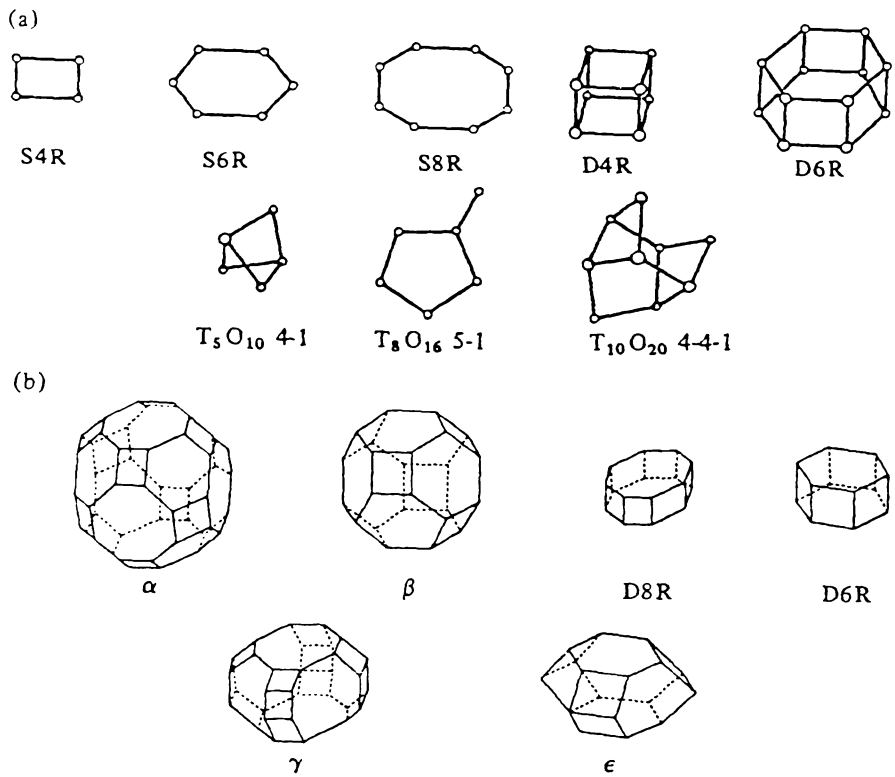


Figure 1.2 (a) The secondary building units (SBU) in zeolite structures according to Meier.[12] Only the positions of the tetrahedral silicon and aluminium atoms are shown. Oxygen atoms lie near the connecting solid lines, which are not intended to mean bonds. (b) Some polyhedra in zeolite frameworks: a (26-hedron Type I) or truncated cuboctahedron; b (14-hedron type I) or truncated octahedron; d or double 8-ring; D6R or double 6-ring (hexagonal prism); g or 18-hedron; and e or the 11-hedron.[13]

1.2.2 Framework Structures

Mutual sharing of all oxygen atoms in the tetrahedra between silicon and aluminium atoms results in framework structures. The three main classes of framework aluminosilicates are feldspars, feldspathoids, and zeolites.

Noselite and Sodalite

Chromate nosean belongs to the small noselite sub-group of the sodalite family of aluminosilicates. The basic structural unit of the sodalite group is the cuboctahedron (or β-cage or sodalite cage) composed of 24 (Si or Al)-O

tetrahedra forming six four-membered rings and eight six-membered rings (see Figure 1.3).

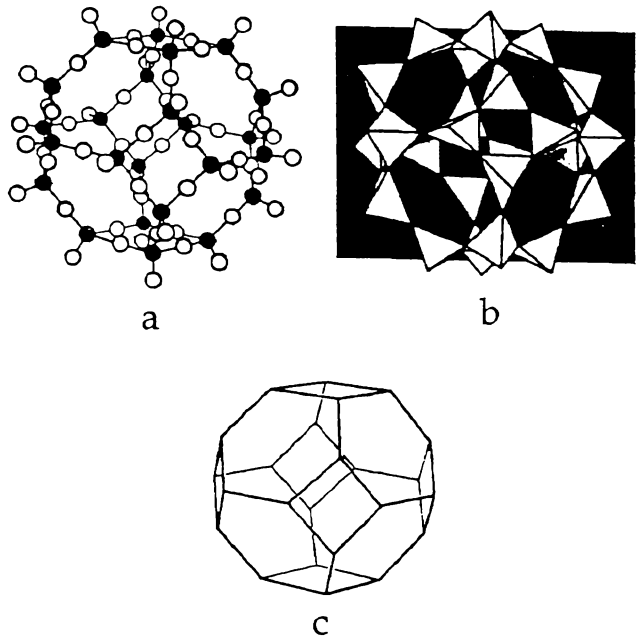


Figure 1.3 Three ways of depicting the truncated octahedron (or sodalite unit or β-cage) in aluminosilicate frameworks.

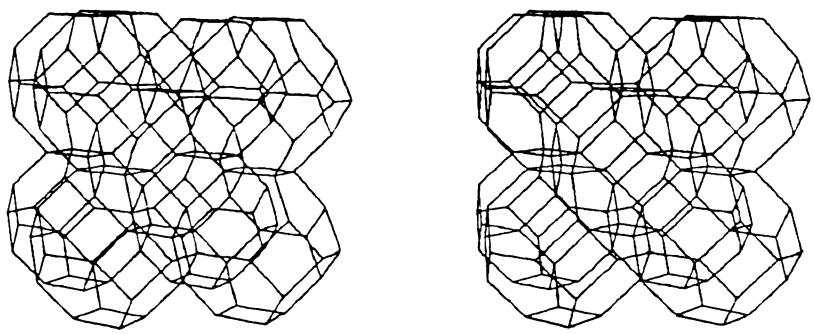


Figure 1.4 Stereodiagram of the framework of sodalite.

Sodalite and nosean have structures topologically similar to that of ultramarine, first determined by Jaeger,[14] and consist of fused sodalite cages (see Figure 1.4). Sodalites are an unusual group of aluminosilicates in that they contain within the framework anionic species such as Cl^-, OH^-, and SO_4^{2-}

occupying positions near the centre of the sodalite cage.[15] They are of the general formula $M_n[SiAlO_4]_6 \cdot X_m$ where M represents monovalent or divalent cations of overall charge +8 and X represents either a monovalent anion (m = 2) or a divalent anion (m = 1). The anion is most commonly a halide but sodalites containing SCN^-, NO_2^-, OH^- and other small inorganic/organic ions are known.[16] Intraframework cations lie near the plane of the six-membered rings on eight crystallographically indistinguishable sites. Intraframework anions occupy sites in the centre of the cuboctahedra at crystallographic coordinates (0,0,0) and (1/2,1/2,1/2) surrounded tetrahedrally by four cations. Members of the noselite subgroup, of general formula $M_n[SiAlO_4]_6 \cdot MO_4^{2-}$, contain divalent anions such as chromate and sulphate in alternate cages. The unit cells of noselites contain only one divalent anion distributed over the two anion sites in the space group $P_{\bar{4}3m}$. Alternately filled and empty cuboctahedra gives two cage sizes with two distinct sets of 12 oxygen positions on 12i sites and two distinct sets of four equivalent cations. Loss of the n-glide plane along the 100 plane results in a significant difference in the X-ray diffraction pattern in the (100) peak which is present for noselites but completely extinguished in sodalites.

As noted by Pauling,[15] the sodalite framework is partially collapsed by rotation of the TO4 tetrahedra to accommodate the intraframework ions.[17] The maximum symmetry for sodalite-type structures is the centrosymmetric space group $Im3m$. and occurs when the framework is in the fully expanded state. Even the slightest collapse destroys the centre of symmetry and the space group becomes $I\bar{4}3m$. Depmeier *et al.*[18] found $Sr_8[Al_{12}O_{24}].(CrO_4)_2$ sodalite could be described equally well by $Im3m$ or $I\bar{4}3m$. In aluminosilicates ordering of Al and Si further reduces the space group to $P_{\bar{4}3n}$.

Zeolite A

Linking sodalite cages through shared oxygen atoms through the four rings produces the framework of zeolite A (see Figure 1.5). An alternative description involves two types of polyhedra, a cubic arrangement of eight metal atoms and the sodalite (β) cage. Placing sodalite units at the corners of a cube and linking them through the four-rings (S4R) produces the zeolite A framework. The large cavity produced, the α-cage, has a diameter of ~11.4 Å. Entry into the α-cage is through an 8-ring (S8R) with a free diameter of 4.2 Å. Zeolite A has a pseudo unit cell containing 24 tetrahedra, 12 AlO_4 and 12 SiO_4 with a pseudo-cell constant of 12.3 Å. The real unit cell contains 192 tetrahedra with a cell constant of 24.6 Å. Zeolites of the A type generally have Si/Al ratios near 1. It is postulated that variations in the Si/Al ratio arise from occlusion of $NaAlO_2$ within the β-cages, similar to feldspathoid behaviour.[19]

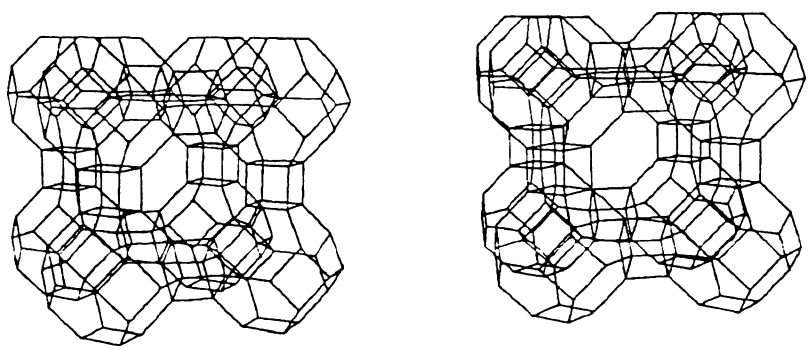


Figure 1.5 Stereodiagram of the framework of zeolite A.

Zeolites X and Y

Zeolite X and Y have structures topologically similar to that of the mineral faujasite (see Figure 1.6). The framework consists of a diamond-like array of sodalite cages linked tetrahedrally through 6-rings (S6R) of sodalite cages. Each sodalite cage is linked to four others in a tetrahedral configuration through hexagonal prisms (D6R) attached to four of the eight S6R. Linking the

octahedra is this way forms an α-cage with a diameter of ~13 Å, entry into which is through a 12-ring (S12R) with a free diameter of ~7.4 Å.

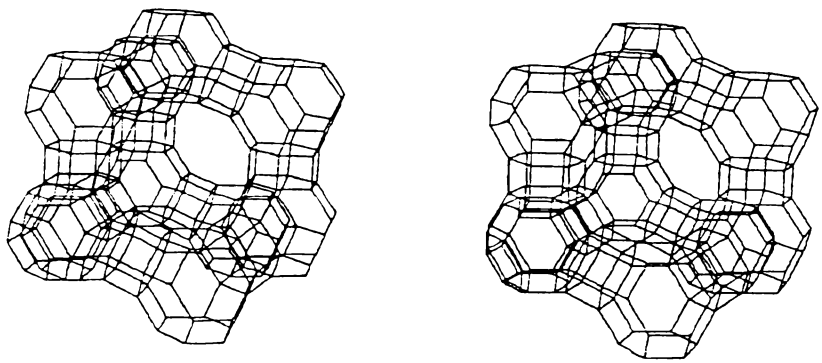


Figure 1.6 Stereodiagram of the framework of faujasite.

Zeolites X and Y can be differentiated on the basis of their chemical composition, structure, and physical and chemical properties. Cation composition and distribution and the Si/Al ratio also differ. In zeolite X the number of aluminium ions in the unit cell varies from about 96 to 77 while that of zeolite Y varies from about 76 to 48. These aluminium contents correspond to Si/Al ratios between 1 and 1.5 for zeolite X and between 1.5 and 3 for zeolite Y.

Mordenite

The structure of mordenite consists of chains containing five rings, such as those shown in Figure 1.7, cross linked by the sharing of neighbouring oxygen atoms to form four rings. Mordenite contains S12R perpendicular to the *c*-axis of free diameter 6.7x7.0 Å and S8R perpendicular to the *b*-axis of free diameter 2.9x5.7 Å.

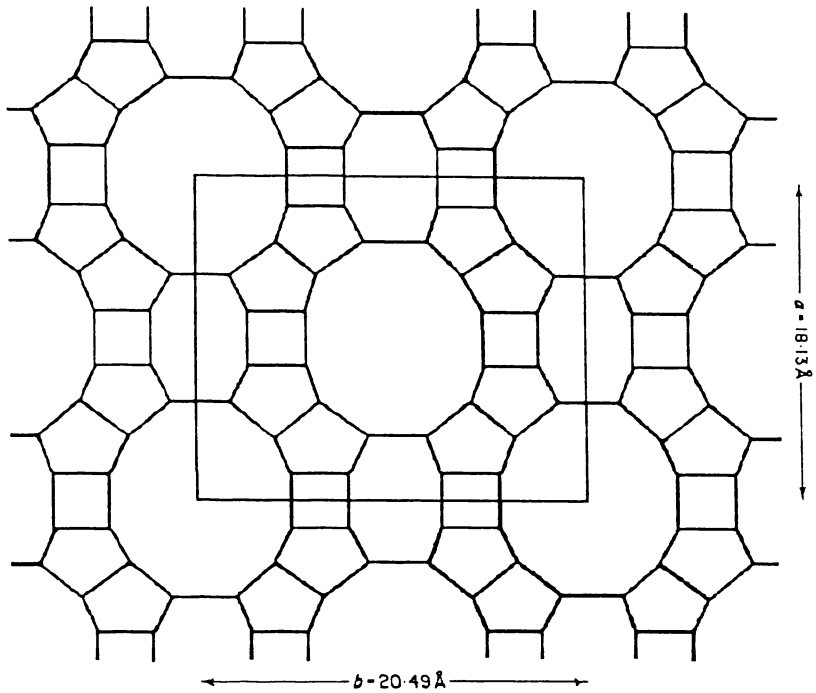


Figure 1.7 The framework structure of mordenite in cross-section normal to the wide channels.

1.3 Adsorption by Zeolites

One of the most useful properties of zeolites is their ability to occlude and release small molecules. Zeolites upon formation contain large quantities of water. Removal of this water is often a reversible process having little effect on the aluminosilicate framework but leaving large void spaces capable of occluding small molecules. Upon dehydration cations lose their coordination sphere and seek coordination with framework oxygens. In most cases the framework does not provide sites of high enough coordination and at least some of the cations must occupy sites of low coordination. In zeolites X and Y each unit cell contains 16 cation sites of near octahedral symmetry in the hexagonal prisms while the rest of the cations occupy sites of lower symmetry and coordination in the sodalite cages and in the supercage. Binding of cations to surface oxygens on one side only results in a large electrostatic field adjacent to the large cavity. This electrostatic field is responsible for the characteristic adsorption properties of zeolites. Adsorption is favourable when the process

results in a zeolite-adsorbate system of lower free-energy than the separate zeolite and adsorbate. Attainment of equilibrium results in the configuration of the adsorbate-adsorbent pair to the lowest free-energy. Cation-cation repulsions and the large electrostatic field within the supercage resulting upon dehydration are undesirable for an ideal ionic lattice and make the adsorption of polar, polarisable or ionic species favourable. Methods commonly employed for the introduction guest compounds into zeolite host crystals include salt introduction from melts, ion-exchange (both from solution and via solid-state reactions), and gaseous adsorption of volatile species. Because of the high temperatures required to occlude chromate within zeolites we are interested, in addition to salt-zeolite interactions, in solid-state ion-exchange reactions. Examples of such reactions follow.

1.3.1 Ion-Exchange via Solid-State Reactions

Barrer[20] reported cation exchange between NH_4Cl and zeolites in the anhydrous state. Nearly complete cation exchange resulted from extended exposure of anhydrous zeolites and NH_4Cl vapours at 300°C. Barrer and Kanellopoulos[21] studied the cation exchange between HCl and NaY showing replacement of zeolite Na^+ by H^+. Rabo *et al.*[4,22,23] reported the release of HCl during calcination of mixtures of NaY, CaY, BaY, or ZnY and salt halides at temperatures above 500°C. The amount of HCl released depended on the H content of the zeolite indicating replacement of the protons of structural hydroxyls by the cations of the halide salt. Investigations by Liquornik and Marcus[24,25] showed cation exchange between molten nitrate salts and A type zeolites. Clearfield *et al.*[26] observed solid-state exchange reactions between halides ($ZnCl_2$, $CuCl_2$, $NiCl_2$, $CoCl_2$, $MnCl_2$, and $CrCl_3$) and the hydrogen forms of A, X and Y type zeolites. More recently, Beyer *et al.*[27] reported the release of hydrogen chloride during the solid-state interactions between alkali

metal chlorides (NaCl, KCl, RbCl, and CsCl) and NH_4-ZSM-5, H-ZSM-5 and silicalite. Fornes *et al.*[28] studied the interactions of NiO, MoO_3 and their mixtures with the acid surface of an H-Y ultrastable zeolite. Kucherov and Slinkin[29] reported the migration of Cu(II) or Cu(I) ions into zeolite channels upon calcination of H-mordenite or H-ZSM-5 and CuO, $CuCl_2$, CuF_2, $Cu_3(PO_4)_2$ or CuS_2 and showed coordination in the same positions as copper ions introduced by aqueous ion-exchange. Migration of Fe(III) ions onto cationic positions results during the solid-state interaction between H-ZSM-5 and $FeCl_3$.[30] Solid-state reactions of V_2O_5 with H-ZSM-5[31] and H-Y[32] introduced vanadyl species onto cationic sites. Slinkin *et al.*[33,34] introduced chromium cations onto the cationic positions of H-ZSM-5 via solid-state reaction with CrO_3. Kucherov *et al.*[35] reported a comparative study of the introduction of Cu, Fe, Cr, and V cations into H-ZSM-5 and H-[Ga]ZSM-5 via solid-state reactions.

1.3.2 Salt Occlusion or Imbibation

Barrer *et al.*[36] observed the reversible occlusion of iodide and fluoride salts within Linde A and Linde X zeolites. An enhanced high temperature stability of the zeolite lattice was observed for the zeolite-salt systems. Heating AgA zeolite and $AgNO_3$ melt at 250-260°C for at least eight hours resulted in the occlusion of 9 $AgNO_3$ molecules per pseudo unit cell.[37] According to X-ray evidence the nitrate guest salt formed an octahedral $(AgNO_3)_9$ cluster in each large cavity. All the $AgNO_3$ was removed by washing in hot water. Heating $NaNO_3$ and NaA zeolite at 350°C occluded up to two nitrate ions per sodalite cage.[38] The infrared and Raman spectra of the nitrate ions in the large cages and the small cages differed appreciably, the former resembling those of solid $NaNO_3$. Washing removed all nitrate in the large cages leaving only those bands caused by nitrate ions trapped in the sodalite cages. Zeolite A

occludes NaCl and $CaCl_2$ from solution with kinetics that follow a $\sqrt{t}$ law over the initial stages of salt occlusion and indicate activation energies of 106 kJ mol^{-1} for sodium chloride and 114 kJ mol^{-1} for calcium chloride.[39] Saturated Na_2SO_4 solution in contact with zeolite A for a week at 190°C showed no occlusion of the sulphate ion. The sulphate ion with a diameter of 5.5 Å is excluded.[39]

Table 1.1 summarises the work of Rabo *et al.* showing the effect of temperature on the uptake of sodium halides[40] and $NaNO_3$/ClO_3^-[41] into the sodalite cages of zeolite Na-Y. An increase in temperature with increasing anion radius is required to allow passage into the sodalite cages.

Table 1.1 Solid-state reactions between various anions and zeolite Y from Rabo *et al.*[40,41].

Guest Salt	Thermal Treatment T/°C	Time/hr	Anion per β-cage	X-Ray crystallinity
NaCl	200	24	0.02	excellent
	330	24	0.04	excellent
	440	24	0.29	excellent
	550	24	1.02	excellent
NaBr	550	24	0.16	excellent
	700	24	0.98	excellent
	785	24	0.64	fair
NaI	550	24	0.06	excellent
	645	24	0.33	fair-good
	700	24	0.25	poor
$NaNO_3$	550	64	0.59	excellent
	650	24	1.32	excellent
$AgNO_3$	550	48	0.37	excellent
$NaClO_3$	650	16	0.9	excellent

1.4 Intracage Reactions of Feldspathoids

Intracage reactions and decomposition of salt species within feldspathoids have been known for some time. Barrer *et al.*[42] followed the kinetics of oxygen release as functions of temperature and time during the thermal decomposition of $NaClO_2$, $NaClO_3$ and $NaClO_4$ to NaCl within sodalite cages. Weller and Haworth[43] observed decomposition of MnO_4^- to MnO_2^- and ClO_4^- to Cl^- in sodalites. Lattice parameters for both sodalites contracted due to formation of smaller occluded salt species. Weller *et. al*[44] observed the appearance of the (100) X-ray diffraction peak when the sodalite $Na_8[AlSiO_4]_6.(SCN)_2.xH_2O$ was heated in air at 850°C for 24 hours. Conversion of a sodalite phase to a noselite phase and the increase in unit cell edge, was attributed to the formation of sulphate nosean, $Na_8[AlSiO_4]_6.(SO_4)$. Brown[9] reported the loss of the (100) X-ray diffraction peak when chromate nosean was reduced by $H_{2(g)}$ at temperatures above 500°C while the loss was not observed for reductions performed below 500°C. The (100) peak loss was attributed to the formation of reduced chromate sodalite at the higher temperatures. Heating reduced chromate sodalites in oxygen at temperatures up to 670°C formed chromate sodalites that were converted to chromate noseans by heating in air at 1000°C.

1.5 Catalytic Activity of Supported Chromium Species

Catalysts based on chromium, molybdenum and tungsten oxides have attracted considerable interest in recent years. High activity in alkene polymerisation reactions, particularly that of ethylene, has resulted in a focussing of research and development on silica supported chromium oxide catalysts.[45] These types of catalysts also exhibit varying degrees of activity towards other reactions such as the decomposition of H_2O_2,[46] the reduction of

N_2O by CO,[47] the exchange of H_2 and D_2,[48] the oxidation of CO,[49,50] the hydrogenation of olefins,[51,52,53] and the oxidation of alcohols.[54,55,56] Chromia-alumina catalysts are active in alkane dehydrogenation, dehydrocyclisation, and in oxidation reactions.[57,58,59] Activity towards ethylene hydrogenation[60] and ammonia oxidation by nitric oxide[61] have been reported. Chromium on various other supports or alone in various forms exhibits activity in a wide range of reactions. Some examples are the oxidation of carbon monoxide by chromium-promoted Raney copper catalysts,[62] the water-gas shift reaction over iron oxide/chromium oxide,[63] the hydrogenation of dienes by copper chromite,[64] ethylene by chromia,[65] and the oxidation of methanol over chromium containing corundum catalyst.[66] Zeolites loaded with chromium ions are active in hydrogen oxidation,[67] hydration of olefins,[68] and ethylene polymerisation.[69]

1.6 Previous Zeolite Studies at The University of Waikato

Moroney[6] synthesised chromate nosean via the solid-state reaction of mixtures of hydroxysodalite and sodium chromate. X-ray diffraction indicated hydroxysodalite decomposition to an amorphous aluminosilicate precursor prior to nosean formation. Chromate occluded within the cages of nosean was found to reduce in hydrogen gas at elevated temperatures. The formulated product of the reduction of chromium was Cr_2O_3.

Shanmugam[7] produced highly crystalline chromate, molybdate and tungstate noseans via solid-state reactions of mixtures of the sodium salt and a variety of aluminium and silicon starting materials. Chromate nosean was reduced by hydrogen gas at elevated temperatures. Electron Paramagnetic Resonance indicated the formation of paramagnetic chromium species during

reductions. Also reported were preliminary kinetic studies of the reoxidation of reduced chromate nosean by oxygen gas.

Brown[9] synthesised chromate, molybdate, and tungstate nosean via solid-state reactions. Laser Raman spectra of chromate nosean and EPR spectra of Cr(V) and Cr(III), formed upon reduction by hydrogen gas, provided spectroscopic fingerprints of chromate occluded within sodalite cages. The kinetics of reduction and reoxidation reactions showed diffusion of the reactant gas through the nosean framework to be rate-limiting.

Martinus[8] investigated the crystallisation of various salt-loaded aluminosilicates via solid-state reactions using kaolinite as a starting material.

Snowdon[10] investigated the solid-state reactions between sodium chromate and zeolites of the types A and Y in the temperature range 500°C to 800°C. Substantial levels of chromate were irreversibly occluded. Raman spectra were characteristic of discrete chromate oxyanions and the occlusion of chromate within sodalite cages was postulated.

1.7 Scope of this Investigation

Preliminary research by Snowdon[10] showed that the solid-state reaction between sodium chromate salt and zeolites of the types Y and A results in the irreversible occlusion. Extensions to Snowdon's work were envisaged.

Snowdon reported Raman spectra characteristic of discrete chromate oxyanions and it was postulated that occlusion within the sodalite cages occurred. As complex anions are known to occupy, and indeed stabilise, this type of cage in both zeolites and feldspathoids, occlusion within sodalite cages is a conceivable outcome of the solid-state reaction of zeolites and sodium chromate. The complex structures of zeolites mean that they offer more

possible sites for occlusion than the simpler feldspathoids. For example, zeolites of the types A and Y contain sodalite cages and supercages both capable of occluding salt species. Raman spectra characteristic of discrete chromate oxyanions may result from the occlusion of such species within supercages. A more rigorous physical and spectroscopic study of chromate-loaded zeolites was planned to determine the means of occlusion. In addition, a detailed study of the uptake kinetics during salt occlusion offers a possible means for deducing the mechanism of oxyanion uptake.

An aim of this and earlier work was to determine whether occlusion of chromate within the sodalite cages of zeolites X, Y, and A is possible. The devising of a strategy for chromate based on consideration of the literature on salt loading phenomena was planned. Extension of the work to include molybdate and tungstate occlusion by zeolites was planned. These results and those for sodium chromate then would allow a comparison of the occlusion chemistry of oxyanions of the first to third transition series of Group VI. Differences arising from the larger anion radii of molybdate and tungstate and their greater tendency to condense to poly-oxyanions may be present.

Investigations of the occlusion of oxyanions by zeolites without sodalite cages such as M5 (mordenite) and S115 (silicalite) were planned to determine the role of sodalite cages in oxyanion occlusion. Solid-state reactions between sodium chromate and the hydrogen form of Y were envisaged to assess the role of acid sites in oxyanion occlusion.

An aspect of the chemistry of oxyanion-loaded zeolites of significant interest is the reactivity of the occluded species. The kinetics of the redox reactions is of interest as it is the rate at which these reactions proceed that will determine whether occluded species can function effectively as catalysts or reagents. It is also of interest to know how these systems respond, with respect

to structural stability, to the often harsh conditions encountered in the pretreatments (activation) or actual use of catalysts. Such extremes include high temperatures and long periods of time under vacuum or in oxidising or reducing atmospheres. Kinetic studies offer a means of accessing reactivity and may allow the reaction mechanism to be deduced. Such a study of the $H_{2(g)}/O_{2(g)}$ redox reactions of chromate nosean was performed by Brown.[9] The rate determining step for both reactions was found to be the diffusion of the reactant gas through the dense framework of this felspathoid. The more open structures of zeolites may afford different kinetics with faster reaction rates and/or alternative rate determining steps. In a manner similar to the way in which pore size governs sorption processes, pore size may also control kinetics of redox reactions of occluded chromates. A systematic study of the reactivity of occluded chromates in different zeolites would allow the effect of other variables such as channel structure, and Si/Al ratio also to be determined.

The extent to which occlusion modifies redox chemistry is of interest. Zeolites offer void spaces that can be filled by salt species. Upon occlusion these species are separated to various extents depending on the number of oxyanions per unit cell. Void spaces in zeolites can be considered as reaction chambers of nanometer dimensions. Interactions between occluded species will be limited to those in close proximity (for example those within one α-cage) particularly if constrictions within the structure (eg S8R, S10R, S12R) or a strong interaction with the lattice prevents migration of occluded species. Even if migration can occur, the nanometer dimensions of zeolite cavities will prevent the formation of stable macroscopic crystalline or polymeric phases. For example, since reduction of sodium chromate salt by hydrogen gas forms crystalline $NaCrO_2$, one might expect the product of the reduction occluded species to be different from that of the pure salt. This difference might give rise

to interesting chemistries involving novel oxyanion species unobtainable via other means in alternative systems.

An insight into the reaction chemistry can be gained from stoichiometries of gas uptakes. However, little more than an average oxidation state can be deduced by this method alone. Investigations using spectroscopic techniques (Raman, EPR, FTIR) were envisaged to provide discrimination between the possible combinations of oxidation states consistent with a given average oxidation state.

Investigations of the reactivity of chromate zeolites towards ethylene polymerisation and oxidation of low molecular weight alcohols were envisaged.

Brown[9] reported the loss of the 100 X-ray diffraction peak of chromate noselite upon reduction under certain conditions indicating a transformation to a sodalite framework. Only reductions performed at temperatures above 500°C resulted in the framework transformation and the need for the acquisition of the fully expanded state was postulated. Later work by Martinus[8] showed that framework changes correlated with the loss of the chromate infrared band suggesting that the degree of reduction affected the framework structure. Combined X-ray diffraction and spectroscopic analyses and further consideration of space group criteria were planned to deduce the mechanism of the framework changes.

References in Chapter One

1) Barrer, R.M. and Cole, J.F., *J. Chem. Soc. A*, **9** (1970) 1516.

2) Barrer, R.M., Cole, J.F. and Villiger, H., *J. Chem. Soc. A*, **9** (1970) 1523.

3) Barrer, R..M. and Marcilly, C., *J. Chem. Soc. A*, **16** (1970) 2735.

4) Rabo, J.A., Poutsma, M.L. and Skeels, G.W., *Proc. Int. Congr. Catal. 5th*, North Holland Publishing Co., pp. 1353-1363.

5) Tomisaka, T. and Eugster, H.P., *Mineral. Jour. Japan*, **5(4)** (1968) 249 .

6) Moroney, L., in "**Preparation and Properties of Some Salt-Encapsulated Feldspathoids**", M.Sc. Thesis, The University of Waikato, Hamilton, New Zealand (1978).

7) Shanmugam, S., in "**Some Apsects of the Chemistry of CrO_4-Noseans**", M.Sc. Thesis, The University of Waikato, Hamilton, New Zealand (1983).

8) Martinus, D.D., in "**The Synthesis and Characterisation of Oxyanion-Salt Loaded Noseans**", M.Sc. Thesis, The University of Waikato, Hamilton, New Zealand (1989).

9) Brown, M.L., in "**Some Aspects of the Reactivity of Chromate Nosean**", M.Sc. thesis, The University of Waikato, Hamilton, New Zealand (1989).

10) Snowdon, T. J., in "**Some Aspects of the Loading of Zeolites with Sodium Chromate**", M.Sc. Thesis, The University of Waikato, Hamilton, New Zealand (1989).

11) Breck, D. W. and Flanigen, E. M., in "**Molecular Sieves**", Society of Chemical Industry, London (1968) pp. 47.

12) Meier, W.M., in "**Molecular Sieves**", Society of Chemical Industry, London (1968) pp.10.

13) Barrer, R.M., *Chem. Ind.*, (1963) 1203.

14) Jaeger, F. M., *Trans. Faraday Soc.*, **25** (1929) 320.

15) Pauling, L., *Z. Kristallogr.*, **74** (1930) 213.

16) Barrer, R.M. and Cole, J.F., *J. Chem. Soc A*, (1970) 1516.

17) Hassan, I. and Grundy, H.D., *Acta Cryst.*, **B40(1)** (1984) 6.

18) Depmeier, W., Schmid, H. and Setter, N., *Acta Cryst.*, **C43** (1987) 2251.

19) Sekanina, J. and Wyart, J., *Mineral. Cristallogr.*, **59** (1936) 377.

20) Barrer, R.M., Nature, **164** (1949) 112.

21) Barrer, R.M. and Kanellopoulos, A. G., *J. Chem. Soc. A*, **5** (1970) 765.

22) Rabo, J.A. and Kasai, P.H., *Progress in Solid State Chemistry*, Pergamon Press, Oxford (1975) pp. 1-19.

23) Rabo, J.H., "Salt Occlusion in Zeolite Crystals" in "**Zeolite Chemistry and Catalysis**", (Ed. Rabo, J.A.) ACS Monograph 171, Am. Chem. Soc., Washington, D.C., USA (1976) pp. 332-349.

24) Liqournik, M. and Marcus, Y., *J. Phys. Chem.*, **72** (1968) 2885.

25) Liqournik, M. and Marcus, Y., *J. Phys. Chem.*, **72** (1968) 4704.

26) Clearfield, A., Saldarriaga, C.H. and Buckley, R.C., *Proc. 3rd Int. Conf. on Molecular Seives* , Zurich (1973) pp. 241-245.

27) Beyer, H.K., Karge, H.G. and Borbely, G., *Zeolites*, **8(1)** (1988) 79.

28) Fornes ,V., Vazquez, M.I. and Corma, A., *Zeolites*, **6(2)** (1986) 125.

29) Kucherov, A.V. and Slinkin, A.A., *Zeolites*, **6(3)** (1986) 175.

30) Kucherov, A.V. and Slinkin, A.A., *Zeolites*, **8(2)** (1988) 110.

31) Kucherov, A.V. and Slinkin, A.A., *Zeolites*, **7(6)** (1987) 583.

32) Huang, M., Shan, S., Yuan, C., Li, Y. and Wang, Q., *Zeolites*, **10** (1990) 772.

33) Kucherov, A.V. and Slinkin, A.A., *Zeolites*, **7(1)** (1987) 38.

34) Slinkin, A.A. , Kucherov, A.V., Gorjachenko, S.S., Aleshin, E.G. and Slovetskaja, K.I., *Zeolites*, **10(2)** (1990) 111.

35) Kucherov, A.V., Slinkin, A.A., Beyer, G.K. and Borbely, G., *J. Chem. Soc. Faraday Trans I*, **85(9)** (1989) 2737.

36) Barrer, R.M. and Wasilewski, S., *Trans. Faraday Soc.*, **57** (1961) 1140.

37) Barrer, R.M. and Meier, W.M., *J. Chem. Soc.*, (1958) 299.

38) Loos, K.R. and Cole, J.F., in "**Raman Spectra of Polyatomic Ions in Zeolites**", Proc. Int. Conf. Zeolites, 3rd, Leven University Press (1973) pp. 230-234.

39) Breck, D.W., *J. Chem. Ed.*, **41** (1964) 678.

40) Rabo, J.A. and Kasai, O.H., in "**Progress in Solid State Chemistry**", (Ed. McCaldin, J.O.), Pergamon Press (Oxford), 1975, Vol. 9 , pp. 1.

41) Rabo, J.A., in "**Zeolite Chemistry and Catalysis**", (Ed. Rabo, J.A.) American Chemical Society Monograph 171 (1976) pp. 344.

42) Barrer, R.M. Daniels, E.A. and Madigan, G.A., *J. Chem. Soc. Dalton*, **18** (1976) 1805.

43) Weller, M.T. and Haworth, K.E., *J. Chem. Soc. Chem. Commun.*, **10** (1991) 734.

44) Weller, M.T., Wong, G., Adamson, C.L., Dodd, S.M. and Roe, J.J.B., *J. Chem. Soc. Dalton Trans.*, **2** (1990) 593.

45) Hogan, J.P., *Polym. Sci.*, **A1 8(9)** (1970) 2637.;
Spitz, R., Revillon, A. and Guyot, A., *J. Catal.*, **35** (1974) 335.;
Groeneveld, C., Wittgen, P.P.M.M., van Kersbergen, A.M., Mestrom, P.L.M., Nuijten, C.E. and Schuit, G.C.A., *J. Catal.*, **59(2)** (1979) 153.;
McDaniel, M.P., *J. Catal.*, **67(1)** (1981) 71.;
Beck, D.D. and Lunsford, J.H., *J. Catal.*, **68** (1981) 121.;

McDaniel, M.P., *J. Catal.*, **76(1)** (1982) 17, 29, 37.;
Merryfield, R., McDaniel, M.P. and Parks, G., *J. Catal.*, **77(2)** (1982) 360.;
Wittgen, P.P.M.M., Groeneveld, C., Zwaans, P.J.C.J.M., Morgenstern, H.J.B., van Heughten, A.H., van Heumen, C.J.M. and Schuit, G.C.A., *J. Catal.*, **77** (1982) 340.;
McDaniel, M.P. and Welch, M.B., *J. Catal.*, **82(1)** (1983) 98.;
Welch, M.B. and McDaniel, M.P., *J. Catal.*, **82(1)** (1983) 110.;
McDaniel, M.P., Welch, M.B. and Dreiling, M.J., *J. Catal.*, **82(1)** (1983) 118.;
Groeneveld, C., Wittgen, P.P.M.M., Swinnen, H.P.M., Wernsen, A., and Schuit, G.C.A., *J. Catal.*, **83(2)** (1983) 346.;
Ellison, A., *J. Chem. Soc. Faraday Trans. I*, **80(9)** (1984) 2567.;
Myers, D.L. and Lunsford, J.H., *J. Catal.*, **92** (1985) 260.;
Indovina, V., Cimino, A. and Invers, M., *J. Phys. Chem.*, **82** (1978) 285.;
McDaniel, M.P. and Johnson, M.M., *J. Catal.*, **101** (1986) 446.;
Lunsford, J.H., Fu, S-L. and Myers, D.L., *J. Catal.*, **111** (1988) 231.;
Myers, D.L. and Lunsford, J.H., *J. Catal.*, **99** (1986) 140.;
Rebenstorf, B. and Larsson, R., *J. Catal.*, **84** (1983) 240.;
Weiss, K. and Krauss, H-L., *J. Catal.*, **88** (1984) 424.;
Groeneveld, C., Wittgen, P.P.M.M., Lavrijsen, J.P.M. and Schuit, G.C.A., *J. Catal.*, **82** (1983) 77.;

46) Deren, J., Haber, J. and Siechowski, J., *Proc. 3 rd Int. Cong. Cat.*, Amsterdam, **Vol II** (1965) 993.

47) Shih, S.S., Shihabi, D.S. and Squires, R.G., *Proc. 6 th Int. Cong. Cat.*, London, **Vol 2** (1976) 978.

48) Indovina, V., Cimino, A. and Invers, M., *J. Phys. Chem.*, **82** (1978) 285.

49) Shvets, V.A., Lipatkina, N.I., Kansanky, V.V. and Chuvylkin, N.D., "Magnetic Resonance in Colloid and Interface Science " (NATO advanced study institutes series), Dordrecht (1980) 521.

50) Iwasawa, Y., Sasaki, Y. and Ogasawara, S., *J. Mol. Cat.*, **16** (1982) 27.

51) Iwasawa, Y., Sasaki, Y. and Ogasawara, S., *J. C. S. Chem. Comm.*, (1981) 140.

52) Lugo, H.J. and Lunsford, J.H., *J. Catal.*, **91** (1985) 155.

53) Iwasawa, Y., Chiba, T. and Ito, N., *J. Catal.*, **99** (1986) 95.

54) Richter, M. and Ohlmann, G., *Applied Catalysis*, **36** (1988) 81.

55) Parlitz, B., Hanke, W., Fricke, R., Richter, M., Roost, U. and Ohlmann, G., *J. Catal.*, **94** (1985) 24.

56) Richter, M., Alsdorf, E., Fricke, R., Jancke, K. and Ohlmann, G., *Applied Catalysis*, **24** (1986) 117.

57) Grunert, W., Saffert, W., Feldhaus, R. and Anders, K., *J. Catal.*, **99** (1986) 149.
58) Grunert, W., Shipiro, E.S., Feldhaus, R. and Anders, K., Anstoshin, G.V. and Minachev, KH.M., *J. Catal.*, **100** (1986) 138.
59) Zaki, M.I. and Fouad, N.E., *Applied Catalysis*, **21** (1986) 359.
60) Khodakov, Y.S., Makarov, P.A., Delzer, G. and Minachev, Kh.M., *J. Catal.*, **61** (1980) 138.
61) Niiyama, H., Murata, K., Can, H.V. and Echigoya, E., *J. Catal.*, **62** (1980) 1.
62) Laine, J., Ferrer, Z. and Labady, M., *Applied Catalysis*, **44** (1988) 11.
63) Chinchen, G.C., Logan, R.H. and Spencer, M.S., *Applied Catalysis*, **12** (1984) 69.
64) Jalowiecki, L., Daage, M. and Bonnelle, J.P., *Applied Catalysis*, **16** (1985) 1.
65) Khodakov, Yu.S., Makarov, P.A., Delzer, G. and Minachev, Kh.M., *J. Catal.*, **61(1)** (1980) 184.
66) Awe, A.A., Miliades, G. and Vickerman, J.C., *J. Catal.*, **62(2)** (1980) 202.
67) Krauss, H.L., *Proc. 5 th Int. Cong. Cat.* , Amsterdam (1973) 207.
68) Patzelova, V. and Tvaruzkova, Z., *React. Kinet. Catal. Lett.*, **16** (1981) 65.
69) Przhevalskaya, L.K., Shvets, V.A. and Kazanskii, V.B., *J. Catal.*, **39(3)** (1975) 363.;
Breck, D.D. and Lunsford, J.H., *J. Catal.*, **68** (1981) 121.;
Kazanskii, V.B. and Pecherskaya, Y.I., *Kinet. Katal.*, **2** (1961) 454.;
Eley, D.D., Rochester, C.H. and Scurrell, M.S., *Proc. Roy. Soc. London, Ser. A*, **329** (1972) 361.;
Yashima, T., Nagata, J., Shimazaki, Y. and Hara, N., *Molecular Seives II* (American Chemical Society, Washington D.C. (1977) pp. 626.;
Atanasova, V.D., Shvets, V.A. and Kazanskii, V.B., *Kinet. Katal.*, **28** (1973) 1033.;
Wichterlova, B., Tvaruzkova, Z. and Novakova, J., *J. Chem. Soc. Faraday Trans. I*, **79(7)** (1983) 1573.;
Beran, S., Jiru, P. and Wichterlova, B., *J. Chem. Soc. Faraday Trans. I*, **79(7)** (1983) 1585.

Chapter Two

Methods & Materials

Chapter Two

Methods and Materials

2.1 Introduction

Salt-loaded zeolites were produced by a solid-state reaction between zeolites and the sodium salts of chromate, molybdate, and tungstate as described in Section 2.3. Loaded samples were characterised by a variety of methods including X-Ray Diffraction (Section 2.5), Electron Paramagnetic Resonance (Section 2.6), X-Ray Fluorescence (Section 2.7), Laser Raman Spectroscopy (Section 2.8), Differential Thermal Analysis (Section 2.9), surface area (BET) studies (Section 2.10), X-Ray Photoelectron Spectroscopy (Section 2.11), Scanning Electron Microscopy (Section 2.12) and Fourier Transform Infrared (Section 2.13). The reactivities of loaded zeolites towards reduction by hydrogen gas and reoxidation by oxygen gas were assessed volumetrically on a modified BET line (Section 2.14).

2.2 Materials

Zeolites LZ-Y52, LZ-Y72, LZ-M5, and S115 (silicalite) powders were supplied by Union Carbide. Zeolites 13X, 3A, 4A, and 5A were laboratory reagent molecular sieves (0.5 to 5 μm) from BDH. The various other reagents used are given in Table 2.1.

Table 2.1 Sources and grades of the various reagents used.

Reagent	Grade	Source
Sodium chromate	laboratory reagent	Unilab
Sodium Tungstate	analytical	M&B
Sodium Molybdate	analytical	M&B
Sodium hydroxide	AR	SS

2.3 Solid-State Reactions

A reaction mixture was prepared by placing the zeolite in a porcelain crucible and then adding a known quantity of a strong solution of the oxyanion salt. The reaction mixture was placed in a muffle furnace and the temperature raised to 150°C and left for ~1 hour to remove excess water. The furnace temperature was then raised at 10°/min until the desired temperature was reached. After a certain period of time the mixture was removed from the furnace and the salt not irreversibly bound to the zeolite was removed. Initially samples were washed by soxhlet extraction with water for at least 72 hours. Later tests showed that ~2 hours in 250 ml water at 100°C achieved the same result as prolonged soxhlet extraction. Surface water was removed by heating the washed zeolite at 120°C in an oven for at least 2 hours. Samples were stored in a desiccator over saturated ammonium nitrate until use.

2.4 Loaded Samples and Sample Notation

Salt contents were determined using X-ray fluorescence. Results were obtained as wt% figures for Cr_2O_3 and SiO_2 etc. These values were manipulated into the form of unit cell compositions based on the number of metal atoms (Al and Si) per unit cell (192 for X, Y, and A and 48 for M5). Samples were named on the basis of the number of salt molecules per unit cell. A sample containing $x.x$ moles of oxyanion M per unit cell of a zeolite Z was referred to in the form $x.xMZ$. For example, a 5A zeolite was found to contain 32.3 chromates per unit cell and was named 32.3Cr5A.

Various loaded zeolites were examined in this work. The details of the syntheses of the loaded samples are given in Table 2.2.

Table 2.2 Details of the syntheses of the loaded zeolites. The number in brackets is the ratio of the moles oxyanion per mole of zeolite.

Sample	Reaction Mixture	Conditions
5.8CrX	25.0 g of 13X + 25 ml of 1 mol L^{-1} Na_2CrO_4 (17.5)	670°C for 7 hours
13.6CrX	13.8 g of 13X + 35 ml of 2 mol L^{-1} Na_2CrO_4 (111)	620°C for 20 hours
2.1CrX	5 g of 13.6CrX + 150 ml of 2 mol L^{-1} NaOH	80°C for 24 hours
13.4CrY	3.0 g of Y52 + 13 ml of 2 mol L^{-1} Na_2CrO_4 (185)	620°C for 23 hours
2.8CrY	5.4 g of Y52 + 5 ml of 1 mol L^{-1} Na_2CrO_4 (15.8)	600°C for 21 hours
4.8Cr5A	5.1 g of 5A + 5 ml of 1 mol L^{-1} Na_2CrO_4 (16.7)	600°C 93 hours
32.3Cr5A	20.0 g of 13X + 175 ml of 1 mol L^{-1} Na_2CrO_4 (149)	620°C for 20 hours
10.7CrY72	5.0 g of Y72 + 5 ml of 1 mol L^{-1} Na_2CrO_4 (17.1)	565°C for 7 hours
2.3Cr3A	4.9 g of 3A + 5 ml of 1 mol L^{-1} Na_2CrO_4 (17.4)	565°C for 7 hours
3.3Cr4A	4.9 g of 4A + 5 ml of 1 mol L^{-1} Na_2CrO_4 (17.0)	650°C for 7 hours
1.0CrM5	4.6 g of M5 + 5 ml of 1 mol L^{-1} Na_2CrO_4 (5.6)	565°C for 7 hours
0.9CrS115	4.2 g of 3A + 5 ml of 1 mol L^{-1} Na_2CrO_4 (5.3)	565°C for 7 hours
2.3MoX	5.0 g of 13X + 5 ml of 1 mol L^{-1} Na_2CrO_4 (17.5)	565°C for 7 hours
1.9WX	5.0 g of 13X + 5 ml of 1 mol L^{-1} Na_2CrO_4 (17.4)	565°C for 7 hours
Cr^{nos}	10 g of kaolinite + 4 g of Na_2CrO_4 (slurried)	820°C for 72 hours

2.5 Powder X-Ray Diffraction (PXRD)

XRD is a convenient and powerful method for analysing crystalline solids. Zeolites used in this work were highly crystalline powders. PXRD was used to measure framework crystallinity and thereby assess lattice stability under the thermal treatment employed in the solid-state reactions. PXRD patterns were recorded using a *Philips PW1729* X-ray generator in conjunction with a *Philips PW1840* diffractometer control and a *Philips PM8203A* one line

recorder. Samples were packed into holders 1 cm x 1.5 cm of 2 mm depth. The settings generally used are given in Table 2.3.

Table 2.3 Settings generally used for the recording of PXRD patterns.

Scan Rate /°2θ s^{-1}	0.1 qualitative
	0.01 quantitative
Range	2x10^3
Time constant /s	0.1
Chart /mm s^{-1}	10

Accurate determinations of unit cell edge dimensions of chromate nosean and the products after various redox treatments were required in this work. What follows is the calculation of the unit cell edge of a nosean using PXRD data and an estimate of the error in the determination. Noise appeared to be the major source of random error. Since the signal to noise ratio decreases with increasing intensity of the signal the measurement of the position of the most intense peak in the PXRD pattern of noseans (hkl = 211 peak at d = 3.72 Å) was judged to be the most reliable means of unit cell edge determination. The magnitude of random errors was assessed by repeated measurements on several sample packings. Halite was used as an internal standard.

Calculation of Unit Cell Edge

The positions of the halite and nosean 211 PXRD peak were measured. The magnitude of systematic errors was determined through comparison of the position of the halite peak with the literature value from Powder Diffraction File (PDF) 5-628 (d = 2.821 Å). The nosean peak was then corrected for this systematic error. For example, the 211 peak (in °2θ) for Cr^{nos} occurred at 23.79° and halite at 31.57 for one sample packing. The halite peak should be at 31.70°

indicating a systematic error of 0.13°. Correcting the nosean peak by this amount gives $2\theta^{211} = 23.92°$.

$$d = \frac{\lambda}{2\,\mathrm{Sin}\theta} = \frac{1.5410\ \text{Å}}{2\,\mathrm{Sin}(23.92/2)} = 3.718\ \text{Å}$$

$$a_0 = d\sqrt{h^2 + k^2 + l^2} = 3.718\sqrt{2^2 + 1^2 + 1^2} = 9.107\ \text{Å}$$

Estimation of the Random and Instrumental Errors in a_0

The PXRD machine increased the value of 2θ in increments of 0.01°. The estimated instrumental error was half of the smallest increment, i.e. 0.005°. This absolute error in a 2θ value of ~24° is 0.042% or an absolute error of ± 0.002 Å in the a_0 value. The PXRD machine is therefore not capable of measuring a_0 values to greater accuracy than ± 0.002 Å.

Random error, most likely to be introduced through noise or variations in packing, is a further source of uncertainty in the a_0 determination. Table 2.4 shows the values of a_0 derived from several different sample packings. In this case, the random errors were smaller than the instrumental errors indicating that determination of a_0 was limited by the size of the increments of the XRD machine, i.e. ± 0.002 Å.

Table 2.4 Data for the estimation of random errors in the determination of unit cell edge (a_0) from PXRD peaks. Where $\bar{x}$ is the average, σ^{n-1} is the standard deviation, and λ^{95} is the 95% confidence interval.

a_0 /Å	$\bar{x}$ /Å	σ^{n-1}	λ^{95}
9.107, 9.107, 9.106, 9.108, 9.107, 9.107	9.107	± 0.0006	0.001

The unit cell edges of other systems were determined by averaging at least three measurements of a_0 derived from the 211 reflection. Random errors were assessed from the variation in a_0.

2.6 Electron Paramagnetic Resonance (EPR)

Powder EPR spectra of chromium containing zeolites were obtained at room temperature on a Varian E-104 9.5 GHz Spectrometer. Approximately 0.01 g of sample was placed in a quartz-glass capillary tube with a diameter of 2 mm. Spectra were recorded at room temperature. DPPH was used as an external standard. Standard spectrometer settings that were used are shown in Table 2.5.

Table 2.5 Settings generally used for the recording of EPR spectra.

Field /G	4000
Range /G	5000
Gain	as required
Modulation	0.25
Time constant /s	10
Attenuation /dB	15

The ratio of the Cr(III) EPR signals of two zeolites was needed in this work. The factors that will affect the intensity of EPR signals are :

1) the density of the sample packing

2) the temperature at which the signal is measured

3) random instrumental errors

What follows are the results of an experiment designed to estimate the contributions of these factors to the overall error in the ratio value. No assessment of the effect of sample temperature was made on the basis that samples were run at the same room temperature. The effect of sample packing was assessed by measuring the intensity of the Cr(III) signal of four sample packings. Random instrumental errors were assessed by measuring the signal intensity of one packing four times. The results are shown in Table 2.6.

Table 2.6 Results of the experiment to determine the errors in the recording of EPR signal intensities. Where $\bar{x}$ is the average, σ^{n-1} is the standard deviation, and λ^{95} is the 95% confidence interval.

Packing No.	Signal Intensity
#1	8.25, 8.30, 8.40, 8.25 : $\bar{x}$ = 8.30, σ^{n-1} = 0.07, λ^{95}=0.14
#2	8.68
#3	9.40
#4	8.70
	$\bar{x}$ = 8.76, σ^{n-1} = 0.48, λ^{95}=0.94

The data indicates that random instrumental error (λ^{95}=0.14) is negligible compared to packing error (λ^{95}=0.94). The λ^{95} in the ratio of two signals is 15.5%. For the calculated ratio of 2.2 the 95% confidence interval is 2.2 ± 0.3.

Reduction of sodium chromate salt gave a green powder that gave an XRD pattern characteristic of $NaCrO_2$. The reduced sample, named Na_2CrO_4(R), gave an EPR signal characteristic of a Cr(III) species. It was possible to quantify the Cr(III) EPR signals of reduced chromate zeolites using Na_2CrO_4(R). What follows are the experimental procedure and results of the EPR experiment. Because the densities of $NaCrO_2$ and 13.6CrX(873) were different the EPR tube was filled to a known height and the sample weight measured. It was noted that the Cr(III) signal for Na_2CrO_4(R) was significantly narrower than that of 13.6CrX(873). This is the result of line narrowing in a magnetically concentrated sample as has previously been observed for $NaCrO_2$.[1] Line narrowing made quantification through ratios of peak intensities inaccurate so peak areas were used. Peak areas were calculated by cutting out the EPR signal, measuring the paper weight of the signal, and division by the gain. Table 2.7 shows the EPR data.

Table 2.7 Results of the EPR signal quantification.

Sample	Wt sample /g	Peak Wt /g	Gain	Area x100 / arbitrary units
Na_2CrO_4(R)	0.54	0.2374	8 x 1	296.8
13.6CrX(R873)	0.78	0.3312	1.6×10^2	20.7

Calculation of Spin Concentrations

Sample Na_2CrO_4(R) was $NaCrO_2$.NaOH (MW = 147).

=> Moles Cr(III) in EPR tube with Na_2CrO_4(R) = $\frac{0.54}{147} = 3.67 \times 10^{-3}$

Ratio of EPR signal of $\frac{Na_2CrO_4(R)}{13.6CrX(R873)} = \frac{296.8}{20.7} = 14.34$

=> Moles Cr(III) in EPR tube with 13.6CrX(R873) = $\frac{3.67 \times 10^{-3}}{14.34} = 2.56 \times 10^{-4}$

=> Moles Cr(III)/g of 13.6CrX(R873) = $\frac{2.56 \times 10^{-4}}{0.78} = 3.28 \times 10^{-4}$

Minimal errors due to changes in density arising from packing fluctuations were introduced as each sample was weighed. From the earlier experiment it was shown that the error (λ^{95}) in the absence of density fluctuations was 1.69% in each reading giving 2.4% error in the ratio. An error (λ^{95}) in the Cr(III) content in the EPR tube arising from variations in the height to which the EPR tube was filled is estimated to be 3.4%. The overall error is 4.2%. The 95% confidence interval for the moles of Cr(III) in 13.6CrX(R873) is therefore $(3.3 \pm 0.2) \times 10^{-4}$.

2.7 X-Ray Fluorescence (XRF)

Zeolite samples were sent to The Analytical Facility at Victoria University for XRF analysis. The instrumentation used for XRF analysis was a *Philips PW1404* automatic sequential X-ray spectrometer fitted with *V1.3* firmware and a *PW1500 72* position sample changer. The on-line computer comprised a *DEC Professional 350, VR-241* colour monitor and a *LA210* printer. The operating system was *POS-V2.0A* running *V2.0 Philips X-44* software. Fused glass disks were prepared using procedures modified from Norrish and Hutton.[2] *Sigma Chemicals* Norrish Formula X-ray flux was used with 0.25 to 0.75g of zeolite powder and 0.040g of AR ammonium nitrate in a covered Pt-5%Au crucible in a muffled gas flame. The exact weight of sample powder used was recorded and entered into the computer at run-time. Glass disks were pressed on a graphite die using Al plunger and annealed for several hours before being cooled, labelled and stored in plastic containers in a desiccator. Loss on ignition (LOI) was determined gravimetrically by heating each sample in an electric furnace at 1100°C for 1 hour using ceramic crucibles. Determinations were carried out under vacuum using the *Ka* line and Sc/Mo dual anode X-ray tube operated at 45 kV / 50 mA. The detection system comprised a flow proportional counter fitted with a 1 mm polypropylene window and using P10 gas (10% methane in argon). The course collimator and large aperture were used in all cases. Regression lines were calculated using the *Philips* mathematical model, with loss eliminated empirical alphas calculated from factors provided by K. Norrish for the Sc tube.

2.8 Laser Raman Spectroscopy

Raman spectra were recorded on a Spex Ramalog-9 system which consisted of five components:

(1) monochromatic light source was generated by either a He-Ne laser operated in the red region (laser line at 149038.1 nm) or a Ar laser operated in the green region (laser line at either 15802.8 cm^{-1} or 19435 cm^{-1}).

(2) Spex 1459 UVISIR Raman illuminator.

(3) Spex model 1403, 0.85 m double monochromator.

(4) signal processing system consisting of an RCA C31034 photomultiplier tube, amplification system, and DM1B Spectroscopy Laboratory Coordinator.

Zeolite samples were pressed into self-supporting wafers, 1 cm in diameter and 1 to 2 mm in thickness, using a conventional infrared KBr disc cast under a pressure of 1425 Psi for two minutes. Zeolite wafers were placed in a mount to give a laser beam to surface angle of ~45°. Chromate zeolites in the unreacted form were a yellow colour that warranted the use of the red He-Ne laser with a line at 15802.8 cm^{-1}. Samples reduced in hydrogen gas were varying shades of green and were found to adsorb the red laser line. For these samples the green Ar laser line at 19435 cm^{-1} was used successfully. Spectra of liquids were recorded on samples contained within glass capillary tubes. Potassium sulphate was used as an external standard. Slit widths of 200 pre-sample and 250 post-sample gave a spectral bandpass of 1.5 cm^{-1}. Signal to noise ratios were increased by cumulative scanning.

2.9 Differential Thermal Analysis (DTA)

Differential thermal curves were obtained using a *Stone P-202* furnace platform in conjunction with a *Stone LB-202* recorder and controller. Alumina was used as an inert reference material. The zeolite sample (~0.2g) was mixed with alumina (~0.5g). Sample and reference were heated from 20°C to 1100°C at a heating rate of 30°C/min in air.

2.10 BET Surface Area

Nitrogen adsorption at liquid nitrogen temperature can be used to evaluate the surface areas of porous solids. Surface areas were determined using a BET line shown in Figure 2.1. An accurately weighed zeolite sample (0.2g to 0.4 g) was outgassed to ~ 10^{-5} Torr by heating the sample at 350°C for at least 24 hours to remove zeolitic water. Volumes of the various parts of the line were calibrated using helium. To measure the N_2 adsorption isotherm the line was completely outgassed and the manifold and sample chamber were isolated from the rest of the vacuum line. With the sample chamber isolated from the manifold and the gas burette empty an accurately measured nitrogen pressure of about 7 cmHg was introduced into the manifold. The sample was immersed in liquid nitrogen and opened to the manifold. The pressure after equilibration was recorded using a cathetometer when no further adsorption occurred over a five minute period. The level of mercury in the gas burette was raised successively up to each calibration mark and the pressure recorded after equilibrium at each level was reached. Adsorption data was analysed on a *Microsoft Excel* spreadsheet based on the equations given by Brunauer *et al.*[3]

2.11 X-Ray Photoelectron Spectroscopy (XPS)

XPS is a convenient and powerful technique for the structural elucidation of the surface layers of solids. Samples were sent to The University of Auckland for XPS analysis. Spectra were recorded on a *KRATOS XSAM-800.* The set-up consisted of XPS/SAM (Scanning Auger Microprobe), dual anode X-ray source (Mg Kα and Al Kα), and a hemispherical analyser. Al Kα radiation was used.

2.12 Scanning Electron Microscopy (SEM)

SEM is a powerful technique for analysis of solid samples. Synthetic zeolites that are crystallised from aqueous hydrogels or conversion of various aluminosilicates, such as kaolin, generally exhibit well defined geometries and relatively uniform particle sizes in the micron range.

SEM photographs were recorded on a *Hitachi S4000* scanning electron microscope located at the Microscope Unit at the Meat Industry Research Institute of New Zealand (MIRINZ). Samples were coated with Pt-Au to minimise charging. An accelerating voltage of 5 keV was used.

2.13 Fourier Transform Infrared (FTIR)

FTIR spectra were recorded on a *BIO RAD (DIGILAB DIVISION) FTS*-40/1. Settings used are shown in Table 2.8. Samples were prepared by pressing a physical mixture consisting of the zeolite and KBr in a ratio of ~1:10 at 1425 psi for two minutes to give a disk of ~ 0.5 mm. In the discussions of the following chapters "IR" and "Infrared" refer to Fourier Transform Infrared.

Table 2.8 Settings used for the recording of FTIR spectra.

Range /cm^{-1}	1300 to 350
Aperture /cm^{-1}	2
Scan Speed /kHz	10
Resolution /cm^{-1}	2
Sample Beam	internal
Detection	internal
Background Scans	16
Sample Scans	16
Purge Time /min	1 to 5

2.14 Reactivity Studies

The reactivities of chromate, molybdate and tungstate containing zeolites towards reduction by hydrogen and carbon monoxide gases and reoxidation by oxygen gas were determined by following gaseous uptakes on a modified BET vacuum line, shown diagrammatically in Figure 2.1. A known weight of zeolite was outgassed for at least 24 hours (to ~ 10^{-5} Torr) in the sample chamber positioned within a furnace at 500°C. Appendix Eleven shows the thermal characteristics of the furnace. The average temperature was constant near the centre of the furnace and varied only through fluctuations arising from the control unit. Providing the sample was placed within ~5 cm of the centre of the furnace the temperature could be measured to within ± 10°. Volumes of the manifold and the total volume of the system were calibrated using helium. With the sample chamber evacuated, an accurately measured pressure of gas was introduced into the manifold. Reactions were initiated by opening the tap between the sample chamber and the manifold. Gaseous uptakes were determined volumetrically by following the level of mercury in the manometer using a cathetometer. The level of mercury in the left side of the manometer was kept adjusted to a set mark during the reaction to keep the volume (V_{tot}) constant. Because of the speed of the reaction over small reaction times it was not possible to measure the levels of both sides of the manometer

with one cathetometer sight so two sights were used. Maximum uptakes were generally measured after reaction times of at least 20 hours although some reactions required shorter or longer periods of time for the reaction to reach completion. When an accurate final uptake was required the reaction was left until no observable uptake was observed over a significant period of time. The moles of gas adsorbed at any given time was calculated from the initial pressure and the pressure at that time. This value was then converted into moles of gas reacted per mole of oxyanion. A model calculation follows including error estimates. Data is from Red#40 (see Appendix 7/1).

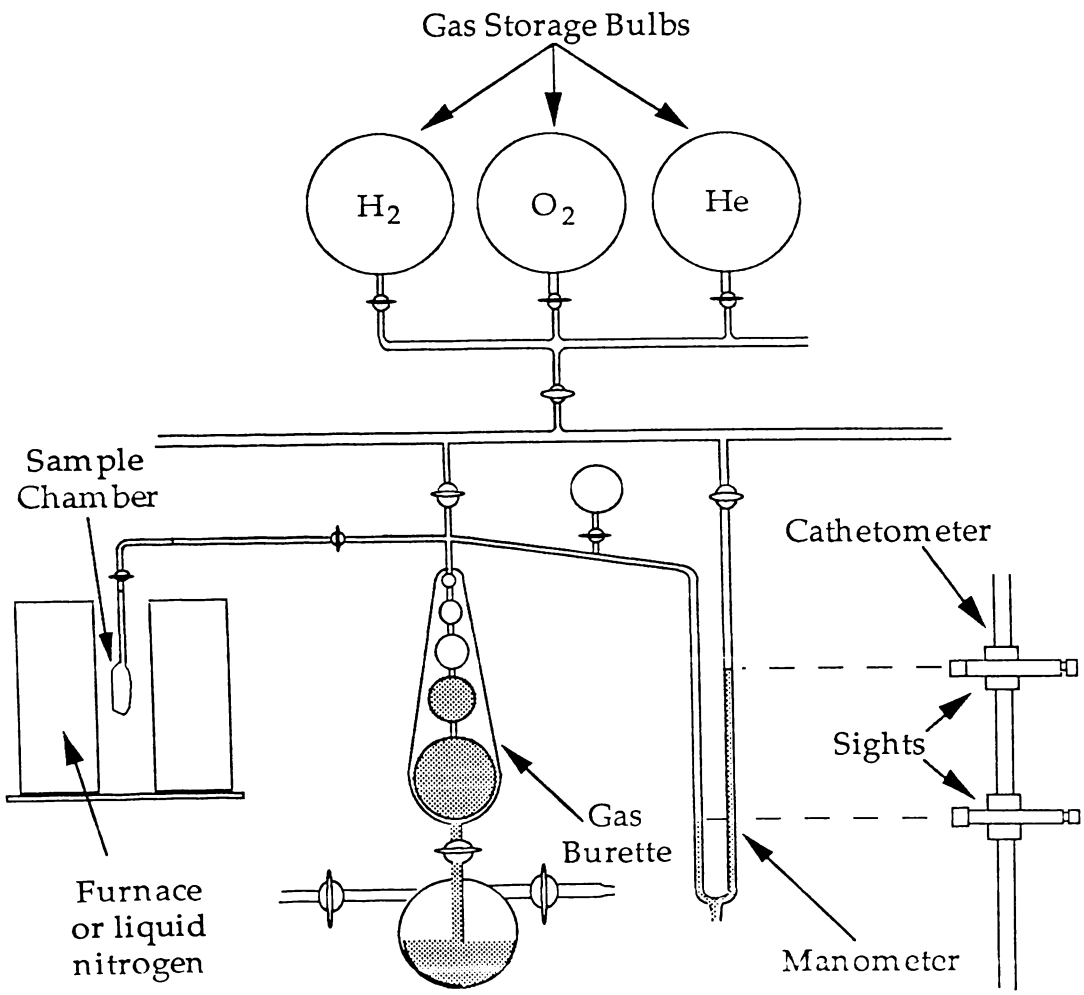


Figure 2.1 Diagram of the modified BET line used for surface area determinations and reactivity studies.

Model Calculation

$$N_i = \frac{P_i V_{man}}{R T} = 1.2791 \times 10^{-3} (\pm 0.55\%)$$

$$N_\infty = \frac{P_i V_{tot}}{R T} = 5.840 \times 10^{-4} (\pm 0.68\%)$$

$$N_{ads} = N_i - N_\infty = 6.95 \times 10^{-4} \pm 1.1 \times 10^{-5} (1.58\%)$$

$$H_2/Cr = \frac{N_{ads}}{N_{Cr}} = 1.45 (\pm 2.62\%)$$

$$= 1.45 \pm 0.04$$

Where

T_r = room temperature / K
= 295 ± 0.2 K (0.08%)

V_{man} = volume of the manifold with the sample chamber closed / cm^3
= 44.3 ± 0.2 cm^3 (0.45%)

V_{tot} = volume of the manifold + sample chamber / cm^3
= 72.0 ± 0.4 cm^3 (0.56%)

P_i = initial pressure in V_{man} / cmHg
= 53.13 ± 0.01 cmHg (0.02%)

P_∞ = pressure in V_{tot} at t_∞ / cmHg
= 14.88 ± 0.01 cmHg (0.07%)

N_{Cr} = moles of chromium in sample
= $(4.79 \pm 0.05) \times 10^{-4}$ (1.04%)

N_i = initial moles of reactant gas

N_∞ = moles of reactant gas remaining after t_∞

N_{ads} = moles of reactant gas adsorbed

R = 82.0575 atm cm^3 $mole^{-1}$ K^{-1}

H_2/Cr = moles of $H_{2(g)}$ reacted per mole of chromium

References in Chapter Two

1) Angelov, S., Darriet, J., Delmas, C., and Le Flem, G., *Solid State Communications*, **50(4)** (1984) 345.

2) Norrish, K. and Hutton, J.T., *Geochim Cosmochim. Acta*, **33** (19)431.

3) Brunauer, S., Emmett, P.J., and Teller, E., *J. Am. Chem. Soc.*, **59** (1937) 2682; *J. Am. Chem. Soc.*, **60** (1938) 309.

Chapter Three

Solid-State Reactions Between Zeolites and Group(VI) Oxyanions

Chapter Three

Solid-State Reactions Between Zeolites and Group (VI) Oxyanions

3.1 Introduction

Studies of sodium chromate, sodium molybdate, and sodium tungstate occlusions by A, 13X, Y52, Y72 (the hydrogen form of Y52), M5 (mordenite) and S115 (silicalite) zeolites were performed. The effects of temperature, zeolite, and zeolite to chromate mole ratio on the occlusion process were determined. The kinetics of chromate uptake by 13X at various temperatures was determined and details of the mechanism were deduced. The effect of sodium chromate on the thermochemistry (DTA) and lattice stability (PXRD) of 13X are reported. A strategy for chromate occlusion based upon consideration of the literature on salt occlusion phenomena was devised.

3.2 Methods and Materials

All zeolites used have been described previously, see Section 2.2. The procedure for occluding salts was outlined in Section 2.3. Unit cell contents were calculated from XRF analyses as outlined in Section 2.7.

3.3 Results and Interpretation

3.3.1 Hydrothermal Uptake from Strong Salt Solution

When 1 g of 13X was contacted with 250 ml of 2.5 mol L^{-1} Na_2CrO_4 solution at 80°C for 24 hours followed by filtering and washing with 200 ml of distilled water at ~20°C no sodium chromate was retained by the zeolite.

Treatment similar to that above except with 125 ml of 2.5 mol L^{-1} Na_2CrO_4 solution and 125 ml of 2 mol L^{-1} NaOH resulted in the retention of chromate as evidenced by the yellow colour of the washed product.

3.3.2 Reaction of 13X and Sodium Chromate at 800°C

Occlusion of salt species such as $NaNO_3$ within the sodalite cages of faujasite type zeolites requires temperatures above the melting point of the salt. As sodium chromate melts at ~800°C a firing temperature of 800°C might be necessary to achieve chromate occlusion within sodalite cages. A reaction mixture was prepared containing 5 g of 13X and 20 ml of 2.5 mol L^{-1} Na_2CrO_4 solution. Firing for 24 hours at 800°C followed by the standard washing and drying treatment formed a product that gave a PXRD pattern that indicated the complete loss of zeolite peaks and the appearance of extraneous peaks characteristic of chromate nosean. Many sodium-aluminium-silicon oxide materials (such as nepheline, kaolin, and some aluminosilicate gels) react with sodium chromate at temperatures above 800°C to form chromate nosean. Similar reaction temperature and reaction product indicates that 13X acts as a source of Na, Al, and Si in a similar manner to other amorphous and crystalline aluminosilicates capable of producing sodalites such as nosean.

3.3.3 DTA Analysis of the Chromate-Zeolite Interaction

Results

Figure 3.1 shows the DTA patterns of zeolite 13X, a chromate-zeolite reaction mixture named 13X/Na_2CrO_4 (as described in Section 3.2.2), and pure sodium chromate. The DTA pattern of 13X shows a broad endothermic peak centred at ~150°C and three sharp exothermic peaks at 837°C, 949°C and 1037°C. Sodium chromate salt gave very sharp endothermic peaks at 430°C and 805°C. The reaction mixture gave a broad endothermic peak at ~150°C, two sharp overlapping exothermic peaks at 796°C and 843°C, and a broad exothermic peak at ~900°C.

Interpretation

The broad exothermic peaks at ~150°C for the zeolite samples results from the loss of zeolitic water. The three endothermic peaks in the DTA pattern of 13X are consistent with the literature and are assigned, in order of increasing temperature, to zeolite lattice decomposition forming amorphous phases, recrystallisation of carnegiete from amorphous phases, and decomposition of carnegiete.

It is apparent from the DTA patterns that the presence of sodium chromate has a dramatic effect on the thermochemistry of zeolite 13X. Temperatures slightly above the melting point of a salt are generally chosen for occlusion of salts within β-cages. The melting point of sodium chromate (805°C) and the temperature of lattice decomposition (837°C) appeared to offer a small temperature window in which, through careful control over reaction temperature, occlusion of chromate oxyanions in β-cages may have been achieved. The melting of sodium chromate, however, rather than facilitating penetration into β-cages, promotes an alternative process involving the production of chromate nosean.



Figure 3.1 DTA patterns of sodium chromate salt (top), 13X (middle) and a reaction mixture of 13X and sodium chromate salt (bottom). DTA patterns recorded at a scan rate of 30°C/min in air.

3.3.4 Occlusion of Chromate, Molybdate, and Tungstate

Effect of Temperature and Time

Occlusion of sodium chromate, sodium molybdate, and sodium tungstate by zeolites of the types A, X, Y, M5, and S115 was investigated. The method of sample preparation was outlined in Section 2.3. Raw data for XRF analysis of a variety of zeolite-sodium chromate, zeolite-sodium molybdate and zeolite-sodium tungstate systems were converted into unit cell contents. Unit cell contents were evaluated based on 192 (Si+Al) atoms per unit cell for X, Y, and A zeolites and 48 (Si+Al) atoms for mordenite. Reaction mixtures contained 4 g of dehydrated zeolite and 5 ml of 1 mol L^{-1} Na_2MO_4 (M = Cr, Mo, W) to give oxyanion to zeolite mole ratios of ~22 : 1. Such mixtures were heated at 465°C, 565°C, and 650°C for periods of 2 and 7 hours and washed and dried in the usual manner. Sample notation is as follows. A sample of zeolite *Z* heated with Na_2MO_4 at *X*°C for *Y* hours was named *M.Z.X/Y*, eg a zeolite 13X heated in Na_2CrO_4 at 565°C for 7 hours was named Cr.13X.565/7. Results of chromate occlusion are shown in Table 3.1 and Table 3.2. Sodium molybdate and sodium tungstate occlusions are shown in Table 3.3 and Table 3.4 respectively.

Table 3.1 Reaction of faujasite type zeolites and sodium chromate.

Sample	Unit Cell Composition
13X	$Na_{83.8}Si_{106.2}Al_{85.8}O_{768}{\cdot}227.5H_2O$
Cr.13X.465/2	$Na_{79.2}Si_{106.6}Al_{85.4}O_{768}{\cdot}232.2H_2O{\cdot}0.4Na_2CrO_4$
Cr.13X.650/2	$Na_{77.1}Si_{106.5}Al_{85.5}O_{768}{\cdot}227.5H_2O{\cdot}1.7Na_2CrO_4$
Cr.13X.465/7	$Na_{81.6}Si_{106.4}Al_{85.6}O_{768}{\cdot}225.5H_2O{\cdot}0.9Na_2CrO_4$
Cr.13X.565/7	$Na_{80.9}Si_{106.4}Al_{85.6}O_{768}{\cdot}209.5H_2O{\cdot}1.8Na_2CrO_4$
Cr.13X.650/7	$Na_{77.4}Si_{106.1}Al_{85.9}O_{768}{\cdot}208.5H_2O{\cdot}3.0Na_2CrO_4$
Y52	$Na_{51.2}Si_{136.7}Al_{55.3}O_{768}{\cdot}248.0H_2O$
Cr.Y52.465/2	$Na_{50.1}Si_{137.5}Al_{54.5}O_{768}{\cdot}233.0H_2O{\cdot}0.5Na_2CrO_4$
Cr.Y52.650/2	$Na_{49.0}Si_{137.4}Al_{54.6}O_{768}{\cdot}179.2H_2O{\cdot}2.3Na_2CrO_4$
Cr.Y52.465/7	$Na_{49.1}Si_{137.0}Al_{55.0}O_{768}{\cdot}174.6H_2O{\cdot}1.3Na_2CrO_4$
Cr.13X.565/7	$Na_{48.9}Si_{137.0}Al_{55.0}O_{768}{\cdot}150.9H_2O{\cdot}2.7Na_2CrO_4$
Cr.13X.650/7	$Na_{48.3}Si_{137.6}Al_{54.4}O_{768}{\cdot}163.3H_2O{\cdot}3.0Na_2CrO_4$
Y72	$Na_{9.6}Si_{136.7}Al_{55.3}O_{768}{\cdot}187.6H_2O$
Cr.Y72.465/2	$Na_{16.5}Si_{136.5}Al_{55.5}O_{768}{\cdot}182.5H_2O{\cdot}2.8Na_2CrO_4$
Cr.Y72.650/2	$Na_{13.0}Si_{137.1}Al_{54.9}O_{768}{\cdot}171.5H_2O{\cdot}6.1Na_2CrO_4$
Cr.Y72.465/7	$Na_{15.1}Si_{136.7}Al_{55.3}O_{768}{\cdot}171.7H_2O{\cdot}5.3Na_2CrO_4$
Cr.Y72.565/7	$Na_{6.6}Si_{136.6}Al_{55.4}O_{768}{\cdot}150.6H_2O{\cdot}10.7Na_2CrO_4$
Cr.Y72.650/7	$Na_{6.0}Si_{137.1}Al_{54.9}O_{768}{\cdot}181.6H_2O{\cdot}13.0Na_2CrO_4$

Table 3.2 Reaction of A and mordenite type zeolites and sodium chromate.

Sample	Unit Cell Composition
M5	$Na_{7.2}Si_{40.3}Al_{7.7}O_{192}\cdot 31.3H_2O$
Cr.M5.465/2	$Na_{6.5}Si_{40.3}Al_{7.7}O_{192}\cdot 29.1H_2O\cdot 0.4Na_2CrO_4$
CrM5.650/2	$Na_{5.9}Si_{40.3}Al_{7.7}O_{192}\cdot 26.7H_2O\cdot 1.0Na_2CrO_4$
Cr.M5.465/2	$Na_{7.1}Si_{40.3}Al_{7.7}O_{192}\cdot 28.1H_2O\cdot 0.6Na_2CrO_4$
Cr.M5.565/7	$Na_{6.1}Si_{40.3}Al_{7.7}O_{192}\cdot 25.7H_2O\cdot 1.0Na_2CrO_4$
Cr.M5.650/7	$Na_{6.9}Si_{40.3}Al_{7.7}O_{192}\cdot 24.1H_2O\cdot 1.1Na_2CrO_4$
3A	$Na_{49.0}K_{34.6}Si_{96.2}Al_{95.8}O_{768}\cdot 201.0H_2O$
Cr.3A.465/2	$Na_{59.4}K_{26.2}Si_{95.9}Al_{96.1}O_{768}\cdot 195.9H_2O\cdot 0.9Na_2CrO_4$
Cr.3A.650/2	$Na_{57.6}K_{23.8}Si_{94.9}Al_{97.1}O_{768}\cdot 198.6H_2O\cdot 1.6Na_2CrO_4$
Cr.3A.465/7	$Na_{57.6}K_{30.6}Si_{94.8}Al_{97.2}O_{768}\cdot 186.6H_2O\cdot 1.2Na_2CrO_4$
Cr.3A.565/7	$Na_{57.8}K_{26.6}Si_{94.9}Al_{97.1}O_{768}\cdot 185.9H_2O\cdot 2.1Na_2CrO_4$
Cr.3A.650/7	$Na_{61.5}K_{29.4}Si_{95.0}Al_{97.0}O_{768}\cdot 197.4H_2O\cdot 3.3Na_2CrO_4$
4A	$Na_{88.3}Si_{95.0}Al_{97.0}O_{768}\cdot 200.6H_2O$
Cr.4A.465/2	$Na_{87.0}Si_{95.5}Al_{96.5}O_{768}\cdot 207.6H_2O\cdot 1.2Na_2CrO_4$
Cr.4A.650/2	$Na_{83.3}Si_{95.9}Al_{96.1}O_{768}\cdot 210.7H_2O\cdot 2.3Na_2CrO_4$
Cr.4A.465/7	$Na_{87.6}Si_{95.7}Al_{96.3}O_{768}\cdot 190.7H_2O\cdot 1.7Na_2CrO_4$
Cr.4A.565/7	$Na_{85.8}Si_{95.7}Al_{96.3}O_{768}\cdot 193.6H_2O\cdot 2.1Na_2CrO_4$
Cr.4A.650/7	$Na_{84.3}Si_{95.4}Al_{96.6}O_{768}\cdot 196.6H_2O\cdot 3.3Na_2CrO_4$
5A	$Na_{25.8}Ca_{35.0}Si_{96.7}Al_{95.3}O_{768}\cdot 201.0H_2O$
Cr.5A.465/2	$Na_{28.7}Ca_{32.7}Si_{95.6}Al_{96.4}O_{768}\cdot 214.0H_2O\cdot 0.4Na_2CrO_4$
Cr.5A.650/2	$Na_{28.1}Ca_{33.0}Si_{96.2}Al_{95.8}O_{768}\cdot 216.4H_2O\cdot 0.7Na_2CrO_4$
Cr.5A.465/7	$Na_{27.8}Ca_{34.2}Si_{95.7}Al_{96.3}O_{768}\cdot 197.8H_2O\cdot 1.4Na_2CrO_4$
Cr.5A.565/7	$Na_{27.6}Ca_{34.2}Si_{96.4}Al_{95.6}O_{768}\cdot 197.3H_2O\cdot 2.4Na_2CrO_4$
Cr5A.650/7	$Na_{24.4}Ca_{34.5}Si_{96.9}Al_{95.1}O_{768}\cdot 205.2H_2O\cdot 4.0Na_2CrO_4$

Table 3.3 Reaction of faujasite type and mordenite zeolites and sodium molybdate.

Sample	Unit Cell Composition
Y72	$Na_{9.6}Si_{136.7}Al_{55.3}O_{768}\cdot 187.6H_2O$
Mo.Y72.475/7	$Na_{14.4}Si_{136.9}Al_{55.1}O_{768}\cdot 191.6H_2O\cdot 1.4Na_2MoO_4$
Mo.Y72.565/7	$Na_{14.0}Si_{136.7}Al_{55.3}O_{768}\cdot 146.1H_2O\cdot 5.3Na_2MoO_4$
Mo.Y72.650/7	$Na_{14.8}Si_{136.8}Al_{55.2}O_{768}\cdot 89.7H_2O\cdot 7.0Na_2MoO_4$
Y52	$Na_{51.2}Si_{136.7}Al_{55.3}O_{768}\cdot 248.0H_2O$
Mo.Y52.475/7	$Na_{50.0}Si_{136.8}Al_{55.2}O_{768}\cdot 217.1H_2O\cdot 0.8Na_2MoO_4$
Mo.Y72.565/7	$Na_{49.9}Si_{137.5}Al_{54.5}O_{768}\cdot 182.0H_2O\cdot 1.9Na_2MoO_4$
Mo.Y72.650/7	$Na_{47.8}Si_{137.7}Al_{54.3}O_{768}\cdot 90.0H_2O\cdot 5.5Na_2MoO_4$
13X	$Na_{83.8}Si_{106.2}Al_{85.8}O_{768}\cdot 227.5H_2O$
Mo.13X.475/7	$Na_{76.9}Si_{106.1}Al_{85.9}O_{768}\cdot 232.1H_2O\cdot 0.4Na_2MoO_4$
Mo.13X.565/7	$Na_{74.9}Si_{106.3}Al_{85.7}O_{768}\cdot 203.0H_2O\cdot 2.3Na_2MoO_4$
Mo.13X.655/7	$Na_{76.2}Si_{106.4}Al_{85.6}O_{768}\cdot 175.2H_2O\cdot 2.7Na_2MoO_4$
M5	$Na_{7.2}Si_{40.3}Al_{7.7}O_{192}\cdot 31.3H_2O$
Mo.M5.565/7	$Na_{6.6}Si_{40.2}Al_{7.8}O_{192}\cdot 26.5H_2O\cdot 0.5Na_2MoO_4$
Mo.M5.650/7	$Na_{7.1}Si_{40.4}Al_{7.6}O_{192}\cdot 16.5H_2O\cdot 0.8Na_2MoO_4$

Table 3.4 Reaction of faujasite type and mordenite zeolites and sodium tungstate.

Sample	Unit Cell Composition
Y72	$Na_{9.6}Si_{136.7}Al_{55.3}O_{768}\cdot 187.6H_2O$
W.Y72.475/7	$Na_{16.9}Si_{136.9}Al_{55.1}O_{768}\cdot 186.2H_2O\cdot 4.7Na_2WO_4$
W.Y72.565/7	$Na_{12.5}Si_{136.7}Al_{55.3}O_{768}\cdot 163.9H_2O\cdot 8.7Na_2MoO_4$
W.Y72.650/7	$Na_{10.8}Si_{136.4}Al_{55.6}O_{768}\cdot 117.6H_2O\cdot 10.6Na_2MoO_4$
Y52	$Na_{51.2}Si_{136.7}Al_{55.3}O_{768}\cdot 248.0H_2O$
W.Y52.475/7	$Na_{47.8}Si_{137.4}Al_{54.6}O_{768}\cdot 227.2H_2O\cdot 2.0Na_2WO_4$
W.Y52.565/7	$Na_{48.7}Si_{137.1}Al_{54.9}O_{768}\cdot 211.1H_2O\cdot 1.9Na_2WO_4$
W.Y52.650/7	$Na_{48.5}Si_{137.4}Al_{54.6}O_{768}\cdot 55.9H_2O\cdot 5.5Na_2WO_4$
13X	$Na_{83.8}Si_{106.2}Al_{85.8}O_{768}\cdot 227.5H_2O$
W.13X.475/7	$Na_{77.5}Si_{106.2}Al_{85.8}O_{768}\cdot 217.7H_2O\cdot 1.8Na_2WO_4$
W.13X.565/7	$Na_{77.9}Si_{106.4}Al_{85.6}O_{768}\cdot 221.0H_2O\cdot 2.7Na_2WO_4$
W.13X.650/7	$Na_{75.1}Si_{106.3}Al_{85.7}O_{768}\cdot 186.6H_2O\cdot 3.4Na_2WO_4$
M5	$Na_{7.2}Si_{40.3}Al_{7.7}O_{192}\cdot 31.3H_2O$
W.M5.465/7	$Na_{6.6}Si_{40.3}Al_{7.7}O_{192}\cdot 26.0H_2O\cdot 0.3Na_2WO_4$
W.M5.565/7	$Na_{6.5}Si_{40.3}Al_{7.7}O_{192}\cdot 25.6H_2O\cdot 0.5Na_2WO_4$
W.M5.650/7	$Na_{6.7}Si_{40.4}Al_{7.6}O_{192}\cdot 20.7H_2O\cdot 0.7Na_2WO_4$

Effect of Chromate to Zeolite Mole Ratio on the Occlusion of Sodium Chromate by 5A

Two reaction mixtures were prepared containing 30 g of 5A and 30 ml of 1 mol L^{-1} Na_2CrO_4 solution and 20 g 5A and 175 ml of 1 mol L^{-1} Na_2CrO_4 solution. The former mixture contained a chromate to zeolite mole ratio of 16 while that of the latter mixture was 149, i.e. if all the chromate in the reaction mixtures was occluded within the zeolite then 16 and 140 chromates would be occluded per unit cell. Uptakes were 1.5 Cr/uc (chromates per unit cell) after 107 hours at 620°C from the mixture containing the low ratio and 32.3 Cr/uc after 20 hours at 620°C from that containing the high ratio.

Maximum Uptake Levels of Sodium Chromate

The reaction mixtures used in Section 3.2.4 contained sufficient Na_2CrO_4 to load 54 chromates per unit cell or 6.75 chromates per α-cage. Reaction mixtures were prepared containing higher chromate to zeolite ratios. Heating these mixtures at 620°C for 20 hours gave loaded zeolites with compositions shown in Table 3.5.

Table 3.5 Reaction mixtures and maximum chromate uptakes.

Zeolite	Reaction Mixture	Moles Cr/zeolite	Cr/uc	Sample
13X	13.8 g 13X + 35 ml 2.5 mol L^{-1} Na_2CrO_4	111	13.6	13.6CrX
Y52	3.0 g Y52 + 7 ml 2.5 mol L^{-1} Na_2CrO_4	100	13.4	13.4CrY
5A	20.0 g 5A + 175 ml 1.0 mol L^{-1} Na_2CrO_4	149	32.3	32.3Cr5A

Factors Affecting the Reaction Between Zeolites and Sodium Chromate, Sodium Molybdate and Sodium Tungstate

The work described in this chapter investigated the effect of temperature, time, zeolite structure, and chromate to zeolite mole ratio on the occlusion of sodium chromate, sodium molybdate, and sodium tungstate.

Preliminary investigations of the effect of temperature and time indicated that uptake increased with increasing temperature and time.

Chromate uptakes after 7 hours at 655°C (as Cr/uc) of 3.0, 3.0, 3.3, 3.3, and 4.0 for 13X, Y52, 3A, 4A, and 5A, respectively, indicate that zeolite structure plays no significant role in the rate of occlusion under the conditions of the experiment.

Similar maximum uptakes for 13X and Y52 were observed (~13.5 Cr/uc) while 5A was found to occlude a higher amount (32.3 Cr/uc). The fact that zeolites with similar structures occluded similar amounts while zeolites with different structures occluded different amounts indicates that zeolite structure governs the maximum amount of occlusion.

Chromate to zeolite mole ratio was found to affect the rate of occlusion. The reaction mixture with a chromate to zeolite ratio of 16 contained insufficient chromate to achieve the maximum loading of 32.3 Cr/uc. The occlusion of only 1.5 Cr/uc after 107 hours at 620°C indicates that reaction did not reach completion suggesting either an equilibrium or an order dependence on chromate concentration was involved in the rate of uptake. Increasing the chromate to zeolite mole ratio to 149 allowed maximum uptake to achieved within only 20 hours at the same temperature.

3.3.5 Kinetics of Sodium Chromate Uptake by 13X

Results

The kinetics of the occlusion of sodium chromate was investigated at various temperatures. A reaction mixture was prepared by drying a mixture of 80 g of 13X and 250 ml of 1 mol L^{-1} Na_2CrO_4 at 150°C for 1 hour. A sample of this mixture was placed in the furnace and the temperature raised at 20°/min until the desired temperature was reached. Samples were removed after various reaction times. Figure 3.2 shows the chromate uptake as functions of time at various temperatures.

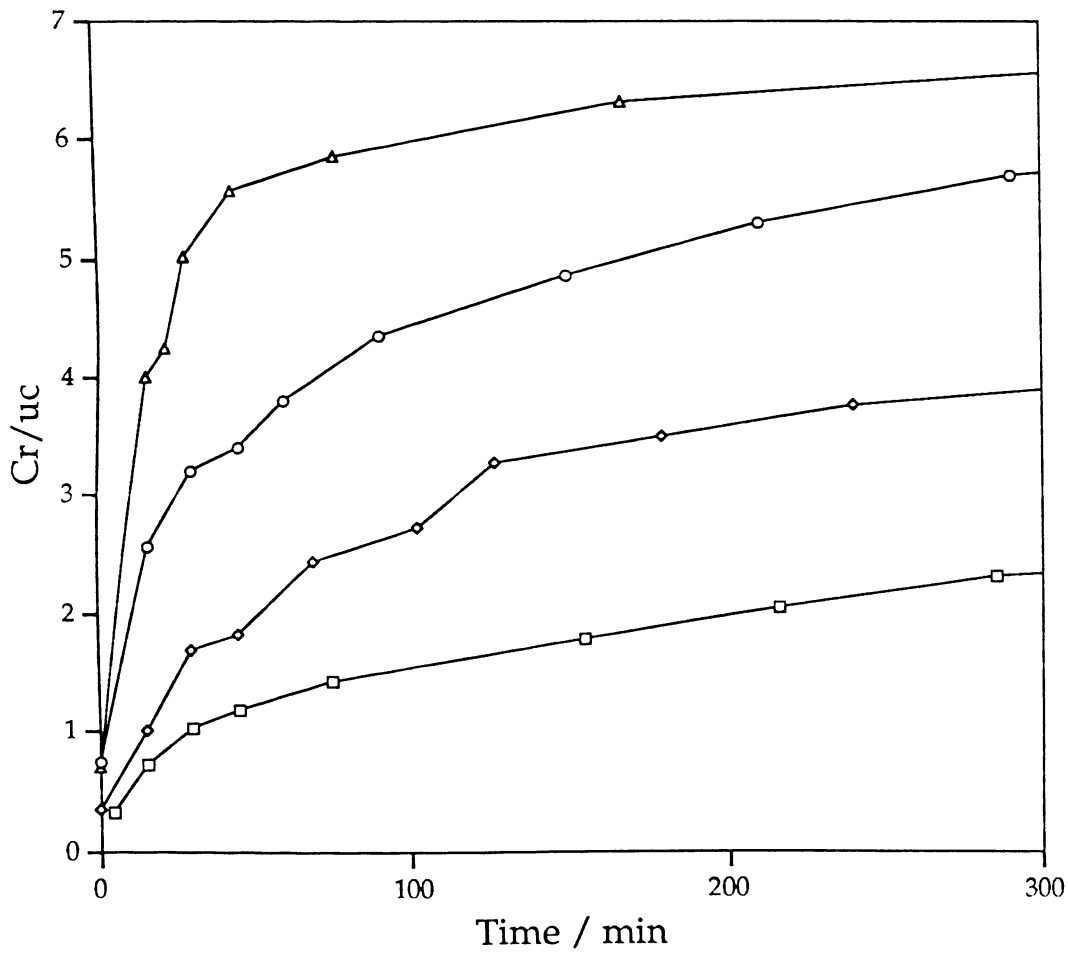


Figure 3.2 Uptakes of sodium chromate by zeolite 13X via the solid-state reaction between sodium chromate and zeolite 13X at various temperatures. Reaction temperatures are (△) 720°C, (○) 670°C, (◇) 600°C, and (□) 540°C.

Figure 3.3 shows fractional uptakes (θ) of sodium chromate as functions of $\sqrt{t}$ and indicates a linear relationship over the initial stages of the reactions. Values of θ were calculated from uptake data by dividing the uptake at any given time by 8.35, the uptake value after 1300 minutes at 720°C.

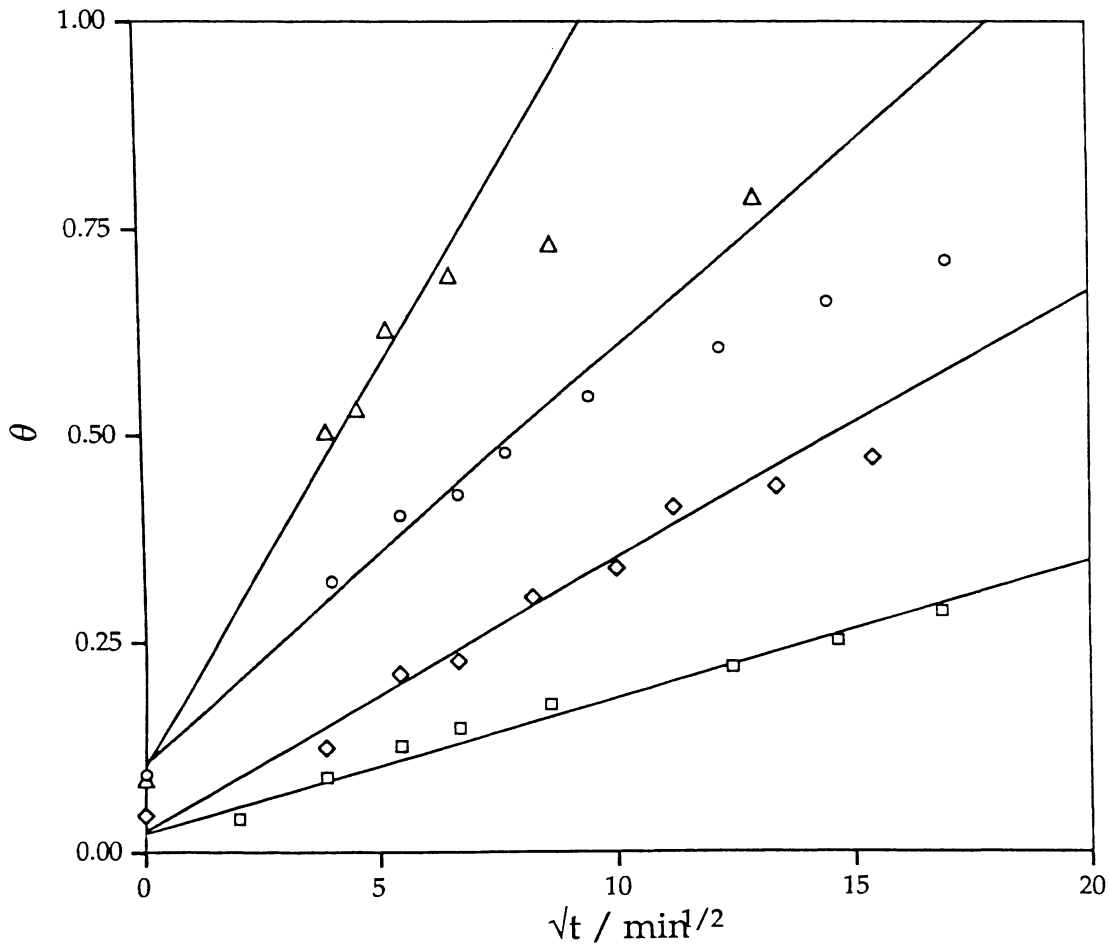


Figure 3.3 $\sqrt{t}$ dependency of sodium chromate uptake by zeolite 13X at various temperatures. Reaction temperatures are (△) 720°C, (○) 670°C, (◇) 600°C, and (□) 540°C.

A $\sqrt{t}$ dependence is often observed for ion-exchange processes involving zeolites, the kinetics of which are controlled by diffusion of the ions through the zeolite crystals. Barrer derived the following relationship between the extent of reaction over the initial stages of reaction.

$$\theta = \frac{6}{r_o}\sqrt{\frac{Dt}{\pi}} \qquad 3.1$$

where θ = extent of reaction, D = diffusion coefficient, r_o = radius of the crystallites, and t = time. Values of D obtained from the slopes of the lines shown in Figure 3.4 using an average crystallite radius of 1 μm (estimated from SEM photographs) are given in Table 3.6. Figure 3.4 shows the Arrhenius relationship $\left(D = D_0 e^{-E_a / RT} \right)$ for the process. The slope and intercept of the line of best fit correspond to an apparent activation energy of 124 ± 10 kJ mol^{-1} and a D_0 value of 2.18x10^4 m^2 s^{-1}.

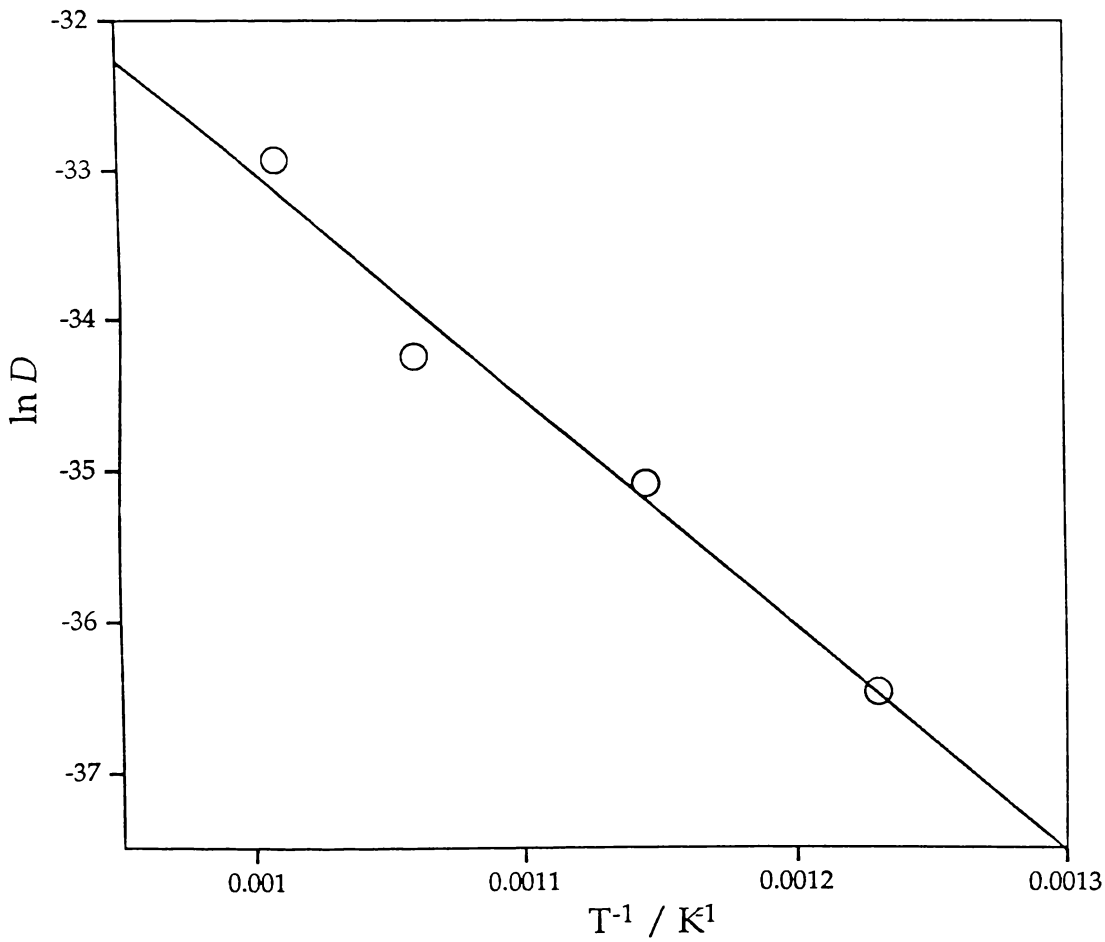


Figure 3.4 Arrhenius plot for the uptake of sodium chromate by zeolite 13X.

Table 3.6 Diffusion coefficient data obtained from the √t plot for the uptake of sodium chromate by zeolite 13X.

T/°C	D /m^2 s^{-1} x10^{17}
540	0.245
600	0.963
670	2.245
720	8.320

Interpretation

Uptake of sodium chromate by zeolite 13X was consistent with diffusion control as reported in the literature for many salt exchange and ion-exchange reactions. The CrO_4^{2-} anion, with a thermochemical radius of 2.56 ± 0.03 Å,[1] is one of the largest oxyanions while Na^+ cation is moderately small cation of radius 0.98 Å.[2] The rate of the diffusion process is therefore likely to be limited by the diffusion of the chromate anion rather than by the sodium cation. Figure 3.5 compares the effect of temperature on the coefficient of self-diffusion for sodium cations in zeolite Y[3] and coefficient of diffusion for sodium chromate into zeolite X. Extrapolation of the sodium chromate data to a $10^3/T$ value of 1.5 (394°C) gives a diffusion coefficient of 10^{-12} compared to 10^{-9} for self-diffusion of sodium cations in Y.

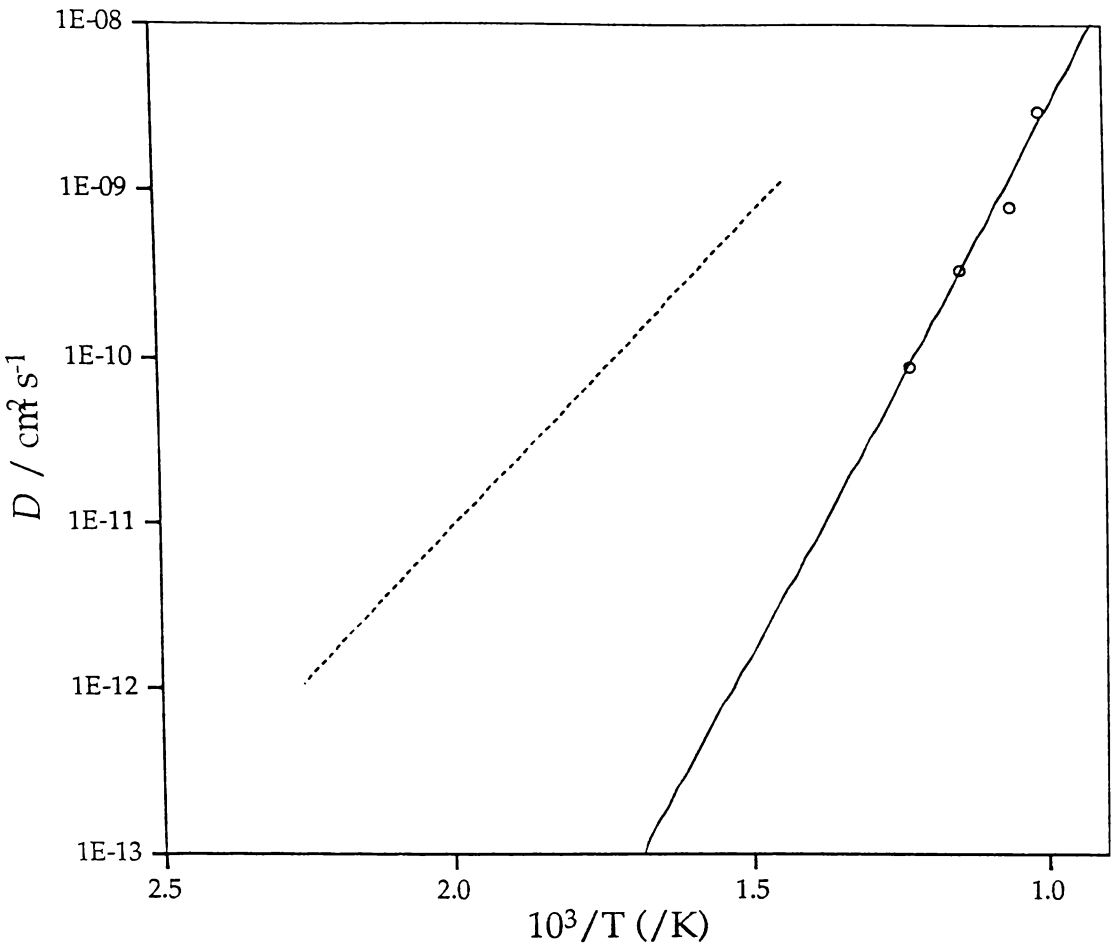


Figure 3.5 Comparison of the effects of temperature on the coefficients of self-diffusion for sodium cations in zeolite Y and the diffusion coefficients of sodium chromate into zeolite 13X.

Araya and Dyer[4] observed diffusion controlled kinetics for the elution of chloride and fluoride compounds from zeolite A and the activation energies shown in Table 3.7 were derived. The activation energy of 124 ± 10 kJ mol^{-1} for sodium chromate diffusion into zeolite 13X is slightly larger than the activation energy for diffusion of sodium chloride into zeolite A. Anions such as the halides show an anion sieve effect whereby the temperature required to achieve penetration of the anion into sodalite cages of Na-Y zeolite increases with increases in the anion radius.[3] The increase in activation energy can therefore be related to the larger radius of the chromate anion compared to that of the

chloride anion. It must however be realised that the zeolite adsorbent is different. Larger diffusion coefficients and lower activation energies are the likely results of diffusion through the larger S12R pore openings of 13X compared to diffusion through the S8R of zeolite A. The expectation is that the activation energy for the diffusion of sodium chromate into zeolite A would be greater than that observed in these studies of zeolite 13X.

Table 3.7 Activation energies (E_a) for the elution of chloride and fluoride compounds from zeolite A (after Araya and Dyer[4]). Also shown are the radius of the anions (r_a).

Salt	(Li,Na)Cl	KF
E_a/ kJ mol^{-1}	107	34
r_a/Å	1.72	1.26

3.4 Discussion

3.4.1 Hydrothermal Reactions of 13X and Salts

Contact with strong salt solutions is generally sufficient to load salt species into α-cages. With chromate, however, treatment of 13X with 2.5 mol L^{-1} Na_2CrO_4 solution for 24 hours at 80°C resulted in no occlusion. As the thermochemical diameter of the CrO_4^{2-} anion (5.12 ± 0.06 Å) is significantly smaller than the kinetic diameter of the S12R (8.0 Å) the lack of chromate occlusion is not the result of size exclusion. Low diffusion coefficients may be the cause of the lack of occlusion. In Section 3.2.5 it was shown that solid-state occlusions followed diffusion controlled kinetics. Extrapolation of the Arrhenius plot to 80°C gives a diffusion coefficient of 3.4x10^{-26} m^2 s^{-1} at this temperature. This diffusion coefficient and equation 3.1 were used to evaluate a half-life of 2.3x10^{13} s (7,300,00 years) for occlusion at 80°C. Similarly, a θ value of 0.000001 was calculated for θ after 24 hours at 80°C. The absence of

significant occlusion after 24 hours is consistent with half-life and θ value calculated from the extrapolated diffusion coefficient. A possible explanation of the low diffusion coefficients is that chromate is strongly adsorbed by sites within the pore structure of the zeolite. The diffusion coefficients for migration of species that are undergoing adsorption are often given by the equation $D_{eff} = \frac{D}{1+K}$ where D_{eff} is the effective diffusion coefficient, D is the diffusion coefficient in the absence of adsorption, and K is the equilibrium constant of the adsorption process.[5] In the case of chromate adsorption on 13X the equilibrium might be given by $Na_2CrO_4 + S \overset{K}{\rightleftharpoons} S\cdots Na_2CrO_4$ (where S is the adsorption site). Under conditions of strong adsorption the equilibrium will lie towards the product side giving a large value of K and a decrease in the effective diffusion coefficient. Removal of all occluded chromate from 13.4CrY within 24 hours by salt solutions indicated large diffusion coefficients of chromate under the conditions of the experiment. Substantial uptakes of chromate from salt solution in the presence of NaOH indicated a similar increase in diffusion coefficient of chromate. Such an increase is consistent with a decrease in the strength of chromate adsorption. If the other salt completed for sites then an equilibrium such as $S\cdots Na_2CrO_4 + NaOH \overset{K'}{\rightleftharpoons} S\cdots NaOH + Na_2CrO_4$ would exist. Such an equilibrium would lower the equilibrium constant of the earlier equilibrium thereby increasing the effective diffusion coefficient.

3.4.2 Devised Strategy for Oxyanion Occlusion

Hydrothermal salt uptake was hindered by slow diffusion rates. Although increased rates could be achieved through the addition of NaOH or salt species such and NaCl and Na_2SO_4, uptake under these conditions would result in mixed salt species. While mixed salt species may be adequate, or even desirable, under certain circumstances, they were deemed unsuitable for this

work. Solid-state reactions provided a convenient means of chromate occlusion by allowing reactions to be performed at much higher temperatures thereby affording larger diffusion coefficients even in the absence of other salts. Zeolites with faujasite structures offer two types of cages (α and β) each capable of occluding salt species. Temperatures above the melting point of the salt are generally required for β-cage occlusion, with occlusion being limited to α-cages at temperatures below the melting point. Most salt of practical interest have melting points well below the decomposition temperature of many zeolites. As such there is a range of temperatures over which β-cage occlusion can be achieved without zeolite decomposition. DTA and PXRD studies have shown that the melting point of sodium chromate is sufficiently close to the temperature of zeolite decomposition that reactions at temperatures even slightly below the melting point of sodium chromate result in the production of chromate nosean. Preservation of zeolite lattice crystallinity therefore required that solid-state reactions be performed at temperatures well below 800°C. The likelihood of chromate occlusion in β-cages under the conditions employed in the solid-state reactions is discussed in Section 3.4.3.

3.4.3 Possibility of Chromate Occlusion Within β-Cages

It was of interest to investigate the possibility of loading sodalite cages of zeolites with sodium chromate. Some idea of the likelihood of chromate occlusion in β-cages at employed temperatures between 465°C and 650°C can be obtained from consideration of the literature on solid-state occlusions of other salt species.

The results of Rabo *et al.* given in Table 1.1 (see Section 1.3.2) indicated that an increase in temperature as radius of the anion increased was required to load the β-cages of Na-Y. A temperature of 645°C was required for even

moderate levels β-cage occlusion of NaI. within 24 hours As the thermochemical radii of CrO_4^{2-}, 2.56 ± 0.03 Å,[1] is substantially greater than that of I^-, 2.10 ± 0.08 Å,[1] the expectation is that higher temperatures would be required for the passage of chromate anions into β-cages than would be required for iodide anions. It is therefore reasonable to expect that sodium chromate occluded at temperatures up to 650°C would lie within α-cages.

It has been suggested that decomposition of large complex oxyanions to form smaller molecules is a means by which penetration into β-cages is achieved. For example, Rabo considered it rather surprising that while I^- was too large to penetrate β-cages at 650°C the "substantially larger" NO_3^- anion reached anion/β-cage ratios greater than one at 650°C.[6] The ease of nitrate occlusion was attributed to the formation of smaller molecules, through decomposition by loss of oxygen, to form NO and NO_2 followed by reformation of NO_3^- subsequent to occlusion in β-cages. In the case of sodium chromate, decomposition could form species such as Na_2CrO_3, Na_2CrO_2, and CrO_3 with symmetry below tetrahedral and with anion radii below that of CrO_4^{2-}. Lower radii would facilitate β-cage occlusion. Decomposition of chromate as a means of β-cage occlusion is eliminated below.

Examination of the thermochemical radii of anions places some doubt on the decomposition of oxyanions as a means of β-cage penetration. Jenkins and Thakur[1] evaluate the thermochemical radius of the NO_3^- anion at 1.79 ± 0.06 Å. This radius, contrary to the beliefs of Rabo, is significantly lower than that of I^- and is intermediate between those of Cl^- (1.72 ± 0.05 Å) and Br^- (1.88 ± 0.05).[1] Rapid occlusion of $NaNO_3$ at temperatures around 650°C is not surprising given that the occlusions of NaCl at 550°C and NaBr at 700°C reach anion to β-cage ratios of near unity. Postulates of NO_2^- formation are therefore not necessary to explain rapid NO_3^- occlusion. Consideration of the thermochemical radius of NO_2^-, 1.92 ± 0.11 Å,[1] suggests that its formation may even have a detrimental effect on the occlusion process. Rapid occlusion

of $NaClO_3$ again is not surprising given that the radius of ClO_3^- (1.71 ± 0.06 Å)[1] is indistinguishable from that of Cl^- (1.72 ± 0.05 Å).[1]

Chapter Three References

1) Jenkins, H.D.B. and Thakur, K.P., *J. Chem. Educ.*, **56(9)** (1979) 576.

2 MacKay, K.M. and MacKay, R.A., in "**Introduction to Modern Inorganic Chemistry**", 3rd edition, International Textbook Company (Glasgow), 1981, pp. 25.

3) Freeman, D.C., Jr and Stamires, D.N., *J. Chem. Phys.*, **35** (1961) 799.

4) Araya, A. and Dyer, A., *Zeolites*, **1** (1981) 35.

5) Crank, J., in "**The Mathematics of Diffusion**", 2nd Edn, Clarendon Press, Oxford (1975) pp. 326.

6) Rabo, J.A., in "**Zeolite Chemistry and Catalysis**" (Ed. Rabo, J.A.), American Chemical Society Monograph 171 (1976) pp. 344.

Chapter Four

Structural Elucidation of Chromate Zeolites

Chapter Four

Structural Elucidation of Chromate Zeolites

4.1 Introduction

Solid-state reactions between zeolites of the types A, 13X, Y52, Y72, M5, and S115 and the sodium salts of chromate, molybdate and tungstate resulted in substantial irreversible uptakes of the transition metal oxyanions (see Chapter Three). This chapter describes the physical and spectroscopic characterisation of these loaded zeolites. A model of the chromate to zeolite interaction is proposed.

4.2 Methods and Materials

Techniques available to study the loaded zeolites systems were: Surface area determination by the BET method, Scanning Electron Microscopy (SEM), Laser Raman Spectroscopy, Differential Thermal Analysis (DTA), Electron Paramagnetic Resonance (EPR), Fourier Transform Infrared Spectroscopy (FTIR), powder X-Ray Diffraction (PXRD), and X-Ray Photo-electron Spectroscopy (XPS). The application of these methods was discussed in Chapter Two. The zeolites examined in this chapter were 13X, 2.1CrX, 5.8CrX, 13.6CrX, 13.4CrY, 32.3Cr5A, chromate nosean (Cr^{nos}), LZ-Y72, 10.3CrY72, 2.3Cr3A, 3.3Cr4A, 1.0CrM5, and 0.9CrS115.

4.3 Possible Means of Occlusion

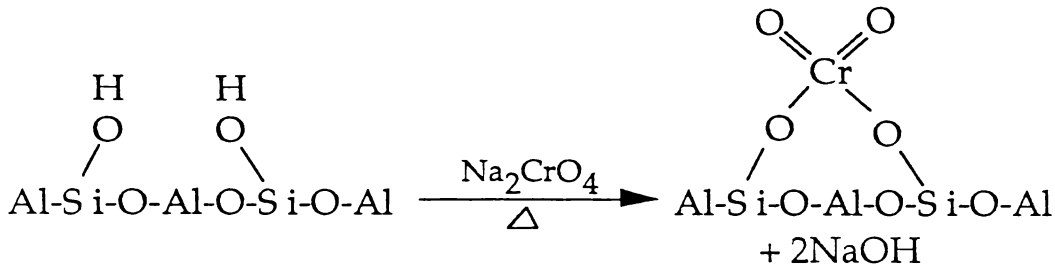
Several reactions between the zeolite and the oxyanion can be envisaged. These include (i) adsorption onto the surface of the zeolite crystals by reaction with surface hydroxyls, (ii) formation of chromyl cations and solid-state ion-exchange with the protons of structural hydroxyls, (iii) formation of chromyl cations and solid-state ion-exchange with zeolite cations, (iv) occlusion of microcrystalline sodium chromate phases within the zeolite cages or channels, (v) replacement of framework atoms, (vi) encapsulation within the sodalite cages of A, X, and Y type zeolites, (vii) coordination to the lattice through sodium cations in the supercage, (viii) formation of sodium chromate phases on the surface of the zeolite crystals (ix) occlusion of chromate into a newly formed aluminosilicate, silicate, or alumina phase. These possible means of oxyanion retention and their anticipated physical and spectroscopic properties that may allow discrimination are discussed in detail in the following sections.

4.3.1 Reaction with Surface Hydroxyls

At the surface of a zeolite crystal there exists tricoordinated metal atoms. In the tricoordinated state Al^{3+} atoms are charge balanced but Si^{4+} possesses a nett positive charge. Thus for each silicon atom on the external surface of the zeolite crystal there exists one surface hydroxyl species. At elevated temperatures the replacement of two OH^- groups by one oxyanion might be envisaged to occur in a process as outlined in Scheme 4.1. If the sodium hydroxide formed was removed during the washing step then we would expect no nett sodium uptake to occur. If this process was the sole means of uptake then XPS would detect high oxyanion concentrations at the surface of the crystals. Raman spectra would be characteristic of discrete oxyanions. No

loss of BET surface area would occur unless oxyanions blocked the external pore system.

Scheme 4.1 Reaction of sodium chromate with zeolitic surface hydroxyls.



4.3.2 Formation of Chromyl Cations and Solid-State Reaction with the Protons of Structural Hydroxyls

It is known that structural hydroxyls formed as a result of deammoniation of NH_4^+ exchanged zeolites act as powerful cation traps. For example, the anhydrous high temperature reaction between CrO_3 and HY results in the solid-state ion-exchange of chromyl cations onto cationic positions, see Section 1.3.1. This process can be represented as follows:

Scheme 4.2 Solid-state reaction between chromium trioxide and hydrogen zeolites involving the replacement of the protons of structural hydroxyls by chromyl cations (CrO_2^{2+}).

$$CrO_3 + 2\,(ZO\text{-}H) \xrightarrow{\Delta} (ZO)_2\,CrO_2 + H_2O$$

One can formulate a scheme involving the formation of a chromyl cation from a chromate oxyanion through reaction with the protons of hydroxyls and ion-exchange of chromyl cations onto cationic positions as shown in Scheme 4.3.

Scheme 4.3 Possible reaction between the H^+ forms of zeolites and sodium chromate involving the replacement of the protons of structural hydroxyls by chromyl cations.

$$Na_2CrO_4 + 2\,(ZO\text{-}H) \xrightarrow{\Delta} (ZO)_2\,CrO_2 + 2\,NaOH$$

Uptake as in Scheme 4.3 would result in no loss of surface area. If the NaOH was removed during the washing step then no nett uptake of sodium would occur. Raman spectra would be characteristic of discrete oxyanions.

Another process involving the exchange of the protons of structural hydroxyls by sodium cations from sodium chromate can be envisaged to occur and involves the stoichiometry shown in Scheme 4.4.

Scheme 4.4 Reaction between zeolites and sodium chromate involving the replacement of the protons of structural hydroxyls by sodium cations.

$$Na_2CrO_4 + 2\ (ZO\text{-}H) \xrightarrow{\Delta} 2\ (ZO\text{-}Na) + H_2CrO_4$$

The consequences of this process would be the uptake two sodium cations per chromium and the formation of a chromic acid type species that would most likely decompose.

4.3.3 Formation of Chromyl Cations and Solid-State Reaction with Zeolite Cations

Occlusion of oxyanions within the sodium forms of zeolites might occur in a reaction analogous with Scheme 4.3 with the stoichiometry shown in Scheme 4.5. This reaction represents the formation of a zeolitic chromyl cation and disodium oxide from a chromate oxyanion through reaction with, and replacement of, zeolitic sodium cations. If the washing step removed the introduced sodium as sodium hydroxide then no nett uptake of sodium would occur. If the disodium oxide becomes irreversibly occluded within the zeolite, for example by encapsulation within a sodalite cage, then uptake of two sodium cations per oxyanion would result. Little or no loss of surface area would result from such an uptake. Raman spectra would be characteristic of discrete oxyanions.

Scheme 4.5 Possible reaction of zeolitic sodium cations and sodium chromate involving the replacement of zeolitic sodium cations by chromyl cations.

$$Na_2CrO_4 + 2\,(ZO\text{-}Na) \xrightarrow{\Delta} (ZO)_2\,CrO_2 + 2\,Na_2O$$

4.3.4 Occlusion of Microcrystalline Sodium Chromate Phases within Supercages or Channels

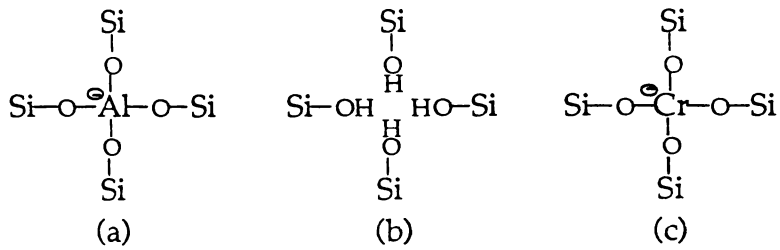
The supercage and channels of zeolites provide void spaces that might be filled with microcrystalline lattices of oxyanions in a process analogous to uptake of salts such as $AgNO_3$. Zeolite A was found to occlude nine $AgNO_3$ per α-cage to give a pseudo unit cell composition of $Na_{12}[Al_{12}Si_{12}O_{24}].9AgNO_3$, see Section 1.3.2. The salt formed an octahedral $(AgNO_3)_9$ cluster in each α-cage. The Raman spectrum of the nitrate inclusion compound was not characteristic of discrete anions but was similar to that of the pure salt. Raman spectra similar to that of the pure oxyanion salt would be expected upon the formation of an intrazeolitic sodium chromate phase. Uptake of two sodium cations per oxyanion and loss of BET surface area are likely outcomes of such occlusion.

4.3.5 Replacement of Framework Atoms

Chromium is isomorphically substituted into the framework of zeolites when a chromium compound is used in the crystallisation of the zeolite.[1] Garwood *et al.*[2] have reported significant chromium uptakes when X and Y zeolites were refluxed with $CrCl_3$. Treatment of NaY and NaX with 15 mL of refluxing 1.0 mol L^{-1} chromium chloride per gram of zeolite removed 32% and 46% of the aluminium, respectively, with 7 wt% and 13 wt% chromium remaining in the washed residue. Removal of aluminium ruptures the lattice leaving "ghost" sites. The ruptured lattice is "healed" to the extent that chromium reacts with the silicon to form Si-O-Cr bonds, see Scheme 4.6. The atomic dimensions of chromium and stability of the tetrahedral configuration

are such that it fits easily into the ghost site. Oxyanion uptake via this mechanism would involve reduction of chromate to Cr(III). If this occurred then one sodium would be required to neutralise the monovalent negative charge of the transition metal lattice site. In the absence of reduction the site would be trivalent and three sodium cations would be required to neutralise the charge of the site. A loss of aluminium would occur. Providing the structure remained intact no loss of BET surface area would result.

Scheme 4.6 Isomorphous replacement of aluminium by chromium during refluxing of zeolites X and Y with $CrCl_3$. (a) shows the original site. (b) removal of aluminium creates "ghost" sites. (c) ruptures in the lattice are "healed" by reaction with chromium to form Cr-O-Si bonds.



4.3.6 Encapsulation within Sodalite Cages

Encapsulation of oxyanions within the sodalite cages in zeolites of the type A, X, and Y could occur by passage of the chromate oxyanion through the six-membered rings of sodalite units facing the supercage or on the external surface of the crystal. This type of occlusion should be similar to occlusion of anions within the sodalite cages of feldspathoid type aluminosilicates such as sodalites and noselites. Uptake of two sodium cations per oxyanion would result. No loss of surface area would be expected as nitrogen does not penetrate the sodalite cages under the conditions of the BET method. Raman spectra would indicate discrete oxyanions.

4.3.7 Coordination to the Lattice through Cations

The positive charge of cations might act as sites for oxyanion adsorption through the formation of Na···O-Cr interactions. Retention of overall charge neutrality would require the uptake of two sodium cations per oxyanion. Raman spectra would be characteristic of discrete oxyanions and loss of BET surface area would result.

4.3.8 Formation of Crystalline Phases on Crystal Surfaces

Uptake might occur via growth of crystalline phases on the surface of zeolite crystals. Such phases would have little effect on surface area unless blocking of external pores prevented the passage of nitrogen into the crystals. Uptakes of two sodium cations per oxyanion would result. Raman bands characteristic of the crystalline oxyanion phase would be evident. PXRD peaks of the crystalline oxyanion phase would be superimposed upon the zeolite peaks if the concentration was sufficiently high. Such phases might be visible in SEM photographs.

4.3.9 Formation of a New Oxyanion Containing Aluminosilicate Phases

The presence of some salt species, including sodium chromate, molybdate and tungstate, and elevated temperatures promotes phase transitions of aluminosilicate frameworks. For example, sodium chromate reacts with a variety of amorphous aluminosilicates (eg aluminosilicate gels) and crystalline aluminosilicates (eg kaolinite) at elevated temperatures to form chromate nosean.[1,2] Oxyanion occlusion might involve the breakdown of zeolite framework and the formation of a new oxyanion containing phase(s). Sodium uptake levels through this process would depend on the mode of

chromate bonding in the new aluminosilicate phase. Loss of XRD peaks and IR framework bands would accompany lattice degradation and other XRD peaks would appear if the new phase was crystalline. Zeolite framework degradation would be evident in SEM photographs as changes in crystal morphology.

4.4 Results and Interpretation

4.4.1 Chromate Leaching By NaOH, NaCl, and Na_2SO_4

Leaching Results

While chromates occluded in zeolite of X and Y types zeolites were resistant to leaching with boiling water, heating in NaOH solution was found to rapidly remove sodium chromate yet leave the zeolite lattice intact. Heating 13.6CrX in 2 mol L^{-1} NaOH at 80°C for 24 hours followed by washing to remove NaOH gave a lighter coloured zeolite that contained only 2.1 chromates per unit cell. This zeolite was named 2.1CrX. The same treatment of 13.4CrY removed all the chromate. Similar NaOH treatment on 10.3CrY72 removed substantial quantities of chromate.

Heating 13.6CrX in 2 mol L^{-1} NaCl and Na_2SO_4 solutions removed a similar amount of chromate as did the NaOH solution .

Interpretation of Chromate Leaching

The complete removal by NaOH solution of chromate from 13.4CrY indicates that the occlusion process can be reversed in at least some cases. Retention of some chromates in 13.6CrX indicates that both reversible and irreversible occlusion can occur to give two types of chromates. Removal of chromate by NaCl and Na_2SO_4 salts indicates that removal by NaOH is a general effect and is not caused by the caustic nature of NaOH or the properties

of the OH^- anion. This suggests that salt exchange is an integral step in the leaching process.

4.4.2 SEM Analysis of Zeolite Morphologies

SEM Results

Plates 4.1 to 4.18 show the SEM photographs of the various parent zeolites and their chromate loaded counterparts.

Zeolite 13X (Plates 4.1 and 4.2) displayed uniform crystal sizes in the range 1-5 μm. There appears to be no uniformity in particle geometry. Individual particles show various degrees of apparent cracking possibly a result of twinning however individual crystal faces are flat. Small clumps on the surface of the crystals could be amorphous material or small incompletely formed zeolite particles. Zeolite 5.8CrX (Plate 4.3 and 4.4) displayed similar size and shape distribution to that of the parent 13X zeolite. A small amount of etching appeared as roughening of crystal surfaces. Holes and gaps appeared at the surface of some crystals possibly due to chromate attack or damage resulting from gaseous or water release during firing. Zeolite 13.6CrX (Plates 4.5 and 4.6) displayed similar crystal morphology to that of 13X. Small amount of etching was suggested by the roughening of surface faces. The holes and gaps present in 5.8CrX are absent for 13.6CrX. Zeolite 2.1CrX (Plates 4.7 and 4.8) had similar morphology to 13X and 13.6CrX from which it was derived.

Zeolite 5A (Plates 4.9 and 4.10) consisted of cube shaped crystals with flat surfaces with particle sizes ranging from 1-5 μm. Broken faces, particle twinning and particle budding are evident but the particles are generally cubic with flat surfaces and well defined edges and vertices. No significant change to the size distribution between 5A and zeolite 4.8Cr5A (Plate 4.11) was evident.

The crystal surface of 4.8Cr5A appeared to exhibit only small amounts of etching with retention of the cubes with well defined edges and flat faces. Zeolite 32.3Cr5A (Plate 4.12) had similar shape characteristics with edges and vertices being well defined. Roughening of the faces indicated etching and/or surface deposition.

Zeolite LZ-Y52 (Plates 4.13 and 4.14) exhibited particle sizes in the range 0.1-1 μm. Particle geometries varied to a greater extent than other zeolites and agglomerates were evident to a greater degree than other zeolites. Zeolite 2.8CrY (Plates 4.15 and 4.16) displayed no significant changes in geometry or particle size distribution to those of Y52.

LZ-Y72 (Plate 4.17) exhibited similar particle morphology as LZ-Y52. Zeolite 10.3CrY72 (Plate 4.18) showed no changes to particle size or shape compared to those of LZ-Y72. An extraneous phase is apparent on crystal surfaces.

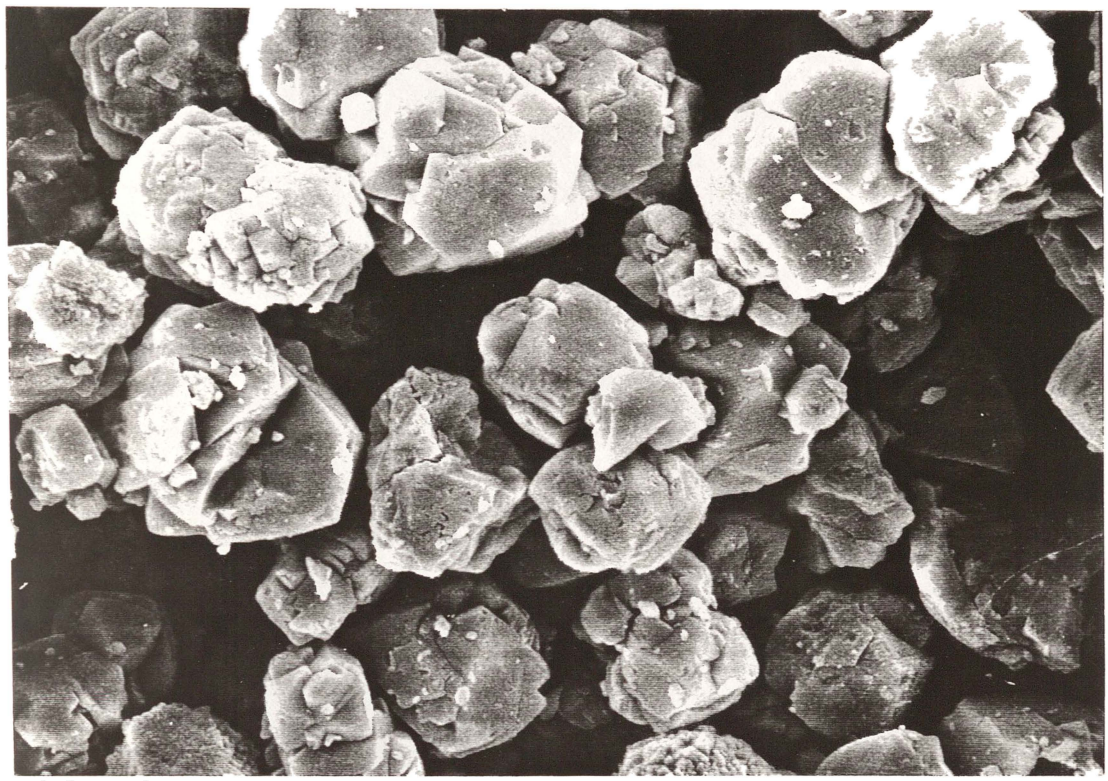


Plate 4.1 SEM photograph of zeolite 13X at a magnification of 8.0 k showing the uniformity of particle size and variation in particle geometry. 1 cm on the plate equals 0.93 μm.

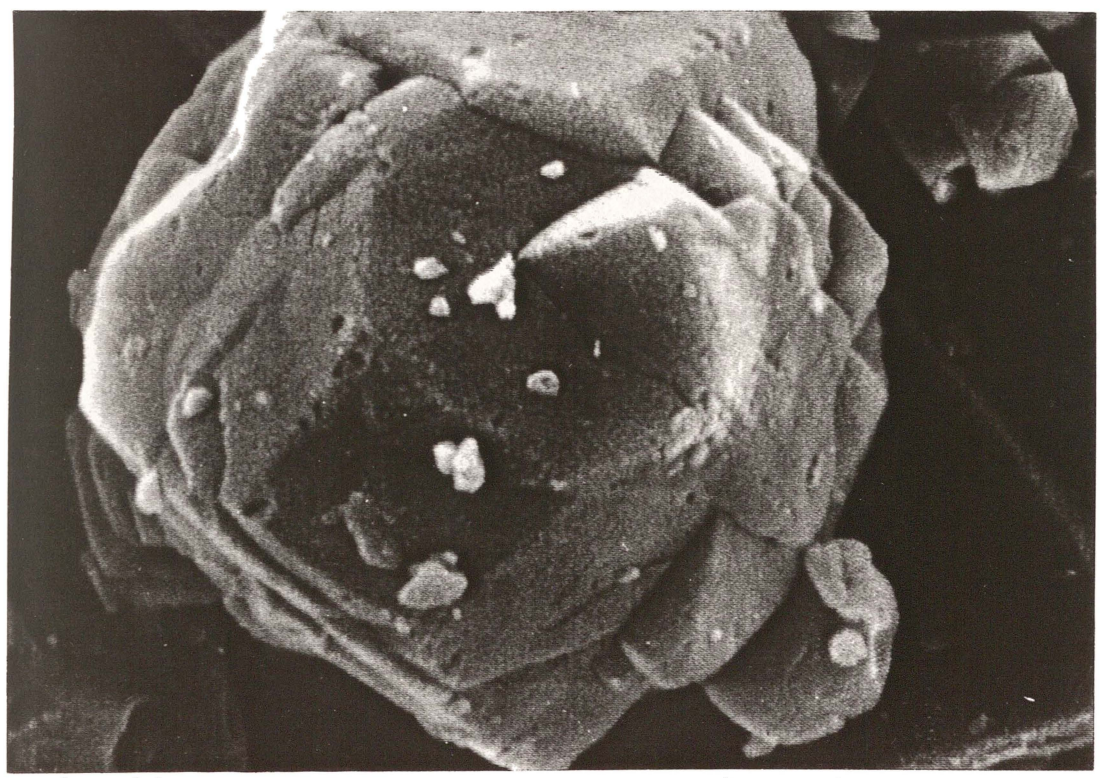


Plate 4.2 SEM photograph of zeolite 13X at a magnification of 18.0 k showing the smooth crystal surfaces. 1 cm on the plate equals 0.26 μm.

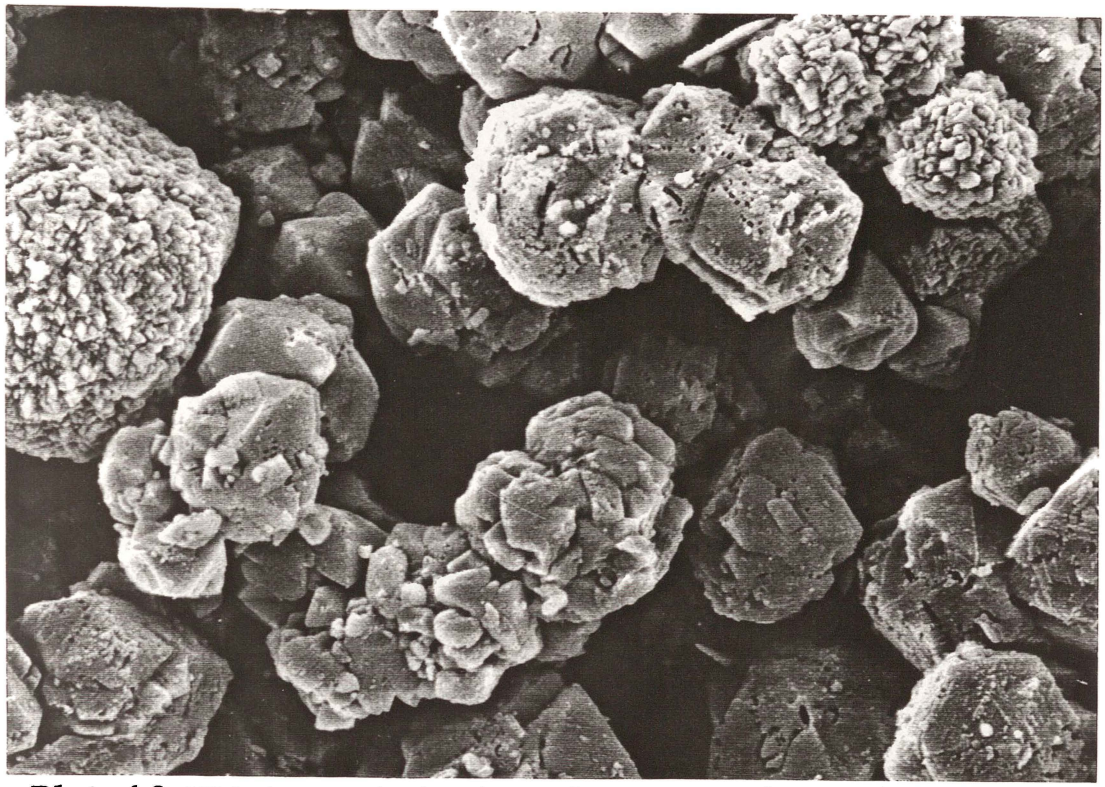


Plate 4.3 SEM photograph of zeolite 5.6CrX at a magnification of 8.0 k. Note the similar crystal size and shape to those of 13X. 1 cm on the plate equals 0.93 μm.

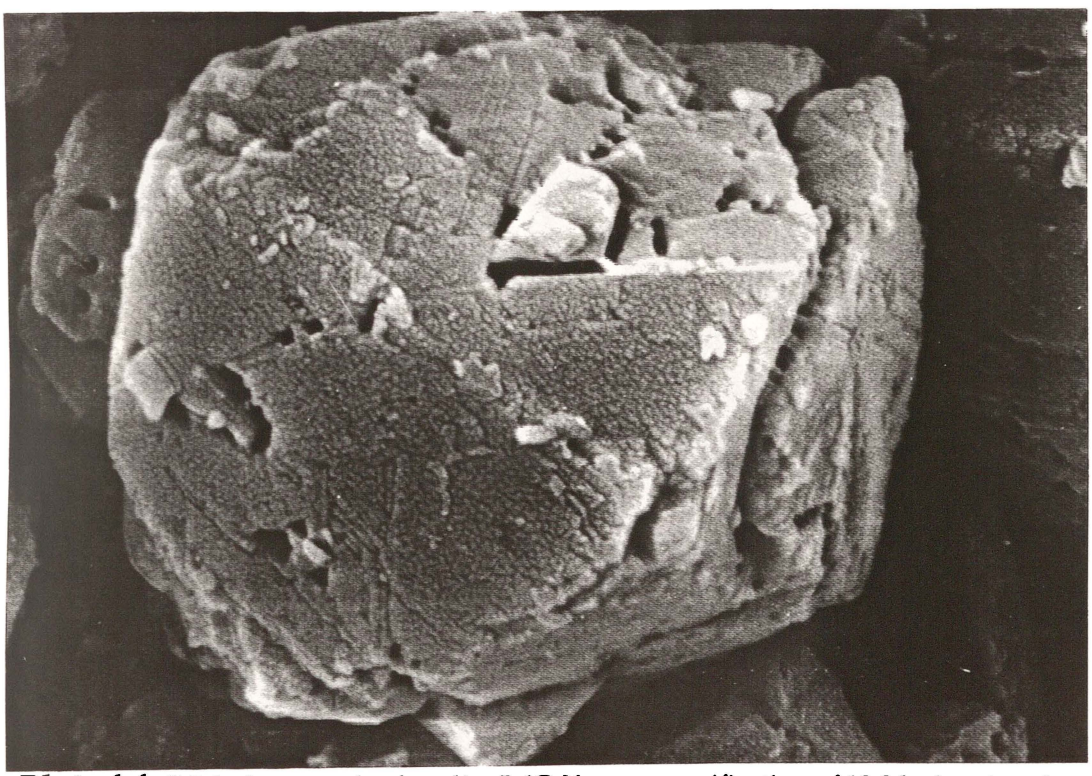


Plate 4.4 SEM photograph of zeolite 5.6CrX at a magnification of 18.0 k showing the cracking and etching resulting from the solid-state reaction at 670°C for 7 hours. 1 cm on the plate equals 0.26 μm.

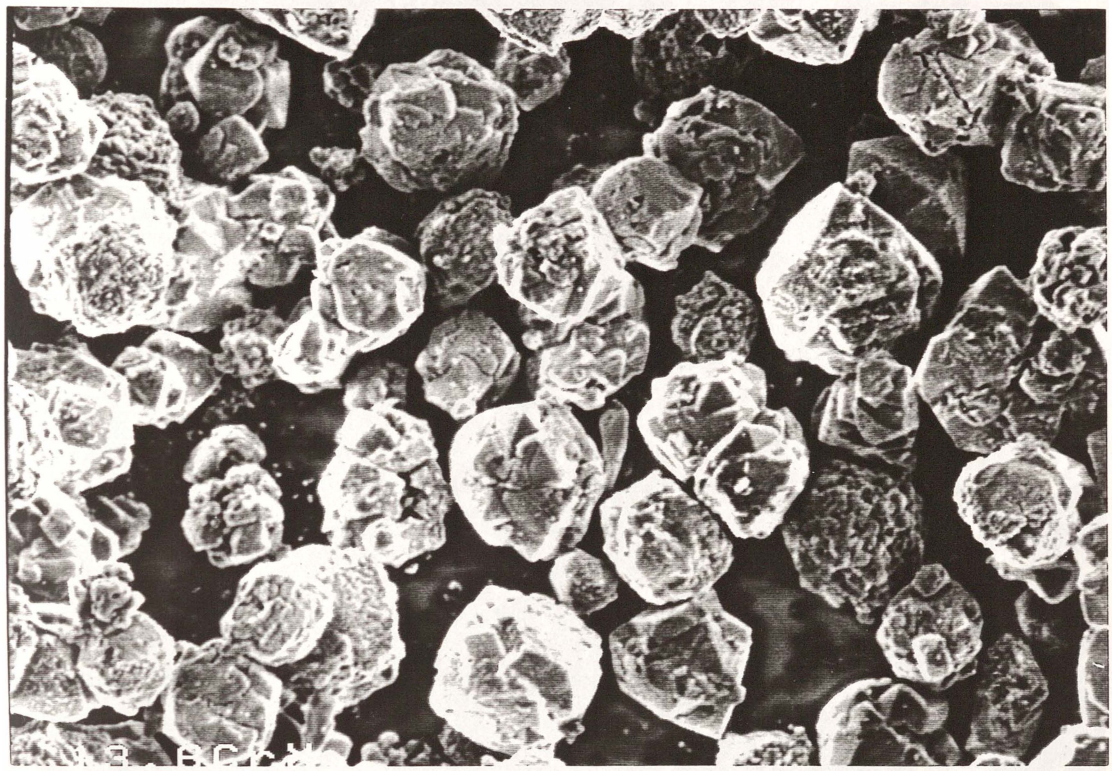


Plate 4.5 SEM photograph of zeolite 13.6CrX at a magnification of 6.0 k. Note the similar crystal morphology to that of 13X. 1 cm on the plate equals 1.29 μm.

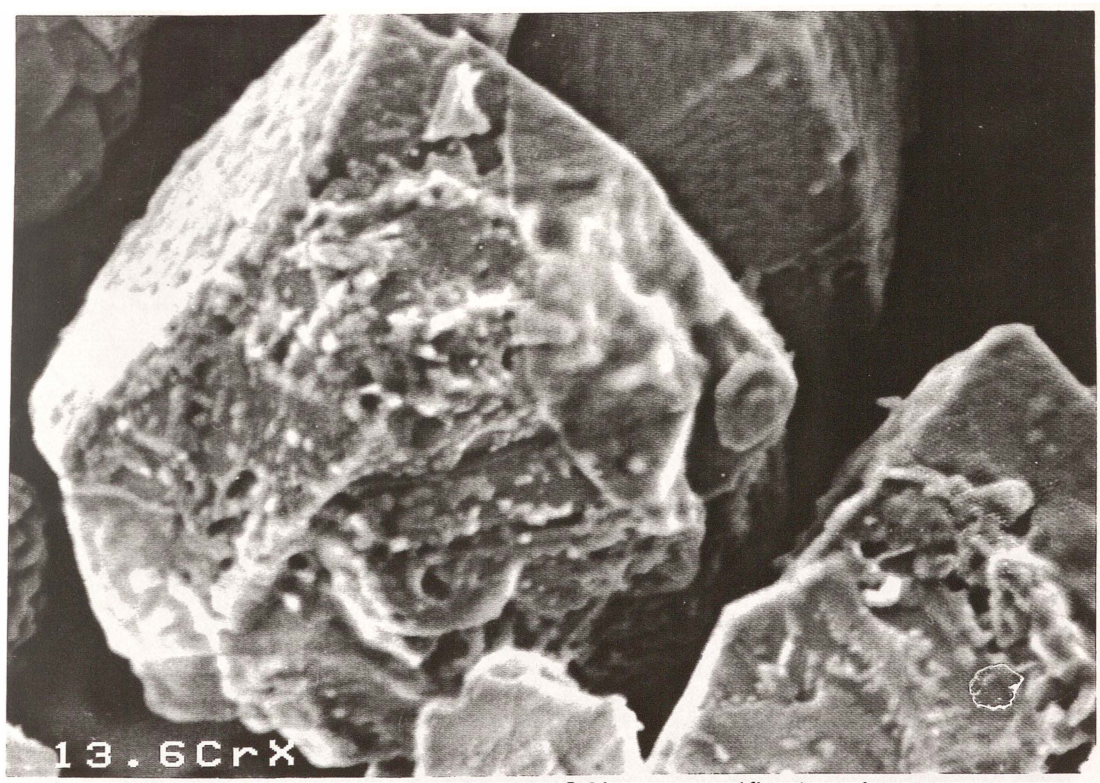


Plate 4.6 SEM photograph of zeolite 13.6CrX at a magnification of 25.0 k. Note the similar crystal morphology to that of 13X . Also evident is the absence of etching seen for 5.8CrX presumably due to the milder conditions of the solid-state reaction (620°C) despite the longer reaction time of 20 hours. 1 cm on the plate equals 0.31 μm.

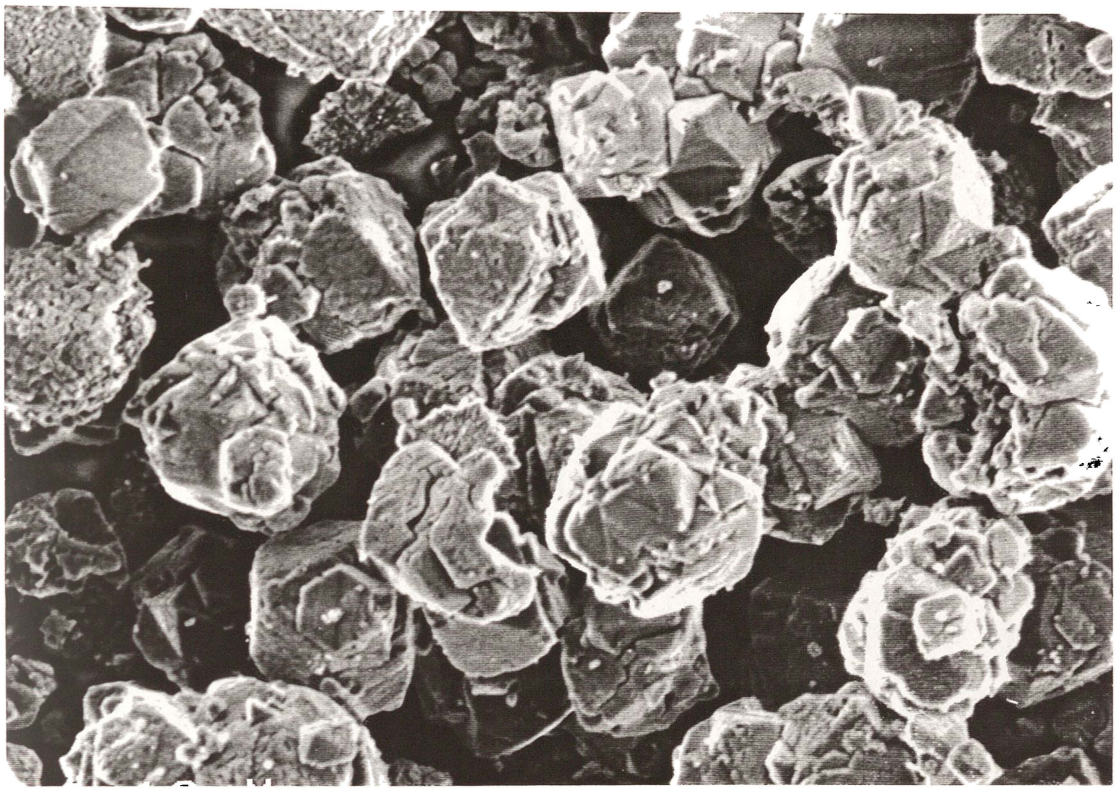


Plate 4.7 SEM photograph of zeolite 2.1CrX at a magnification of 8.0 k. Note the similar crystal morphology to that of 13.6CrX (from which it was derived) indicating NaOH treatment has no significant effect on the zeolite lattice. 1 cm on the plate equals 0.97 μm.

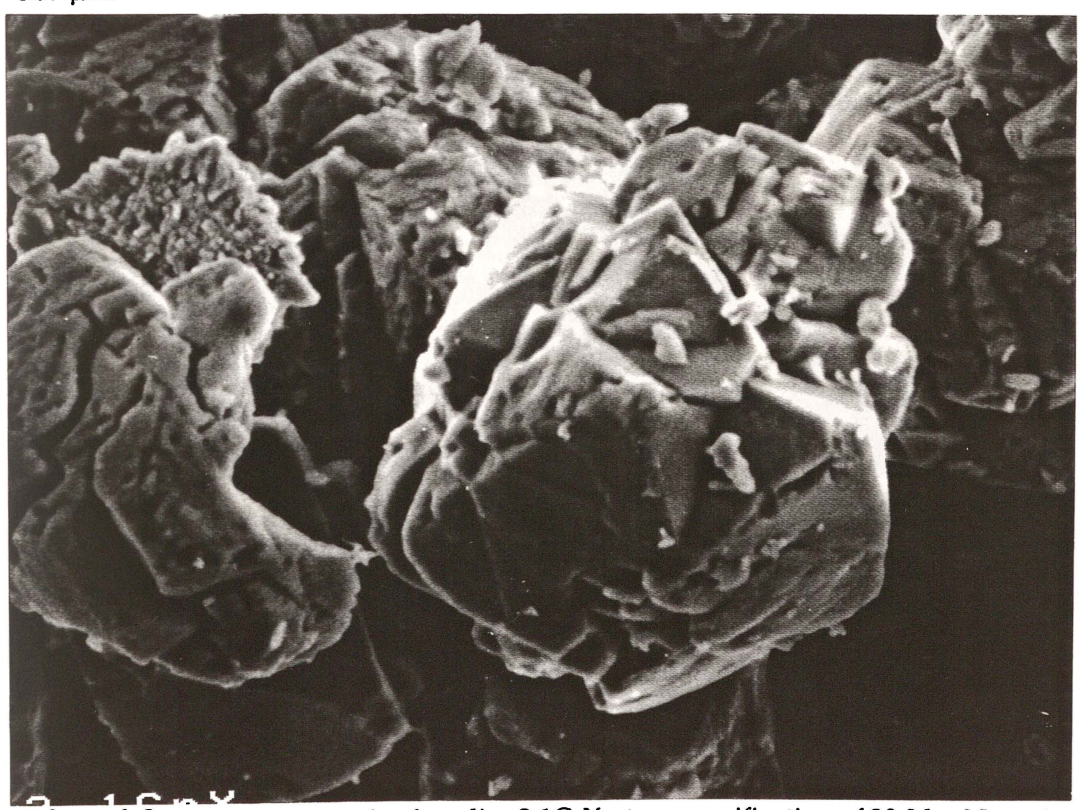


Plate 4.8 SEM photograph of zeolite 2.1CrX at a magnification of 20.0 k. Note the similar surface properties to those of 13.6CrX. 1 cm on the plate equals 0.39 μm.

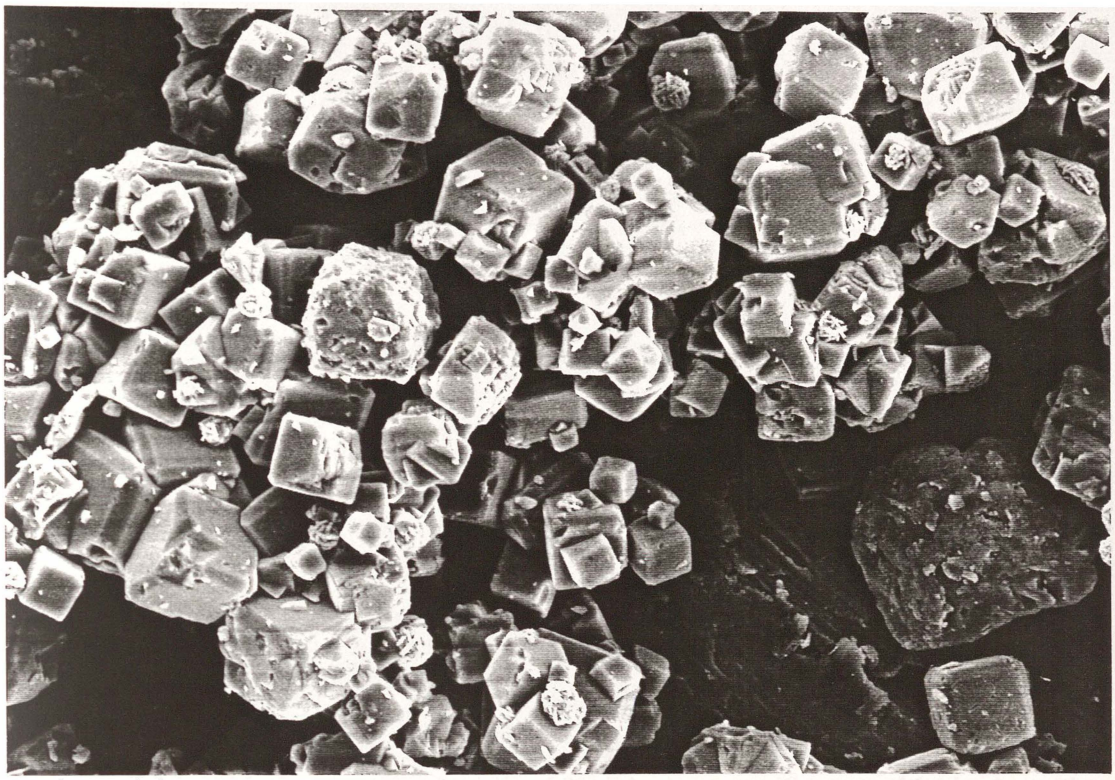


Plate 4.9 SEM photograph of zeolite 5A at a magnification of 1.8 k showing the uniformity in crystal size and shape. 1 cm on the plate equals 2.58 μm.

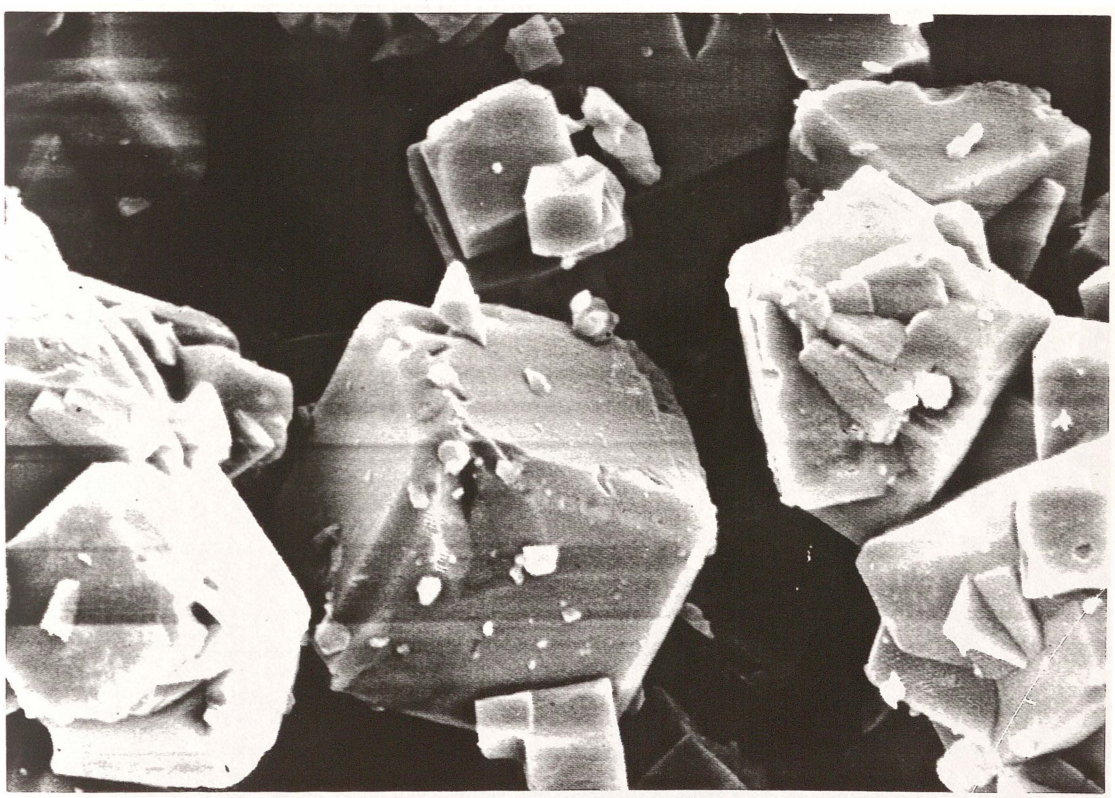


Plate 4.10 SEM photograph of zeolite 5A at a magnification of 6.0 k showing the cube shaped crystals with sharp crystal vertices and flat faces. 1 cm on the plate equals 0.78 μm.

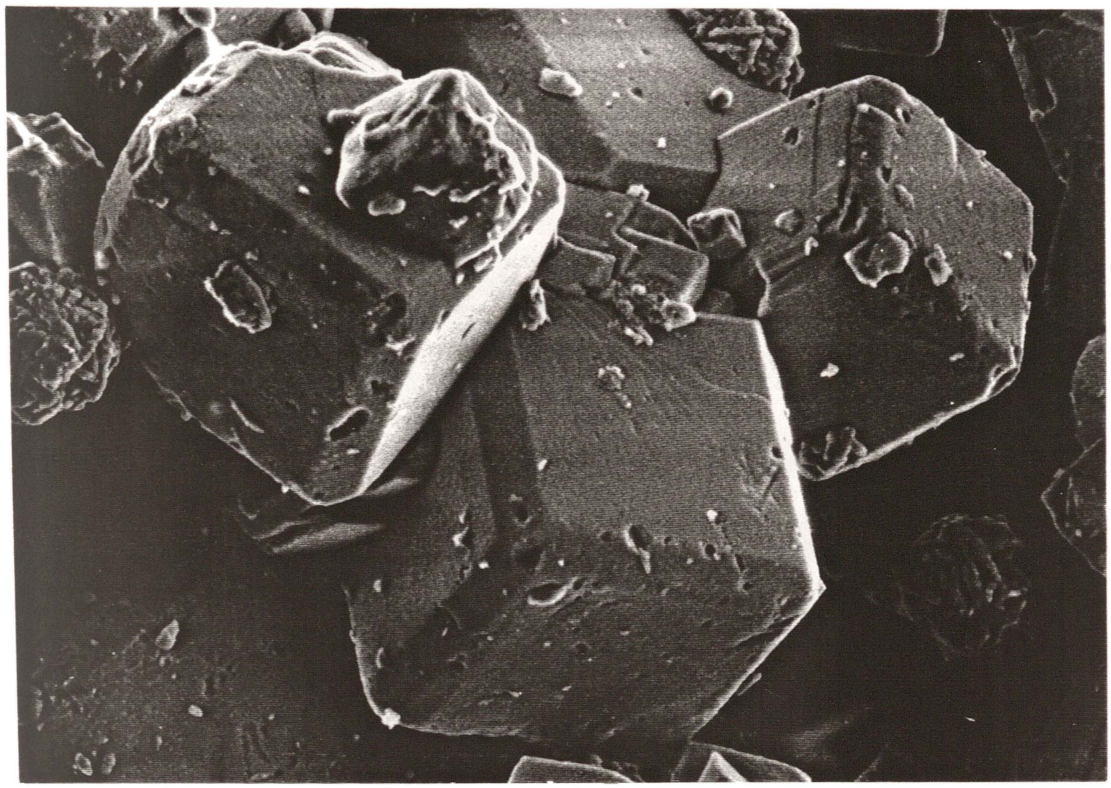


Plate 4.11 SEM photograph of zeolite 4.8Cr5A at a magnification of 6.6 k. Note the lack of significant change to crystal shape or surface properties upon low chromate loading. 1 cm on the plate equals 0.71 μm.

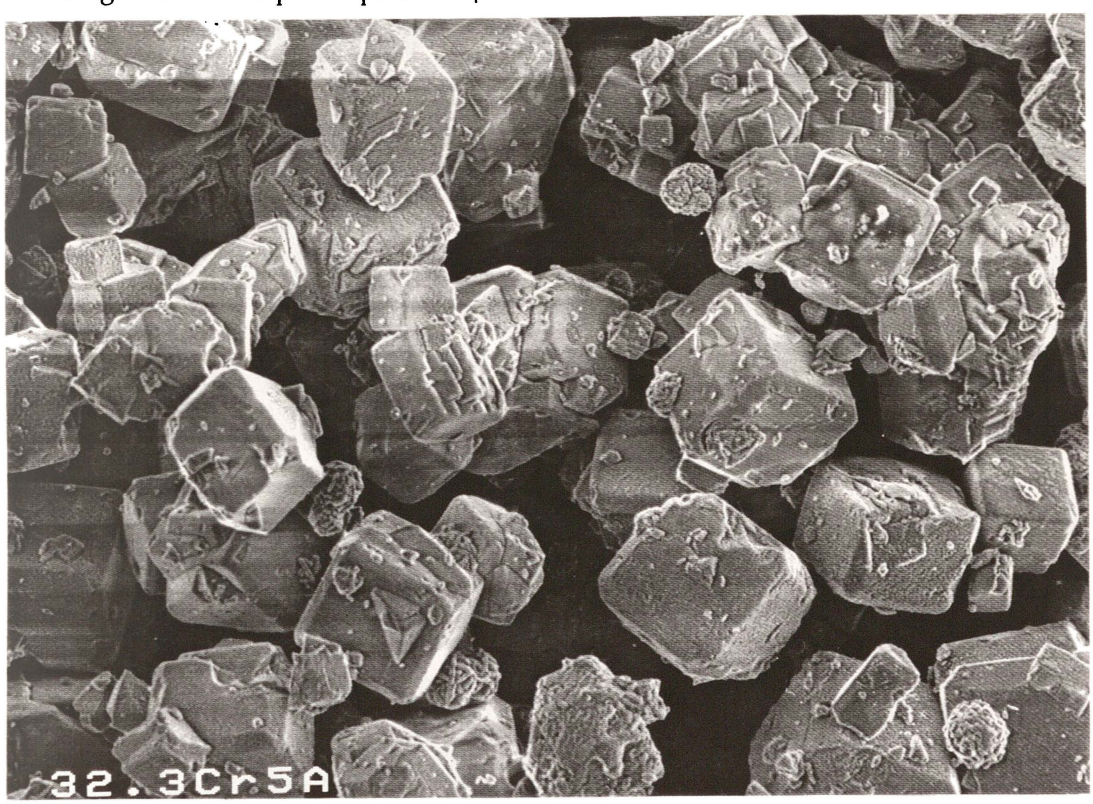


Plate 4.12 SEM photograph of zeolite 32.3Cr5A at a magnification of 4.5 k. Note the lack of significant change to crystal shape or surface properties upon high chromate loading. 1 cm on the plate equals 1.72 μm.

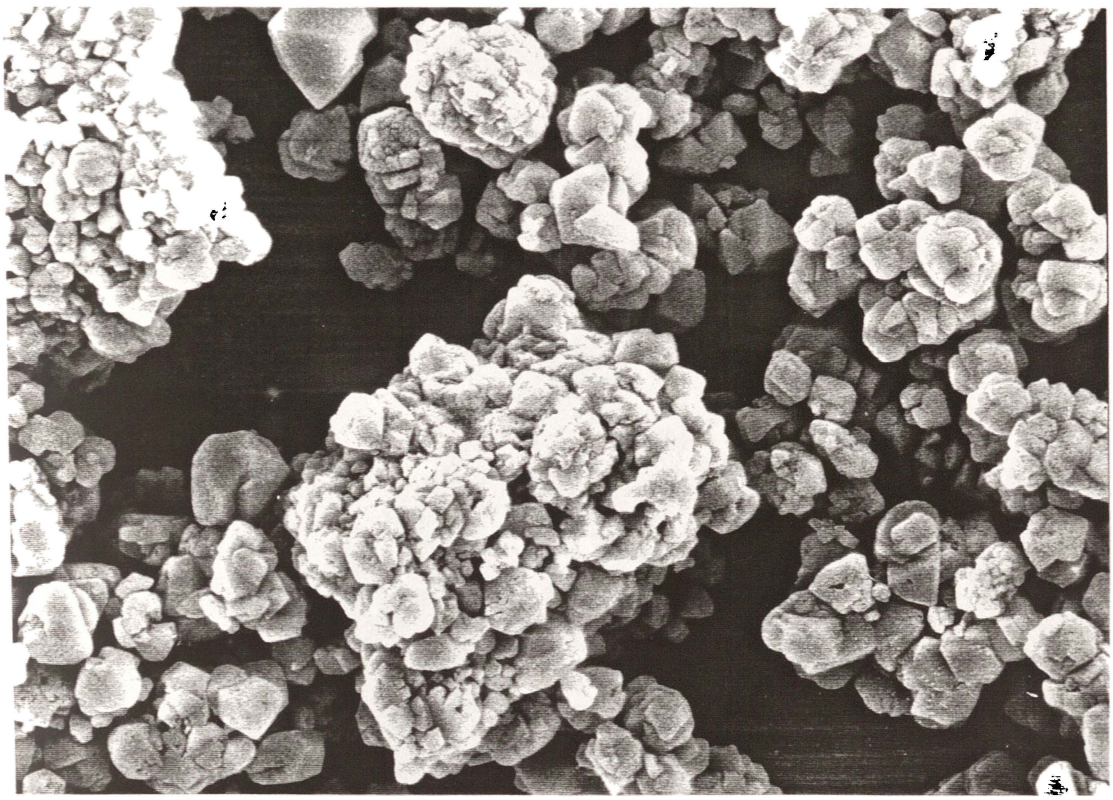


Plate 4.13 SEM photograph of zeolite Y52 at a magnification of 8.0 k showing the large variation in particle size and geometry and the presence of agglomerates. 1 cm on the plate equals 0.93 μm.

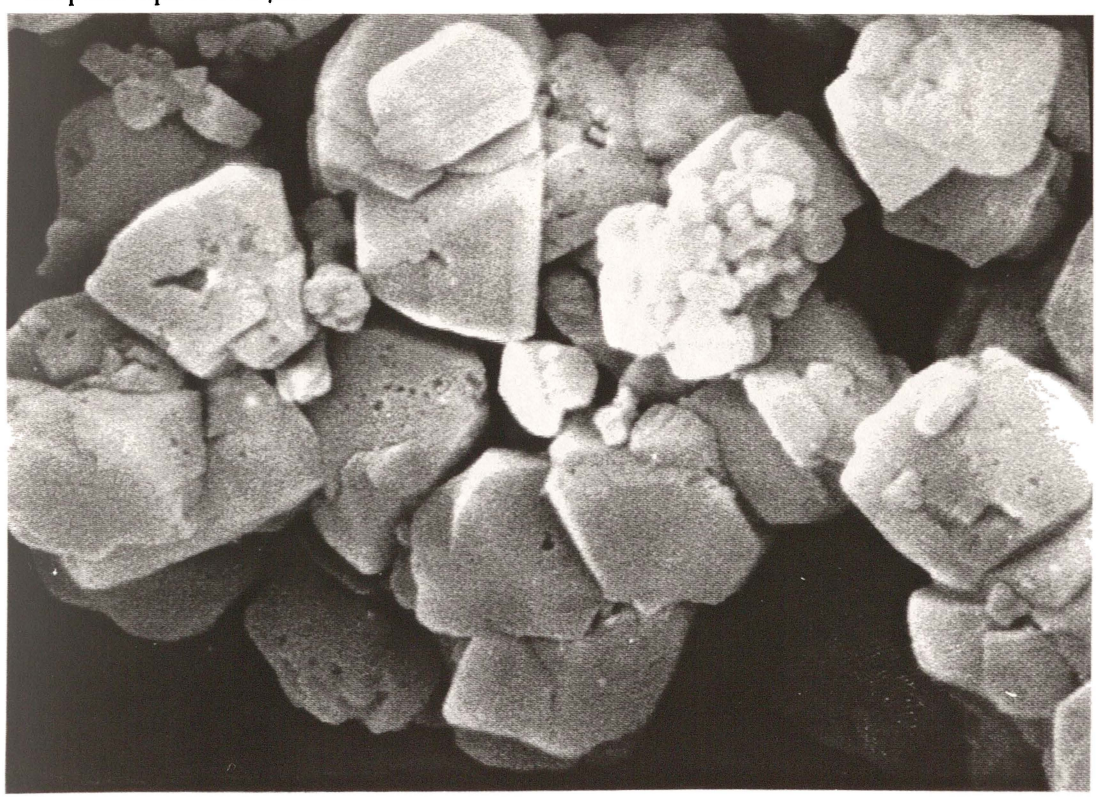


Plate 4.14 SEM photograph of zeolite Y52 at a magnification of 18.0 k showing the smoothness of the crystal surfaces. 1 cm on the plate equals 0.26 μm.

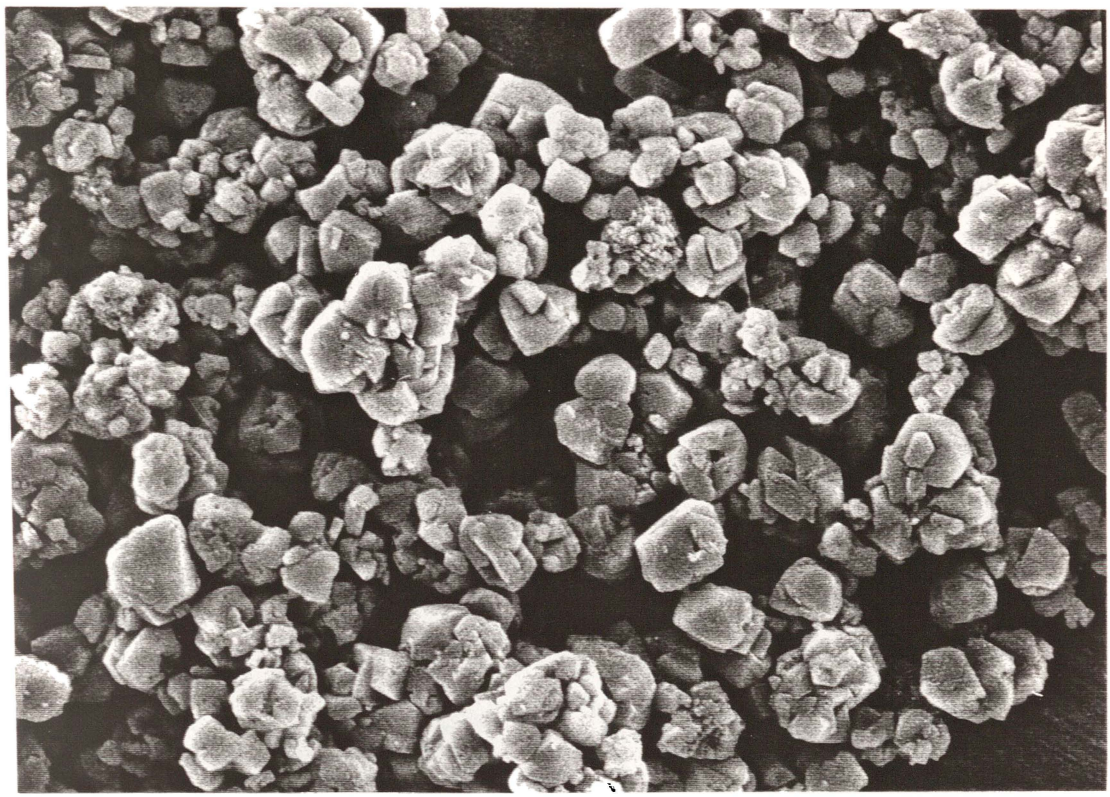


Plate 4.15 SEM photograph of zeolite 2.8CrY at a magnification of 8.0 k. Note the lack of change to crystal shape and size upon chromate loading. 1 cm on the plate equals 0.93 μm.

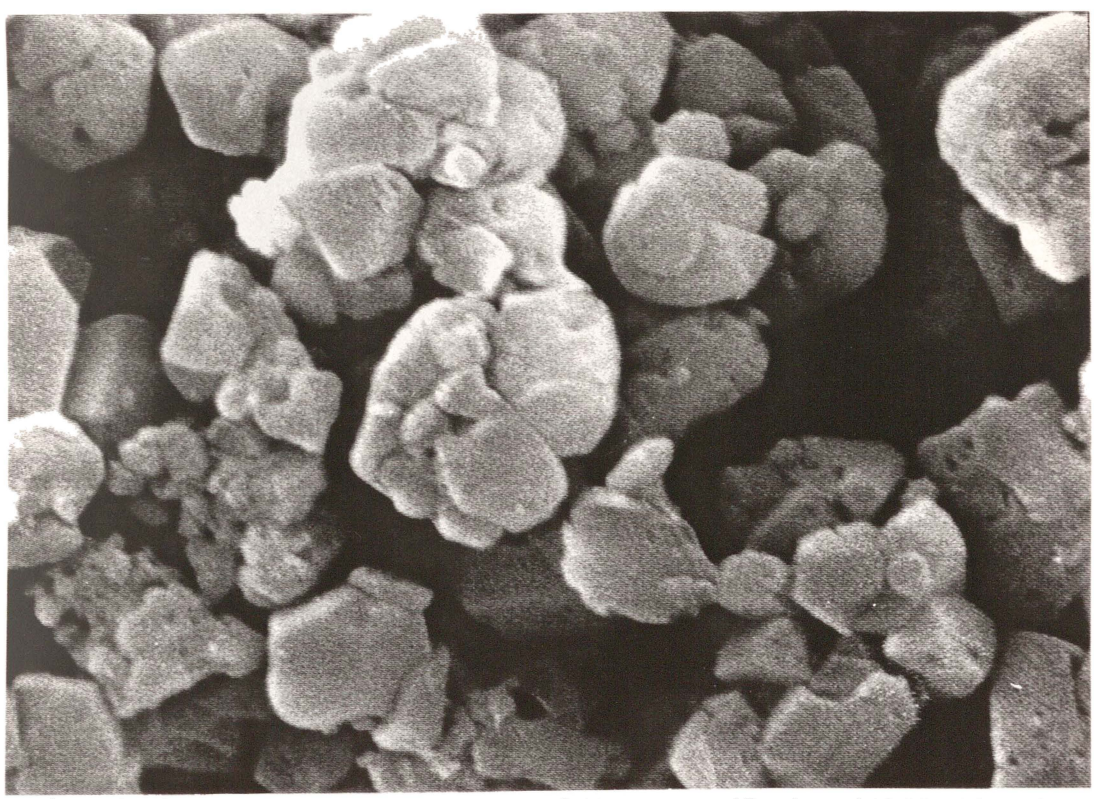


Plate 4.16 SEM photograph of zeolite 2.8CrY at a magnification of 18.0 k. Note the absence of change to the smooth crystal surfaces upon chromate loading. 1 cm on the plate equals 0.26 μm.



Plate 4.17 SEM photograph of zeolite LZ-Y72 on a magnification of 15.0 k. Note the smooth crystal surfaces. 1 cm on the plate equals 0.58 μm.



Plate 4.18 SEM photograph of zeolite 10.3CrY72 at a magnification of 15.0 k. Note the retention of crystal morphology but the deposition of an extraneous phase on zeolite crystal surfaces. 1 cm on the plate equals 0.58 μm.

SEM Interpretation

The absence of significant change in the crystal morphology of any of the zeolites examined upon loading with sodium chromate is consistent with the results of Snowdon.[3] Structural degradation involving collapse of the zeolite framework to give phases such as sodalite would result in the loss of void space. For example, transformation of 13X to sodalite would result in a change in pore volume from 0.50 cc/cc[4] to 0.35 cc/cc.[5] Loss of pore volume would involve collapse of the zeolite cavities that would be evidenced as changes to the crystal size and/or shape. Little change suggests the absence of lattice collapse and therefore the retention of the zeolite framework.

Cracks and holes were present in the surface of 5.8CrX while the surface of 13.6CrX remained relatively smooth. These changes in surface morphology are therefore not related to the degree of chromate loading. Degradation of the surface of 5.8CrX resulting from reaction with sodium chromate and promoted by the higher temperature employed in the synthesis, 670°C compared to 620°C for 13.6CrX, is the likely cause of the difference in surface morphology.

Minor roughening of the surface of 13.6CrX indicated the presence of an extraneous material. This material is absent from the surface of 2.1CrX indicating that the material was removed by the NaOH treatment. The material may be a layer of chromium compounds around the crystal.

The roughness of the surface of 10.3CrY72 crystals indicates deposition of an extraneous phase. The green colour of 10.3CrY indicated reduction of chromates during the solid-state reaction. The extraneous phase may be the product of this reduction.

4.4.3 PXRD Analysis of Chromate Zeolites

PXRD Results

The PXRD patterns of zeolite 13X and various chromate-loaded zeolites are shown in Figure 4.1. Zeolite 13X was highly crystalline giving sharp and intense PXRD peaks. 13.6CrX gave sharp but less intense PXRD peaks. Zeolite 2.1CrX gave PXRD peak intensities similar to those of 13X. Figure 4.2 shows the PXRD pattern of LZ-Y72 and 10.3CrY72. In addition to peaks of the zeolite, additional peaks are evident as indicated by the arrows in Figure 4.2(b). Table 4.1 lists the XRD peak positions (2θ), d-spaces, and relative intensities of the non-zeolite peaks and compares them to those of Cr_2O_3 (Powder Diffraction File (PDF) 6-504).

Table 4.1 Non-zeolite peaks in the PXRD pattern of 10.3CrY72. (I/I_1 are calculated relative to the 016 plane while numbers in brackets are calculated relative to the 014 plane to be consistent with PDF 6-504).

CrY72			Cr_2O_3		
2θ	d	I/I_1	hkl	d	I/I_1
24.2	3.68	57 (50)	012	3.63	75
33.4	2.69	100 (88)	014	2.67	100
35.6	2.52	80 (71)	110	2.48	95
54.3	1.69	113 (100)	116	1.67	90

PXRD Interpretation

PXRD patterns indicated the loss of zeolite peak intensities upon loading. For example 13.6CrX had peak intensities only ~40% of those of 13X. Removal of most of the chromate by NaOH to form zeolite 2.1CrX resulted in an increase in the PXRD peaks to intensities similar to those of 13X. Loss in intensity of PXRD peaks of 13.6CrX was therefore not the result of lattice

degradation. The loss is also unlikely to have arisen from physical dilution of the lattice with sodium chromate as the intensity losses far exceed the dilution (11.2 wt% Na_2CrO_4). Adsorption of X-rays by the occluded chromate oxyanions is the most likely cause of the intensity losses.

Extraneous peaks in the PXRD pattern of 10.3CrY72 were due to Cr_2O_3. The most intense peak for pure Cr_2O_3 (PDF 6-504) is the (014) diffraction plane while that of Cr_2O_3 in 10.3CrY72 was the (116) diffraction plane. As the (116) peak is close to the zeolite peak at $2\theta \approx 54°$, the increase in the intensity of the (116) peak can be attributed to superimposition upon the zeolite peak. For this reason, and to be consistent with PDF 6-504, the relative intensities have also been evaluated relative to the (014) plane. A relative intensity greater than 100 is thereby obtained for the (016) peak.

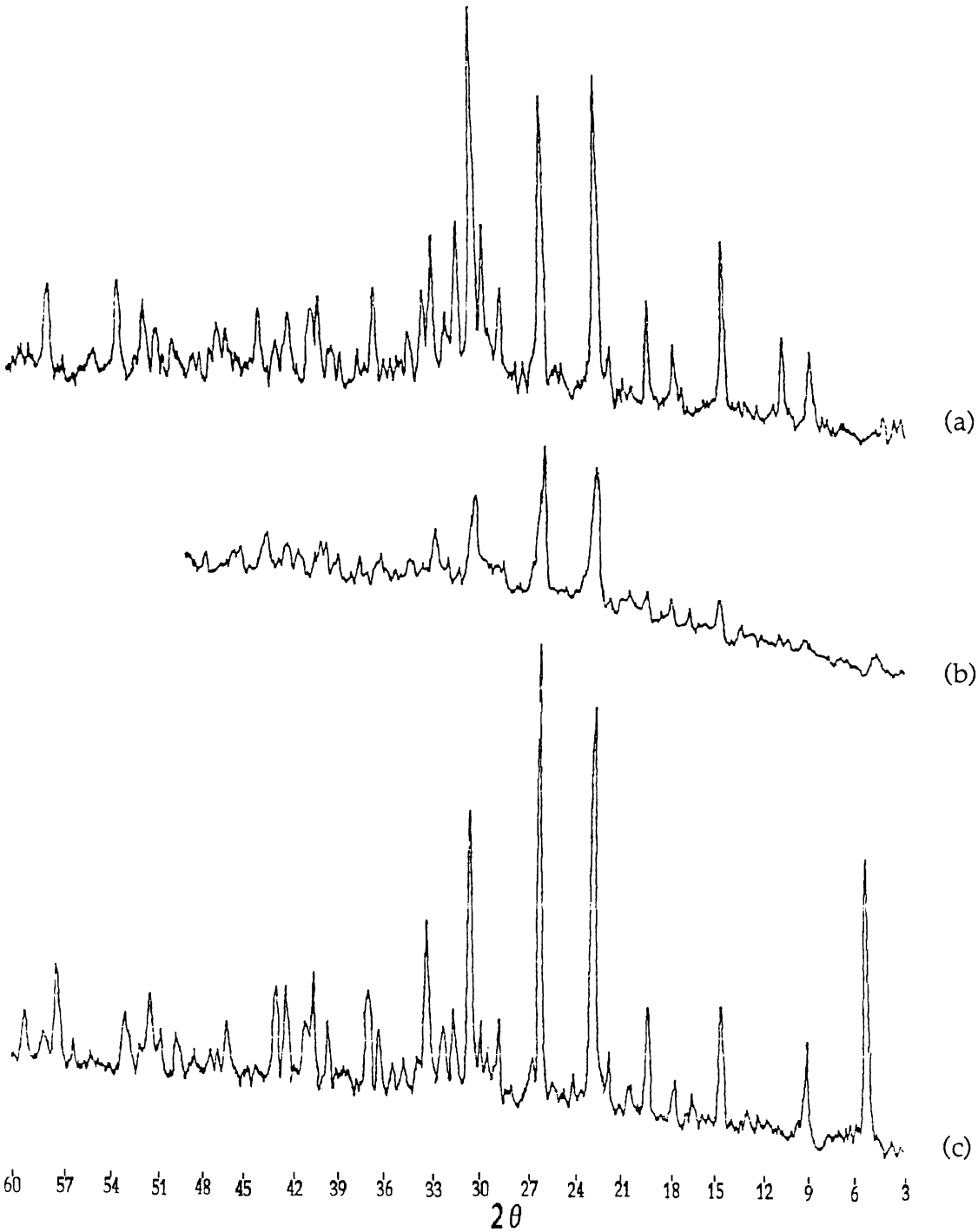


Figure 4.1 PXRD patterns of (a) 13X, (b) 13.6CrX, and (c) 2.1CrX. All patterns were recorded on a range of $1x10^3$ and have the same vertical scale in the figure. 1 cm on the figure equals 2.88 cm on the original trace or 11.5% of full scale deflection.

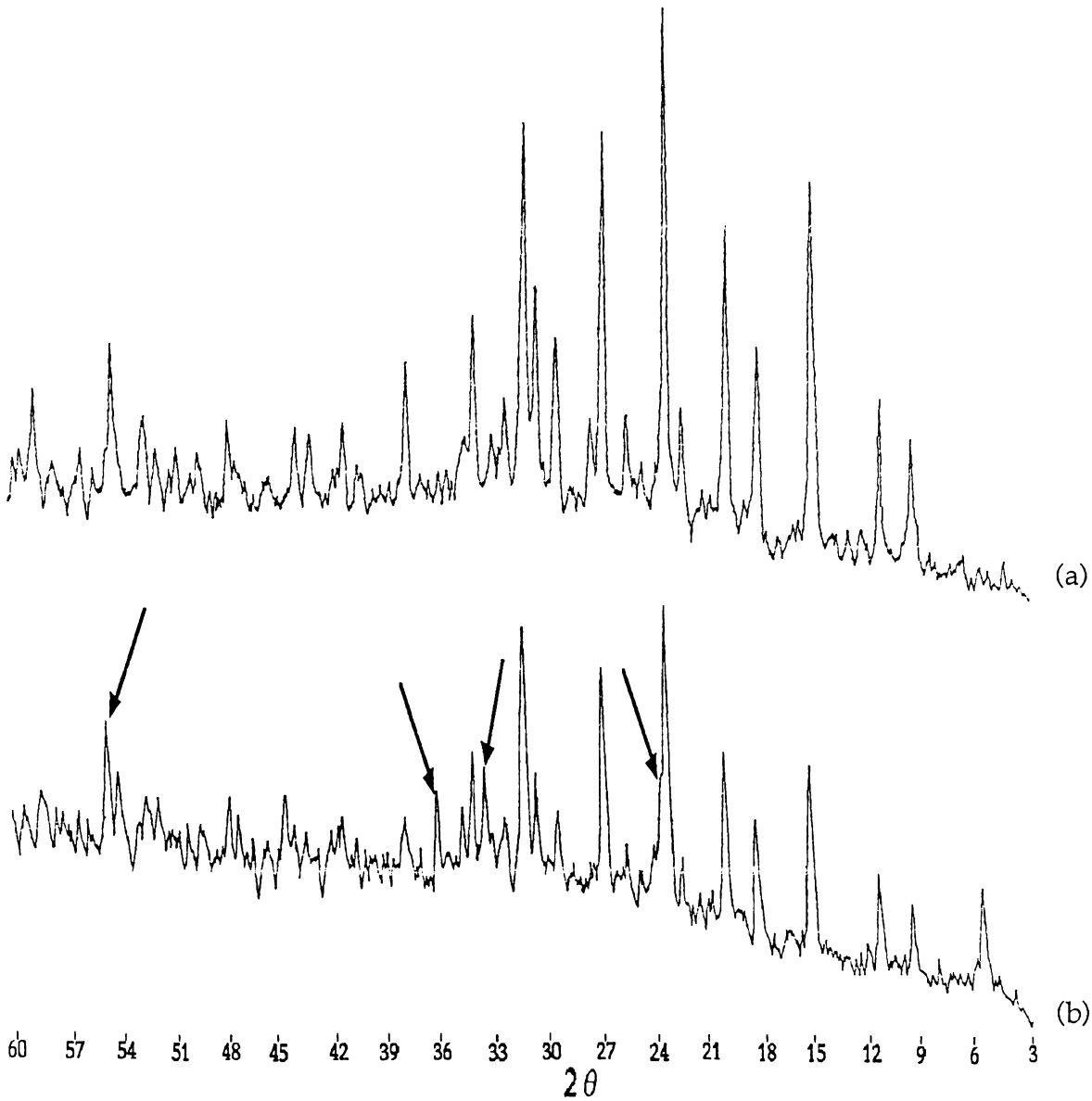


Figure 4.2 PXRD patterns of (a) LZ-Y72 and (b) 10.3CrY72. Arrowed are the non-zeolite peaks. Both patterns were recorded on a range of $1x10^3$ and have the same vertical scale in the figure. 1 cm on the figure equals 2 cm on the original pattern or 8% of full scale deflection.

4.4.4 Laser Raman Spectroscopic Analysis of Loaded Zeolites

Laser Raman spectroscopy is a useful technique for the detection and elucidation of species on the surface of solids. The gaining of information about chromates in the bulk zeolite phase relies on sufficient laser beam penetration to excite occluded chromates. In the absence of sufficient penetration the bands of surface bound species would dominate the spectrum. Under such conditions the spectrum would not be indicative of the bulk phase. In the discussions that follow, care is taken to differentiate between the bands of surface and bulk species to maximise the information obtained from spectra.

Laser Raman Results

Raman spectra of sodium chromate salt (Cr^{salt}), sodium chromate solution (Cr^{sol}), and chromate nosean (Cr^{nos}) are shown in Figure 4.3. Chromate-loaded zeolites of the types X and Y gave the Raman spectra shown in Figure 4.4. Figure 4.5 shows the Raman spectra of chromate-loaded A type zeolites. The Raman spectra of M5 and S115 zeolites loaded with chromate are shown in Figure 4.6. Table 4.2 summarises the positions of the Raman bands for all the zeolites examined. Evacuation of 13.6CrX at 350°C for 2 hours resulted in a change in colour to light green and the complete loss of all Raman bands.

Laser Raman Interpretation

Sodium chromate salt gave sharp Raman bands in the regions 300-500 cm^{-1} and 800-1000 cm^{-1}. The spectrum was consistent with the literature[6] and the assignment of the bands is shown in Table 4.3. Bands in the region 300-500 cm^{-1} are bending modes and are not as intense or sharp as the stretching modes in the region 800-1000 cm^{-1}. For this reason it was decided that attention would be focussed on the stretching bands of chromate zeolites. Chromate

solution (Cr^{sol}) gave a band at 847 ± 1 cm-1, a value identical to that observed by Stammerich et *al.*[7].

Table 4.2 Positions of the chromate Raman bands for the various chromate-loaded zeolites. (sh = sharp, br = broad, s = strong, m = medium, w = weak, and vw = very weak).

Sample	Peak Position /cm^{-1}					G^P
	ν_1 CrO_4^{2-}	ν_1 Si-CrO_4-Si	ν_3 CrO_4^{2-}	ν_1 $Cr_2O_7^{2-}$	ν_3 $Cr_2O_7^{2-}$	
Cr^{salt}	851±1(sh,s)		899±1(sh,s)			---
			932±1(sh,s)			
Cr^{sol}	847±1(sh,s)		900±3(br,w)			---
Cr^{nos}	856±1(sh,s)		900±3(sh,m)			1
2.1CrX	850±1(sh,s)		897±3(sh,s)			1
13.6CrX	850±1(sh,s)		894±3(sh,m)	905±3(sh,m)	940±6(sh,w)	2
13.4CrY	849±3(sh,s)		897±3(sh,s)	905±3(sh,s)	940±6(sh,m)	2
1.0CrM5	849±1(sh,s)	880±5(sh,m)	897±1(sh,s)	905±3(sh,s)	938±6(sh,m)	2
0.9CrS115	849±1(sh,s)	880±5(sh,m)	898±1(sh,s)	904±3(sh,s)	939±6(sh,m)	2
3.3Cr4A	849±3(br,w)			905±3(sh,s)	940±6(sh,m)	2
2.3Cr3A	849±3(br,w)			905±3(sh,s)	940±6(sh,m)	2
32.3Cr5A	849±3(br,w)	880±5(sh,s) ($CaCrO_4$)		905±3(sh,s)		3

Table 4.3 Positions of the Raman bands of sodium chromate salt and chromate solution and their assignments to the various vibrational modes.[6]

Assignment	ν_2	ν_4	ν_1	ν_3
Sodium Chromate Salt	349 ± 2 360 ± 2	390 ± 2 406 ± 2	851 ± 1	899 ± 1 932 ± 1
Chromate Solution			847 ± 1	900 ± 3

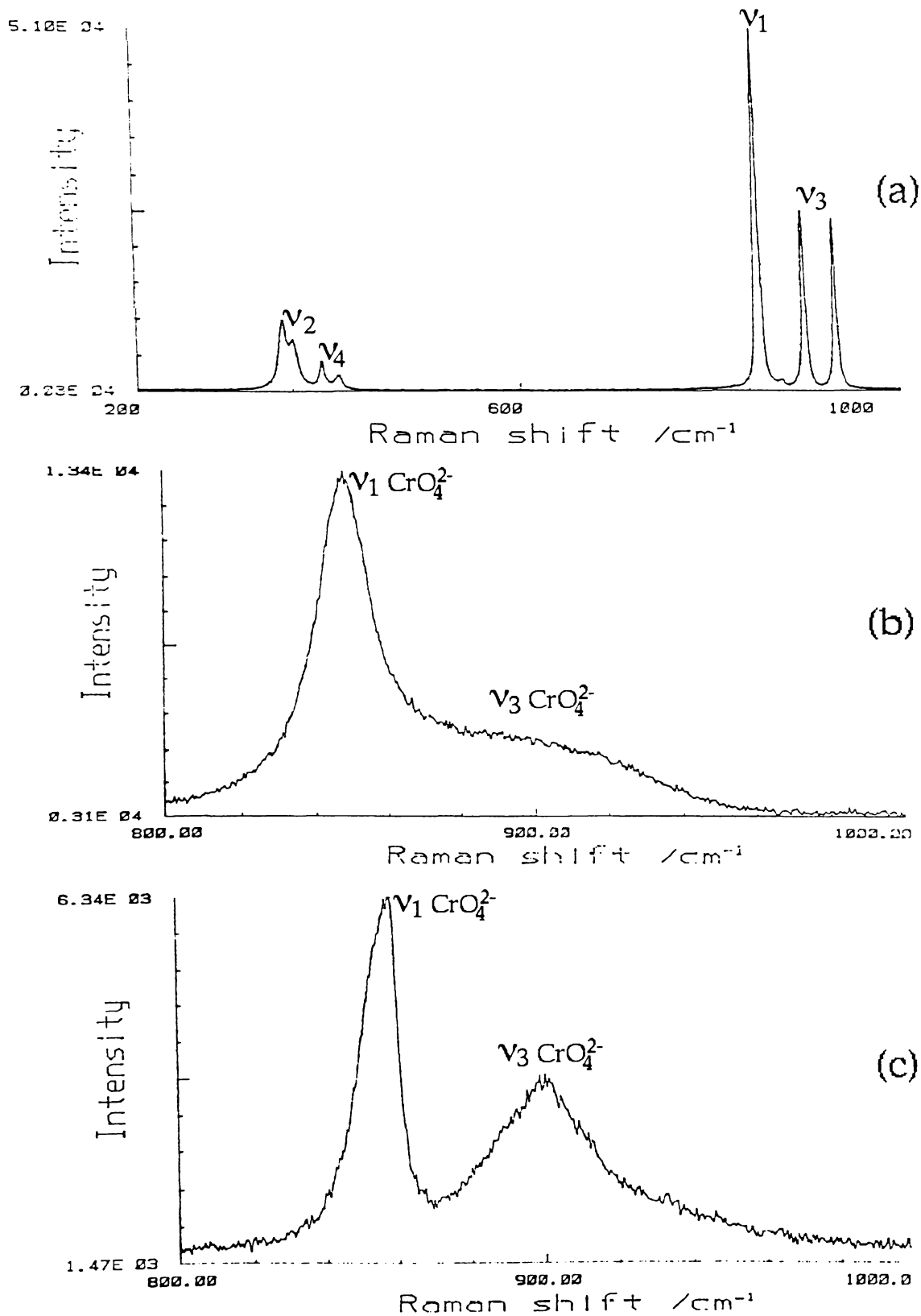


Figure 4.3 Raman spectra of (a) anhydrous chromate salt, (b) chromate solution, (c) chromate nosean. The spectrum of Cr^{nos} indicates the occlusion of discrete chromate oxyanions of tetrahedral symmetry.

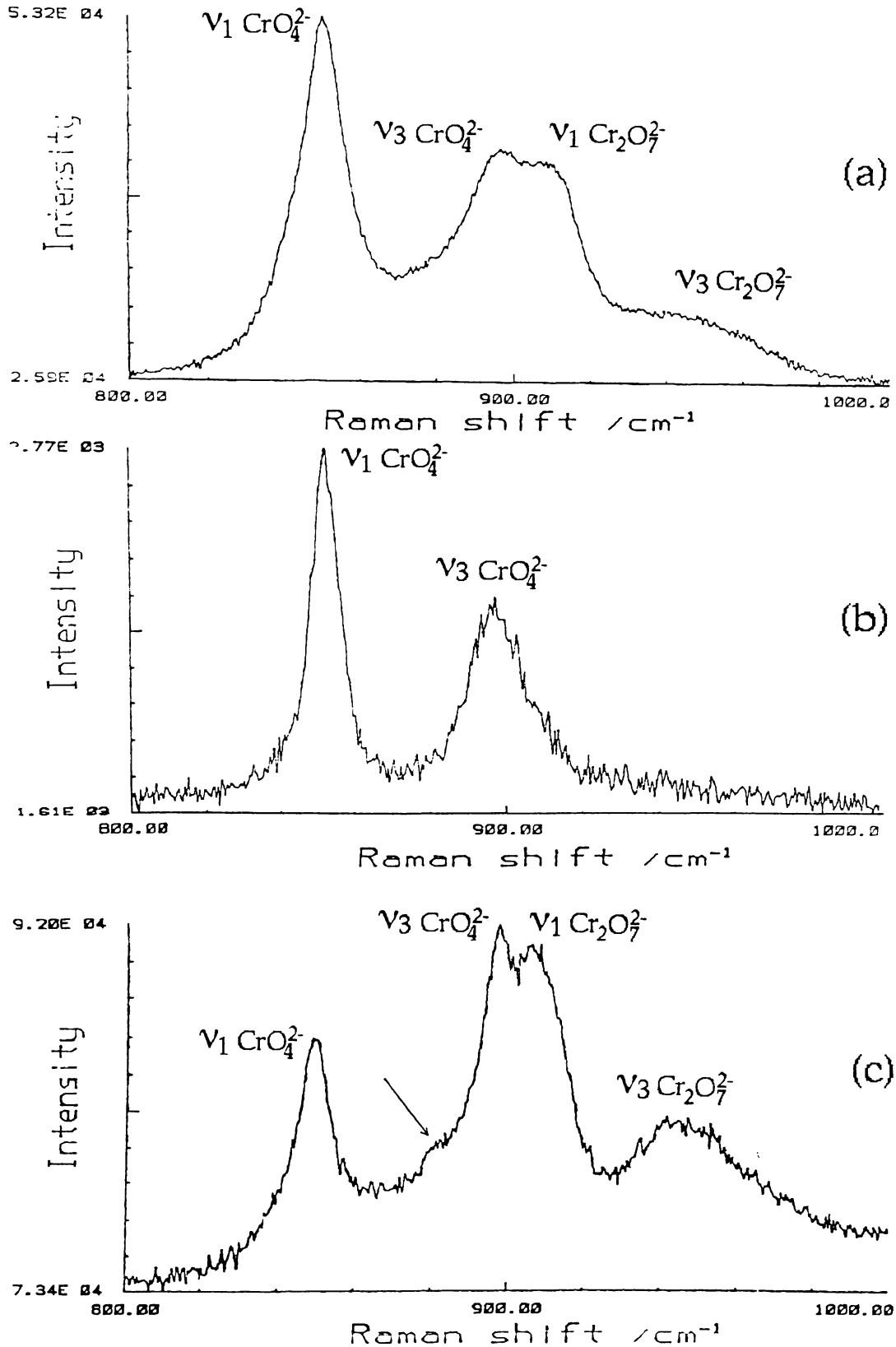


Figure 4.4 Raman spectra of (a) 13.6CrX, (b) 2.1CrX, and (c) 13.4CrY. Bands assignments are shown. The arrow indicates the barely visible band at 880 ± 5 cm-1 assigned to an anchored chromate of the type Si···O_2-Cr-O_2···Si.

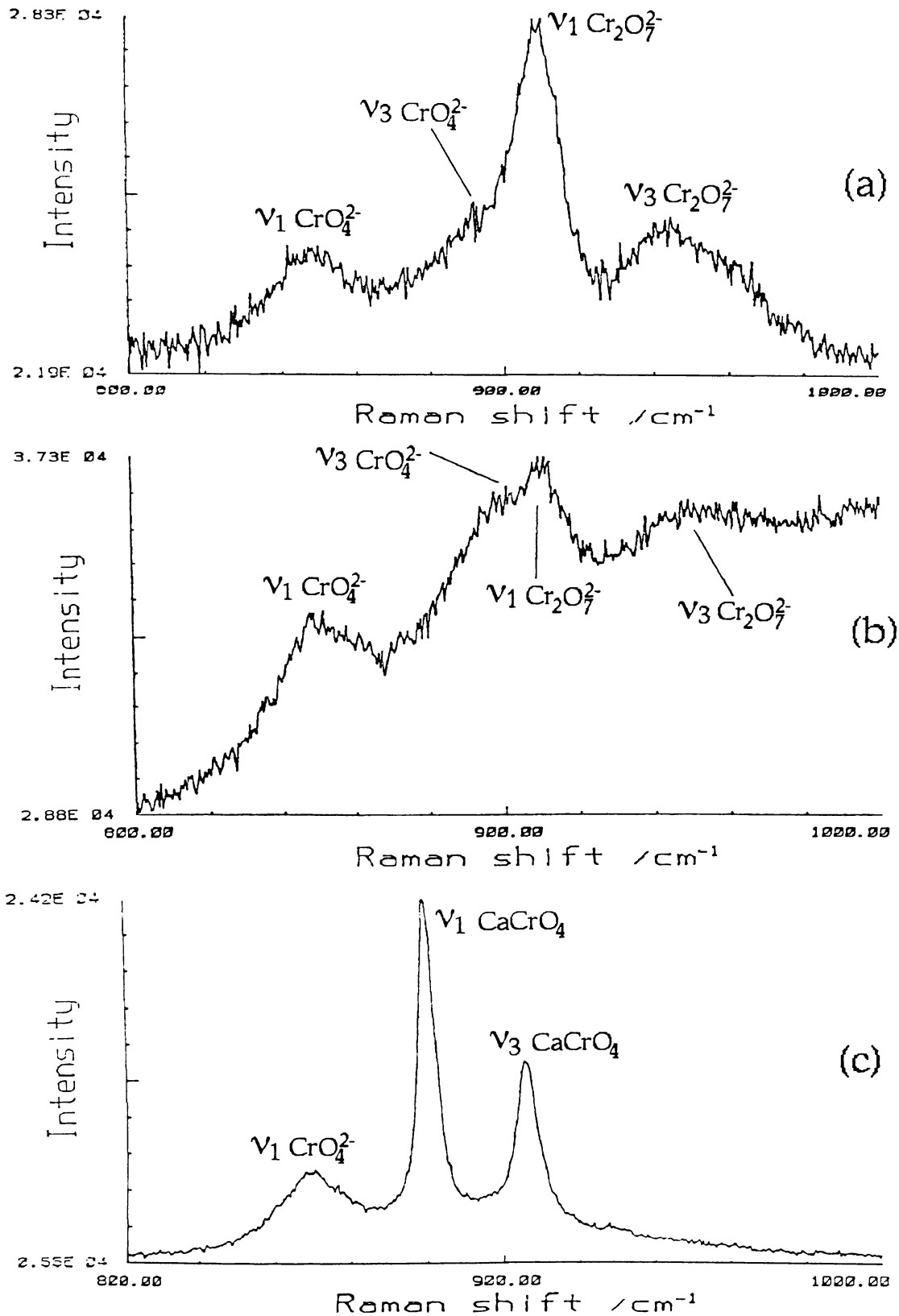


Figure 4.5 Raman spectra of (a) 3.3Cr4A, (b) 2.3Cr3A, and (c) 32.3Cr5A. Chromate and dichromate bands are present in the spectra of 3.3Cr4A and 2.3Cr3A. The spectrum of 32.3Cr5A is dominated by a band at 880 cm^{-1} not visible in the spectra of many other zeolites and attributed to a $CaCrO_4$ species.

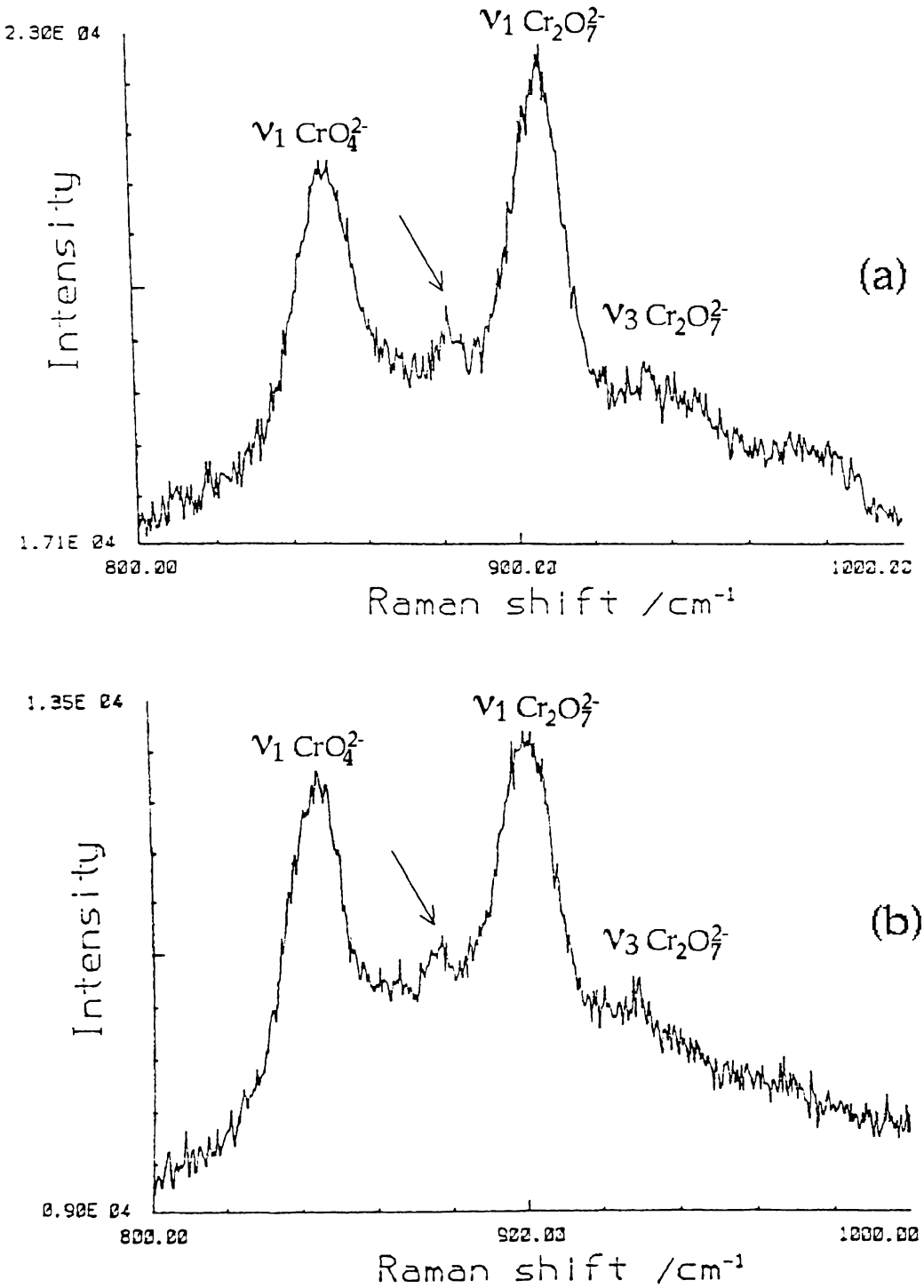


Figure 4.6 Raman spectra of (a) 0.9CrS115 and (b) 1.0CrM5. Both chromate and dichromate bands are present in the spectra. The arrows indicates the barely visible band at 880 ± 5 cm-1 assigned to an anchored chromate of the type Si···O_2-Cr-O_2···Si.

Aqueous sodium chromate, 2.1CrX, and Cr^{nos} gave much simpler spectra than the pure salt owing to the loss of lattice site effects of the crystal. A strong peak at 847 ± 1 cm^{-1} for Cr^{sol}, 850 ± 1 cm^{-1} for 2.1CrX, and 856 ± 1 cm^{-1} for Cr^{nos} is due to the ν_1 stretching mode and the weak broad band at 890 ± 5 cm^{-1} is due to the IR and Raman active ν_3 band. Chromate zeolites gave Raman spectra with qualitative similarities to both the spectra of Cr^{sol} and Cr^{salt} with the overall shape resembling Cr^{sol} while narrower peak widths were similar to Cr^{salt}. The shapes of the spectra indicate the occlusion of sodium chromate as discrete chromate oxyanions of tetrahedral symmetry. Peak broadening upon dissolution can be ascribed to the heterogeneous nature of the chromate environment in solution arising from rotational and solvation sphere fluctuations. Sharpening of the bands upon occlusion in zeolites indicates a more homogeneous environment around the chromate oxyanion and is consistent with oxyanions being fixed on similar sites within the framework.

Assignments of the Raman Bands

Bands at ~850 cm^{-1} and ~900 cm^{-1}

The spectra of all the chromate zeolites showed bands at ~850 cm^{-1} and ~900 cm^{-1} with characteristics similar to those of Cr^{sol}. These bands are therefore assigned as the ν_1 and ν_3 bands, respectively, of a chromate species.

Bands at ~905 cm^{-1} and ~940 cm^{-1}

Superimposed upon the bands at ~850 cm^{-1} and ~900 cm^{-1} in the spectra of 13.6CrX, 13.4CrX, 0.9CrS115, 1.0CrM5, 2.3Cr3A, and 3.3Cr4A were two more bands at ~905 cm^{-1} and ~940 cm^{-1}. Increases in wavenumber positions are often related to increased polarity of the chromate unit. For example the increase in frequency of the ν_1 band along the series CrO_2Cl_2,[8] CrO_2F_2,[9] and the esters of chromic acid[10] is essentially related to the bond-order increase in

the two outer chromium to oxygen bonds. Bands at high wavenumber may therefore have arisen from highly polarised chromate species. Such large shifts as seen here (~850 cm^{-1} to ~905 cm^{-1}) are, however, unlikely to be the effect of polarisation. The positions of the bands are close to those observed for free dichromate at 904 cm^{-1} and 950 cm^{-1}.[11,12] These two bands are therefore assigned to a dichromate species.

Band at ~880 cm^{-1}

The often barely visible band at ~880 cm^{-1} shown by the arrows in the spectra of some chromate zeolites may have arisen from several sources. These include the Raman activation of the otherwise IR only band of free chromate at either 880 cm^{-1} (ν_{as}) or 870 cm^{-1} (ν_s). For example, the ν_{as} mode of chromate is observed in the Raman spectra of chromate adsorbed onto colloidal silver.[13] Another possibility is that the band is the ν_1 vibration of an anchored chromate species. The fact that there is no correlation between the intensity of this band and those of the other bands in the spectra of the various zeolites suggests that it arises from a different species. The increase from ~850 cm^{-1} to ~880 cm^{-1} is within the range explainable by increased polarisation of the chromate unit, for example the ν_1 band of CrO_2Cl_2 occurs at 875 cm^{-1}. The band is at a similar position to that of chromates anchored to alumina of 875 cm^{-1}.[14] Anchoring of chromates through replacement of surface hydroxyls would form Si···O_2-Cr-O_2···Si species.

The band at 880 cm^{-1} is present at low intensities in the spectra of 4A, 3A, M5, 13X, and Y type zeolites but is very intense in the spectrum of 32.3Cr5A. Much higher intensity for 5A compared to 4A and 3A despite their identical frameworks and similar Si/Al ratios suggests that the intensity of the band is enhanced by Ca^{2+}. Coordination of a chromate to a Ca^{2+} cation on the

S_{II} site, about 1.2Å from the centre of the 8-ring, would form a $CaCrO_4$ type species. Increase in the wavenumber position of the ν_1 band from ~850 cm^{-1} to 880 cm^{-1} would arise from increased polarisation caused by coordination to a divalent cation. The lack of a dichromate band at ~940 cm^{-1} for 32.3Cr5A indicates that the band at 905 ± 3 cm^{-1} does not arise from a dichromate species. This combined with the general features of the ν_1 and ν_3 bands of other species suggests that the band at 905 ± 3 cm^{-1} is the ν_3 band of the $CaCrO_4$ species.

Correlation Between the Raman Bands and Ring Sizes

The samples can be divided into three groups based on the number and positions of the Raman bands in their spectra, see Table 4.2. Group 1 contains Cr^{nos} and 2.1CrX with spectra exhibiting only chromate bands. Zeolites 13.6CrX, 1.0CrM5, 0.9CrS115, 2.3Cr3A, 3.3Cr4A, and 13.4CrY were placed in Group 2 due to the presence of both dichromate and chromate bands in their spectra. Group 3 contains only 32.3Cr5A whose spectrum exhibited only chromate and $CaCrO_4$ bands.

A relationship exists between the occurrence or absence of the various bands and the types of windows present in the various zeolites. Cr^{nos} and all zeolites gave CrO_4^{2-} bands. Since the only rings common to all the samples are the S4R and S6R these species could be associated with hexagonal or square faces.

The absence of $Cr_2O_7^{2-}$ bands for nosean and intense bands for chromate loaded 3A, 4A, M5, 13X, and Y52 type zeolites suggests that these species are associated with S8R, S10R and S12R rather than S4R and/or S6R. Higher $Cr_2O_7^{2-}$ band intensities for Y52 than for 13X suggests that the Si/Al ratio might control the concentration of such species. High Si content appears to

favour the formation of $Cr_2O_7^{2-}$ suggesting that the dichromate species is anchored through Si atoms. The formation of Si bound species is consistent with the replacement of surface hydroxyls. In the case of dichromate, species of the type Si···O_3-Cr-O-Cr-O_3···Si would form. Dichromate association with S12R, S10R and S8R suggests that larger ring sizes offer a configuration more suitable for dichromate adsorption. Interatomic distances of dichromate bonded to two silicon atoms, representing atoms on the surface of zeolite crystal, were estimated using Chem3D™ molecular modelling application using the structural data shown in Table 4.4. Structures containing either sp^2 or sp^3 hybridised oxygen atoms bridging between chromium and silicon and a combination of both were prepared and interatomic Si-Si distances calculated, see Table 4.5. The maximum Si-Si distance is obtained when both oxygen atoms linking Cr and Si are sp^2 hybridised, see Model (A), and is 7.24 Å. A smaller Si-Si distance of 5.55 Å is obtained when the dichromate consists of one sp^2 hybridised oxygen atom and one sp^3 hybridised oxygen atom, see in Model (B). The smallest distance between Si-Si atoms is 4.08 Å and occurs when both oxygen atoms linking Cr and Si are sp^3 hybridised, as shown in Model (C).

Table 4.4 Structural data of dichromate.

Element	Cr-O	Si-O	O-Cr-O	Cr-O-Cr	Cr-O-Si
Value	1.910 Å	1.840 Å	109.47°	180.00°	180° (sp^2), 109.47 (sp^3)

Table 4.5 Structures and derived structural data of the possible configurations of anchored dichromates.

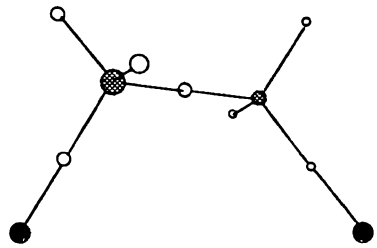
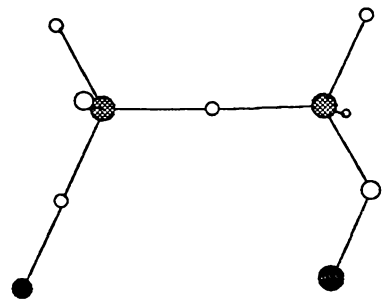
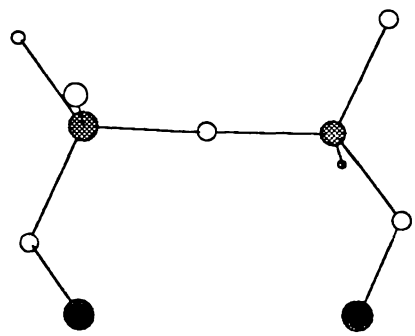
Hybridisation of the oxygen linking Si and Cr	Chem3D™ Structure ● = Si, ◍ = Cr, ○ = O	Si-Si distance	Model
2x sp^2		7.24 Å	(A)
1x sp^2 1x sp^3		5.55 Å	(B)
1x sp^3		4.08 Å	(C)

Table 4.6 Distances between Si atoms in the rings of various sizes. Numbers in brackets refer to the position in the ring. Atoms are numbered consecutively around the ring.

Ring	Distance to Si(1)					
	Si(2)	Si(3)	Si(4)	Si(5)	Si(6)	Si(7)
S6R	3.09	5.35	6.18	---	---	---
S8R	3.09	5.71	7.46	8.07	---	---
S10R	3.09	5.88	8.09	9.51	10.00	---
S12R	3.09	5.97	8.44	10.34	11.53	11.94

The Si atoms of the structures shown in Table 4.5 are supplied by the surface of the zeolite crystal and will be members of the rings forming the external pore system. Dichromate adsorption will occur when a ring offers a site with a Si-Si distance close to the optimum Si-Si distance of the favoured $Si\text{-}O_2\text{-}Cr\text{-}O_2\text{-}Si$ unit. The distances between metal atoms of the rings of various sizes is therefore of interest and have been calculated. The ring model consisted of a planar ring with metal to metal distances of 3.09 Å corresponding to the Si-Al distance found in a S6R of hydroxysodalite. The number in the brackets refers to the position of the Si atom in the ring. Atoms are numbered consecutively around the ring. Interatomic distances between Si atoms in rings of various sizes are given in Table 4.6. A S6R offers Si atoms separated by distances of 5.35 Å (Si(1)-Si(3)) and 6.18 Å (Si(1)-Si(4)). The apparent lack of dichromate adsorption to silicon atoms of S6R, despite the fact that the Si-Si distances are similar to the optimum Si-Si distance for Model (B) (5.55 Å) and Model (C) (4.08 Å), suggests that these models are inappropriate. Model (A) with the larger Si-Si distances is favoured. Anchoring of dichromates will therefore be favourable when a ring affords Si-Si distances near 7.24 Å.

Dichromate Raman bands are evident in the spectra of the zeolites containing S8R, S10R, and S12R. The S12R offers a range of sites with Si-Si distances ranging between 3.09 Å and 11.94 Å. Distances closest to the optimum value of 7.24 Å are offered by Si(1)-Si(4) (5.97 Å) and Si(1)-Si(5) (8.44 Å). A S10R offers distances of 5.88Å, by Si(1)-Si(3), and 8.09 Å, by Si(1)-Si(4), while S8R offers Si-Si distances of 8.07 Å, by Si(1)-Si(5), and 7.46 Å, by Si(1)-Si(4). Sites suitable for dichromate adsorption are therefore present on the surfaces of all the zeolites studied and replacement of surface hydroxyls to form anchored dichromates provides a viable mechanism for adsorption.

The more intense dichromate bands for 13.4CrY relative to those of 13.6CrX indicates higher dichromate concentrations for the Y zeolite. Adsorption would be prevented if an Al atom was at the (4) position in the S12R. Adsorption of dichromate probably requires the correct Si/Al ordering in the ring. A higher Si content will increase the probability of an Si atom in any given position in the ring thereby affording a greater chance for dichromate adsorption.

It is clear that higher Si/Al ratios favour dichromate adsorption. More intense dichromate band intensities in the spectrum of 3.3Cr4A, despite the lower Si/Al (1.08) compared to that of both Y52 (2.67) and 13X (1.27), indicates that structure also plays an important role in dichromate adsorption. If it is assumed that the surface concentration of chromates in the various zeolites was similar then the intensity of the dichromate band relative to the chromate band (evaluated from peak heights) can be used to order the zeolites with respect to the amount of dichromate they contain. Table 4.7 shows the ratio of the dichromate to chromate band intensities and the properties of various ring sizes. The ratio of the dichromate and chromate band intensities follows the sequence Cr4A >> CrM5 ≈ CrY52 > Cr13X. It is evident from Table 4.7 that the ratio of dichromate to chromate band intensities increases as the difference between the optimum Si-Si distance of the anchored dichromate (7.24 Å) and the Si-Si distance of the most favourable adsorption site decreases. The high concentration of dichromates on the surface of Cr4A can therefore be attributed to the S8R having a site that offers a Si-Si distance (7.46 Å) that is very close to the optimum Si-Si distance of an anchored dichromate (7.24 Å) of Model (A).

Table 4.7 Ratio of the dichromate and chromate Raman band intensities and the structural data of the various ring sizes.

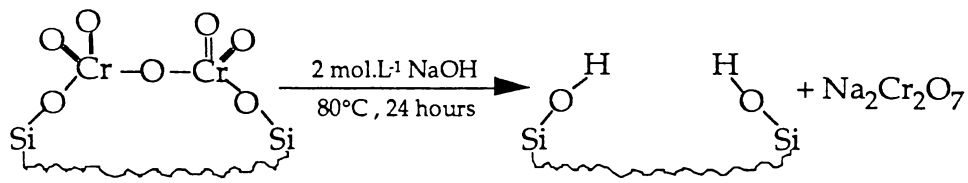
Zeolite	$I(\frac{Cr_2O_7^{2-}}{CrO_4^{2-}})$	Ring	Adsorption Site	Si-Si Dist.	(Si-Si)/Å - 7.24Å
Cr^{nos}	0	S6R	Si(1)-Si(4)	6.18	-1.04
4A	2.7	S8R	Si(1)-Si(4)	7.46	0.22
M5	1.1	S10R	Si(1)-Si(4)	8.09	0.85
Y52	1.3	S12R	Si(1)-Si(4)	8.44	1.20
13X	0.6	S12R	Si(1)-Si(4)	8.44	1.20

Occluded vs Surface Chromate

All the zeolites contain rings that offer sites for the adsorption of chromate onto zeolite surfaces. The ν_1 and ν_3 bands at ~850 cm^{-1} and ~900 cm^{-1} could therefore be due to chromates on the zeolite surfaces or chromates occluded within zeolite pores. The bands are assigned to occluded chromates for the reasons that follow. Firstly, ν_1 band frequencies of ~850 cm^{-1} show no significant shifts relative to the 851 ± 1 cm^{-1} of Cr^{salt}. Coordination to surfaces generally results in significant blue-shifts that have been attributed to increases in bond order of the outer Cr-O bonds resulting from the increased polarisation of the chromate unit.[14] The absence of a blue-shift is therefore inconsistent with a surface bound species. Adsorbed chromate typically have a ν_1 band at around 880 cm^{-1} and there is evidence in some zeolites of such bands. Secondly, detection of occluded chromates requires penetration of the laser beam into at least the first level of α-cages. No literature giving levels of beam penetration are available but it has been suggested that penetration would be to the order of 20 Å.[15] Such penetration would be sufficient to detect species occluded in the α-cages on the outer surface of the crystals. The band at ~880 cm-1 was enhanced by the presence of Ca^{2+}. As there are no cations on the outer surface of zeolite crystals, detection of a $CaCrO_4$ species

indicates sufficient beam penetration to detect occluded species. Thirdly, the spectrum of 2.1CrX displayed only chromate bands. Bands attributable to dichromate species in the spectrum of 13.6CrX disappeared after NaOH treatment used to form 2.1CrX. Apparently NaOH is therefore capable of breaking Si-O-Cr bonds, see Scheme 4.7

Scheme 4.7 Proposed mechanism for the removal of surface bound dichromates by NaOH solution.



If surface bound chromates were present then the expectation is that the ability of NaOH to break Si-O-Cr bonds would result in the removal of these species. The bands at ~850 cm^{-1} and ~900 cm^{-1} in the spectrum of 2.1CrX that survived after NaOH treatment are most likely to have arisen from occluded chromates and can be considered to be characteristic of this type of species. Fourthly, the ν_1 band at 856 ± 1 cm^{-1} in the spectrum of Cr^{nos} displayed a small but significant blue-shift attributable to a decrease in the Na-Cr distances that is consistent with occlusion within the β-cages of this dense felspathoid, see Section 4.4.8, but inconsistent with the blue-shift expected for adsorption. Detection of chromates occluded in nosean indicates laser beam penetration into at least the first layer of β-cages. Chromate occluded in the α-cages of zeolites are therefore also likely to receive beam excitation.

4.4.5 FTIR Analysis of Loaded Zeolites

FTIR Results

The FTIR spectra of sodium chromate, 13X, 13.6CrX and Cr^{nos} are shown in Figure 4.7. Zeolite 13X gave a spectrum consistent with the literature[16] containing sharp well defined bands associated with vibrations of the aluminosilicate framework. Zeolites give a strong and broad ν_{as}(T-O-T) vibration around 1000 cm^{-1} that masks, to various extents, the important chromate vibrational bands in this region. Only in the spectra of highly loaded samples, i.e Cr^{nos} and 13.6CrX was there a chromate band visible at around ~900 cm^{-1}.

FTIR Interpretation

FTIR, because of its full penetration through zeolite crystals, offers a means of analysing bulk phase chromate. The presence of chromate was indicated by the ν_3 IR band at ~900 cm^{-1} in the spectra of 13.6CrX and Cr^{nos} as a shoulder on the broad and intense ν_{as}(T-O-T) zeolite band at ~1000 cm^{-1}. The IR active ν_{as} dichromate band at 950 cm^{-1} was not visible in the spectra of even the most highly loaded zeolites. The absence of dichromates within nosean is to be expected as the anion is too large to fit in the β-cage. The larger cages of zeolites however could offer sites for dichromate occlusion. FTIR however indicates the presence of few dichromates in the bulk of the zeolite crystals.

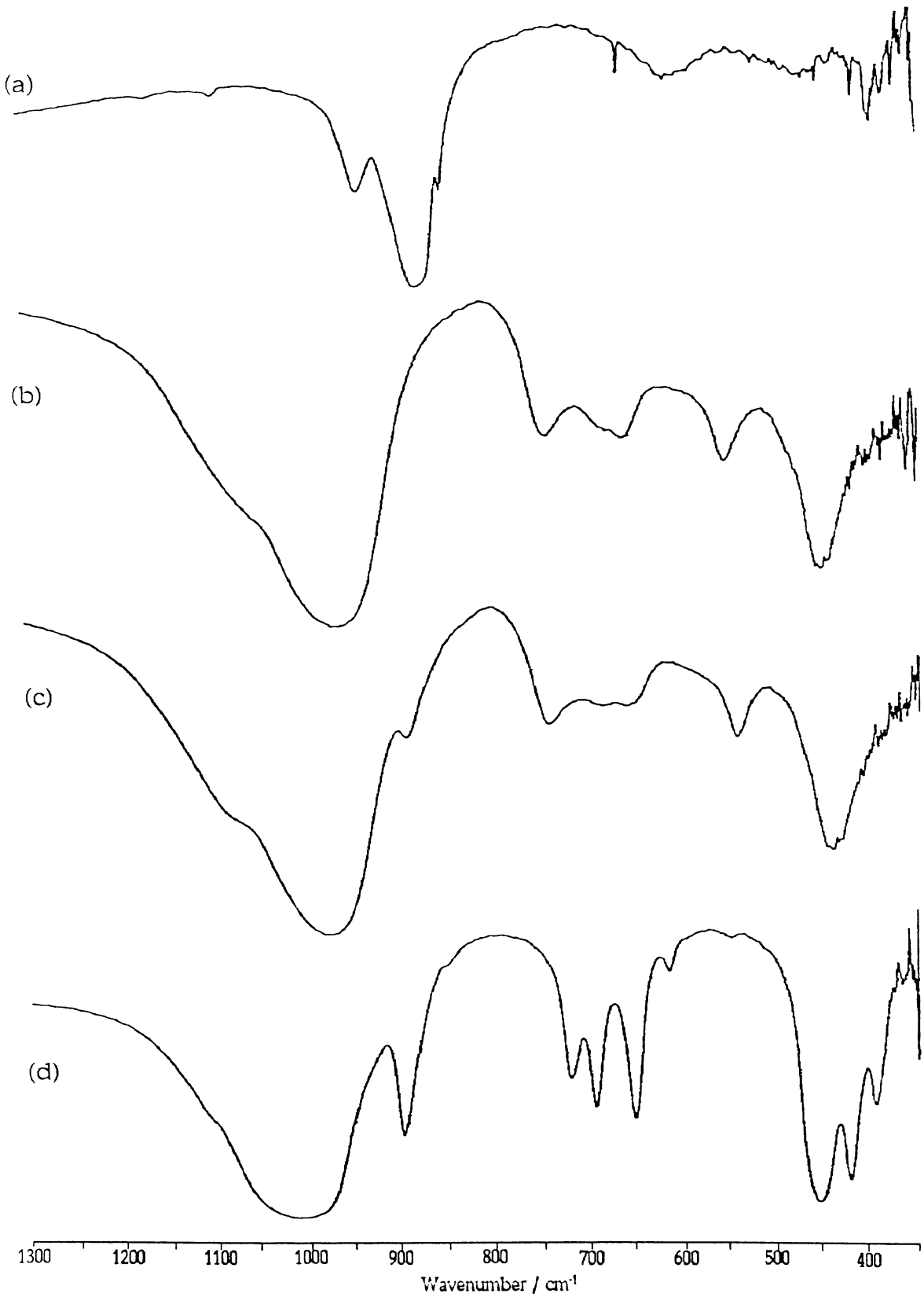


Figure 4.7 FTIR spectra of (a) sodium chromate salt, (b) 13X, (c) 13.6CrX, and (d) chromate nosean. Note the ν_3 chromate band at ~900 cm^{-1} in the spectra of chromate nosean and 13.6CrX.

4.4.6 DTA Analysis of X-Type Zeolites

DTA Results and Interpretation

The temperatures of lattice degradation (T_d) and recrystallisation (T_r) for 13X and 5.8CrX are given in Table 4.8.

Table 4.8 DTA data of various X-type zeolites. (T_d = temperature of lattice breakdown, T_r = temperature of recrystallisation)

Zeolite	T_d/°C	T_r/°C
13X	837	949
5.8CrX	864	937

Loading 5.6 chromates per unit cell into zeolite 13X increased T_d by 27°C while T_r was lowered by 12°C upon chromate occlusion. An increase in stability upon salt loading is a common phenomenon. Recrystallisation in the presence of chromate forms chromate noselite while carnegiete is formed for pure 13X. A change is recrystallisation product is likely to involve a change in recrystallisation mechanism. The lowering of T_r may in part be caused by such a change in mechanism. As seen in Section 3.2.3 the presence of excess sodium chromate salt resulted in a new endothermic peak at 796°C attributable to the production of either chromate nosean or chromate zeolite promoted by the melting of sodium chromate. Occluded chromates are present as discrete oxyanions thereby lacking the crystal and thermochemical properties of the pure salt. The absence of an endothermic melting process is evidenced by the absence of an endothermic peak at ~800°C. The occluded chromates act as a filler of zeolite pores and increase T_d compared to that of the parent zeolite.

4.4.7 EPR Analysis of Chromate Zeolites

EPR Results and Interpretation (10.3CrY72)

All the sodium zeolites produced yellow chromate zeolites which had no chromium EPR signals. The hydrogen form of Y zeolite, LZ-Y72, reacted with chromate to produce the green 10.3CrY72. Figure 4.8 shows the EPR spectra of LZ-Y72 and 10.3CrY72. The signal of 10.3CrY72 is complex consisting of a broad symmetrical signal (ΔH = 4700 G, g = 1.98 ± 0.01) and a narrow slightly asymmetric signal (ΔH = 100 G, g = 1.976 ± 0.002). These signals are characteristic of chromic oxide (Cr_2O_3), see for example the spectra from Cordischi *et al.*[17] showing the signal arising from Cr_2O_3 in the polycrystalline MgO-Cr_2O_3 phases.

EPR Results and Interpretation (13.6CrX)

The effect of various redox treatments on the EPR spectrum of 13.6CrX is shown in Figure 4.9. Outgassing at 375 ± 5°C to form 13.6CrX(evac) resulted in the appearance of a narrow asymmetric EPR signal (ΔH = 175 G, $g_\perp$ = 1.986 ± 0.002, $g_{||}$ = 1.917 ± 0.002) characteristic of a Cr(V) species of distorted tetrahedral symmetry. Reaction with hydrogen gas at 375 ± 5°C to form 13.6CrX(R375) resulted in the uptake of 1.26 ± 0.02 moles of $H_{2(g)}$ per mole of Cr, the loss of the Cr(V) signal, and the appearance of a broad symmetrical signal (ΔH = ~4000 G, g = 1.98 ± 0.01) characteristic of a Cr(III) species. The ratio of the areas of the Cr(V) peak of 13.6CrX(evac) and Cr(III) peak of 13.6CrX(R375) is 0.043 indicating very little Cr(V) was present in 13.6CrX(evac). The absence of chromate Raman bands in the spectrum of 13.6CrX(evac) indicates that chromates occluded in the α-cages adjacent to the surface of the crystals are reduced upon evacuation. Reduction of these occluded chromates and/or reduction of surface bound species would be consistent with small amounts of reduction and the loss of Raman bands. Reaction with oxygen gas at 500°C resulted in full reoxidation and the loss of

the Cr(III) signal.

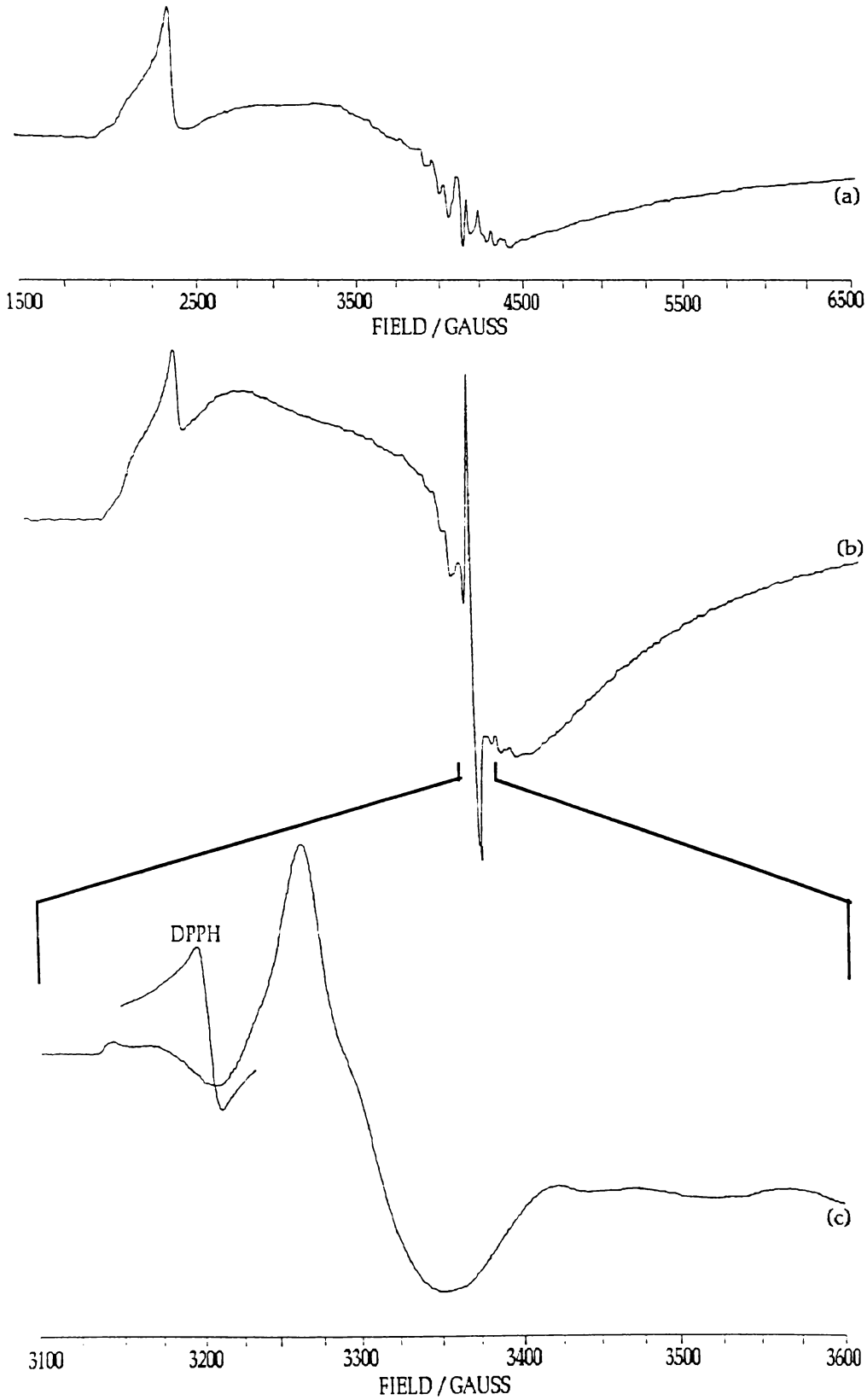


Figure 4.8 EPR spectra of (a) LZ-Y72, (b) 10.3CrY72 on range 5000 G, and (c) 10.3CrY72 on range 500 G. All spectra were recorded on a gain of 2.5×10^3 and have the same vertical range in the figure. 1 cm in the figure equals 2.74 cm in the original trace.

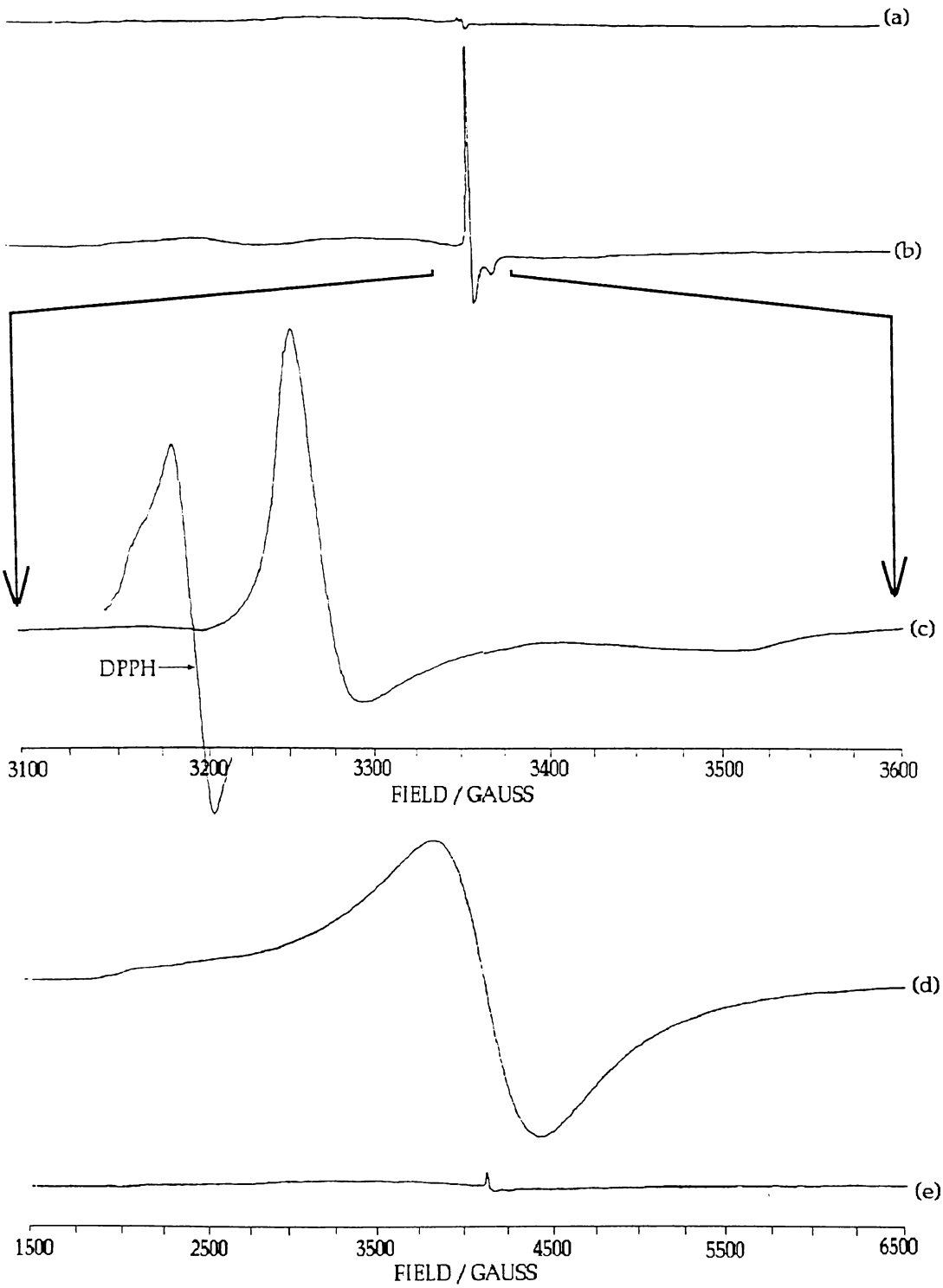


Figure 4.9 Effect of various redox treatments on the EPR spectrum of the zeolite 13.6CrX. Samples are: (a) parent zeolite 13.6CrX, (b) 13.6CrX(evac) (range 5000 G), (c) 13.6CrX(evac) range 500 G, (d) 13.6CrX(R375), and (e) 13.6CrX(O500). All spectra were recorded with a gain of 1.6×10^2 and have the same range in the vertical figure. Spectrum (c) has a range of 500 G as shown by the axis below this spectrum. 1 cm on this figure equals 2.72 cm on the original trace.

4.4.8 Analysis of Sodium Uptakes

Results

XRF analysis gave sodium and chromium contents allowing calculation of sodium uptakes per chromium. Table 4.9 shows these values. Only the highest loaded zeolites are considered. In the tables the contents of M5 are calculated based on 192 metal atoms per unit cell instead of the usual 48 to allow direct comparison with A, X, and Y type zeolites.

Interpretation

Uncertainties are large in the Na/Cr values because the increases in sodium and the chromium content are small resulting in large percentage errors. Added to these errors is the uncertainty arising from the apparent leaching of sodium from the zeolites indicated by the negative sodium increases of some lowly loaded zeolites. The problem is severe for 13X zeolites but less so for Y52, M5, and 4A zeolites. Partial hydrolysis of sodium cations to form structural hydroxyls is the most likely cause of the effect and is consistent with higher levels of hydrolysis of 13X compared to that of Y52. Zeolites with higher aluminium contents are more susceptible to this phenomenon.[18] The Na/Cr value in the absence of hydrolysis would allow the determination of the stoichiometry of occlusion as increases in sodium would result from the uptake of sodium cations counteracting the charge of the chromate anion. Cation hydrolysis would lower the apparent sodium uptake giving misleading Na/Cr values that do not reflect the occlusion stoichiometry. Although the extent of hydrolysis is unknown its effect will always be to lower sodium levels thereby giving smaller Na/Cr values. The evaluated Na/Cr can be considered to be underestimates. Values of Na/Cr for zeolites Y52, M5, and 4A were generally between one and two. Although these values can not be used to differentiate between occlusion as dichromates (Na/Cr = 1) and chromates (Na/Cr = 2),

values at least as high as one indicate chromium uptake as an oxyanion as opposed to uptake as a chromyl cation.

Table 4.9 Sodium uptakes during solid-state reactions of various zeolites with sodium chromate.

Sample No.	Na increase per unit cell (± 0.6)	Cr per uc (± 0.3)	Na/Cr
4A.500.2	1.0	1.0	1.1 ± 0.9
4A.700.2	-0.4	1.8	---
4A.500.7	2.7	1.4	2.0 ± 0.9
4A.600.7	1.7	1.7	1.0 ± 0.5
4A.700.7	2.6	2.6	1.0 ± 0.4
M5.500.2	-0.1	1.2	---
M5.700.2	0.6	3.1	0.8 ± 0.3
M5.500.7	1.1	2.0	2.2 ± 0.7
M5.600.7	0.8	3.2	1.1 ± 0.3
M5.700.7	1.8	3.5	2.1 ± 0.4
Y72.500.2	12.6	2.3	---
Y72.700.2	15.5	4.8	---
Y72.500.7	16.0	4.2	---
Y72.600.7	18.4	8.6	2.1 ± 0.2
Y72.700.7	22.2	10.3	2.1 ± 0.1
Y52.500.2	-0.1	0.4	---
Y52.700.2	2.5	1.9	1.3 ± 0.5
Y52.500.7	0.6	1.0	---
Y52.600.7	3.2	2.1	1.5± 0.5
Y52.700.7	4.1	3.1	1.3± 0.3
13X.500.2	-3.8	0.3	---
13X.700.2	-3.3	1.3	---
13X.500.7	-0.4	0.8	---
13X.600.7	0.6	1.4	---
13X.700.7	-0.4	2.4	---

4.4.9 BET Surface Area Analyses

Table 4.10 shows the surface area of various zeolites. Losses of BET surface area from 387 ± 8 m^2/g for 13X to 170 ± 15 m^2/g and 135 ± 10m^2/g for

5.8CrX and 13.6CrX respectively and from 352 ± 10 m^2/g for 5A to 13 ± 7 m^2/g for 32.3Cr5A could be due to structural degradation, prevention of N_2 adsorption through the blocking of surface pores, and/or the filling of zeolite pores. If the blocking of surface pores occurred then one might expect surface sites to saturate quickly thereby causing significant loss of surface area even at low chromate loading. The similar surface areas of 5A and 4.8Cr5A indicate the blocking of surface pores does not occur. The increase to 385 ± 10 m^2/g upon removal of chromate from 13.6CrX by NaOH to form 2.1CrX indicates that structural degradation was not the cause of the low surface area of 13.6CrX. The filling of zeolitic pores is the most likely cause of the losses of surface area.

Table 4.10 Surface areas of various zeolites.

Sample	13X	5.8CrX	13.6CrX	2.1CrX	5A	4.8Cr5A	32.3Cr5A
SA/$m^2\,g^{-1}$	387 ± 8	170 ± 15	135 ± 10	385 ± 10	352 ± 10	348 ± 10	13 ± 7

4.4.10 XPS Analysis of Chromate Zeolites

XPS Results

Tables 4.11 to 4.14 show the XPS data of various X-type zeolites. All binding energies (BE) are corrected to C 1s as 285.0 eV.

Table 4.11 XPS data of 13X.

Element	BE (eV)	Width (eV)	Atomic conc%	Mass conc %
Na 1s	1072.5	2.62	15.38	18.32
O 1s	531.5	2.70	54.89	45.46
C 1s	284.5	2.77	7.07	4.40
Si 2p	102.0	2.40	12.18	17.72
Al 2p	74.0	2.36	9.10	12.72
Cr 2p	---	---	0.01	0.03

Table 4.12 XPS data of 5.8CrX.

Element	BE (eV)	Width (eV)	Atomic conc%	Mass conc %
Na 1s	1073.0	2.45	16.90	19.97
O 1s	532.0	2.63	53.37	43.87
C 1s	285.0	2.47	6.07	3.75
Si 2p	102.5	2.29	11.68	16.87
Al 2p	74.5	2.13	8.82	12.24
Cr 2p	575.5	0.52	0.13	0.34

Table 4.13 XPS data of 13.6CrX.

Element	BE (eV)	Width (eV)	Atomic conc%	Mass conc %
Na 1s	1072.5	2.51	11.97	14.41
O 1s	531.5	2.93	54.58	45.68
C 1s	285.0	2.72	9.38	5.90
Si 2p	101.5	2.50	12.22	17.97
Al 2p	73.5	2.50	9.03	12.75
Cr 2p	576.5	3.74	0.28	0.76

Table 4.14 XPS data of 2.1CrX.

Element	BE (eV)	Width (eV)	Atomic conc%	Mass conc %
Na 1s	1073.0	2.57	9.21	11.65
O 1s	532.0	2.80	47.33	41.63
C 1s	285.0	2.51	24.38	16.13
Si 2p	102.5	2.47	10.06	15.53
Al 2p	74.5	2.56	7.59	11.27
Cr 2p	---	---	0.00	0.00

XPS Interpretation

The depth of XPS beam penetration is not known so it is not clear to what extent bulk phase chromates were detected. Chromium detected by XPS may be the surface bound dichromates detected by Raman or chromates occluded within the first layer of α-cages, or a combination of both. Higher chromium contents were detected for 13.6CrX than for 5.8CrX. As surface sites

would saturate rapidly, the increase may reflect the increase in the number of occluded chromates.

Bulk phase compositions (from XRF) of zeolites 13.6CrX and 5.8CrX were 12.50 atom% Cr and 5.6 atom% Cr respectively. XPS determined contents were 0.28 and 0.13 atom% for 13.6CrX and 5.8CrX, respectively, indicating much lower chromium contents in the surface layers than in the bulk phase. The XPS and XRF contents differed by a factor of ~45. This discrepancy is much larger than can be attributed to calibration errors. Low chromium contents may have resulted from a depletion of chromate in the α-cages on crystal surfaces. These chromates may be more prone to removal during the washing step subsequent to the solid-state reaction.

XPS indicated the absence of chromium in the surface layers of 2.1CrX. The chromium present in this region of 13.6CrX was therefore removed by the treatment with NaOH. The absence of dichromate bands in the Raman spectrum of 2.1CrX and the lower intensities of the chromate bands in the spectrum of 2.1CrX compared to those in the spectrum of 13.6CrX are consistent with the removal of chromium species from the surface layers upon NaOH treatment.

Binding energy values of 5.8CrX and 13.6CrX were 575.5 eV and 576.5 eV respectively. Both BE values are significantly lower than that observed for Na_2CrO_4[19] (579.6 eV) and other Cr(VI) species such as CrO_3 (578.3 eV to 580.3 eV).[20] The value for 13.6CrX is within the range exhibited by Cr(III) species such as Cr_2O_3 (576.2 eV to 576.8).[20] That of 5.8CrX is significantly lower, however the low chromium content made detection difficult casting some doubt on the BE values. Low BE values indicate reduction of the chromium detected by XPS. Reduction presumably occurs during evacuation prior to XPS analysis. The Cr(III) could be Cr_2O_3 on the surface of zeolite crystals formed upon reduction of surface dichromates or $NaCrO_2$ formed upon reduction of chromates occluded in α-cages on the outer

surface of crystals. Evacuation prior to kinetic studies resulted in a change in the colour of the zeolite from yellow to bright green, the appearance of a Cr(V) EPR signal, and the loss of chromate and dichromate Raman bands. These observations are consistent with the reduction of chromium species on or near the surface layers of chromate zeolites.

Concerns over beam penetration, low chromium contents, and the reduction prior to examination make structural elucidation of occluded chromates on the basis of BE values impossible. Importantly, the low chromium contents indicate the absence of chromium rich phases on the surface of chromate-loaded zeolites.

4.4.11 Analysis of Maximum Chromate Uptakes

Maximum Chromate Uptake Results

Table 4.15 shows the maximum chromate uptakes of the various zeolites.

Table 4.15 Maximum chromate uptakes of various zeolites.

Zeolite	13X	Y52	5A
Cr/uc (± 1.5%)	13.6	13.4	32.3

Interpretation of Maximum Chromate Uptake

If chromates coordinated to one specific type of site within the frameworks of X, Y, and A zeolites then the maximum uptake will reflect the number of such sites. What follows is an analysis the number of the various structural features (rings, prisms, and cages) contained within the unit cells of various zeolites. A correlation between these numbers and the maximum chromate uptake is determined.

Numbers of the Various Ring Sizes in Zeolite A

The unit cell of zeolite A consists of eight α-cages and eight β-cages. β-cages are linked to others through each of the six square faces leaving all eight S6R faces free. The eight β-cages of the unit cell of A therefore contribute sixty-four S6R. For each eight α-cages of the unit cell there are eight D4R giving sixty-four D4R per unit cell.

Numbers of the Various Ring Sizes in Zeolites 13X and Y52

The unit cell of zeolites X and Y consist of eight α-cages and eight β-cages. β-cages are linked through four of the eight S6R faces leaving four S6R faces adjacent to α-cages. The eight β-cages per unit cell thereby supply thirty-two S6R faces. Each α-cage supplies six D6R and six S4R giving forty-eight of both D6R and S4R per unit cell.

Relationships Between the Maximum Chromate Uptakes and the Number of the Various Structural Features

In Table 4.16 the maximum chromate uptakes are related to the number of the various structural features of the various zeolites. A significant relationship exists when the ratio between the maximum number of chromates and a structural feature is common to the three zeolites. The ratio should also be a chemically sensible. If occlusion occurred in cages or double prisms then a whole number of chromates per these structural features would occur. Rings might coordinate one chromate, or one chromate per two rings if coordination across two rings was possible. Chromate to ring ratios lower than 0.5 would indicate the lack of a significant relationship as coordination of one chromate across three or more rings is unlikely

As the unit cells of A, X, and Y all contain eight α-cages and eight β-cages the difference in the maximum uptake levels for A and X or Y indicates

that the number of such cages does not control uptake levels. There appears to be no meaningful correlation between the maximum uptake and the numbers of S12R of X and Y and the S8R of 5A. Ratios between the maximum number of chromates and the number of D6R of X and Y and the D4R of 5A were similar however the Cr to structural feature ratio eliminates occlusion within these prisms. A correlation also exists between chromate uptake and the number of S6R for A (0.50), X (0.43) and Y (0.42) suggesting the number of S6R may control the levels of chromate uptake. The fractional uptake corresponds to one chromate per two S6R suggesting coordination across two of these structural feature.

Table 4.16 Relationship between the numbers of the various structural features (cages, rings and prisms) of the various zeolites and the maximum chromate uptakes.

Zeolite	Cr/uc	Structural Feature	No./uc	Cr/Structural Feature
13X	13.6	α	8	1.7
		β	8	1.7
		S12R	2	6.8
		S6R	32	0.43
		D6R	32	0.43
		S4R	48	0.27
Y52	13.4	α	8	1.7
		β	8	1.7
		S12R	2	6.7
		S6R	32	0.42
		D6R	32	0.42
		S4R	48	0.28
5A	32.3	α	8	4
		β	8	4
		S8R	2	16
		S6R	64	0.50
		D4R	64	0.50

4.4.12 Summary of the Experimental Results

Table 4.17 summarises the experimental results.

Table 4.17 Summary of the experimental results.

Method	Results
BET	Loss of surface area upon loading. Surface area regained upon chromate removal by NaOH.
PXRD	Loss of XRD peak intensities upon loading. Peaks intensities increased upon chromate removal.
SEM	No change to zeolite crystal morphology. Some surface modification for Na zeolites. Extraneous surface phases on 10.3CrY72.
Raman	Chromate, dichromate and anchored chromates detected on or near the surface of the crystals.
FTIR	Chromate detected in highly loaded zeolites.
EPR	No EPR active Cr species in chromate loaded Na zeolites. Cr(V) species of distorted tetrahedral symmetry detected upon evacuation. Cr(III) species detected upon reduction. Cr_2O_3 detected in 10.3CrY72.
XPS	Low chromium contents near surface.
DTA	Temperature of breakdown raised and recrystallisation temperature lowered by occlusion of chromate.
Sodium Uptakes	Na/Cr for 4A, Y52, Y72, and Y72 were usually between 1 and 2.

4.5 Discussion

4.5.1 Framework Stability

Retention of crystal morphology and the regaining of the PXRD peaks upon chromate removal indicates that the no framework degradation upon chromate occlusion. Maximum uptake levels can be achieved with no lattice decomposition indicating that chromates are occluded within zeolite cavities.

4.5.2 Modes of Occlusion that can be Eliminated

Based on the results of the various experimental techniques several of the possible occlusion mechanisms can be eliminated.

Replacement of Framework Atoms

XRF, see Section 3.2.4, indicated no change to the silicon to aluminium contents upon loading. The absence of aluminium or silicon loss from the framework indicates no replacement of framework atoms.

Replacement of Surface Hydroxyls

Sodium uptakes per chromium, molybdenum and tungsten between 1 and 2 indicate that principal uptake was as oxyanions as opposed to uptake via replacement of surface hydroxyls. Loss of surface area indicates that the α-cage is the major site for occlusion. Raman spectra, however, showed the presence of chromate and dichromate species on or near the surface of the crystals indicating the likelihood that replacement of surface hydroxyls was also occurring.

Similar maximum chromate uptakes by 13X and Y52 zeolites despite the fact that both the smaller crystal size and higher silicon content of Y52 would afford a greater number of surface hydroxyls indicates the likelihood that uptake by reaction with surface hydroxyls did not significantly contribute to

the overall chromate uptake. The contribution of uptake by replacement of surface hydroxyls can be estimated from the concentration of such species. The number of surface hydroxyls varies as a function of crystal size and has been estimated to range between $0.15x10^{19}$ per gram for a 1 micron particle to $1.4x10^{20}$ per gram for a 0.1 micron particle.[21,22] Based on these figures maximum uptakes of 0.07 wt% Cr for a 1 micron particle and 0.61 wt% Cr for a 0.1 micron crystal are expected. These values are significantly lower than the chromium contents of the maximum loaded zeolites (3.59 wt% Cr for 13.6CrX, 3.55 wt% Cr for 13.4CrY, and 8.16 wt% Cr for 32.3Cr5A) indicating that replacement of surface hydroxyls is not the sole or even a major mode of uptake. This conclusion is further supported by the low levels of surface chromium detected in the XPS experiments.

Occlusion within Sodalite-Cages

Loss of surface area upon chromate loading roughly proportional to loading indicates that chromate oxyanions occupied positions within the supercages of X and A-type zeolites rather than within sodalite cages.

Replacement of Structural Hydroxyls

The concentration of structural hydroxyls should be low in the sodium forms of zeolites. There may however be structural hydroxyls resulting from partial hydrolysis of cations and replacement by hydronium, H_3O^+.[23,24] XRF indicated cation deficiencies for all zeolites. Sodium contents were lower than aluminium contents, see Table 4.18. These deficiencies could be the result of cation hydrolysis and/or the presence of amorphous phases. Even assuming the cation deficiencies arose solely from cation hydrolysis the numbers of such sites for the sodium zeolites were much smaller than the numbers of oxyanions taken up indicating replacement of structural hydroxyls could only be a minor mode of uptake.

Table 4.18 Sodium deficiencies and maximum chromate uptakes of the zeolites examined.

Zeolite type	Na per uc	Al per uc	Na deficiency per uc	Cr per uc
Y72	9.63	55.34	45.71	---
13X	83.76	85.84	2.08	13.6
Y52	51.16	54.53	3.37	13.4

Formation of Chromyl Cations and Reaction with Zeolite Cations

Cationic positions occupied by Na^+ are not considered to be ion-exchange traps for cations during high temperature reactions, see Section 1.3.1 for accounts of such phenomena. For example, Kucherov and Slinkin[25] found that the solid-state interactions with Cr(III), Cr(VI), Mo(V), and V(V) at temperatures up to 820°C did not permit the exchange of sodium cations for polyvalent cations. The replacement of sodium cations by chromyl cations, even if such species formed during the solid-state reaction with sodium chromate, is unlikely to have occurred.

Formation of Sodium Chromate Phases within Zeolite Cavities or on Crystal Surfaces

Occlusion via the formation of sodium chromate phases on the surface of zeolite crystals can be eliminated based on the Raman spectra which indicate the occlusion of discrete chromate oxyanions of tetrahedral symmetry. In addition, sodium chromate phases on the surface were not detected in SEM photographs or indicated by high XPS chromium contents.

Nitrate occlusion in A zeolite, in which a crystalline nitrate phase is observed, results in an uptake of ten nitrate molecules per pseudo unit cell or eighty nitrates per real unit cell. Maximum chromate uptake levels were only 1.7 and 4.0 per unit cell for 13X and 5A zeolites respectively. An intrazeolitic

sodium chromate phase with a substructure based on such low chromate levels would not be possible.

Occlusion of Sodium Chromate in a New Aluminosilicate Phase

No zeolite lattice breakdown occurred indicating no significant formation of other aluminosilicate phases.

4.5.3 Proposed Mode of Chromate Occlusion: Coordination to Zeolitic Sodium Cations

These systems were deemed unsuitable for Rietveld PXRD analysis due to the fluorescence of occluded chromates.[26] In the absence of definitive structural evidence the chromate to zeolite interaction can only be speculated upon. Consideration of the literature on the types of interactions between transition metal species and zeolites allows a mode of coordination to be proposed.

Interactions between Zeolites Transition Metal Oxo- and Carbonyl Species

Hexacarbonylmetal(0), $M(CO)_6$ (M = Cr, Mo, W), sorbed from the vapour phase into $M'_{56}Y$ (Si/Al = 2.5, M' = Li, Na, K, Rb, Cs) displayed the characteristic pattern of ν(CO) stretching modes for a molecule of octahedral symmetry slightly perturbed by interaction with an extraframework cation(s).[27] Similar results have been reported for $Mo(CO)_6$ in $Na_{56}Y$ and $H_{56}Y$.[28] $M(CO)_6$-$M'_{56}Y$ had the hexacarbonylmetal(0) guest anchored to two α-cage extraframework cations (or Brønsted protons) via the oxygen end of two trans bonded carbonyl ligands, see Figure 4.10. Saturation loading was $2M(CO)_6$/α-cage or one metal carbonyl per two S6R.

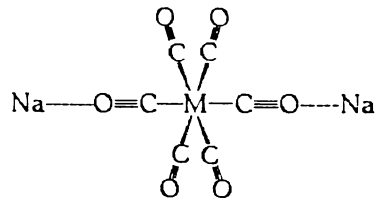


Figure 4.10 Anchoring site for hexacarbonylmetal(0) complex in alkali metal zeolite Y.

Work on the photoxidation of intrazeolite $M(CO)_6$ was prompted by organometallic and matrix isolated rhenium(I)[29] and molybdenum(0)[30] systems, see Figure 4.11:

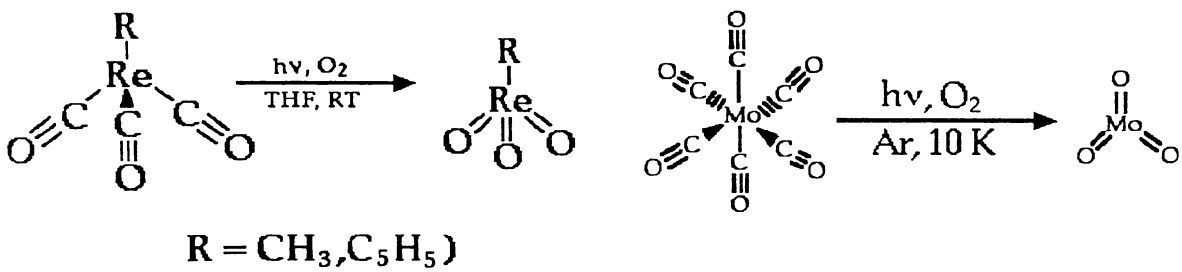


Figure 4.11 Photoxidaton products of matrix isolated rhenium(I) and molybdenum(0).

Moller *et al.*[31] demonstrated that photoxidation of α-cage encapsulated hexacarbonyltungsten(0), $n\{W(CO)_6\}$-$Na_{56}Y$, forms single size tungsten(VI) oxide clusters $n(WO_3)$-$Na_{56}Y$ according to the reaction scheme

$$n\{W(CO)_6\}\text{-}Na_{56}Y + \tfrac{9}{2}nO_2 \xrightarrow{h\nu} n(WO_3)\text{-}Na_{56}Y + 6nCO_2$$

It was also found that the following sequential saturation loading/photoxidation scheme satisfactorily accounted for the chemistry and spectroscopy of the system.

$$16\{W(CO)_6\}\text{-}Na_{56}Y \longrightarrow 16(WO_3)\text{-}Na_{56}Y$$
$$8\{W(CO)_6\}\text{-}16(WO_3)\text{-}Na_{56}Y \longrightarrow 24(WO_3)\text{-}Na_{56}Y$$
$$4\{W(CO)_6\}\text{-}24(WO_3)\text{-}Na_{56}Y \longrightarrow 28(WO_3)\text{-}Na_{56}Y$$
$$\downarrow \qquad\qquad\qquad\qquad \downarrow$$
$$0.1\{W(CO)_6\}\text{-}31.9(WO_3)\text{-}Na_{56}Y \longrightarrow 32(WO_3)\text{-}Na_{56}Y$$

Based of EXAFS the structure of $16(WO_3)$-$Na_{56}Y$ in Figure 4.12 was proposed.

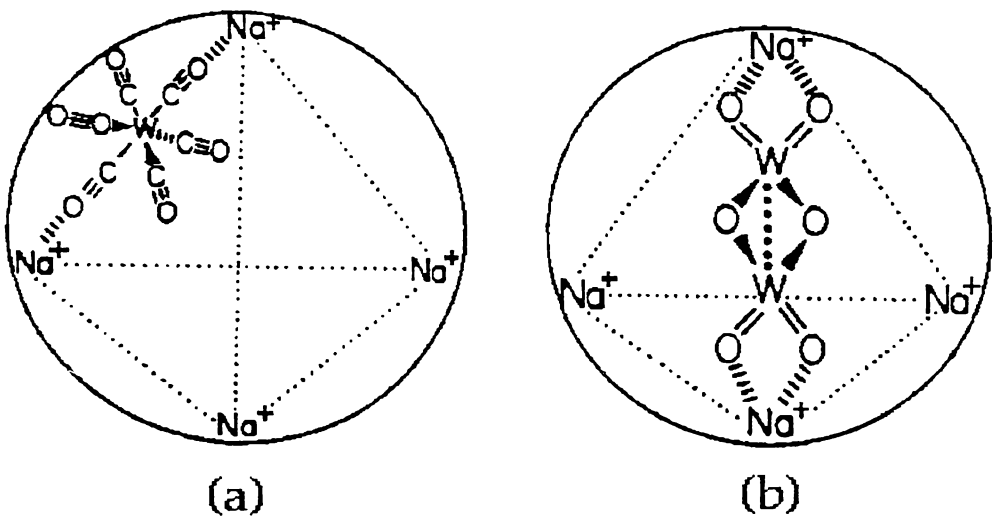


Figure 4.12 Structural illustration of (a) $8\{W(CO)_6\}$-$Na_{56}Y$ and (b) $16(WO_3)$-$Na_{56}Y$.

Later work by Özkar *et al.*[32] found α-cage encapsulated hexacarbonyl-molybdenum(0) underwent the following photoxidation reaction

$$n\{Mo(CO)_6\}\text{-}Na_{56}Y + \tfrac{9}{2}nO_2 \xrightarrow{h\nu} n(MoO_3]\text{-}Na_{56}Y + 6nCO_2$$

Vacuum thermally induced reductive elimination of O_2 from the molybdenum(VI) oxide yielded molybdenum(IV) oxide. This reduction process was quantitatively reversed by exposure of the molybdenum(IV) oxide product to O_2 at 400°C.

$$n\ (MoO_3)\text{-}Na_{56}Y \underset{400°C,\ O_{2(g)}}{\overset{400°C,\ vacuum}{\rightleftharpoons}} n\ (MoO_2)\text{-}Na_{56}Y + \tfrac{1}{2}n\ O_2$$

Structural and spectroscopic analyses demonstrated that over the loading range $0 < n \leq 16$ the molybdenum oxides were located in the α-cages as the redox inter convertible monomers shown in Figure 4.13.

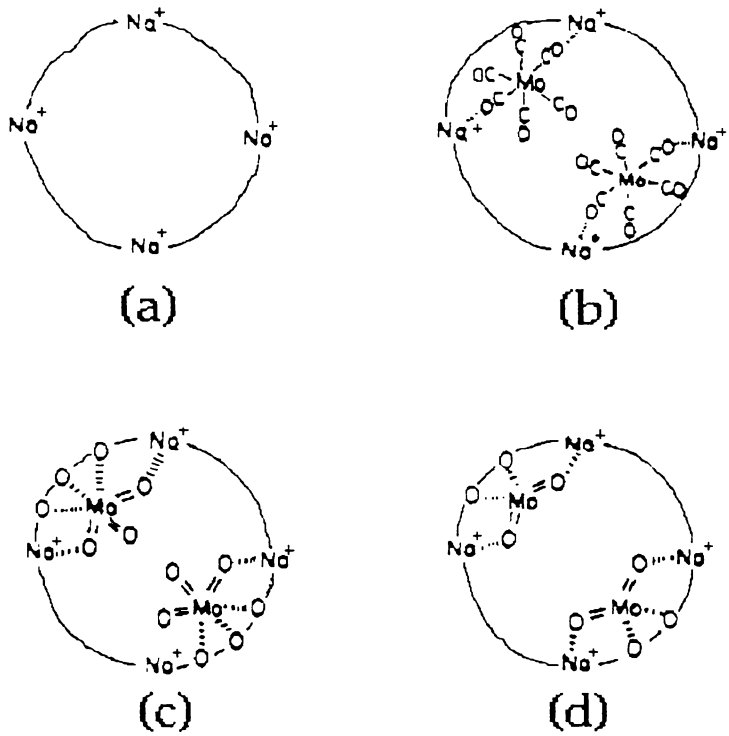


Figure 4.13 Structures proposed by Özkar[29] of (a) dehydrated $Na_{56}Y$, (b) 16{$Mo(CO)_6$}-$Na_{56}Y$, (c) 16(MoO_3)-$Na_{56}Y$, and (d) 16(MoO_2)-$Na_{56}Y$.

Based on curve fitting procedures of EXAFS spectra the coordination numbers in MoO_3 were determined to be 3.25 oxygen atoms at a distance of 1.73 Å and 2.77 oxygen atoms at a distance of 1.88 Å. The model proposed consistent with these calculations is that of a monomeric *fac*-MoO_3 moiety with three shorter Mo=O bonds and stabilised by coordination through three long bonds to framework oxygen atoms of a six-ring lattice site, see Figure 4.14. It was noted that it would also be reasonable to assign the spectrum to a moiety anchored through a four-ring (with two long Mo-O bonds) as the error in the EXAFS calculation was ± 1 atom.

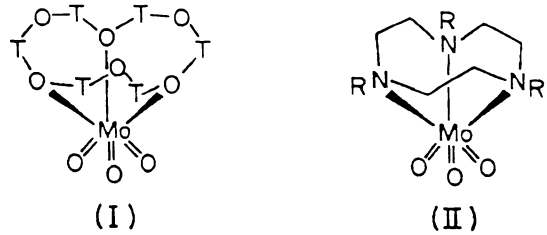


Figure 4.14 Model proposed by Özkar[29] for the "zeolate" ligation bonding in the *fac*-trioxomolybdenum(VI) unit of (MoO_3)-$Na_{56}Y$ (I). The bonding is compared to that in an $LMoO_3$ complex such as 1,4,7-triazocyclononane (II).

Proposed Interaction Between Chromate and Zeolites

A relationship was observed between the number of S6R and the maximum chromate uptake. Such a relationship was also observed for $M(CO)_6$ (for M = Cr, Mo, and W) in Y zeolite in which coordination across two S6R through Na^+ cations located on the S_{II} site was invoked. Subsequent redox treatments on $Mo(CO)_6$ forms MoO_3 and MoO_2 moieties remaining anchored across two S6R and consisting of interactions between oxygen atoms of the molybdenum species and two Na^+ cations on the S_{II} site. Similar relationships between the number of occluded species and the number of S6R suggests that the mode of occlusion is similar. Chromate oxyanions are similar to the tungsten and molybdenum oxide compounds and possess metal to oxygen bonds capable of coordination to zeolite sodium cations. Coordination of a chromate across two S6R is therefore feasible.

Chromate differs from the molybdenum and tungsten oxides in that chromate is an oxyanion while the oxides are neutral species. Maintenance of charge neutrality therefore the uptake of two sodium cations per chromate oxyanion. The mode of occlusion is therefore likely to be more complicated than that of the oxides. Cation distributions given by Breck[33] show full occupancy of the 32 S_{II} sites for X and Y zeolites. This corresponds to a sited cation for each of the S6R facing the α-cage. A model of chromate to zeolite interaction must therefore involve the two zeolitic sodium cations, two S6R,

one chromate oxyanion, and two sodium cations neutralising anion charge. Figure 4.15 shows the geometry of two possible configurations involving chromate to sodium interactions. In (I) the zeolite sodium cations, Na(z), migrate into the sodalite cage and occupy a position on or near the $S_{II'}$ site. The sodium cations associated with the divalent chromate oxyanion, Na(Cr), occupy positions near the S_{II} cation site and have three close zeolite oxygen contacts. In (II) the negative charge of the framework is neutralised by the two Na(Z) occupying their normal positions on S_{II} sites. The chromate oxyanion is coordinated to two Na(Z) with its divalent negative neutralised by two Na(Cr) within the α-cage. The configurations which best describes the coordination is rationalised below.

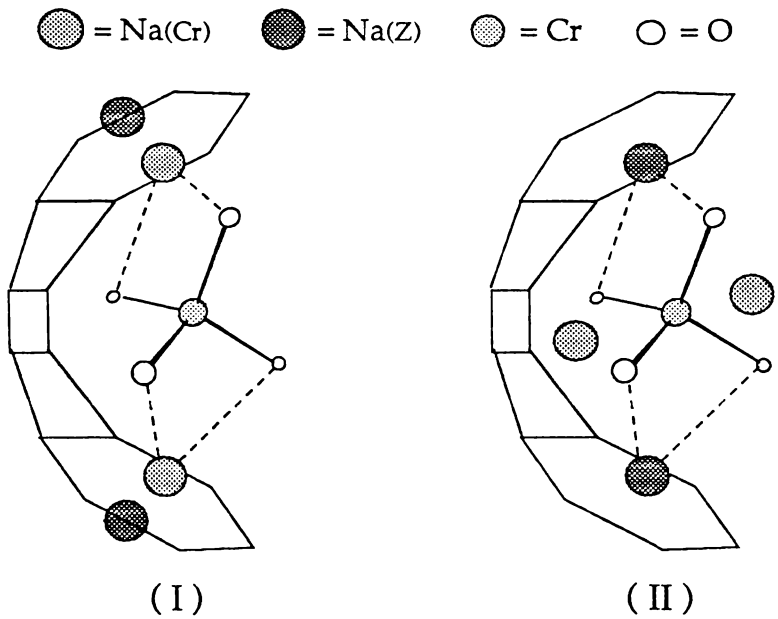


Figure 4.15 Two possible configurations of occluded chromates. The lines represent two S6R adjacent to the α-cage. In (I) the zeolitic sodium that occupied the S_{II} site move into the sodalite cage and locate on the $S_{II'}$ site and the sodium cations accompanying the chromate and neutralising its charge locate near the S_{II} site. The chromate oxyanion coordinates across these two sodium cations. In (II) the chromate oxyanion coordinates to the two zeolitic sodium cations that remain on the S_{II} site. The sodium cations neutralising the charge of the chromate oxyanion lie within the α-cage.

Uptake by S115, the all silica version of M5, is evidence for type (I) coordination. The absence of zeolitic sodium cations simplifies the bonding

scheme to the extent that only the two $Na_{(Cr)}$ need to be considered. S115 was found to occlude a similar amount of chromate as M5 and gave a similar Raman spectrum indicating the same mode of coordination was responsible for occlusion in these zeolites. Uptake into S115 despite the lack of zeolitic sodium cations indicates that the presence of zeolitic sodium cations is not a pre-requisite for the occlusion process. This implies that the sodium cations entering S115 with the chromate unit locate on S5R, analogous to the S6R of X, Y, and A type zeolites. Location of a sodium cation on an S5R face defined by five silicon atoms would normally be energetically unfavourable. However coordination of the sodium to the chromate oxyanion will effectively disperse the positive charge of the sodium to minimise sodium to zeolite interaction. Two S5R can therefore be seen to merely offer sites consisting of two sets of zeolitic oxygen atoms of the correct geometrical arrangement to allow coordination of the Na_2CrO_4 unit.

The situation is more complex for X, Y, and A as the S_{II} cation site already contains sited cations. In these zeolites retention of overall charge neutrality requires the presence of two $Na_{(Z)}$ and two $Na_{(Cr)}$. Spectroscopic similarities between S115 and M5 suggests that the chromate unit has only two sodium cations around it and that configuration (I) best describes the coordination. Movement of the two $Na_{(Z)}$ from their S_{II} sites to the $S_{II'}$ sites near the plane of the S6R but within the sodalite cages would satisfy both the charge neutralisation of the S6R and the opening up of the S_{II} site for coordination.

Coordination in 2.1CrX

Incomplete chromate removal of chromates from X zeolites after NaOH treatment indicates that this type of zeolite occluded two types of chromate. Similar maximum uptakes for both 13X and Y52 indicates that the two types of

chromates occupy the same sites within the α-cage. The cation deficiency of 13X (2.1 ± 0.1 Na/uc) has the same value as the amount of chromate resistant to leaching by NaOH (2.1 Cr/uc). Assuming that the cation deficiency of 13X arose from partial hydrolysis of sodium cations then the unit cell of 13X contained 2.1 ± 0.1 structural hydroxyls. The irreversible occlusion of 2.1 chromates per unit cell corresponds to one chromate per one structural hydroxyl. Interaction through two S6R could be similar to that shown in Figure 4.19 but with coordination through one proton and one sodium cation. The resistance of these chromates to removal by NaOH suggests a stronger interaction with the lattice than chromates coordinated through two sodium cations.

Coordination in CrY72 Zeolites

Solid-state reactions between the hydrogen zeolite Y72 and sodium chromate were unique in that green powders were formed. Extraneous PXRD peaks and EPR spectra were characteristic of crystalline Cr_2O_3 as was the green colour. The material observed by SEM on the surface of zeolite crystals is likely to have been this Cr_2O_3. The formation of Cr_2O_3 for chromate-loaded Y72 zeolites while Y52 gave yellow samples and no Cr_2O_3 indicates the acid sites of H^+ zeolites play a significant role in solid state reactions. As shown in Section 1.3.1 acid sites are considered to be powerful traps for cations. In the case of Na_2CrO_4, the trapping of Na^+ and CrO_2^{2+} was discussed in Section 4.3.2. The formation of Cr_2O_3 is evidence that Na^+ cations rather than CrO_2^{2+} cations are involved. Replacement of protons of structural hydroxyls by sodium cations could occur in a process similar to that observed by Rabo[34] for the reaction of H-Y with NaCl in which NaY and HCl gas were formed. The analogous reaction for Y72 and Na_2CrO_4 would form chromic acid type species. Such species would be prone to dehydration at elevated temperatures to form CrO_3. Decomposition of occluded CrO_3 to form crystalline Cr_2O_3

phases would be prevented by the isolating effect of the nanometer dimensions of the zeolite cavities. The formation of crystalline Cr_2O_3 therefore implies that the chromium species migrate out of the zeolite crystals prior to decomposition. This is supported by the observation of extraneous material on crystal surfaces. Such a migration process would be promoted by the concentration gradient that would result from the continual production of intrazeolitic CrO_3. Once free from the confines of zeolitic cavities formation of a crystalline phase is no longer inhibited by the zeolite framework and decomposition to highly stable Cr_2O_3 results. The stoichiometry of this process could be that shown in Scheme 4.8.

Scheme 4.8 Proposed scheme for the reaction of sodium chromate with the acid sites of hydrogen zeolite LZ-Y72. Ion-exchange of zeolite protons for sodium results in the formation of chromic acid type species that decompose to form Cr_2O_3 once free from zeolite pores.

$$4\,ZOH + 2\,Na_2CrO_4 \xrightarrow{\Delta} 4\,ZONa + 2\,H_2CrO_4$$

$$2\,H_2CrO_4 \xrightarrow{\Delta} 2\,CrO_3 + H_2O$$

$$2\,CrO_3 \xrightarrow{\Delta} Cr_2O_3 + \tfrac{3}{2}\,O_2$$

$$4\,ZOH + 2\,Na_2CrO_4 \xrightarrow{\Delta} 4\,ZONa + Cr_2O_3 + 2\,H_2O + \tfrac{3}{2}\,O_2$$

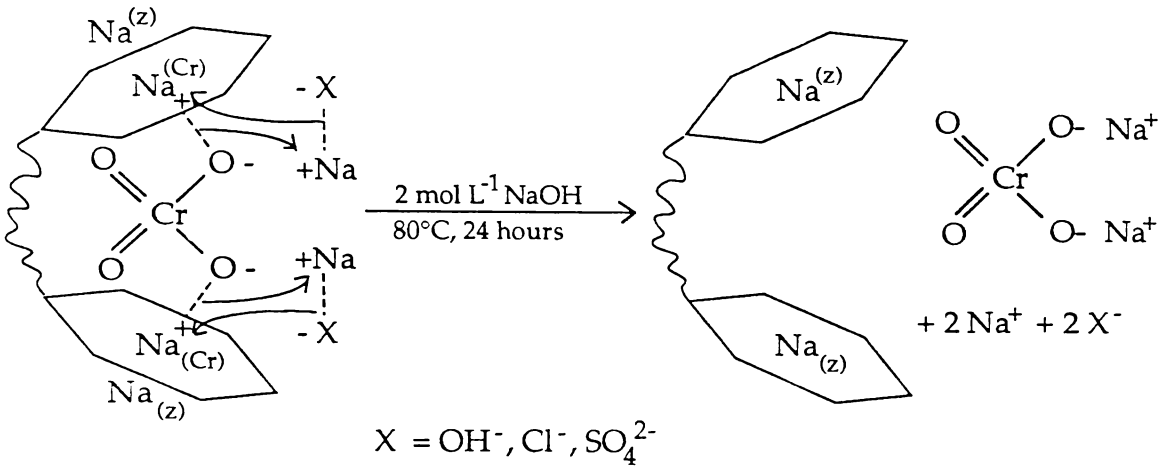
In addition to cation exchange, and subsequent decomposition, occlusion of chromate without decomposition was shown by the leaching of chromates from 10.3CrY72 with NaOH, see Section 4.4.1. Occlusion of chromates would occur as the ion-exchange described above converted the hydrogen form of the zeolite into the sodium form. Each of these processes would result in the uptake of two sodium cations per chromium. Sodium uptakes per chromium of 2.1 ± 0.2 for 8.6CrY72 and 2.1 ± 0.1 for 10.3CrY72 are consistent with this reaction scheme.

Green powders were often formed during the solid-state synthesis of chromate noseans from kaolinite.[2] The addition of small amounts of sodium hydroxide ensured bright yellow chromate nosean. The role of sodium hydroxide in the production of yellow nosean was explained by the suppression of chromate reduction due to the neutralisation of acid sites of the kaolinite. Interaction of sodium chromate with the acid sites of zeolites formed upon deammoniation can be expected to be similar to that of acid sites of other aluminosilicates, i.e. they act as traps for migrating cations.

4.5.4 Proposed Mechanism of Chromate Removal

A mechanism of chromate removal may be developed now that a chromate-zeolite interaction has been proposed. The inability of boiling water to remove chromate reflects the strong interaction between chromate and the zeolite. Rapid removal of chromate by NaOH, NaCl, and Na_2SO_4 suggested an electrolyte mediated process. Removal of the chromate oxyanion as the $(Na^+)_2/CrO_4^{2-}$ ion "triplet" requires movement of the two Na^+ cations. The presence of cations from the salt/NaOH solution in the vicinity of the chromate could weaken the chromate to $Na_{(Cr)}$ interaction while the temperature of 80°C employed provides sufficient activation energy to break the $Na_{(Cr)}$ to chromate interaction. Once the chromate to sited cation interaction was broken these ions would be free to migrate away from the site. Migration out of the zeolite crystal would be promoted by the concentration gradient from the zeolite crystal to the surrounding solution. Scheme 4.9 would account for release of the chromate.

Scheme 4.9 Proposed mechanism for the removal of occluded chromates by electrolyte such as NaOH.



4.5.5 Usefulness of Raman for the Differentiation Between Chromates in α- and β-cages of Zeolites

One reason for investigating nosean systems was that these systems with their relatively simple structures appeared to be ideal models for the characterisation of species occluded within β-cages. It was initially thought that differentiation between species occluded in the α-cages and β-cages of zeolites could be achieved through the comparison of the Raman spectra with that of Cr^{nos}. Snowdon observed similarities between the Raman spectra of Cr^{nos} and chromate zeolites and attributed these to the occlusion of chromate in β-cages of A, X, and Y type zeolites. These similarities were confined to the general features of the spectra such as shape which can only indicate the symmetry of the chromate unit. Loss of the site effects are therefore evidence only for the occlusion of discrete chromate oxyanions of tetrahedral symmetry. We have now shown that chromates are occluded within the α-cages of zeolites X, Y, and A and in the channels of M5 zeolite. Raman spectra indicate that the occluded chromates are monomeric and have tetrahedral symmetry. A difference in the frequencies of the ν_1 band was observed and appeared to offer a means of differentiating α-cage and β-cage occluded chromates. To evaluate

the potential effect of occlusion within the β-cages of zeolites the source of the blue-shift must be understood. It has been shown that the frequencies of chromate internal modes in the series (K, Rb, $Cs)_2CrO_4$ decrease linearly with an increase in the square of the cation to chromium distance.[35] The very similar electronegativities of the cations indicate that there is no significant difference in covalent bonding in the compounds. It was therefore concluded that the shifts to lower frequencies resulted from the falling off of the coulombic forces in the crystal as the cation to chromium distance increased. Movement of the ν_1 band from 851 ± 1 cm^{-1} to 847 ± 1 cm^{-1} upon dissolution of the salt may therefore be ascribed to the spatial separation of the anion and cation resulting from the formation of a solvation sphere around the chromate oxyanion.

The blue-shift from 847 ± 1 cm^{-1} for Cr^{sol} to 850 ± 1 cm^{-1} for 13.6CrX suggests a small contraction of the cation to anion distance and is consistent with the loss of the solvation sphere upon occlusion. A frequency of the ν_1 band similar to that of Cr^{salt} indicates similar cation to anion distances. During formation, sodium and chromate species are labile within the α-cage and will move to minimise free-energy as the system cools. The similar frequencies of the ν_1 band for Cr^{salt} and 13.6CrX indicate that the lowest free-energy of occluded chromates arises when the cation to anion distances are similar to those of the pure salt.

In a similar manner, the blue-shift of the ν_1 peak from 851 ± 1 cm^{-1} for Cr^{salt} to 856 ± 1 cm^{-1} for Cr^{nos} suggests a decrease in the sodium to chromate distance. It is known that the Na to Br distances within the $[Na_4.Br]^{3+}$ clusters in bromosodalite are smaller than those of the pure NaBr salt.[36] The blue-shift of the ν_1 chromate band upon occlusion in nosean is consistent with the smaller cation to anion distances found for this mineral type.

If Raman is to be able to differentiate between chromates occluded in α-cages and β-cages of zeolites then a pre-requisite for this would be similar cation environments in zeolite and nosean β-cages. The unit cell of nosean consists of two β-cages each containing four cations. Each β-cage consists of eight S6R half of which have a sodium cation near their planes but displaced slightly towards the centre of the sodalite cage. The four S6R rings that have a sited cation give a tetrahedral arrangement around the anion. Small cation to anion distances causes the blue-shift of the ν_1 band. A similar blue-shift for chromates occluded in β-cages of zeolites would require small cation to anion distances and therefore the occupation by sodium cations of four of the eight S6R rings of the β-cage. The zeolite cation site equivalent to those of nosean is $S_{II'}$ the occupancy of which is low for X and Y type zeolites.[30] A chromate occluded within a β-cage is therefore likely to be surrounded by only the two sodium cations that accompanied it into the cage. These two cations would locate near the $S_{II'}$ site, would be coordinated with the chromate anion, and would give a similar ν_1 frequency to that of α-cage occluded chromate. Such coordination within the β-cages of Cr^{nos} has been inferred in later work (see Section 5.4.13) from the red-shift of the ν_1 Raman band from 856 ± 1 cm^{-1} for Cr^{nos} to 851 ± 1 cm^{-1}. The expectation therefore is that differentiation between α-cage and β-cage occluded chromates on the basis of their Raman spectra would not be possible.

Chapter Four References

1) Ermolenko, N.F, Levina, S.A., and Pansevitch-Kolada, L.V., *Dokl. Akad. Nauk B. SSR*, **8**(6) (1964) 394.

2) Garwood, W.E., Lucki, S.J., Chen, N.Y., and Bailar (Jr), J.C., *Inorganic Chemistry*, **17**(3) (1978) 610.

3) Snowdon, T.J., in "**Some Aspects of theLoading of Zeolites with Sodium Chromate**", M.Sc. Thesis, The University of Waikato, Hamilton, New Zealand (1989).

4) Breck, D.W, in "**Zeolite Molecular Sieves**", John Whiley & Sons (Canada), 1974, pp. 176.

5) as in Ref. 4, pp. 155.

6) Carter, R.L. and Bricker, C.E., *Spectrochimica Acta*, **30A** (1974) 1793.

7) Stammerich, H., Bassi, D., and Sala, O., *Spectrochimica Acta*, **13** (1958) 403.

8) Miller, F.A., Carlson, G.L., and White, W.B., *Spectrochimica Acta*, **14** (1959) 709.

9) Hobbs, W.E., *J. Chem. Phys.*, **28** (1958) 1220.

10) Richer, J.C. and Hachey, J.M., *Can. J. Chem.*, **53** (1975) 3087.

11) Stammerich, H., Bassi, D., and Sala, O., *Spectrochimica Acta*, **13** (1950) 403.

12) Campbell, J.A., *Spectrochimica Acta*, **21** (1965) 1333.

13) Feilchenfeld, H. and Siiman, O., *J. Phys. Chem.*, **90** (1986) 4590.

14) Iannibello, A., Marengo, S., Tittarelli, P., *J. Chem. Soc. Faraday Trans. I*, **80** (1984) 2209.

15) Cartner, A.M., *personal communication*, (June, 1993).

16) Henderson, C.M.B. and Taylor, D., *Spectrochimica Acta*, **33A** (1977) 283.

17) Cordischi, D., Vickerman, J.C., and Cimino, A., *Trans. Faraday Soc.*, (1970) 1312.

18) Breck, D.W, in "**Zeolite Molecular Sieves**", John Whiley & Sons (Canada), 1974, pp. 461.

19) Contarini, S. Aduru. S., and Rabalais, J.W., *J. Phys. Chem..*,**90** (1986) 3202.

20) Merryfield, R., McDaniel, M., and Parks, G., *J. Catal.*, **77** (1982) 348.;
Okamoto, Y., Fujii, M., Imanaka, T, and Teraniski, S., *Bull. Chem. Soc. Japan*, **49(4)** (1976) 859.;
Cimino, A., DeAngelis, B.A., Luchetti, A., and Minelli, G., *J. Catal.*, **45** (1976) 316.;
Allen, G.C., Curtis, M.T., Hooper, A.J., and Tucker, P.H., *J. Chem. Soc., Dalton Trans.*, (1973) 1675.

21) G.T. Kerr, E. Dempsey and R.J. Mikovsky, *J. Phys. Chem.*, **69** (1965) 4050 .

22) J. Uytterhoeven, L.G. Christner and W.K. Hall, *J. Phys. Chem.*, **69** (1965) 2117.

23) C.L. Angell and P.C. Schaffer, *J. Phys. Chem.*, **69** (1965) 3463 .

24) J.W. Ward, *J. Catal.*, **10** (1968) 34 .

25) A.V. Kucherov and A.A. Slinkin, *Zeolites*, **7** (1987) 38-46.

26) Gainsford, G., *personal communication*, (November, 1992)

27) Özkar, S., Ozin, G.A., Moller, K., and Bein, T., *J. Am. Chem. Soc.*, **112** (1990) 9575.

28) Abdo, S., Howe, R.F., *J. Phys. Chem.*, **87** (1983) 1713;
You-Sing, Y. and Howe, R.F., *J. Chem. Soc. Faraday Trans. I*, **82** (1986) 2887;
Okamoto, Y., Maezawa, A., Kane, H., Mitsushima, I. and Imanaka, T., *J. Chem. Soc. Faraday Trans.*, **84** (1988) 851;
Coddington, J.H., Howe, R.F., Yong, Y.S. Asakara, K. and Iwasawa, Y, *J. Chem. Soc. Faraday Trans.*, **86(6)** (1990) 1015.

29) Hermann, W.A., *J. Organomet. Chem.*, **300** (1986) 111.

30) Almond, M.J., Crayston, J.A., Downs, A.J., Poliakoff, M., Turner, J., *Inorg. Chem.*, **25** (1986) 19.

31) Moller, K. Bein, T., Özkar, S. and Ozin, G.A., *J. Phys. Chem.*, **95** (1991) 5276.

32) Özkar, S., Ozin, G.A. and Prokopowicz, R.A., *Chem. Mater.*, **4** (1992) 1380.

33) Breck, D.W, in "**Zeolite Molecular Sieves**", John Whiley & Sons (Canada), 1974, pp. 100-101.

34) Rabo, J.A., Poutsma, M.L., and Skeels, G.W., *Proc. Int. Congr. Catalysis* 5^{th}, North Holland Publishing Co., pp. 1353.

35) Carter, E.L. and Bricker, C.E., *Spectrochimica Acta*, **27A** (1971) 569.

36) Ozin, G.A., *Advanced Materials*, **4(10)** (1992) 612.

Chapter Five

Intracage Reactions of Chromate Zeolites

Chapter Five

Intracage Reactions of Chromate Nosean and Chromate Zeolites

5.1 Introduction

Within this work we have prepared several types of zeolites containing various amounts of occluded chromate, molybdate, and tungstate oxyanions. In this chapter, studies of the redox reactions of sodium chromate salt and a variety of loaded zeolites are reported and details of the mechanisms of these reactions are deduced. An effect of the degree of chromate loading on the redox products was observed and rationalised. Differences between occluded chromate, molybdate, and tungstate were observed and explained.

5.2 Methods and Materials

Methods and materials involved in the work reported in this chapter were discussed in Chapter Two. Samples examined are sodium chromate salt, Cr^{nos}, 2.1CrX, 5.8CrX, 13.6CrX, 4.8Cr5A, 32.3Cr5A, 2.3MoX and 1.9WX. Details of the syntheses of the zeolites can be seen in Table 2.2.

5.3 Results

5.3.1 Redox Reactions of Sodium Chromate Salt

A sample of sodium chromate was heated in a porcelain crucible at 850°C for 24 hours followed by cooling to 120°C in an oven and storage in a desiccator over dry silica gel. This treatment ensures that sodium chromate is anhydrous Na_2CrO_4 and not the tetrahydrate $Na_2CrO_4.4H_2O$.[1]

Redox Products

Reaction of sodium chromate and hydrogen at 400 ± 5°C formed a dark green crystalline powder, Na_2CrO_4(R), that gave the PXRD pattern shown in Figure 5.1 (a). PXRD data obtained from the pattern is given in Table 5.9 and is characteristic of a $NaCrO_2$ phase (PDF 18-1209). Na_2CrO_4(R) exhibited a strong symmetrical EPR signal characteristic of a Cr(III) species.

Na_2CrO_4(R) did not appear to dissolve or react with water. Where the chromium solid touched the quartz glass reaction chamber the surface was deeply etched. Removal of Na_2CrO_4(R) left the surface covered with a small amount of a lumpy white material. This material was washed from the glass by distilled water at 90°C to form a basic solution. Uptake of 1.58 ± 0.04 moles of H_2 per mole of Cr at 400 ± 5°C indicated reduction to an average oxidation state of Cr(+2.84 ± 0.08).

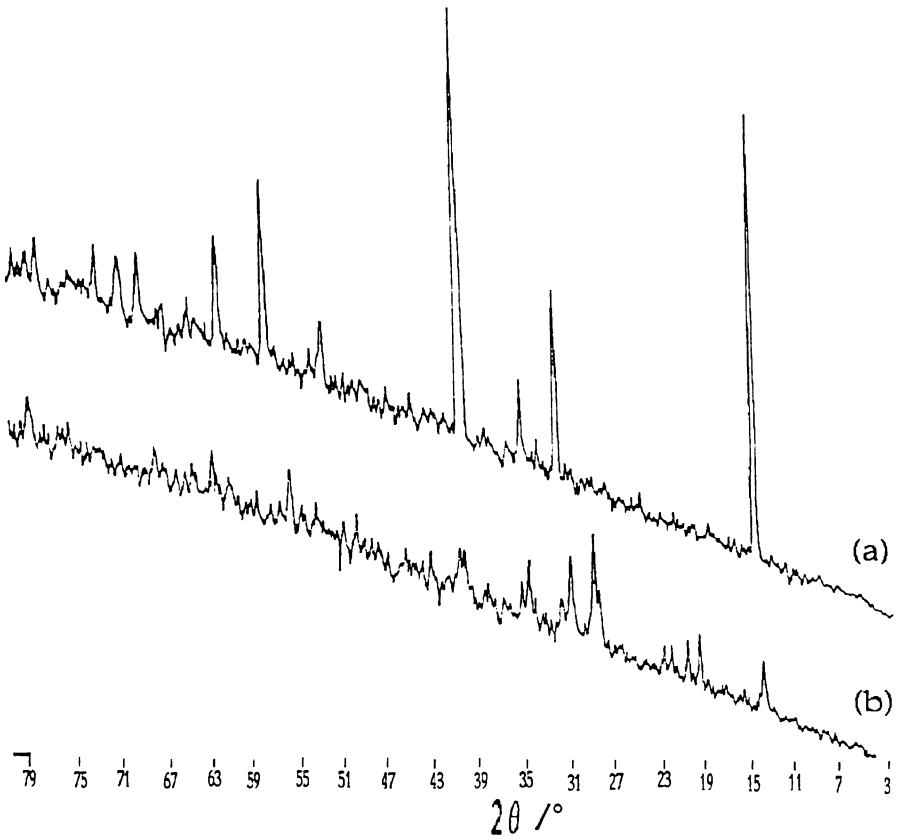


Figure 5.1 PXRD patterns of the products of the redox reactions of sodium chromate salt: The pattern of Na_2CrO_4(R), (a), is that of the product of the reduction of sodium chromate salt by hydrogen gas at 500°C and is characteristic of $NaCrO_2$. The pattern of Na_2CrO_4(R,O), (b), is that of the product of the reoxidation of Na_2CrO_4(R) by oxygen gas at 600°C and indicates the presence of $NaCrO_2$ and Na_2CrO_4 phases. Both patterns were recorded on the intensity range of $2x10^3$ and have the same vertical scale in the figure. 1 cm on the figure equals 2.73 cm on the original pattern or 10.9% of full scale deflection.

Reoxidation of Na_2CrO_4(R) by oxygen gas at 600 ± 5°C gave a lighter green coloured solid, Na_2CrO_4(R,O), that gave the PXRD pattern shown in Figure 5.1 (b). PXRD data obtained from the pattern is given in Table 5.1 and indicates the presence of Na_2CrO_4 and $NaCrO_2$ phases. Product Na_2CrO_4(R,O) was highly hygroscopic adsorbing water from the atmosphere and when added to water gave a yellow solution containing chromate and a green precipitate. A 0.745 g sample of Na_2CrO_4(R,O) gave 0.596 g of soluble chromate and 0.159 g of green precipitate. Atomic adsorption analysis of soluble product gave a Na to Cr ratio of 1.9 ± 0.1 consistent with Na_2CrO_4. Na_2CrO_4(R,O) exhibited the EPR signal observed for Na_2CrO_4(R) but with an intensity only 3% that of

Na_2CrO_4(R). A sample, named Na_2CrO_4(0.4), was prepared from a physical mixture of 0.4008 g Na_2CrO_4, 0.5961 g silica gel, and 0.0314 g Na_2CrO_4(R). Table 5.2 shows the PXRD data for the intensities of the Na_2CrO_4 peaks for Na_2CrO_4(R,O) and Na_2CrO_4(0.4).

Heating a physical mixture containing 0.50 g of Na_2CrO_4(R,O) and 0.21 g of NaOH at 500°C for 2 hours resulted in the formation of a bright yellow solid with a PXRD pattern characteristic of Na_2CrO_4.

Table 5.1 Data obtained from the PXRD patterns of Na_2CrO_4(R), Na_2CrO_4(R,O), and compared to the PXRD data of $NaCrO_2$ (PDF 18-1209) and Na_2CrO_4 (PDF 22-1365). The pattern of Na_2CrO_4(R,O) exhibits peaks of both $NaCrO_2$ and Na_2CrO_4 .(*) indicates the most intense peak of Na_2CrO_4 to which all other Na_2CrO_4 peaks are evaluated. (#) indicates the most intense peak of $NaCrO_2$ to which all other $NaCrO_2$ peaks are evaluated.

Na_2CrO_4(R)		$NaCrO_2$	Na_2CrO_4		Na_2CrO_4(R,O)
d/Å	I/I_1	d and (I/I_1)	d and (I/I_1)	d/Å	I/I_1
5.34	100	5.32 (70)		5.57	95
			5.073 (65)	5.15	53
			3.885 (65)	3.95	44
			3.574 (40)	3.63	32
			2.932 (60)	2.97	59
			2.897 (100)	2.93	100(*)
			2.733 (70)	2.75	76
2.66	42	2.66 (20)		2.69	59
2.55	8	2.542 (20)		2.53	47
2.46	19	2.451 (40)		2.49	100
			2.477 (25)	2.46	44
2.16	100	2.164 (100)		2.19	100(#)
			2.171(13)	2.17	44
			2.036 (19)	2.05	35
			1.944 (12)	1.96	29
			1.795 (15)	1.80	41
1.71	15	1.707 (10)	1.787 (18)	1.76	29
			1.651 (11)	1.65	29
1.58	40	1.578 (20	1.620 (19)	1.63	56
1.49	26	1.487 (40)		1.48	42
			1.495 (14)	1.47	47

Table 5.2 Intensities of the Na_2CrO_4 peaks in the PXRD patterns of samples Na_2CrO_4(R,O)(I^*) and Na_2CrO_4(0.4) ($I^{\#}$).

d :	5.40	4.11	3.93	3.60	2.95	2.92	2.75	2.49
$I^{\#}$:	4	8	7	4	8	11	12	7
I^* :	4	9	8	5	10	17	12	10

XPS Analysis of Sodium Chromate and Redox Products

Cr 2p binding energies of 578.0 ± 0.2 and 579.4 ± 0.2 eV are characteristic of Cr(III) and Cr(VI) species respectively. The O 1s binding energies of Na_2O, Na_2CrO_4, $NaCrO_2$, and Cr_2O_3 are identical so the stoichiometries of mixed oxides cannot be determined from O chemical shifts.[2] The O 1s binding energies of M-O and H-O, however, differ appreciably from 530.0 ± 0.2 eV to 531.5 ± 0.5 eV respectively. This difference in O 1s binding energy and the difference in Cr 2p binding energy of Cr(VI) and Cr(III) allowed the atomic concentrations of Cr(III), Cr(VI), M-O, and H-O shown in Table 5.3 to be calculated from the XPS spectra of Na_2CrO_4, Na_2CrO_4(R) and Na_2CrO_4(R,O). The atomic concentrations of sodium chromate given by Contarini *et al.*[2] and those determined is this study are similar. Compositions of the samples are $Na_{2.0}CrO_{4.0}$ for chromate salt, $Na_{3.9}CrO_{8.1}$ for Na_2CrO_4(R), and $Na_{2.0}CrO_{3.8}$ for Na_2CrO_4(R,O).

Table 5.3 Binding energies and atomic concentrations of species in the surface layers of sodium chromate salt and its redox products. Samples are sodium chromate (Na_2CrO_4), reduced sodium chromate (Na_2CrO_4(R)), and the oxidised product of reduced sodium chromate (Na_2CrO_4(R,O)). Binding energies were calculated relative to C 1s at 285.0 eV.

Sample	Species	Binding Energy	Atomic Conc. /%	
Na_2CrO_4	Na 1s	1071.4	28.9	28.9
	Cr 2p Cr(VI)	579.4	12.3	
	Cr(III)	577.9	2.1	14.4
	O 1s O-M	529.8	51.2	
	O-H	532.9	6.4	57.6
Na_2CrO_4(R)	Na 1s	1071.7	29.8	29.8
	Cr 2p Cr(VI)	580.1	1.7	
	Cr(III)	577.1	6.0	7.7
	O 1s O-M	530.3	8.6	
	O-H	532.9	53.8	62.4
Na_2CrO_4(R,O)	Na 1s	1071.3	29.0	29.0
	Cr 2p Cr(VI)	579.3	13.0	
	Cr(III)	577.2	1.8	14.8
	O 1s O-M	529.8	47.2	
	O-H	531.6	8.9	56.1

Significant quantities of Cr(III) are present in the surface layers of Na_2CrO_4 and Na_2CrO_4(R,O). While the presence of Cr(III) in Na_2CrO_4(R,O) could be interpreted in terms of incomplete reoxidation, that in Na_2CrO_4 can only be explained in terms of reduction during evacuation prior to XPS analysis. Quantitative XPS data has shown that fresh Li, Na, and K chromates have a chromate substrate with a thin overlayer of oxides and hydroxides.[2] Such an overlayer presumably forms during outgassing prior to XPS analysis. Under ion and electron radiation the overlayer grows. Increases in Cr(III) and (OH) concentrations were attributed to decomposition of chromate as shown below.

$$2\,Na_2CrO_4 + 2\,H_2O \longrightarrow Cr_2O_3 + 4\,NaOH + \frac{3}{2}O_2$$

The formation of an overlayer was consistent with the proposed mechanism involving the formation of a non-volatile chromium species with a large negative free energy of formation.

Reduction resulted in a loss of Cr(VI) and an increase in Cr(III) and an overall depletion of Cr in the surface layer. The concentration of M-O decreased while that of H-O increased. These changes in concentrations suggest an accumulation of NaOH in the surface layer. The composition of Na_2CrO_4(R) of $Na_{3.9}CrO_{8.1}$ reflects these changes The Na to Cr ratio and the O-H content are consistent with the formation of a $NaCrO_2{\cdot}3NaOH{\cdot}3H_2O$ phase. Retention of water during redox reactions is unlikely due to the vacuum and elevated temperatures employed. The adsorption of water upon exposure of the sample to air subsequent to redox reactions would increase the H-O content. Pure NaOH is deliquescent. Similar hygroscopic properties of NaOH in Na_2CrO_4(R) would promote the adsorption of water from the atmosphere. Strong adsorption of such water by the NaOH may be the cause of the retention of water. Another possibility is that the overlayer prevents outgassing. Such a phenomenon has been reported upon Ar^+ bombardment of $(NH_4)_2CrO_4$ prior to XPS analysis.[2]

Cyclic Redox Reactions

The effect of cyclic redox reactions of chromate salt on the average chromium oxidation state is shown in Figure 5.2. Reaction with O_2 at 600 ± 5°C for 23.3 hours subsequent to the first reduction to ~Cr(III) reoxidised the chromium to an average oxidation state of Cr(+4.6 ± 0.2). Subsequent redox reactions resulted in average oxidation state transitions between ~Cr(+4.7) and ~Cr(+3.0).

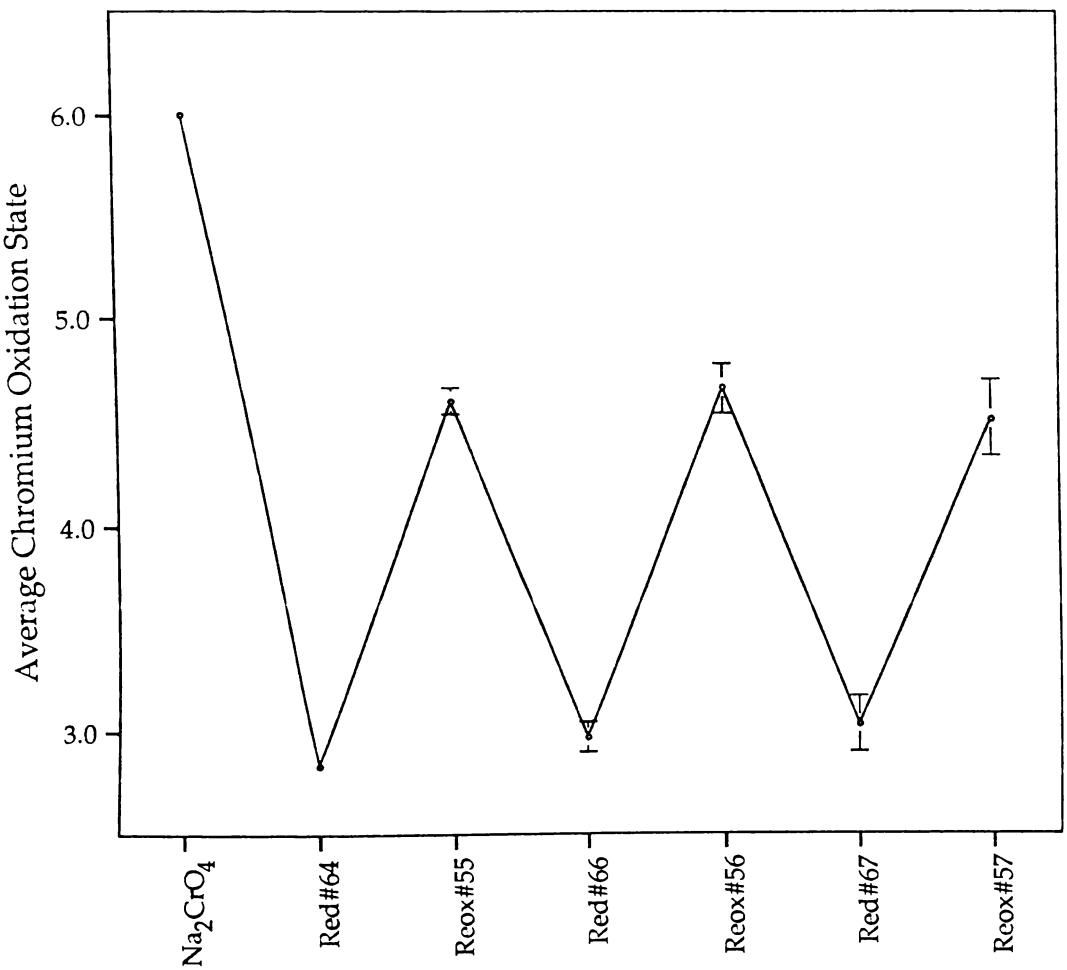


Figure 5.2 Average chromium oxidation state as a function of cyclic redox reactions on sodium chromate salt. Reaction temperatures are: Red#64 (400°C), Reox#55 (600°C), Red#66 (400°C), Reox#56 (600°C), Red#67 (600°C), and Reox#57 (600°C).

5.3.2 Redox Reactions of 13.6CrX

Figure 5.3, Figure 5.4, and Figure 5.5 show the PXRD, FTIR and EPR spectra, respectively, of 13.6CrX and the products of various redox treatments.

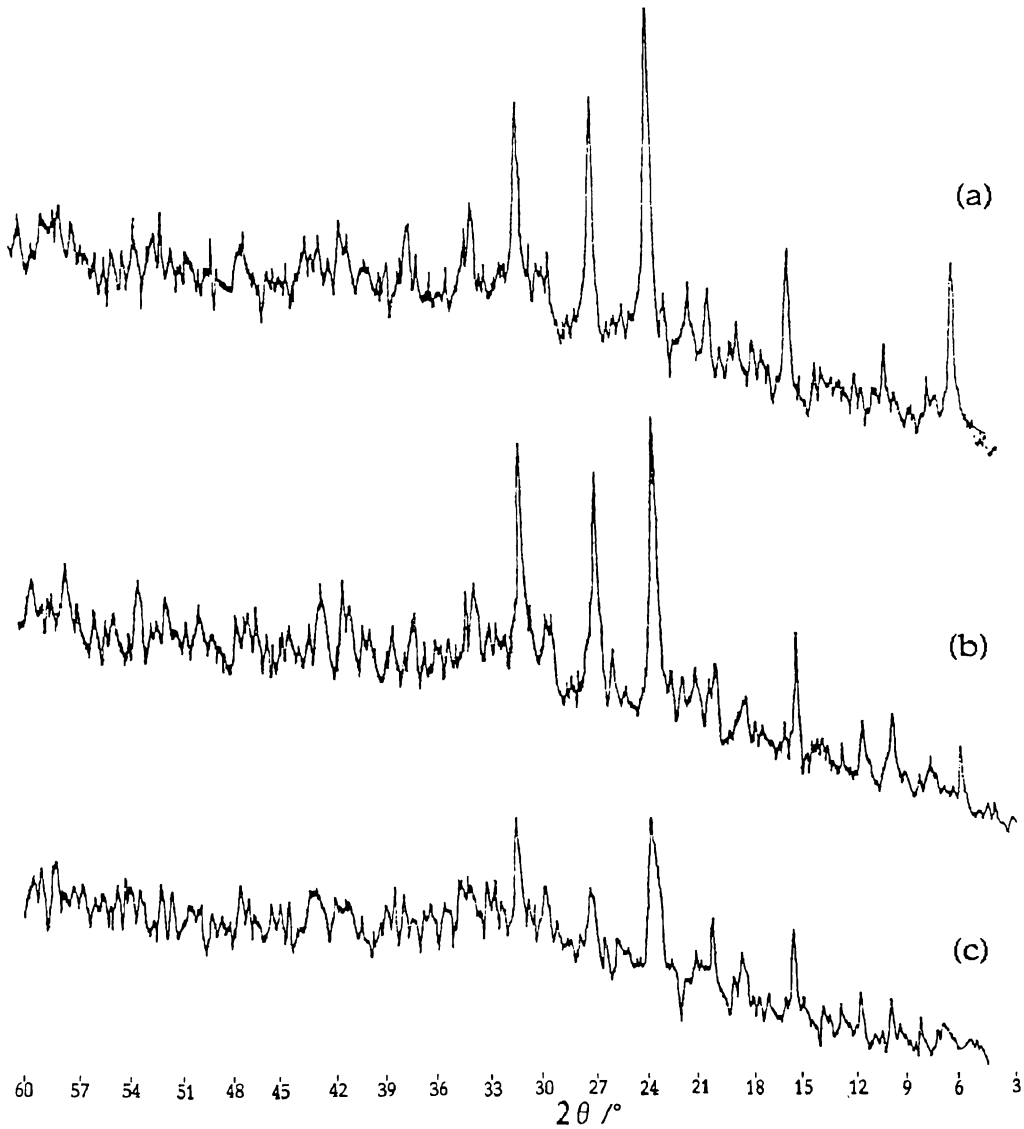


Figure 5.3 Effect of various redox treatments on the PXRD pattern of the zeolite 13.6CrX. Samples are: (a) parent zeolite 13.6CrX, (b) reduction by hydrogen gas at 250°C to form 13.6CrX(R250), (c) reduction by hydrogen gas at 375°C to form 13.6CrX(R375). All patterns were recorded on the intensity range of $1x10^3$. 1 cm on the figure equals 2.71 cm on the original pattern or 10.8% of full scale deflection.

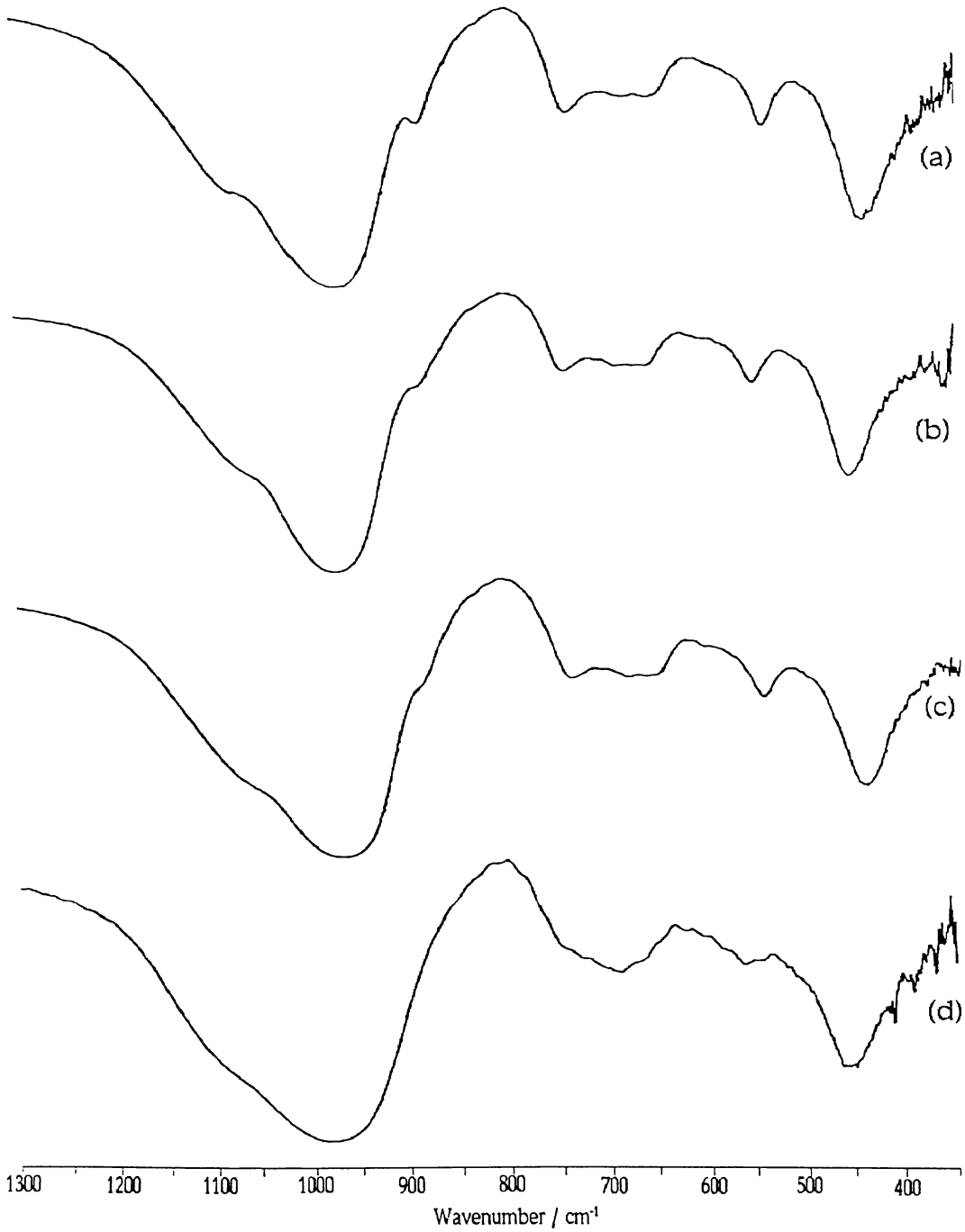


Figure 5.4 Effect of various redox treatments on the IR spectrum of the zeolite 13.6CrX. Samples are: (a) parent zeolite 13.6CrX, (b) evacuation at 375°C for 24 hours to form 13.6CrX(evac), (c) reduction by hydrogen gas at 250°C to form 13.6CrX(R250), and (d) reduction by hydrogen gas at 375°C to form 13.6CrX(R375).

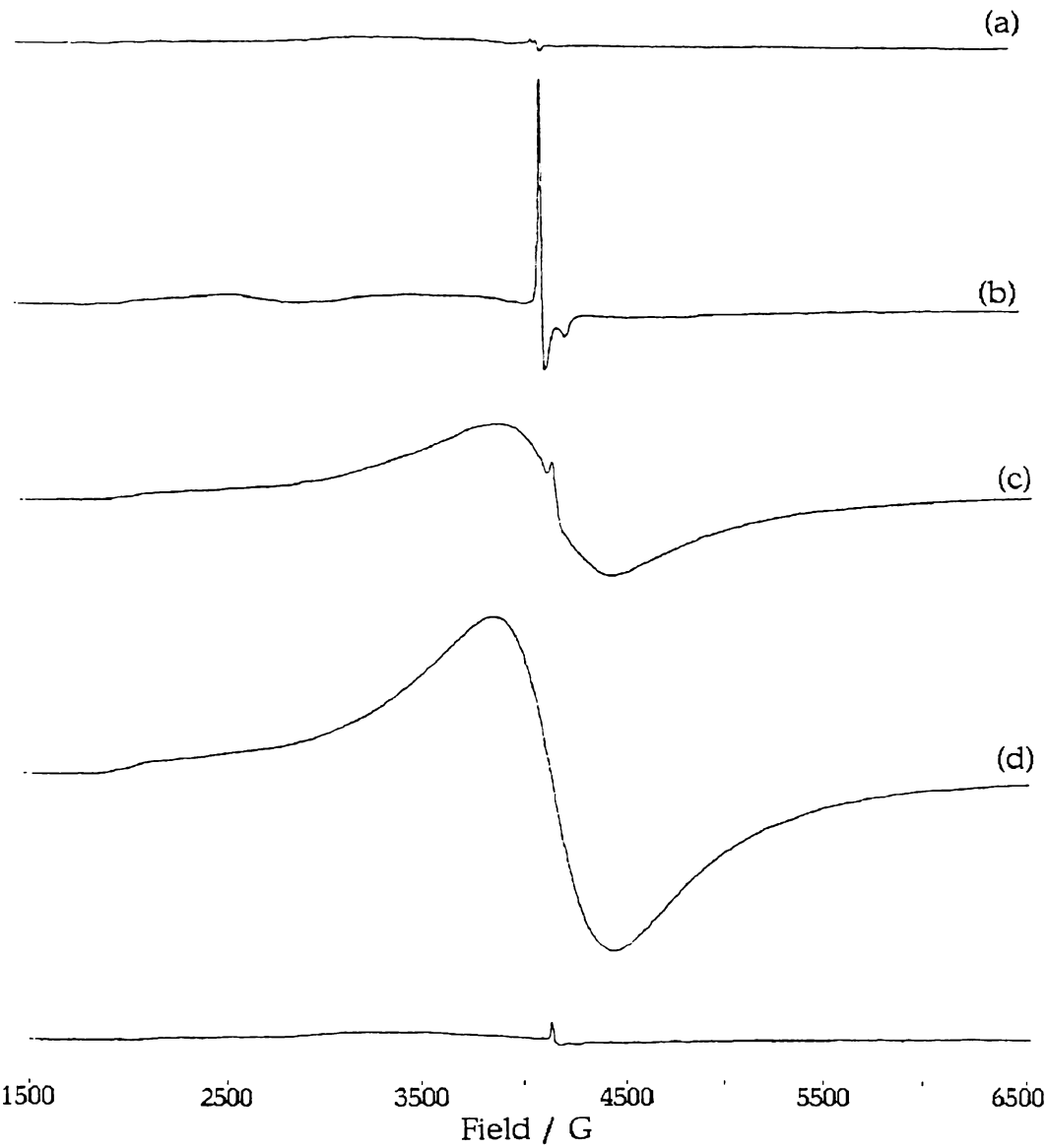


Figure 5.5 Effect of various redox treatments on the EPR spectrum of the zeolite 13.6CrX. Samples are: (a) parent zeolite 13.6CrX, (b) evacuation at 375°C to form 13.6CrX(evac), (c) reduction by hydrogen gas at 250°C to form 13.6CrX(R250), (d) reduction by hydrogen gas at 375°C to form 13.6CrX(R375), and (e) oxidation of 13.6CrX(R375) by oxygen gas at 500°C to form 13.6CrX(O500). All spectra were recorded with a gain of 1.6×10^2 and have the same range in the vertical figure. 1 cm on this figure equals 2.72 cm on the original trace.

Product 13.6CrX(evac)

Evacuation of 13.6CrX at 375 ± 5°C for 24 hours resulted in the appearance of a sharp anisotropic EPR signal (ΔH = 175 G, $g_{\perp} = 1.986 \pm 0.002$, $g_{\parallel} = 1.917 \pm 0.002$), see Figure 5.5 (b), characteristic of a Cr(V) species of distorted tetrahedral symmetry. The ν_3 chromate IR band at 900 ± 2 cm^{-1} is clearly evident in the spectrum of 13.6CrX. A slight loss of intensity of the ν_3 chromate IR band, see Figure 5.4 (b), was observed while no change to the PXRD pattern occurred. The sample became slightly green.

Product 13.6CrX(R250)

Reaction with hydrogen at 250 ± 5°C resulted in the uptake of 0.63 ± 0.02 moles of H_2 per mole of Cr and a change in colour to yellow-green. The absence of significant change to the PXRD pattern or lattice IR bands indicated no framework degradation. A slight loss of intensity of the ν_3 chromate IR band was observed. Loss of intensity of the Cr(V) EPR signal was accompanied by the appearance of a broad symmetric signal (ΔH = ~4500 G, g = 1.98 ± 0.01) characteristic of a Cr(III) species.

Product 13.6CrX(R375)

Reaction of 13.6CrX with hydrogen at 375 ± 5°C resulted in uptake of 1.26 ± 0.02 moles of H_2 per mole of Cr and a change in colour to dark green. Loss of intensities of the lattice IR bands and the PXRD peaks indicated framework degradation. Zeolite 13.6CrX(R375) gave a broad EPR signal characteristic of a Cr(III) species. The ratio of the Cr(III) EPR peak intensities of 13.6CrX(R375) and 13.6CrX(R250) was 2.2 ± 0.3. In Section 2.6 the concentration of Cr(III) in 13.6CrX(R375) was calculated to be $(3.3 \pm 0.2) \times 10^{-4}$ moles Cr(III)/g.

5.3.3 Redox Reaction of 2.1CrX and 5.8CrX

Average chromium oxidation state as functions of successive redox reactions for 2.1CrX and 5.8CrX are shown in Figure 5.6 and Figure 5.7, respectively. Cyclic redox reactions on the anchored chromates of 2.1CrX resulted in average chromium oxidation state transitions between Cr(VI) and Cr(IV). The EPR spectra of a reduced sample and the levels of hydrogen uptake indicated a lack of reduction to Cr(III) despite an excess of hydrogen gas and prolonged reaction times.

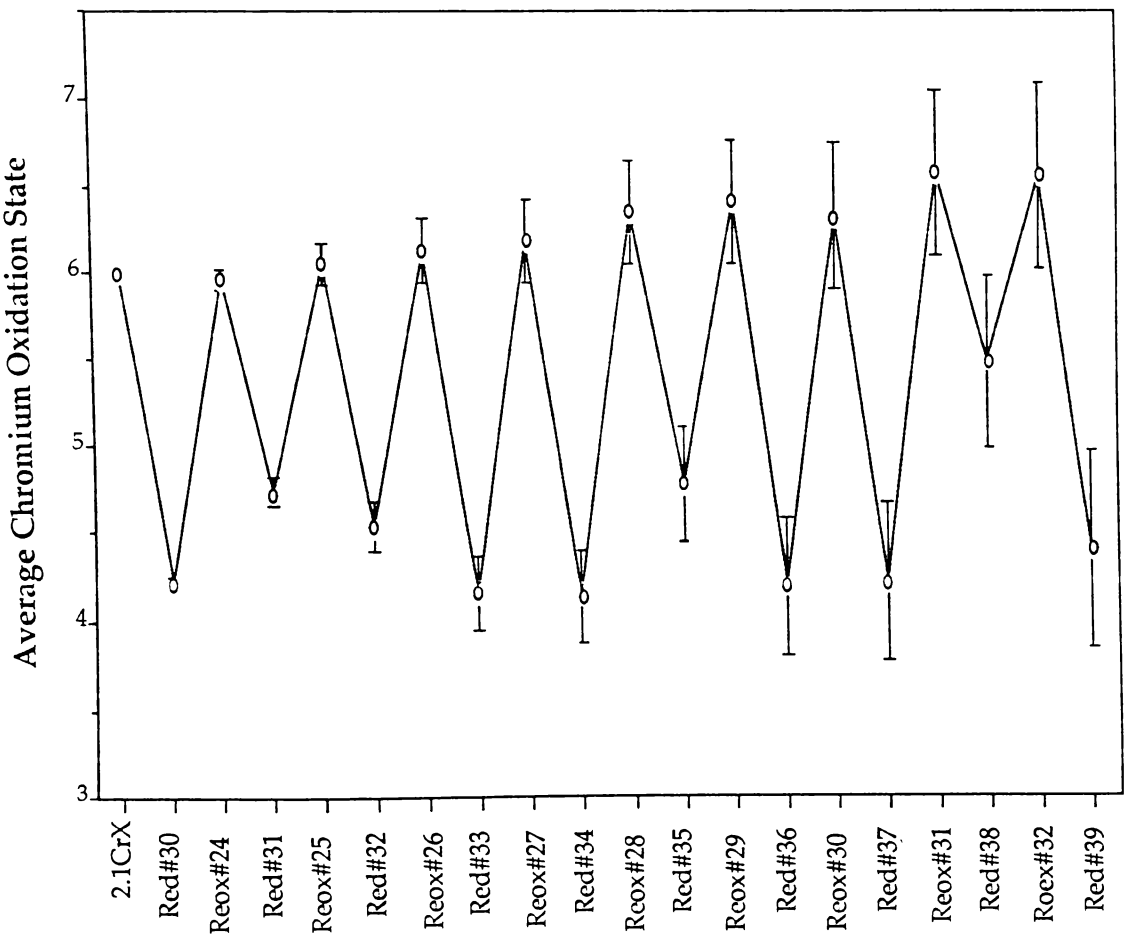


Figure 5.6 Average chromium oxidation state as functions of successive redox reactions of zeolite 2.1CrX. Full reaction conditions can be seen in Appendix Five (Reductions) and Appendix Six (Reoxidations). Given below are the reaction temperatures. Red#30(300°C), Reox#24 (300°C), Red#31 (250°C), Reox#25 (250°C), Red#32 (275°C), Reox#26 (325°C), Red#33 (315°C), Reox#27 (275°C), Red#34 (325°C), Reox#28 (315°C), Red#35 (250°C), Reox#29 (250°C), Red#36 (335°C), Reox#30 (250°C), Red#37 (350°C), Reox#31 (285 C), Red#38 (225°C), Reox#32 (275°C), and Red#39 (375°C).

Chromates of 5.8CrX were reduced to Cr(IV) during the first reduction by reaction with the stoichiometric amount of hydrogen gas. Reoxidation of these Cr(IV) species back to Cr(VI) was possible. Reaction with excess hydrogen during the second reduction lowered the average chromium oxidation state from Cr(VI) to Cr(III). Reoxidation of these Cr(III) species was incomplete ceasing at an average oxidation state of Cr(V) despite prolonged reaction times and an excess of oxygen gas. Stoichiometries of subsequent redox reactions indicated average chromium oxidation state transitions between Cr(III) and Cr(V) or Cr(IV) depending on reoxidation temperature.

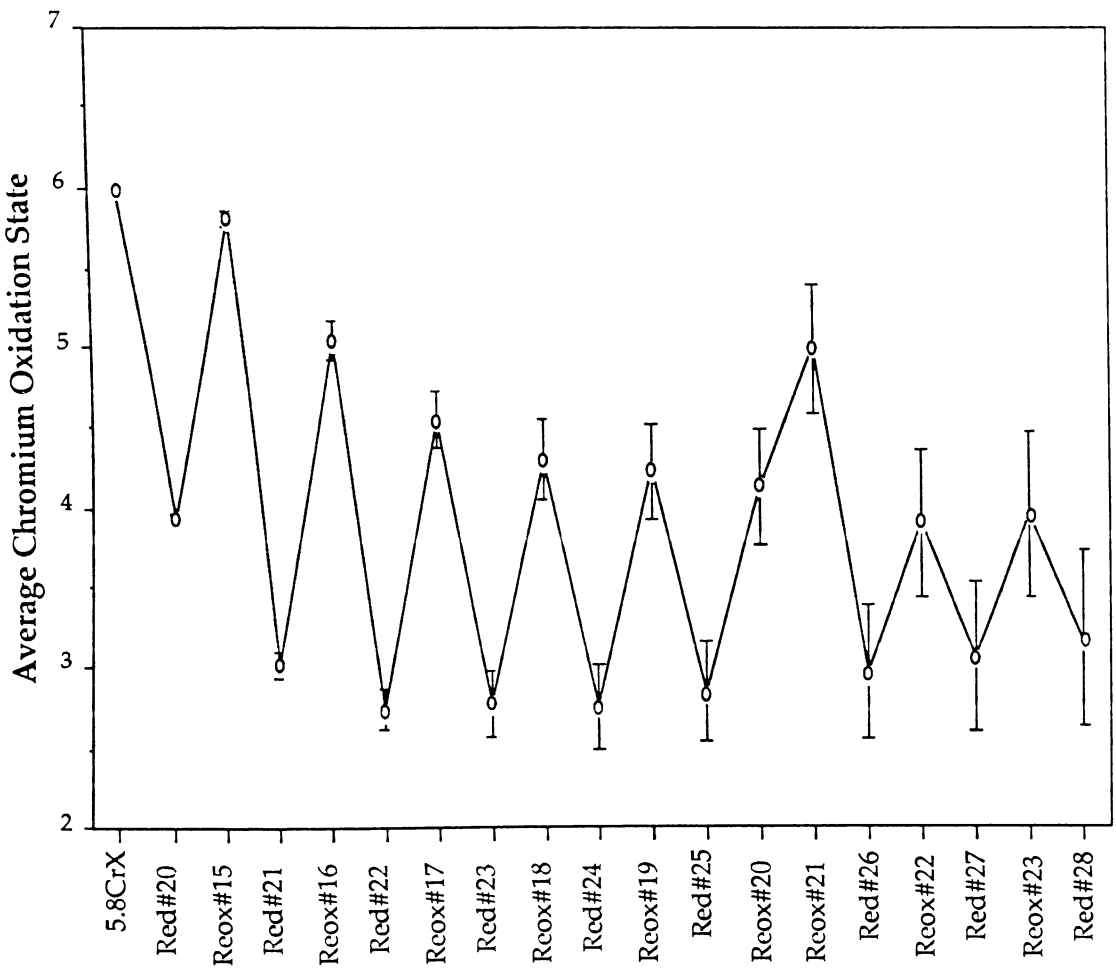


Figure 5.7 Average chromium oxidation state as functions of successive redox reactions of zeolite 5.8CrX. Full reaction conditions can be seen in Appendix Three (Reductions) and Appendix Four (Reoxidations). Given below are the reaction temperatures. Red#20 (350°C), Reox#15 (400°C), Red#21 (350°C), Reox#16 (400°C), Red#22 (350°C), Reox#17 (400°C), Red#23 (325°C), Reox#18 (400°C), Red#24 (375°C), Reox#19 (350°C), Red#25 (300°C), Reox#20 (375°C), Reox#21 (620°C), Red#26 (325°C), Reox#22 (300°C), Red#27 (275°C), Reox#23 (275°C), Red#28 (250°C).

5.3.4 Redox Reactions of 13.4CrY and 2.8CrY

13.4CrY

Figure 5.8 shows the average oxidation state of chromium as a function of successive redox reactions on 13.4CrY. Hydrogen uptake of the first reduction was 1.16 ± 0.04 moles of $H_{2(g)}$ per mole of Cr indicating incomplete reduction to an average oxidation state of Cr(+3.7). Full reoxidation to Cr(VI) occurred at temperatures of 450°C and above while the reoxidation at 400°C resulted in partial reoxidation to an average oxidation state of ~Cr(V). Subsequent redox reactions resulted in transitions between ~Cr(+6) and ~Cr(+3.7).

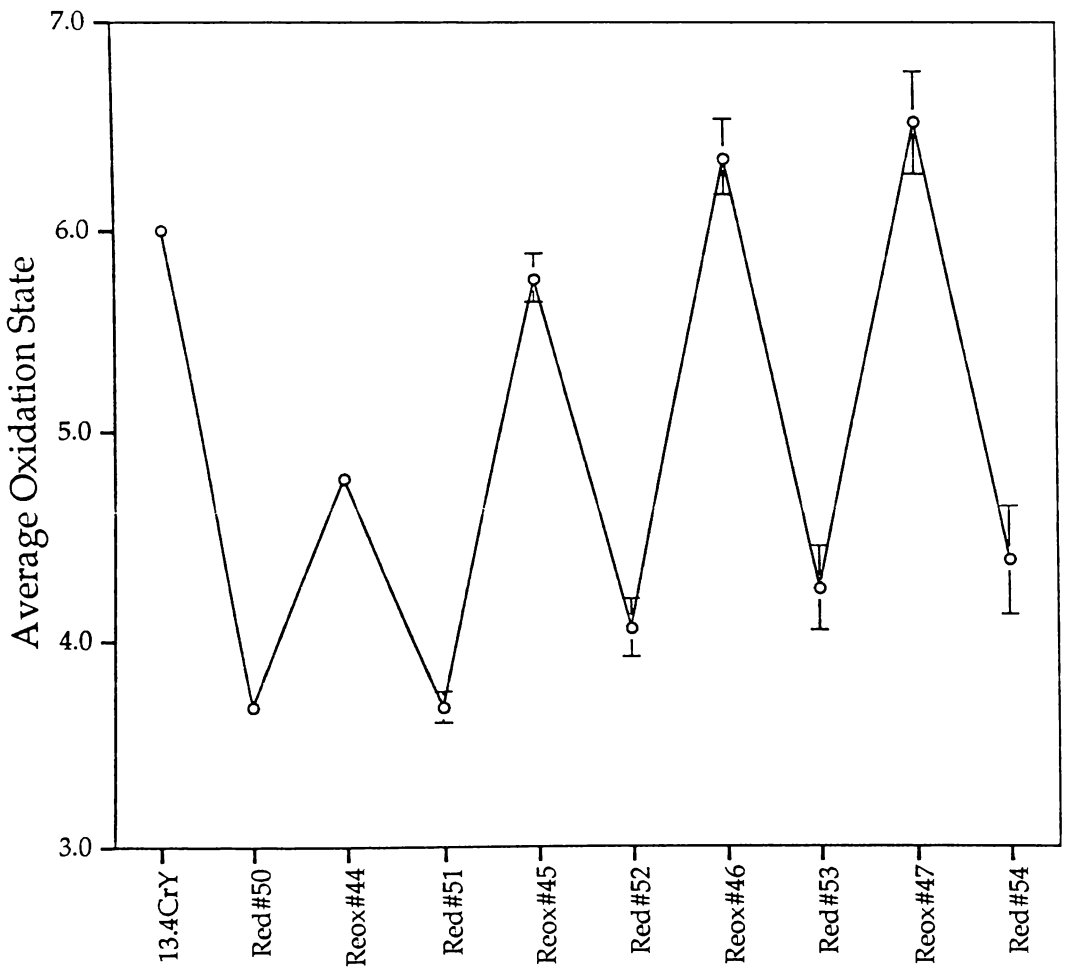


Figure 5.8 Effect of cyclic redox reactions on the average chromium oxidation state of chromates occluded in 13.4CrY. Full reaction conditions can be seen in Appendix Nine (Reductions) and Appendix Ten (Reoxidations). Given below are the reaction temperatures. Red#50 (375°C), Reox#44 (400°C), Red#51 (450°C), Reox#45 (450°C), Red#52 (450°C), Reox#46 (500°C), Red#53 (475°C), Reox#47 (500°C), and Red#54 (475°C).

2.8CrY

Data of the redox reactions of 2.8CrY are shown in Appendix One (Reductions) and Appendix Two (Reoxidations). Hydrogen uptakes per mole of chromium were generally between ~0.4 and ~0.7 indicating average oxidation state changes between ~1 and ~1.5. Oxygen uptakes per mole of chromium were generally between ~0.3 and ~0.6. Oxygen uptakes were greater than expected considering the hydrogen uptakes. This and a change in colour from yellow to yellow-green upon evacuation indicated self-reduction. It was therefore not possible to determine precise oxidation states but reliable oxidation state changes of between ~1.2 and ~2.4 were calculated from the oxygen uptake data.

5.3.5 Redox Reactions of 4.8Cr5A and 32.3Cr5A

Figure 5.9 shows the EPR spectra of a sample of 4.8Cr5A after evacuation and various redox treatments. Few paramagnetic chromium species are present in the original sample. Evacuation at 425 ± 5°C for 24 hours, to form 4.8Cr5A(evac), resulted in the appearance of a narrow asymmetric EPR signal characteristic of a Cr(V) species in a distorted tetrahedral environment. Reduction of 4.8Cr5A(evac) by hydrogen gas at 425 ± 5°C for 24 hours, to form 4.8Cr5A(R425), resulted in the loss of this EPR signal. Evacuation of 4.8Cr5A(R425) at 425 ± 5°C for 24 hours to form 4.8Cr5A(R425e) resulted in no change to the EPR spectrum. Oxidation of 4.8Cr5A(R425) by oxygen gas at 425 ± 5°C for 24 hours, to form 4.8Cr5A(O425), resulted in the reappearance of the Cr(V) signal but of lower intensity than that for 4.8Cr5A(evac).

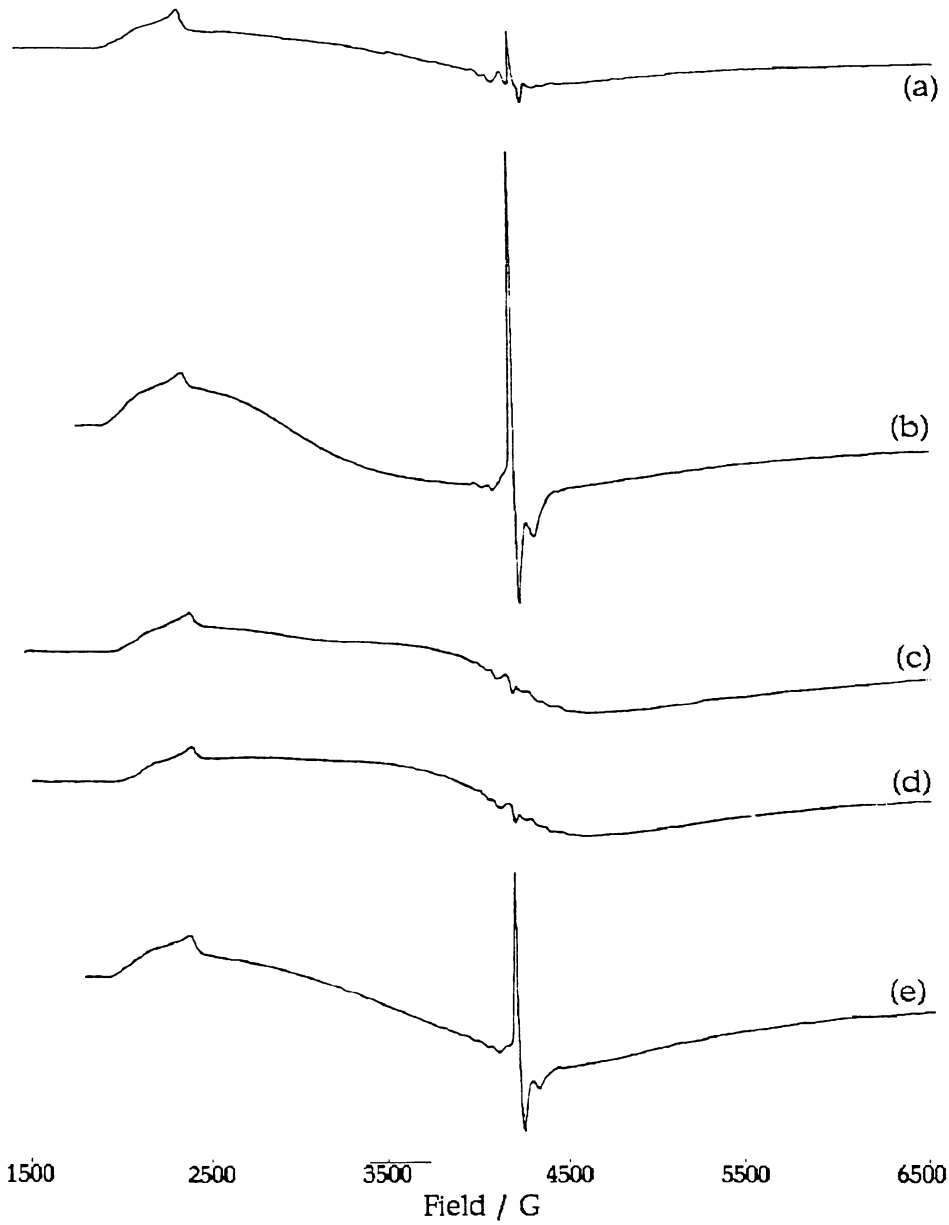


Figure 5.9 Effect of various redox treatments on the EPR spectrum of 4.8Cr5A. Samples are (a) parent zeolite 4.8Cr5A, (b) evacuated at 425°C for 24 hours to form 4.8Cr5A(evac), (c) 4.8Cr5A(evac) reduced by hydrogen gas for 24 hours at 425°C to form 4.8Cr5A(R425), (d) 4.8Cr5A(R425) evacuated at 425°C for 24 hours to form 4.8Cr5A(R425e), (e) 4.8Cr5A(R425e) reoxidised by oxygen gas at 425°C for 24 hours to form 4.8Cr5A(O425). All spectra were recorded on a gain of $4x10^3$. 1 cm on the figure equals 2.70 cm on the original spectrum.

Figure 5.10 shows the average oxidation state of chromium in 4.8Cr5A as a function of successive redox reactions. Results indicate reduction to Cr(III) during the first reduction at 400 ± 5°C. Reoxidation ceased at an average oxidation state of Cr(V) despite prolonged reaction times and excess oxygen gas. Subsequent redox reactions resulted in average oxidation state transitions between Cr(III) and Cr(V) except at 650 ± 5°C where increased oxygen uptake indicated that some Cr(VI) may have been formed.

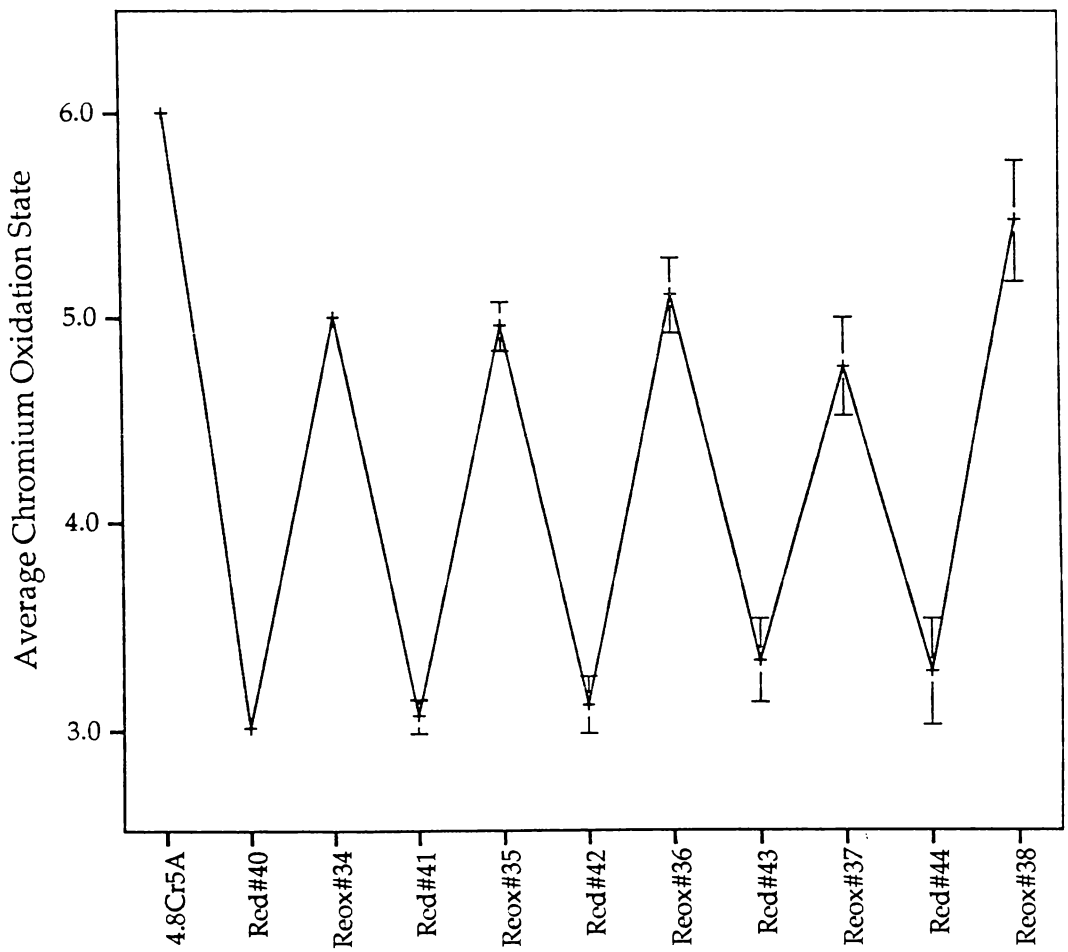


Figure 5.10 Chromium oxidation state as a function of successive redox reactions on zeolite 4.8Cr5A. Full reaction conditions can be seen in Appendix Seven (Reductions) and Appendix Eight (Reoxidations). Given below are the reaction temperatures. Red#40 (400°C), Reox#34 (400°C), Red#41 (450°C), Reox#35 (450°C), Red#42 (500°C), Reox#36 (500°C), Red#43 (400°C), Reox#37 (350°C), Red#44 (550°C), and Reox#38 (650°C).

Reduction of 32.3Cr5A by hydrogen gas at 500°C resulted in the uptake of 1.24 ± 0.04 moles of $H_{2(g)}$ per mole of Cr indicating incomplete reduction to an average oxidation state of Cr(+3.5).

5.3.6 Redox Reactions of Chromate Nosean

Various redox treatments were performed on chromate nosean (Cr^{nos}) to form the products outlined in Table 5.4. Figure 5.11, Figure 5.12, and Figure 5.13 show the PXRD patterns, IR spectra and Raman spectra, respectively, of Cr^{nos} and the products obtained after various redox treatments. Table 5.5 shows the unit cell edges (a_o) and the positions of the framework IR bands of Cr^{nos} and the products after the various redox treatments.

Table 5.4 Products obtained from various redox treatments on Cr^{nos}.

Sample	Redox Treatment
Cr^{nos}	Nil
$Cr^{nos}_{R400/Cr(4.5)}$	Cr^{nos} heated in $H_{2(g)}$ at 400°C for 28 hours. $H_2/Cr = 0.75$
$Cr^{nos}_{R600/Cr(3.5)}$	Cr^{nos} heated in $H_{2(g)}$ at 600°C for 219 minutes. $H_2/Cr = 1.27$
$Cr^{nos}_{R400/Cr(3.5)}$	Cr^{nos} heated in $H_{2(g)}$ at 400°C for 95 hours. $H_2/Cr = 1.26$
$Cr^{nos}_{R400.O600}$	$Cr^{nos}_{R400/Cr(3.5)}$ heated in $O_{2(g)}$ at 600°C for 18 hours. $O_2/Cr = 0.66$
$Cr^{nos}_{R400.O1000}$	$Cr^{nos}_{R400.O600}$ heated in air at 1000°C for 3 hours

Table 5.5 a_os and position of the framework IR bands for Cr^{nos} and the products obtained after various redox treatments.

Sample	a_o / Å	ν_{as}(T-O-T) ± 5 /cm^{-1}	ν_s(T-O-T)[a] ± 1 /cm^{-1}	ν_s(T-O-T)[b] ± 1 /cm^{-1}	ν_s(T-O-T)[c] ± 1 /cm^{-1}	δ(O-T-O)[d] ± 1 /cm^{-1}	δ(O-T-O)[e] ± 1 /cm^{-1}
Cr^{nos}	9.107(2)	1008	721	697	654	457	422
$Cr^{nos}_{R600/Cr(3.5)}$	9.073(6)	999	729	701	658	460	431
$Cr^{nos}_{R400/Cr(3.5)}$	8.916(6)	992	737	715	668	465	440
$Cr^{nos}_{R400.O600}$	9.093(2)	1009	722	696	655	458	424
$Cr^{nos}_{R400.O1000}$	9.111(2)	1007	722	696	654	455	422
$Cr^{nos}_{R400/Cr(4.5)}$	9.119(3)	1007	721	695	654	453	419

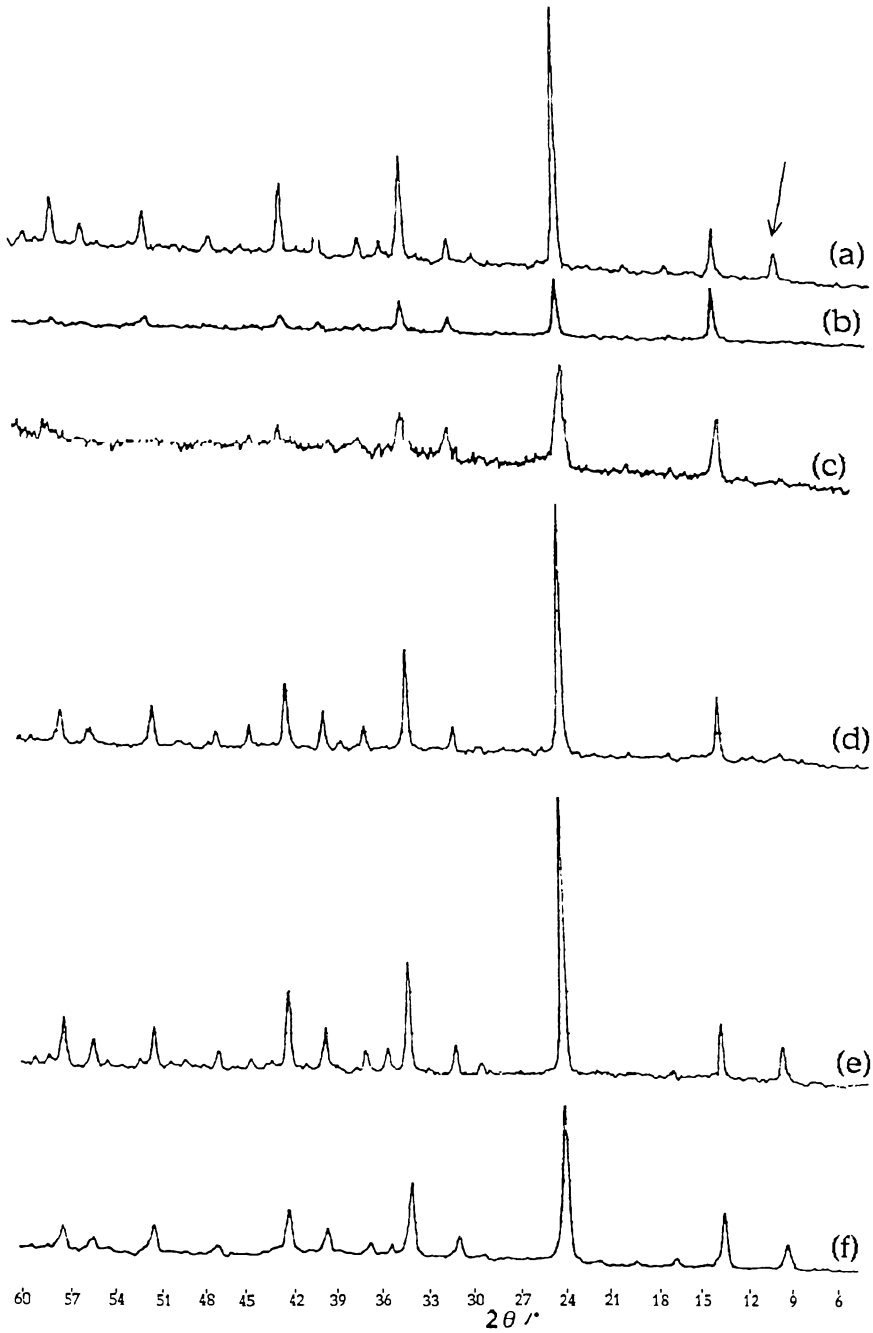


Figure 5.11 PXRD patterns of chromate nosean and products of various redox treatments. Samples are: (a) Cr^{nos} (chromate nosean), (b) $Cr^{nos}_{R600/Cr(3.5)}$ (reduced chromate sodalite), (c) $Cr^{nos}_{R400/Cr(3.5)}$ (reduced chromate sodalite), (d) $Cr^{nos}_{R400.O600}$ (chromate sodalite), (e) $Cr^{nos}_{R400.O1000}$ (chromate nosean), and (f) $Cr^{nos}_{R400/Cr(4.5)}$ (chromate nosean). The arrowed peak arises from the 100 diffraction plane of the noselite framework, the absence of which in the patterns of some samples indicates a sodalite framework. All patterns were recorded on a range of $5x10^3$ and have the same vertical scale in the figure. 1 cm on the figure equals 2.80 cm on the original pattern or 11.2% of full scale deflection.

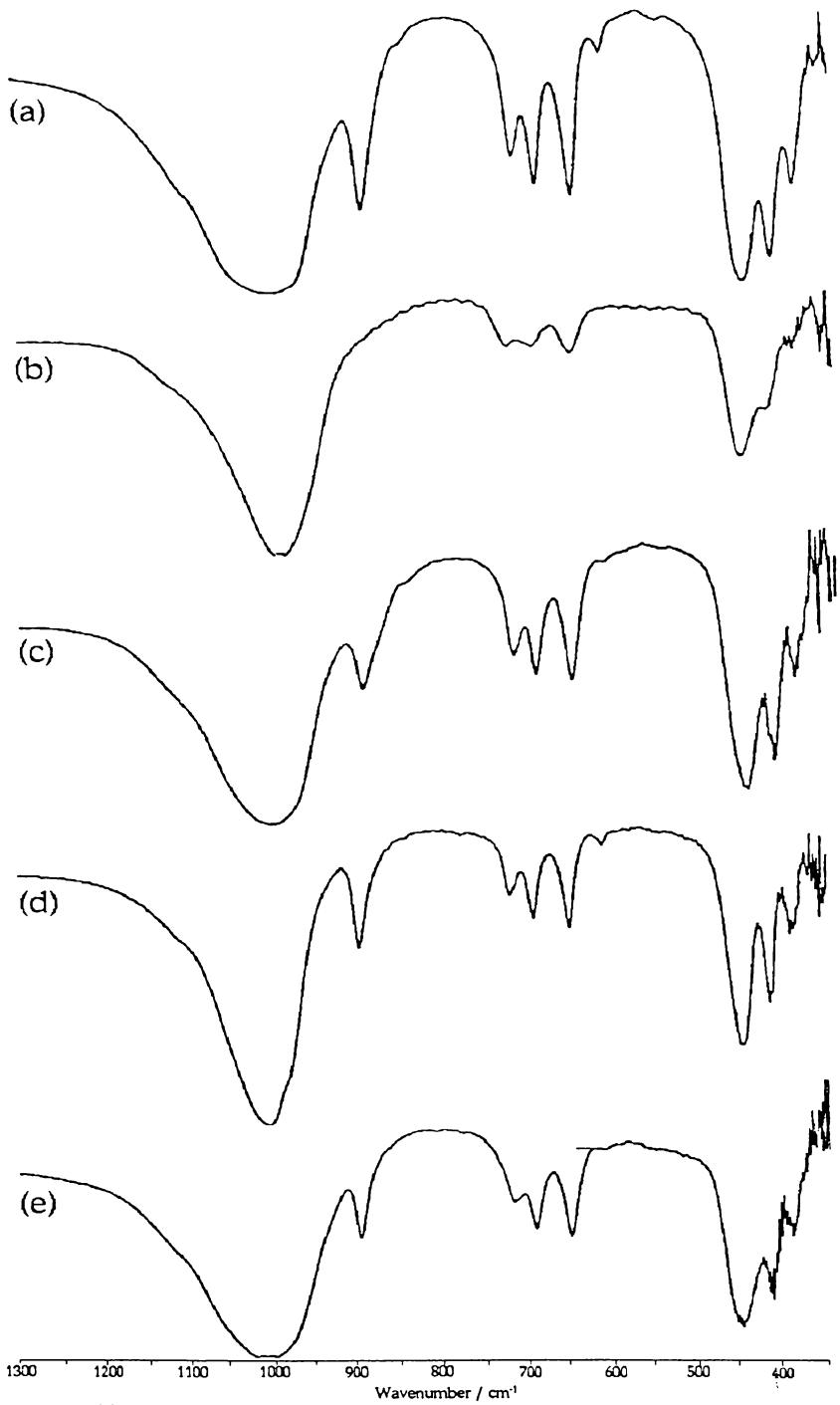


Figure 5.12 Infrared spectra of chromate nosean and products of various redox treatments. Samples are: (a) Cr^{nos} (chromate nosean), (b) $Cr^{nos}_{R400/Cr(3.5)}$ (reduced chromate sodalite), (c) $Cr^{nos}_{R400.O600}$ (chromate sodalite), (d) $Cr^{nos}_{R400.O1000}$ (chromate nosean), and (e) $Cr^{nos}_{R400/Cr(4.5)}$ (chromate nosean). Note the loss of the v_3 chromate band at ~900 cm^{-1} and loss of framework band intensities in the spectrum of reduced chromate sodalite (b). Also evident is the broader chromate v_3 band for chromate sodalite (c) compared to that of chromate nosean (d).

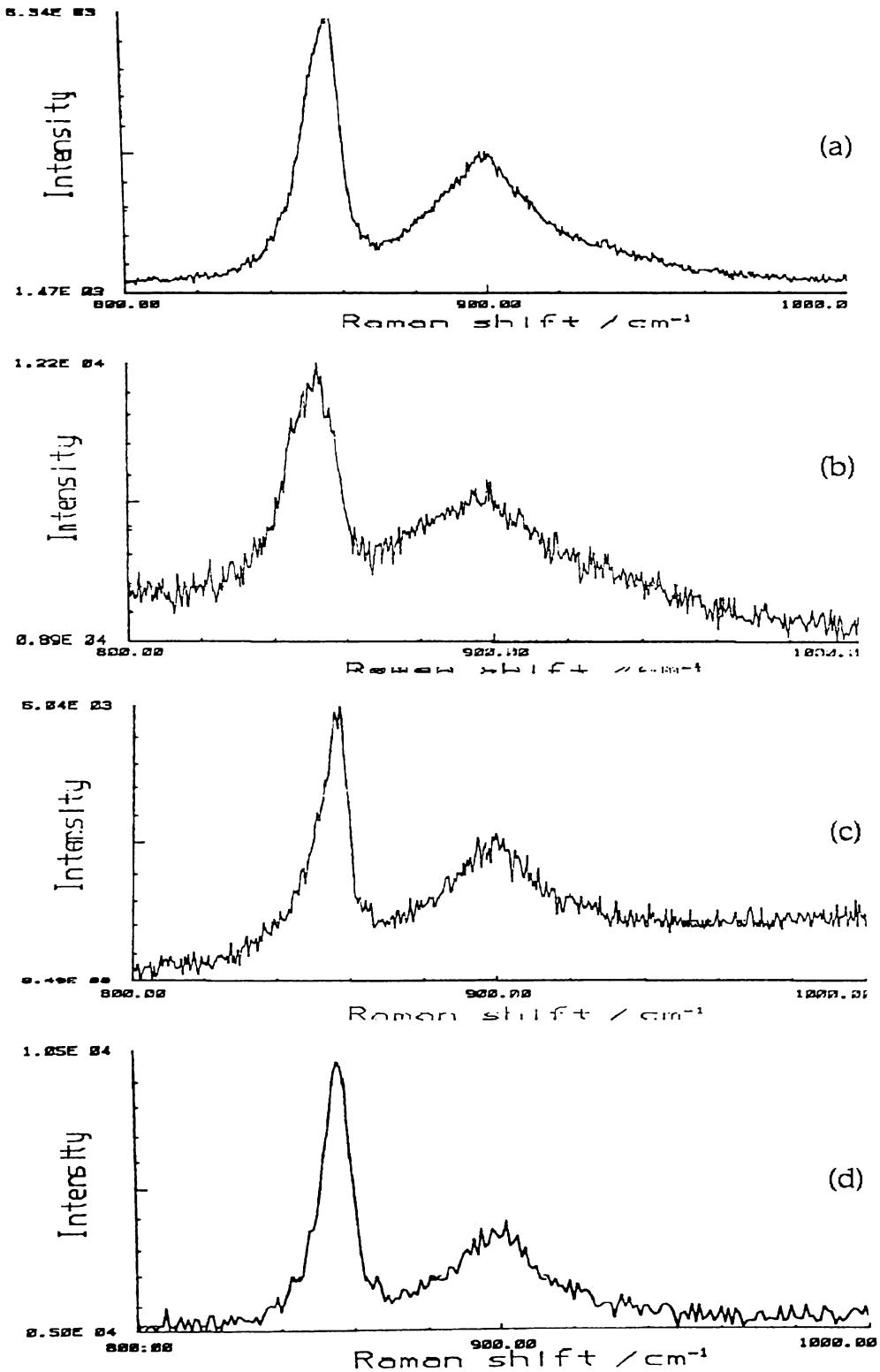


Figure 5.13 Raman spectra of chromate nosean and products of various redox treatments. Samples are: (a) Cr^{nos} (chromate nosean), (b) $Cr^{nos}_{R400.O600}$ (chromate sodalite), (c) $Cr^{nos}_{R400.O1000}$ (chromate nosean), and (d) $Cr^{nos}_{R400/Cr(4.5)}$ (chromate nosean). Note the lower wavenumber position of the ν_1 band of chromate sodalite (b) compared to those of the chromate noselites.

Cr^{nos}

Sharp and intense peaks in the PXRD pattern of Cr^{nos}, see Figure 5.11 (a), indicated high crystallinity. This was reflected by the sharp bands in the FTIR spectrum (Figure 5.12 (a)). Assignment of the bands in the FTIR spectrum, see Table 5.5, was made by comparison to similar systems.[3] Evident in the FTIR spectrum is the ν_3 chromate band at ~900 cm^{-1}. Assignment of the bands in the Raman spectrum were considered earlier (Section 4.4.4) and are ν_1 (856.5 ± 1 cm-1) and ν_3 (900 ± 3 cm^{-1}).

Product $Cr^{nos}_{R400/Cr(4.5)}$

Heating Cr^{nos} in $H_{2(g)}$ at 400 ± 5°C for 28 hours resulted in the uptake of 0.75 ± 0.02 moles of H_2 per mole of Cr and a change in colour to a bright green. Such an uptake corresponds to an average chromium oxidation state of +4.5 and the sample was referred to as $Cr^{nos}_{R400/Cr(4.5)}$. A decrease in the intensity of the (211) peak (at $2\theta = 24.03°$, $d = 3.72$ Å) to ~62% that of Cr^{nos} was the only significant change to the PXRD pattern, see Figure 5.11 (f). PXRD peak positions indicated an increase in a_o from 9.107(2) Å to 9.119(3) Å. The wavenumber frequencies of the ν_s(T-O-T)^b, δ(T-O-T)^d, and δ(T-O-T)^e decreased. No significant changes to the chromate Raman and IR bands or nosean framework IR bands occurred upon reduction.

Products $Cr^{nos}_{R400/Cr(3.5)}$ and $Cr^{nos}_{R600/Cr(3.5)}$

Total uptake by Cr^{nos} of 1.27 ± 0.02 moles of H_2 per mole of Cr at 600°C and 1.26 ± 0.02 moles of H_2 per mole of Cr at 400°C indicated consistent reduction to Cr(+3.5). The samples became dark green in colour. Contractions of a_o from 9.107(2) Å for Cr^{nos} to 9.073(6) Å for $Cr^{nos}_{R600/Cr(3.5)}$ and 8.916(6) Å for $Cr^{nos}_{R400/Cr(3.5)}$ were observed through changes in PXRD peak positions. The wavenumber frequencies of the ν_{as}(T-O-T) bands decreased for both samples while those of the ν_s(T-O-T) and δ(O-T-O) bands increased. The PXRD

patterns of $Cr^{nos}_{R600/Cr(3.5)}$ and $Cr^{nos}_{R400/Cr(3.5)}$, Figures 5.11 (b) and 5.11 (c) respectively, indicated the extinction of the (100) peak (at $2\theta = 9.67°$, $d = 9.146$ Å). The (211) PXRD peak (at $2\theta \approx 24°$) decreased in intensity to ~24% and ~40% that of Cr^{nos} for $Cr^{nos}_{R600/Cr(3.5)}$ and $Cr^{nos}_{R400/Cr(3.5)}$ respectively. The ν_3 chromate IR band at ~900 cm^{-1} for $Cr^{nos}_{R400/Cr(3.5)}$ completely disappeared upon reduction, see Figure 5.12 (b), as did the chromate Raman bands. Framework ν_s(T-O-T) and δ(O-T-O) IR bands became less intense.

Product $Cr^{nos}_{R400.O600}$

Heating $Cr^{nos}_{R400/Cr(3.5)}$ at 600 ± 5°C in oxygen resulted in a total uptake of 0.66 ± 0.02 moles of O_2 per mole of Cr indicating full reoxidation to Cr(VI). The (100) PXRD peak reappeared only slightly, see Figure 5.11 (d). The (211) PXRD peak increased in intensity to ~100% of that of Cr^{nos} and, apart from the extinction of the (100) peak, the PXRD pattern was almost indistinguishable from that of Cr^{nos}. PXRD peak positions indicated an increase in a_o from 8.916(6) Å of $Cr^{nos}_{R400/Cr(3.5)}$ to 9.093(2) Å. The wavenumber position of the ν_{as}(T-O-T) band increased while those of the ν_s(T-O-T) and δ(O-T-O) bands decreased. Chromate Raman bands reappeared upon reoxidation and the ν_3 chromate IR band reappeared to an intensity similar to that for Cr^{nos}. The frequency of the ν_1 chromate Raman band was 851 ± 1 cm^{-1}. Both the IR and Raman chromate band widths were greater than for Cr^{nos}. Nosean framework IR bands gained in intensity upon reoxidation.

Product $Cr^{nos}_{R400.O1000}$

Further heating of $Cr^{nos}_{R400.O600}$ at 1000 ± 20°C in air for 3 hours resulted in the reappearance of the (100) PXRD peak to give a pattern indistinguishable to that of Cr^{nos}, see Figure 5.11 (e). PXRD peak positions indicated an increase in a_o from 9.093(2) Å of $Cr^{nos}_{R400.O600}$ to 9.111(2) Å. No significant change to the intensity of the ν_3 chromate IR band occurred but the band became sharper.

The ν_1 chromate Raman band was sharper than that of $Cr^{nos}_{R600.O600}$ and was at the higher wavenumber of 855.5 ± 1 cm^{-1}.

5.3.7 Redox Reactions of Na_2MoO_4 and Na_2WO_4 Loaded Zeolites

Occluded Na_2MoO_4 was found to react with $H_{2(g)}$ and $O_{2(g)}$ at temperatures of 450°C and 550°C. Figure 5.14 shows the average oxidation state of molybdenum in 2.3MoX as functions of successive redox reactions. Stoichiometries of $H_{2(g)}$ and $O_{2(g)}$ reactions indicated reduction to ~Mo(V) and reoxidation to ~Mo(VI). Two reactions of 1.9WX and hydrogen at 450°C each resulted in the uptake of 0.05 ± 0.04 moles of $H_{2(g)}$ per mole of W indicating that occluded sodium tungstate can not be reduced by hydrogen gas at 450°C.

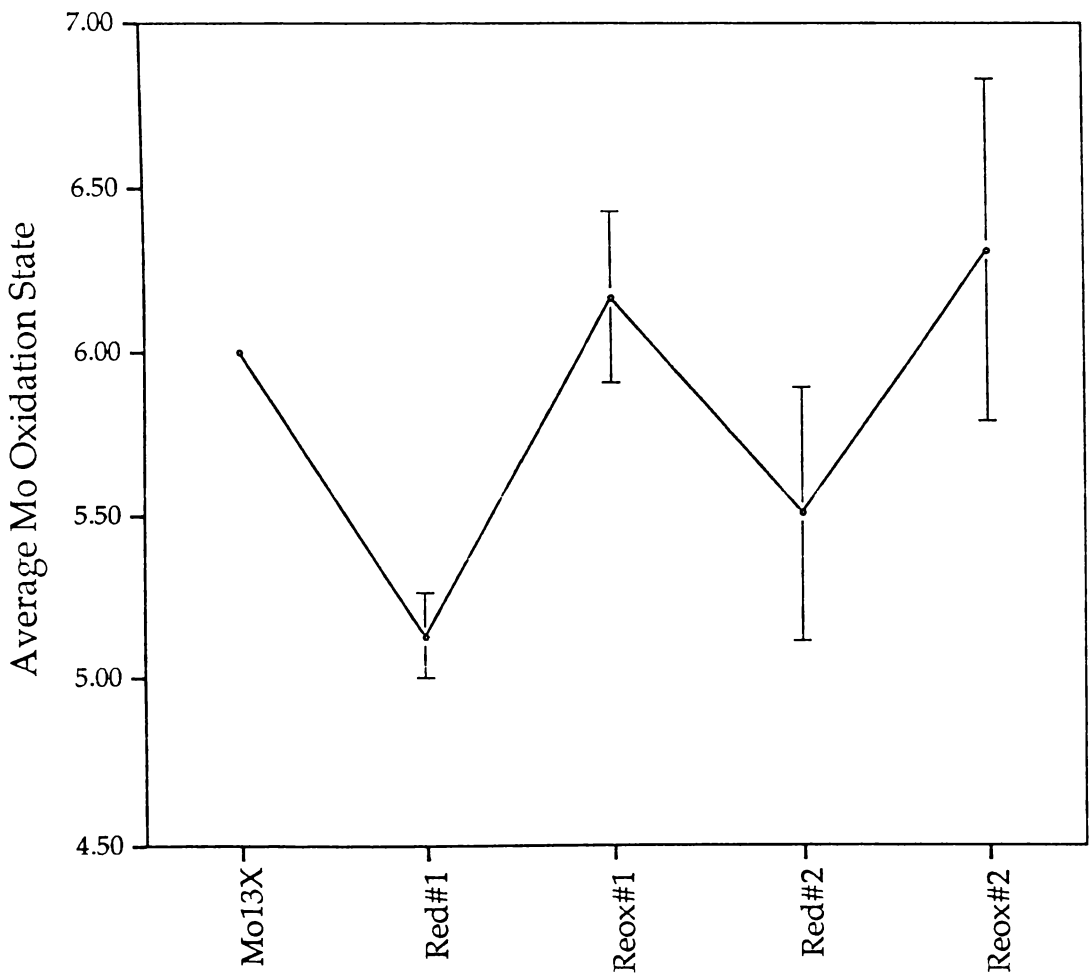


Figure 5.14 Average oxidation state of molybdenum upon cyclic redox reactions on 2.3MoX. The plot illustrates the reduction of molybdates to ~Mo(V) and full reoxidation to Mo(VI). Reaction temperatures are: Red#1 (550°C), Reox#1 (550°C), Red#2(450°C) and Reox#2 (450°C).

5.4 Discussion

5.4.1 Redox Reactions of Sodium Chromate

The Chemistry of Reduction and Reduction Product

The green crystalline powder formed upon reduction of sodium chromate gave a PXRD pattern characteristic of the compound $NaCrO_2$. Hydrogen uptake that indicated full reduction to Cr(III). Reduction of sodium chromate to form $NaCrO_2$ and NaOH as shown in Scheme 5.1 is consistent with these observations. Chromium-oxygen and chromium-sodium-oxygen species such as Cr_2O_3, Na_3CrO_4, and Na_4CrO_4 were eliminated due to the absence of their characteristic PXRD peaks.

Scheme 5.1 Stoichiometry consistent with reduction of sodium chromate by hydrogen gas to form $NaCrO_2$.

$$Na_2CrO_4 + \frac{3}{2}H_{2(g)} \xrightarrow{600^\circ C} NaCrO_2 + NaOH + H_2O$$

Although there was evidence for the production of a small amount of NaOH, i.e. the etching of the reaction chamber, no significant quantity of pure NaOH was observed. The inability to leach NaOH from Na_2CrO_4(R) by water indicates that the NaOH was firmly held within the crystals of this compound. Reaction as in Scheme 5.1, while adequately describing the stoichiometry and individual reaction products, does not account for the complex nature of the reduction product. The distribution of NaOH within Na_2CrO_4(R) is not known. An even distribution of the NaOH depleted and rich areas would account for the lack of free NaOH as the bulk of the NaOH would lie in the depths of the crystals. Reaction of a gas with a crystalline lattice can involve rapid reaction near the surface of crystals followed by slow reaction towards the centre of crystals. Under such reaction conditions a skin of $NaCrO_2$ would form rapidly on the surface of Na_2CrO_4 crystals followed by growth of the $NaCrO_2$ phase towards the centre of the crystal. Passage of NaOH into internal

areas of unreacted Na_2CrO_4 may have been promoted by the ability of Na_2CrO_4 to form binary mixtures with NaOH. For example, Khitrov and Khitrova[4] and Khitrov and Bergman[5] observed $2NaOH{\cdot}Na_2CrO_4$ and $4NaOH{\cdot}Na_2CrO_4$ phases, considered as representatives of the higher orthochromates $Na_4H_2CrO_6$ and $Na_6H_4CrO_8$, when NaOH and Na_2CrO_4 were heated. Reaction as above would explain the absence of leachable NaOH in Na_2CrO_4(R). What little NaOH was observed, i.e. the etching of the reaction chamber, may have been released from the crystal during the production of the outer skin of $NaCrO_2$. As an overlayer of Cr_2O_3 forms during outgassing at room temperature prior to XPS analysis, one would certainly form during evacuation prior to redox reactions due to the elevated temperatures employed. An overlayer could contribute to the prevention of NaOH passage out of crystals. What little NaOH was indicated may be the NaOH produced during the formation of an overlayer.

Composition of Na_2CrO_4(R,O)

The average oxidation state in Na_2CrO_4(R,O) evaluated from the cumulative stoichiometries of hydrogen and oxygen uptakes was Cr(+4.60 ± 0.24). Such an unusual oxidation state must be the average of a mixture of oxidation states. Confirmation of the average oxidation state by an alternative method and assessments of the physical and spectroscopic properties of Na_2CrO_4(R) follow.

PXRD indicated that the green precipitate formed upon the dissolving of Na_2CrO_4(R,O) was chromic oxide (Cr_2O_3), presumably formed by disproportionation of chromates of higher oxidation state. Addison and Barker[6] reported the formation of Cr_2O_3 upon addition of Na_2CrO_3 to water through disproportionation of Cr(IV) to Cr(III) and Cr(VI) in the proportion required by the equation:

$$3\ Na_2CrO_3 + 2\ H_2O \longrightarrow Na_2CrO_4 + Cr_2O_3 + 4\ NaOH$$

Likewise, Cr(V) could disproportionate to give Cr(VI) and Cr(III):

$$6\ Cr(V) \longrightarrow 2\ Cr(III) + 2\ Cr(VI)$$

The amount of either Cr(IV) or Cr(V) present in a sample can be evaluated from the amount of Cr_2O_3 formed upon disproportionation. Each mole of Cr_2O_3 is formed from either three moles of Cr(IV) or six moles of Cr(V). The calculation of the average oxidation state will therefore not be affected by whether the Cr_2O_3 was formed from Cr(IV) or Cr(V). It will be assumed that Cr_2O_3 was formed from Cr(IV). The addition of 0.75 ± 0.01 g of $NaCrO_2$(O) to water formed 0.16 ± 0.01 g of Cr_2O_3. This value corresponds to 1.05×10^{-3} moles of Cr_2O_3 indicating that 3.14×10^{-3} moles of Cr(IV) were present in Na_2CrO_4(R,O) prior to dissociation. This amount of Cr(IV) indicates an average chromium oxidation state of Cr(+4.77 ± 0.09).

Reoxidations of Na_2CrO_4(R) to form Na_2CrO_4(R,O) involved uptakes of 0.44 ± 0.04, 0.42 ± 0.04, and 0.37 ± 0.04 moles of O_2 per mole of Cr indicating incomplete reoxidations. The simplest oxidation process that would lead to such oxygen consumption would be reaction of 1.25 moles of O_2 per 3 moles of Cr (five oxidation state jumps over three chromium atoms). The average chromium oxidation state in Na_2CrO_4(R,O) based on the theoretical uptakes is Cr(+4.67). In order to account for an average oxidation state of 4.67 it is necessary to envisage a combination of oxidation states over three chromium atoms. Products consistent with average oxidation state are $Na_2CrO_4 \cdot 2\ Na_2CrO_3$ {A}, $Na_2CrO_3 \cdot 2\ NaCrO_3$ {B}, and $NaCrO_2 \cdot NaCrO_3 \cdot Na_2CrO_4$ {C}. PXRD and EPR indicated that there were only traces of $NaCrO_2$ in Na_2CrO_4(R,O) eliminating the possibility that {C} is the reoxidation product. EPR also indicated the absence of Cr(V) indicating that {B} is not the reoxidation product. Sample Na_2CrO_4(0.4) contained 40 wt% Na_2CrO_4. Similar Na_2CrO_4 PXRD peak intensities for Na_2CrO_4(R,O) and

Na_2CrO_4(0.4) indicated that Na_2CrO_4(R,O) also contained ~40 wt% Na_2CrO_4 and is consistent with the formation of product {A}.

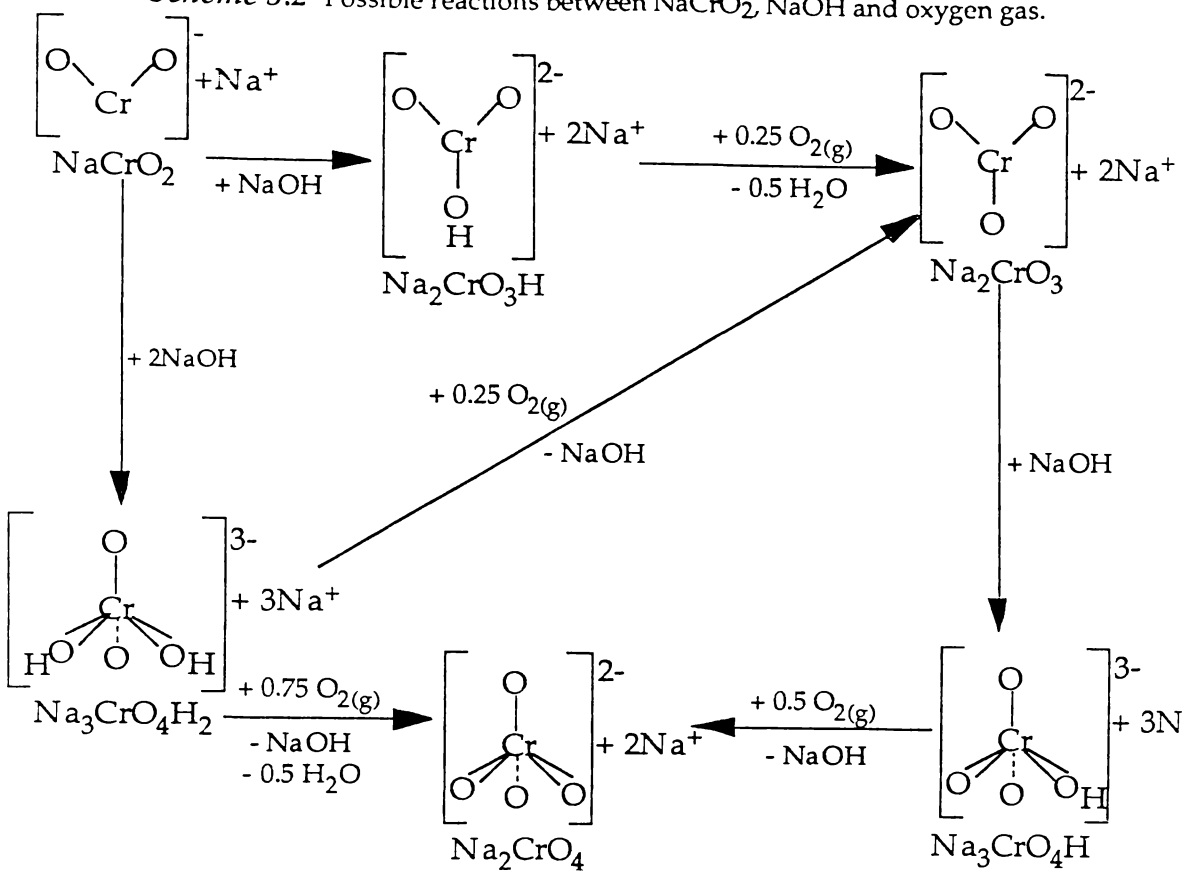
The cumulative stoichiometries of hydrogen and oxygen uptakes, the stoichiometry of disproportionation, PXRD patterns, and EPR spectra are all consistent with Na_2CrO_4(R,O) being $Na_2CrO_4 \cdot 2Na_2CrO_3$.

The Mechanism of Reoxidation

Incomplete reoxidation of Na_2CrO_4(R) despite 23.3 hours at 600°C and an excess of oxygen gas indicated the inability of Na_2CrO_3 species to further oxidise to Na_2CrO_4. The reduction step was therefore not completely reversible under the conditions of the experiment. Addition of NaOH to Na_2CrO_4(R,O) allowed full oxidation to Na_2CrO_4 upon further heating in air at a lower temperature of 500°C for only 2 hours.

The formation of both Na_2CrO_4 and Na_2CrO_3 require the recombination of $NaCrO_2$ and NaOH. Two different reoxidised species must be the result of two different interactions between NaOH and $NaCrO_2$. Scheme 5.2 shows possible reactions between $NaCrO_2$, NaOH and oxygen. According to the model, a molecule of $NaCrO_2$ can reoxidise in the presence of one NaOH molecule to produce Na_2CrO_3 or in the presence of two NaOH to form Na_2CrO_4. These two distinct reoxidation reactions could proceed in different proportions to give a variety of average oxidation states. Reaction as shown in Scheme 5.3 is consistent with the formation of a $Na_2CrO_4 \cdot 2Na_2CrO_3$ reoxidation product.

Scheme 5.2 Possible reactions between $NaCrO_2$, NaOH and oxygen gas.



Scheme 5.3 Mechanism consistent with the stoichiometry of the reoxidation of reduced sodium chromate salt.

$$NaCrO_2 + 2\,NaOH + \tfrac{3}{4}\,O_{2(g)} \xrightarrow{600\,^\circ C} Na_2CrO_4 + NaOH + \tfrac{1}{2}H_2O$$

$$2\,NaCrO_2 + 2\,NaOH + \tfrac{1}{2}\,O_{2(g)} \xrightarrow{600\,^\circ C} 2\,Na_2CrO_3 + H_2O$$

$$3\,NaCrO_2 + 3\,NaOH + \tfrac{5}{4}\,O_{2(g)} \xrightarrow{600\,^\circ C} Na_2CrO_4 + 2\,Na_2CrO_3 + \tfrac{3}{2}H_2O$$

Reaction to form Na_2CrO_4 as in Scheme 5.3 requires two moles of NaOH to react with one mole of $NaCrO_2$ and will be favoured in regions of high NaOH concentration. The formation of Na_2CrO_4 in the surface layer is therefore consistent with the finding of high NaOH concentration in this region.

The inability of Na_2CrO_3 to oxidise to Na_2CrO_4 in the absence of NaOH indicates that uptake of oxygen directly from the gas phase by a Cr species does not occur. This suggests that oxygen ligands acquired by the Cr species during the reactions of Scheme 5.2 are derived from NaOH. The stoichiometry of the reoxidation of reduced sodium chromate salt in the presence of excess NaOH is that given in Scheme 5.4. As the stoichiometric amount of $NaCrO_2$ and NaOH results in incomplete reoxidation, overall stoichiometry does not reflect the reaction mechanism. Not only are two NaOH molecules per molecule of $NaCrO_2$ involved in the reaction but also oxygen uptake from the gas phase as suggested by the overall stoichiometry is not believed to occur.

Scheme 5.4 Stoichiometry of the reoxidation reduced sodium chromate salt to sodium chromate in an excess of NaOH.

$$NaCrO_2 + NaOH + \frac{3}{4}\,O_{2(g)} \xrightarrow{600°C} Na_2CrO_4 + \frac{3}{2}H_2O$$

The Overall Redox Chemistry

The observations that all reductions formed ~Cr(+3) and all reoxidations formed ~Cr(+4.67) indicate that the reduction and reoxidation products were not affected by cyclic redox reactions. Since reoxidation is limited by the amount of NaOH available, the observation of cyclic redox reactions indicates that no NaOH was lost from the system. The sodium-chromium-oxygen phase is therefore conserved with redox reactions occurring via the uptake and loss of hydrogen. Scheme 5.5 is proposed for the cyclic redox chemistry of sodium chromate salt.

Scheme 5.5 Proposed redox reactions of sodium chromate salt.

Reduction of Na_2CrO_4 to give Na_2CrO_4(R)

$$Na_2CrO_4 + \frac{3}{2} H_{2(g)} \xrightarrow{600°C} NaCrO_2 + NaOH + H_2O$$

Reoxidations of Na_2CrO_4(R) to give Na_2CrO_4(R,O)

$$3\ NaCrO_2 + 3\ NaOH + \frac{5}{4} O_{2(g)} \xrightarrow{600°C} Na_2CrO_4 + 2\ Na_2CrO_3 + \frac{3}{2} H_2O$$

Reductions of Na_2CrO_4(R,O) to give Na_2CrO_4(R)

$$Na_2CrO_4 + 2\ Na_2CrO_3 + \frac{5}{2} H_{2(g)} \xrightarrow{600°C} 3\ NaCrO_2 + 3\ NaOH + H_2O$$

5.4.2 Redox Reactions of 13.6CrX

Uptake of 1.26 ± 0.02 moles of $H_{2(g)}$ per mole of chromium at 375 ± 5°C by 13.6CrX to give 13.6CrX(R375) indicated incomplete reduction to an average chromium oxidation state of Cr(+3.5). Zeolite 13.6CrX contained 3.59 ± 0.05 wt% Cr equivalent to (6.9 ± 0.1)x10^{-4} moles of Cr/g. The ratio of the areas of the EPR signals of Na_2CrO_4(R) and 13.6CrX(R375) indicated that the latter contained a Cr(III) concentration of (3.3 ± 0.2)x10^{-4} moles Cr(III)/g. This EPR determined Cr(III) concentration indicates that 48 ± 2% of the chromium in 13.6CrX(R375) was in the Cr(III) oxidation state. The observed uptake was 1.26 ± 0.02 moles of H_2 per mole of Cr or 8.7 ± 0.2 moles $H_{2(g)}$/g. Reduction of (3.3 ± 0.2)x10^{-4} moles Cr/g to Cr(III) would require 4.95 ± 0.06 moles $H_{2(g)}$/g. This implies that 3.74 ± 0.23 moles $H_{2(g)}$/g reacted with the remaining 3.60 ± 0.24 moles Cr/g corresponding to 1.04 ± 0.09 moles $H_{2(g)}$/Cr. The remaining 52 ± 2% of the chromium was therefore in the Cr(IV) oxidation state

indicating an equimolar mixture of Cr(III) and Cr(IV). The reaction in Scheme 5.6 is consistent with the reduction of chromates occluded in 13.6CrX to an average oxidation state of Cr(+3.5). Oxygen uptakes by reduced 13.6CrX indicated full reoxidation to Cr(VI). Scheme 5.7 shows the stoichiometry of the reoxidation reaction.

Scheme 5.6 Proposed reaction scheme for the reduction of 13.6CrX by hydrogen gas at 375°C. Reduction proceeds to an average state of Cr(+3.5) through the formation of Cr(III) and Cr(IV).

$$2\,Na_2CrO_4 + \frac{5}{4}H_{2(g)} \xrightarrow{375°C} NaCrO_2\text{-}Na_2CrO_3 + NaOH + 2\,H_2O$$

Scheme 5.7 Proposed reaction scheme for the reoxidation of reduced 13.6CrX by oxygen gas at temperatures between 450°C and 500°C. Reoxidation to Cr(VI) was possible.

$$NaCrO_2\text{-}Na_2CrO_3 + NaOH + \frac{5}{4}O_{2(g)} \xrightarrow{450-500°C} 2\,Na_2CrO_4 + \frac{1}{2}H_2O$$

The lower reaction temperature of 250 ± 5°C during the reduction to form 13.6CrX(R250) resulted in the uptake of 0.63 ± 0.02 moles of $H_{2(g)}$ per mole of Cr after 23.5 hours. The Cr(III) EPR signal of 13.6CrX(R250) was about half that of 13.6CrX(R375) as was the hydrogen uptake indicating a direct relationship between Cr(III) content and hydrogen consumption. Through careful control of reaction conditions it is therefore possible to control the concentrations of some oxidation states during reduction of chromate zeolites.

5.4.3 Redox Reactions of 4.8Cr5A and 32.3Cr5A

Redox Reactions of 32.3Cr5A

Stoichiometries of hydrogen and oxygen reactions indicated transitions between average oxidation states of Cr(+3.5) and Cr(VI). The redox chemistry

was similar to that of 13.6CrX, for which reaction stoichiometries were given, and will not be considered further.

Reductions of 4.8Cr5A

The uptake of 1.45 ± 0.02 moles of H_2 per mole of Cr by 4.8Cr5A indicated full reduction of Cr(VI) to Cr(III). The reaction in Scheme 5.8 is consistent with the stoichiometry of the reduction.

Scheme 5.8 Proposed reaction between 4.8Cr5A and hydrogen gas.

$$Na_2CrO_4 + \frac{3}{2}H_{2(g)} \xrightarrow{400°C} NaCrO_2 + NaOH + H_2O$$

Reduction of occluded chromates to Cr(III) involves the loss of H_2O and NaOH. From the kinetics of the initial reduction of 4.8Cr5A (see Section 6.6.2, Figure 6.20 and Figure 6.21) it was proposed that a fast two electron process occurs which is followed by a slower one-electron process. It is the migration of NaOH that appears to have caused the subsequent complex reoxidation chemistry. The fact that full reoxidation of Cr(IV) formed during the initial reduction of the other *MLZ* (5.8CrX) occurred (see Section 5.4.4) implies that NaOH is not liberated during this step. It is concluded that rapid reduction of Cr(VI) to Cr(IV) involves the loss of H_2O while NaOH is lost during the subsequent slower reduction of Cr(IV) to Cr(III), as shown in Scheme 5.9.

Scheme 5.9 Proposed reaction mechanism for the reduction of 4.8Cr5A by hydrogen gas.

$$Na_2CrO_4 + H_{2(g)} \xrightarrow{\Delta, \text{fast}} Na_2CrO_3 + H_2O$$

$$Na_2CrO_3 + \frac{1}{2}H_{2(g)} \xrightarrow{\Delta, \text{ slow}} NaCrO_2 + NaOH$$

Reoxidations of 4.8Cr5A

The first reoxidation of reduced 4.8Cr5A involved the uptake of 0.50 ± 0.04 mole of O_2 per mole of Cr indicating reoxidation to an average oxidation state of Cr(V). Reoxidation to an average oxidation state of Cr(V) could occur

through the formation of equal amounts of Cr(IV) and Cr(VI) in the forms of Na_2CrO_4 and Na_2CrO_3 species or the formation of Cr(V) in the form of $NaCrO_3$ and NaOH species. Because the initial hydrogen uptake of 1.45 ± 0.04 moles of $H_{2(g)}$ per mole of Cr is close to the expected uptake of 1.5 for reduction of Cr(VI) to Cr(III) it can be concluded that little self-reduction occurred during outgassing. The Cr(V) signal of 4.8Cr5A(evac) therefore arose from a very small concentration of Cr(V). The smaller Cr(V) signal of 4.8Cr5A(O425) indicates an even lower Cr(V) concentration in the reoxidised zeolite. This suggests the formation of a equal amounts of Cr(IV) and Cr(VI). The redox chemistry of the chromates of 4.8Cr5A was similar to that of the pure sodium chromate salt with full reductions to Cr(III) and incomplete reoxidations. Occluded Na_2CrO_4 and Na_2CrO_3 species formed upon reoxidation of 4.8Cr5A would be analogous to the Na_2CrO_4 and Na_2CrO_3 phases formed upon reoxidation of reduced sodium chromate salt. The formation of two different oxidised chromium species and incomplete reoxidation of reduced chromate salt were attributed to dependence of reoxidation product on the NaOH concentration, see Section 5.4.1. Formation of $2NaCrO_3 \cdot Na_2CrO_4$ upon reoxidation of reduced sodium chromate salt was explained in terms of different reactions of $NaCrO_2$ in the presence of one NaOH and two NaOH, see Scheme 5.3. Reoxidation of 4.8Cr5A to an average oxidation state of Cr(V) can be accounted for in terms of the same individual reactions as for the pure salt but in different proportions, see Scheme 5.10.

Scheme 5.10 Proposed mechanism of the reoxidation of $NaCrO_2$ within the pores of 4.8Cr5A by oxygen gas.

$$NaCrO_2 + 2\,NaOH + \tfrac{3}{4}\,O_{2(g)} \xrightarrow{\Delta} Na_2CrO_4 + NaOH + \tfrac{1}{2}\,H_2O$$

$$NaCrO_2 + NaOH + \tfrac{1}{4}\,O_{2(g)} \xrightarrow{\Delta} Na_2CrO_3 + \tfrac{1}{2}\,H_2O$$

$$NaCrO_2 + 2\,NaOH + O_{2(g)} \xrightarrow{\Delta} Na_2CrO_4 + Na_2CrO_3 + H_2O$$

5.4.4 Redox Reactions of 2.1CrX and 5.8CrX

Redox reactions of 5.8CrX were very similar to those of 4.8Cr5A which were discussed in detail in Section 5.4.3 with full reductions to Cr(III) and incomplete reoxidations to an average oxidation state of Cr(V).

Redox reactions of 2.1CrX resulted in transitions between average oxidation states of Cr(IV) and Cr(VI). Stoichiometries of oxygen uptakes indicated reoxidation to Cr(VI). Scheme 5.11 is proposed for the these reactions. The chromates in 2.1CrX are thought to be bound to the lattice through one proton and one sodium cation and will be referred to as $NaHCrO_4$ species.

Scheme 5.11 Proposed redox reactions of the chromates in 2.1CrX.

$$NaHCrO_4 + H_{2(g)} \xrightarrow{\Delta} NaHCrO_3 \quad \text{(Reductions)}$$

$$NaHCrO_3 + \tfrac{1}{2}O_{2(g)} \xrightarrow{\Delta} NaHCrO_4 \quad \text{(Reoxidations)}$$

Zeolite 5.8CrX contained 2.1 proton bound chromates and 3.7 sodium bound chromates per unit cell. Full reduction to Cr(III) indicated that all the chromates in this system behaved identically. Reduction of proton bound chromates to Cr(III) is therefore possible under certain circumstances.

5.4.5 Effect of Encapsulation on Maximum Hydrogen Uptakes

The majority of the chromate zeolites examined were found to take up less hydrogen per mole of chromium than pure sodium chromate salt when exposed under the same conditions. For example, uptakes (moles of H_2 per mole of Cr) of 1.26 ± 0.02 for Cr^{nos}, 1.26 ± 0.02 for 13.6CrX and 1.24 ± 0.02 for 32.3Cr5A were significantly less than that for chromate salt of 1.58 ± 0.04. Two

possible reasons for the lower uptakes are self-reduction of chromates or incomplete reduction. Self-reduction would be a means by which chromates could reduce without uptake of hydrogen thereby giving lower hydrogen uptakes than expected for a given average oxidation state change. The change in colour of 13.6CrX from yellow to light green and the appearance of an EPR signal characteristic of a Cr(V) species upon evacuation prior to redox reactions indicated a certain amount of self-reduction. Quantitative EPR indicated that $48 \pm 2\%$ of the Cr in 13.6CrX(R375) was in the Cr(III) oxidation state (see Section 5.4.2). Lower hydrogen uptakes for this zeolite was therefore due to incomplete reduction and not self-reduction.

5.4.6 Comparison of the Redox Behaviours of Chromate Zeolites

Table 5.6 summarises the redox reactions of the materials examined. The chromate zeolites can be divided into three groups on the basis of the redox chemistry of their occluded chromates.

Zeolites 13.6CrX, 13.4CrY, 32.3Cr5A, and Cr^{nos} displayed similar redox chemistries. Reductions were consistently incomplete ceasing at an average oxidation state of ~Cr(+3.5). Reoxidations to an average oxidation state of Cr(VI) indicated full reoxidation. Cyclic redox reactions resulted in transitions between average oxidation states of Cr(VI) and Cr(+3.5). As these zeolites contain high levels of chromate they were referred to as highly-loaded zeolites or *HLZ*.

Zeolites 4.8Cr5A and 5.6CrX displayed full reductions to Cr(III) and incomplete reoxidation to an average oxidation state of Cr(V) (or Cr(IV) at lower reaction temperatures). Cyclic redox reactions resulted in transitions between average oxidation states of Cr(III) and Cr(V). Due to the moderate loading of these zeolites they were referred to as a moderately-loaded zeolites or *MLZ*.

The redox chemistry of 2.1CrX involved reductions average oxidation state transitions between ~Cr(IV) and Cr(VI). This zeolite contained a low level of chromate and was referred to as a lowly-loaded zeolite or *LLZ*.

Highly-loaded zeolites (*HLZ*), moderately-loaded zeolites (*MLZ*), and lowly-loaded zeolites (*LLZ*) exhibited quite different reduction chemistries. Full reduction to Cr(III) for *MLZ* is in contrast to incomplete reduction to an average oxidation state of Cr(+3.5) for *HLZ* and incomplete reduction to an average oxidation state of ~Cr(IV) for *LLZ*.

Table 5.6 Summary of the redox chemistries of chromate zeolites and sodium chromate.

Zeolite	Minimum Oxidation State	Oxidation State Transitions	Zeolite Group
Na_2CrO_4	Cr(III)	Cr(III) $\longleftrightarrow$ ~Cr(+4.67)	n.a.
4.8Cr5A	Cr(III)	Cr(III) $\longleftrightarrow$ Cr(V)	*MLZ*
5.8CrX	Cr(III)	Cr(III) $\longleftrightarrow$ Cr(V)	
13.6CrX	Cr(+3.5)	Cr(+3.5) $\longleftrightarrow$ Cr(VI)	
13.4CrY	Cr(+3.7)	Cr(+3.7) $\longleftrightarrow$ Cr(VI)	*HLZ*
32.3Cr5A	Cr(+3.5)	Cr(+3.5) $\longleftrightarrow$ Cr(VI)	
Cr^{nos}	Cr(+3.5)	Cr(+3.5) $\longleftrightarrow$ Cr(VI)	
2.1CrX	Cr(IV)	Cr(IV) $\longleftrightarrow$ Cr(VI)	*LLZ*

5.4.7 Reasons for the Differences in Reduction Chemistries

The reduction chemistry of occluded chromate is affected by the degree of loading. There is, however, no correlation between degree of loading and degree of chromate reduction. Incomplete reductions and complete reoxidations for *HLZ* and *LLZ* are in contrast to the redox reactions of *MLZ*.

This suggests that more than one process inhibiting reduction is involved. Possible reasons for incomplete reductions of *LLZ* and *HLZ* follow.

Incomplete Reductions of *LLZ*

Reduction of Cr(IV) to Cr(III) involves the acquisition of three electrons. Because hydrogen gas is a two electron reducing agent, such reduction requires reaction of three moles of hydrogen per two moles of chromium. Reduction of Cr(VI) to Cr(IV) occurs via reaction of one hydrogen molecule with one chromium atom while reduction of Cr(IV) to Cr(III) involves the reaction of one hydrogen molecule with two chromium atoms. The reduction involving two chromium atoms, in the absence of chemisorption of the hydrogen atom across two chromium atoms, would require a hydrogen atom transfer. If a maximum possible distance for a hydrogen atom transfer existed and the chromates were separated by a distance greater than this then reduction would be prevented. If chromate loading is homogeneous then chromates in *LLZ* will be dispersed more sparsely throughout the zeolite crystals than those in *MLZ* and *HLZ*. Reduction of chromates in *LLZ* to Cr(IV) may therefore be the result of sufficient spatial separation to prevent the reduction involving two chromium atoms.

Incomplete Reductions of *HLZ*

Full reduction of *MLZ* implies that chromates in these zeolites were sufficiently close as to allow reductions involving two chromium atoms. As the greater loading of *HLZ* further reduces the inter-chromate distance, spatial separation was not the cause of incomplete reductions in *HLZ*. Two possible reasons for incomplete reductions of *HLZ* are that an equilibrium is involved or that there is an interaction between chromium species.

NaOH is produced during reduction of chromate. If no sink exists for this NaOH then equilibria of the type shown below may be involved.

$$Na_2CrO_3 + 0.5\ H_{2(g)} \rightleftharpoons NaCrO_2 + NaOH$$

According to this model the presence of NaOH could favour the higher oxidation state species. The zeolite pore and cavity system offers a sink for NaOH through occlusion within void spaces. Incomplete reduction of chromates in *HLZ* would then be the result of insufficient void space to occlude all the NaOH produced. Reduction of two of the four chromates in the α-cage of 32.3Cr5A but only one of the two chromates in the α-cage of 13.6CrX, despite the larger α-cage of X zeolite, indicates that lack of void space is not the reason for lower reduction in the latter zeolite. Void space, or the equilibrium indicated above, thus appear to play no significant role in reduction.

Reduction to Cr(III) of one of the two chromates of the α-cages of 13.6CrX and 13.4CrY zeolites and two of the four chromates in the α-cage of 32.35A indicates that the reduction of one chromate to Cr(III) inhibits the reduction of one other presumably neighbouring chromate. A chromate-chromate interaction such as the formation of a Cr-O-Cr bond, similar to those found in dichromate species, is suggested. Linking $NaCrO_2$ and Na_2CrO_3 species through one of the oxygen ligands of the latter species would form a "dimer" of the type $NaCrO_2$-O-CrO_2Na_2. If the loading of chromates in *MLZ* is homogeneous then the chromates will be dispersed more sparsely throughout the zeolite crystals than those in *HLZ*. The lack of chromates in close proximity within *MLZ* would eliminate the possibility of "dimer" formation thereby allowing the full reduction of chromates to Cr(III). Both $NaCrO_2$ and Na_2CrO_3 have independent existences as crystalline solids. Formation of a mixed oxidation state "dimer" from discrete monomers of these two species is conceivable. A possible structure and the likely existence of such a species is discussed below.

5.4.8 Model Structure of the "Dimer"

Movement of occluded chromates and their reduced counterparts in the α-cage will be restricted by the strong interaction with lattice bound Na^+ cations. Rather than forming the two moieties and then allowing them to configure to the lowest free energy as single entities it may be more appropriate to form the constituent monomers and, with the restrictions on movement imposed by the lattice in mind, study the effect that available movement has on a pair of such species. The Na^+ cations of the $NaCrO_2$ and Na_2CrO_3 moieties are thought to be sited on or near the S_{II} cation site, near the planes of the S6R facing the α-cage. The atomic distance between Na^+ cations sited on S_{II} was calculated using the atomic coordinates from a single crystal XRD study of X-type zeolite[7] and is 7.46 Å.

The most stable configuration of monomeric chromium moieties is likely to be midway between two Na^+ sites and sited so as to minimise the distance between charge bearing oxygen atoms and the Na^+ cations. Because the chromium moieties are much smaller than the size of the coordination site, the smallest Na^+ to O distances will occur when the O atoms lie on the axis defined by the two Na^+ cations as shown in Figure 5.15.

Rotation about the Na^+-Na^+ axis will allow minimisation of the system free energy. The four Na^+ atoms of the two chromium species lie near the four S6R facing the α-cage and have a tetrahedral configuration as shown in Figure 5.16. The distance between the centres of the two axes defined by the Na^+ cations (labelled a and b on the Figure) is 6.46 Å. The shortest distance between the Cr atom of the CrO_2^- species and the oxygen atom of the CrO_3^{2-} species is obtained when both these atoms lie on the line between a and b, as shown in the Figure, and is 2.63 Å. This value is significantly larger than the normal Cr to O bond length of 1.91 Å indicating that, for an unperturbed system, the bond-order would be well below one. The interaction between the

Cr(III) and Cr(IV) species would therefore be weak unless the chromium species (and possibly the Na^+ cations as well) move off the axis between the S_{II} sites. It is clearly evident, however, that two chromates occluded within one α-cage are in close enough proximity to allow "dimers" to form.

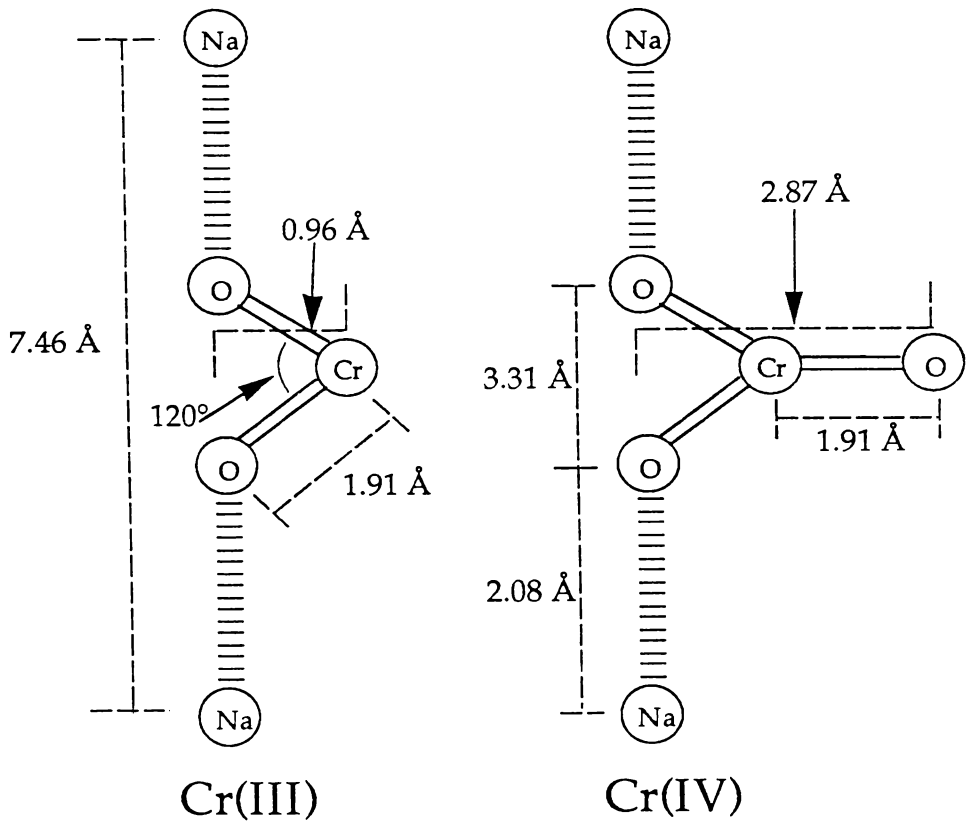


Figure 5.15 Structures of the model Cr(III) and Cr(IV) compounds. Note that the oxygen atoms of the chromium species lie on the axis defined by the two Na^+ cations to which they are coordinated. Movement if these species within the α-cage is assumed to occur through rotation around the Na^+-Na^+ axis.

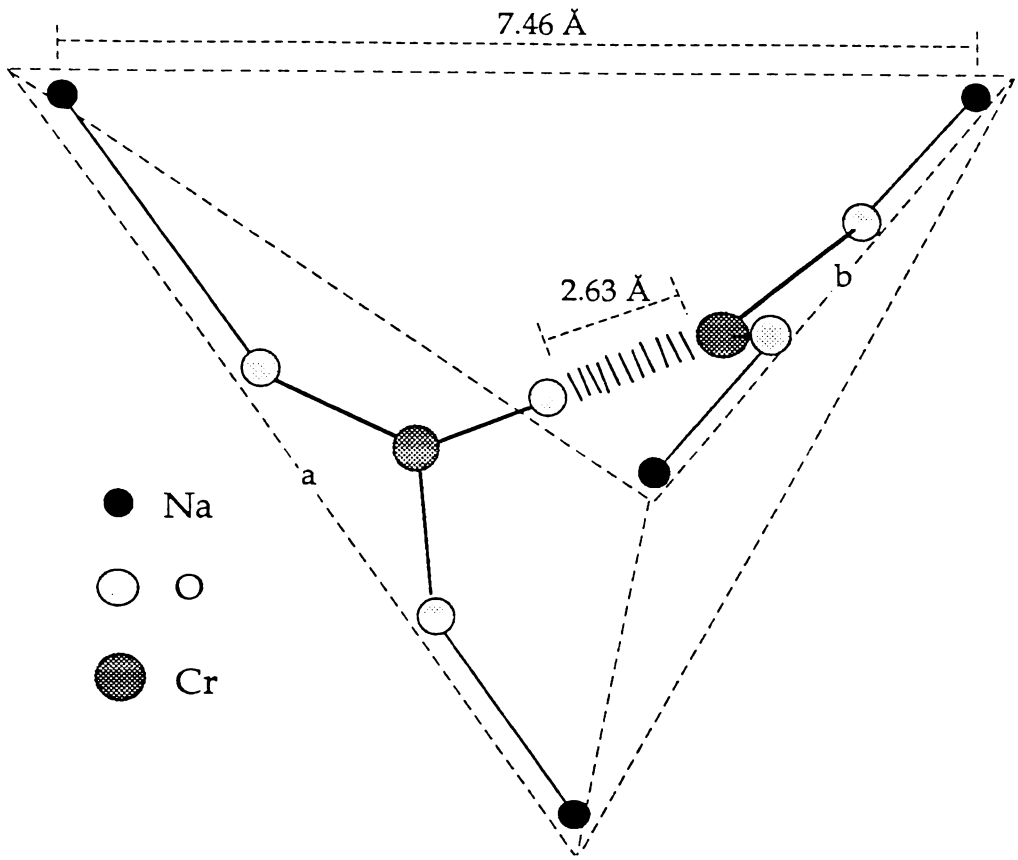


Figure 5.16 Model used to calculate interatomic distance between the oxygen atom of CrO_3^{2-} and the Cr atom of CrO_2^- in the Na_3CrO_5 "dimer" occluded in the α-cage of X zeolite.

5.4.9 Stability of the "Dimer": Resistance to Reduction to Cr(III)

The oxidation state free energy diagram for chromium[8] indicates that Cr(III) is stable, Cr(VI) is highly oxidising, Cr(V) and Cr(IV) species are oxidising, while Cr(II) and Cr(0) are reducing. Reductions of sodium chromate and chromates of *MLZ* to Cr(III) are consistent with the stability of the +III oxidation state. Stabilisation of the +IV oxidation state would appear, in the light of conventional wisdom, to be anomalous and the probability of the existence of a mixed Cr(III)-Cr(IV) system in the pure crystalline state or in solution to be low. This is examined below.

It might be expected that the oxidising power of the Cr(IV) fragment would destabilise a Cr(IV)-Cr(III) "dimer". There must therefore be some reason for the resistance of the Cr(IV) group to reduction. In the crystalline

solid-state the coordination number of chromium would be increased by the site effects in the crystalline lattice. Discrete $NaCrO_2$ monomers in zeolite pores have low coordination and C_{2V} symmetry. The formation of a "dimer" is a means by which higher coordinative saturation and trigonal planar (C_{3V}) symmetry can be maintained. The higher coordination number can be expected to stabilise the "dimer" relative to any combination of the constituent monomer species.

5.4.10 Reason for the Differences in Reoxidation Chemistries

Incomplete reoxidation of reduced chromate salt was attributed to the effect of NaOH concentration on the reoxidation mechanism. By analogy incomplete reoxidation of chromates in *MLZ* may be the result of a similar dependence of reoxidation product on NaOH concentration. Differing reoxidation chemistries of reduced chromates in *HLZ* and of reduced sodium chromate salt and reduced chromates in *LLZ* is due to the formation of different reduction products, i.e. Cr(III) in *MLZ* and sodium chromate as opposed to a Cr(III)-Cr(IV) system in *HLZ* and Cr(IV) in *LLZ*.

5.4.11 Proposed Structures of the Occluded Chromate Species

Occluded Na_2CrO_4

Figure 5.17 shows the proposed structures of occluded chromates and the reduced products. It has been proposed that occluded chromates consist of a chromate oxyanion coordinated to the lattice through two cations, $Na_{(Cr)}$, located near the planes of the two S6R, see Figure 5.17 (a). It is not clear where the cations that neutralise framework charge, $Na_{(Z)}$, that originally occupied the S_{II} site are sited but they are likely to be near S6R to counteract the negative charge of the six-ring. They have been placed on the $S_{II'}$ site in these diagrams.

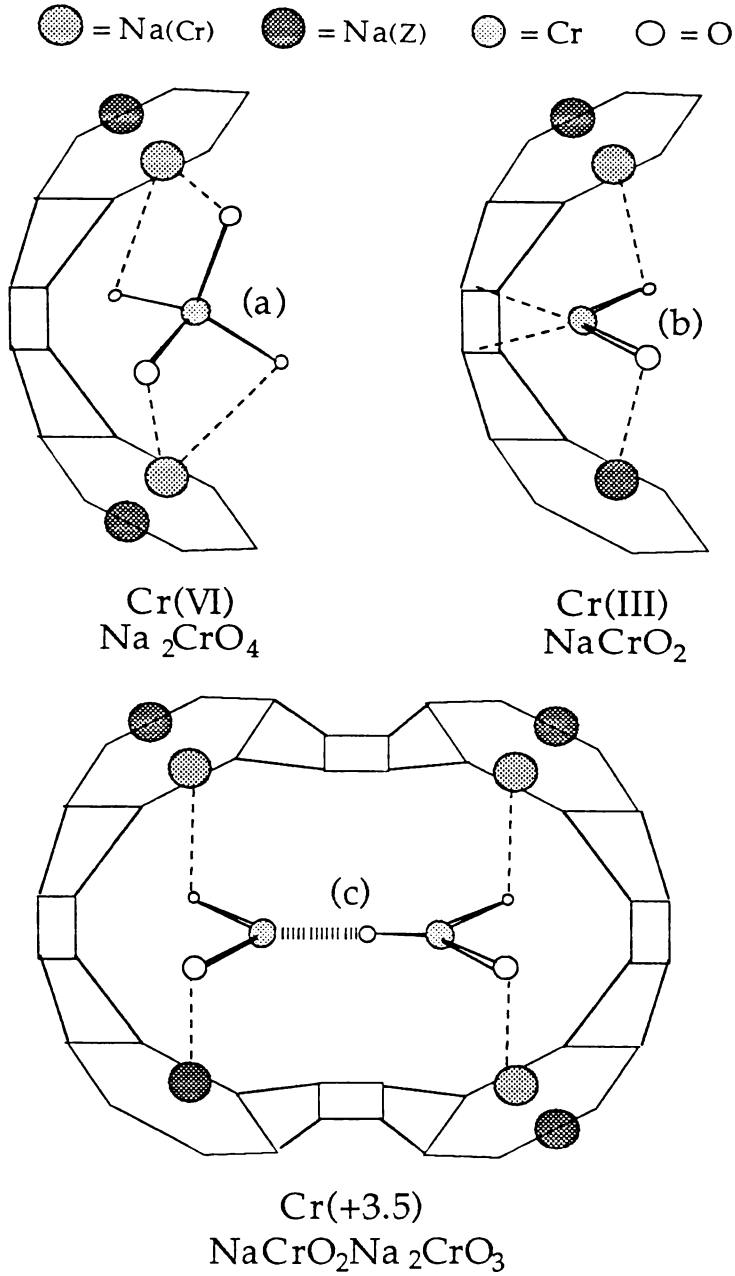


Figure 5.17 Proposed structures of occluded chromates and the various reduced species.

Occluded $NaCrO_2$

Figure 5.17 (b) shows the proposed structure of the Cr(III) species. Reduction to Cr(III) forms a $NaCrO_2$ species through the loss of H_2O and NaOH from Na_2CrO_4. Migration of NaOH away from the $NaCrO_2$ species would open up the S_{II} site and may allow one of the $Na_{(Z)}$ to adopt its favoured configuration on the S_{II} site. In the figure this is shown to have occurred.

Destabilisation caused by low coordinative saturation could be minimised by coordination of the CrO_2^- moiety to the framework through two or more lattice oxygen atoms of an S4R to increase coordination to pseudo tetrahedral or higher. The S4R is provided by a face of the D4R or D6R that link the sodalite cages in A and X zeolites respectively.

Occluded $NaCrO_2$-Na_2CrO_3 "Dimer"

It has been proposed (Section 5.4.4) that reduction to an average oxidation state of Cr(+3.5) forms a $NaCrO_2$-Na_2CrO_3 "dimer" with a structure shown in Figure 5.17 (c). The CrO_2^- moiety is shown coordinated to the lattice through one $Na_{(Cr)}$ and one $Na_{(Z)}$. Coordination of the CrO_3^{2-} moiety to the lattice is shown through two $Na_{(Cr)}$. The four Na cations lie on the four S6R facing the α-cage of X and Y zeolites in a tetrahedral configuration. "Dimerisation" is considered to occur through the formation of a long range interaction between the oxygen atom of the Cr(VI) species and the chromium atom of the Cr(III) species.

5.4.12 Redox Reactions of Chromate Nosean

5.4.12.1 Space Group and Cluster Considerations

Constraints on anion valence and distribution are imposed by the sodalite framework and must be considered when formulating redox products. There are eight cation sites per unit cell located near the planes of the eight hexagonal faces of the two sodalite cages. A combined cation charge of +6 is required to neutralise the charge of the $[Al_6Si_6O_{24}]^{6-}$ framework anion leaving only two cation sites to be filled by cations counteracting anion charge. When a salt species, such as NaCl, is occluded within a sodalite cage the Na^+ cation of the salt becomes indistinguishable from the three other cations. For this reason the intraframework species of sodalites are often referred to in the form of clusters.

A cage containing an NaCl salt contains a $[Na_4.Cl]^{3+}$ cluster consisting of a Cl^- anion at the centre of the cage surrounded by a tetrahedral arrangement of four Na^+ cations. Noselites, with alternate cages containing divalent anions, have two cluster types per unit cell for example $[Na_4.SO_4]^{2+}$ and $[Na_4.H_2O]^{4+}$ in sulphate nosean. The nosean framework also restricts possible reaction products to discrete monomeric oxyanions. Species such as Cr_2O_3 can not form as these would require the co-existence of two crystalline phases and the absence of salt species within the sodalite cages. Any consideration of the redox products of noseans should describe the clusters in the two cages of the unit cell and should not deal merely with species present in the free salt such as Na_2CrO_4. Table 5.7 lists possible products of the redox reactions of Cr^{nos}. The formation of NaOH occurs during the reduction of sodium chromate, see Section 5.4.1. Many of the possible redox products therefore involve the cleavage of OH^- and formation of a cage containing the $[Na_4.OH]^{3+}$ cluster.

Reduction of chromate nosean by hydrogen gas at 600°C resulted in a transformation from a noselite framework to a sodalite framework. In addition to the constraints imposed by the framework, space group criteria of the sodalite and noselite groups must be considered. Table 5.8 summarises the differences between the noselite and sodalite frameworks.

Transformation from a noselite framework to a sodalite was evidenced by the loss of the 100 PXRD peak (see Figure 5.11). The 100 peak is systematically absent from the patterns of sodalites. Processes consistent with the transformation follow.

Table 5.7 Possible cage clusters in the cages of the redox products of Cr^{nos}.

Chromium Oxidation State	Species Designation	Occluded Species Cage A	Cage B
Cr(VI)	A	$[Na_4.CrO_4]^{2+}$	$[Na_4]^{4+}$
	B	$[Na_4.CrO_3]^{4+}$	$[Na_4.O]^{2+}$
Cr(V)	C	$[Na_4.CrO_4.H]^{2+}$	$[Na_4]^{4+}$
	D	$[Na_4.CrO_2(OH)]^{2+}$	$[Na_4]^{4+}$
	E	$[Na_4.CrO_3]^{3+}$	$[Na_4.OH]^{3+}$
Cr(IV)	F	$[Na_4.CrO_4.H_2]^{2+}$	$[Na_4]^{4+}$
	G	$[Na_4.CrO_2(OH)_2]^{2+}$	$[Na_4]^{4+}$
	H	$[Na_4.CrO_3.H]^{3+}$	$[Na_4.OH]^{3+}$
	I	$[Na_4.CrO_2(OH)]^{3+}$	$[Na_4.OH]^{3+}$
	J	$[Na_4.CrO_3]^{2+}$	$[Na_4]^{4+}$
Cr(III)	K	$[Na_4.CrO_4.H_3]^{2+}$	$[Na_4]^{4+}$
	L	$[Na_4.CrO(OH)_3]^{2+}$	$[Na_4]^{4+}$
	M	$[Na_4.CrO_3.H_2]^{3+}$	$[Na_4.OH]^{3+}$
	N	$[Na_4.CrO(OH)_2]^{3+}$	$[Na_4.OH]^{4+}$
	O	$[Na_4.CrO_3.H]^{2+}$	$[Na_4]^{4+}$
	P	$[Na_4.CrO_2]^{3+}$	$[Na_4.OH]^{3+}$

1) The occupation of all anion sites through conversion of the divalent anion into two monovalent anions

Sodalites contain two monovalent anions per unit cell, i.e. one per β-cage. Formation of two monovalent anions from the divalent chromate anion and passage of one anion into the empty cage would fill all anion sites and thereby form a sodalite.

2) Conversion of the divalent anion into an anion and a neutral species

It is not clear whether anions must occupy the anion sites for the n-glide to be produced or whether a neutral species can fill the role of an anion. The formation of a neutral species such as CrO_3 must be addressed.

3) Non-occupation of all anion sites

A sodalite framework is observed for hydrosodalite ($Na_6[AlSiO_4]_6.nH_2O$, $0 \leq n \leq 8$)[9]that contains no anions. The n-glide must result from all anion sites being vacant. Chromate oxyanions show high affinity for aluminosilicate frameworks as evidenced by their irreversible binding to the internal surfaces of various zeolites. Coordination of the reduced chromium species to the lattice would result in movement off the anion site. This process would generate the n-glide necessary for the extinction of the 100 peak.

Table 5.8 Differences between the frameworks of sodalite and noselite.

Structural Feature	Sodalite Framework	Noselite Framework
Anion Valence	Monovalent	Divalent
Anion number	Two per unit cell	One per unit cell
Anion Symmetry	Spherical eg. Cl^-, Br^-, I^- Other eg. OH^-	Tetrahedral eg. SO_4^{2-}, CrO_4^{2-}
Space Group	$P_{\bar{4}3n}$	$P_{\bar{4}3m}$
Atomic Positions	One set of 24 equivalent oxygen positions. One set of 8 equivalent sodium positions	Two sets of 12 equivalent oxygen positions . Two sets of 4 equivalent sodium positions
Cage Dimensions	Two equivalent sized cages per unit cell	Two different sized cages per unit cell

Before proceeding to formulate redox products some possible routes consistent with the space group criteria are discussed below and outlined in Figure 5.18. Conversion of noselite (N/I) to sodalite upon reduction could occur via coordination of the reduced chromates to the lattice (S/II) or through the formation of two monovalent anions (S/III). Reoxidation of (S/II) without

release from the lattice would form chromate sodalite (S/IV) due the absence of anions on anion sites. Reoxidation of (S/III) to give (S/V) could form sodalite containing a neutral species through the occupation of all anion sites. Reoxidation of (S/III) gives chromate sodalite (S/IV) if the divalent anion is not cleaved from the lattice. Formation of chromate noselite (N/VII) from (S/IV) would occur if the divalent anion was cleaved from the lattice. Reformation of a divalent anion from (S/V) would form a chromate noselite (N/VII). On the basis of crystallographic space group criteria three possible reaction routes can be envisaged to account for the transformation of noselite to sodalite and the subsequent transformation of sodalite back to noselite, see Figure 5.18.

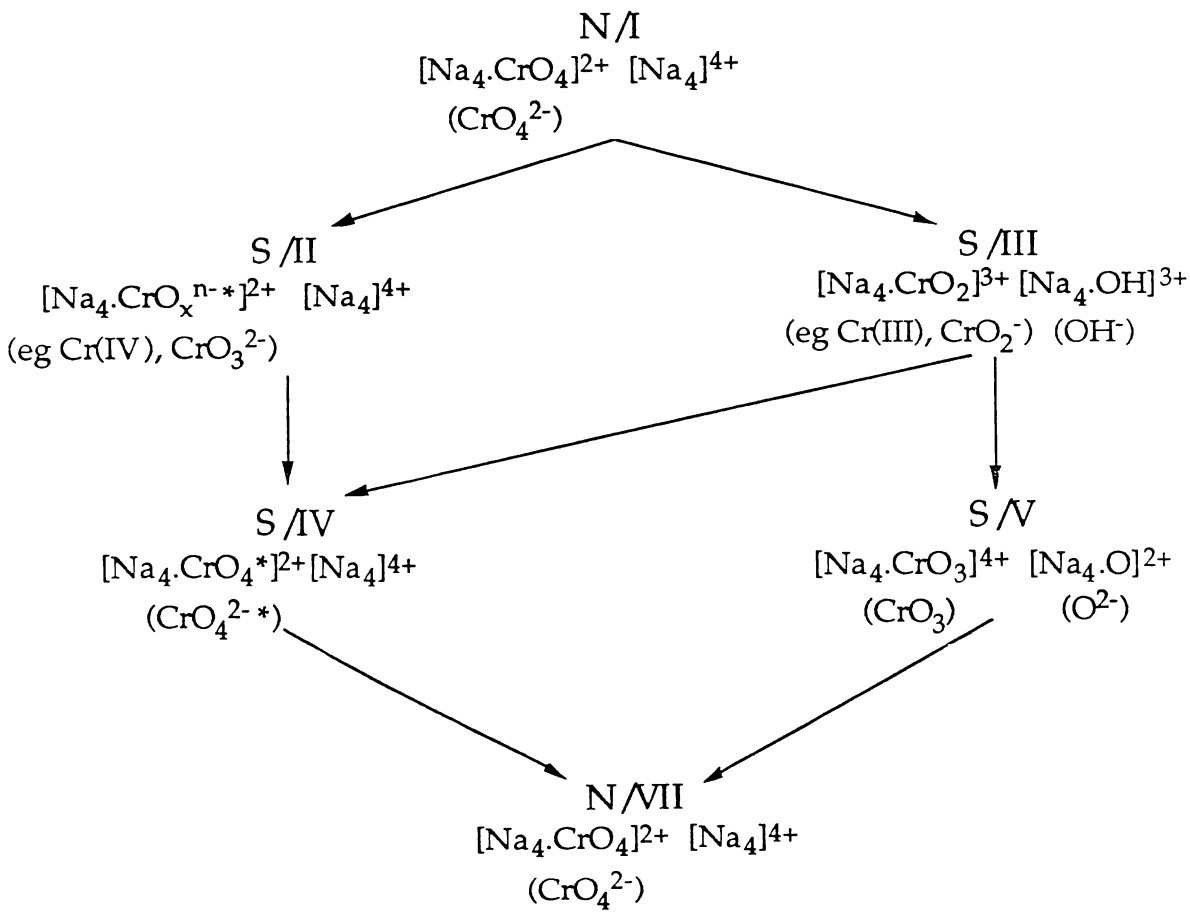


Figure 5.18 Possible reaction routes for the redox reactions of chromate noselite (see text). Shown are the cluster compositions below which in brackets are shown the species occupying the sodalite cage(s) of the unit cell.

5.4.12.2 Correlation between IR Band Frequencies and Unit Cell Edge (a_o)

Henderson and Taylor[3] observed a relationship between the a_o and the positions of the IR adsorption bands of anhydrous synthetic and natural aluminosilicates in the region 600-1000 cm^{-1} and gave equations relating the a_o of sodalites to the mean sizes of the cavity cation and anion. Figure 5.19 shows the relationship between the a_o and framework IR band frequencies of Cr^{nos} and the products after various redox treatments. Increases in the frequencies of the ν_{as}(T-O-T) bands and decreases in the frequencies of the ν_s(T-O-T) and δ(O-T-O) bands upon increasing a_o are consistent with the work of Henderson and Taylor.

5.4.12.3 Interpretation of a_o Contraction upon Chromate Reduction

Calculation of Mean Anion Radius (r_a) from a_o

Reduction at 400 ± 5°C for 95 hours to produce $Cr^{nos}_{R400/Cr(3.5)}$ resulted in an a_o contraction from 9.107(2) Å for Cr^{nos} to 8.916(6) Å. A linear relationship between a_o and mean cation and anion radii was observed by Henderson and Taylor[3] for Li, Na, and K forms of halide sodalites. PXRD measurement of the a_o of a nosean or sodalite may provide a means by which the radius of the occluded anion might be estimated. Structural elucidation of the reduced system on the basis of the radius of the occluded oxyanion might also be possible. Estimation of anion radii from measurements of a_o requires that the a_o and anion radius relationship is valid for complex anions. The sizes of both cages of the unit cell must also be known accurately. Calibration against actual (or estimated) thermochemical radii of the reduced chromium species will also be necessary. These three factors are considered in the following sections.

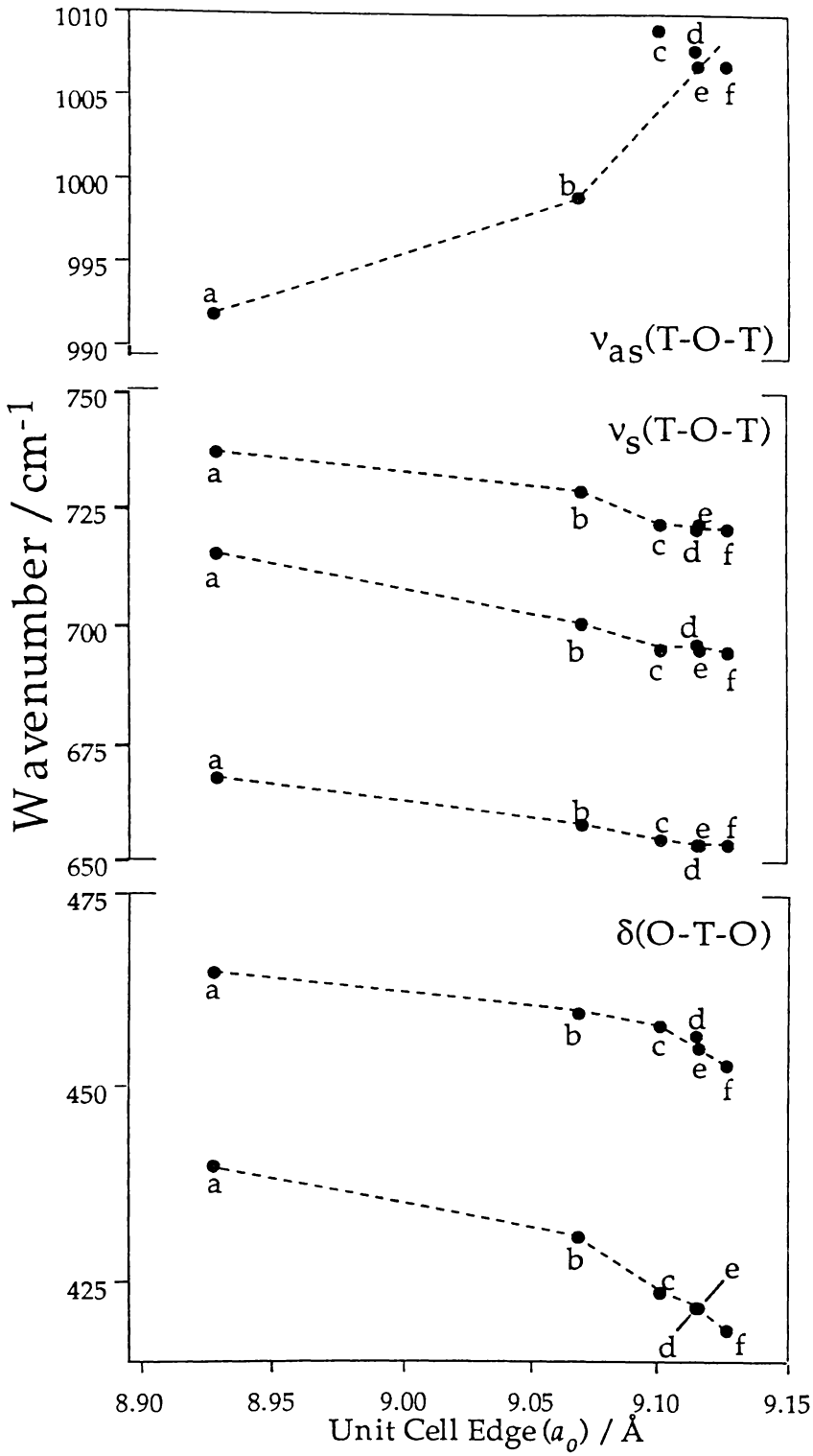


Figure 5.19 Relationship between the frequencies of the IR bands of the framework and the a_0 of Cr^{nos} and the products after various redox treatments. Products are (a) $Cr^{nos}_{R400/Cr(3.5)}$, (b) $Cr^{nos}_{R600/Cr(3.5)}$, (c) $Cr^{nos}_{R400.O600}$, (d) Cr^{nos}, (e) $Cr^{nos}_{R400.O1000}$ and (f) $Cr^{nos}_{R400/Cr(4.5)}$. Errors in the unit cell edges and wavenumbers positions of the framework bands are given in Table 5.5.

Relationship between a_o and r_a

The relationship between a_o and r_a for the Na forms of various sodalites is shown in Figure 5.20. All anion radii were obtained from an article by Jenkins and Thakur.[10] Relevant radii and a_o are shown in Table 5.9. Figure 5.20 indicates that the complex anions show the expected trend. Values for the a_o of the sodalites containing OH^-, Cl^-, Br^-, and I^- are those of dehydrated systems and that of sulphate nosean was determined from single crystal XRD. The line of best fit passes directly through the points of these five systems indicating that a_o is linearly related to anion radius. Sodalites containing the complex anions were subject to less stringent control over composition. Deviation of the a_o values of these systems from the line of best fit could be the result of fluctuations in composition.

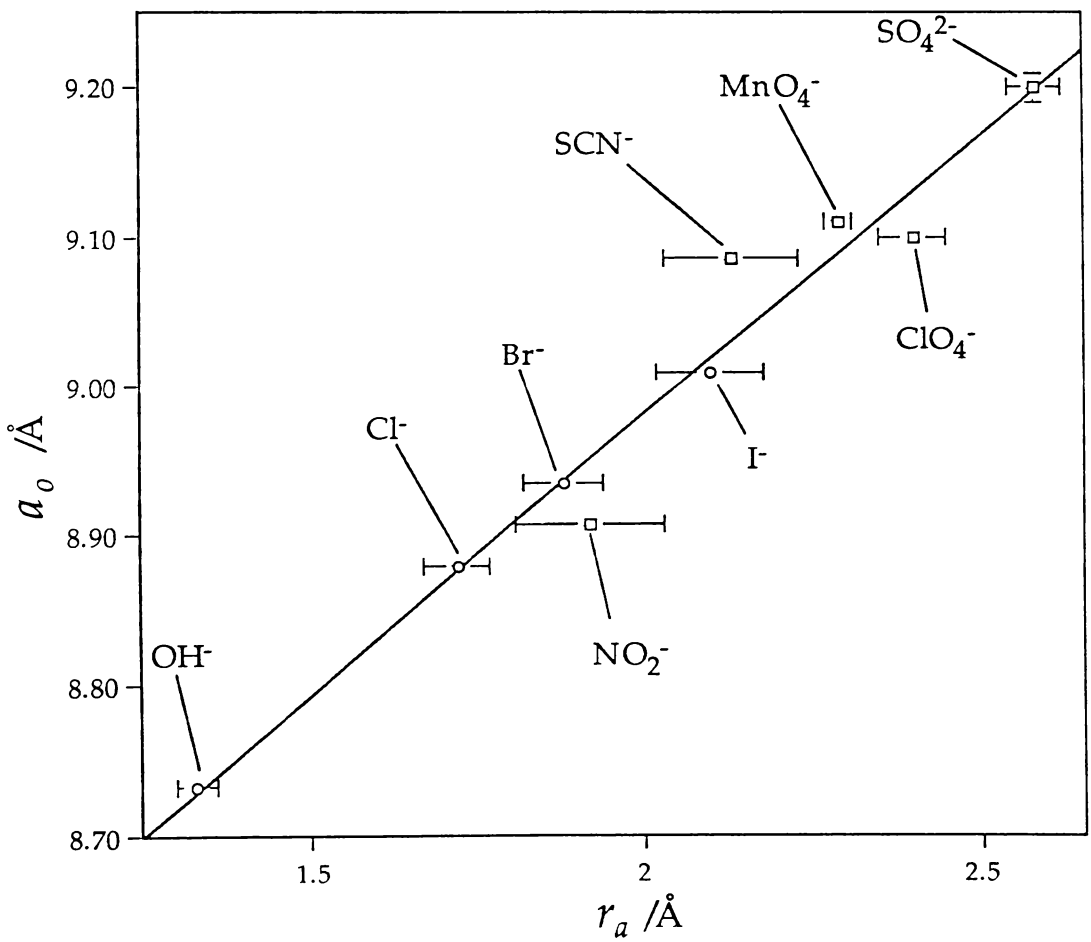


Figure 5.20 Plot showing the linear relationship between the a_o of Na sodalites (and a_o^{O2} of sulphate nosean) and the radius of the occluded anion. Shown are the occluded anions.

Table 5.9 Thermochemical radii of various anions (r_a) and the unit cell edges (a_0)[11] of the corresponding sodalite or nosean. The a_0s of sulphate nosean marked by (*) are the sizes of the two cages as determined from single crystal XRD, see text.

Zeolite	Anion	r_a / Å	a_0 / Å	XRD Ref
Chlorine Sodalite	Cl^-	1.72 ± 0.05	8.881(2)	11
Bromine Sodalite	Br^-	1.88 ± 0.06	8.935(2)	13
Iodine Sodalite	I^-	2.10 ± 0.08	9.015(2)	13
Hydroxysodalite	OH^-	1.33 ± 0.03	8.754(2)	13
Isocyanate Sodalite	SCN^-	2.13 ± 0.10	9.086(2)	12
Nitrate Sodalite	NO_2^-	1.92 ± 0.11	8.906(1)	14
Permanganate Sodalite	MnO_4^-	2.29 ± 0.02	9.111(1)	13
Perchlorate Sodalite	ClO_4^-	2.40 ± 0.05	9.101(1)	15
Sulphate Nosean	SO_4^{2-}	2.58 ± 0.04	9.090(1)	13
Sulphate Nosean	SO_4^{2-}	2.58 ± 0.04	9.20(2) *	14
			8.90(2) *	
Hydrosodalite	------	----------	8.888(1)	15

The line of best fit shown in Figure 5.20, including the standard deviations of the slope and intercept, is given by equation 5.1.

$$a_0\,(/\text{Å}) = 0.337(\pm 0.009)r_a + 8.30\ (\pm 0.02) \qquad (5.1)$$

Values in the brackets of the above equation are standard deviations obtained from a least squares regression analysis. Errors in thermochemical radii given by Jenkins and Thakur[11] are assumed to also be standard deviations.

Unit Cell Edges of Noseans

Hassan and Grundy[16] have shown that sulphate nosean contains two sets of framework oxygen atoms, *O1* and *O2*, within its unit cell. The atomic coordinates of the *O1* and *O2* oxygen atoms were used to estimate cell edges and the sizes of the two different cages in sulphate nosean. A unit cell edge (a_0^{O1}) of 8.94(2) Å was obtained for *O1* while that of *O2* (a_0^{O2}) was 9.20(2) Å. The resulting average cell edge of 9.07(2) Å was close to their observed average a_0 of 9.084Å. It was suggested[16] that *O2* oxygens were associated with the

cages containing larger $[Na_4.SO_4]^{2+}$ clusters and *O1* oxygens were associated with the cages containing smaller $[Na_4.H_2O]^{4+}$ clusters.

Comparison of a_o^{O1}, 8.94(2), and the a_o of hydrosodalite, 8.888(1) Å,[17] indicates that the water containing cage in sulphate nosean is the same size as the water containing cage in hydrosodalite. The size of a water containing cage in a nosean appears to be unaffected by the size of the anion containing cage. It is therefore reasonable to expect an OH^- containing cage in a nosean or sodalite to have the same size as found in hydroxysodalite, i.e. 8.754(1) Å.[13]

Heat treatment on sulphate nosean increased its a_o from 9.075(2) Å to 9.090(2) Å.[13] Such treatment will have little or no effect on the SO_4^{2-} anion so the a_o expansion presumably arose from changes to a_o^{O1}. The likely cause of an increase to a_o^{O1} is cage expansion to counteract increased Na-Na repulsions upon dehydration of $[Na_4.H_2O]^{4+}$ to form $[Na_4]^{4+}$. It can be inferred that a_o is dependent on the level of hydration. Reduction to form $Cr^{nos}_{R400/Cr(3.5)}$ was performed at 400°C. At this temperature the outgassing for 24 hours under vacuum would form a dehydrated system. Similarly any water produced during the reduction reaction at 400°C would be removed from nosean pores. In the discussion that follows all water is considered to have been removed. It is therefore necessary to know the size of an empty cage. Equation 5.1 and a radius of 2.56 ± 0.03 Å[11] allows the calculation of a_o^{O2} for a cage containing CrO_4^{2-} to be 9.17(5) Å. From this value and the a_o of Cr^{nos} of 9.107(2) Å an a_o^{O1} of 9.05(4) Å is derived for an empty cage. This value compares favourably with the a_o of dehydrated hydrosodalite of 9.11 Å[16] supporting the view that the size of a cage is not affected by the size of neighbouring cages.

Anion Radii of Reduced Chromium Species

Estimation of the sizes of the cages containing the CrO_2^- and CrO_3^{2-} from equation 5.1 requires the radii of these anions. No thermochemical radii are available for CrO_3^{2-} and CrO_2^- species, but one can estimate their radii by

analogy with the effect of changes in structure on the anion radius of other oxide containing anions. Table 5.10 list some relevant anion radii.

Table 5.10 Thermochemical radii[11] of various anions relevant to this work. Estimated radii for reduced chromium species are indicated by (#).

Anion	Shape	r_a / Å
ClO_3^-	trigonal planar	1.71 ± 0.06
ClO_4^-	tetrahedral	2.40 ± 0.05
VO_3^-	trigonal planar	1.82 ± 0.02
VO_4^{3-}	tetrahedral	2.60 ± 0.06
HCO_2^-	bent	1.69 ± 0.01
HCO_3^-	trigonal planar	1.56± 0.02
NO_2^-	bent	1.92 ± 0.11
NO_3^-	trigonal planar	1.79 ± 0.06
SO_4^{2-}	tetrahedral	2.58 ± 0.04
CrO_4^{2-}	tetrahedral	2.56 ± 0.03
CrO_3^{2-}	trigonal planar	1.82 ± 0.10 (#)
CrO_2^-	bent	1.96 ± 0.12 (#)

Formation of CrO_3^{2-} from CrO_4^{2-} involves the loss of an oxide ligand to form a trigonal planar species from the tetrahedral chromate anion. Ratios of the radii of ClO_3^-/ClO_4^- of 0.71 ± 0.04 and VO_3^-/VO_4^{3-} of 0.70 ± 0.02 indicate a lowering of anion radius by a factor of 0.71 ± 0.03 upon loss of an oxygen ligand from a tetrahedral anion to form a trigonal planar anion. Ratios of NO_2^-/NO_3^- of 1.07 ± 0.10 and HCO_2^-/HCO_3^- of 1.08 ± 0.02 suggests that the radius increases by a factor of about 1.08 upon the loss of an oxygen ligand from the trigonal planar anion to form a bent species. The error in the NO_2^-/NO_3^- ratio is large due to the large errors in the NO_2^- radius. For this reason the HCO_2^-/HCO_3^- ratio of 1.08 ± 0.02 is considered to be the most reliable value. Applying these trends to the chromium system and using an anion radius for CrO_4^{2-} of 2.56 ± 0.03 Å gives radii of 1.82 ± 0.10 Å for CrO_3^{2-} and 1.96 ± 0.12 Å for CrO_2^-.

Estimation of a_0

The possible formation of mixtures of two oxidation states complicates estimation of a_0. Stoichiometry of hydrogen uptake indicated reduction to an average oxidation state of Cr(+3.5), see Section 5.3.6. The simplest scheme to account for this observation is the formation of equimolar proportions of Cr(III) and Cr(IV). As two chromium species are needed to account for the chemistry but only one chromium is occluded per unit cell, description of the contents and sizes of two unit cells is required to characterise the system. In the following discussion two *O2* cages and two *O1* cages of the two unit cells are represented by *O2*, *O2'*, *O1*, and *O1'* with cell dimensions given by a_0^{O2}, $a_0^{O2'}$, a_0^{O1}, and $a_0^{O1'}$.

From Equation 5.1 and the radii of the reduced chromium species, a_0^{O2} values of 8.97(6) Å and 8.92(6) Å were calculated for cages containing CrO_2^- and CrO_3^{2-} respectively. These values and a_0^{O1} values of 9.05(4) Å for an empty cage and 8.784(1) Å for the OH^- containing cage allows the average a_0 for three combinations of possible cage clusters shown in Table 5.11 to be evaluated.

Table 5.11 Average unit cell edge (a_0) expected for various cluster formations in reduced chromate nosean. Shown are the clusters in the four cages of two unit cells and the unit cell edges of the individual cages. Numbers in brackets are the standard deviations.

	Cage				
	O1	*O2*	*O1'*	*O2'*	a_0 /Å
Cluster	$[Na_4.OH]^{3+}$	$[Na_4.CrO_2]^{3+}$	$[Na_4.OH]^{3+}$	$[Na_4.CrO_2]^{3+}$	
a_0^{OX}	8.754(1)	8.97(6)	8.754(1)	8.97(6)	8.86(3)
Cluster	$[Na_4.OH]^{3+}$	$[Na_4.CrO_2]^{3+}$	$[Na_4]^{4+}$	$[Na_4.CrO_3]^{2+}$	
a_0^{OX}	8.754(1)	8.97(6)	9.05(4)	8.92(6)	8.92(4)
Cluster	$[Na_4]^{4+}$	$[Na_4.CrO_3]^{2+}$	$[Na_4]^{4+}$	$[Na_4.CrO_3]^{2+}$	
a_0^{OX}	9.05(4)	8.92(6)	9.05(4)	8.92(6)	8.98(5)

Of the three combinations of Cr(III) and Cr(IV) only the formation of both CrO_2^- and CrO_3^{2-} to give an a_o of 8.921(26) Å agrees with the experimentally observed a_o of 8.92(4) Å. Formation of Cr(III) and Cr(IV) as in Scheme 5.12 is consistent with both the stoichiometry of gas uptake and the estimated a_o.

Scheme 5.12 Possible cluster formation during the reduction of Cr^{nos} to Cr(+3.5).

$$2([Na_4.CrO_4]^{2+}/[Na_4]^{4+}) + \frac{5}{2} H_{2(g)}$$

$$\Delta \downarrow$$

$$([Na_4.CrO_2]^{3+}/[Na_4.OH]^{3+}) + ([Na_4.CrO_3]^{2+}/[Na_4]^{4+}) + 2\,H_2O$$

Effect of Reaction Time on a_o

Reduction at 600°C for 219 minutes to form $Cr^{nos}_{R600/Cr(3.5)}$ resulted in an uptake of 1.27 ± 0.02 moles of $H_{2(g)}$ per mole of Cr and an a_o contraction to 9.073(6) Å. Loss of Raman and IR bands upon formation of $Cr^{nos}_{R600/Cr(3.5)}$ is consistent with the formation CrO_2^- and CrO_3^{2-} species. Formation of a sodalite and loss of the intensities of framework IR bands are also consistent with this change. The a_o contraction from 9.107(2) Å to 9.073(6) Å was much smaller than expected for full reduction and is inconsistent with the formation of the clusters shown in Scheme 5.12. As the migration of OH^- from *O2* into empty *O1* cages to form $[Na_4.CrO_2]^{3+}$ and $[Na_4.OH]^{3+}$ clusters results in major a_o contraction, one possible cause of the lack of contraction could be that the OH^- remains in the *O2* cage. The absence of migration of OH^- into *O1* cages during reduction to Cr(+3.5) would form the clusters shown below.

$$[Na_4.CrO_2.OH]^{2+} + [Na_4]^{4+} + [Na_4.CrO_3]^{2+} + [Na_4]^{4+}$$

Estimation of the expected a_o of a nosean containing the clusters shown above is not possible as the size of the $[Na_4.CrO_2.OH]^{2+}$ containing cage is unknown. The observed average a_o and the estimated a_os of the other three cages suggests that the a_o for the $[Na_4.CrO_2.OH]^{2+}$ containing cage is 9.28(6) Å. This value is significantly larger than that expected for a cage containing CrO_2^-, 8.97(6) Å, or

OH^-, 8.754(1) Å. The a_o of the CrO_2^-/OH^- containing cage is significantly larger than that of a cage containing CrO_4^{2-}, 9.17(4) Å despite the fact that the occluded species contain one less oxygen atom. Expansion of the cage to counteract anion-anion interactions between CrO_2^- and OH^- may be the cause of this phenomenon.

Longer reaction times, as experienced by $Cr^{nos}_{R400/Cr(3.5)}$, resulted in an a_o contraction consistent with passage of OH^- anions into *O1* cages. This process proceeds at a slower rate than reduction as complete reduction can occur with little a_o contraction. As the movement of OH^- anions into the *O1* cage requires passage through S6R, hindrance to such passage will be afforded by the oxygen atoms of the six-ring. Slower passage of OH^- anion through S6R than diffusion of $H_{2(g)}$ molecules through the noselite framework would account for the difference in the rates of the reduction and a_o contraction processes. Completion of reduction before passage of OH^- anions into the *O1* cage would require that the presence of OH^- in the *O2* cage does not inhibit reduction. Reduction as in Scheme 5.13 is proposed. Reaction involves the rapid reduction to Cr(III) and Cr(IV) to form CrO_2^-, CrO_3^{2-}, and OH^- species within *O2* cages. A slower process then occurs involving the passage of OH^- anions into the *O1* cages.

Scheme 5.13 Possible cage clusters and reaction sequence involved in the reduction of Cr^{nos} by hydrogen gas at 400°C.

$$[Na_4.CrO_4]^{2+} + [Na_4]^{4+} + [Na_4.CrO_4]^{2+} + [Na_4]^{4+} + \frac{5}{2}H_{2(g)}$$

$$\text{fast} \downarrow \Delta$$

$$[Na_4.CrO_2.OH]^{2+} + [Na_4]^{4+} + [Na_4.CrO_3]^{2+} + [Na_4]^{4+} + 2\,H_2O$$

$$\text{slow} \downarrow \Delta$$

$$[Na_4.CrO_2]^{3+} + [Na_4.OH]^{3+} + [Na_4.CrO_3]^{2+} + [Na_4]^{4+}$$

Longer reaction time under hydrogen results in anion redistribution while reoxidation reforms a divalent anion. It would appear that, through appropriate choice of reaction temperature and time, an otherwise unstable system can be produced. A sodalite system with a configuration as in $Cr^{nos}_{R600/Cr(3.5)}$ is therefore best regarded as being in a metastable state.

Alternative Method of a_o Determination

PXRD gives an a_o that is an average of two cage sizes in noseans. Assumptions about the size of unoccupied cages and of cages containing reaction products were needed before a_o could be related to anion radius. Single crystal XRD of chromate nosean and reduced samples would allow the precise determination of the various individual cage sizes and therefore estimation of anion radii without the need for these assumptions. Chromate nosean is prepared via high temperature reactions giving fine powders unsuitable for single crystal work. Hydrothermal synthetic methods allow the production of larger crystals of zeolites and feldspathoids. Unfortunately chromate nosean cannot be prepared hydrothermally as the presence of chromate salt promotes the formation of cancrinite.[17,18]

5.4.12.4 Reduction to Cr(+4.5)

Reduction to an average oxidation state of Cr(+4.5) appears to be a simple reaction which results in no significant spectroscopic or crystallographic changes. The absence of a significant difference in the intensity of the ν_3 chromate IR band between Cr^{nos} and $Cr^{nos}_{R400/Cr(4.5)}$ indicated little change in the concentration of chromate or change to the bond order or symmetry upon reduction to Cr(V) and Cr(IV). The Raman and IR spectra were characteristic of tetrahedral chromate indicating no change in symmetry of the chromate oxyanion. Formulation of the reduced species with formal hydroxy groups (Species D, G, I, L and N of Table 5.7) is therefore inappropriate. A process

involving electron transfers from a hydrogen molecule to the chromate(VI) to form a CrO_4^{3-} and CrO_4^{4-} species and encapsulated hydrogen ions within the sodalite cage is consistent with the retention of chromate IR and Raman bands upon reduction. Formation of tetrahedral chromate(V) species, CrO_4^{3-}, would be consistent with the work of Brown[1] where an isotropic EPR signal observed upon reduction of chromate nosean was characteristic of a Cr(V) species of high tetrahedral symmetry. A Cr(V) species having one hydroxyl group would be asymmetric and give an anisotropic EPR signal.

The increase in the a_o from 9.107(2) Å to 9.119(3) Å and the changes in the frequencies of the IR bands of the framework indicated an enlargement of the sodalite cage(s) consistent with the encapsulation of hydrogen ions. Retention of the noselite framework indicated occupation of alternate cages by divalent anions. Redistribution of anions to form $[Na_4.CrO_3.H]^{3+}$ and $[Na_4.OH]^{3+}$ clusters (H) is inconsistent with the retention of chromate IR and Raman bands and the retention of the noselite framework. In addition the formation of a smaller trigonal planar chromium species and migration of OH^- into empty cages would result in a decrease in the a_o. Scheme 5.14 shows the proposed stoichiometry for the formation of $Cr^{nos}_{R400/Cr(4.5)}$ from Cr^{nos}.

Scheme 5.14 Reaction of Cr^{nos} to the average oxidation state of Cr(+4.5) through the formation of Cr(IV) and Cr(V) species.

$$2\,([Na_4.CrO_4]^{2+}/\,[Na_4]^{4+}) + \frac{3}{4}H_{2(g)}$$

$$\xrightarrow{400^\circ C,\ 28\ hrs}$$

$$\underset{Cr(IV)}{([Na_4.CrO_4H_2]^{2+}\,/\,[Na_4]^{4+})} + \underset{Cr(V)}{([Na_4.CrO_4H]^{2+}\,/\,[Na_4]^{4+})}$$

5.4.12.5 Conversion of Chromate Nosean to Reduced Chromate Sodalite

The significant features of the reduction of chromate nosean to reduced chromate sodalite were incomplete reductions, loss of IR and Raman chromate bands, decreases in the intensities of the ν_{as}(T-O-T) and δ(O-T-O) framework IR bands, a_o contractions, and conversion of the noselite framework into a sodalite framework.

Raman and IR bands of chromate were observed for CrO_4^{3-} and CrO_4^{4-} species in $Cr^{nos}_{R400/Cr(4.5)}$. Loss of chromate IR and Raman bands for $Cr^{nos}_{R600/Cr(3.5)}$ upon reduction to an average oxidation state of Cr(+3.5) indicated a fundamental change to the symmetry of the chromate unit upon reduction. Such a change is consistent with the formation of CrO_2^- and CrO_3^{2-} species as observed or postulated for reduction of chromate occluded in zeolite cages. The magnitude of the a_o contraction from 9.107(2) Å to 8.916(6) Å for $Cr^{nos}_{R400/Cr(3.5)}$ was shown to be consistent with the production of the clusters shown below.

$$[Na_4.CrO_2]^{3+} + [Na_4.OH]^{3+} + [Na_4.CrO_3]^{2+} + [Na_4]^{4+}$$

Extinction of the (100) PXRD peak indicated the conversion of the noselite to a sodalite framework. Such a conversion could occur via movement of anions from the anion sites (S/II) or through the occupation of all anions sites by formation of two monvalent anions from the divalent anion (S/III). Reduction to Cr(III) forms CrO_2^- and OH^- thereby allowing occupation of the adjacent empty cage by the OH^- anion. Reduction to Cr(IV) forms divalent CrO_3^{2-} anions, the cage containing which will be accompanied by an empty cage. The n-glide responsible for the loss of the 100 peak is therefore not the result of the occupation of all anion sites. It must therefore arise from movement of the reduced chromium species from the anion sites.

Decreases in the intensities of the ν_{as}(T-O-T) and δ(O-T-O) framework IR bands were not caused by structural degradation as subsequent reoxidation

increased their intensities to values comparable to those of Cr^{nos}. Inhibition of lattice vibrations must be the result of movement of the reduced anions from the anion site and an increased interaction with the lattice.

Reduction of Cr^{nos} was incomplete ceasing at an average oxidation state of Cr(+3.5). As in the case of chromate zeolites, incomplete reduction could be the result of an interaction between chromium species such as the formation of a "dimer". Formation of a "dimer" species within the sodalite framework would involve an interaction between species in adjacent β-cages. A possible structure of the sodalite "dimer" is shown in Figure 5.21. Details of the production of the diagram and structural features of the "dimer" are given below.

the diagram was created in CHEM3D™ molecular modelling application for Macintosh computers. Framework atom positions were obtained from a study of hydroxysodalite.[19] The narrow lines define the framework of two adjacent β-cages. Bolder lines of the framework define the four S6R on which the four Na^+ cations coordinated to the two chromium species lie. The chromium species were prepared using the standard Cr to O bond lengths (1.91 Å) of CHEM3D™. The sizes of the chromium species are in proportion to the size of the sodalite cage. No energy minimisation procedures were performed on the system. Chromium species have simply been placed within the sodalite cages in positions consistent with the experimental observations. The diagram is therefore merely a pictorial representation meant to convey the approximate positions of the intraframework species and should not be taken as indicative of exact atomic positions. The high symmetry of the sodalite structure results in a tetrahedral arrangement of cations within and between adjoining cages. Placing the chromium species in a similar manner to that shown in Figure 5.16 for X type zeolite results in the "dimer" arrangement shown. Interaction between the CrO_3^{2-} and the CrO_2^- species could occur through the S4R that links the four S6R.

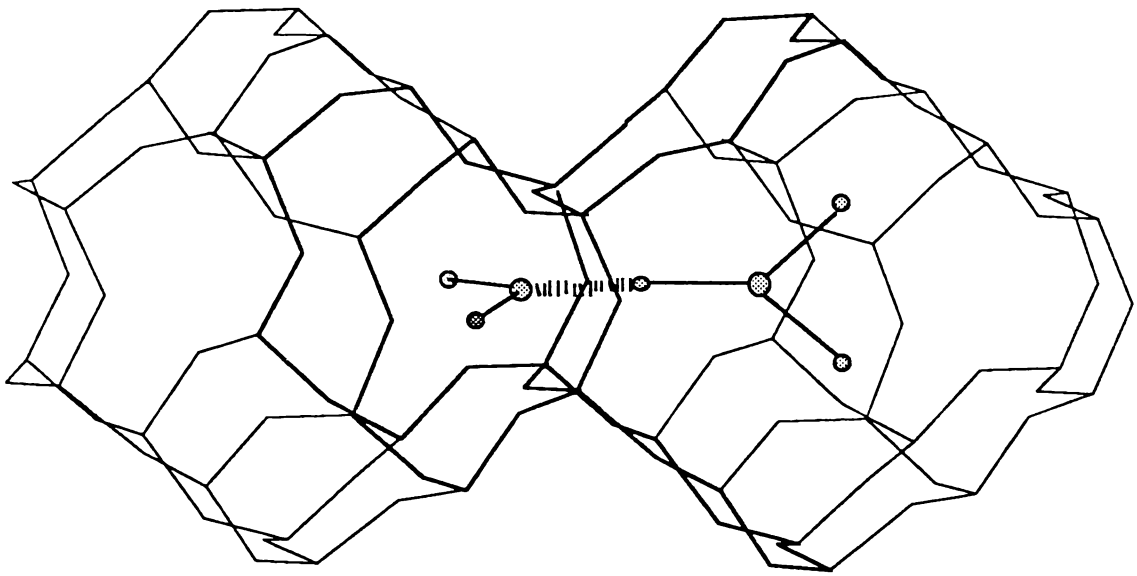


Figure 5.21 Pictorial representation of the proposed "dimer" in the reduced chromate sodalite. See text for details of the production of the diagram. Interaction between the chromium species is shown to occur through the S4R linking two adjacent sodalite cages.

Anion Distributions and Structure in $Cr^{nos}_{R400/Cr(3.5)}$.

There is formally only one anion site per sodalite cage. This conclusion is based on the fact that sodalites and noseans contain no more than one anion per cage and that the anion occupies a position near the centre of the cage. The absence of literature reports of a sodalite or nosean containing anions in positions other than on the anion site can be found. Because very few sodalites or noseans containing transition metal compounds can or have been synthesised, little is known about the redox chemistry of anions in sodalite structures. Redox reactions offer a means of producing novel oxyanion redox products with concomitant formation of unique sodalite structures.

An anion located on the anion site will most effectively reduce cation-cation repulsions and will allow the charge of the anion to be most effectively dispersed. A system with the lowest free energy will therefore occur when the anion is located on the anion site. Movement of the anion from the anion site would normally be an unfavourable process due to the increase the free energy of the system. The conclusion that anion movement occurs upon reduction of

Cr^{nos} suggests that this process can result in an overall lowering of the free energy of the system. Reduction of CrO_4^{2-} forms CrO_3^{2-} and CrO_2^-. The low coordinative saturation of these species, especially that of CrO_2^-, would result in destabilisation. In the absence of an alternative source of ligands, the formation of weak interactions with the oxygen atoms of the lattice or of other chromium species are the only means by which coordination number, and therefore stability, can be increased. These interactions, however, require movement of the chromium species from the anion site. The fact that anion movement occurs indicates that the stabilisation resulting from the increase in coordination number upon the movement of the anion from the anion site outweighs the destabilisation resulting from the increase in cation-cation repulsions. The oxidising conditions employed in solid-state syntheses of noselites would result in oxyanions of high coordinative saturation, such as SO_4^{2-} and CrO_4^{2-}, which have little affinity for the framework oxygen atoms. Anions such as the halides will also have little affinity for the framework. As such sodalites and noselites when synthesised invariably contain anions located on the anion site. Only through the production of species with low coordinative saturation is it likely that the anion will migrate from the anion site.

5.4.12.6 Conversion of Reduced Chromate Sodalite to Chromate Sodalite

Reappearance of the chromate IR and Raman bands indicated reformation of the divalent chromate oxyanion. According to the model, reduction of CrO_4^{2-} anions forms lattice bound CrO_3^{2-} and CrO_2^- species coordinated to two sodium cations. Reoxidation could occur without movement of the CrO_4^{2-} species back to the anion site. Coordination of the chromate anions to lattice oxygen atoms is unlikely given their high coordinative saturation. The chromates could, however, remain coordinated to only the two sodium cations to which the reduced species were coordinated.

The sodalite framework is consistent with all anions lying off the anion sites. Incomplete expansion of the a_o from 8.916(6) Å of $Cr^{nos}_{R400/Cr(3.5)}$ to 9.093(2) Å for $Cr^{nos}_{R400.O600}$ compared to 9.107(2) Å for Cr^{nos} indicated that the structures of $Cr^{nos}_{R400.O600}$ and Cr^{nos} were significantly different. Coordination of the oxyanion to the lattice could be the cause of this difference. Lowering of the ν_1 Raman band from 856.5 ± 1 cm^{-1} for Cr^{nos} to 851 ± 1 cm^{-1} for $Cr^{nos}_{R400.O600}$ is a small but significant red-shift that indicates a difference in the environment of the chromate oxyanions of these systems. A difference in the broadness of the chromate Raman and IR bands of $Cr^{nos}_{R400.O600}$ compared to those of Cr^{nos} is further evidence for such an effect. Sharp bands for Cr^{nos} reflects the uniformity of chromate anion sites within the nosean structure. Broader bands for $Cr^{nos}_{R400.O600}$ indicates a greater environmental variation of chromates in this nosean. It is interesting to note that the position of the ν_1 band for $Cr^{nos}_{R400.O600}$ was almost identical to that of 2.1CrX and 13.6CrX and various other chromate-loaded zeolites. Constant frequencies of the ν_1 Raman band for chromate loaded zeolites are evidence for a uniform mode of chromate coordination for the different zeolite types. The value of 851 ± 1 cm^{-1} was taken to be indicative of chromate oxyanions coordinated to aluminosilicate lattices through two zeolitic cations (see proposed model for chromate zeolites in Figure 5.17 (a). It was deduced in Section 4.5.5 that the blue-shift of the ν_1 Raman band from 851 ± 1 cm^{-1} to 856.5 ± 1 cm^{-1} was caused by the smaller cation to anion distances of salt species in nosean than in the pure salt. The value of 856.5 ± 1 cm^{-1} was taken to be characteristic of chromate anions located on the anion sites of sodalite cages. The frequency of the ν_1 Raman band of 851 ± 1 cm^{-1} for $Cr^{nos}_{R400.O600}$ is consistent with coordination of chromate oxyanions to the surface of the sodalite cages through two sodium cations.

Spectroscopic and crystallographic data indicates that reoxidation of lattice bound species occurs without movement back to the anion site resulting

in the formation of chromate anions coordinated to only two of the four sodium cations per sodalite cage. It would appear that the temperature of 600 ± 5°C was sufficient to reform divalent chromate oxyanions but insufficient to allow movement back to the anion site in the time scale of the experiment. A system with chromates lying off the anion site is likely to be in a strained configuration having a higher free-energy than that of a system with the chromates located on anion sites. Relaxation of the system back to the lowest free-energy state must be prevented by the strong interaction between chromate and intrazeolitic sodium cations. Chromate sodalite is presumably a metastable state.

5.4.12.7 Conversion of Chromate Sodalite to Chromate Noselite

Reappearance of the (100) PXRD peak indicated that $Cr^{nos}_{R400.O1000}$ had a noselite crystal structure. An increase in a_o from 9.093(2) Å for $Cr^{nos}_{R600.O600}$ to 9.111(2) Å for $Cr^{nos}_{R400.O1000}$ indicated movement of framework atoms and intraframework ions. The a_o value was indistinguishable from that of Cr^{nos}, 9.107(2) Å, indicating that the framework atoms, and therefore the intraframework ions, of $Cr^{nos}_{R400.O1000}$ and Cr^{nos} were located on identical crystallographic positions. Release of the oxyanion from the lattice and migration onto the anion site at the centre of the cage would account for the reformation of the noselite framework. The increase in wavenumber position of the ν_1 Raman peak from 851 ± 1 cm^{-1} to 855.5 ± 1 cm^{-1} (a value equivalent within experimental error to that of Cr^{nos}, 856.5 ± 1 cm^{-1}) and the narrowing of the widths of the chromate IR and Raman bands are consistent with the smaller cation to anion distances and uniformity of chromate environment that would result from migration of chromates back to anion sites.

Presumably the increase in temperature from 600 ± 5°C to 1000 ± 20°C provides the activation energy for release of the chromate oxyanion from the

lattice. Relaxation of the system is inhibited by the high affinity of chromate oxyanions for zeolitic sodium cations. The high temperatures required for the sodalite to noselite transformation indicates that a large energy barrier exists between the sodalite and noselite configurations. Increasing the temperature overcomes this barrier. If the thermal displacement of the lattice bound chromate oxyanion from its equilibrium position increased to the extent that the cation-oxyanion interaction was broken then the oxyanion could migrate back to the anion site.

Beuhrer *et al.*[20] investigated the dynamic properties of hydrogen in hydroxysodalite using quasieleastic neutron scattering. A loss in neutron intensity above ~250°C suggested increasing disorder in the sodium-hydrogen system and a jump rotation of the complete complex cation $(Na_4OH)^{3+}$ was proposed, see Figure 5.22. A model can be proposed in which a jump rotation of the sodium tetrahedra in chromate sodalite allows the cleavage of the chromate oxyanion from the lattice via interruption of the sodium to oxyanion interaction.

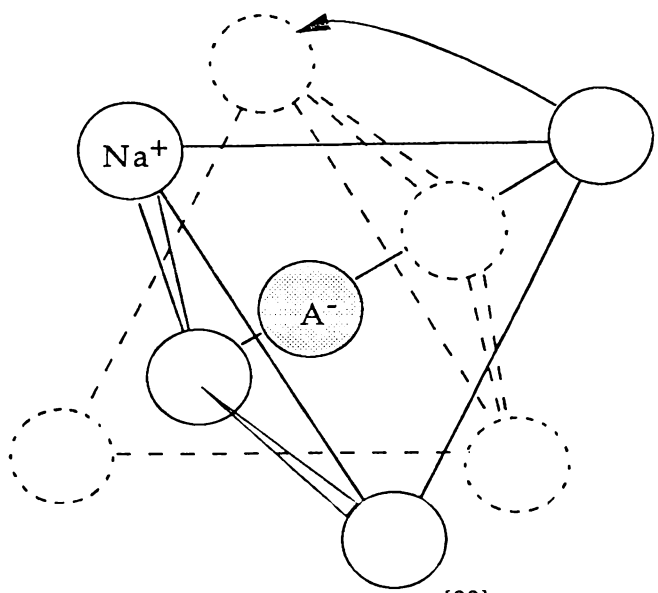


Figure 5.22 Model proposed by Beuhrer et *al.*[22] of the jump rotation of the $(Na_4.OH)^{3+}$ complex cation responsible for the loss of neutron intensity above ~250°C.

5.4.12.8 Summary of Model for the Redox Reactions of Chromate Nosean

The redox reactions of chromate nosean are summarised below.

Reduction of Chromate Nosean to Reduced Chromate Sodalite

Reduction of the $[Na_4.CrO_4]^{2+}/[Na_4]^{4+}$ clusters of Cr^{nos} by hydrogen gas at 400 ± 5°C for 95 hours produced Cr(III) and Cr(IV) in the forms of $[Na_4.CrO_2]^{3+}/[Na_4.OH]^{3+}$ and $[Na_4.CrO_3]^{2+}/[Na_4]^{4+}$ clusters possibly consisting of a Cr(III)-Cr(IV) "dimer". Movement of the reduced chromium oxyanions from the anion sites resulted in the loss of the n-glide along the 100 diffraction plane, hence the observation of the change from a noselite framework to a sodalite framework. The formation of the "dimer" or interactions with lattice atoms inhibited vibrations of the framework tetrahedra resulting in the loss of intensity of framework IR bands.

Reoxidation of Reduced Chromate Sodalite to Chromate Sodalite

Heating reduced chromate sodalite in oxygen at 600 ± 5°C for 24 hours resulted in full reoxidation. Chromate IR and Raman bands reappeared indicating the reformation of divalent chromate oxyanions. The intensities of lattice IR vibrations increased to values similar to those of Cr^{nos} indicating the loss of the "dimer" or loss of interaction between the chromium anions and lattice atoms. Retention of the sodalite framework resulted from the anion sites being vacant due to the coordination of the CrO_4^{2-} species to the lattice through two of the four Na^+ cations of the β-cage. This interaction resulted in a red-shift in the chromate ν_1 Raman band from 856.5 ± 1 cm^{-1} to 851 ± 1 cm^{-1} and a broadening of the chromate IR and Raman bands compared to those of Cr^{nos}.

Formation of Chromate Nosean from Chromate Sodalite

Chromate noselite reformed upon heating in air at 1000 ± 20°C through cleavage of the chromate oxyanion from the lattice and re-positioning of the tetrahedral chromate oxyanion on the anion site. A blue-shift in the ν_1 Raman band from 851 ± 1 cm^{-1} to 855.5 ± 1 cm^{-1} and the sharpening of the chromate IR and Raman bands resulted from this movement.

5.4.12.9 Differences Between the High and Low Temperature Reductions

Brown[21] observed the formation of sodalites at reduction temperatures above 500°C while at temperatures below 500°C the noselite framework was retained. It was suggested that the fully expanded state was necessary to allow the transition as this is reached at ~500°C.[22] Later work by Martinus[23] showed that the transition correlated with the loss of the chromate FTIR band indicating that the full reduction of chromate was required. Combined FTIR and kinetic studies have shown that heating chromate nosean in hydrogen gas at 400 ± 5°C for 95 hours produced sodalite indicating that a fully expanded state is not necessary for the noselite to sodalite transition. Uptake data indicates that full reduction at 600 ± 5°C occurs after about 120 minutes while reaction at 400 ± 5°C was still occurring after 80 hours. Current work has shown that partial reduction to Cr(V) and Cr(IV) results in no space group changes. Since samples in previous work were typically removed after about 24 hours, it can now be concluded that incomplete reduction is the reason why sodalite was not formed in previous work at furnace temperatures up to 400°C.

5.4.13 Comparison of the Redox Chemistries of Occluded Chromates and Chromium Ions in Zeolites

Chromate occluded within the cages of zeolites exhibit a different chemistry to that of chromium present as cations in zeolites. To appreciate

these differences the chemistry of chromium cations in zeolites must be understood.

The Chemistry of Chromium Ions in Zeolites

Chromium cations can be introduced into zeolite cavities either as Cr^{3+} by reaction of the sodium or ammonium forms of zeolites and chromium salts such as $CrCl_3$. Crystallographic studies of X- and Y-type zeolites indicate that polyvalent transition metal ions locate preferentially on site I at the centre of the double six-ring (D6R). This results in the attainment of the highest coordination (sixfold) whereby the high charge of the cation can be most effectively dispersed. The site preference of chromium ions is somewhat different to other polyvalent cations. A crystal structure of CrY zeolite containing 1.2 wt% chromium showed that Cr^{3+} cations occupy preferentially the site I' after dehydration and were three coordinate.[24] The preference of chromium for site I' arises from its small ionic radius (0.069 nm) requiring chromium cations to occupy a site offering the closest cation to zeolite lattice contacts. Exchange of transition metal ions into A-type zeolites and subsequent dehydration leaves the exchanged ion in trigonal coordination in a distorted six-ring which links the α and β cages of the zeolite.[25,26,27]

Oxidation of Cr^{3+} ions to Cr^{5+} and Cr^{6+} have been reported.[28,29,30] The presence of chromate type structures formed via oxidation of chromium exchanged zeolite has been shown by temperature programmed desorption measurements of the removal of extra-framework oxygen ligands as gaseous oxygen.[31] Oxidation also resulted in the appearance of an IR band at 900 cm^{-1} which was assigned to a Cr=O bond vibration of the chromate type complex. Outgassing of chromium ion-exchanged zeolites at high temperatures followed by exposure to atmospheric oxygen at room temperature resulted in the formation of Cr(VI) and Cr(IV) species within zeolite cavities.[32] Reduction of

Cr^{3+} ions by carbon monoxide forms Cr^{2+} ions.[33] The species in Figure 5.23 are envisaged. Oxidation of Cr^{3+} ions to Cr^{5+} involves the acquisition of one extralattice oxygen ligand. The Cr ion moves out of the plane of the six-ring resulting in a distorted tetrahedral complex. Oxidation of Cr^{5+} to Cr^{6+} involves the acquisition of another oxygen ligand and the breaking of a chromium to framework oxygen contact to form intrazeolitic chromate complex.

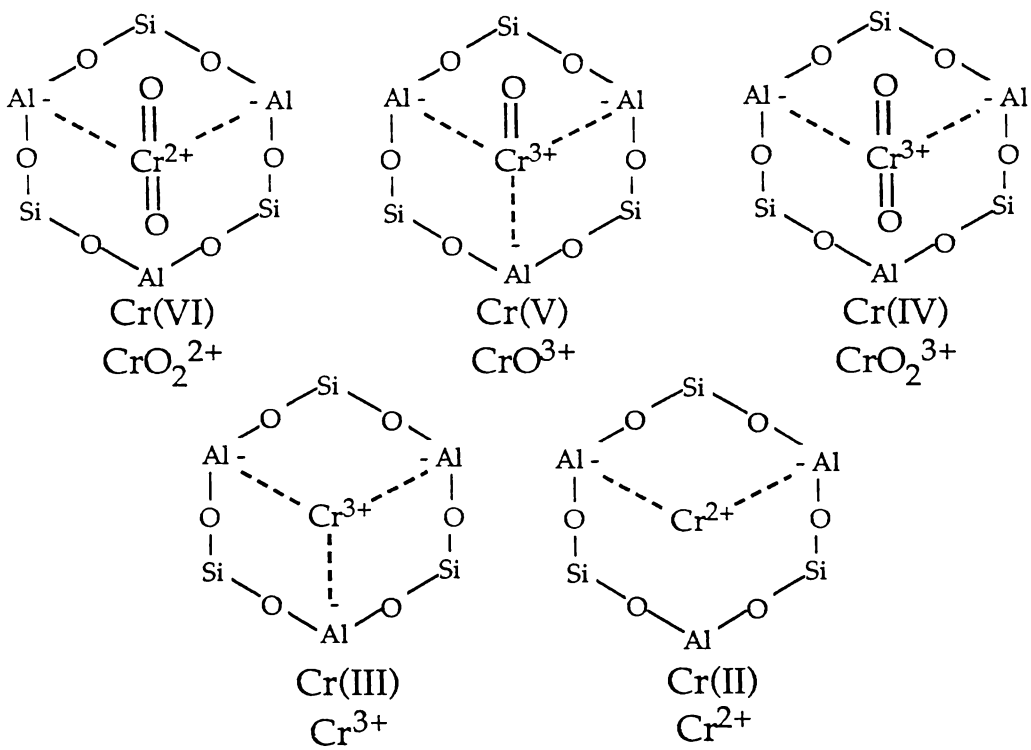


Figure 5.23 Proposed species involved in the redox chemistry of chromium cations in zeolites. Silicon and aluminium atoms belong to an S6R. Below the structure is the chromium oxidation state and the chromium species.

Interpretation of Differences Between the Chemistries of Occluded Chromates and Chromium Ions in Zeolites

Intrazeolitic chromate complexes formed by oxidation of chromium ion-exchanged zeolites and occluded chromates display some structural and spectroscopic similarities, eg the ν_3 chromate IR band at ~900 cm^{-1}, yet they display vastly different redox chemistries.

Occluded chromates display a smaller range of oxidation states than chromium ions in zeolites. While reduction of Cr^{3+} ions forms Cr^{2+}, occluded chromates can not be reduced with $H_{2(g)}$ to below Cr(III). Intrazeolitic chromate complexes can reduce to Cr^{3+} through loss of an oxygen ligand while maintaining high coordinative saturation through the adoption of three-fold coordination to the lattice. Chromium ions balance the charge of the lattice and coordinate tightly to it upon dehydration. They are therefore best regarded as an integral part of the zeolite structure possessing the ability to coordinate extrazeolitic ligands to form intrazeolitic chromate complexes of higher oxidation state. Occluded chromates are extralattice with interaction to the lattice being through the coordination with two sodium cations on S6R. Reduction of occluded chromate to Cr(II) would require the formation of species such as CrO and Na_2CrO_2. The configuration affording the highest coordinative saturation is CrO_2^{2-} with two-fold coordination and C_{2v} symmetry. Reduction to CrO would be prevented by the destabilisation arising from the low coordinative saturation of this species. Reduction to Cr(II) in the form of CrO_2^{2-} would require the formation of $NaHCrO_2$ since one sodium cation is necessarily lost as NaOH during the reduction of Cr(IV), Na_2CrO_3, to Cr(III), $NaCrO_2$. No evidence was found was found for such a species. Reduction is apparently limited to Cr(III) in the form of $NaCrO_2$ species. The stability of this species of two-fold coordination is probably increased through coordination to lattice oxygen atoms, see Figure 5.17 (b).

Reduction of chromates in *HLZ* was limited to an average oxidation state of Cr(+3.5), a result attributed to an interaction between chromium species to form "dimers" promoted by the low coordinative saturation of the CrO_2^- species and the close proximity to the oxygen atom of a neighbouring CrO_3^{2-} species. No evidence for "dimer" formation during redox reactions of chromium cations is observed.

Occluded chromates could not be reduced by $CO_{(g)}$ while $CO_{(g)}$ can reduce chromium cations in zeolites to Cr(II). Since $CO_{(g)}$ is a stronger reducing agent than hydrogen the reason why $H_{2(g)}$ can reduce occluded chromates while $CO_{(g)}$ cannot may be mechanistic rather than thermodynamic. The formation of hydroxyl groups could favour the hydrogen reaction.

5.4.14 Comparison of the Redox Reactions of Occluded Chromate, Molybdate, and Tungstate

Occluded chromate, molybdate, and tungstate displayed significant differences in their redox chemistries. While reduction to Cr(III) was possible for chromate, reduction of molybdate was limited to ~Mo(V), and reduction of tungstate below W(VI) was not possible. The systems can be ordered with respect to the ability to reduce to low oxidation states according to the sequence chromate>molybdate> tungstate. This sequence mirrors that of the relative stabilities of the various oxidation states of the elements, see Figure 5.24. Molybdenum and chromium are qualitatively similar with VI being strongly oxidising. They differ appreciably, however, at lower oxidation states with III being very stable for chromium but less so for molybdenum. Tungsten differs from both chromium and molybdenum with VI being most stable. Reduction of chromates occluded in *MLZ* to Cr(III) was consistent with the stability of the III oxidation state for this element. Likewise, reduction of occluded molybdate to Mo(V) is consistent with the instability of VI and stability of V for this element. The absence of reduction of occluded tungstates can be ascribed to the stability of the VI oxidation state.

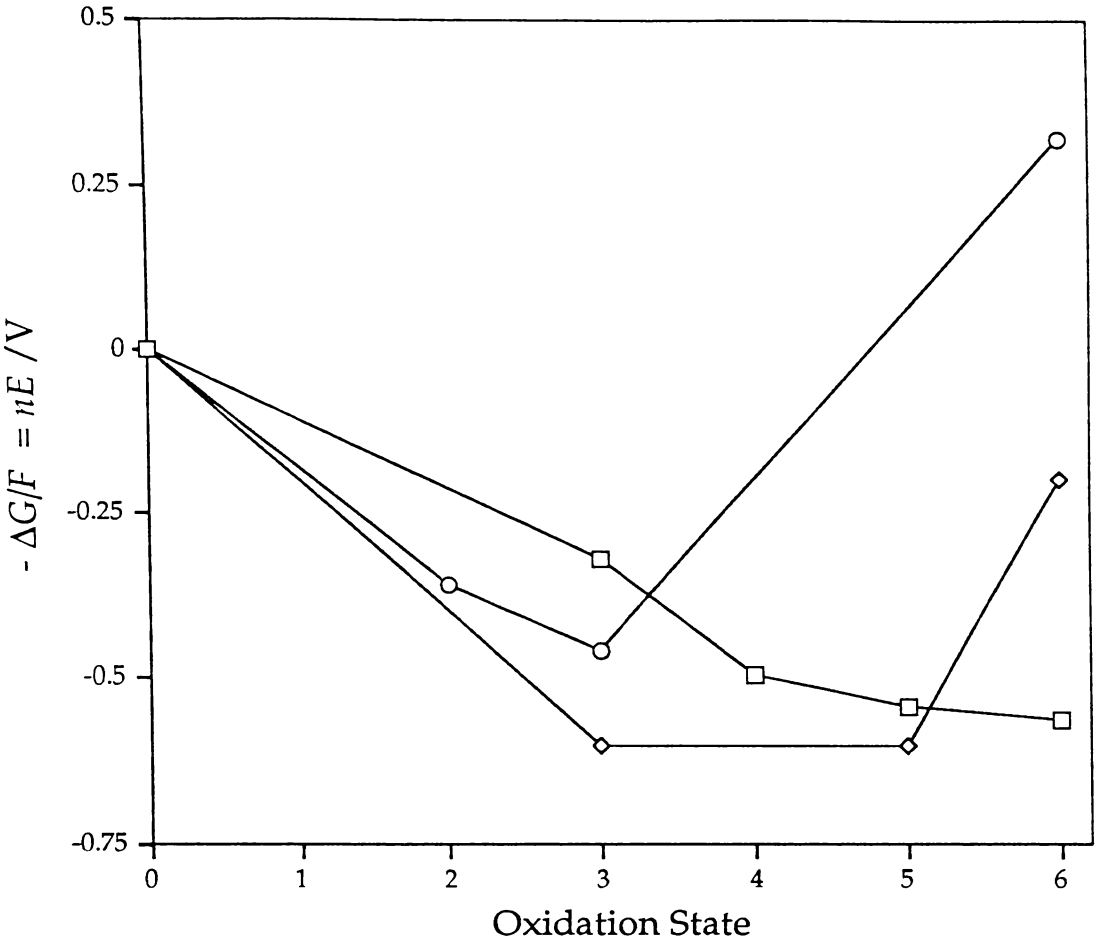


Figure 5.24 Oxidation state free energy diagram for chromium (○), molybdenum (◇), and tungsten (□). This illustrates the greater relative stability of the lower oxidation states according to the sequence chromium>molybdenum>tungsten. ΔG/F values for chromium were divided by 5 to allow their presentation on the same plot as molybdenum and tungsten.

References in Chapter Five

1) Carter, R.L. and Bricker, C.E., *Spectrochimica Acta*, **30A** (1974) 1793.

2) Contarini, S., Aduru. S., and Rabalais, J.W., *J. Phys.* Chem., **90** (1986) 3202.

3) Henderson, C.M.B. and Taylor, D., *Spectrochimica Acta*, **33A** (1977) 283.

4) Khitrov, V.A. and Khitrova, N.N., *Doklady Akad. Nauk. S.S.S.R.*, **88** (1953) 853.

5) Khitrov, V.A. and Bergman, A.G., *Doklady Akad. Nauk. S.S.S.R.*, **24** (1954) 204.

6) Addison, C.C and Barker, M.G., *J. Chem. Soc.*, (1965) 5534.

7) Olson, D.H., *J. Phys. Chem.*, **74(14)** (1970) 2758.
8) MacKay, K.M. and MacKay, R.A., in " **Modern Inorganic Chemistry**", 3rd Edition, International Textbook Company (London), 1981, pp. 209.
9) Buehrer, W., Felsche, J., and Luger, S., *J. Chem. Phys.*, **87**(4) (1987) 2316
10) Jenkins, H.D.B. and Thakur, K.P, *J. Chem. Educ.*, **56** (1979) 577.
11) Tomisaka, T. and Eugster, H.P., *Mineral. Jour. Japan*, **5** (1968) 249.
12) Weller, M.T, Wong, G., Adamson, C.L., Dodd, S.M., and Roe, J.J.B., *J. Chem. Soc. Dalton Trans.*, (1990) 593.
13) Weller, M.T. and Haworth, K.E., *J. Chem. Soc. Chem. Commun.*, (1991) 734.
14) Hassan, I. and Grundy, H.D., *Acta Cryst.*, **B40** (1984) 6.
15) Bondareva, O.S. and Malinovskii, Yu.A., *Sov. Phys. Crystallogr.*, **28(3)** (1983) 273.
16) Denks, V.P., *Tr. Inst. Fiz. Akad. Nauk Est. SSR*, **55** (1984) 14.
17) Barrer, R.M., Cole, J.F., and Villager, H., *J. Chem. Soc. (A)*, (1970) 1523.
18) Barrer, R.M. and Raitt, J.S., *J. Chem. Soc.*, (1954) 4641.
19) Luger, S., Felsche, J., and Fischer, P., *Acta Cryst.*, **C43** (1987) 1.
20) Beuhrer, W., Felsche, J. and Luger, S., *J. Chem. Phys.*, **87(4)** (1987) 2316.
21) Brown, M.L., in "**Some Aspects of the Reactivity of Chromate Nosean**", M.Sc. thesis, The University of Waikato, Hamilton, New Zealand (1989).
22) Taylor, D., *Mineralogical Magazine*, **38** (1972) 593.
23) Martinus, D.D., in "**The Synthesis and Characterisation of Oxyanion-Salt Loaded Noseans**", M.Sc. Thesis, The University of Waikato, Hamilton, New Zealand (1989).
24) Pearce, J.R. and Mortier, W.J., *J. Chem. Soc. Faraday Trans. I*, **77** (1981) 1935.
25) Klier, K. and Ralek, M., *J. Phys. Chem. Solids*, **29** (1968) 951 .
26) Polak, R. and Cerny, V., *J. Phys. Chem. Solids*, **29** (1968) 945.
27) Riley, P.E. and Seff, K., *J. Chem. Soc. Chem. Commun.*, (1972) 1287.
28) Naccache, C. and Taarit, Y. ben, *J. Chem. Soc. Faraday Trans. I*, **69** (1973) 1475.
29) Pearce, J.R., Sherwood, D.E. and Lunsford, J.H., *J. Phys. Chem.*, **84** (1980) 3215.
30) Hemidy, J.F., Goupil, J.M. and Cornet, D., *J. Chim. Phys.*, **74** (1977) 74.
31) Iwamoto, M. , Nakamura, W. , Nagano, H. and Kagawa, S., *J. Phys. Chem.*, **86** (1982) 153.
32) Coughlan, B., M^{c}Cann, W.A. and Carroll, W.M., *J. Colloid and Interface Sci.*, **74** (1979) 136.
33) Kellerman, R., Hutta, P.J., and Klier, K., *J. Am. Chem. Soc.*, **96(18)** (1974) 5946

Chapter Six

Kinetics of the Redox Reactions of Chromate Zeolites

Chapter Six

Kinetics of the Reactions of Chromate Zeolites

6.1 Introduction

Studies of the kinetics of redox reactions of various chromate-loaded zeolites were performed. The effects of zeolite structure, degree of chromate loading, and temperature on reaction rate and kinetics were determined. Fitting reaction data to kinetic models allowed details of reaction mechanisms to be deduced.

6.2 Methods and Materials

Redox reactions at temperatures ranging between 250°C and 650°C were performed on zeolites 5.8CrX, 2.1CrX, 4.8Cr5A, 2.8CrY, and 13.4CrY. These zeolites were chosen to give a range of different zeolites with similar loadings and also different loadings for one type of zeolite. The data obtained should thereby allow the effects of zeolite structure and degree of loading on the rates of redox processes to be deduced. Reactions were performed under conditions outlined in Section 2.14.

Uptake data were converted into values of θ (extent of reaction). The validity of several kinetic models was tested by inspection of how well the data fitted the kinetic equations. The derivations and graphical implications of the various kinetic models are given in Section 6.3.

6.3 Heterogeneous Reaction Kinetics

6.3.1 The Consecutive Steps

A heterogeneous catalytic reaction involving a porous solid can be divided into the following elementary steps. 1) diffusion of gas molecules to the surface of the crystal, 2) diffusion of gas molecules into the crystal, 3) adsorption of the gas molecules at the active site, 4) chemical reaction, 5) desorption of the product(s) from the active site, 6) diffusion of the product(s) out of the crystal, 7) diffusion of the product(s) away from the surface of the crystal. Any of these steps, through which the reaction proceeds, may be rate limiting under certain conditions.

6.3.2 Diffusion of Reactant Molecules to the Surface

Transport of gaseous reactant molecules to the surface of the solid catalysts is controlled by the rate of molecular diffusion. This process is expected to be rapid at the temperatures of the reactions.

6.3.3 Diffusion of Gas Molecules into the Crystals

Once the reactant molecule has reached the surface of a porous solid it must then penetrate in order to reach active sites. Solid state reactions between zeolites and sodium chromate loads chromate oxyanions throughout the entire zeolite crystal. Reaction of all but the chromates adsorbed to the surface of the crystals will require the passage of reactant gases through zeolite pores and channels. If zeolite pore openings offer a barrier to such passage then the rate of diffusion of reactant gases to the active site may be rate limiting. Many zeolitic processes, such as gaseous adsorption and ion-exchange, display diffusion controlled kinetics. Barrer[1] described in detail the kinetics of

intracrystalline diffusion and derived equations 6.1 and 6.2 for the fractional uptake (θ) as functions of large t and small t, respectively.

$$\ln\theta = \ln\left(\frac{6}{\pi^2}\right) - \frac{D\pi^2 t}{r_o^2} \qquad 6.1$$

$$\theta = \frac{6}{r_o}\sqrt{\frac{Dt}{\pi}} = \frac{2A}{V}\sqrt{\frac{Dt}{\pi}} \qquad 6.2$$

where A is the total external surface and V is the total volume of the crystallites of radius r_o, and D is the diffusion coefficient. A plot of extent of reaction against $\sqrt{t}$ will have a slope equal to $6 / r_o \sqrt{D / \pi}$.

In large crystals one measures intracrystalline diffusion. Examples are water diffusion in chabazite, heulandite and gmelinite,[2] diffusion of ammonia in analcime,[3] diffusion of Ne and Kr into mordenite,[4] imbibation of NaCl and $CaCl_2$ salts from aqueous solutions into Na-A,[5] elution of LiCl and NaCl from salt loaded A-type zeolite.[6] However, in beds of fine synthetic zeolite powders or powder compacts, in which the individual crystals are normally in the range 0.1 to 10 μm, the situation is more complex. Some possible rate controlling steps which can arise are:

1) Intracrystalline diffusion, i.e. diffusion within crystals.

2) Intercrystalline diffusion, i.e. diffusion in intercrystalline void spaces.

3) Control by passage through surface skins on crystal surfaces.

Surface Skins

The equation for the fractional uptake for rate control by transmission through a surface skin into spheres all of the same radius, r_o, and of total external surface area, A, from constant external pressure is given in equation 6.3

$$\theta = 1 - \exp\left(-\frac{3\alpha t}{r_o}\right) = 1 - \exp\left(-\frac{\alpha A t}{V}\right) \qquad 6.3$$

where α is the transmission coefficient through the skin.[7]

Intercrystalline Diffusion

Consider linear diffusion into a cylindrical column of zeolite powder bounded top and bottom by the planes x = 0 and x = *l*. Sorption occurs only after flow through x = 0, all other surfaces being impermeable due to the container walls. For control, at constant pressure through crystallites all of radius r_o, by intracrystalline Knudsen flow the early time √t equation is

$$\theta = \frac{2}{l}\sqrt{\frac{D_g t}{\pi}} \qquad 6.4$$

where D_g is the diffusion coefficient. A plot of θ against √t will be linear over the initial stages of the reaction and will have a slope equal to $\frac{2}{l}\sqrt{D_g / \pi}$.

6.3.4 Chemisorption Processes.

Once a reactant molecule has penetrated through the crystal it must adsorb onto the active site. If the reaction of chemisorbed species, i.e step 4, is rate determining then processes involving the adsorption and desorption of reactants reach equilibrium. If this situation is fulfilled then the Langmuir isotherm can be used to estimate the concentrations of adsorbed reactants. If the reaction at the surface is rapid then the adsorption at the gas-solid interface, i.e. step 3, may be rate determining. Two main types of gas-solid adsorptions may be distinguished. In the first type, the interactions are weak and are regarded as arising from van der Waals-type interactions, with heats of adsorption, ΔH_a, typically being about -20 kJ mol^{-1}. More exothermic heats

of adsorption, in the range -40 to -400 kJ mol^{-1}, are involved in the second type of interaction. The strength of the bonds between the surface atoms and the adsorbate in this second type are in the same range as those between bonded atoms in molecules and this type of interaction is referred to as chemisorption to distinguish it from van der Waals' or physical adsorption. Physical adsorption equilibria are usually established rapidly except when limited by diffusion into porous solids. Chemisorption, however, may be either rapid or slow. For slow activated chemisorption the experimental results often fit the so-called Elovich equation, i.e.

$$\frac{dq}{dt} = a \exp(-\alpha q) \qquad 6.5$$

where a and α are constants and q is the amount adsorbed. The integrated form of equation 6.5 can be written in the form

$$q = (2.3/\alpha)\log(t + t_0) - (2.3/\alpha)\log t_0 \qquad 6.6$$

$$\text{with } t_0 = 1/a\,\alpha \qquad 6.7$$

With a correctly chosen t_0, the plot of q against log $(t + t_0)$ should give a straight line with a slope = $2.3/\alpha$. Equation 6.7 then gives a which represents the initial rate of adsorption for $q = 0$. The test involves one disposable parameter t_0 which is found by trial and error. With too small a t_0 value one obtains a curve convex to the log $(t + t_0)$ axis whereas too large a value of t_0 will give a concave curve. This is illustrated in a plot drawn by Tayler and Thon[8] for the adsorption of H_2 on Cr_2O_3.

The literature on the kinetics of chemisorption shows that the Elovich equation is often valid for systems in which the adsorbing surface is heterogeneous. This applies to many chemisorption processes of practical interest, such as adsorption of gases on industrial catalysts and other

powdered or granular materials and adsorption on imperfectly cleaned metal surfaces.

6.3.5 Chemical Reaction

Ritchie showed that in many cases where unsatisfactory Elovich plots were obtained that good fits could be obtained to the equations for the adsorption of gases on solids based simply on the adsorption of gases at vacant surface sites.[9] The theory Ritchie used was elementary. Let θ be the fraction of surface sites which are occupied by the adsorbed gas, let n be the number of surface sites occupied by each molecule of adsorbed gas and let α be the rate constant. Assume that the rate of chemisorption is independent of gas pressure, or occurs at constant pressure, and depends solely on the fraction of sites which are unoccupied at time t, then

$$\frac{d\theta}{dt} = \alpha (1-\theta)^n \qquad 6.8$$

Equation (6.8) integrates to

$$\frac{1}{(1-\theta)^{n-1}} = (n-1)\alpha t + 1, \text{ for } n \neq 1 \qquad 6.9$$

or

$$\theta = 1 - e^{-\alpha t}, \text{ for } n = 1. \qquad 6.10$$

6.3.6 Complexities of Gas-Solid Reactions

Reactions between gases and solids are often complex. The models described earlier are some of the simplest examples of kinetic models. For examples of more complex models see Levenspiel.[10] Generally the objective of kinetic studies is to elucidate the mechanism(s) of the process being

investigated. The simplest model that can describe the kinetics is regarded as a good starting point for the kinetic assignment. The models discussed earlier were found to adequately describe the kinetics of the most reactions in this work.

6.4 The Activation Energy

The magnitude of a rate constant, k, depends on the magnitude of the activation energy, E_a, and on the absolute temperature, T. Quantitatively, k is related to E_a and T by the Arrhenius equation:

$$k = A\, e^{-E_a/RT} \qquad 6.11$$

where A is a proportionality constant, R is the gas constant, and e is the base of the natural logarithms. Taking the natural logarithm of equation 6.11 gives:

$$\ln k = \ln A - \frac{E_a}{RT} \qquad 6.12$$

Thus a plot of $\ln k$ versus $1/T$ gives a straight line whose slope is equal to $-Ea/R$ and whose intercept with the ordinate is $\ln A$. Similarly, activated diffusion controlled reactions show an Arrhenius dependency of the form:

$$\ln D = \ln D_0 - \frac{E_a}{RT} \qquad 6.13$$

6.5 Results

6.5.1 Rate Dependence on Gas Pressure

Reaction and adsorption studies are generally performed under constant pressure conditions using continuous flow apparatus. Under these conditions the effect of gas pressure on reaction rate can be removed from the kinetic equation and is effectively accounted for in the rate constant. The vacuum line used in this work is a constant volume/changing pressure system. Under these conditions the effect of gas pressure on rate must be assessed and accounted for in the kinetic equations.

Two experiments were performed with different hydrogen pressures to assess the effect of hydrogen pressure on rate of reduction. Reactions were performed as outlined in Section 2.14. All other variables were kept constant by examining the same zeolite for both experiments and using the same sample weight (~0.5 g) and furnace temperature (250°C). Any changes in rate of uptake under these conditions would be related to the hydrogen pressure. The reactions were performed with initial hydrogen pressures, after the manifold was opened to the sample chamber, of 31.4 cmHg and 20.5 cmHg. From the similarity of the kinetics of the hydrogen uptake at the two different pressures it was concluded that the instantaneous rate of uptake was independent of the hydrogen pressure. This allowed the unmodified use of the kinetic models described earlier.

Total uptakes of oxygen were approximately half those of hydrogen. For example during the reoxidations of 5.8CrX the initial and final oxygen pressures were ~22 cmHg to ~18 cmHg indicating a change of only about 20%. Furthermore, most of this change ocurred over the rapid initial stages of the oxidation where uptake was too rapid to be monitored. Over the majority of the oxidation for which data was obtained the $O_{2(g)}$ pressure was constant to

within about 2 cmHg. Unmodified models discussed earlier were used in the analysis of the data.

6.5.2 Reactivity of Chromate Zeolite 5.8CrX

Reductions

Uptakes of hydrogen by 5.8CrX as functions of time at various temperatures are shown in Figure 6.1. Data collected for the reduction reactions are given in Appendix Three. Of the kinetic models described earlier, only the second-order kinetic model gave linear plots. Plots of $1/(1-\theta)$ against time, corresponding to second-order reaction kinetics, are shown in Figure 6.2. Linearity over substantial extents of the overall reactions was shown by regression analysis, the results of which are shown in Table 6.1 along with the calculated values of the second-order rate constants, k_2. The Arrhenius plot for the reduction process, see Figure 6.3, had an intercept of 15.32 corresponding to an A value of 2.22×10^{-7} and a slope of -10984 ($r^2 = 0.996$) giving an apparent activation energy of 91 ± 5 kJ mol^{-1}.

Reoxidations

Oxygen uptakes during the reoxidation of 5.8CrX against time are shown in Figure 6.4. Data collected for the reoxidation reactions are given in Appendix Four. A plot of $1/(1-\theta)^3$ against time, corresponding to four-order kinetics, for Reox#19 is shown in Figure 6.5. The intercept of the line of best fit shown in Figure 6.5 was 4.46, a value significantly higher than unity predicted by the fouth-order kinetic model. Plots of θ against the natural logarithm of time, corresponding to chemisorption kinetics, can be seen in Figure 6.6. Of the kinetic models described earlier, only fourth-order reaction and chemisorption kinetic models gave linear plots.

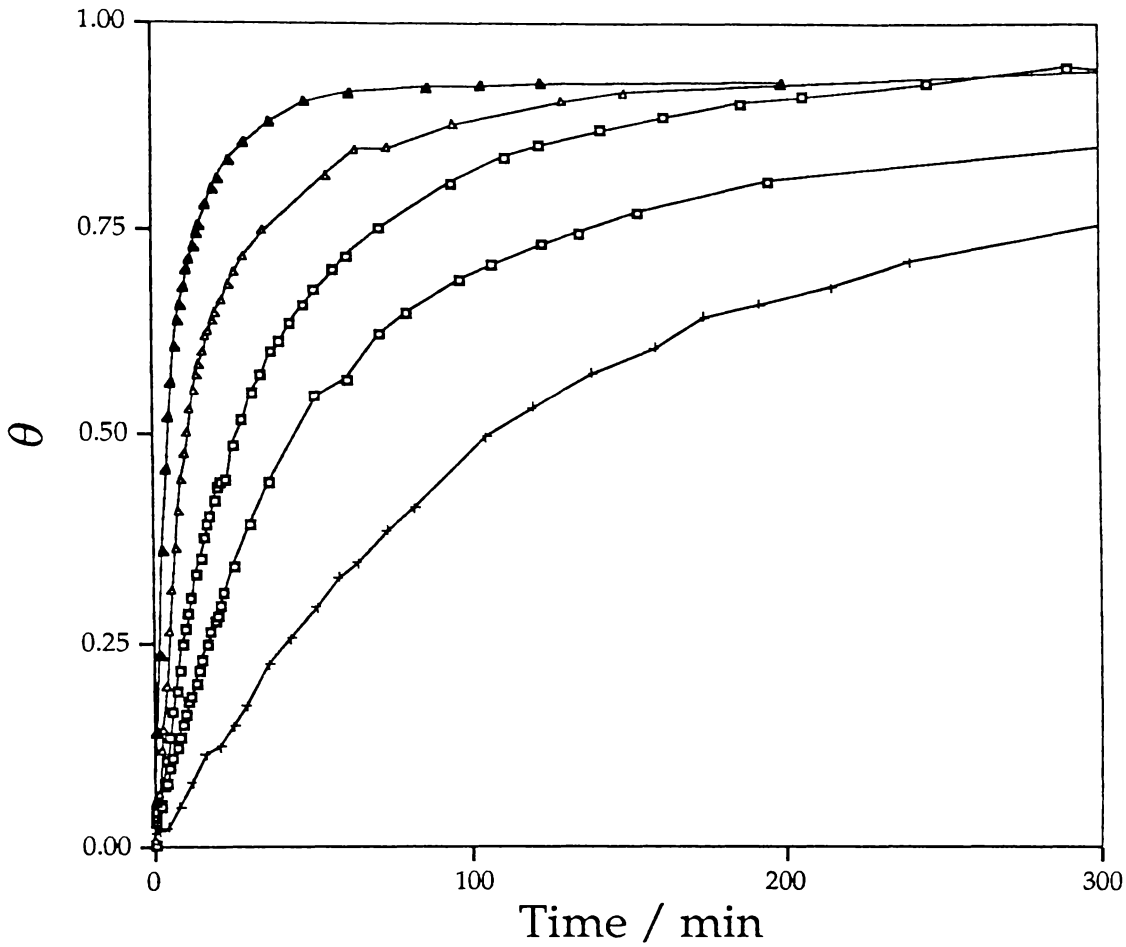


Figure 6.1 Hydrogen uptakes by 5.8CrX as functions of time at various temperatures. Reaction temperatures are: (+ Red#27, 275°C), (▫ Red#25, 300°C), (▪ Red#26, 325°C), (▲ Red#22, 350°C), and (▲ Red#24, 375°C).

Table 6.1 Kinetic analysis of the reduction of 5.8CrX by hydrogen gas. k_2 is the second-order rate constant. θ_{max} is the maximum value of θ included in the least squares fit, *nd* is the number of data points included in the least squares fit and r^2 is the correlation coefficient.

Red#	T/°C	k_2	θ_{max}	*nd*	r^2
24	375	0.19697	0.90	22	0.998
20	350	0.07247	0.87	23	0.994
23	325	0.04526	0.93	25	0.996
25	300	0.02197	0.81	32	0.999
27	275	0.01020	0.71	23	0.997

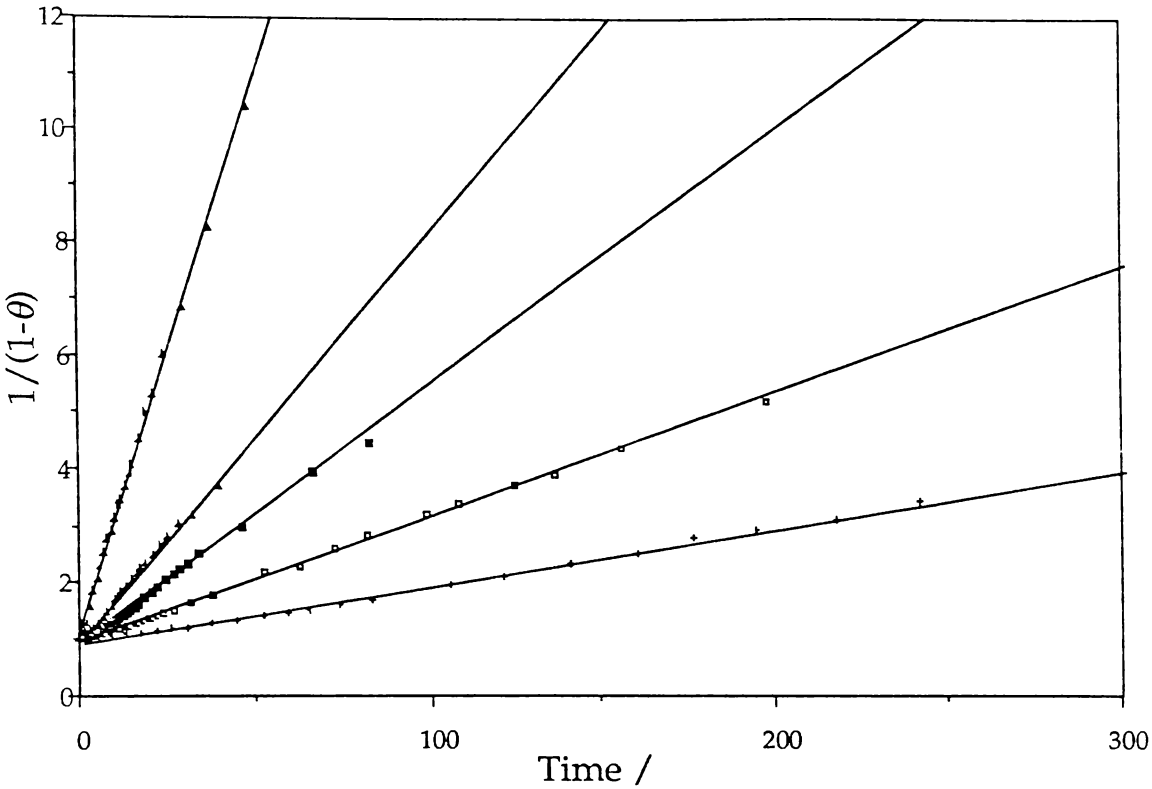


Figure 6.2 Second-order reaction kinetics plot for reductions of 5.8CrX at various temperatures. Reaction temperatures are: (+ Red#27, 275°C), (▫ Red#25, 300°C), (▪ Red#23, 325°C), (▲ Red#20, 350°C), and (▲ Red#24, 375°C).

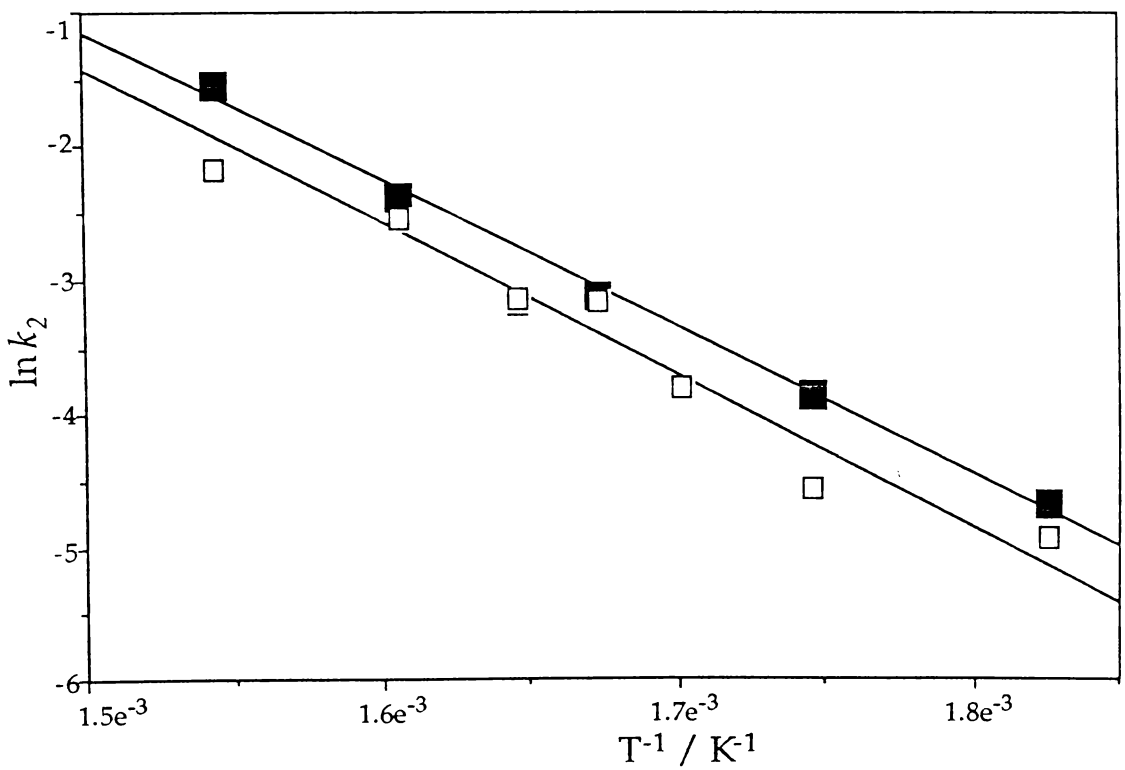


Figure 6.3 Arrhenius plot for the reduction of zeolites 2.1CrX (□) and 5.8CrX (■). by hydrogen gas.

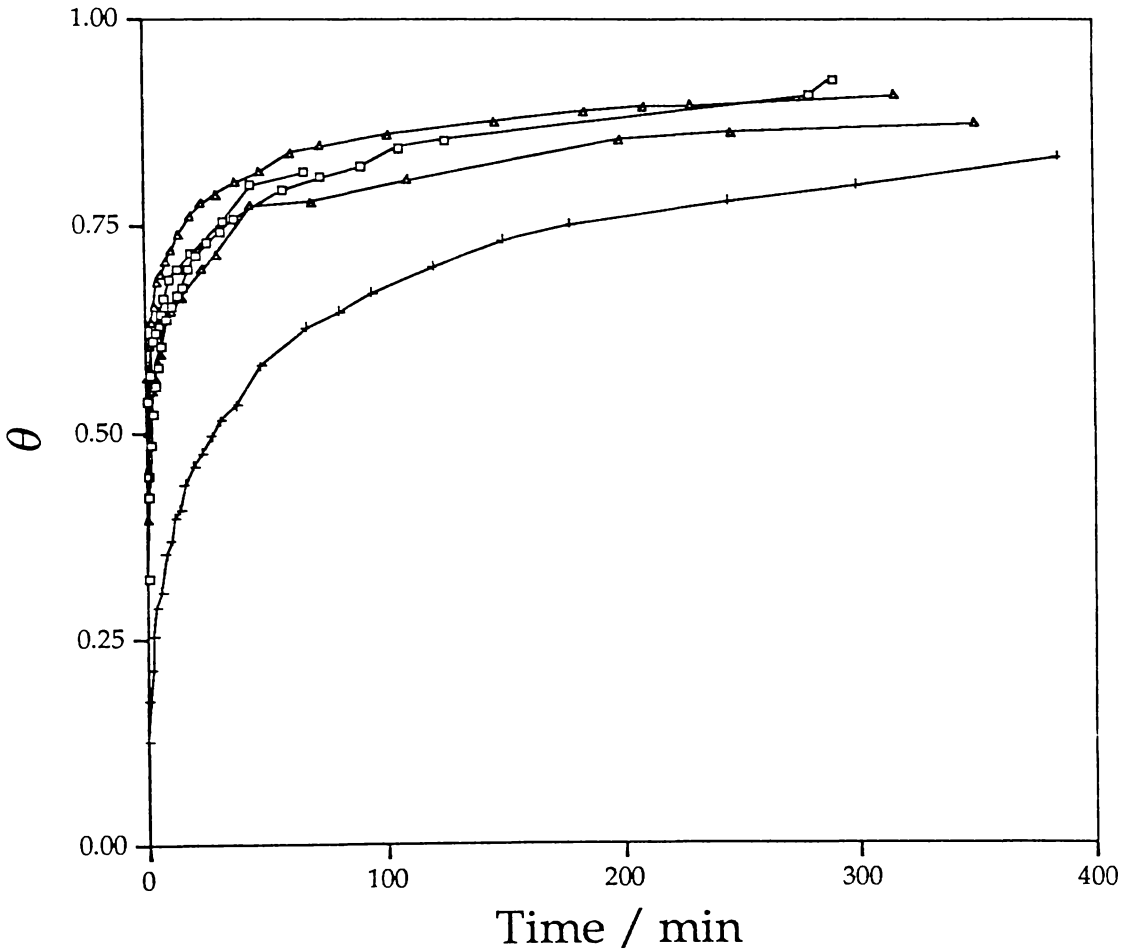


Figure 6.4 Oxygen uptakes by reduced 5.8CrX as functions of time at various temperatures. Reaction temperatures are: (+ Reox#22, 300°C), (▲ Reox#17, 400°C), (■ Reox#19, 350°C) (▫ Reox#18, 400°C), and (△ Reox#20, 375°C).

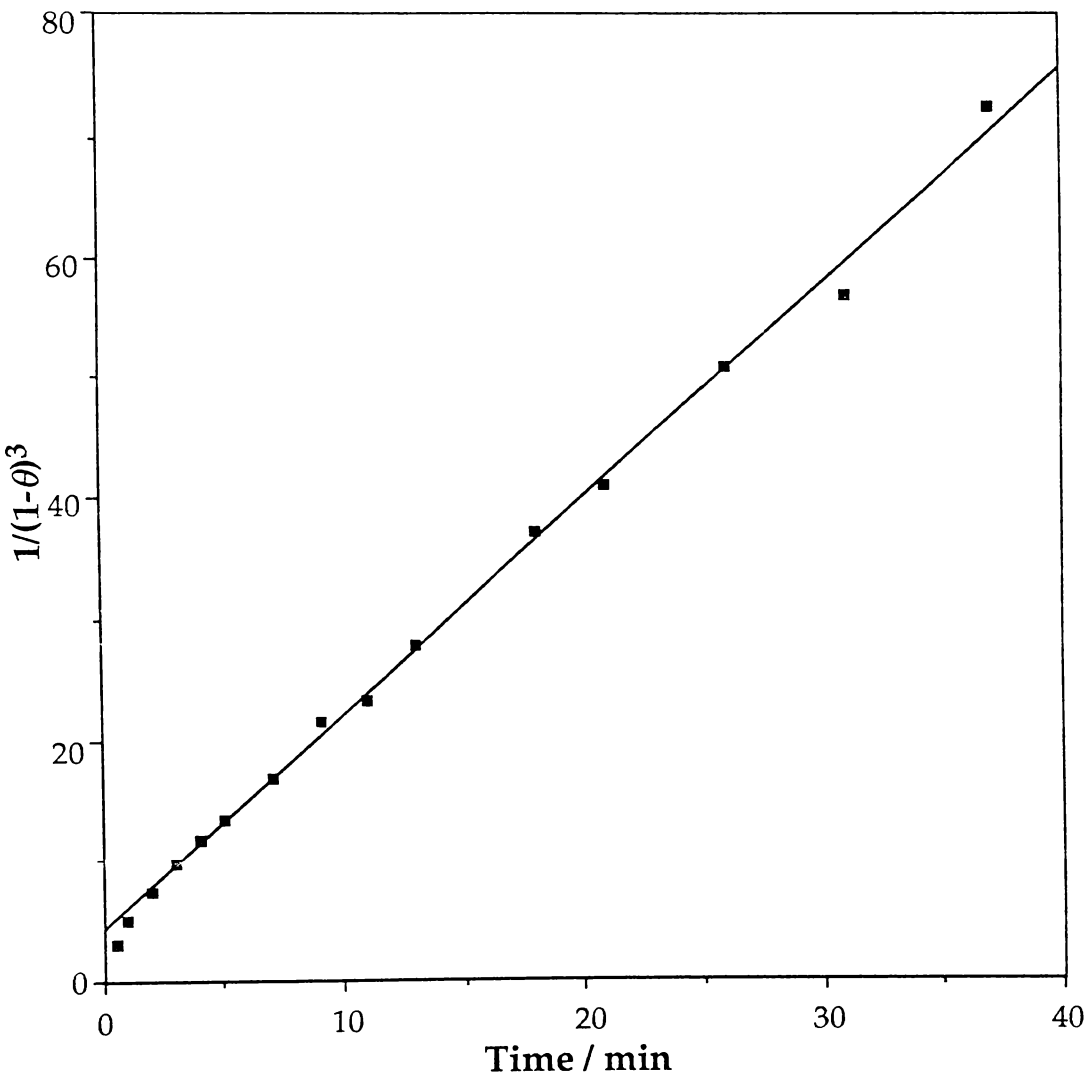


Figure 6.5 Plot of $1/(1-\theta)^3$, corresponding to fourth-order kinetics, for a reoxidation of reduced 5.8CrX by oxygen gas at 350°C (Reox#19).

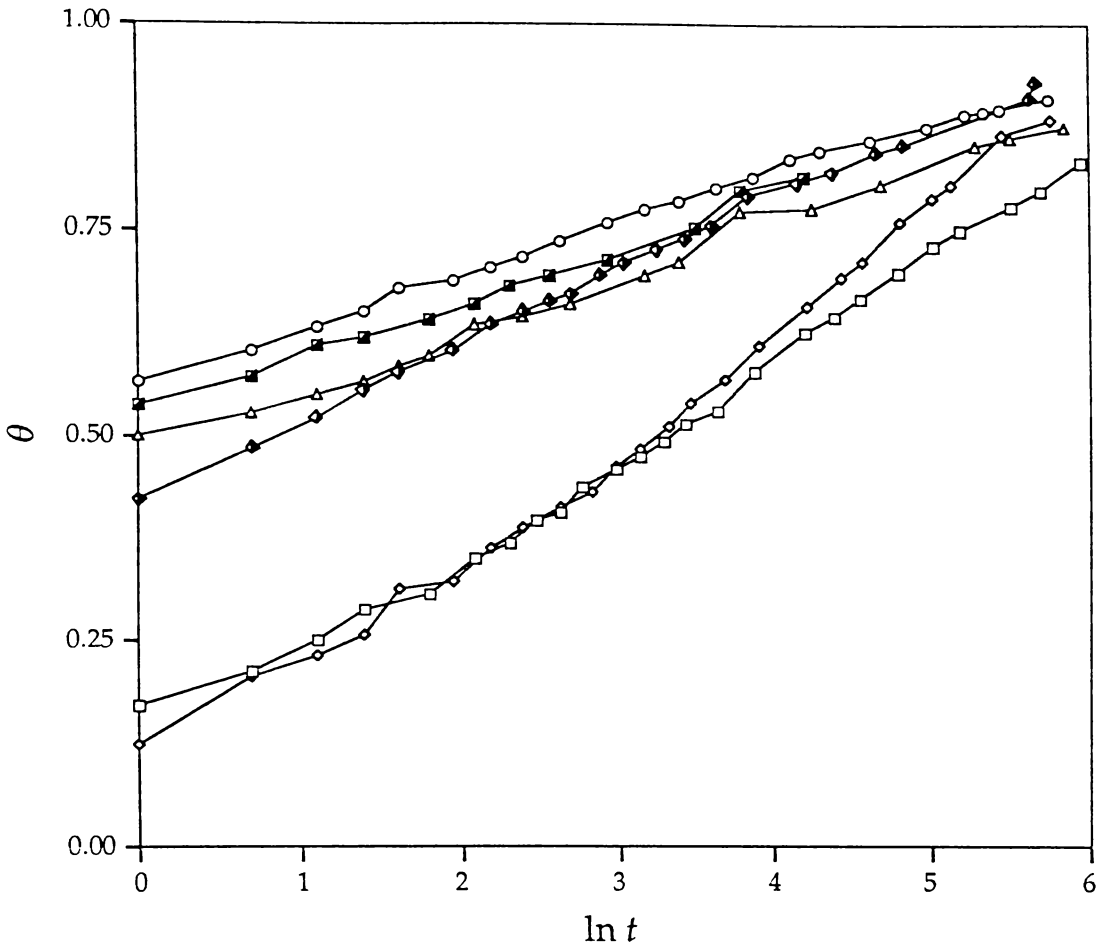


Figure 6.6 Plot of θ against ln$t$ for reoxidations of reduced 5.8CrX. Reactions are (○ Reox#20, 375°C), (□ Reox#22, 300°C), (◗ Reox#19, 350°C), (◢ Reox#18, 400°C), (△, Reox#17, 400°C), and (◇ Reox#15, 400°C).

6.5.3 Reactivity of Chromate Zeolite 2.1CrX

Reductions

Uptakes of hydrogen against time for the reductions of 2.1CrX at various temperatures are shown in Figure 6.7. Data collected for the reduction reactions are given in Appendix Five. Of the kinetic models described earlier, only the second-order kinetic model gave linear plots. Plots corresponding to second-order kinetics are shown in Figure 6.8. Linearity over substantial extents of the overall reactions was shown by regression analysis, the results of

which are shown in Table 6.2 along with the calculated values of the second-order rate constants, k_2. The Arrhenius plot for the reduction of chromate zeolite 2.1CrX by hydrogen gas is shown in Figure 6.3. The line of best fit for the data displayed in Figure 6.3 had an intercept of 15.72 (ln A) and a slope of -11426 ($r^2 = 0.943$) corresponding to a value for A of 1.489×10^{-7} and an apparent activation energy of 95 ± 7 kJ mol^{-1}.

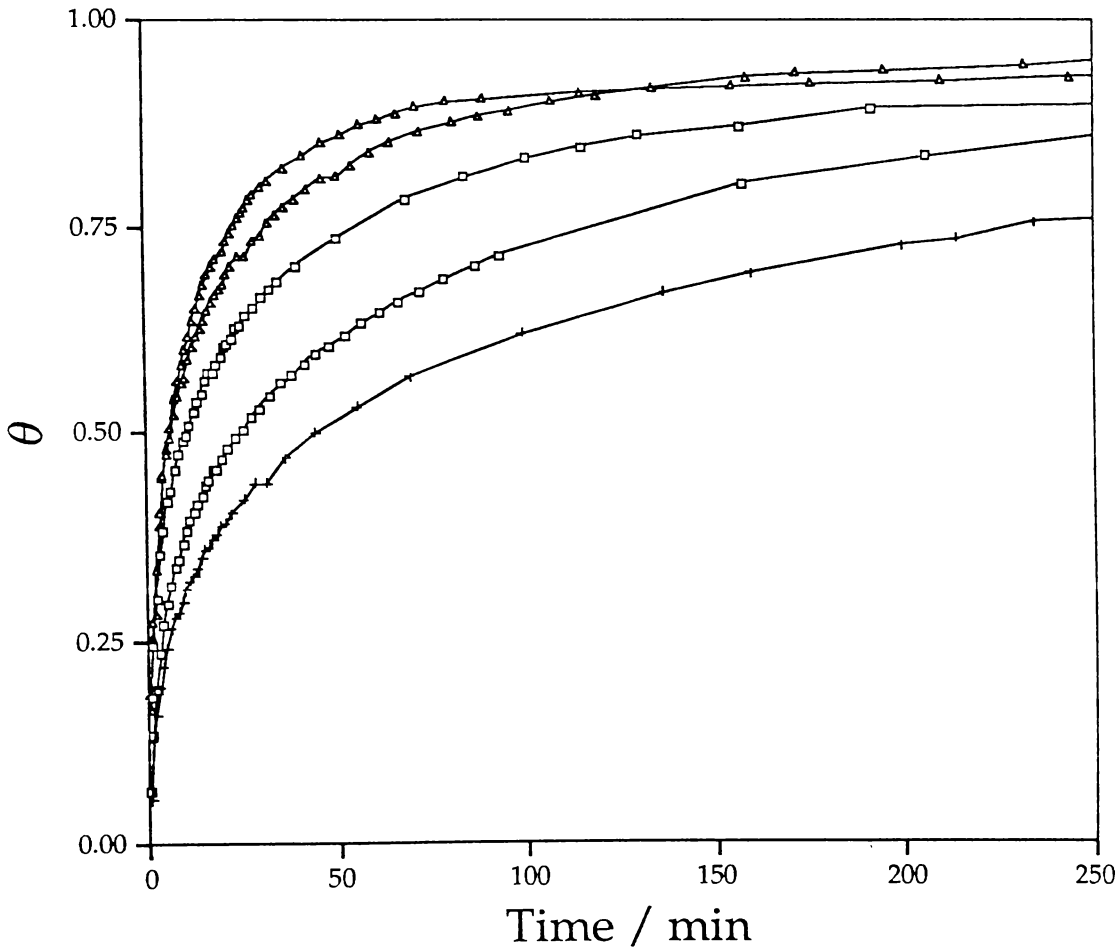


Figure 6.7 Hydrogen uptakes by 2.1CrX as functions of time at various temperatures. Reaction temperatures are: (+ Red#30, 300°C), (▫ Red#33, 315°C), (▪ Red#36, 335°C), (▲ Red#37, 350°C), and (▲ Red#39, 375°C).

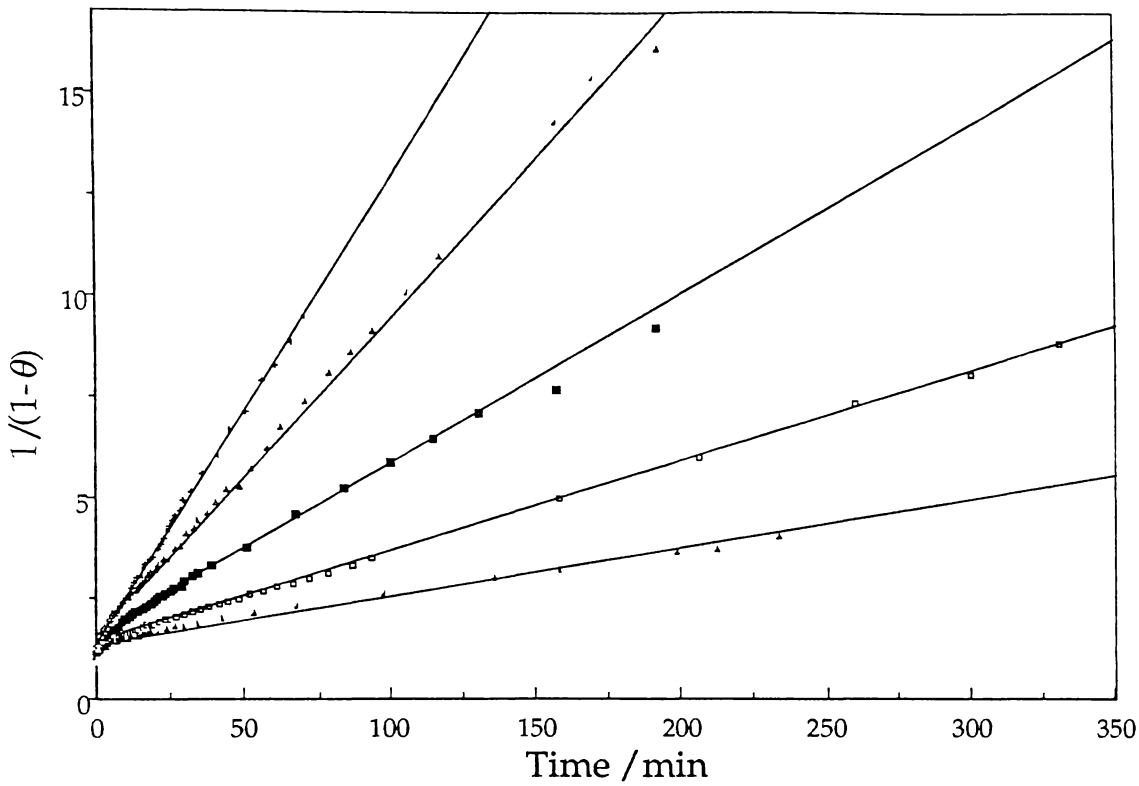


Figure 6.8 Second-order reaction kinetics plot for reductions of 2.1CrX at various temperatures. Reaction temperatures are: (▲ Red#30, 300°C), (▫ Red#33, 315°C), (▪ Red#36, 335°C), (▲ Red#37, 350°C), and (+ Red#39, 375°C).

Table 6.2. Kinetic analysis of the reduction of chromate zeolite 2.1CrX by hydrogen gas. k_2 is the second-order rate constant. θ_{max} is the maximum value of θ included in the least squares fit, *nd* is the number of data points included in the least squares fit and r^2 is the correlation coefficient.

Red#	T /°C	k_2	θ_{max}	*nd*	r^2
38	225	0.00614	0.453 - 0.710	9	0.999
31	250	0.00663	0.483 - 0.737	7	0.995
32	275	0.00724	0.494 - 0.756	10	0.996
33	315	0.02243	0.441 - 0.887	27	0.997
34	350	0.08066	0.524 - 0.809	29	0.998
36	335	0.04200	0.547 - 0.859	22	0.993
37	350	0.07966	0.448 - 0.953	40	0.990
39	375	0.1147	0.445 - 0.895	33	0.999

Reoxidations

Reoxidations of 2.1CrX were investigated in the temperature range 250°C to 375°C. Data collected for the reoxidation reactions are given in Appendix Six. Plots of the extent of reaction, θ, against time for reoxidations are shown in Figure 6.9.

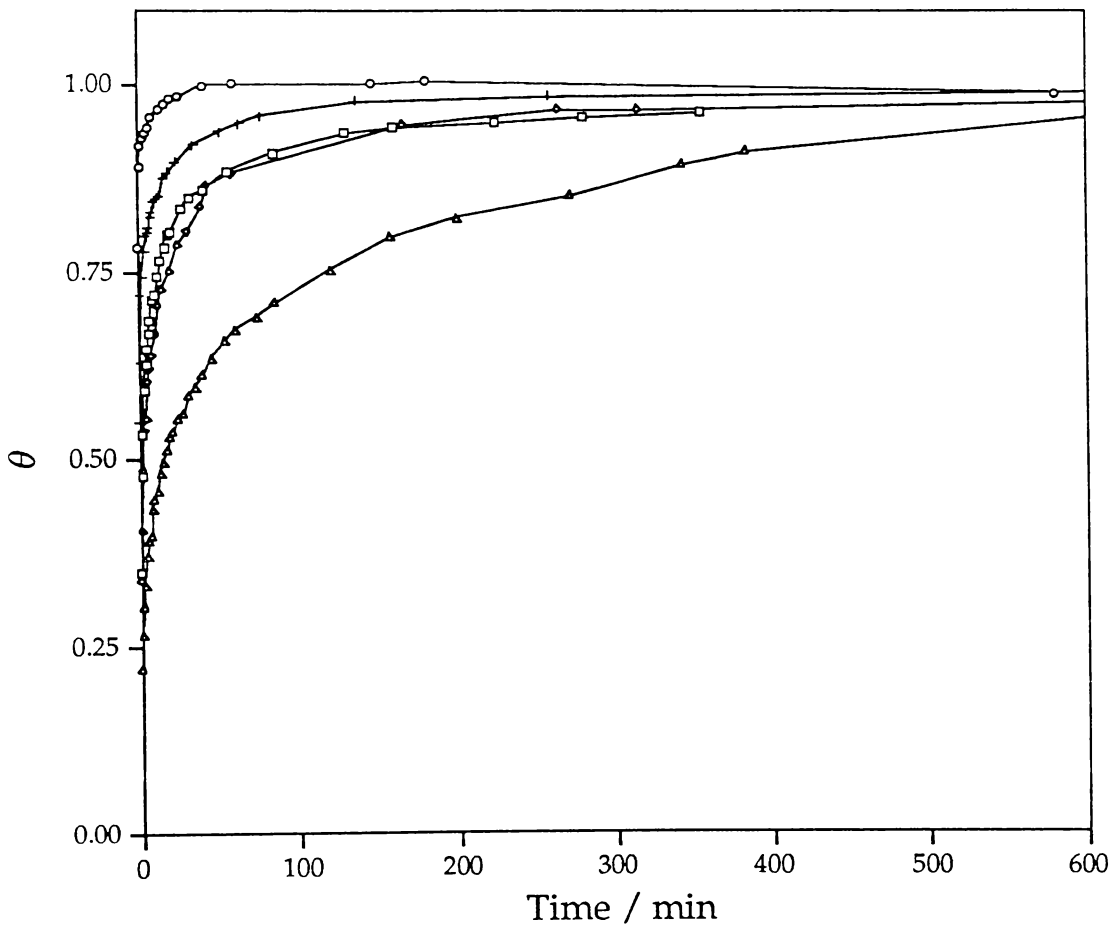


Figure 6.9 Kinetics of the reoxidation of reduced 2.1CrX by oxygen gas at various temperatures. Reaction temperatures are (◇ Reox#25, 250°C), (△ Reox#27, 275°C), (□ Reox#24, 300°C), (+ Reox#28, 315°C), and (○ Reox#26, 325°C).

6.5.4 Reactivity of Chromate Zeolite 2.8CrY

Uptakes of hydrogen gas by chromate zeolite 2.8CrY as functions of time at various temperatures are shown in Figure 6.10. Data collected for the reduction reactions are given in Appendix One. Of the kinetic models

described earlier, only the second-order kinetic model gave linear plots. Plots testing for second-order reaction kinetics are shown in Figure 6.11. Least squares regression analysis of the lines in Figure 6.11 gave the second-order rate constants shown in Table 6.3. Figure 6.12 shows the temperature dependence on the second-order rate constants. The slope and intercept of the Arrhenius plot were 15.7 and -11610 respectively, corresponding to an A value of 1.52×10^{-7} and an activation energy of 97 ± 10 kJ mol^{-1}. Uptakes of oxygen gas by reduced 2.8CrY as functions of time at various temperatures are shown in Figure 6.13.

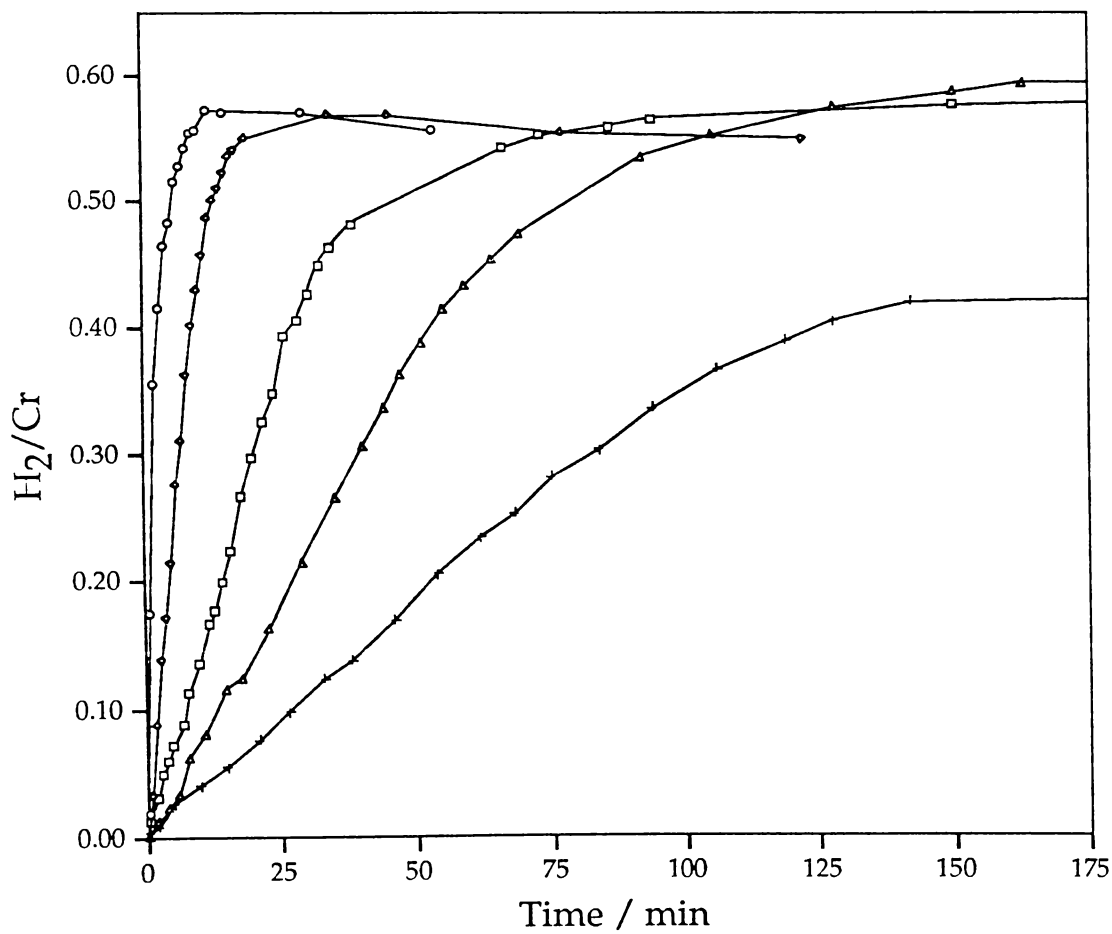


Figure 6.10 Hydrogen uptakes by 2.8CrY as functions of time at various temperatures. Reaction temperatures are (+ Red#10, 300°C, (▵ Red#15, 315°C), (▫ Red#16, 350°C), (◆ Red#14, 375°C), and (○ Red#6, 400°C).

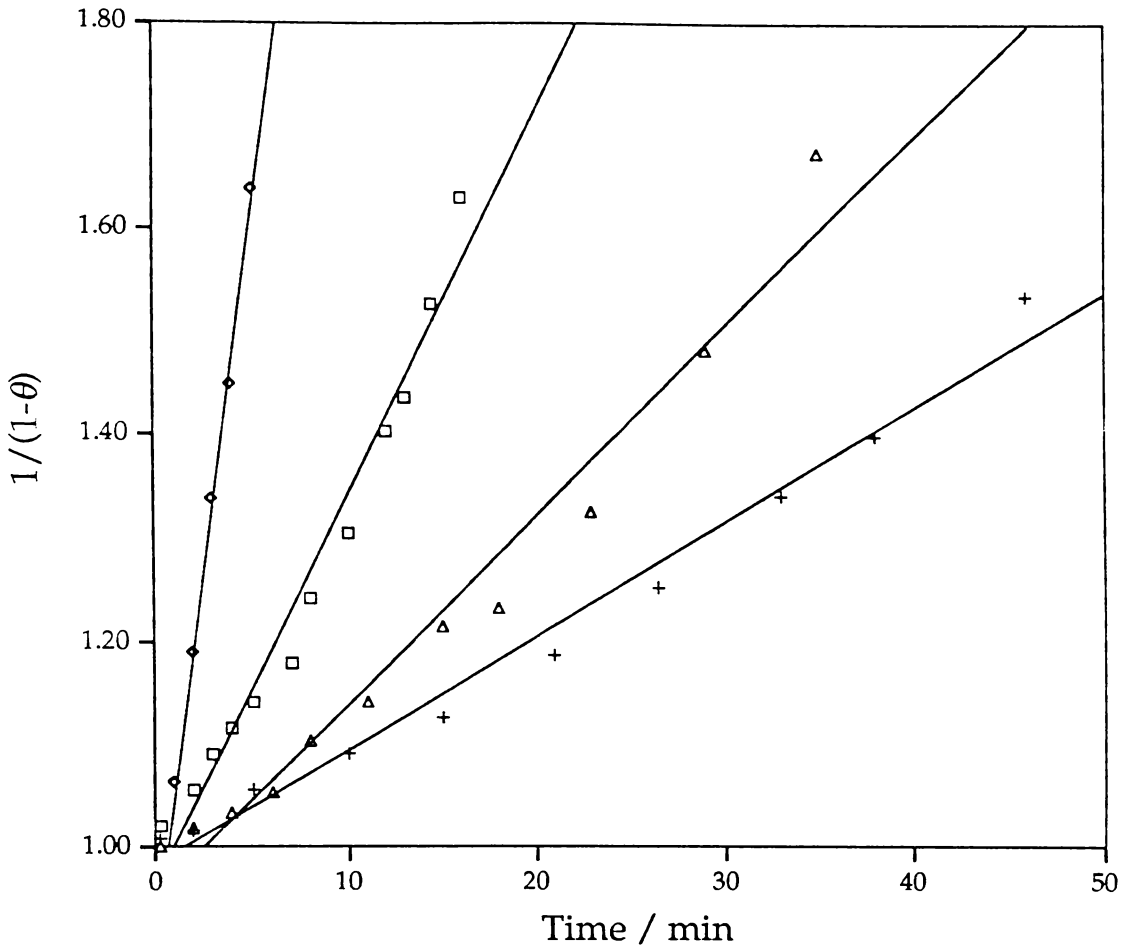


Figure 6.11 Second-order kinetics plots for the reductions of 2.8CrY. Reaction temperatures are (+ Red#10, 300°C), (△ Red#15, 315°C), (□ Red#16, 350°C), and (◇ Red#14, 375°C).

Table 6.3 Kinetic analysis of the reduction of chromate zeolite 2.8CrY by hydrogen gas. k_2 is the second-order rate constant and θ_{max} is the maximum value of θ included in the least squares fit.

Red#	T/°C	θ_{max}	k_2
14	375	0.39	0.141
16	350	0.39	0.038
15	315	0.40	0.018
10	300	0.35	0.011

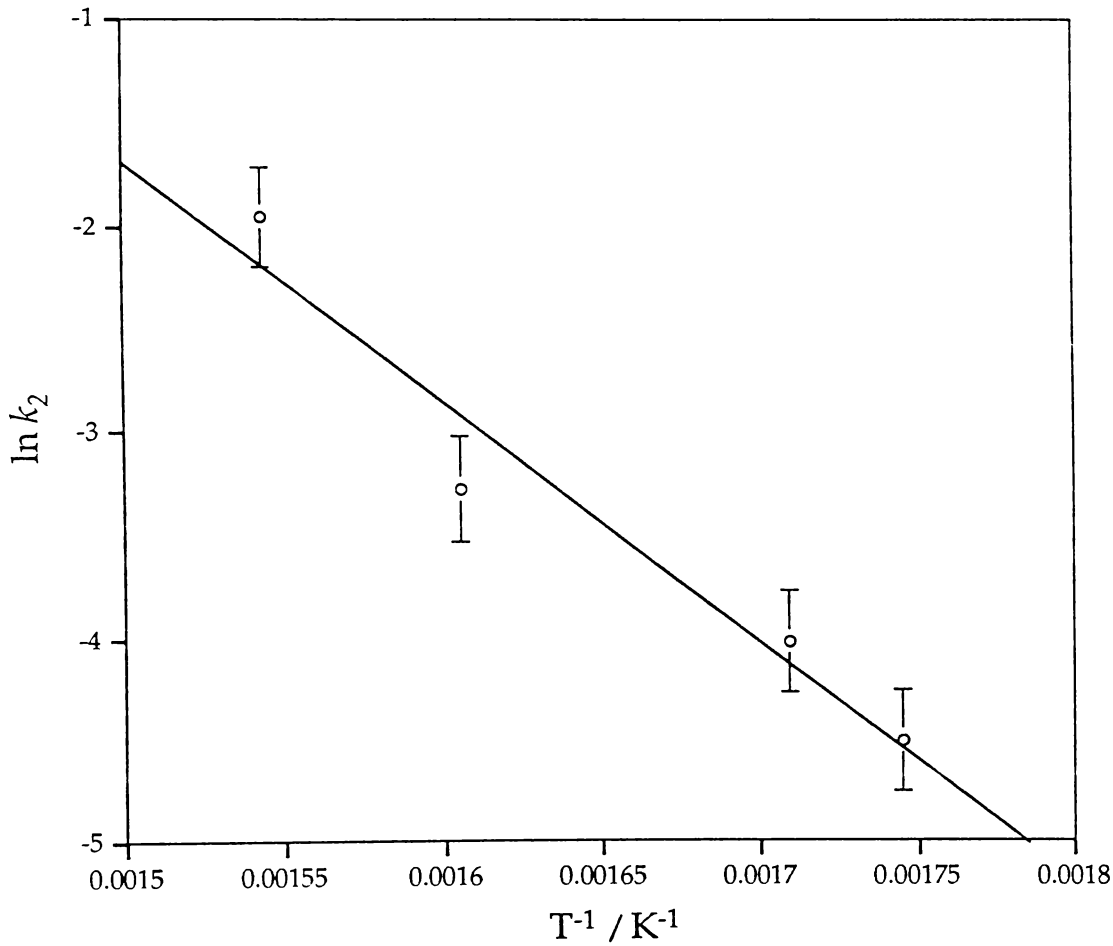


Figure 6.12 Arrhenius plot for the reduction of 2.8CrY by hydrogen gas.

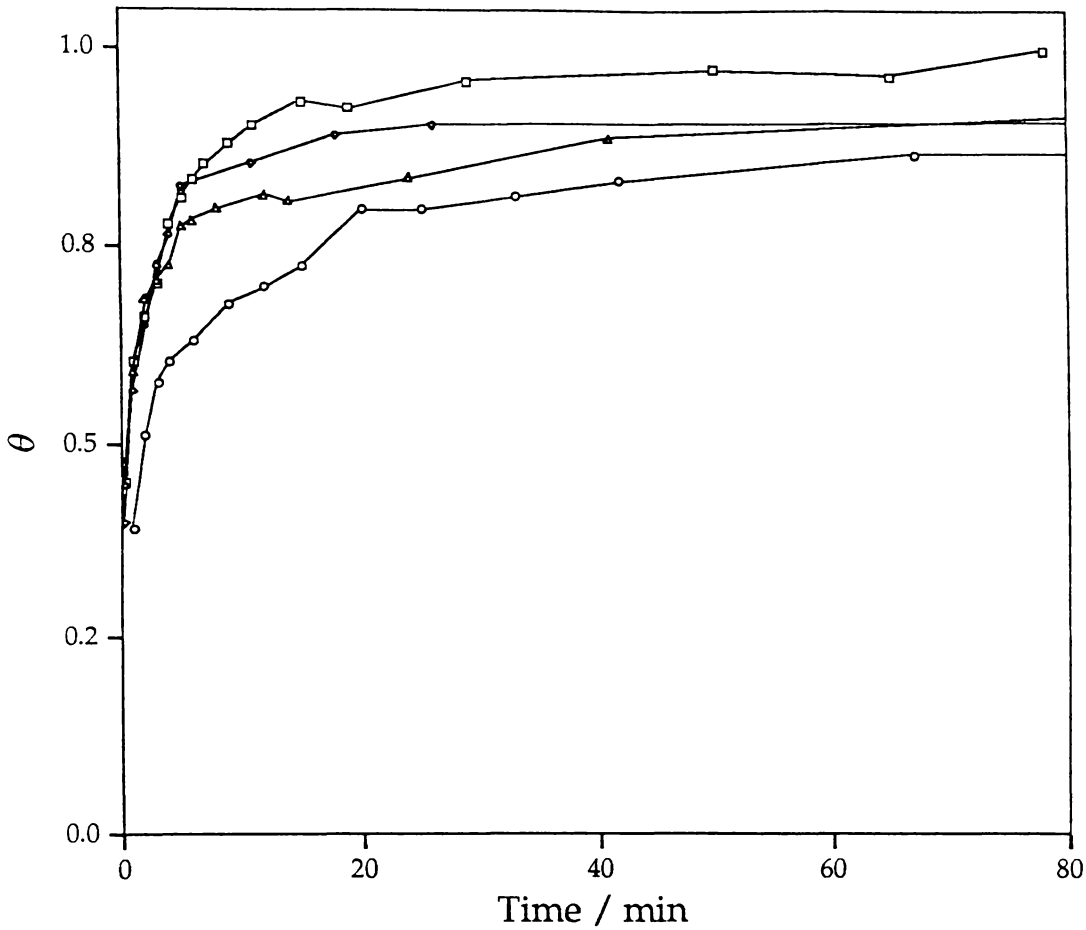


Figure 6.13 Uptakes of oxygen gas by reduced 2.8CrY at 300°C (bottom two curves) and 400°C (top two curves).

6.5.5 Reactivity of Chromate Zeolite 13.4CrY

Reductions

Uptakes of hydrogen gas by chromate zeolite 13.4CrY as functions of time at various temperatures are shown in Figure 6.14. Data collected for the reduction reactions are given in Appendix Nine. Of the kinetic models described earlier, only the second-order kinetic model gave linear plots. Plots of $1/(1-\theta)$ for the reductions, see Figure 6.15 , were linear up to 75% of the overall reaction. Table 6.4 summarises the kinetic data of the reductions. Figure 6.16 shows the temperature dependence of the second-order rate

constant. The intercept of 12.05 and the slope of -10346 correspond to an A value of 5.84×10^{-6} and an apparent activation energy of 86 ± 2 kJ mol^{-1}.

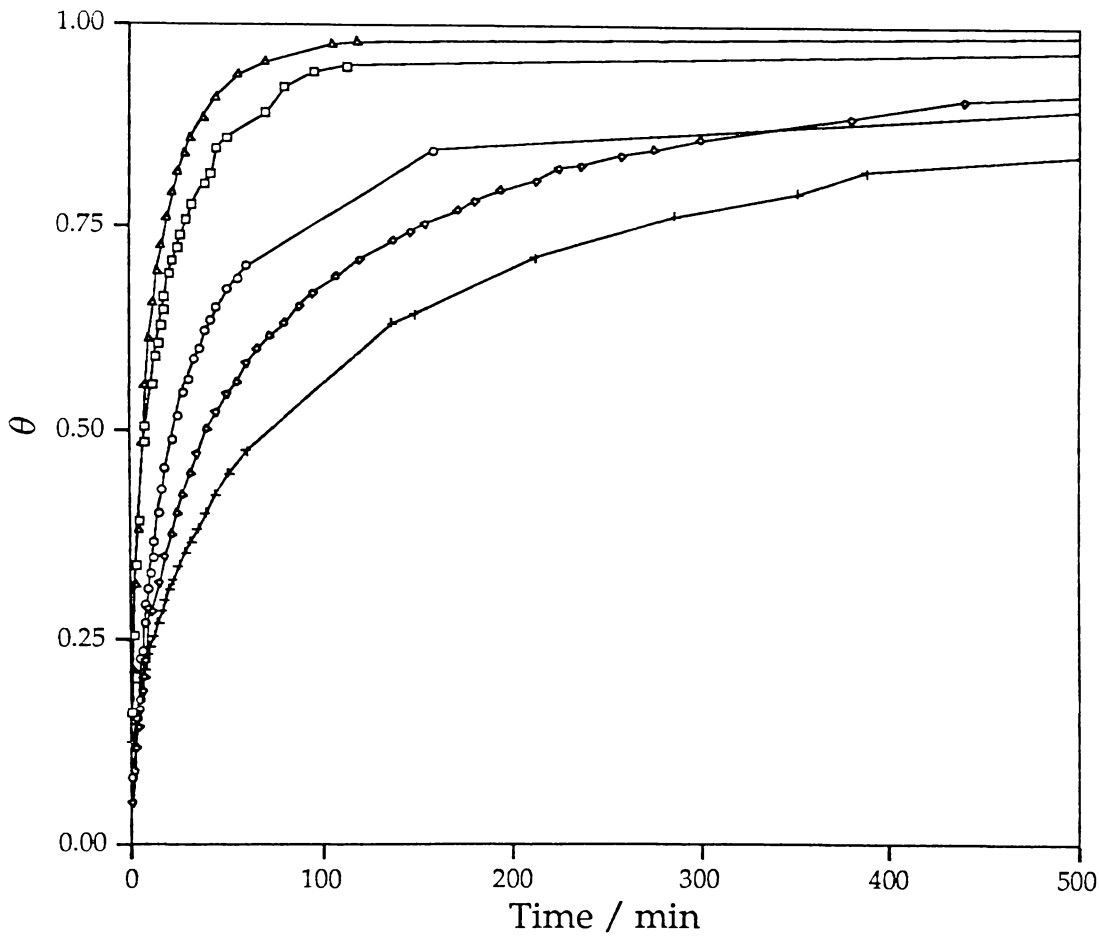


Figure 6.14 Plots of extent of reaction against time for the reductions of 13.4CrY by hydrogen gas at various temperatures. Reaction temperatures were: (△ Red#53, 475°C), (□ Red#52, 450°C), (○ Red#55, 400°C), (◇ Red#50, 375°C), and (+ Red#56, 350°C).

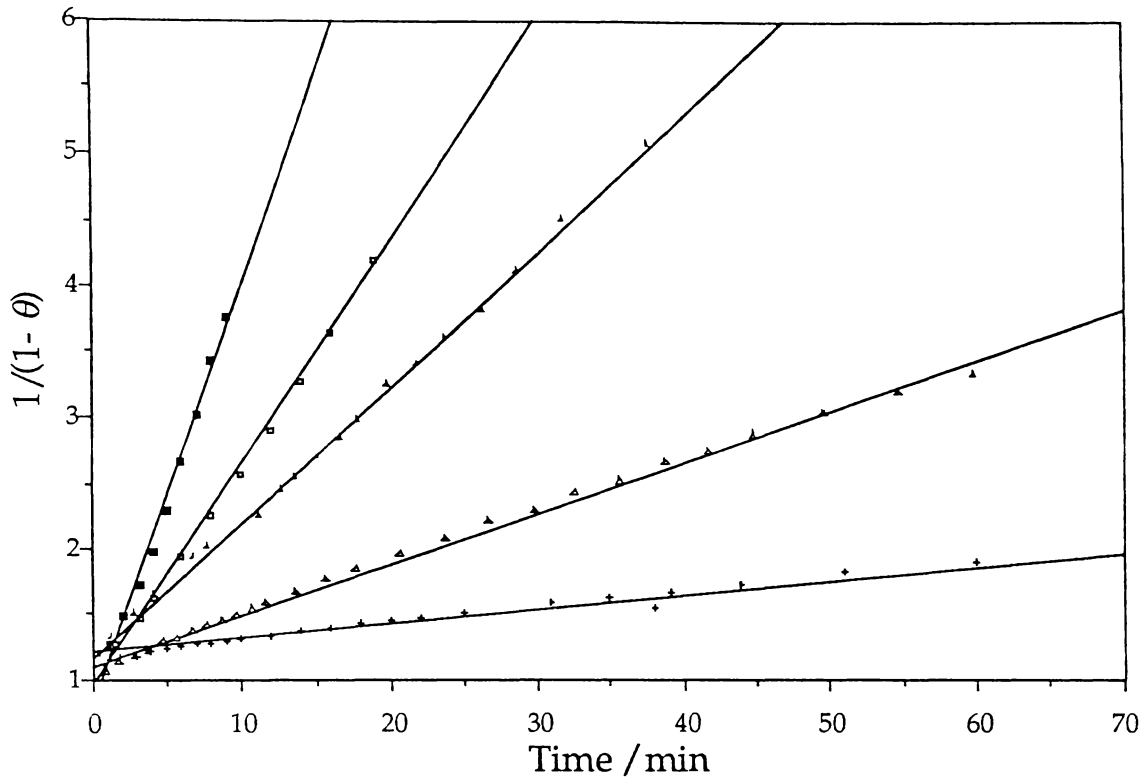


Figure 6.15 Second-order reaction kinetics plot for reductions of 13.4CrY at various temperatures. Reaction temperatures are: (◆ Red#56, 350°C), (▲ Red#50, 375°C), (▲ Red#55, 400°C), (■ Red#52, 450°C), and (■ Red#53, 475°C).

Table 6.4 Kinetic analysis of the reduction of chromate zeolite 13.4CrY by hydrogen gas. k_2 is the second-order rate constant. θ_{max} is the maximum value of θ included in the least squares fit, *nd* is the number of data points included in the least squares fit and r^2 is the correlation coefficient.

Red#	T/°C	θ_{max}	k_2	r^2	*nd*
53	475	0.76	0.1675	0.998	10
52	450	0.80	0.1024	0.998	19
55	400	0.70	0.0389	0.997	27
50	375	0.86	0.0193	0.999	41
56	350	0.79	0.0104	0.998	29

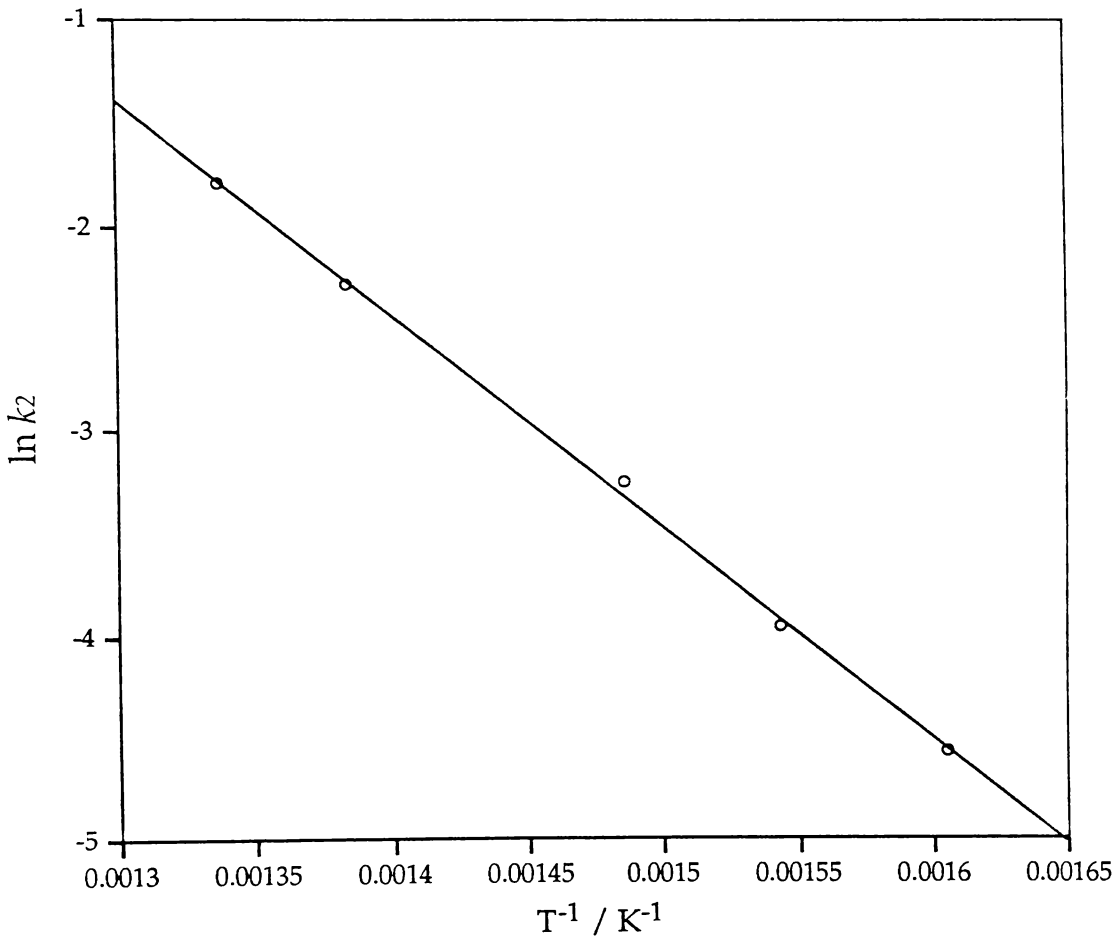


Figure 6.16 Arrhenius plot for the reduction of 13.4CrY by hydrogen gas.

Reoxidations

Oxygen uptakes as functions of time at various temperatures are shown in Figure 6.17. Data collected for the reoxidation reactions are given in Appendix Ten. None of the kinetic models described earlier adequately fitted the uptake over substantial range of θ. The best fit of the uptake data was obtained from a third-order kinetics treatment, shown in Figure 6.18, and display high degrees of linearity over the range of θ between ~0.3 and ~0.75.

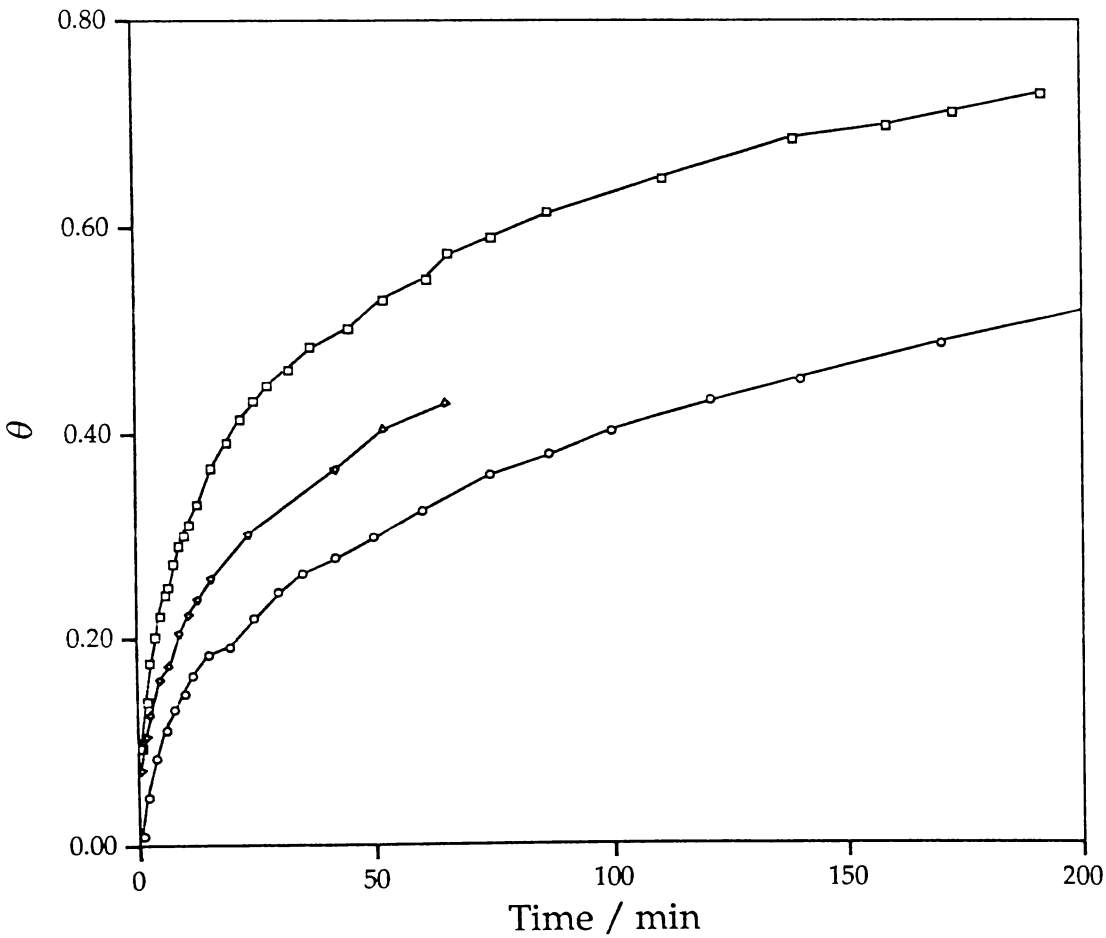


Figure 6.17 Plots of extent of reaction against time for reoxidations of reduced 13.4CrY by oxygen gas. Reaction temperatures are: (▫ Reox#46, 500°C), (◦ Reox#45, 450°C), and (○ Reox#44, 400°C).

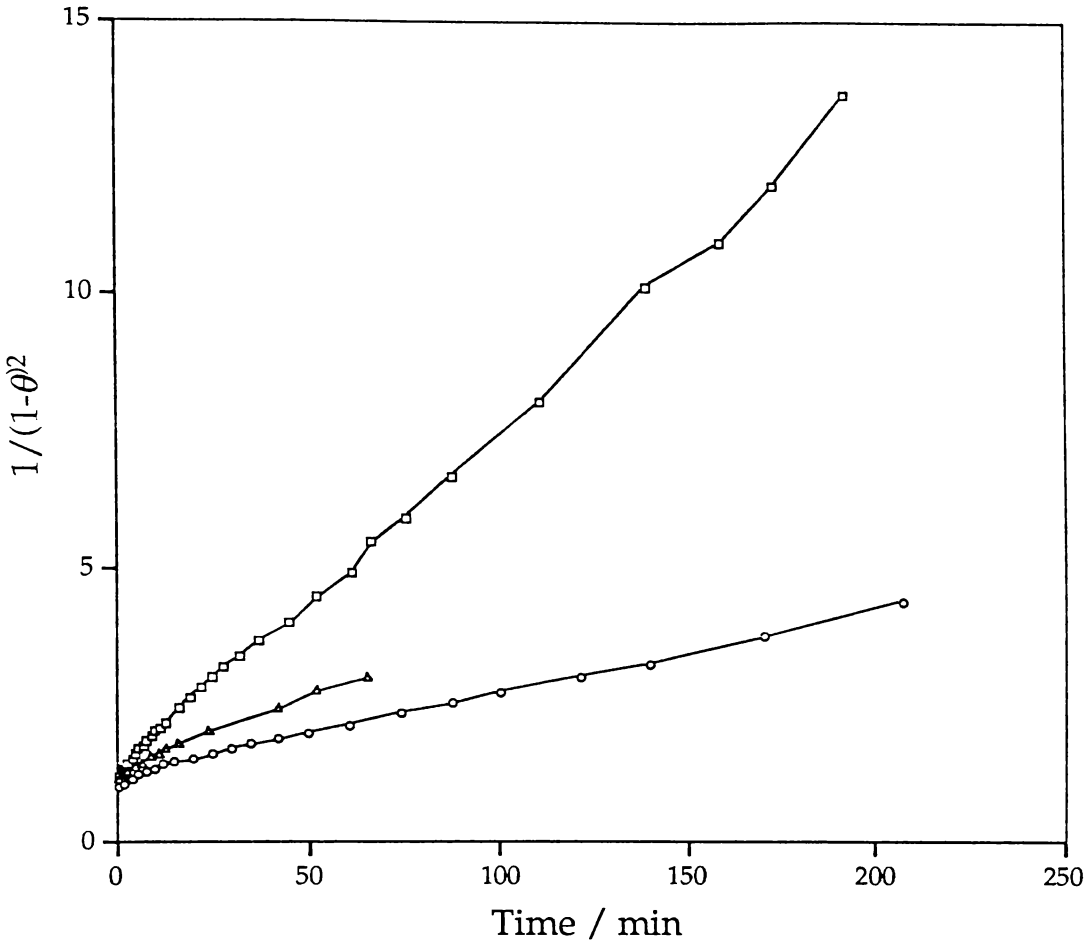


Figure 6.18 Third-order kinetics plots for the reoxidations of reduced 13.4CrY by oxygen gas at various temperatures. Reaction temperatures are: (▫ Reox#46, 500°C), (◇ Reox#45, 450°C), and (○ Reox#44, 400°C).

6.5.6 Reactivity of 4.8Cr5A

Reductions

Uptakes of hydrogen gas by 1.784 g of chromate zeolite 4.8Cr5A as functions of time at various temperatures are shown in Figure 6.19. Data collected for the reduction reactions are given in Appendix Seven. Hydrogen uptakes (as moles of H_2 per mole of Cr) at $t\infty$ for the first to fourth successive reductions were 1.45 ± 0.04, 0.97 ± 0.04, 0.92 ± 0.04, and 0.89 ± 0.04 respectively. The first reduction had a higher hydrogen uptake than any successive reduction with the uptake level corresponding to a three electron reduction

while later reductions indicated two electron reduction processes. Because of the difference between the first reduction to Cr(III) and all subsequent reductions, the reduction to Cr(III) was referred to as the primary reduction while subsequent reductions were referred to as secondary reductions. Figure 6.20 shows the average chromium oxidation state and $1/(1-\theta)$ against time for the primary reduction of 4.8Cr5A at 400°C. None of the kinetic models described earlier could describe the kinetics of the primary reduction.

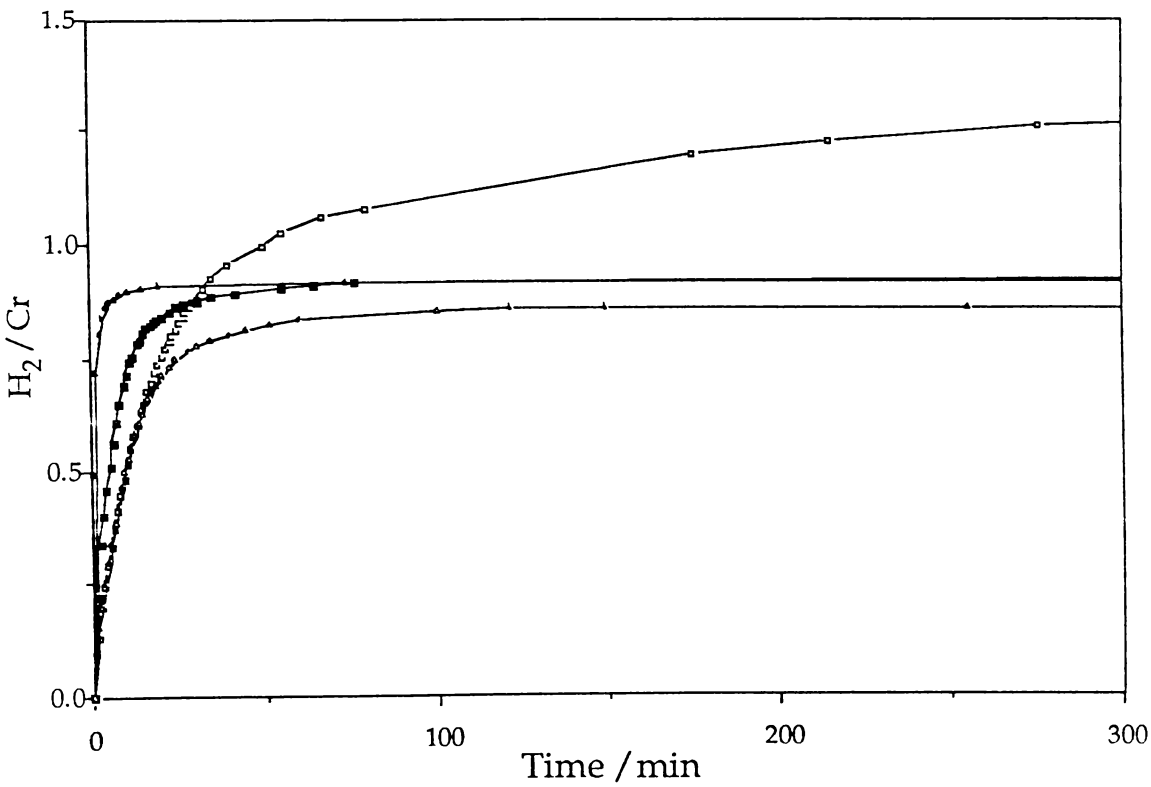


Figure 6.19 Uptake of hydrogen gas as functions of time by 4.8Cr5A at various temperatures. Temperatures are: (▫ Red#40, 400°C), (▪ Red#41, 450°C), (▲ Red#42, 500°C), and (◆ Red#43, 400°C).

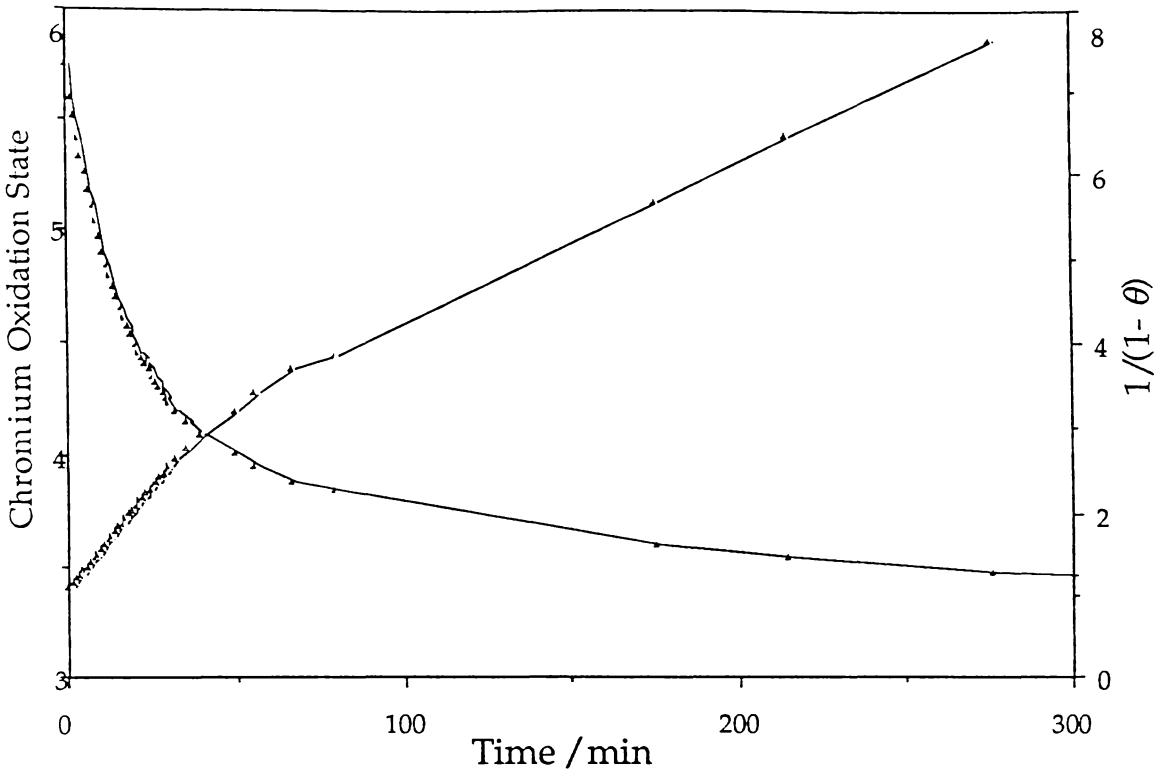


Figure 6.20 Plots of chromium oxidation state, ♦, and $1/(1-\theta)$, ◇, as functions of time for the primary reduction of 4.8Cr5A by hydrogen gas at 400°C.

Reoxidations

Uptakes of oxygen gas by 1.784 g of reduced chromate zeolite 4.8Cr5A as functions of time at various temperatures are shown in Figure 6.21. Data collected for the reoxidation reactions are given in Appendix Eight. The immediately obvious feature of the reoxidations is the lack of a temperature dependence on the rate of oxygen uptake in the range 350°C to 650°C. Oxygen per chromium uptakes at t_∞ for reoxidations at 350°C, 400°C, 450°C, 500°C and 650°C were 0.35 ± 0.02, 0.50 ± 0.02, 0.48 ± 0.02, 0.49 ± 0.02 and 0.55 ± 0.02 respectively. Of the kinetic models described earlier, only the diffusion controlled kinetic model gave linear plots. Plots of uptakes against $\sqrt{t}$ are shown in Figure 6.22.

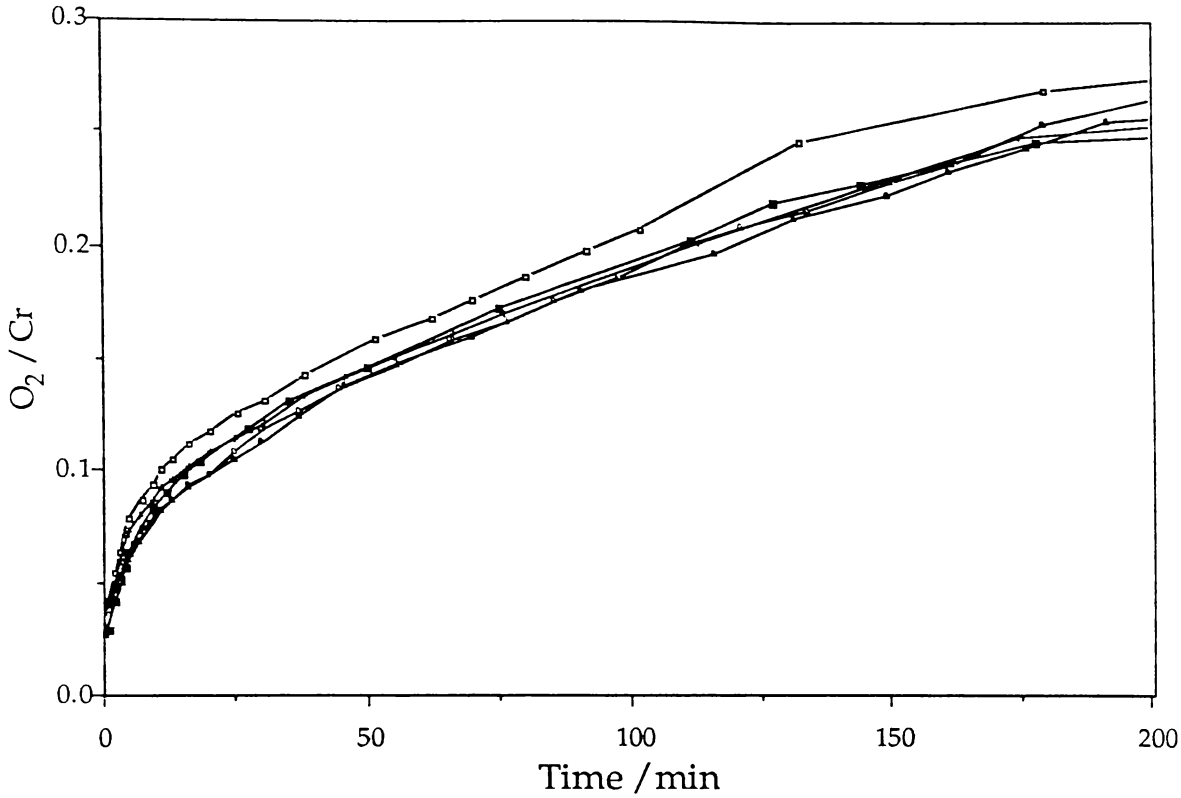


Figure 6.21 Oxygen uptakes as functions of time by reduced 4.8Cr5A at various temperatures. Reaction temperatures are: (■ Reox#37, 350°C), (◇ Reox#34, 400°C), (◆ Reox#35, 450°C), (◂ Reox#36, 500°C), and (□ Reox#38, 650°C).

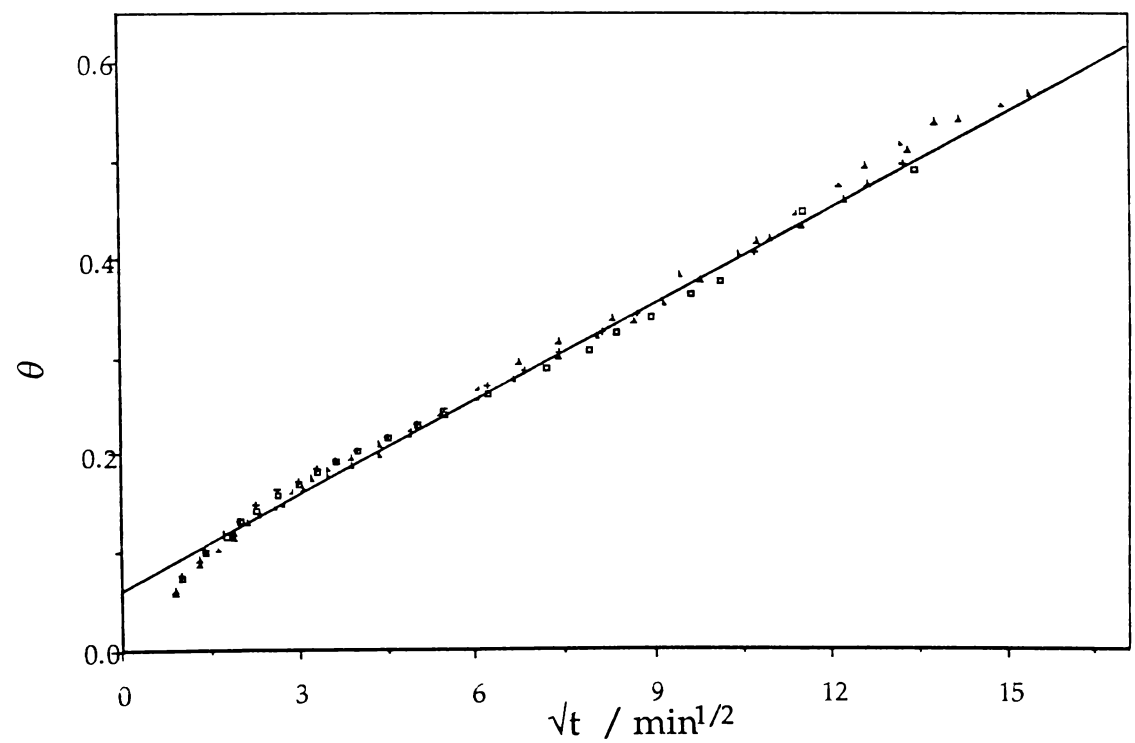


Figure 6.22 Oxygen uptakes as functions of √t by reduced 4.8Cr5A at various temperatures. Reaction temperatures are: (■ Reox#37, 350°C), (◇ Reox#34, 400°C), (◆ Reox#35, 450°C), and (□ Reox#38, 650°C).

A reoxidation of a 0.830 g sample of reduced 4.8Cr5A at 400°C is compared to a reoxidation of the 1.784 g sample at the same temperature in a plot of θ against $\sqrt{t}$ in Figure 6.24. While a $\sqrt{t}$ law was observed for the 1.784 g sample this was not the case for the 0.830 g sample. A change in kinetics from diffusion control to an alternative control, resembling chemisorption kinetics, is evident.

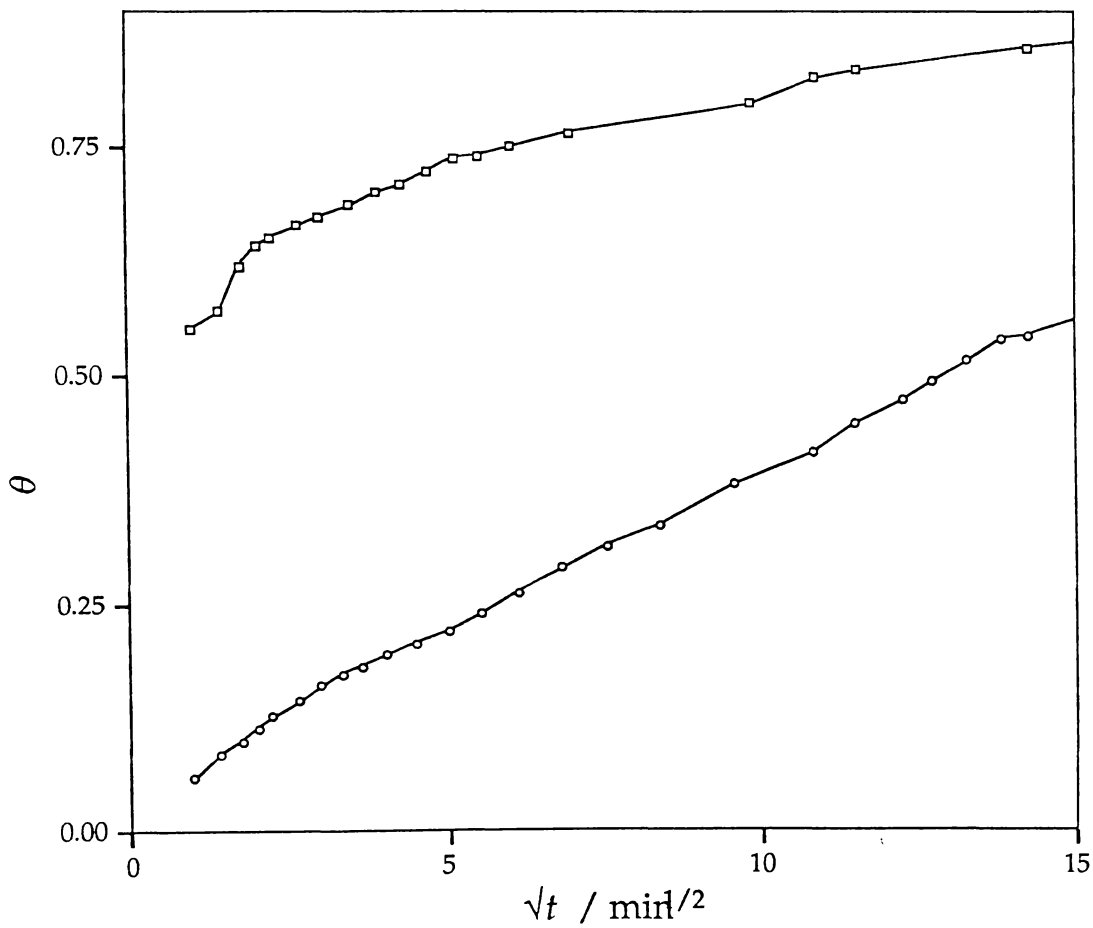


Figure 6.23 Plots of θ against $\sqrt{t}$ for the reoxidations of two sample weights of 4.8Cr5A at 400°C. Sample weights are 1.784 g (∘ Reox#34) and 0.830 g sample (▫ Reox#52). The plots indicates a change in kinetics upon the change in sample bed weight.

6.5.7 Reactions Between Chromate Zeolites and other Gases

Analysis of the reactivity of 2.1CrX and 5.8CrX to the oxidation of $CO_{(g)}$ and $CH_{4(g)}$ were performed under similar conditions to the $H_{2(g)}$ reactions. The lack of gas uptake in both cases indicated an inability of these systems to oxidise $CO_{(g)}$ and $CH_{4(g)}$.

The reactivity of the above systems in ethylene polymerisation and oxidation of methanol was assessed at Industrial Research Limited (IRL).[11] No activity in either reaction was observed at temperatures up to 400°C.

6.6 Discussion

6.6.1 Reductions of 4.8Cr5A

The primary reduction of 4.8Cr5A was unusual in that the $1/(1-\theta)$ plot was curved indicating the inability of second-order kinetics to fit the data. Uptake data indicates rapid adsorption up to a $H_{2(g)}$ to Cr ratio of about one followed by a slower rate of uptake consistent with rapid reduction of Cr(VI) to Cr(IV) and a subsequent slower reduction of Cr(IV) to Cr(III) occurring as consecutive and segregated reactions. The plots showing $1/(1-\theta)$ and average chromium oxidation state against time (Figure 6.20) were also consistent with a change in mechanism at an average oxidation state of ~Cr(IV). Reaction as in Scheme 6.1 provides a possible explanation of these observations.

Scheme 6.1 Proposed mechanism and overall stoichiometry for the primary reduction of 4.8Cr5A.

$$Na_2CrO_4 + H_{2(g)} \xrightarrow{fast} Na_2CrO_3 + H_2O$$

$$Na_2CrO_3 + \tfrac{1}{2}H_{2(g)} \xrightarrow{slow} NaCrO_2 + NaOH$$

$$Na_2CrO_4 + \tfrac{3}{2}H_{2(g)} \longrightarrow NaCrO_2 + NaOH + H_2O$$

6.6.2 Second-Order Dependence of the Reductions

Linear plots of $1/(1-\theta)$ against time were observed for the reductions of all the zeolites examined, with the exception of the primary reduction of 4.8Cr5A. Such plots are often observed for the chemisorption of hydrogen onto various solids and interpreted in terms of dissociative chemisorption resulting in the loss of two adsorption sites per hydrogen molecule. Since hydrogen is a two electron reducing agent, linear second-order plots for reductions can be interpreted in terms of the loss of two active sites of the chromium through reaction with each hydrogen molecule.

6.6.3 Kinetics of Reoxidations

Reoxidations of 5.8CrX

Both fourth-order reaction kinetics (see Figure 6.5) and chemisorption kinetics (see Figure 6.6) can be used to fit the kinetic data for the reoxidations of 5.8CrX over certain ranges of θ values. Deviation of the data from linearity at early times and the non unity intercept of the fourth-order plot indicates the inappropriateness of this model. Although the non-linear region is limited to low values of t, it accounts for more than 50% of the overall reaction. The range of θ over which linearity in the fourth-order plot is observed is only from ~0.5 to ~0.8. A mechanism consistent with fourth-order kinetics is not immediately obvious and reports of such high orders in one reactant are rare. For these reasons it was decided that a mechanistic interpretation of fourth-order kinetics was not warranted. In contrast, the chemisorption model was able to fit the uptake data over the important initial stages of reaction. Considerations of the reaction mechanism and the response of the kinetic data to the procedures commonly employed in the analysis of chemisorption data follow.

The general features of the plots of θ against time for the reoxidations of 5.8CrX are those observed for chemisorption processes. These features are rapid and often unmeasurable rates at small reaction times followed by a much slower rate at longer reaction times. See Manchado *et al.*[12] for examples of chemisorption processes. When the kinetics of activated chemisorption are depicted as plots of the amount adsorbed against the logarithm of time, sigmoid curves are obtained.[13] At the region of greatest slope, around the point of inflection, the plots often approach linearity, a property known as the "Elovich equation". The Elovichian region is preceded by a "pre-Elovichian" region and followed by a "post-Elovichian" region. The relative importance of these regions varies with adsorbent-adsorbate pairs. Characteristic sigmoid shape is evident for the two lower lines in Figure 6.7 while the region concave to the θ axis is absent for the upper set of lines. Reox#22 is one of the lower lines displaying sigmoid shape. It has been found by trial and error that a value between 1.1 and 1.4 for t_0 maximises the linearity of the $\ln(t + t_0)$ plot (see Figure 6.24).

Figure 6.25 shows θ against $\ln t$ for Reox#19. A high degree of linearity is apparent up to a θ value of about 0.8. From Figure 6.25 it is clear that adjustment using t_0 had little effect on the linearity of the plot above about $\theta = 0.5$. This is to be expected as the logarithm scale emphasises low values. Adjustment using t_0 affects the plot only at small t thereby "correcting" for the rapid adsorption in the pre-Elovichian region, which in this case covers $0 < \theta < \sim 0.4$. The data for Reox#19 required no adjustment, however no data were obtained below $\theta = 0.42$ suggesting that the pre-Elovichian region had occurred prior to the first reading. Reactions of Scheme 6.2 have been devised to be consistent with chemisorption kinetics.

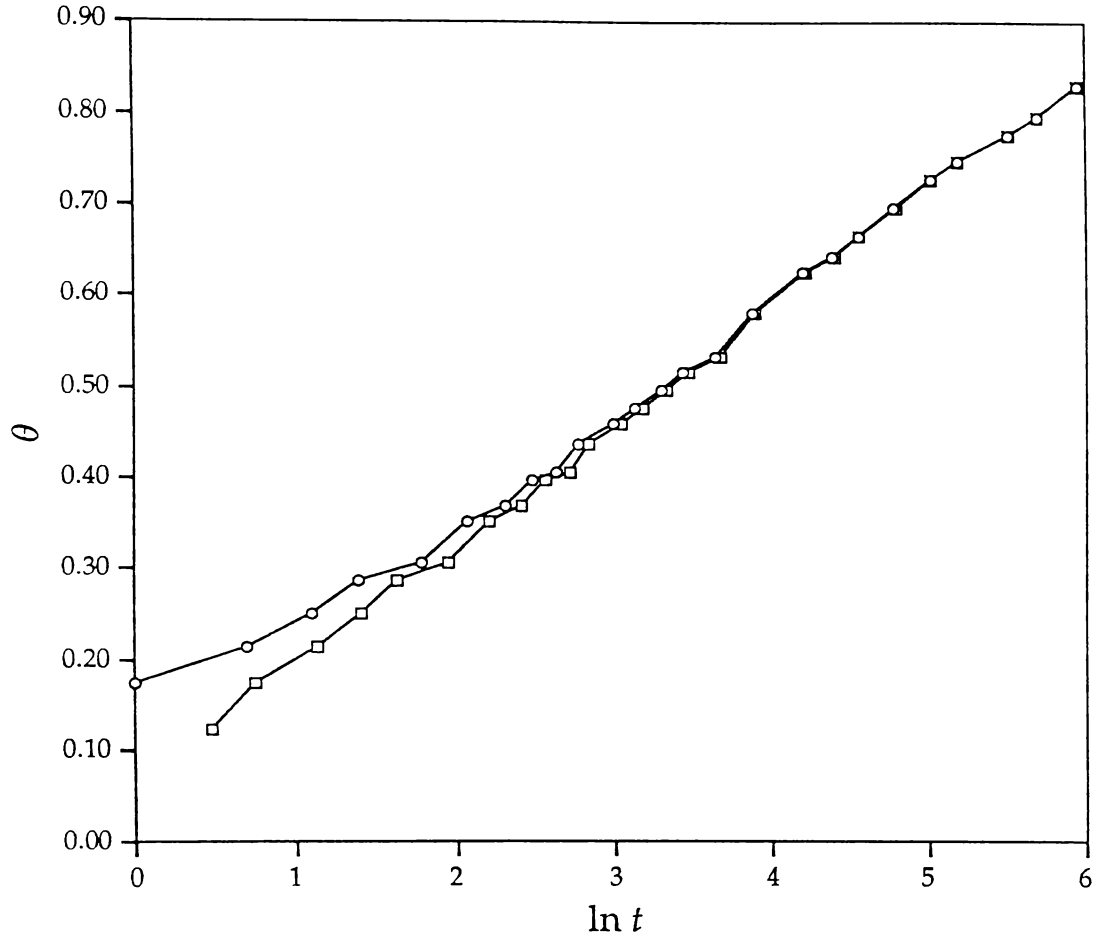


Figure 6.24 Plots of θ against ln$t$, (∘), and ln(t + 1.1), (▫), for reoxidation of reduced 5.8CrX by oxygen gas at 300°C (Reox#22).

Scheme 6.2 Reaction of reduced 5.8CrX and oxygen gas consistent with chemisorption kinetics. The individual steps are: (1) Rapid transport of a gaseous oxygen molecule to the zeolite surface. (2) Rapid diffusion of the gaseous oxygen molecule through zeolite crystals. (3) Slow chemisorption of the gaseous oxygen molecule onto active site(s). (4) Rapid reaction of the adsorbed oxygen molecule with chromium.

$$O_{2(g)} \xrightarrow{fast} O_{2(g,surface)} \quad (1)$$

$$O_{2(g,surface)} \xrightarrow{fast} O_{2(g,zeolite)} \quad (2)$$

$$(n\mathrm{Cr}^{(m)+}) + O_{2(g,zeolite)} \xrightarrow{slow} (n\mathrm{Cr}^{(m)+})\cdot\cdot O_{2(ads)} \quad (3)$$

$$(n\mathrm{Cr}^{(m)+})\cdot\cdot O_{2(ads)} \xrightarrow{fast} (n\mathrm{Cr}^{(m+4)+}) + 2\,O^{2-} \quad (4)$$

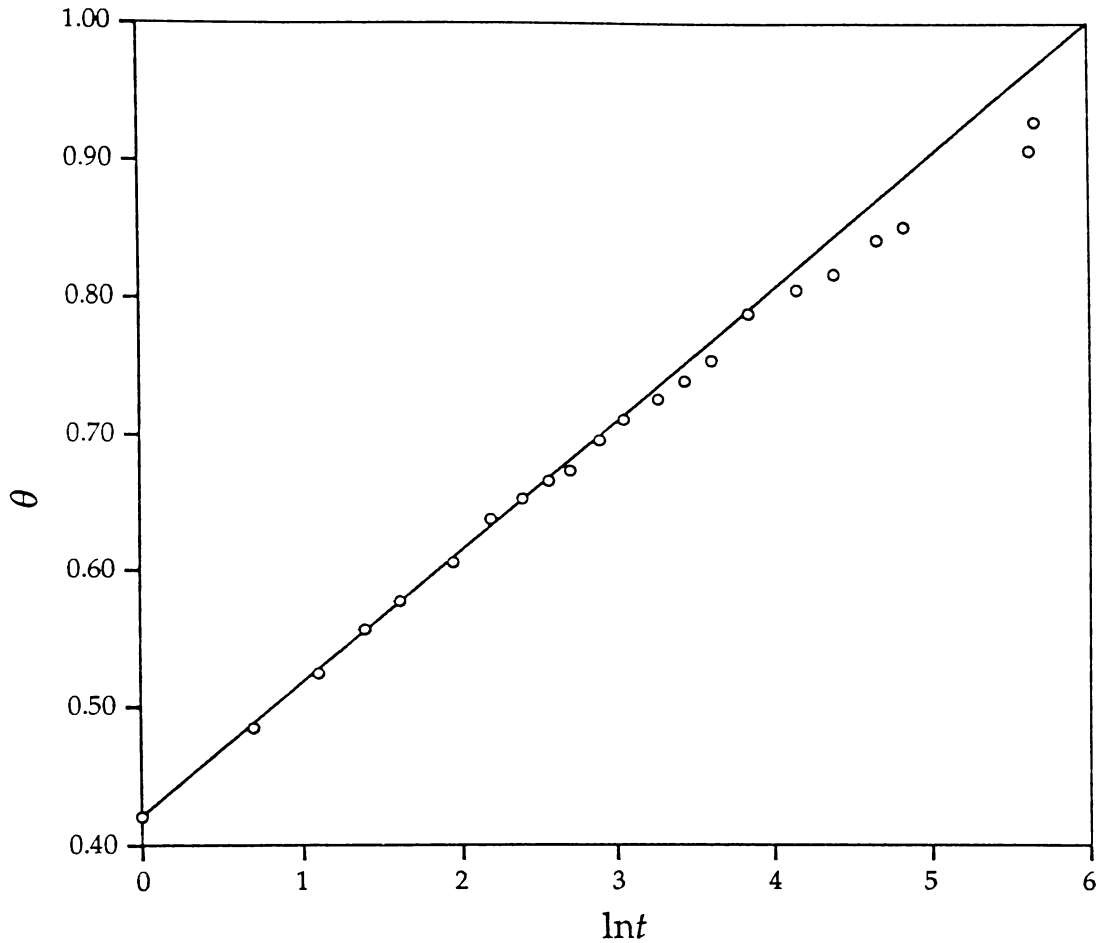


Figure 6.25 Plot of θ against ln$t$ for a reoxidation of reduced 5.8CrX by oxygen gas at 350°C (Reox#19).

Reoxidations of 4.8Cr5A

Both intra- and intercrystalline diffusion give linear plots of θ against $\sqrt{t}$. The temperature coefficient is a simple method for the differentiation between intra- and inter-crystalline diffusions. The apparent coefficient for intra-crystalline diffusion, D_i, is normally exponentially dependent ($D_i = D_o \exp(-E_a/RT)$ on the reaction temperature whereas Knudsen intercrystalline diffusivity, D_g, depends on $\sqrt{T}$. The rate of intercrystalline diffusion is also dependent on the size and shape of the bed while intra-crystalline diffusion is dependent on the surface area to volume ratio of the crystallites which is not dependent on the bed dimensions. Changing the bed

characteristics by halving the bed weight resulted in a change in kinetics from diffusion control. This fact and the low temperature coefficient indicate that intercrystalline diffusion was the rate limiting step in the reoxidation of the 1.784 g sample.

For intercrystalline diffusion to be rate limiting the oxygen molecules must spend considerable time within intercrystalline voids. SEM photographs indicated that the A-type zeolites were of fairly uniform size (0.1 to 5 μm) with almost perfectly cubic crystallites and having well defined flat surfaces and sharp edges. The uniform size and the cubic shape would allow close packing to occur without the large void spaces between individual crystallites as observed in a bed of spherically shaped X type zeolite. This close packing could be expected to inhibit intercrystalline diffusion to the extent that it became rate limiting.

Reoxidations of 13.4CrY

Of the kinetic models examined only third-order kinetic displayed any degree of linearity. The region of linearity was between θ values of ~0.3 and ~0.7. For similar reasons as given for the apparent fourth-order kinetics of 5.8CrX, a mechanistic interpretation involving third-order kinetics was considered to be not warranted. More importantly, 13.4CrY displayed kinetics different from the reoxidations of other systems for which chemisorption kinetics were followed. A reason for this is suggested below.

6.6.4 Effect of Degree of Loading on Reoxidation Kinetics

Reoxidations of 2.1CrX, 2.8CrY, and 5.8CrX displayed similar chemisorption features which contrasted with the slower non-chemisorption reactions of 13.4CrY. Similar bed weights and $O_{2(g)}$ to chromium ratios indicated that the differences arose from the degree of loading. In earlier

discussions (see Section 5.4.4) it was deduced that the reduction of chromates in *LLZ* and *MLZ* formed monomeric CrO_3^{2-} (Cr(IV)) and CrO_2^{-} (Cr(III)) species. In *HLZ* the reduced species was of mixed oxidation state of average oxidation number 3.5. The fact that the reactions were not diffusion controlled eliminated effect of loading on transport as an explanation of the differences in the kinetics. If the mixed oxidation state of the reduced *HLZ* was due to discrete Cr(IV) and Cr(III) species, it would be expected to react at a similar rate to that observed for *LLZ* and *MLZ*. The fact that the kinetics of the *HLZ* were much slower therefore indicated the likelihood that the Cr species were not monomeric. This finding lends support to the suggestion made in Section 5.4.7 that the mixed oxidation state formed in *HLZ* was due to "dimerisation". The relative reaction rates in these systems could then be explained by the lower reactivity of the more highly coordinated "dimer".

6.6.5 Discussion of Reaction Kinetics

Earlier work by Brown reported a study of the kinetics of the $H_{2(g)}/O_{2(g)}$ redox reactions of chromate nosean. In chromate nosean the location of the chromate oxyanion within the aluminosilicate framework is precisely defined by the crystallographic parameters of the $P_{\bar{4}3m}$ space group and lies at the centre of the sodalite cage. For this reason chromate nosean was considered to be an ideal model system for the analysis of the physiochemical nature of chromate oxyanions encapsulated in sodalite cages. Processes involving the uptakes of $H_{2(g)}$ by chromate nosean and $O_{2(g)}$ by reduced chromate nosean in the temperature range 500°C to 670°C were found to be diffusion controlled with activation energies of 73 ± 2 kJ mol^{-1} and 95 ± 13 kJ mol^{-1} respectively. The diffusion controlled rate-determining-step was attributed to the hindered passage of reactant molecules through the S6R windows of the sodalite cages due to the kinetic diameter of hydrogen and

oxygen being larger than the kinetic diameter of the S6R. The observations of chemical reaction and chemisorption kinetics for the redox reactions of chromate zeolites indicates that transport through the zeolite matrix is not a rate limiting step. Reaction of chromates located in α-cages of faujasite type zeolites requires passage of the reactant gas through S12R. As the kinetic diameter of S12R (8.0 Å) is larger than the kinetic diameter of hydrogen (2.89 Å) and oxygen (3.56 Å) these rings will offer little resistance to the diffusion of the gases through the framework. The observations of faster rates of hydrogen and oxygen uptakes by chromate zeolites than for chromate nosean at any given temperature is consistent with the greater accessibility of chromate in α-cages to reactant gaseous molecules than chromates in β-cages.

6.6.6 Comparison with the Chemistry of Intrazeolitic Chromate Complexes

Apparent activation energies for the oxidation of hydrogen gas by the chromates in various zeolites are given in Table 6.5. The zeolites examined showed similar activation energies from 86 ± 2 kJ mol^{-1} to 97 ± 10 kJ mol^{-1} with an average of 91 ± 4 kJ mol^{-1}. .

Table 6.6 Apparent activation energies of the reduction of various chromate-loaded zeolites by hydrogen gas.

Zeolite	2.1CrX	5.8CrX	2.8CrY	13.4CrY	Average
Ea	95 ± 7	91 ± 5	97 ± 10	86 ± 2	91 ± 6

Mahoney *et al.*[14] found the oxidation of hydrogen catalysed by X-type zeolite containing chromium ions had an apparent activation energy of 88.4 kJ mol^{-1}. This value is within the experimental error of the average E_a for the oxidation of hydrogen by occluded chromates in this study suggesting that similarities between the two processes may exist. This is examined below.

Mahoney's zeolites were prepared via ion-exchange of X zeolite using chromic nitrate. Catalytic activity was determined using 1% H_2 in air in a flow system operating at atmospheric pressure. Elevated temperatures and oxidising conditions causes oxidation of Cr^{3+} ions to Cr(VI) moieties in the form of intrazeolitic chromate complexes (*ICC*), see Section 5.4.14. Such species are likely to have been the catalytically active sites in Mahoney's studies given that the gas stream was highly oxidising consisting mainly of air. Similar E_as indicate the likelihood that reduction of *ICC*s is the rate limiting step in the process. Catalytic oxidation of hydrogen may therefore occur by reduction of *ICC*s by hydrogen followed by rapid reoxidation of the reduced *ICC*s by oxygen in the air stream resulting in the rejuvenation of the active site. This is consistent with the kinetics of redox reactions of *LLZ* and *MLZ*, for which reoxidations proceeded at significantly faster rates than reductions at all temperatures examined. The sites for hydrogen attack of *ICC*s and occluded chromates are the extrazeolitic oxygen atoms of the chromate type species The reductions should be mechanistically very similar. The similarity between the E_as for the catalytic oxidation of $H_{2(g)}$ by Cr(III) exchanged zeolite and the oxidation of $H_{2(g)}$ by chromate zeolite is therefore explained.

The rapid rates of hydrogen and oxygen uptakes indicates that chromate zeolites may function adequately in the catalytic oxidation of hydrogen.

References in Chapter Six

1) Barrer, R.M., in "**Zeolites and Clay minerals as Sorbents and Molecular Sieves**", Academic Press (London), 1978, pp. 256-338.
2) Barrer, R.M. and Fender, B.E.F., *J. Phys. and Chem. Solids*, **21** (1961) 12.
3) Tiselius, A., *Z. Phys. Chem.*, **A174** (1935) 401.
4) Barrer, R.M., *Trans. Faraday Soc.*, **45** (1949) 358.
5) Barrer, R.M. and Walker, A.J., *Trans. Faraday Soc.*, **60** (1964) 171.

6) Araya, A. and Dyer, A., *Zeolites*, **1** (1981) 35.

7). Kärger, J and Hermann, P., *Ann. Phys. (Leipzig)*, **257** (1976) 209.

8) Tayler, A.A. and Thon, N., *J. Am. Chem. Soc.*, **74** (1952) 4169.

9) Ritchie, A. G., *J. Chem. Soc., Faraday Trans. I*, **73(10)** (1977) 1650.

10) Levenspiel, O., in "**Chemical Engineering**", 2nd Edn, John Whiley & Sons, New York (1972) pp. 359.

11) N. Milestone, *personal communication*.

12) Manchado, M.C., Guil, J.M., and Paniego, A.R., *J. Chem. Soc. Faraday Trans. I*, **85(7)** (1989) 1775.

13) Ungarish, M. and Attaroni, C, *J. Chem. Soc. Faraday Trans. I*, **79** (1983) 119.

14) Mahoney, F., Rudham, R., and Summers, J.V., *J. Chem. Soc. Faraday Trans. I*, **75(2)** (1979) 314.

Chapter Seven
Conclusions

Chapter Seven

Summary of Conclusions

Solid-State Reactions Between Zeolites and Group (VI) Oxyanions

Solid-state reactions between zeolites of the types A, X, Y, M5 and S115 and the sodium salt of chromate, molybdate, and tungstate at temperatures between 465°C and 650°C resulted in substantial levels of salt uptake. Reaction of 13X and sodium chromate at 800°C resulted in lattice degradation and the formation of chromate nosean. The rate of salt uptake depended on the temperature at which the reaction is performed and the zeolite to salt ratio. At any given temperature the rate of uptake followed the sequence $Na_2CrO_4 > Na_2MoO_4 > Na_2WO_4$ with the decreases being related to the increase in oxyanion size.

Uptake of sodium chromate by 13X at temperatures between 520°C and 720°C followed diffusion controlled kinetics over the initial stages of the reaction. The temperature dependence on the apparent diffusion coefficient indicated an apparent activation energy of 124 ± 10 kJ mol^{-1}. A diffusion coefficient at 394°C, extrapolated from the solid-state reaction data, was ~1000 times lower than that of sodium cations in Y zeolite at this temperature indicating that the diffusion coefficient of the CrO_4^{2-} anion limited diffusion.

Hydrothermal reaction of 13X with 2.5 mol L^{-1} Na_2CrO_4 solution at 80°C resulted in no sodium chromate uptake. This was attributed to a low effective diffusion coefficient at this temperature resulting from a strong interaction with the lattice. Sodium chromate was entrained when NaOH was added to the Na_2CrO_4 solution. An increase in the effective diffusion coefficient by

lowering the equilibrium constant of the sodium chromate adsorption reaction was postulated.

Structure of Chromate Zeolites

Providing a suitable temperature was chosen, sodium chromate could be occluded into the structures of 3A, 4A, 5A, 13X, Y52, Y72, M5, and S115 with little framework degradation. Combined spectroscopic and physical probes located sodium chromate within the α-cages of A, X, and Y zeolites and the channels of M5 and S115 zeolites. Maximum uptakes by X, Y, and A type zeolites equalled half the number of S6R faces adjacent to the α-cages and coordination through sodium cations located near two S_{II} sites was proposed.

The acid sites of hydrogen zeolites played an important role in the occlusion process. Solid-state reaction between sodium chromate and hydrogen zeolite LZ-Y72 produced green powders that gave EPR signals and extraneous PXRD peaks characteristic of Cr_2O_3. Formation of Cr_2O_3 on crystal surfaces (SEM) was attributed to decomposition of chromic acid species formed by ion-exchange of the protons of structural hydroxyls for sodium cations of sodium chromate. Conversion of the hydrogen zeolite into a sodium zeolite allowed subsequent occlusion of sodium chromate without decomposition.

Redox Reactions of Occluded Oxyanions

Sodium chromate salt and sodium chromate occluded within the α-cages of A, X, and Y type zeolites were reduced by hydrogen gas and reoxidised by oxygen gas.

Sodium chromate salt was reduced by hydrogen gas to Cr(III) in the form of $NaCrO_2$ and NaOH. Reoxidations were incomplete ceasing at an average oxidation state of ~Cr(+4.67) despite excess oxygen gas and prolonged reaction times. The reoxidised product was Na_2CrO_3 and Na_2CrO_4 in a 2:1

ratio. Addition of NaOH to the partially oxidised sample allowed oxidation to Na_2CrO_4 indicating that an excess of NaOH was required for full oxidation. A mechanism consistent with the degree of oxidation was postulated consisting of oxidation to Na_2CrO_4 in the presence of excess of NaOH and oxidation to Na_2CrO_3 in the presence of a stoichiometric amount of NaOH.

Redox reactions of occluded chromates were dependent on the concentration of oxyanion. Highly loaded zeolites were reduced to an average oxidation state of Cr(+3.5). Quantitative EPR and stoichiometry of hydrogen uptake indicated the formation of equimolar amounts of Cr(III) and Cr(IV). The inability to reduce all the chromates to Cr(III) was attributed to "dimerisation" of neighbouring Cr(III) and Cr(IV) species in an α-cage. Preliminary molecular modelling studies enabled a structure of the "dimer" to be proposed. This consisted of a long range interaction between an oxygen atom of the CrO_3^{2-} species and the Cr atom of the CrO_2^- species. Reaction with $O_{2(g)}$ resulted in full reoxidation to Cr(VI) in the form of occluded Na_2CrO_4 species. Cyclic redox reactions resulted in transitions between average oxidation states of Cr(+3.5) and Cr(VI).

Moderately-loaded zeolites were reduced to Cr(III). Reoxidation ceased at an average oxidation state of Cr(V) in the form of equimolar amounts Na_2CrO_3 and Na_2CrO_4 species. The formation of two oxidised species was attributed to a similar dependence of oxidation product on NaOH concentration as observed for the oxidation of reduced sodium chromate salt. Cyclic redox reactions resulted in transitions between average oxidation states of Cr(III) and Cr(V).

Reaction of chromate nosean with $H_{2(g)}$ at 600°C for 219 minutes and 400°C for 95 hours converted the noselite framework to a sodalite framework. Movement of reduced chromate anions from the anion sites was envisaged. As in the case of *HLZ*, maximum hydrogen uptakes indicated reduction to Cr(+3.5). Reaction of the reduced sodalite with $O_{2(g)}$ at 600°C resulted in full

reoxidation and retention of the sodalite framework. Spectroscopic evidence indicated the formation of chromate anions coordinated to two of the four sodium cations of alternate sodalite cages. Retention of the sodalite framework was attributed to the anion sites remaining vacant. Heating the chromate sodalite in air at 1000°C reformed a noselite framework. Based of crystallographic considerations and spectroscopic changes, cleavage of the chromate oxyanions from the lattice and movement back to anion sites was envisaged.

Redox reactions of sodium molybdate and sodium tungstate occluded in 13X indicated that sodium tungstate could not be reduced by $H_{2(g)}$ at 450°C while sodium molybdate was reduced to an average oxidation state of ~Mo(V) under similar conditions. Consideration of the oxidation state free energy diagrams for Cr, Mo, and W allowed the stability of the W(VI) oxidation state and the lower tendency of Mo to reduce to lower oxidation states compared to that of Cr to be attributed to the relative stabilities of the various oxidation states for these elements.

Kinetics of the Reactions of Occluded Chromates

Reactions of occluded chromates within the α-cages of X and Y type zeolites and $H_{2(g)}$ generally followed second-order reaction kinetics attributed to the loss of two active sites per hydrogen molecule. The apparent activation energies of these zeolites of various loadings were similar, ranging from 86 ± 2 kJ mol^{-1} to 97 ± 10 kJ mol^{-1}. Most reoxidations could be described by chemisorption kinetics. Observations of reaction and chemisorption kinetics for redox reactions of chromate zeolites were in contrast to diffusion kinetics observed for chromate nosean. This was attributed to hindered passage of hydrogen and oxygen molecules through S6R of nosean but free passage through S10R and S12R of zeolites. The significantly lower reaction temperatures required to achieve a given reaction rate for chromate zeolites

relative to chromate nosean reflected the greater accessibility to $H_{2(g)}$ and $O_{2(g)}$ of the chromates in supercages than in sodalite cages.

Zeolites 2.1CrX and 5.8CrX were not active as reagents or catalyts in $CO_{(g)}$, $CH_{4(g)}$, and methanol oxidations or ethylene polymerisation.

Suggestions for Further Work

On the Structure of Chromate Zeolites

Prior to this work no structural studies of chromate loaded zeolites had been reported. A tentative model for the chromate-zeolites interaction has been proposed. The assignment of chromate positions between two S6R was based on a correlation between the maximum chromate uptake and the number of S6R present in the various zeolites. Many techniques have recently been applied to structural elucidation of similar systems. These include Far-IR and ^{23}Na MAS-NMR. These techniques were not available for the present studies. Their application to chromate zeolites should provide the information to precisely determine the location and nature nature of the chromate to zeolite interaction.

Far-IR: Extraframework alkali metal and alkaline earth metal cations in dehydrated zeolites have been shown to behave as essentially decoupled harmonic oscillators.[1] Each crystallographically distinct cation displays a diagnostic far-IR adsorption (200-30 cm^{-1}) corresponding to the most dipole active translatory mode of the cation with respect to its oxygen framework site. The frequency and intensity of the bands reflect the charge and mass, site

symmetry, geometry, and distribution of the extraframework Na^+ cations.[2] For dehydrated $Na_{56}Y$ four well resolved far-IR bands are observed at 186 cm^{-1} (II), 160 cm^{-1} (I), 105 cm^{-1} (I'), and 90 cm^{-1} (III).[3] Far-IR appears to offer the possibility of locating the Na^+ cations in chromate-loaded zeolites. Effects resulting from migration of cations (eg the proposed movement from S_{II} to $S_{II'}$) may be evident as could shifts resulting from chromate coordination.

^{23}Na MAS-NMR: Dehydrated $Na_{56}Y$ gives a broad asymmetric ^{23}Na resonance at -12 ppm arising from a convolution of signals due to cations mainly in sites II, I, I', and III.[3] Chemical shifts arsing from interactions with molybdenum hexacarbonyl and molybdenum oxides were observed. Similar chemical shifts in spectra of chromate-loaded zeolites may facilitate the locating of the chromate oxyanions.

Single Crystal XRD: Single crystal XRD is a powerful technique for the structural elucidation of crystalline phases. Chromate zeolites of this work were microcrystalline powders unsuitable for single crystal work. Rietveld analysis of powder patterns is often successful in locating extraframework species in zeolites. Chromate zeolites were deemed to be unsuitable for such work due to the fluorescence of occluded chromate. Analysis of chromate zeolites by the single crystal XRD method will depend on whether sufficiently large crystals can be prepared. This work has shown that solid-state reactions can load powder zeolites to high levels with minimal change in crystal morphology. A similar lack of change to large single crystals would allow the preparation of single crystals of chromate zeolites via solid-state reactions of the parent zeolite crystal and sodium chromate. Hydrothermal uptakes may be possible in favourable cases.

On "Dimer" Formation

Evidence for "dimer" formation was based on EPR and stoichiometry of hydrogen uptake. The postulate of "dimer" formation involves a sufficiently novel chromium species to warrant further investigation. Unfortunately, due to its broadness the Cr(III) EPR signal could not be used to provide definitive evidence for the presence of a "dimer". Single crystal studies of the reduced chromate zeolite offer the possibility of locating the key atoms to give direct evidence for an interaction between Cr(III) and Cr(IV). Molecular modelling studies may also be warranted.

The ability to load Na_2MoO_4 and Na_2WO_4 should allow mixed phases (Na_2CrO_4/Na_2MoO_4, Na_2CrO_4/Na_2WO_4, Na_2MoO_4/Na_2WO_4, and $Na_2CrO_4/Na_2MoO_4/Na_2WO_4$) to be produced. The structures and redox chemistries of these systems represent a logical extension of the present studies. Mixed oxidation state heteronuclear "dimers" (containing Cr-O-Mo, Cr-O-W, or Mo-O-W bonds) are an interesting possibility!

On the Redox Reactions of Chromate Nosean

Combined spectroscopic and PXRD analysis were sufficient to characterise the redox products of chromate nosean. PXRD changes were assessed through analyses of space group criteria of the sodalite and noselite groups. An obvious extension to this work is Rietveld analysis. Sodalites are ideal systems for Rietveld analysis due to their relatively simple, highly symmetric, and static structures that yield diffraction patterns with minimal peak overlap.[4] The lack of an accurate base structure often hinders Rietveld analysis. Chromate nosean, however, should be ideally suited for Rietveld analysis due to the similarity between the unit cell edges, and therefore intraframework ions, of chromate nosean and sulphate nosean for which accurate atomic positions have been obtained from single crystal work.[5] Due to the similarity between the thermochemical radii of chromate (2.56 ± 0.03 Å)

and sulphate (2.58 ± 0.04)[6] it may be possible to deal solely with sulphate species in the Rietveld analysis. The formation of "dimer" in sodalite is less easy to envisage than in zeolite pores due to the greater isolation of species occluded in β-cages. Rietveld offers the possibility of locating the Cr(III) and Cr(IV) species. If they lie on opposite sides of one ring, for example an S4R as proposed in this work, this would be good evidence of an interaction. Rietveld analysis of powder neutron diffraction data, such as that performed for hydroxysodalite,[7] may complement the XRD analysis. Again the use of sulphate nosean crystallographic data will assist the analysis.

On the Reactivity of Chromate Zeolites

Preliminary reactivity studies were confined to redox reactions involving hydrogen and oxygen gases. The catalytic activity of chromate loaded zeolites is an area available for study (see below).

Catalytic Oxidation of Hydrogen

Rates of the individual redox reactions were rapid at temperatures above 250°C. The catalytic oxidation of hydrogen by chromate zeolites is a logical extension to the redox reactions.

The Lack of Ethylene Polymerisation

Preliminary studies indicated that 2.1CrX and 5.8CrX were inactive in ethylene polymerisation and oxidation of methanol. Reactions such as polymerisation require a vacant coordination site. High coordinative saturation of the chromates may be the cause of the lack of activity. High coordination numbers, despite reduction to CrO_2^-, can be maintained through coordination to lattice oxygen atoms. As such, no species of low coordination can be produced via the means used in this study. Reactivity may be enhanced

by the occlusion of more active species or the formation of lower oxidation state species using stronger reducing agents. This is considered briefly below.

Use of Stronger Reducing Agents

Reduction to oxidation states below Cr(III) was not possible using hydrogen. Reduction in Na vapour may allow reduction to lower oxidation states. The removal of a greater number of the oxygen ligands could allow the formation of species such as CrO (Cr(II)), NaCrO Cr(I), Na_2CrO Cr(O) or metallic chromium. These species may possess catalytic activity.

The Hydrogen form of Occluded Chromates

Replacement of the sodium cations of occluded chromates by protons would form a solid chromic acid type species. that may possess a chemistry different to that of sodium bound occluded chromates. Attempts to form such species by ion-exchange subsequent to chromate loading were unsuccessful. It may be possible to form the ammonium bound chromates through solid-state or hydrothermal uptake of ammonium chromate by the ammonium form of Y zeolite. Subsequent heat treatment could form the proton bound chromates.

Loading More Active Oxidising Agents into Zeolites

Loading more active oxidising agents into zeolite pores, such as OsO_4, may provide a means for the production of low temperature oxidation reagents or catalysts.

On the Redox Reactions of Sodium Chromate Salt

The stoichiometries of the redox reactions of sodium chromate indicated that the reduction reaction was not completely reversible and a mechanism consistent with the degree of reoxidation was postulated. According to the model, the oxygen ligands acquired by chromium species were derived form

NaOH and no uptake of oxygen directly from the gas phase by a chromium species occurred. The model predicts that, in the absence of oxygen exchange between the gas and solid phases, little O^{18} would end up on the chromium if labelled oxygen gas was used. A small amount of labelled chromate would result due to the fact that some NaOH would be the labelled product of the reaction to form Na_2CrO_4. Uptake by the means, however, would be significantly lower than that predicted for uptake of oxygen ligands by chromium directly from the gas phase

References

1) Ozin, G.A., Baker, M.D., and Godber, J., *J. Phys. Chem.*, **93** (1989) 2899.
2) Godber, J., and Ozin, G.A., *J. Phys. Chem.*, **92** (1988) 2841;
Godber, J., Baker, M.D., and Ozin, G.A., *J. Phys. Chem.*, **93** (1989) 1409.
3) Ozin, G.A., Ozkar, S., and Macdonald, P., *J. Phys. Chem.*, **94** (1990) 6939.
4) Stein, A., Ozin, G.A., Macdonald, P.M., and Jelinek, R., *J. Am. Chem. Soc.*, **114** (1992) 5171.
5) Hassan, I. and Grundy, H.D., *Acta Cryst.*, **B40** (1984) 6.
6) Jenkins, H.D.B. and Thakur, K.P, *J. Chem. Educ.*, **56** (1979) 577.
7) Luger, S., Felsche, J., and Fischer, P., *Acta Cryst.*, **C43** (1987) 1.

Appendix One

APPENDIX 1/1

Red#3

Zeolite 2.8CrY, (1.305g), 1.27 Wt%Cr_2O_3, N_{Cr} = (2.18 ± 0.04)x10^{-4}
Vman = 45.0±0.2 cm^3, Vtot = 62.3±0.4 cm^3, P_i = 31.82±0.01 cmHg, Tr = 22.0±0.2°C
N_i = (7.78 ± 0.04)x10^{-4}, Tf = 400°C, $H_2/Cr(\infty)$ = 0.35 ± 0.08.

Time/min	T/K	P/cmHg ± 0.01	(Moles Ads ± 0.09) x1e^4	H_2/Cr ± 0.08	θ ± 0.16
0.25	295	22.98	0.00	0.00	-0.01
1	295	22.74	0.08	0.04	0.10
2	295	22.65	0.11	0.05	0.14
3	295	22.63	0.12	0.05	0.15
5	295	22.47	0.17	0.08	0.22
7.5	295	22.25	0.24	0.11	0.32
10	295	22.00	0.33	0.15	0.43
14	295	21.81	0.39	0.18	0.52
20.5	295	21.75	0.41	0.19	0.54
37	295	21.53	0.49	0.22	0.64
45	295	21.29	0.57	0.26	0.75
52	295	21.12	0.62	0.29	0.82
64	295	21.07	0.64	0.29	0.85
75	295	21.07	0.64	0.29	0.85
112	295	20.99	0.67	0.31	0.88
129	295	20.97	0.68	0.31	0.89
145	295	20.89	0.70	0.32	0.93
170	295	20.85	0.72	0.33	0.94
195	295	20.84	0.72	0.33	0.95
1400	295	20.73	0.76	0.35	1.00

APPENDIX 1/2

Red# 4

Zeolite 2.8CrY, (1.305g), 1.27 Wt%Cr_2O_3, N_{Cr} = (2.18±0.04)x10^{-4}
V_{man} = 45.0±0.2 cm^3, V_{tot} = 62.3±0.4 cm^3, P_i = 28.70±0.01 cmHg, T_r = 22.5±0.2°C
N_i = (7.00±0.04)x10^{-4}, T_f = 400°C, $H_2/Cr(\infty)$ = 0.55±0.08

Time/min	T/°C	P/cmHg ± 0.01	(Moles Ads ±0.09) x10^4	H_2/Cr ± 0.08	θ ± 0.16
0.25	22.5	19.97	0.25	0.12	0.21
1.5	22.5	18.69	0.68	0.31	0.57
2	22.5	18.15	0.87	0.40	0.72
3	22.5	17.92	0.94	0.43	0.79
4	22.5	17.69	1.02	0.47	0.85
5	22.5	17.65	1.03	0.47	0.86
6	22.5	17.58	1.06	0.49	0.88
7.5	22.5	17.54	1.07	0.49	0.89
9	22.5	17.50	1.09	0.50	0.90
12	22.5	17.43	1.11	0.51	0.92
27	22.5	17.36	1.13	0.52	0.94
45	22.5	17.34	1.14	0.52	0.95
60	22.5	17.32	1.15	0.53	0.95
75	22.5	17.31	1.15	0.53	0.96
135	22.5	17.26	1.17	0.54	0.97
170	22.5	17.21	1.18	0.54	0.98
220	22.5	17.15	1.20	0.55	1.00

APPENDIX 1/3

Red# 5

Zeolite 2.8CrY, (1.305g), 1.27 Wt%Cr_2O_3, N_{Cr} = (2.18±0.04)x10^{-4}
V_{man} = 45.0±-.2 cm^3, V_{tot} = 62.3±0.4 cm^3, P_i = 28.43±0.01 cmHg, T_r = 22.0±0.2°C
N_i = (6.95±0.04)x10^{-4}, T_f = 400°C, $H_2/Cr(\infty)$ = 0.39±0.08.

Time/min	T/°C	P/cmHg 0.01	(Moles Ads ± 0.09) x10^5	H_2/Cr ±0.08	θ ±0.16
0.25	22	20.50	0.05	0.00	0.01
1	22	20.00	1.73	0.08	0.20
2	22	19.76	2.55	0.12	0.30
3	22	19.54	3.31	0.15	0.39
4	22	19.31	4.08	0.19	0.48
5	22	19.27	4.23	0.19	0.50
6	22	19.13	4.70	0.22	0.55
8	22	19.07	4.89	0.22	0.57
10	22	18.96	5.27	0.24	0.62
12	22	18.92	5.40	0.24	0.63
14	22	18.88	5.54	0.25	0.65
17	22	18.84	5.66	0.26	0.66
20	22	18.58	6.55	0.30	0.77
22	22	18.56	6.62	0.30	0.78
30	22	18.53	6.73	0.31	0.79
49	22	18.47	6.93	0.32	0.81
59	22	18.41	7.13	0.33	0.83
72	22	18.35	7.34	0.34	0.86
78	22	18.32	7.44	0.34	0.87
94	22	18.27	7.61	0.35	0.89
127	22	18.23	7.74	0.36	0.91
217	22	18.14	8.03	0.37	0.94
283	22	18.13	8.08	0.37	0.95
330	22	18.09	8.22	0.38	0.96
1400	22	17.99	8.54	0.39	1.00

APPENDIX 1/4

Red# 7

Zeolite 2.8CrY, (1.305g), 1.27 Wt%Cr_2O_3, N_{Cr} = (2.18±0.04)x10^{-4}
V_{man} = 45.0±0.2 cm^3, V_{tot} = 62.3±0.4 cm^3, P_i = 28.57±0.01 cmHg, Tr = 24.0±0.2°C
N_i = (6.94±0.04)x10^{-4}, T_f = 400°C, $H_2/Cr(\infty)$ = 0.57±0.08.

Time/min	T/°C	P/cmHg ±0.01	(Moles Ads ±0.09) x10^4	H_2/Cr ± 0.08	θ ± 0.16
0.25	24	20.50	0.04	0.02	0.03
1	24	19.48	0.38	0.18	0.31
2	24	18.31	0.78	0.36	0.62
3	24	17.92	0.91	0.42	0.73
4	24	17.60	1.01	0.47	0.81
5	24	17.49	1.05	0.48	0.84
6	24	17.27	1.13	0.52	0.90
7	24	17.20	1.15	0.53	0.92
8	24	17.10	1.18	0.54	0.95
9	24	17.02	1.21	0.56	0.97
10	24	17.00	1.22	0.56	0.97
12	24	16.91	1.25	0.57	1.00
15	24	16.91	1.25	0.57	1.00
29	24	16.92	1.24	0.57	1.00
53	24	17.01	1.21	0.56	0.97

APPENDIX 1/5

Red# 8

Zeolite 2.8CrY, (1.305g), 1.27 Wt%Cr_2O_3, N_{Cr} = (2.18±0.04)x10^{-4}
V_{man} = 45.0±0.2 cm^3, V_{tot} = 62.8±0.4 cm^3, P_i = 28.35±0.01 cmHg, T_r = 22.0±0.2°C
N_i = (6.93±0.01)x10^{-4}, T_f = 300°C, $H_2/Cr(\infty)$ = 0.43±0.08.

Time/min	T/°C	P/cmHg ± 0.01	(Moles Ads ±0.09) x10^5	H_2/Cr ± 0.08	θ ± 0.16
0.25	22	20.28	0.01	0.00	0.00
1	22	20.26	0.10	0.00	0.01
2	22	20.23	0.19	0.01	0.02
5	22	20.18	0.36	0.02	0.04
10	22	20.02	0.91	0.04	0.10
17	22	19.81	1.61	0.07	0.17
24	22	19.72	1.94	0.09	0.21
32	22	19.47	2.78	0.13	0.30
38	22	19.36	3.17	0.15	0.34
42	22	19.27	3.46	0.16	0.37
50	22	19.09	4.06	0.19	0.44
56	22	18.93	4.64	0.21	0.50
64	22	18.73	5.30	0.24	0.57
67	22	18.70	5.41	0.25	0.58
76	22	18.47	6.21	0.29	0.67
83	22	18.35	6.59	0.30	0.71
91	22	18.27	6.88	0.32	0.74
97	22	18.24	6.98	0.32	0.75
102	22	18.21	7.10	0.33	0.77
107	22	18.10	7.46	0.34	0.80
113	22	18.04	7.67	0.35	0.83
117	22	18.00	7.81	0.36	0.84
202	22	18.08	7.52	0.35	0.81
230	22	18.02	7.73	0.36	0.83
1400	22	17.57	9.28	0.43	1.00

APPENDIX 1/6

Red# 9

Zeolite 2.8CrY, (1.305g), 1.27 Wt%Cr_2O_3, N_{Cr} = (2.18±0.04)x10^{-4}
V_{man} = 45.0±0.2 cm^3, V_{tot} = 62.8±0.4 cm^3, P_i = 28.05±0.01 cmHg, T_r = 23.0±0.2°C
N_i = (6.83±0.04)e^{-4}, T_f = 300°C, $H_2/Cr(\infty)$ = 0.51±0.08.

Time/min	T/°C	P/cmHg ± 0.01	(Moles Ads ± 0.09)x10^4	H_2/Cr ± 0.08	θ ± 0.16
0.25	23	20.10	-0.01	0.00	-0.01
2	23	20.05	0.00	0.00	0.01
5	23	19.98	0.03	0.01	0.03
11	23	19.75	0.11	0.05	0.10
15	23	19.59	0.16	0.07	0.15
20	23	19.49	0.20	0.09	0.18
26	23	19.33	0.25	0.11	0.23
33	23	19.13	0.32	0.15	0.29
38	23	18.90	0.40	0.18	0.36
44	23	18.81	0.43	0.20	0.39
50	23	18.70	0.47	0.21	0.42
57	23	18.45	0.55	0.25	0.50
68	23	18.11	0.67	0.31	0.60
75	23	18.05	0.69	0.32	0.62
80	23	17.97	0.71	0.33	0.65
86	23	17.91	0.74	0.34	0.66
93	23	17.79	0.78	0.36	0.70
99	23	17.71	0.80	0.37	0.72
106	23	17.62	0.83	0.38	0.75
113	23	17.56	0.85	0.39	0.77
124	23	17.48	0.88	0.40	0.80
130	23	17.41	0.90	0.42	0.82
1400	23	16.81	1.11	0.51	1.00

APPENDIX 17

Red# 10

Zeolite 2.8CrY, (1.305g), 1.27 Wt%Cr_2O_3, N_{Cr} = (2.18±0.04)x10^{-4}
V_{man} = 45.0±0.2 cm^3, V_{tot} = 62.8±0.4 cm^3, P_i = 28.82±0.01 cmHg, T_r = 23.0±0.2°C
N_i = (7.02±0.04)x10^{-4}, T_f = 300°C, $H_2/Cr(\infty)$ = 0.48±0.08.

Time/min	T/°C	P/cmHg ± 0.01	(Moles Ads ±0.09)x10^4	H_2/Cr ± 0.08	θ ± 0.16
0.25	23	20.60	0.00	0.00	0.01
2	23	20.57	0.02	0.01	0.02
5	23	20.46	0.06	0.03	0.05
10	23	20.37	0.09	0.04	0.08
15	23	20.27	0.12	0.05	0.11
21	23	20.14	0.16	0.08	0.16
26.5	23	20.00	0.21	0.10	0.20
33	23	19.84	0.27	0.12	0.25
38	23	19.75	0.30	0.14	0.28
46	23	19.55	0.36	0.17	0.35
54	23	19.32	0.44	0.20	0.42
62	23	19.11	0.50	0.23	0.48
68	23	19.01	0.55	0.25	0.52
75	23	18.83	0.61	0.28	0.58
84	23	18.69	0.66	0.30	0.63
94	23	18.48	0.73	0.34	0.70
106	23	18.28	0.80	0.37	0.76
119	23	18.14	0.85	0.39	0.81
128	23	18.04	0.88	0.40	0.84
142	23	17.94	0.91	0.42	0.87
1400	22	17.49	1.05	0.48	1.00

APPENDIX 1/8

Red# 12

Zeolite 2.8CrY, (1.305g), 1.27 Wt%Cr_2O_3, N_{Cr} = (2.18±0.04)x10^{-4}
V_{man} = 45.0±0.2 cm^3, V_{tot} = 62.3±0.4 cm^3, P_i = 28.30±0.01 cmHg, T_r = 23.0±0.2°C
N_i = (6.89±0.04)x10^{-4}, T_f = 350°C, $H_2/Cr(\infty)$ = 0.43±0.08.

Time/min	T/°C	P/cmHg ± 0.01	(Moles Ads ± 0.09)x10^4	H_2/Cr ± 0.08	θ ± 0.16
0.25	23	20.29	0.05	0.02	0.05
1	23	20.17	0.09	0.04	0.09
2	23	19.97	0.15	0.07	0.16
3	23	19.68	0.25	0.12	0.27
4	23	19.51	0.31	0.14	0.33
5	23	19.37	0.36	0.16	0.38
6	23	19.21	0.41	0.19	0.44
7	23	19.03	0.47	0.22	0.51
8	23	18.91	0.51	0.24	0.55
9	23	18.79	0.55	0.25	0.59
10	23	18.59	0.62	0.29	0.67
11	23	18.45	0.67	0.31	0.72
12	23	18.41	0.68	0.31	0.73
13	23	18.32	0.71	0.33	0.76
14	23	18.22	0.74	0.34	0.80
15	23	18.16	0.76	0.35	0.82
16	23	18.09	0.79	0.36	0.85
17	23	18.02	0.81	0.37	0.87
18	23	17.96	0.83	0.38	0.89
19	23	17.95	0.83	0.23	0.53
20	23	17.93	0.84	0.39	0.91
22	23	17.80	0.88	0.41	0.95
25	23	17.77	0.90	0.41	0.96
38	23	17.69	0.92	0.42	0.99
69	23	17.67	0.93	0.43	1.00
124	23	17.66	0.93	0.43	1.00

APPENDIX 1/9

Red# 13

Zeolite 2.8CrY, (1.305g), 1.27 Wt% Cr_2O_3, N_{Cr} = (2.18±0.04)x10^{-4}
V_{man} = 45.0±0.2 cm^3, V_{tot} = 62.3±0.4 cm^3, P_i = 28.70±0.01 cmHg, T_r = 22.5±0.2°C
N_i = (7.00±0.04)x10^{-4}, T_f = 325°C, $H_2/Cr(\infty)$ = 0.38±0.08.

Time/min	T/°C	P/cmHg ± 0.01	(Moles Ads ± 0.05) x10^4	H_2/Cr ± 0.08	θ ± 0.16
0.25	22.5	20.56	0.05	0.02	0.06
1	22.5	20.44	0.09	0.04	0.11
2	22.5	20.34	0.13	0.06	0.15
3	22.5	20.19	0.18	0.08	0.21
4	22.5	19.99	0.24	0.11	0.29
6	22.5	19.87	0.28	0.13	0.34
7	22.5	19.73	0.33	0.15	0.40
8	22.5	19.66	0.36	0.16	0.43
9	22.5	19.58	0.38	0.18	0.46
10	22.5	19.51	0.41	0.19	0.49
11	22.5	19.42	0.44	0.20	0.53
12	22.5	19.34	0.47	0.21	0.56
13	22.5	19.26	0.49	0.23	0.59
14	22.5	19.22	0.50	0.23	0.60
16	22.5	19.09	0.55	0.25	0.66
18	22.5	19.02	0.57	0.26	0.69
20	22.5	18.90	0.61	0.28	0.73
22	22.5	18.84	0.63	0.29	0.76
24	22.5	18.74	0.66	0.31	0.80
27	22.5	18.62	0.71	0.33	0.85
30	22.5	18.52	0.74	0.34	0.89
35	22.5	18.43	0.77	0.36	0.93
40	22.5	18.35	0.80	0.37	0.96
50	22.5	18.29	0.82	0.38	0.98
63	22.5	18.24	0.84	0.38	1.00
94	22.5	18.26	0.83	0.38	1.00
107	22.5	18.25	0.83	0.38	1.00

APPENDIX 1/10

Red# 14

Zeolite 2.8CrY, (1.305g), 1.27 Wt%Cr_2O_3, N_{Cr} = (2.18±0.04)x10^{-4}
V_{man} = 45.0±0.2 cm^3, V_{tot} = 62.3±0.4 cm^3, P_i = 28.61±0.01 cmHg, T_r = 21.0±0.2°C
N_i = (7.02±0.04)x10^{-4}, T_f = 375°C, $H_2/Cr(\infty)$ = 0.55±0.08.

Time/min	T/°C	P/cmHg ± 0.01	(Moles Ads ± 0.05)x10^4	H_2/Cr ± 0.08	θ ± 0.16
0.25	21	20.68	-0.01	-0.01	-0.01
1	21	20.44	0.07	0.03	0.06
2	21	20.08	0.19	0.09	0.16
3	21	19.76	0.30	0.14	0.25
4	21	19.55	0.37	0.17	0.31
5	21	19.278	0.47	0.21	0.39
6	21	18.87	0.60	0.28	0.50
7	21	18.65	0.68	0.31	0.57
8	21	18.31	0.79	0.36	0.66
9	21	18.07	0.87	0.40	0.73
10	21	17.89	0.94	0.43	0.78
11	21	17.71	1.00	0.46	0.83
12	21	17.52	1.06	0.49	0.89
13	21	17.43	1.09	0.50	0.91
14	21	17.37	1.11	0.51	0.93
15	21	17.30	1.14	0.52	0.95
16	21	17.21	1.17	0.54	0.98
17	21	17.18	1.18	0.54	0.99
19	21	17.12	1.20	0.55	1.00
34	21	17.00	1.24	0.57	1.04
45	21	17.00	1.24	0.57	1.04
77	21	17.09	1.21	0.55	1.01
122	21	17.12	1.20	0.55	1.00

APPENDIX 1/11

Red# 15

Zeolite 2.8CrY, (1.305g), 1.27 Wt%Cr_2O_3, N_{Cr} = (2.18±0.04)x10^{-4}
V_{man} = 45.0 cm^3, V_{tot} = 62.8±0.04 cm^3, P_i= 28.82±0.01 cmHg, T_r = 20.0±0.2°C
N_i = (7.09±0.04)x10^{-4}, T_f = 315°C, $H_2/Cr(\infty)$ = 0.66±0.08.

Time/min	T/°C	P/cmHg ± 0.01	(Moles Ads ± 0.05)x10^4	H_2/Cr ± 0.08	θ ± 0.16
0.25	20	20.62	0.00	0.00	0.00
2	20	20.54	0.03	0.01	0.02
4	20	20.48	0.05	0.02	0.03
6	20	20.40	0.07	0.03	0.05
8	20	20.22	0.13	0.06	0.09
11	20	20.10	0.18	0.08	0.12
15	20	19.88	0.25	0.12	0.18
18	20	19.84	0.27	0.12	0.19
23	20	19.59	0.35	0.16	0.25
29	20	19.26	0.47	0.21	0.33
35	20	18.94	0.58	0.26	0.40
40	20	18.69	0.66	0.31	0.46
44	20	18.49	0.73	0.34	0.51
47	20	18.32	0.79	0.36	0.55
51	20	18.16	0.84	0.39	0.59
55	20	18.00	0.90	0.41	0.63
59	20	17.88	0.94	0.43	0.66
64	20	17.76	0.98	0.45	0.69
69	20	17.62	1.03	0.47	0.72
92	20	17.23	1.17	0.54	0.82
105	20	17.12	1.20	0.55	0.84
128	20	16.98	1.25	0.57	0.88
150	20	16.90	1.28	0.59	0.89
163	20	16.85	1.30	0.59	0.91
1400	20	16.45	1.43	0.66	1.00

APPENDIX 1/12

Red# 16

Zeolite 2.8CrY, (1.305g), 1.27 Wt%Cr_2O_3, N_{Cr} = (2.18±0.04)x10^{-4}
V_{man} = 45.0±0.2 cm^3, V_{tot} = 62.8±0.4 cm^3, P_i= 28.82±0.01 cmHg, T_r = 20.0±0.2°C
N_i = (7.09±0.04)x10^{-4}, T_f = 350°C, $H_2/Cr(\infty)$ = 0.58±0.08.

Time/min	T/°C	P/cmHg ± 0.01	(Moles Ads ± 0.05) x10^4	H_2/Cr ± 0.08	θ ± 0.16
0.25	22.5	14.43	0.03	0.01	0.02
2	22.5	14.31	0.07	0.03	0.05
3	22.5	14.19	0.11	0.05	0.08
4	22.5	14.12	0.13	0.06	0.10
5	22.5	14.04	0.16	0.07	0.12
7	22.5	13.94	0.19	0.09	0.15
8	22.5	13.78	0.25	0.11	0.20
10	22.5	13.63	0.29	0.14	0.23
12	22.5	13.43	0.36	0.17	0.29
13	22.5	13.37	0.38	0.18	0.30
14.5	22.5	13.22	0.43	0.20	0.35
16	22.5	13.07	0.49	0.22	0.39
18	22.5	12.78	0.58	0.27	0.46
20	22.5	12.59	0.65	0.30	0.52
22	22.5	12.40	0.71	0.33	0.57
24	22.5	12.26	0.76	0.35	0.60
26	22.5	11.97	0.86	0.39	0.68
28	22.5	11.89	0.88	0.41	0.70
30	22.5	11.76	0.93	0.43	0.74
32	22.5	11.61	0.98	0.45	0.78
34	22.5	11.52	1.01	0.46	0.80
36	22.5	11.60	0.98	0.45	0.78
38	22.5	11.40	1.05	0.48	0.84
66	22.5	11.01	1.18	0.54	0.94
73	22.5	10.94	1.20	0.55	0.96
86	22.5	10.90	1.22	0.56	0.97
94	22.5	10.86	1.23	0.57	0.98
150	22.5	10.78	1.26	0.58	1.00
190	22.5	10.78	1.26	0.58	1.00
220	22.5	10.78	1.26	0.58	1.00

APPENDIX 1/13

Red# 17

Zeolite 2.8CrY, (1.305g), 1.27 Wt%Cr_2O_3, N_{Cr} = (2.18±0.04)x10^{-4}
V_{man} = 45.0±0.2 cm^3, V_{tot} = 62.3±0.4 cm^3, P_i = 28.67±0.01 cmHg, T_r = 20.5±0.2°C
N_i = (7.04±0.04)x10^{-4}, T_f = 350°C, $H_2/Cr(\infty)$ = 0.64±0.08.

Time/min	T/°C	P/cmHg ± 0.01	(Moles Ads ± 0.05) x10^4	H_2/Cr ± 0.08	θ ± 0.16
0.25	20.5	20.52	0.06	0.03	0.04
1	20.5	20.48	0.07	0.03	0.05
3	20.5	20.37	0.11	0.05	0.08
5	20.5	20.20	0.17	0.08	0.12
7	20.5	20.03	0.22	0.10	0.16
9	20.5	19.83	0.29	0.14	0.21
11	20.5	19.61	0.37	0.17	0.26
13	20.5	19.23	0.50	0.23	0.36
15	20.5	19.17	0.52	0.24	0.37
17	20.5	18.93	0.60	0.28	0.43
19	20.5	18.64	0.70	0.32	0.50
21	20.5	18.45	0.76	0.35	0.55
23	20.5	18.15	0.87	0.40	0.62
25	20.5	18.02	0.91	0.42	0.65
27	20.5	17.86	0.96	0.44	0.69
29	20.5	17.74	1.01	0.46	0.72
31	20.5	17.63	1.04	0.48	0.75
37	20.5	17.39	1.12	0.52	0.80
41	20.5	17.25	1.17	0.54	0.84
55	20.5	17.08	1.23	0.56	0.88
65	20.5	17.03	1.25	0.57	0.89
96	20.5	17.02	1.25	0.57	0.89
105	20.5	16.99	1.26	0.58	0.90
110	20.5	16.95	1.27	0.58	0.91
130	20.5	16.94	1.28	0.59	0.91
138	20.5	16.92	1.28	0.59	0.92
196	20.5	16.87	1.30	0.60	0.93
1400	20.5	16.59	1.40	0.64	1.00

APPENDIX 1/14

Red# 18

Zeolite 2.8CrY, (1.305g), 1.27 Wt%Cr_2O_3, N_{Cr} = (2.18±0.04)x10^{-4}
V_{man} = 45.0±0.2 cm^3, V_{tot} = 62.3±0.4 cm^3, P_i = 23.05±0.01 cmHg, T_r = 21.5±0.2°C
N_i = (5.64±0.04)x10^{-4}, T_f = 350°C, $H_2/Cr(\infty)$ = 0.62=0.08.

Time/min	T/°C	P/cmHg ± 0.01	(Moles Ads ± 0.05) x10^4	H_2/Cr ± 0.08	θ ± 0.16
0.25	21.5	16.56	0.02	0.01	0.02
1	21.5	16.53	0.04	0.02	0.03
2	21.5	16.42	0.07	0.03	0.06
4	21.5	16.25	0.13	0.06	0.10
6	21.5	15.99	0.22	0.10	0.16
8	21.5	15.92	0.24	0.11	0.18
10	21.5	15.76	0.30	0.14	0.22
12	21.5	15.54	0.37	0.17	0.28
14	21.5	15.41	0.42	0.19	0.31
16	21.5	15.21	0.48	0.22	0.36
18	21.5	14.93	0.58	0.27	0.43
20	21.5	14.75	0.64	0.29	0.48
22	21.5	14.56	0.70	0.32	0.52
24	21.5	14.35	0.77	0.36	0.57
26	21.5	14.20	0.83	0.38	0.61
28	21.5	14.03	0.88	0.41	0.66
30	21.5	13.87	0.94	0.43	0.69
32	21.5	13.75	0.98	0.45	0.73
34	21.5	13.63	1.02	0.47	0.76
36	21.5	13.57	1.04	0.48	0.77
38	21.5	13.48	1.07	0.49	0.79
45	21.5	13.27	1.14	0.52	0.85
54	21.5	13.14	1.18	0.54	0.88
85	21.5	13.01	1.23	0.56	0.91
104	21.5	12.99	1.24	0.57	0.92
150	21.5	12.97	1.24	0.57	0.92
175	21.5	12.98	1.24	0.57	0.92
1400	21.5	12.66	1.35	0.62	1.00

APPENDIX 1/15

Red# 19

Zeolite 2.8CrY, (1.305g), 1.27 Wt%Cr_2O_3, N_{Cr} = (2.18±0.04)x10^{-4}
V_{man} = 45.0±0.2 cm^3, Vt_{ot} = 62.3±0.4 cm^3, P_i= 23.05±0.01 cmHg, T_r = 21.5±0.2°C
N_i = (5.64±0.04)x10^{-4}, T_f = 350°C, $H_2/Cr(\infty)$ = 0.52±0.08.

Time/min	T/°C	P/cmHg ± 0.01	(Moles Ads ± 0.05) x10^4	H_2/Cr ± 0.08	θ ± 0.16
0.5	23	5.03	0.02	0.01	0.02
1	23	4.97	0.04	0.02	0.04
2	23	4.91	0.07	0.03	0.06
3	23	4.82	0.10	0.04	0.09
4	23	4.71	0.13	0.06	0.12
5	23	4.62	0.16	0.08	0.14
6	23	4.51	0.20	0.09	0.18
7	23	4.39	0.24	0.11	0.21
8	23	4.26	0.29	0.11	0.25
9	23	4.17	0.32	0.15	0.28
10	23	4.03	0.36	0.17	0.32
11	23	3.92	0.40	0.18	0.35
12	23	3.84	0.43	0.20	0.37
13	23	3.72	0.47	0.21	0.41
14	23	3.59	0.51	0.24	0.45
15	23	3.54	0.53	0.24	0.47
16	23	3.45	0.56	0.26	0.49
18	23	3.26	0.62	0.29	0.55
20	23	3.10	0.68	0.31	0.59
22	23	3.02	0.70	0.32	0.62
24	23	2.90	0.74	0.34	0.65
26	23	2.80	0.78	0.36	0.68
28	23	2.70	0.81	0.37	0.71
30	23	2.61	0.84	0.39	0.74
32	23	2.52	0.87	0.40	0.77
35	23	2.48	0.88	0.41	0.78
38	23	2.40	0.91	0.42	0.80
44	23	2.29	0.95	0.44	0.84
51	23	2.26	0.96	0.44	0.84
60	23	2.21	0.98	0.45	0.86
75	23	2.09	1.02	0.47	0.89
129	23	2.03	1.04	0.48	0.91
200	23	1.92	1.07	0.49	0.94
1400	23	1.73	1.14	0.52	1.00

Appendix Two

APPENDIX 2/1

Reox # 3

Zeolite 2.8CrY, (1.305g), 1.27 Wt%Cr_2O_3, N_{Cr} = (2.18±0.04)x10^{-4}
V_{man} = 45.0±0.2 cm^3, V_{tot} = 62.3±0.4 cm^3, P_i = 24.87±0.01 cmHg, Tr = 21.0±0.2°C
N_i = (6.01±0.04)x10^{-4}, T_f = 400°C, $O_2/Cr(\infty)$ = 0.62±0.08.

Time/min	T/°C	P/cmHg ± 0.01	(Moles Ads ± 0.05) x10^4	O_2/Cr ± 0.08	θ ± 0.16
0.5	21	17.24	0.24	0.11	0.18
2	21	16.99	0.33	0.15	0.24
3	21	16.69	0.43	0.20	0.32
5.5	21	16.50	0.50	0.38	0.62
7.5	21	16.24	0.58	0.27	0.43
9	21	16.10	0.63	0.29	0.47
12	21	15.90	0.70	0.32	0.52
15	21	15.85	0.71	0.33	0.53
17.5	21	15.57	0.81	0,37	0.60
20	21	15.52	0.83	0.38	0.61
23	21	15.34	0.89	0.41	0.65
26	21	15.29	0.91	0.42	0.67
33	21	15.06	0.98	0.45	0.72
36	21	14.95	1.02	0.47	0.75
43	21	14.87	1.05	0.48	0.77
50.5	21	14.75	1.09	0.50	0.80
59	21	14.61	1.14	0.52	0.84
67	21	14.46	1.19	0.54	0.88
75	21	14.40	1.21	0.55	0.89
91	21	14.34	1.23	0.56	0.91
96	21	14.33	1.23	0.56	0.91
117	21	14.30	1.24	0.57	0.92
1400	21	13.96	1.35	0.62	1.00

APPENDIX 2/2

Reox # 4

Zeolite 2.8CrY, (1.305g), 1.27 Wt%Cr_2O_3, N_{Cr} = (2.18±0.04)x10^{-4}
V_{man} = 45.0±0.2 cm^3, V_{tot} = 62.3±0.4 cm^3, P_i = 25.05±0.01 cmHg, T_r = 22.8±0.2°C
N_i = (6.11±0.04)x10^{-4}, T_f = 400°C, $O_2/Cr(\infty)$ = 0.49±0.08.

Time/min	T/°C	P/cmHg ± 0.01	(Moles Ads ± 0.05)X10^4	O_2/Cr ± 0.08	θ ± 0.16
0.25	22.75	17.52	0.19	0.09	0.18
1	22.75	17.40	0.23	0.11	0.22
2	22.75	17.21	0.29	0.13	0.28
3	22.75	17.19	0.30	0.14	0.28
4	22.75	17.10	0.33	0.15	0.31
5	22.75	17.03	0.35	0.16	0.33
6.5	22.75	16.98	0.37	0.17	0.35
8	22.75	16.79	0.43	0.20	0.41
11	22.75	16.73	0.45	0.21	0.43
13	22.75	16.67	0.48	0.22	0.45
16	22.75	16.59	0.50	0.23	0.47
19	22.75	16.53	0.52	0.24	0.49
21.5	22.75	16.44	0.55	0.25	0.52
25	22.75	16.40	0.57	0.26	0.53
30	22.75	16.32	0.59	0.27	0.56
35	22.75	16.24	0.62	0.28	0.58
45	22.75	16.13	0.66	0.30	0.62
55	22.75	16.05	0.68	0.31	0.65
61	22.75	15.99	0.71	0.32	0.67
72	22.75	15.93	0.73	0.33	0.68
84	22.75	15.86	0.75	0.34	0.70
113	22.75	15.75	0.79	0.36	0.74
141	22.75	15.67	0.81	0.37	0.77
1400	22.75	14.93	1.06	0.49	1.00

APPENDIX 2/5

Reox # 5

Zeolite 2.8CrY, (1.305g), 1.27 Wt%Cr_2O_3, N_{Cr} = (2.18±0.04)x10^{-4}
V_{man} = 45.0±0.2 cm^3, V_{tot} = 62.8±0.4 cm^3, P_i= 25.12±0.01 cmHg, Tr = 22.0±0.2°C
N_i = (6.14±0.04)x10^{-4}, T_f = 400°C, $O_2/Cr(\infty)$ = 0.38±0.08.

Time/min	T/°C	P/cmHg ± 0.01	(Moles Ads ± 0.05) x10^4	O_2/Cr ± 0.08	θ ± 0.16
0.25	22	17.66	0.11	0.05	0.13
1	22	17.35	0.21	0.10	0.26
2	22	17.27	0.24	0.11	0.29
3	22	17.21	0.26	0.12	0.31
4	22	17.11	0.30	0.14	0.36
5	22	17.07	0.31	0.14	0.37
7	22	16.97	0.34	0.16	0.41
9	22	16.91	0.36	0.17	0.44
11	22	16.87	0.38	0.17	0.45
13	22	16.81	0.40	0.18	0.48
15	22	16.77	0.41	0.19	0.49
17	22	16.72	0.43	0.20	0.51
20	22	16.69	0.44	0.20	0.53
23	22	16.66	0.45	0.21	0.54
25	22	16.60	0.47	0.25	0.56
30	22	16.58	0.48	0.22	0.57
38	22	16.47	0.51	0.24	0.62
45	22	16.40	0.54	0.25	0.64
50	22	16.40	0.54	0.25	0.64
67	22	16.32	0.57	0.26	0.68
83	22	16.26	0.59	0.27	0.70
107	22	16.17	0.62	0.28	0.74
134	22	16.07	0.65	0.30	0.78
195	22	15.96	0.69	0.32	0.83
245	22	15.89	0.71	0.33	0.85
300	22	15.85	0.73	0.33	0.87
1400	22	15.53	0.84	0.38	1.00

APPENDIX 2/4

Reox # 7

Zeolite 2.8CrY, (1.305g), 1.27 Wt%Cr_2O_3, N_{Cr} = (2.18±0.04)x10^{-4}
V_{man} = 45.0±0.2 cm^3, V_{tot} = 62.3±0.4 cm^3, P_i = 25.03±0.01 cmHg, T_r = 21.0±0.2°C
N_i = (6.14±0.04)x10^{-4}, T_f = 400°C, $O_2/Cr(\infty)$ = 0.33±0.08.

Time/min	T/°C	P/cmHg ± 0.01	(Moles Ads ± 0.05) x10^4	O_2/Cr ± 0.08	θ ± 0.16
0.25	21	17.11	0.32	0.15	0.45
1	21	16.81	0.43	0.20	0.59
2	21	16.61	0.49	0.23	0.68
3	21	16.56	0.51	0.24	0.71
4	21	16.52	0.53	0.24	0.73
5	21	16.41	0.56	0.26	0.77
6	21	16.40	0.57	0.26	0.78
8	21	16.36	0.58	0.27	0.80
12	21	16.33	0.59	0.27	0.82
14	21	16.35	0.58	0.27	0.82
24	21	16.28	0.61	0.28	0.84
41	21	16.17	0.64	0.30	0.89
85	21	16.11	0.66	0.31	0.92
115	21	16.07	0.68	0.31	0.94
300	21	16.02	0.69	0.32	0.96
1400	21	15.93	0.72	0.33	1.00

APPENDIX 2/5

Reox # 8

Zeolite 2.8CrY, (1.305g), 1.27 Wt%Cr_2O_3, N_{Cr} = (2.18±0.04)x10^{-4}
V_{man} = 45.0±0.2 cm^3, V_{tot} = 62.8±0.04 cm^3, P_i = 25.11±0.01 cmHg, T_r = 24.5±0.2°C
N_i = (6.13±0.04)x10^{-4}, T_f = 300°C, $O_2/Cr(\infty)$ = 0.39±0.08.

Time/min	T/°C	P/cmHg ± 0.01	(Moles Ads ± 0.05) x10^4	O_2/Cr ± 0.08	θ ± 0.16
0.25	21.5	16.84	0.38	0.18	0.45
1	21.5	16.46	0.51	0.24	0.60
2	21.5	16.32	0.56	0.26	0.66
3	21.5	16.22	0.60	0.27	0.70
4	21.5	16.02	0.66	0.30	0.78
5	21.5	15.94	0.69	0.32	0.81
6	21.5	15.89	0.71	0.32	0.83
7	21.5	15.84	0.72	0.33	0.85
9	21.5	15.77	0.75	0.34	0.88
11	21.5	15.71	0.77	0.35	0.90
15	21.5	15.64	0.79	0.36	0.94
19	21.5	15.65	0.79	0.36	0.93
29	21.5	15.57	0.82	0.37	0.96
65	21.5	15.55	0.82	0.38	0.97
50	21.5	15.54	0.83	0.38	0.98
78	21.5	15.47	0.85	0.39	1.00

APPENDIX 2/6

Reox # 9

Zeolite 2.8CrY, (1.305g), 1.27 Wt%Cr_2O_3, N_{Cr} = (2.18±0.04)x10^{-4}
V_{man} = 45.0 cm^3, V_{tot} = 62.8±0.4 cm^3, P_i = 25.11±0.01 cmHg, T_r = 22±0.2°C
N_i = (6.14±0.04)x10^{-4}, T_f = 300°C, $O_2/Cr(\infty)$ = 0.30±0.08.

Time/min	T/°C	P/cmHg ± 0.01	(Moles Ads ± 0.05) x10^4	O_2/Cr ± 0.08	θ ± 0.16
1	22	17.22	0.26	0.12	0.39
2	22	16.99	0.33	0.15	0.51
3	22	16.87	0.38	0.17	0.58
4	22	16.82	0.39	0.18	0.60
6	22	16.77	0.41	0.19	0.63
9	22	16.68	0.44	0.20	0.68
12	22	16.64	0.45	0.21	0.70
15	22	16.59	0.47	0.22	0.72
20	22	16.45	0.52	0.24	0.80
25	22	16.45	0.52	0.24	0.80
33	22	16.42	0.53	0.24	0.81
42	22	16.38	0.54	0.25	0.83
67	22	16.31	0.57	0.26	0.87
81	22	16.31	0.57	0.26	0.87
1400	22	16.06	0.65	0.30	1.00

APPENDIX 2/7

Reox # 10

Zeolite 2.8CrY, (1.305g), 1.27 Wt%Cr_2O_3, N_{Cr} = (2.18±0.04)x10^{-4}
V_{man} = 45.0±0.2 cm^3, V_{tot} = 62.8±0.4 cm^3, P_i= 24.97±0.01 cmHg, T_r = 23.0±0.2°C
N_i = (6.08±0.04)x10^{-4}, T_f = 300°C, $O_2/Cr(\infty)$ = 0.39±0.08.

Time/min	T/°C	P/cmHg ± 0.01	(Moles Ads ± 0.05) x10^4	O_2/Cr ± 0.08	θ ± 0.16
0.25	23	16.86	0.34	0.15	0.40
1	23	16.45	0.48	0.22	0.57
2	23	16.24	0.55	0.25	0.65
3	23	16.05	0.62	0.28	0.72
4	23	15.95	0.65	0.30	0.76
5	23	15.79	0.70	0.32	0.83
11	23	15.72	0.73	0.34	0.86
18	23	15.63	0.76	0.35	0.89
26	23	15.60	0.77	0.35	0.90
1400	17	15.05	0.85	0.39	1.00

APPENDIX 2/8

Reox # 11

Zeolite 2.8CrY, (1.305g), 1.27 Wt%Cr_2O_3, N_{Cr} = 2.18±0.04)x10^{-4}
V_{man} = 45.0±0.2 cm^3, V_{tot} = 63.1±0.4 cm^3, P_i= 25.18±0.01 cmHg, T_r = 20.0±0.2°C
N_i = (6.20±0.04)x10^{-4}, T_f = 250°C, $O_2/Cr(\infty)$ = 0.32±0.08.

Time/min	T/°C	P/cmHg ± 0.01	(Moles Ads ± 0.05) x10^4	O_2/Cr ± 0.08	θ ± 0.16
0.25	20	17.49	0.16	0.07	0.23
1	20	17.23	0.25	0.12	0.36
2	20	17.08	0.30	0.14	0.44
3	20	17.02	0.32	0.15	0.47
5	20	16.95	0.35	0.16	0.50
7	20	16.86	0.38	0.17	0.55
10	20	16.83	0.40	0.18	0.66
13	20	16.75	0.42	0.19	0.60
17	20	16.71	0.43	0.20	0.62
23	20	16.63	0.46	0.21	0.66
30	20	16.56	0.48	0.22	0.70
44	20	16.49	0.50	0.23	0.73
59	20	16.43	0.53	0.24	0.76
77	20	16.34	0.56	0.26	0.81
92	20	16.32	0.57	0.26	0.82
1400	22	16.06	0.69	0.32	1.00

APPENDIX 2/9

Reox # 12

Zeolite 2.8CrY, (1.305g), 1.27 Wt%Cr_2O_3, NCr = (2.18±0.04)x10^{-4}
V_{man} = 45.0±0.2 cm^3, V_{tot} = 63.1±0.4 cm^3, P_i = 25.15±0.01 cmHg, T_r = 23.0±0.2°C
N_i = (6.13±0.04)x10^{-4}, T_f = 250°C, $O_2/Cr(\infty)$ = 0.29±0.08.

Time/min	T/°C	P/cmHg ± 0.01	(Moles Ads ± 0.05) x10^4	O_2/Cr ± 0.08	θ ± 0.16
0.25	23	17.58	0.12	0.06	0.19
1	23	17.48	0.16	0.07	0.25
2	23	17.41	0.18	0.08	0.28
3	23	17.37	0.19	0.09	0.31
5	23	17.29	0.22	0.10	0.35
10	23	17.19	0.25	0.18	0.40
12	23	17.13	0.27	0.13	0.43
15	23	17.11	0.28	0.13	0.45
20	23	17.06	0.30	0.14	0.47
36	23	16.95	0.34	0.16	0.54
58	23	16.87	0.36	0.17	0.58
71	23	16.82	0.38	0.17	0.60
89	23	16.78	0.39	0.18	0.62
1400	22.5	16.06	0.63	0.29	1.00

Appendix Three

APPENDIX 3/1

Red#20

Zeolite 5.8CrX, (2.127g), 2.39 Wt%Cr_2O_3, N_{Cr} = (6.70±0.02)x10^{-4}
V_{man} = 44.8±0.2 cm^3, V_{tot} = 64.7±0.4 cm^3, P_i = 29.13±0.01 cmHg, T_r = 22.5±0.2°C
N_i = (7.08±0.04)x10^{-4}, T_f = 350°C, $H_2/Cr(\infty)$ = 1.03±0.04.

Time/min	T/°C	P/cmHg ± 0.01	(Moles Ads ± 0.05) x10^4	H_2/Cr ± 0.04	θ ± 0.08
0.25	22.5	19.796	1.25	0.02	0.02
1	22.5	19.286	3.04	0.05	0.04
2	22.5	18.387	6.20	0.09	0.09
3	22.5	17.644	8.81	0.13	0.13
4	22.5	16.497	1.28	0.19	0.19
5	22.5	16.168	1.40	0.21	0.20
6	22.5	15.155	1.76	0.26	0.25
7	22.5	14.352	2.04	0.30	0.30
8	22.5	13.620	2.29	0.34	0.33
9	22.5	12.836	2.57	0.38	0.37
10	22.5	12.040	2.85	0.43	0.41
11	22.5	11.540	3.02	0.45	0.44
12	22.5	11.114	3.17	0.47	0.46
13	22.5	10.581	3.36	0.50	0.49
14	22.5	10.112	3.53	0.53	0.51
15	22.5	9.786	3.64	0.54	0.53
16	22.5	9.45	3.76	0.56	0.54
17	22.5	9.07	3.89	0.58	0.56
18	22.5	8.80	3.99	0.60	0.58
20.5	22.5	8.31	4.16	0.62	0.60
22	22.5	7.98	4.27	0.64	0.62
23	22.5	7.79	4.34	0.65	0.63
24	22.5	7.62	4.40	0.66	0.64
25	22.5	7.41	4.47	0.67	0.65
28	22.5	6.93	4.64	0.69	0.67
32	22.5	6.60	4.76	0.71	0.69
40	22.5	5.75	5.06	0.76	0.73
80	22.5	3.02	6.02	0.90	0.87
160	22.5	6.54	4.78	0.71	0.69
1000	22.5	0.49	6.90	1.03	1.00

APPENDIX 3/2

Red#21

Zeolite 5.8CrX, (2.127g), 2.39 Wt%Cr_2O_3, N_{Cr} = (6.70±0.02)x10^{-4}
V_{man} = 44.8±0.2 cm^3, V_{tot} = 64.7±0.4 cm^3, P_i = 46.38±0.01 cmHg, T_r = 20.5±0.2°C
N_i = (11.34±0.04)x10^{-4}, T_f = 350°C, $H_2/Cr(\infty)$ = 1.38±0.04.

Time/min	T/°C	P/cmHg ± 0.01	(Moles Ads ± 0.05) x10^4	H_2/Cr ± 0.04	θ ± 0.08
0.5	20.5	31.82	0.15	0.02	0.02
1	20.5	30.82	0.50	0.08	0.05
2	20.5	30.07	0.77	0.12	0.08
3	20.5	28.83	1.20	0.18	0.13
4	20.5	26.76	1.93	0.29	0.21
5	20.5	25.25	2.46	0.37	0.27
6	20.5	24.52	2.72	0.41	0.29
7	20.5	23.28	3.16	0.47	0.34
8	20.5	22.13	3.56	0.53	0.38
9	20.5	21.30	3.85	0.58	0.42
10	20.5	20.72	4.06	0.61	0.44
11	20.5	19.98	4.31	0.64	0.47
12	20.5	19.40	4.52	0.68	0.49
13	20.5	19.09	4.63	0.69	0.50
14	20.5	18.86	4.71	0.70	0.51
15	20.5	18.28	4.91	0.73	0.53
16	20.5	17.93	5.04	0.75	0.54
17	20.5	17.74	5.10	0.76	0.55
18	20.5	17.48	5.20	0.78	0.56
19	20.5	17.19	5.30	0.79	0.57
21	20.5	16.73	5.46	0.82	0.59
23	20.5	16.29	5.61	0.84	0.61
25	20.5	15.97	5.73	0.86	0.62
27	20.5	15.64	5.84	0.87	0.63
29	20.5	15.42	5.92	0.88	0.64
31	20.5	15.15	6.01	0.90	0.65
33	20.5	14.93	6.09	0.91	0.66
35	20.5	14.63	6.20	0.93	0.67
38	20.5	14.38	6.29	0.94	0.68
41	20.5	14.06	6.40	0.96	0.69
45	20.5	13.57	6.57	0.98	0.71
58	20.5	12.71	6.87	1.03	0.74
79	20.5	11.82	7.19	1.07	0.78
95	20.5	11.06	7.45	1.11	0.82
110	20.5	10.71	7.57	1.13	0.82
143	20.5	9.85	7.88	1.18	0.85
1000	20.5	5.92	9.26	1.38	1.00

APPENDIX 3/3

Red#22

Zeolite 5.8CrX, (2.127g), 2.39 Wt%Cr_2O_3, N_{Cr} = (6.70±0.02)x10^{-4}
V_{man} = 44.7±0.2 cm^3, V_{tot} = 63.0±0.4 cm^3, P_i = 44.70±0.01 cmHg, T_r = 19.5±0.2°C
N_i = (10.55±0.04)x10^{-4}, T_f = 350°C, $H_2/Cr(\infty)$ = 1.15±0.04.

Time/min	T/°C	P/cmHg ± 0.01	(Moles Ads ± 0.05) x10^4	H_2/Cr ± 0.04	θ ± 0.08
0.25	19.5	30.40	0.05	0.01	0.01
1.5	19.5	29.15	0.48	0.07	0.06
2.5	19.5	27.92	0.91	0.14	0.12
3	19.5	27.40	1.09	0.16	0.14
4	19.5	26.18	1.51	0.23	0.20
5	19.5	24.69	2.02	0.30	0.26
6	19.5	23.60	2.40	0.36	0.31
7	19.5	22.51	2.78	0.42	0.36
8	19.5	21.49	3.13	0.47	0.41
9	19.5	20.67	3.41	0.51	0.45
10	19.5	19.98	3.65	0.55	0.48
11	19.5	19.44	3.84	0.57	0.50
12	19.5	18.78	4.07	0.61	0.53
13	19.5	18.28	4.24	0.63	0.55
14	19.5	17.90	4.37	0.65	0.57
15	19.5	17.56	4.49	0.67	0.59
16	19.5	17.25	4.60	0.69	0.60
17	19.5	16.85	4.73	0.71	0.62
18	19.5	16.66	4.80	0.72	0.63
19	19.5	16.42	4.88	0.73	0.64
20	19.5	16.19	4.96	0.74	0.65
22	19.5	15.84	5.08	0.76	0.66
24	19.5	15.42	5.23	0.78	0.68
26	19.5	15.10	5.34	0.80	0.70
29	19.5	14.64	5.50	0.82	0.72
35	19.5	13.96	5.73	0.86	0.75
55	19.5	12.48	6.24	0.93	0.81
64	19.5	11.77	6.49	0.97	0.85
74	19.5	11.74	6.50	0.97	0.85
95	19.5	11.12	6.71	1.00	0.88
130	19.5	10.49	6.93	1.04	0.90
150	19.5	10.22	7.02	1.05	0.92
410	19.5	9.29	7.35	1.10	0.96
1000	19.5	8.34	7.67	1.15	1.00

APPENDIX 3/4

Red#23

Zeolite 5.8CrX, (2.127g), 2.39 Wt%Cr_2O_3, N_{Cr} = (6.70±0.02)x10^{-4}
V_{man} = 43.1±0.2 cm^3, V_{tot} = 62.3±0.4 cm^3, P_i = 44.47±0.01 cmHg, T_r = 19.0±0.2°C
N_i = (10.52±0.04)x10^{-4}, T_f = 325°C, $H_2/Cr(\infty)$ = 0.89±0.04.

Time/min	T/°C	P/cmHg ± 0.01	(Moles Ads ± 0.05) x10^4	H_2/Cr ± 0.04	θ ± 0.08
0.5	19.5	30.36	0.15	0.02	0.03
1	19.5	30.24	0.19	0.03	0.03
2	19.5	29.63	0.40	0.06	0.07
3	19.5	29.27	0.52	0.08	0.09
4	19.5	28.81	0.68	0.10	0.11
5	19.5	28.50	0.78	0.12	0.13
6	19.5	27.93	0.98	0.15	0.16
7	19.5	27.45	1.14	0.17	0.19
8	19.5	26.97	1.31	0.20	0.22
9	19.5	26.67	1.41	0.21	0.24
10	19.5	26.16	1.58	0.24	0.27
11	19.5	25.71	1.73	0.26	0.29
12	19.5	25.26	1.89	0.28	0.32
13	19.5	24.95	1.99	0.30	0.34
14	19.5	24.41	2.18	0.33	0.37
15	19.5	24.12	2.28	0.34	0.38
17	19.5	23.23	2.58	0.39	0.43
19	19.5	22.86	2.71	0.40	0.46
21	19.5	22.37	2.88	0.43	0.48
23	19.5	21.85	3.05	0.46	0.51
25	19.5	21.49	3.18	0.47	0.53
27	19.5	21.04	3.33	0.50	0.56
29	19.5	20.81	3.41	0.51	0.57
32	19.5	20.30	3.58	0.54	0.60
44	19.5	19.17	3.97	0.59	0.67
65	19.5	17.77	4.45	0.66	0.75
81	19.5	17.27	4.62	0.69	0.78
124	19.5	16.89	4.75	0.71	0.80
143	20.5	16.43	4.92	0.74	0.83
156	20.5	16.10	5.04	0.75	0.85
169	20.5	15.86	5.12	0.76	0.86
187	20.5	15.57	5.22	0.78	0.88
246	20.5	14.93	5.44	0.81	0.91
280	20.5	14.71	5.51	0.82	0.93
1000	18	13.30	5.95	0.89	1.00

APPENDIX 3/5

Red#24

Zeolite 5.8CrX, (2.127g), 2.39 Wt%Cr_2O_3, N_{Cr} = (6.70± 0.02)x10^{-4}
V_{man} = 43.1±0.2 cm^3, V_{tot} = 62.6±0.4 cm^3, P_i = 45.13±0.01 cmHg, T_r = 18.5±0.2°C
N_i = (10.69±0.04)x10^{-4}, T_f = 375°C, $H_2/Cr(\infty)$ = 0.77±0.04.

Time/min	T/°C	P/cmHg ± 0.01	(Moles Ads ± 0.05) x10^4	H_2/Cr ± 0.04	θ ± 0.08
0.5	18.5	30.53	1.75	0.03	0.03
1	18.5	29.22	6.28	0.09	0.12
2	18.5	27.77	1.13	0.17	0.22
3	18.5	25.86	1.78	0.27	0.35
4	18.5	24.34	2.31	0.35	0.45
5	18.5	23.41	2.63	0.39	0.51
6	18.5	22.75	2.86	0.43	0.55
7	18.5	22.08	3.09	0.46	0.60
8	18.5	21.61	3.25	0.49	0.63
9	18.5	21.29	3.36	0.50	0.65
10	18.5	20.97	3.47	0.52	0.67
11	18.5	20.63	3.59	0.54	0.69
12	18.5	20.45	3.65	0.54	0.71
13	18.5	20.23	3.72	0.56	0.72
14	18.5	19.94	3.82	0.57	0.74
15	18.5	19.84	3.86	0.58	0.75
17	19	19.48	3.99	0.60	0.77
19	19	19.16	4.10	0.61	0.79
21	19.5	19.00	4.17	0.62	0.81
24	19.5	18.66	4.29	0.64	0.83
29	19.5	18.35	4.39	0.66	0.85
37	19.5	17.96	4.53	0.68	0.88
48	19.5	17.57	4.66	0.70	0.90
62	20	17.43	4.72	0.76	0.91
87	20	17.34	4.75	0.71	0.92
104	20	17.31	4.76	0.71	0.92
123	20	17.26	4.78	0.71	0.92
200	20.5	17.28	4.78	0.71	0.93
1000	16.75	15.93	5.17	0.77	1.00

APPENDIX 3/6

Red#25

Zeolite 5.8CrX, (2.127g), 2.39 Wt%Cr_2O_3, N_{Cr} = (6.70±0.02)x10^{-4}
V_{man} = 43.1±0.2 cm^3, V_{tot} = 62.3±0.4 cm^3, P_i = 44.55±0.01 cmHg, T_r = 23.0±0.2°C
N_i = (10.43±0.01)x10^{-4}, T_f = 300°C, $H_2/Cr(\infty)$ = 0.69±0.04.

Time/min	T/°C	P/cmHg ± 0.01	(Moles Ads ± 0.05) x10^4	H_2/Cr ± 0.04	θ ± 0.08
0.5	22	30.30	0.17	0.03	0.04
1	22	30.23	0.19	0.03	0.04
2	22	30.13	0.23	0.03	0.05
3	22	29.80	0.34	0.05	0.07
4	22	29.73	0.36	0.05	0.08
5	22	29.49	0.44	0.07	0.10
6	22	29.33	0.50	0.07	0.11
7	22	29.16	0.55	0.08	0.12
8	22	28.98	0.61	0.09	0.13
9	22	28.74	0.69	0.10	0.15
10	22	28.58	0.75	0.11	0.16
11	22	28.36	0.82	0.12	0.18
12	22	28.30	0.84	0.13	0.18
13	22	28.08	0.92	0.14	0.20
14	22	27.87	0.99	0.15	0.21
15	22	27.67	1.06	0.16	0.23
17	22	27.41	1.15	0.17	0.25
18	22	27.19	1.22	0.18	0.26
19	22	27.02	1.28	0.19	0.28
20	22	26.93	1.31	0.20	0.28
21	22	26.79	1.36	0.20	0.29
22	22	26.55	1.44	0.21	0.31
25	22	26.12	1.58	0.24	0.34
30	22	25.46	1.81	0.27	0.39
36	22	24.78	2.04	0.30	0.44
51	22	23.36	2.52	0.38	0.55
61	22	22.85	2.69	0.40	0.58
71	22	22.33	2.87	0.43	0.62
80	22	21.96	2.99	0.45	0.65
97	22	21.42	3.17	0.47	0.69
107	22	21.17	3.26	0.49	0.71
123	22	20.81	3.38	0.51	0.73
135	22	20.63	3.44	0.51	0.74
154	22	20.28	3.56	0.53	0.77
196	22	19.76	3.73	0.56	0.81
490	22	18.12	4.29	0.64	0.93
1000	18	16.91	4.62	0.69	1.00

APPENDIX 3/7

Red#26

Zeolite 5.8CrX, (2.127g), 2.39 Wt%Cr_2O_3, N_{Cr} = (6.70±0.02)x10^{-4}
V_{man} = 43.1±0.2 cm^3, V_{tot} = 62.0±0.4 cm^3, P_i = 44.56±0.01 cmHg, T_r = 22.0±0.2°C
N_i = (10.43±0.04)x10^{-4}, T_f = 325°C, $H_2/Cr(\infty)$ = 1.01±0.04.

Time/min	T/°C	P/cmHg ± 0.01	(Moles Ads ± 0.05) x10^4	H_2/Cr ± 0.04	θ ± 0.08
0.5	22	30.40	0.02	0.00	0.00
1	22	29.90	0.19	0.03	0.03
2	22	29.46	0.34	0.05	0.050
3	22	28.95	0.52	0.08	0.08
4	22	28.36	0.72	0.11	0.11
5	22	27.80	0.91	0.14	0.13
6	22	27.18	1.12	0.17	0.17
7	22	26.71	1.28	0.19	0.19
8	22	26.18	1.47	0.22	0.22
9	22.25	25.57	1.68	0.25	0.25
10	22.25	25.25	1.79	0.27	0.26
11	22	24.81	1.94	0.29	0.29
12	22	24.48	2.05	0.31	0.30
13	22	23.92	2.24	0.33	0.33
15	22	23.50	2.38	0.36	0.35
16	22	23.00	2.55	0.38	0.38
17	22.5	22.78	2.64	0.40	0.39
18	22.5	22.56	2.72	0.41	0.40
19	22.5	22.19	2.84	0.43	0.42
20	22.5	21.89	2.95	0.44	0.44
21	22.5	21.76	2.99	0.45	0.44
23	22.5	21.69	3.02	0.45	0.45
25	22.5	20.88	3.29	0.49	0.49
28	22.75	20.28	3.50	0.52	0.52
31	22.75	19.65	3.72	0.56	0.55
34	22.5	19.21	3.86	0.58	0.57
37	22.5	18.64	4.06	0.61	0.60
40	22.5	18.40	4.14	0.62	0.61
43	22.75	17.99	4.29	0.64	0.63
47	23	17.57	4.44	0.66	0.66
51	23	17.20	4.56	0.68	0.67
57	23	16.67	4.74	0.71	0.70
61	23	16.34	4.86	0.73	0.72
71	23	15.68	5.08	0.76	0.75

Appendix 3/7 Continued Next Page

Appendix 3/7 Continued

94	23	14.59	5.45	0.81	0.81
111	23.25	13.99	5.66	0.85	0.84
122	23.25	13.72	5.75	0.86	0.85
142	23	13.32	5.88	0.88	0.87
162	23	12.99	6.00	0.90	0.89
187	23.5	12.68	6.11	0.91	0.90
207	23.5	12.52	6.17	0.92	0.91
246	23.5	12.20	6.27	0.94	0.93
340	23	11.95	6.35	0.95	0.94
290	23	11.80	6.40	0.96	0.95
1000	22.5	10.70	6.77	1.01	1.00

APPENDIX 3/8

Red#27

Zeolite 5.8CrX, (2.127g), 2.39 Wt%Cr_2O_3, N_{Cr} = (6.70±0.02)x10^{-4}
V_{man} = 43.1±0.2 cm^3, V_{tot} = 62.3±0.4 cm^3, P_i = 45.24±0.01 cmHg, T_r = 23.0±0.2°C
N_i = (10.55±0.04)x10^{-4}, T_f = 275°C, $H_2/Cr(\infty)$ = 0.42±0.04.

Time/min	T/°C	P/cmHg ± 0.01	(Moles Ads ± 0.05) x10^4	H_2/Cr ± 0.04	θ ± 0.08
0.5	23	30.66	0.06	0.01	0.02
2	23	30.64	0.07	0.01	0.02
4	23	30.60	0.08	0.01	0.03
8	23	30.40	0.15	0.02	0.05
12	23	30.15	0.23	0.04	0.08
16	23	29.87	0.33	0.05	0.12
21	23	29.79	0.36	0.05	0.13
25	23	29.58	0.43	0.06	0.15
29	23	29.38	0.49	0.07	0.18
36	23	28.97	0.60	0.09	0.41
43	23	28.71	0.73	0.11	0.26
51	23	28.40	0.83	0.12	0.30
58	23	28.11	0.93	0.14	0.33
64	23	27.96	0.98	0.15	0.35
73	23	27.65	1.09	0.16	0.39
82	23	27.43	1.16	0.17	0.41
105	23	26.73	1.40	0.21	0.50
120	23	26.44	1.50	0.22	0.53
139	23	26.11	1.61	0.24	0.58
159	23	25.85	1.70	0.26	0.61
175	24	25.63	1.81	0.27	0.64
193	23.5	25.46	1.85	0.28	0.66
216	22.5	25.20	1.91	0.29	0.68
240	23	24.99	2.00	0.30	0.71
373	23	24.18	2.27	0.34	0.81
1000	24	22.71	2.81	0.42	1.00

APPENDIX 3/9

Red#28

Zeolite 5.8CrX, (2.127g), 2.39 Wt%Cr_2O_3, N_{Cr} = (6.70±0.02)x10^{-4}
V_{man} = 43.1±0.2 cm^3, V_{tot} = 64.7±0.4 cm^3, P_i = 46.54±0.01 cmHg, T_r = 23.0±0.2°C
N_i = (10.86±0.04)x10^{-4}, T_f = 250°C, $H_2/Cr(\infty)$ = 0.39±0.04.

Time/min	T/°C	P/cmHg ± 0.01	(Moles Ads ±0.05) x10^4	H_2/Cr ± 0.04	θ ± 0.08
0.5	23	30.97	0.00	0.00	0.00
1	23	30.98	0.00	0.00	0.00
21	23.75	30.56	0.12	0.03	0.07
32	23.75	30.20	0.30	0.05	0.11
43	24	30.14	0.33	0.05	0.13
52	24	30.03	0.37	0.06	0.14
62	24.25	29.81	0.45	0.07	0.17
72	24.5	29.64	0.52	0.08	0.20
87	24.5	29.40	0.60	0.09	0.23
106	24.5	29.07	0.72	0.11	0.28
134	24.5	28.82	0.81	0.12	0.31
148	24.5	28.59	0.89	0.13	0.34
156	24.5	28.53	0.91	0.14	0.35
180	24.5	28.09	1.06	0.16	0.41
214	24.5	27.83	1.15	0.17	0.44
230	24.5	27.68	1.20	0.18	0.46
379	23.5	26.46	1.60	0.24	0.61
540	23	25.45	1.94	0.29	0.74
1000	24.25	23.62	2.61	0.39	1.00

Appendix Four

APPENDIX 4/1

Reox # 15

Zeolite 5.8CrX, (2.127g), 2.39 Wt%Cr_2O_3, N_{Cr} = (6.70±0.02)x10^{-4}
V_{man} = 44.8±0.2 cm^3, V_{tot} = 64.7±0.4 cm^3, P_i = 45.19±0.01 cmHg, T_r = 20.0±0.2°C
N_i = (11.07±0.04)x10^{-4}, T_f = 400°C, $O_2/Cr(\infty)$ = 0.47±0.04.

Time/min	T/°C	P/cmHg ± 0.01	(Moles Ads ± 0.05) x10^4	O_2/Cr ± 0.04	θ ± 0.08
0.5	20	30.32	0.33	0.12	0.12
1	20	29.68	0.55	0.15	0.20
2	20	29.10	0.76	0.18	0.28
3	20	28.93	0.82	0.19	0.30
4	20	28.73	0.89	0.20	0.33
5	20	28.34	1.03	0.22	0.38
7	20	28.28	1.05	0.23	0.38
9	20	27.99	1.15	0.24	0.42
11	20	27.83	1.21	0.25	0.44
14	20	27.63	1.28	0.26	0.47
17	20	27.50	1.33	0.26	0.49
20	20	27.31	1.39	0.27	0.51
23	20	27.14	1.46	0.28	0.53
28	20	26.93	1.53	0.29	0.56
32	20	26.74	1.60	0.30	0.58
40	20	26.53	1.67	0.31	0.61
50	20	26.25	1.77	0.33	0.65
68	20	25.93	1.88	0.34	0.69
84	20	25.69	1.97	0.36	0.72
97	20	25.55	2.02	0.36	0.74
124	20	25.21	2.14	0.38	0.78
152	20	25.02	2.20	0.39	0.81
171	20	24.90	2.25	0.40	0.82
237	20	24.49	2.39	0.42	0.88
322	20	24.36	2.44	0.42	0.89
1000	20	23.53	2.73	0.47	1.00

APPENDIX 4/2

Reox # 16

Zeolite 5.8CrX, (2.127g), 2.39 Wt%Cr_2O_3, N_{Cr} = (6.70±0.02)x10^{-4}
V_{man} = 43.1±0.2 cm^3, V_{tot} = 63.0±0.4 cm^3, P_i = 33.30±0.01 cmHg, T_r = 20.0±0.2°C
N_i = (7.85±0.01)x10^{-4}, T_f = 400°C, $O_2/Cr(\infty)$ = 0.50±0.04.

Time/min	T/°C	P/cmHg ± 0.01	(Moles Ads ± 0.05) x10^4	O_2/Cr ± 0.04	θ ± 0.08
0.25	20	20.65	0.73	0.13	0.22
1.5	20	20.06	0.93	0.16	0.28
3	20	19.36	1.17	0.19	0.36
4	20	19.20	1.23	0.20	0.37
5	20	19.08	1.27	0.21	0.39
7	20	18.81	1.36	0.22	0.42
9	20	18.37	1.51	0.24	0.46
11	20	18.26	1.55	0.25	0.47
13	20	18.16	1.59	0.26	0.48
21	20	17.78	1.72	0.27	0.52
29	20	17.44	1.84	0.29	0.56
36	20	17.35	1.87	0.30	0.57
48	20	17.04	1.97	0.31	0.60
72	20	16.66	2.10	0.33	0.64
86	20	16.56	2.16	0.34	0.66
107	20	16.27	2.24	0.35	0.68
170	20	15.62	2.46	0.38	0.75
226	20	14.49	2.85	0.44	0.87
1000	20	13.25	3.28	0.50	1.00

APPENDIX 4/3

Reox # 17

Zeolite 5.8CrX, (2.127g), 2.39 Wt%Cr_2O_3, N_{Cr} = (6.70±0.02)x10^{-4}
V_{man} = 43.1±0.2 cm^3, V_{tot} = 61.8±0.4 cm^3, P_i = 35.64±0.01 cmHg, Tr = 18.8±0.2°C
N_i = (8.44±0.04)x10^{-4}, T_f = 400°C, $O_2/Cr(\infty)$ = 0.45±0.04.

Time/min	T/°C	P/cmHg ± 0.01	(Moles Ads ± 0.05) x10^4	O_2/Cr ± 0.04	θ ± 0.08
0.25	18.75	21.35	1.18	0.18	0.39
1	18.75	20.39	1.51	0.23	0.50
2	18.75	20.14	1.59	0.24	0.53
3	18.75	19.95	1.66	0.25	0.55
4	18.75	18.81	2.04	0.31	0.68
5	18.75	19.63	1.77	0.26	0.58
6	18.75	19.54	1.80	0.27	0.59
8	18.75	19.19	1.92	0.29	0.63
11	18.75	19.12	1.94	0.29	0.64
15	18.75	18.97	1.99	0.30	0.66
24	18.75	18.67	2.09	0.31	0.69
30	18.75	18.52	2.15	0.32	0.71
44	18.75	18.00	2.32	0.35	0.77
70	18.75	17.96	2.34	0.35	0.77
110	18.75	17.72	2.42	0.36	0.80
200	18.75	17.28	2.57	0.38	0.85
247	18.75	17.20	2.59	0.39	0.86
350	18.75	17.10	2.63	0.39	0.87
1000	18.75	15.91	3.03	0.45	1.00

APPENDIX 4/4

Reox # 18

Zeolite 5.8CrX, (2.127g), 2.39 Wt%Cr_2O_3, N_{Cr} = (6.70±0.02)x10^{-4}
V_{man} = 43.1±0.2 cm^3, V_{tot} = 61.8±0.4 cm^3, P_i = 34.77±0.01 cmHg, T_r = 21.0±0.2°C
N_i = (8.17±0.04)x10^{-4}, T_f = 400°C, $O_2/Cr(\infty)$ = 0.38±0.04.

Time/min	T/°C	P/cmHg ± 0.01	(Moles Ads ± 0.05) x10^4	O_2/Cr ± 0.04	θ ± 0.08
0.25	21	20.70	1.19	0.18	0.47
1	21	20.02	1.42	0.21	0.56
2	21	19.76	1.50	0.23	0.59
3	21	19.47	1.60	0.24	0.63
4	21	19.40	1.63	0.24	0.64
6	21	19.22	1.69	0.25	0.66
8	21	19.08	1.73	0.26	0.68
10	21	18.92	1.79	0.27	0.70
13	21	18.83	1.82	0.27	0.71
19	21	18.69	1.86	0.28	0.73
33	21	18.40	1.96	0.29	0.77
44	21	18.07	2.07	0.31	0.81
67	20.5	18.05	2.07	0.31	0.81
1000	17	16.43	2.55	0.38	1.00

APPENDIX 4/5

Reox # 19

Zeolite 5.8CrX, (2.127g), 2.39 Wt%Cr_2O_3, N_{Cr} = (6.70±0.02)x10^{-4}
V_{man} = 43.1±0.1 cm^3, V_{tot} = 63.0±0.4 cm^3, P_i = 35.48±0.01 cmHg, T_r = 18.5±0.2°C
N_i = (8.40±0.04)x10^{-4}, T_f = 350°C, O_2/Cr(∞) = 0.37±0.04.

Time/min	T/°C	P/cmHg ± 0.01	(Moles Ads ± 0.05) x10^4	O_2/Cr ± 0.04	θ ± 0.08
0.5	18.5	21.96	0.80	0.12	0.32
1	18.5	21.26	1.04	0.16	0.42
2	18.5	20.80	1.20	0.18	0.49
3	18.5	20.52	1.29	0.19	0.53
4	18.5	20.29	1.37	0.21	0.56
5	18.5	20.13	1.43	0.2	0.58
7	18.5	19.95	1.49	0.22	0.61
9	18.5	19.72	1.57	0.23	0.64
11	18.5	19.61	1.61	0.24	0.65
13	18.5	19.52	1.64	0.25	0.67
15	18.5	19.46	1.66	0.25	0.67
18	18.5	19.30	1.72	0.26	0.70
21	18.5	19.19	1.75	0.26	0.71
26	18.5	19.09	1.79	0.27	0.73
31	18.5	18.99	1.82	0.27	0.74
37	18.5	18.88	1.86	0.28	0.76
57	18.5	18.64	1.95	0.29	0.79
74	19.5	18.59	1.99	0.30	0.81
90	19.5	18.50	2.01	0.30	0.82
106	20	18.36	2.08	0.31	0.84
126	20	18.29	2.10	0.31	0.85
280	20	17.90	2.23	0.33	0.91
290	19.5	17.72	2.28	0.34	0.93
1000	18	17.12	2.46	0.37	1.00

APPENDIX 4/6

Reox # 20

Zeolite 5.8CrX, (2.127g), 2.39 Wt%Cr_2O_3, N_{Cr} = (6.70±0.02)x10^{-4}
V_{man} = 43.1±0.2 cm^3, V_{tot} = 62.6±0.4 cm^3, P_i = 35.42±0.01 cmHg, T_r = 22.0±0.2°C
N_i = (8.29±0.04)x10^{-4}, T_f = 375°C, $O_2/Cr(\infty)$ = 0.32±0.04.

Time/min	T/°C	P/cmHg ± 0.01	(Moles Ads ± 0.05) x10^4	O_2/Cr ± 0.04	θ ± 0.08
0.5	22	21.46	0.99	0.15	0.46
1	22	20.74	1.23	0.18	0.57
2	22	20.50	1.31	0.20	0.61
3	22	20.31	1.38	0.21	0.64
4	22.5	20.19	1.43	0.21	0.67
5	22.5	20.05	1.48	0.22	0.69
7	22.5	19.98	1.50	0.22	0.70
9	22.5	19.88	1.54	0.23	0.71
11	22.5	19.80	1.56	0.23	0.73
14	22.5	19.65	1.62	0.24	0.75
19	22.5	19.54	1.65	0.25	0.77
24	23	19.49	1.68	0.25	0.78
30	23	19.41	1.71	0.26	0.79
38	23	19.32	1.74	0.26	0.81
48	23.5	19.21	1.79	0.27	0.83
61	22.5	19.05	1.82	0.27	0.84
74	23	19.04	1.83	0.27	0.85
102	23.5	18.98	1.86	0.28	0.87
147	23.5	18.88	1.90	0.28	0.88
185	23.5	18.79	1.93	0.29	0.90
210	23.5	18.76	1.94	0.29	0.90
230	23.5	18.74	1.94	0.29	0.90
316	22.5	18.61	1.97	0.29	0.92
1000	18.75	17.84	2.15	0.32	1.00

APPENDIX 4/7

Reox # 21

Zeolite 5.8CrX, (2.127g), 2.39 Wt%Cr_2O_3, N_{Cr} = (6.70±0.02)x10^{-4}
V_{man} = 43.1±0.2 cm^3, V_{tot} = 61.0±0.4 cm^3, P_i = 35.66±0.01 cmHg, Tr = 22.8±0.2°C
N_i = (8.33±0.04)x10^{-4}, T_f = 620°C, $O_2/Cr(\infty)$ = 0.33±0.04.

Time/min	T/°C	P/cmHg ± 0.01	(Moles Ads ± 0.05) x10^4	O_2/Cr ± 0.04	θ ± 0.08
0.5	22.5	24.54	0.20	0.03	0.09
1	22.5	24.44	0.23	0.04	0.11
2	22.5	24.35	0.26	0.04	0.12
3	22.5	24.24	0.30	0.05	0.14
4	22.5	24.15	0.33	0.05	0.15
5	22.5	24.07	0.36	0.05	0.16
7	22.5	23.96	0.39	0.06	0.18
9	22.5	23.87	0.43	0.06	0.19
11	22.5	23.75	0.47	0.07	0.21
13	22.5	23.67	0.49	0.07	0.22
15	22.5	23.58	0.52	0.08	0.24
18	23	23.51	0.56	0.08	0.25
21	23	23.45	0.58	0.09	0.26
25	23	23.35	0.61	0.09	0.28
29	23	23.30	0.62	0.09	0.29
34	23	23.21	0.66	0.10	0.30
40	23	23.13	0.68	0.10	0.31
46	22.75	23.00	0.72	0.11	0.33
52	22.75	22.94	0.74	0.11	0.34
70	22.5	22.62	0.84	0.13	0.38
80	23	22.66	0.84	0.13	0.38
97	23.5	22.50	0.90	0.14	0.41
113	23.75	22.32	0.97	0.14	0.44
133	24	22.16	1.03	0.15	0.47
173	24	21.90	1.11	0.17	0.51
230	24	21.48	1.25	0.19	0.57
293	23.5	21.06	1.38	0.21	0.63
324	23.5	20.90	1.43	0.21	0.65
1000	20.5	18.41	2.19	0.33	1.00

APPENDIX 4/8

Reox # 22

Zeolite 5.8CrX, (2.127g), 2.39 Wt%Cr_2O_3, N_{Cr} = (6.70±0.02)x10^{-4}
V_{man} = 43.1±0.2 cm^3, V_{tot} = 62.8±0.4 cm^3, P_i = 45.40±0.01 cmHg, T_r = 25.0±0.2°C
N_i = (10.52±0.04)x10^{-4}, T_f = 300°C, $O_2/Cr(\infty)$ = 0.23±0.04.

Time/min	T/°C	P/cmHg ± 0.01	(Moles Ads ± 0.05) x10^4	O_2/Cr ± 0.04	θ ± 0.08
0.5	25	30.56	0.19	0.03	0.12
1	25	30.33	0.27	0.04	0.17
2	25	30.15	0.33	0.05	0.21
3	25	29.98	0.39	0.06	0.25
4	25	29.81	0.45	0.07	0.29
6	25	29.72	0.48	0.07	0.31
8	25	29.51	0.55	0.08	0.35
10	25	29.43	0.57	0.09	0.37
12	25	29.30	0.62	0.09	0.40
14	25	29.25	0.64	0.10	0.41
16	25	29.11	0.68	0.10	0.44
20	25	29.01	0.72	0.11	0.46
23	25	28.93	0.74	0.11	0.48
27	25	28.84	0.77	0.12	0.50
31	25	28.74	0.81	0.12	0.52
38	25	28.67	0.83	0.12	0.53
48	25	28.45	0.90	0.14	0.58
67	25	28.24	0.98	0.15	0.63
81	25	28.15	1.01	0.15	0.65
95	25	28.05	1.04	0.16	0.67
120	25	27.90	1.09	0.16	0.70
150	25	27.76	1.14	0.17	0.73
179	25	27.67	1.17	0.17	0.75
246	25	27.54	1.21	0.18	0.78
300	25	27.45	1.24	0.19	0.80
385	25	27.30	1.30	0.19	0.83
1000	25	26.52	1.56	0.23	1.00

APPENDIX 4/9

Reox # 23

Zeolite 5.8CrX, (2.127g), 2.39 Wt%Cr_2O_3, N_{Cr} = (6.70±0.02)x10^{-4}
V_{man} = 43.1±0.2 cm^3, V_{tot} = 63.2±0.4 cm^3, P_i = 35.55±0.01 cmHg, T_r = 22.0±0.2°C
N_i = (8.32±0.04,x10^{-4}, Tf = 275°C, $O_2/Cr(\infty)$ = 0.22±0.04.

Time/min	T/°C	P/cmHg ± 0.01	(Moles Ads ± 0.05) x10^4	O_2/Cr ± 0.04	θ ± 0.08
0.5	22	21.60	0.90	0.14	0.60
1	22	21.17	1.05	0.16	0.70
2	22	20.80	1.18	0.18	0.79
3	21.5	20.58	1.24	0.19	0.83
4	21.5	20.30	1.34	0.20	0.89
5	21.5	20.27	1.35	0.20	0.90
6	21.5	20.21	1.37	0.20	0.92
7	21.75	20.18	1.38	0.21	0.93
8	21.75	20.07	1.42	0.21	0.95
9	21.5	20.00	1.44	0.22	0.96
10	21.5	19.98	1.45	0.22	0.97
12	21.5	19.96	1.46	0.22	0.97
16	22	19.91	1.48	0.22	0.99
21	22	19.88	1.49	0.22	1.00
26	22	19.87	1.49	0.22	1.00

Appendix Five

APPENDIX 5/1

Red#30

Zeolite 2.1CrX, (2.127g), 1.02 Wt%Cr_2O_3, N_{Cr} = (3.90±0.02)x10^{-4}
V_{man} = 43.1±0.2 cm^3, V_{tot} = 62.3±0.4 cm^3, P_i = 40.34±0.01 cmHg, T_r = 25.0±0.2°C
N_i = (9.35±0.04)x10^{-4}, T_f = 300°C, $H_2/Cr(\infty)$ = 1.00±0.04.

Time/min	T/°C	P/cmHg ± 0.01	(Moles Ads ± 0.05) x10^4	H_2/Cr ± 0.04	θ ± 0.08
0.5	25	27.26	0.21	0.05	0.05
1	25	26.42	0.49	0.13	0.13
2	25	26.05	0.61	0.16	0.16
3	25	25.66	0.74	0.19	0.19
4	25	25.36	0.84	0.22	0.22
5	25	25.11	0.93	0.24	0.24
6	25	24.83	1.02	0.26	0.26
7	25	24.66	1.08	0.28	0.28
8	25	24.58	1.11	0.28	0.29
9	25	24.46	1.15	0.29	0.30
10	25	24.28	1.21	0.31	0.31
11	25	24.15	1.25	0.32	0.32
12	25	24.11	1.26	0.33	0.33
13	25	23.99	1.30	0.34	0.34
14	25	23.84	1.35	0.35	0.35
15	25	23.72	1.40	0.36	0.36
16	25	23.69	1.41	0.36	0.36
17	25	23.59	1.44	0.37	0.37
18	25	23.50	1.47	0.38	0.38
19	25	23.39	1.50	0.39	0.39
20	25.25	23.36	1.52	0.39	0.39
22	25.25	23.24	1.56	0.40	0.40
25	25.25	23.05	1.63	0.42	0.42
28	25.5	22.85	1.70	0.44	0.44
31	25.25	22.81	1.71	0.44	0.44
36	25.25	22.48	1.82	0.47	0.47
44	25	22.11	1.93	0.50	0.50
55	24.5	21.71	2.06	0.53	0.53
69	298.5	21.36	2.20	0.57	0.57
99	297	20.66	2.40	0.62	0.62
137	23.25	20.02	2.60	0.67	0.67
160	23	19.73	2.69	0.69	0.69
200	22	19.26	2.82	0.73	0.73
214	22	19.18	2.85	0.73	0.73
235	22	18.94	2.93	0.75	0.75
1000	20	16.01	3.89	1.00	1.00

APPENDIX 5/2

Red#31

Zeolite 2.1CrX, (2.127g), 1.02 Wt%Cr_2O_3, N_{Cr} = (3.90±0.02)x10^{-4}
V_{man} = 43.1±0.2 cm^3, V_{tot} = 62.8±0.4 cm^3, P_i = 40.63±0.01 cmHg, T_r = 22.5±0.2°C
N_i = (9.49±0.04)x10^{-4}, T_f = 250°C, $H_2/Cr(\infty)$ = 0.70±0.04.

Time/min	T/°C	P/cmHg ± 0.01	(Moles Ads ± 0.05) x10^4	H_2/Cr ± 0.04	θ ± 0.08
0.5	22.5	27.35	0.17	0.05	0.06
1	22.5	27.00	0.29	0.08	0.11
2	22.5	26.86	0.34	0.09	0.13
3	22.5	26.68	0.40	0.10	0.15
4	22.5	26.56	0.44	0.11	0.16
5	22.5	26.46	0.48	0.12	0.18
6	22.5	26.28	0.54	0.14	0.20
7	22.5	26.17	0.57	0.15	0.21
8	22.5	26.06	0.61	0.16	0.23
10	22.5	25.96	0.65	0.17	0.24
12	22.5	25.72	0.73	0.19	0.27
14	22.5	25.64	0.76	0.19	0.28
16	22.5	25.49	0.81	0.21	0.30
18	22.5	25.43	0.83	0.21	0.31
20	22.5	25.31	0.87	0.22	0.32
23	22.5	25.13	0.93	0.24	0.34
26	22.5	25.09	0.94	0.24	0.35
33	22.5	24.79	1.05	0.27	0.39
37	22.5	24.68	1.08	0.28	0.40
42	22.5	24.55	1.13	0.29	0.42
47	22.5	24.44	1.17	0.30	0.43
54	22.5	24.27	1.22	0.32	0.45
69	22.5	24.00	1.31	0.34	0.48
90	22.25	23.70	1.41	0.36	0.52
109	22.5	23.43	1.51	0.39	0.56
130	22.5	23.23	1.58	0.41	0.58
210	22.5	22.65	1.78	0.46	0.65
245	22.5	22.43	1.85	0.48	0.68
295	22.5	22.27	1.91	0.49	0.70
340	22.5	21.99	2.00	0.51	0.74
1320	20	19.73	2.71	0.70	1.00

APPENDIX 5/3

Red#32

Zeolite 2.1CrX, (2.127g), 1.02 Wt%Cr_2O_3, N_{Cr} = (3.90±0.02)x10^{-4}
V_{man} = 43.1±0.2 cm^3, V_{tot} = 62.8±0.4 cm^3, P_i = 40.76±0.01 cmHg, T_r = 21.3±0.2°C
N_i = (9.57±0.04)x10^{-4}, T_f = 275°C, $H_2/Cr(\infty)$ = 0.70±0.04.

Time/min	T/°C	P/cmHg ± 0.01	(Moles Ads ± 0.05) x10^4	H_2/Cr ± 0.04	θ ± 0.08
0.3	21.25	27.20	0.26	0.05	0.08
1	21.25	26.61	0.46	0.10	0.14
2	21.25	26.31	0.56	0.12	0.17
3	21.25	26.11	0.63	0.13	0.19
4	21.25	25.86	0.72	0.15	0.22
5	21.25	25.63	0.80	0.17	0.24
6	21.25	25.46	0.85	0.18	0.26
7	21.25	25.28	0.91	0.20	0.28
8	21.25	25.23	0.93	0.20	0.28
9	21.25	25.08	0.98	0.21	0.30
10	21.25	24.98	1.02	0.22	0.31
12	21.25	24.84	1.06	0.23	0.32
14	21.25	24.70	1.11	0.24	0.34
17	21.25	24.47	1.19	0.25	0.36
19	21.25	24.41	1.21	0.26	0.37
21	21.25	24.22	1.28	0.27	0.39
23	21.25	24.18	1.29	0.28	0.39
25	21.25	24.06	1.33	0.28	0.40
27	21.25	24.04	1.34	0.29	0.41
30	21.25	23.91	1.38	0.30	0.42
35	21.5	23.65	1.48	0.32	0.45
43	21.5	23.43	1.56	0.33	0.47
50	21.5	23.20	1.63	0.35	0.50
63	21.75	23.06	1.69	0.36	0.51
72	22	22.84	1.77	0.38	0.54
99	22	22.46	1.90	0.41	0.58
124	22	22.10	2.02	0.43	0.61
143	22	21.91	2.09	0.45	0.63
172	22	21.73	2.15	0.46	0.65
196	22	21.54	2.21	0.47	0.67
222	22	21.41	2.26	0.48	0.68
305	22	20.82	2.46	0.52	0.75
341	22	20.71	2.50	0.53	0.76
1350	21.25	18.31	3.30	0.70	1.00

APPENDIX 5/4

Red#33

Zeolite 2.1CrX, (2.127g), 1.02 Wt%Cr_2O_3, N_{Cr} = (3.90±0.02)x10^{-4}
V_{man} = 43.1±0.2 cm^3, V_{tot} = 62.3±0.4 cm^3, P_i = 40.82±0.01 cmHg, T_r = 21.5±0.2°C
N_i = (9.57±0.04)x10^{-4}, T_f = 315°C, $H_2/Cr(\infty)$ = 1.11±0.04.

Time/min	T/°C	P/cmHg ± 0.01	(Moles Ads ± 0.05) x10^4	H_2/Cr ± 0.04	θ ± 0.08
0.3	21.5	27.40	0.27	0.07	0.06
1	21.5	26.50	0.58	0.15	0.14
2	21.5	25.80	0.82	0.21	0.19
3	21.5	25.23	1.01	0.26	0.24
4	21.5	24.80	1.16	0.30	0.27
5	21.5	24.48	1.27	0.33	0.29
6	21.5	24.20	1.36	0.35	0.32
7	21.5	23.93	1.45	0.37	0.34
8	21.5	23.78	1.50	0.39	0.35
9	21.5	23.57	1.58	0.41	0.37
10	21.5	23.35	1.65	0.42	0.38
11	21.5	23.19	1.71	0.44	0.40
12	21.5	23.07	1.74	0.45	0.41
13	21.5	22.94	1.79	0.46	0.42
14	21.5	22.84	1.82	0.47	0.42
15	21.5	22.67	1.88	0.48	0.44
16	21.5	22.62	1.90	0.49	0.44
17	21.5	22.43	1.96	0.50	0.46
18	21.5	22.42	1.96	0.50	0.46
19	21.5	22.29	2.01	0.52	0.47
21	21.5	22.11	2.07	0.53	0.48
23	21.5	21.97	2.12	0.54	0.49
25	21.5	21.84	2.16	0.56	0.50
27	21.5	21.66	2.22	0.57	0.52
29	21.5	21.51	2.27	0.58	0.53
32	21.5	21.32	2.34	0.60	0.54
35	21.5	21.15	2.40	0.62	0.56
38	21.5	21.02	2.44	0.63	0.57
41	21.5	20.85	2.50	0.64	0.58
44	21.5	20.68	2.56	0.66	0.59
48	21.5	20.57	2.59	0.67	0.60
52	21.5	20.40	2.65	0.68	0.62
56	21.5	20.23	2.71	0.70	0.63
61	21.5	20.07	2.76	0.71	0.64
66	21.5	19.88	2.83	0.73	0.66

Appendix 5/4 Continued Next Page

Appendix 5/4 Continued

72	21.5	19.72	2.88	0.74	0.67
78	21.5	19.53	2.95	0.76	0.68
87	21.5	19.31	3.02	0.77	0.70
93	21.5	19.15	3.07	0.79	0.71
158	21.75	18.07	3.45	0.89	0.80
206	22	17.66	3.59	0.92	0.84
260	22	17.28	3.72	0.96	0.86
300	22	17.13	3.77	0.97	0.88
330	22.25	17.00	3.82	0.98	0.89
1365	20	15.45	4.30	1.11	1.00

APPENDIX 5/5

Red#34

Zeolite 2.1CrX, (2.127g), 1.02 Wt%Cr_2O_3, N_{Cr} = (3.90±0.02)x10^{-4}
V_{man} = 43.1±0.2 cm^3, V_{tot} = 62.2±0.4 cm^3, P_i = 40.62±0.01 cmHg, Tr = 21.3±0.2°C
N_i = (9.53±0.04)x10^{-4}, T_f = 325°C, $H_2/Cr(\infty)$ = 1.14±0.04.

Time/min	T/°C	P/cmHg ± 0.01	(Moles Ads ± 0.05) x10^4	H_2/Cr ± 0.04	θ ± 0.08
0.3	21.5	26.15	0.67	0.17	0.15
1	21.5	25.07	1.04	0.27	0.23
2	21.5	24.05	1.39	0.36	0.31
3	21.5	23.42	1.60	0.41	0.36
4	21.5	23.04	1.73	0.44	0.39
5	21.5	22.62	1.87	0.48	0.42
6	21.5	22.43	1.93	0.50	0.43
7	21.5	22.24	2.00	0.51	0.45
8	21.5	21.82	2.14	0.55	0.48
9	21.5	21.62	2.21	0.57	0.50
10	21.5	21.49	2.25	0.58	0.51
11	21.5	21.26	2.33	0.60	0.52
12	21.5	21.08	2.39	0.61	0.54
13	21.5	20.97	2.43	0.62	0.55
14	21.5	20.78	2.49	0.64	0.56
15	21.5	20.67	2.53	0.65	0.57
16	21.5	20.54	2.57	0.66	0.58
17	21.5	20.44	2.61	0.67	0.59
18	21.5	20.36	2.63	0.68	0.59
19	21.5	20.20	2.69	0.69	0.60
20	21.5	20.11	2.72	0.70	0.61
21	21.5	20.12	2.72	0.70	0.61
22	21.5	20.08	2.73	0.70	0.61
23	21.5	19.91	2.79	0.72	0.63
24	21.5	19.82	2.82	0.72	0.63
25	21.5	19.75	2.84	0.73	0.64
26	21.5	19.62	2.89	0.74	0.65
27	21.5	19.64	2.88	0.74	0.65
28	21.5	19.53	2.92	0.75	0.66
29	21.5	19.46	2.94	0.75	0.66
31	21.5	19.40	2.96	0.76	0.67
33	21.5	19.18	3.03	0.69	0.68
35	21.5	19.07	3.07	0.79	0.69
38	21.5	18.92	3.12	0.80	0.70
41	21.5	18.85	3.15	0.81	0.71

Appendix 5/5 Continued Next Page

Appendix 5/5 Continued

44	21.5	18.70	3.20	0.82	0.72
47	21.5	18.51	3.26	0.74	0.73
52	21.5	18.27	3.34	0.86	0.75
59	21	18.08	3.40	0.87	0.76
69	21	17.75	3.51	0.90	0.79
85	21	17.47	3.60	0.92	0.81
249	21.5	16.20	4.05	1.04	0.91
285	21.5	16.12	4.07	1.05	0.91
1320	20.75	14.95	4.45	1.14	1.00

APPENDIX 5/6

Red#35

Zeolite 2.1CrX, (2.127g), 1.02 Wt%Cr_2O_3, N_{Cr} = (3.90±0.02)x10^{-4}
V_{man} = 43.1±0.2 cm^3, V_{tot} = 62.8±0.4 cm^3, P_i = 39.94±0.01 cmHg, T_r = 20.8±0.2°C
N_i = (9.39±0.04)x10^{-4}, T_f = 250°C, $H_2/Cr(\infty)$ = 0.89±0.04.

Time/min	T/°C	P/cmHg ± 0.01	(Moles Ads ± 0.05) x10^4	H_2/Cr ± 0.04	θ ± 0.08
0.5	23.75	27.01	0.22	0.06	0.06
1	23.75	26.84	0.28	0.07	0.08
2	23.75	26.48	0.40	0.10	0.12
3	23.75	26.22	0.49	0.13	0.14
4	23.75	26.13	0.52	0.13	0.15
5	23.75	25.98	0.56	0.41	0.46
6	23.75	25.79	0.64	0.16	0.18
7	23.75	25.67	0.68	0.17	0.20
8	23.75	25.50	0.73	0.19	0.21
10	23.75	25.48	0.74	0.19	0.21
12	23.75	25.27	0.81	0.21	0.23
14	23.75	24.96	0.92	0.24	0.26
16	23.75	24.81	0.97	0.25	0.28
18	23.75	24.70	1.01	0.26	0.29
20	23.75	24.60	1.04	0.27	0.30
22	23.75	24.43	1.10	0.28	0.32
24	23.75	24.31	1.14	0.29	0.33
27	23.75	24.22	1.17	0.30	0.34
32	23.75	23.96	1.26	0.32	0.36
37	23.75	23.71	1.34	0.34	0.39
41	23.75	23.61	1.38	0.35	0.40
46	23.75	23.43	1.44	0.37	0.41
51	23.75	23.26	1.50	0.38	0.43
59	23.75	23.09	1.55	0.40	0.45
77	23.75	22.60	1.72	0.44	0.50
110	23.75	22.06	1.90	0.50	0.55
126	23.75	21.82	1.99	0.51	0.57
159	23.75	21.48	2.10	0.54	0.61
1230	21	17.28	3.47	0.89	1.00

APPENDIX 5/7

Red#36

Zeolite 2.1CrX, (2.127g), 1.02 Wt%Cr_2O_3, N_{Cr} = (3.90±0.02)x10^{-4}
V_{man} = 43.1±0.2 cm^3, V_{tot} = 62.1±0.4 cm^3, P_i = 40.85±0.01 cmHg, T_r = 21.0±0.2°C
N_i = (9.59±0.04)x10^{-4}, T_f = 335°C, $H_2/Cr(\infty)$ = 1.24±0.04.

Time/min	T/°C	P/cmHg ± 0.01	(Moles Ads ± 0.05) x10^4	H_2/Cr ± 0.04	θ ± 0.08
0.5	21	25.73	0.87	0.22	0.18
1	21	24.84	1.18	0.30	0.24
2	21	24.04	1.45	0.36	0.30
3	21	23.25	1.71	0.44	0.35
4	21	22.85	1.85	0.48	0.38
5	21	22.36	2.02	0.52	0.42
6	21	22.19	2.07	0.53	0.43
7	21	21.83	2.19	0.56	0.45
8	21	21.53	2.30	0.59	0.48
9	21	21.31	2.37	0.61	0.49
10	21	21.21	2.41	0.62	0.50
11	21	21.05	2.46	0.63	0.51
12	21	20.82	2.54	0.65	0.52
13	21	20.67	2.59	0.66	0.54
14	21	20.50	2.65	0.68	0.55
15	21	20.32	2.71	0.70	0.56
16	21	20.14	2.77	0.71	0.57
17	21	20.15	2.76	0.71	0.57
18	21.5	20.06	2.81	0.72	0.58
19	21.5	19.90	2.86	0.74	0.59
20	21.5	19.76	2.91	0.75	0.60
21	21.5	19.69	2.93	0.75	0.61
22	21.5	19.59	2.97	0.76	0.61
23	21.5	19.42	3.02	0.78	0.62
24	21.5	19.35	3.05	0.78	0.63
26	21.5	19.19	3.10	0.80	0.64
28	21.5	19.07	3.14	0.80	0.65
30	21.5	18.88	3.21	0.82	0.66
32	21.25	18.73	3.25	0.83	0.67
34	21.25	18.60	3.30	0.85	0.68
39	21.25	18.32	3.39	0.87	0.70
50	21.25	17.83	3.56	0.91	0.74
68	21.25	17.16	3.78	0.97	0.78
84	21.25	16.76	3.92	1.01	0.81
100	21	16.44	4.02	1.03	0.83
115	21	16.24	4.09	1.05	0.85
130	21.5	16.06	4.16	1.07	0.86
157	22	15.93	4.21	1.08	0.87
192	22	15.62	4.32	1.11	0.89
1860	20.5	14.01	4.84	1.24	1.00

APPENDIX 5/8

Red#37

Zeolite 2.1CrX, (2.127g), 1.02 Wt%Cr_2O_3, N_{Cr} = (3.90±0.02)x10^{-4}
Vman = 43.1±0.2 cm^3, V_{tot} = 62.1±0.4 cm^3, P_i = 40.62±0.01 cmHg, T_r = 21.0±0.2°C
N_i = (9.54±0.04)x10^{-4}, T_f = 350°C, $H_2/Cr(\infty)$ = 1.19±0.04.

Time/min	T/°C	P/cmHg ± 0.01	(Moles Ads ± 0.05) x10^4	H_2/Cr ± 0.04	θ ± 0.08
0.4	21	25.69	0.85	0.22	0.18
1	21	24.46	1.26	0.33	0.27
2	21	24.35	1.30	0.33	0.28
3	21	22.68	1.87	0.48	0.40
4	21	22.07	2.07	0.53	0.45
5	21	21.75	2.18	0.56	0.47
6	21	21.45	2.28	0.59	0.49
7	21	21.06	2.41	0.62	0.52
8	21	20.77	2.51	0.65	0.54
9	21	20.55	2.58	0.66	0.56
10	21	20.46	2.61	0.67	0.57
11	21	20.16	2.72	0.70	0.59
12	21	19.94	2.79	0.72	0.60
13	21	19.80	2.84	0.73	0.61
14	21	19.66	2.89	0.74	0.62
15	21	19.54	2.93	0.75	0.63
16	21	19.36	2.99	0.77	0.65
17	21	19.22	3.04	0.78	0.66
18	21	19.12	3.07	0.79	0.66
19	21	19.00	3.11	0.80	0.67
20	21	18.92	3.14	0.81	0.68
21	21	18.76	3.19	0.82	0.69
22	21	18.62	3.24	0.83	0.70
24	21	18.48	3.29	0.84	0.71
26	21	18.46	3.29	0.85	0.71
28	21	18.18	3.39	0.87	0.73
30	21	18.11	3.41	0.88	0.74
32	21	17.88	3.49	0.90	0.76
34	21	17.76	3.53	0.90	0.76
36	21	17.63	3.58	0.92	0.77
39	21	17.49	3.62	0.93	0.78
42	21	17.33	3.67	0.94	0.80
46	21.25	17.17	3.74	0.96	0.81
50	21.25	17.14	3.75	0.96	0.81
54	21.25	16.95	3.81	0.98	0.82

Appendix 5/8 Continued Next Page

Appendix 5/8 Continued

59	21.25	16.75	3.88	1.00	0.84
64	21.25	16.57	3.94	1.01	0.85
72	21.25	16.40	4.00	1.03	0.86
81	21.5	16.26	4.05	1.04	0.88
88	21.5	16.14	4.09	1.05	0.88
96	21.5	16.05	4.12	1.06	0.89
107	21.5	15.91	4.16	1.07	0.90
119	21.5	15.80	4.20	1.08	0.91
159	21.5	15.51	4.30	1.10	0.93
172	21.5	15.45	4.32	1.11	0.94
195	21.75	15.41	4.34	1.11	0.94
232	22	15.35	4.36	1.12	0.94
256	22	15.23	4.40	1.13	0.95
288	22	15.29	4.38	1.13	0.95
1350	21.5	14.56	4.62	1.19	1.00

APPENDIX 5/9

Red#38

Zeolite 2.1CrX, (2.127g), 1.02 Wt%Cr_2O_3, N_{Cr} = (3.90±0.02)x10^{-4}
V_{man} = 43.1±0.2 cm^3, V_{tot} = 62.1±0.4 cm^3, P_i = 40.85±0.01 cmHg, T_r = 20.0±0.2°C
N_i = (9.63±0.01)x10^{-4}, T_f = 225°C, $H_2/Cr(\infty)$ = 0.61±0.04.

Time/min	T/°C	P/cmHg ± 0.01	(Moles Ads ± 0.05) x10^4	H_2/Cr ± 0.04	θ ± 0.08
0.5	23	27.54	0.22	0.06	0.09
1	23	27.42	0.26	0.07	0.11
2	23	27.29	0.30	0.08	0.13
3	23	27.17	0.34	0.09	0.14
4	23	27.04	0.39	0.10	0.16
5	23	26.88	0.44	0.11	0.19
6	23	26.82	0.46	0.12	0.19
7	23	26.71	0.50	0.13	0.21
8	23	26.62	0.53	0.14	0.22
9	23	26.61	0.53	0.14	0.22
10	23	26.59	0.54	0.14	0.23
12	23	26.43	0.59	0.15	0.25
14	23	26.37	0.62	0.16	0.26
17	23	26.28	0.65	0.17	0.27
22	23	26.11	0.70	0.18	0.30
29	23	25.90	0.78	0.20	0.33
37	23	25.68	0.85	0.22	0.36
46	23	25.46	0.93	0.24	0.39
51	23	25.33	0.97	0.25	0.41
70	23	25.01	1.08	0.28	0.45
94	23	24.72	1.18	0.30	0.49
117	23.25	24.53	1.25	0.32	0.53
149	23.5	24.27	1.35	0.35	0.57
169	23.5	24.07	1.42	0.36	0.59
199	23.5	23.87	1.49	0.38	0.62
219	23.5	23.78	1.51	0.39	0.64
244	23.5	23.66	1.56	0.40	0.65
274	23.75	23.53	1.61	0.41	0.67
332	23.5	23.26	1.69	0.43	0.71
1365	22.25	21.14	2.38	0.61	1.00

APPENDIX 5/10

Red#39

Zeolite 2.1CrX, (2.127g), 1.02 Wt%Cr_2O_3, N_{Cr} = (3.90±0.02)x10^{-4}
V_{man} = 43.1±0.2 cm^3, V_{tot} = 61.9±0.4 cm^3, P_i = 40.76±0.01 cmHg, T_r = 24.0±0.2°C
N_i = (9.48±0.04)x10^{-4}, T_f = 375°C, $H_2/Cr(\infty)$ = 1.21±0.04.

Time/min	T/°C	P/cmHg ± 0.01	(Moles Ads ± 0.05) x10^4	H_2/Cr ± 0.04	θ ± 0.08
0.5	24	26.01	0.78	0.20	0.17
1	24	24.77	1.20	0.31	0.25
2	24	23.64	1.58	0.41	0.33
3	24	22.86	1.84	0.47	0.39
4	24	22.08	2.10	0.54	0.45
5	24	21.56	2.27	0.58	0.48
6	24	21.22	2.39	0.61	0.51
7	24	20.76	2.54	0.65	0.54
8	24	20.40	2.66	0.68	0.56
9	24	20.16	2.74	0.70	0.58
10	24	19.90	2.82	0.73	0.60
11	24	19.69	2.90	0.74	0.61
12	24	19.40	2.99	0.77	0.63
13	24	19.18	3.07	0.79	0.65
14	24	18.95	3.14	0.81	0.67
15	24	18.79	3.20	0.82	0.68
16	24	18.63	3.25	0.83	0.69
17	24	18.48	3.30	0.85	0.70
18	24	18.35	3.34	0.86	0.71
20	24	18.21	3.39	0.87	0.72
21	24	18.03	3.45	0.89	0.73
22	24	17.88	3.50	0.90	0.74
23	24	17.78	3.54	0.91	0.75
24	24	17.64	3.58	0.92	0.76
25	24	17.54	3.61	0.93	0.77
26	24	17.44	3.65	0.94	0.77
27	24	17.33	3.69	0.95	0.78
28	24	17.25	3.71	0.95	0.79
30	24	17.09	3.77	0.97	0.80
32	24	17.00	3.80	0.98	0.81
36	24	16.76	3.87	0.99	0.82
41	24	16.56	3.94	1.01	0.84
46	24	16.36	4.01	1.03	0.85
51	24	16.21	4.06	1.04	0.86
56	24.25	16.05	4.12	1.06	0.87

Appendix 5/10 Continued Next Page

Appendix 5/10 Continued

61	24.25	15.96	4.15	1.06	0.88
66	24.5	15.85	4.19	1.07	0.89
71	24.5	15.74	4.22	1.08	0.90
79	24.5	15.68	4.25	1.09	0.90
89	24.5	15.62	4.27	1.09	0.90
115	24.5	15.52	4.30	1.10	0.91
134	24.5	15.43	4.33	1.11	0.92
155	24.5	15.39	4.34	1.16	0.92
176	24.5	15.35	4.36	1.13	0.92
210	24	15.28	4.37	1.12	0.93
244	24	15.23	4.39	1.13	0.93
1350	21.75	14.13	4.72	1.21	1.00

Appendix Six

APPENDIX 6/1

Reox # 24

Zeolite 2.1CrX, (2.127g), 1.02 Wt%Cr_2O_3, N_{Cr} = (3.90±0.02)x10^{-4}
V_{man} = 43.1±0.2 cm^3, V_{tot} = 62.3±0.4 cm^3, P_i = 40.53±0.01 cmHg, T_r = 21.8±0.2°C
N_i = (9.50±0.04)x10^{-4}, T_f = 300°C, $O_2/Cr(\infty)$ = 0.43±0.04.

Time/min	T/°C	P/cmHg ± 0.01	Moles Ads ± 0.05) x10^4	O_2/Cr ± 0.04	θ ± 0.08
0.3	21.75	26.05	0.66	0.15	0.35
1	21.75	25.33	0.91	0.21	0.48
2	21.75	25.01	1.02	0.23	0.53
3	21.75	24.69	1.13	0.26	0.59
4	21.75	24.49	1.20	0.27	0.63
5	21.75	24.38	1.23	0.28	0.65
6	21.75	24.25	1.28	0.29	0.67
7	21.75	24.16	1.31	0.30	0.69
8	21.75	24.00	1.36	0.31	0.71
10	21.75	23.96	1.38	0.31	0.72
12	22	23.85	1.42	0.32	0.74
14	22	23.74	1.46	0.33	0.76
16	22	23.63	1.49	0.34	0.78
18	22	23.53	1.53	0.35	0.80
21	22	23.51	1.53	0.35	0.81
27	22	23.34	1.59	0.36	0.84
32	22	23.26	1.62	0.37	0.85
40	22	23.21	1.64	0.37	0.86
56	22	23.07	1.68	0.38	0.88
85	22	22.92	1.73	0.39	0.91
130	22.5	22.82	1.78	0.41	0.93
159	22.5	22.77	1.80	0.41	0.94
225	22.5	22.74	1.81	0.41	0.95
280	23	22.74	1.82	0.42	0.96
355	22.75	22.68	1.83	0.42	0.96
1000	21.5	22.37	1.91	0.43	1.00

APPENDIX 6/2

Reox # 25

Zeolite 2.1CrX, (2.127g), 1.02 Wt%Cr_2O_3, N_{Cr} = (3.90±0.02)x10^{-4}
V_{man} = 43.1±0.2 cm^3, V_{tot} = 62.3±0.4 cm^3, P_i = 40.57±0.01 cmHg, T_r = 22.0±0.2°C
N_i = (9.50±0.04)x10^{-4}, T_f = 250°C, $O_2/Cr(\infty)$ = 0.37±0.04.

Time/min	T/°C	P/cmHg ± 0.01	Moles Ads ± 0.05) x10^4	O_2/Cr ± 0.04	θ ± 0.08
0.5	22	26.38	0.49	0.13	0.34
1	22	26.10	0.59	0.15	0.41
2	22	25.76	0.70	0.18	0.49
3	22	25.54	0.78	0.20	0.54
4	22	25.47	0.80	0.21	0.55
5	22	25.26	0.87	0.22	0.60
6	22	25.18	0.90	0.23	0.62
7	22	25.11	0.92	0.24	0.64
8	22	25.11	0.92	0.24	0.64
10	22	24.99	0.97	0.25	0.67
12	22	24.82	1.02	0.26	0.77
15	22	24.74	1.05	0.27	0.73
20	22	24.63	1.09	0.28	0.75
25	22	24.49	1.14	0.29	0.79
31	22	24.41	1.16	0.30	0.80
39	22	24.27	1.21	0.31	0.84
43	22	24.15	1.25	0.32	0.87
59	22	24.08	1.27	0.33	0.88
166	22	23.81	1.37	0.35	0.94
265	22	23.72	1.40	0.36	0.97
316	22	23.72	1.40	0.36	0.97
1320	20.5	23.46	1.45	0.37	1.00

APPENDIX 6/3

Reox # 26

Zeolite 2.1CrX, (2.127g), 1.02 Wt%Cr_2O_3, N_{Cr} = (3.90±0.02)x10^{-4}
V_{man} = 43.1±0.2 cm^3, V_{tot} = 62.2±0.4 cm^3, P_i = 40.23±0.01 cmHg, T_r = 22.5±0.2°C
N_i = (9.40±0.04)x10^{-4}, Tf = 325°C, $O_2/Cr(\infty)$ = 0.44±0.04.

Time/min	T/°C	P/cmHg ± 0.01	Moles Ads ± 0.05) x10^4	O_2/Cr ± 0.04	θ ± 0.08
0.5	22.5	23.84	1.35	0.35	0.78
1	22.5	23.29	1.54	0.40	0.89
2	22.5	23.15	1.59	0.41	0.91
3	22.5	23.10	1.61	0.41	0.93
4	22.5	23.06	1.62	0.42	0.93
6	22.5	23.02	1.63	0.42	0.94
9	22.5	22.96	1.65	0.42	0.95
13	22.5	22.90	1.67	0.43	0.96
17	22.5	22.87	1.68	0.43	0.97
21	22.5	22.83	1.70	0.44	0.98
26	22.5	22.82	1.70	0.44	0.98
40	22.5	22.74	1.73	0.44	1.00
60	22	22.69	1.73	0.44	1.00
146	22	22.69	1.73	0.44	1.00
180	21.75	22.66	1.74	0.45	1.00
580	20.25	22.61	1.71	0.44	1.00

APPENDIX 6/4

Reox # 27

Zeolite 2.1CrX, (2.127g), 1.02 Wt%Cr_2O_3, N_{Cr} = (3.90±0.02)x10^{-4}
V_{man} = 43.1±0.2 cm^3, V_{tot} = 62.8±0.4 cm^3, P_i = 40.24±0.01 cmHg, T_r = 21.0±0.2°C
N_i = (9.45±0.04)x10^{-4}, T_f = 275°C, $O_2/Cr(\infty)$ = 0.57±0.04.

Time/min	T/°C	P/cmHg ± 0.01	(Moles Ads ± 0.05) x10^4	O_2/Cr ± 0.04	θ ± 0.08
0.5	21	26.15	0.49	0.13	0.22
1	21	25.87	0.59	0.15	0.27
2	21	25.63	0.67	0.17	0.30
3	21	25.44	0.74	0.19	0.33
4	21	25.21	0.82	0.21	0.37
5	21	25.06	0.87	0.22	0.39
7	21	25.01	0.88	0.23	0.40
8	21	24.80	0.96	0.15	0.43
9	21	24.71	0.99	0.25	0.46
11	21	24.64	1.01	0.26	0.46
13	21	24.48	1.07	0.27	0.48
15	21.25	24.41	1.10	0.28	0.50
17	21.25	24.29	1.14	0.29	0.51
19	21.25	24.19	1.17	0.30	0.53
21	21.25	24.15	1.19	0.30	0.54
24	21.25	24.03	1.23	0.32	0.56
27	21.25	24.00	1.24	0.32	0.56
31	21.25	23.82	1.30	0.33	0.59
35	21.25	23.77	1.32	0.34	0.60
39	21.25	23.66	1.35	0.35	0.61
45	21.25	23.52	1.40	0.36	0.63
54	21.25	23.37	1.45	0.37	0.66
61	21.5	23.29	1.49	0.38	0.67
74	21.5	23.18	1.53	0.39	0.69
85	21.5	23.06	1.57	0.40	0.71
120	21.5	22.77	1.66	0.43	0.75
158	22	22.53	1.76	0.45	0.80
200	22	22.37	1.82	0.47	0.82
273	21.25	22.12	1.88	0.48	0.85
344	22	21.90	1.97	0.51	0.89
385	22.25	21.81	2.01	0.52	0.91
647	22.25	21.47	2.13	0.55	0.96
2100	22	21.21	2.21	0.57	1.00

APPENDIX 6/5

Reox # 28

Zeolite 2.1CrX, (2.127g), 1.02 Wt%Cr_2O_3, N_{Cr} = (3.90±0.02)x10^{-4}
V_{man} = 43.1±0.2 cm^3, V_{tot} = 62.3±0.4 cm^3, Pi = 40.59±0.01 cmHg, T_r = 22.0±0.2°C
N_i = (9.40±0.04)x10^{-4}, T_f = 315°C, $O_2/Cr(\infty)$ = 0.62±0.04.

Time/min	T/°C	P/cmHg ± 0.01	(Moles Ads ± 0.05) x10^4	O_2/Cr ± 0.04	θ ± 0.08
0.5	22	24.15	1.32	0.34	0.55
1	22	23.56	1.52	0.39	0.63
2	22	22.93	1.74	0.45	0.72
3	22	22.75	1.80	0.46	0.74
4	22	22.51	1.88	0.48	0.78
5	22	22.37	1.93	0.50	0.80
6	22	22.33	1.94	0.50	0.80
7	22	22.30	1.95	0.50	0.81
8	22	22.20	1.98	0.51	0.82
9	22	22.13	2.01	0.52	0.83
10	22	22.05	2.03	0.52	0.84
12	22	22.01	2.05	0.53	0.85
14	22	21.99	2.06	0.53	0.85
16	22	21.83	2.11	0.84	0.87
19	22	21.76	2.13	0.55	0.88
24	22	21.67	2.16	0.56	0.90
35	22.25	21.52	2.22	0.57	0.92
51	22.5	21.41	2.26	0.58	0.94
64	22.75	21.36	2.29	0.59	0.95
78	22.75	21.29	2.31	0.59	0.96
136	23	21.16	2.36	0.61	0.98
260	23	21.11	2.38	0.61	0.98
1320	22.25	20.94	2.42	0.62	1.00

APPENDIX 6/6

Reox # 29

Zeolite 2.1CrX, (2.127g), 1.02 Wt%Cr_2O_3, N_{Cr} = (3.90±0.02)x10^{-4}
V_{man} = 43.1±0.2 cm^3, V_{tot} = 62.8±0.04 cm^3, P_i = 40.17±0.01 cmHg, T_r = 22.8±0.2°C
N_i = (9.38±0.04)x10^{-4}, T_f = 250°C, $O_2/Cr(\infty)$ = 0.63±0.04.

Time/min	T/°C	P/cmHg ± 0.01	(Moles Ads ± 0.05) x10^4	O_2/Cr ± 0.04	θ ± 0.08
0.5	22.75	25.63	0.65	0.17	0.36
1	22.75	25.21	0.79	0.20	0.44
2	22.75	24.88	0.91	0.23	0.51
3	22.75	24.67	0.98	0.25	0.54
4	22.75	24.48	1.05	0.27	0.58
5	22.75	24.29	1.11	0.28	0.62
6	22.75	24.17	1.15	0.29	0.64
7	22.75	24.14	1.16	0.30	0.65
9	22.75	24.00	1.21	0.31	0.67
11	22.75	23.96	1.22	0.31	0.68
13	22.75	23.79	1.28	0.33	0.71
15	22.75	23.67	1.32	0.34	0.73
17	22.75	23.63	1.33	0.34	0.74
21	22.75	23.49	1.38	0.35	0.77
30	22.75	23.33	1.44	0.37	0.80
37	22.75	23.28	1.45	0.37	0.81
47	22.75	23.15	1.50	0.38	0.83
59	22.5	23.03	1.53	0.39	0.85
68	22.5	23.01	1.54	0.40	0.86
95	22.5	22.83	1.60	0.41	0.89
120	22.5	22.73	1.63	0.42	0.91
160	22.5	22.52	1.71	0.44	0.95
207	22	22.63	1.65	0.43	0.92
1230	20	22.06	1.80	0.63	1.00

APPENDIX 6/7

Reox # 30

Zeolite 2.1CrX, (2.127g), 1.02 Wt%Cr_2O_3, N_{Cr} = (3.90±0.02)x10^{-4}
V_{man} = 43.1±0.2 cm^3, V_{tot} = 62.8±0.4 cm^3, P_i = 40.41±0.01 cmHg, T_r = 20.5±0.2°C
N_i = (9.51±0.04)x10^{-4}, T_f = 250°C, $O_2/Cr(\infty)$ = 0.60±0.04.

Time/min	T/°C	P/cmHg ± 0.01	(Moles Ads ± 0.05) x10^4	O_2/Cr ± 0.04	θ ± 0.08
0.5	20.5	25.72	0.68	0.18	0.29
1	20.5	25.30	0.83	0.21	0.36
2	20.5	25.00	0.93	0.24	0.40
3	20.5	24.80	1.00	0.26	0.43
4	20.5	24.69	1.04	0.27	0.45
5	20.5	24.53	1.09	0.28	0.47
6	20.5	24.44	1.12	0.29	0.48
7	20.5	24.40	1.13	0.29	0.49
8	20.5	24.28	1.18	0.30	0.52
9	20.5	24.21	1.20	0.31	0.52
10	20.5	24.08	1.25	0.32	0.54
12	20.5	24.05	1.26	0.32	0.54
14	20.5	23.95	1.29	0.33	0.55
16	20.5	23.80	1.34	0.34	0.58
18	20.5	23.77	1.35	0.35	0.58
20	20.5	23.70	1.38	0.35	0.59
24	20.5	23.65	1.39	0.36	0.60
27	20.5	23.47	1.45	0.37	0.63
30	20.5	23.39	1.48	0.38	0.64
34	20.5	23.25	1.53	0.39	0.66
38	20.5	23.16	1.56	0.40	0.67
43	20.5	23.04	1.60	0.41	0.69
54	20.5	22.86	1.66	0.43	0.72
71	20.5	22.63	1.74	0.45	0.75
85	20.5	22.51	1.78	0.46	0.77
93	20.5	22.43	1.81	0.46	0.78
135	20.5	22.26	1.87	0.48	0.80
165	20.5	22.14	1.91	0.49	0.82
179	20.5	22.07	1.94	0.50	0.83
219	20.5	22.06	1.94	0.50	0.83
263	20.75	21.99	1.97	0.51	0.85
300	20.75	21.94	1.99	0.51	0.85
334	20.75	21.91	2.00	0.51	0.86
357	20.75	21.80	2.03	0.52	0.87
1350	19.75	20.87	2.33	0.60	1.00

APPENDIX 6/8

Reox # 31

Zeolite 2.1CrX, (2.127g), 1.02 Wt%Cr_2O_3, N_{Cr} = (3.90±0.02)x10^{-4}
V_{man} = 43.1±0.2 cm^3, V_{tot} = 62.5±0.4 cm^3, P_i = 40.63±0.01 cmHg, T_r = 23.3±0.2°C
N_i = (9.47±0.04)x10^{-4}, T_f = 285°C, $O_2/Cr(\infty)$ = 0.66±0.04.

Time/min	T/°C	P/cmHg ± 0.01	(Moles Ads ± 0.05) x10^4	O_2/Cr ± 0.04	θ ± 0.08
0.5	23.25	24.84	1.06	0.27	0.41
1	23.25	24.16	1.29	0.33	0.50
2	23.25	23.76	1.43	0.37	0.55
3	23.25	23.35	1.56	0.40	0.61
4	23.25	23.23	1.61	0.41	0.62
5	23.25	23.09	1.65	0.43	0.64
6	23.25	23.05	1.67	0.43	0.65
8	23.25	23.03	1.68	0.43	0.65
9	23.25	22.93	1.71	0.44	0.66
10	23.25	22.86	1.73	0.44	0.67
12	23.25	22.75	1.77	0.45	0.69
14	23.25	22.68	1.79	0.46	0.70
16	23.25	22.62	1.81	0.47	0.70
18	23.25	22.52	1.85	0.47	0.72
20	23.25	22.43	1.88	0.48	0.73
23	23.25	22.39	1.89	0.49	0.73
26	23.25	22.30	1.92	0.49	0.75
29	23.25	22.18	1.96	0.50	0.76
34	23.25	22.24	1.94	0.50	0.75
43	23.25	22.01	2.02	0.52	0.78
51	23.25	21.88	2.06	0.53	0.80
61	23.25	21.76	2.11	0.54	0.82
83	23.25	21.59	2.16	0.56	0.84
112	23.5	21.43	2.22	0.57	0.86
138	22.5	21.28	2.25	0.58	0.87
170	23.25	21.18	2.30	0.59	0.89
191	23.25	21.13	2.32	0.60	0.90
232	23.25	21.03	2.35	0.60	0.91
1260	21.75	20.26	2.58	0.66	1.00

APPENDIX 6/9

Reox # 32

Zeolite 2.1CrX, (2.127g), 1.02 Wt%Cr_2O_3, N_{Cr} = (3.90±0.02)x10^{-4}
V_{man} = 43.1±0.2 cm^3, V_{tot} = 62.6±0.4 cm^3, P_i = 41.50±0.01 cmHg, T_r = 22.5±0.2°C
N_i = (9.69±0.04)x10^{-4}, T_f = 275°C, $O_2/Cr(\infty)$ = 0.30±0.04.

Time/min	T/°C	P/cmHg ± 0.01	(Moles Ads ± 0.05) x10^4	O_2/Cr ± 0.04	θ ± 0.08
0.4	22.5	27.83	0.24	0.06	0.21
1	22.5	27.62	0.32	0.08	0.27
2	22.5	27.37	0.40	0.10	0.34
3	22.5	27.16	0.47	0.12	0.40
4	22.5	27.07	0.50	0.13	0.42
5	22.5	27.01	0.52	0.13	0.44
6	22.5	26.94	0.54	0.14	0.46
7	22.5	26.88	0.57	0.15	0.48
8	22.5	26.81	0.59	0.15	0.50
9	22.5	26.77	0.60	0.15	0.51
10	22.5	26.74	0.62	0.16	0.52
12	22.5	26.65	0.64	0.17	0.54
14	22.5	26.60	0.66	0.17	0.56
17	22.5	26.46	0.71	0.18	0.60
20	22.5	26.44	0.72	0.18	0.60
23	22.5	26.44	0.72	0.18	0.60
26	22.5	26.39	0.73	0.19	0.62
29	22.5	26.27	0.77	0.20	0.65
32	22.5	26.21	0.79	0.20	0.67
37	22.5	26.14	0.82	0.21	0.69
44	22.5	26.13	0.82	0.21	0.69
48	22.5	26.09	0.84	0.21	0.70
129	23.5	25.81	0.96	0.25	0.81
157	23.75	25.75	0.99	0.25	0.83
206	23.5	25.66	1.01	0.26	0.85
295	24	25.60	1.05	0.27	0.88
1350	23	25.10	1.19	0.30	1.00

APPENDIX 6/10

Reox # 33

Zeolite 2.1CrX, (2.127g), 1.02 Wt%Cr_2O_3, N_{Cr} = (3.90±0.01)x10^{-4}
V_{man} = 43.1±0.2 cm^3, V_{tot} = 62.2±0.4 cm^3, P_i = 40.33±0.01 cmHg, T_r = 23.0±0.2°C
N_i = (9.41±0.04)x10^{-4}, T_f = 335°C, $O_2/Cr(\infty)$ = 0.70±0.04.

Time/min	T/°C	P/cmHg ± 0.01	(Moles Ads ± 0.05) x10^4	O_2/Cr ± 0.04	θ ± 0.08
0.5	23	23.98	1.33	0.34	0.48
1	23	23.12	1.62	0.42	0.59
2	23	22.16	1.94	0.50	0.71
3	23	22.20	1.93	0.50	0.70
4	23	22.12	1.95	0.50	0.71
5	23	21.88	2.03	0.52	0.74
6	23	21.74	2.08	0.53	0.76
7	23	21.64	2.12	0.54	0.77
8	23	21.57	2.14	0.55	0.78
9	23	21.51	2.16	0.56	0.79
11	23	21.38	2.20	0.57	0.80
13	23	21.23	2.25	0.58	0.82
16	23	21.22	2.26	0.58	0.82
21	23	21.09	2.30	0.59	0.84
28	23	20.96	2.35	0.60	0.86
35	23	20.85	2.38	0.61	0.87
52	23	20.68	2.44	0.63	0.89
70	23	20.58	2.47	0.64	0.90
130	23.5	20.41	2.54	0.65	0.93
1200	21.25	19.67	2.74	0.70	1.00

Appendix Seven

APPENDIX 7/1

Red#40

Zeolite 4.8Cr5A, (1.784g), 2.05 Wt%Cr_2O_3, N_{Cr} = (4.80±0.02)x10^{-4}
V_{man} = 44.3±0.2 cm^3, V_{tot} = 72.0±0.4 cm^3, P_i = 53.13±0.01 cmHg, T_r = 22.0±0.2°C
N_i = (12.79±0.04)x10^{-4}, T_f = 400°C, $H_2/Cr(\infty)$ = 1.45±0.04.

Time/min	T/°C	P/cmHg ± 0.01	(Moles Ads ± 0.05) x10^4	H_2/Cr ± 0.04	θ ± 0.08
1	22	31.09	0.62	0.13	0.09
2	22	30.22	0.97	0.20	0.14
3	22	29.67	1.18	0.25	0.17
4	22	29.08	1.41	0.29	0.20
5	22	28.59	1.60	0.34	0.23
6	22	28.10	1.80	0.38	0.26
7	22	27.63	1.98	0.41	0.29
8	22	27.18	2.16	0.45	0.31
9	22	26.75	2.32	0.49	0.33
10	22	26.35	2.48	0.52	0.36
11	22	25.94	2.64	0.55	0.38
12	22	25.59	2.78	0.58	0.40
13	22	25.26	2.91	0.61	0.42
14	22	24.97	3.02	0.63	0.44
15	22	24.70	3.13	0.65	0.45
16	22	24.40	3.24	0.68	0.47
17	22	24.14	3.34	0.70	0.48
18	22	23.89	3.44	0.72	0.50
19	22	23.69	3.52	0.74	0.51
20	22	23.46	3.61	0.75	0.52
21	22	23.24	3.70	0.77	0.53
22	22	23.05	3.77	0.79	0.54
23	22	22.93	3.82	0.80	0.55
24	22	22.75	3.89	0.81	0.56
25	22	22.55	3.97	0.83	0.57
26	22	22.42	4.02	0.84	0.58
27	22	22.30	4.06	0.85	0.59
28	22	22.14	4.13	0.86	0.59
29	22	22.02	4.18	0.87	0.60
30	22	21.90	4.22	0.88	0.61
32	22	21.66	4.31	0.90	0.62
35	22	21.35	4.44	0.93	0.64
39	22	21.02	4.56	0.95	0.66
49	22	20.50	4.77	1.00	0.69
55	22	20.13	4.91	1.03	0.71

Appendix 7/1 Continued Next Page

Appendix 7/1 Continued

66	22	19.75	5.06	1.06	0.73
79	22	19.53	5.15	1.07	0.74
175	22	18.04	5.73	1.20	0.82
215	22	17.67	5.88	1.23	0.85
276	22	17.25	6.04	1.26	0.87
1320	21.25	14.88	6.95	1.45	1.00

APPENDIX 7/2

Red#41

Zeolite 4.8Cr5A, (1.784g), 2.05 Wt%Cr_2O_3, N_{Cr} = (4.79±0.02)x10^{-4}
V_{man} = 44.3±0.2 cm^3, V_{tot} = 71.7±0.4 cm^3, P_i = 42.05±0.01 cmHg, T_r = 19.0±0.2°C
N_i = (10.23±0.04)x10^{-4}, T_f = 450°C, $H_2/Cr(\infty)$ = 0.98±0.04.

Time/min	T/°C	P/cmHg ± 0.01	(Moles Ads ± 0.05) x10^4	H_2/Cr ± 0.04	θ ± 0.08
1	19	23.13	1.13	0.234	0.24
2	19	21.74	1.67	0.35	0.36
3	19	20.98	1.97	0.41	0.42
4	19	20.31	2.24	0.47	0.48
5	19	19.67	2.49	0.52	0.53
6	19	19.03	2.74	0.57	0.59
7	19	18.48	2.96	0.62	0.63
8	19	17.97	3.16	0.66	0.68
9	19	17.53	3.33	0.69	0.71
10	19	17.21	3.46	0.72	0.74
11	19	16.90	3.58	0.75	0.77
12	19	16.76	3.63	0.76	0.78
13	19	16.41	3.77	0.79	0.81
14	19	16.29	3.82	0.80	0.82
15	19	16.14	3.88	0.81	0.83
16	19	16.00	3.93	0.82	0.84
17	19	15.88	3.98	0.83	0.85
18	19	15.80	4.01	0.84	0.86
19	19	15.74	4.04	0.84	0.86
20	19	15.67	4.06	0.85	0.87
22	19	15.57	4.10	0.86	0.88
24	19	15.42	4.16	0.87	0.89
26	19	15.36	4.18	0.87	0.90
30	19	15.27	4.22	0.88	0.90
35	19	15.14	4.27	0.89	0.91
41	19	15.05	4.30	0.90	0.92
55	19	14.93	4.35	0.91	0.93
64	19	14.87	4.38	0.91	0.94
76	19	14.78	4.41	0.92	0.94
3420	18	14.06	4.68	0.98	1.00

APPENDIX 7/3

Red#42

Zeolite 4.8Cr5A, (1.784g), 2.05 Wt%Cr_2O_3, N_{Cr} = (4.79±0.02)x10^{-4}
V_{man} = 44.3±0.2 cm^3, V_{tot} = 70.9±0.4 cm^3, P_i = 46.34±0.01 cmHg, T_r = 21.0±0.2°C
N_i = (11.20±0.04)x10^{-4}, T_f = 500°C, $H_2/Cr(\infty)$ = 0.92±0.04.

Time/min	T/°C	P/cmHg ± 0.01	(Moles Ads ± 0.05) x10^4	H_2/Cr ± 0.04	θ ± 0.08
1	21	22.80	2.38	0.50	0.54
2	21	20.06	3.44	0.72	0.78
3	21	18.96	3.86	0.81	0.88
4	21	18.52	4.03	0.84	0.91
5	21	18.28	4.12	0.86	0.94
6	21	18.13	4.18	0.87	0.95
7	21	18.02	4.23	0.88	0.96
9	21	17.89	4.28	0.89	0.97
11	21	17.81	4.31	0.90	0.98
15	21	17.76	4.32	0.90	0.98
20	21	17.69	4.35	0.91	0.99
74	21	17.62	4.38	0.91	0.99
1320	20	17.48	4.41	0.92	1.00

APPENDIX 7/4

Red#43

Zeolite 4.8Cr5A, (1.784g), 2.05 Wt%Cr_2O_3, N_{Cr} = (4.79± 0.02)x10^{-4}
V_{man} = 44.3±0.2 cm^3, V_{tot} = 72.0±0.4 cm^3, P_i = 50.05±0.01 cmHg, T_r = 20.5±0.2°C
N_i = (12.11±0.04)x10^{-4}, T_f = 400°C, $H_2/Cr(\infty)$ = 0.89±0.04.

Time/min	T/°C	P/cmHg ± 0.01	(Moles Ads ± 0.05) x10^4	H_2/Cr ± 0.04	θ ± 0.08
1	20.75	29.66	0.46	0.10	0.11
2	20.75	28.93	0.74	0.16	0.17
3	20.75	28.32	0.98	0.21	0.23
4	20.75	27.75	1.20	0.25	0.28
5	20.75	27.16	1.44	0.30	0.34
6	20.75	26.65	1.64	0.34	0.38
7	20.75	26.09	1.86	0.39	0.44
8	20.75	25.61	2.05	0.43	0.48
9	20.75	25.13	2.23	0.47	0.52
10	20.75	24.75	2.39	0.50	0.56
11	20.75	24.35	2.54	0.53	0.60
12	20.75	24.01	2.68	0.56	0.63
13	20.75	23.73	2.79	0.58	0.65
14	20.75	23.44	2.90	0.61	0.68
15	20.75	23.19	3.00	0.63	0.70
16	20.75	22.95	3.09	0.65	0.73
17	20.75	22.77	3.16	0.66	0.74
18	20.75	22.57	3.24	0.68	0.76
19	21	22.41	3.31	0.69	0.78
20	21	22.25	3.37	0.70	0.79
21	21	22.16	3.41	0.71	0.80
23	21	21.93	3.50	0.73	0.82
25	21	21.73	3.58	0.75	0.84
28	21	21.52	3.66	0.76	0.86
31	21	21.35	3.73	0.78	0.88
35	21	21.19	3.79	0.79	0.89
40	21	21.06	3.84	0.80	0.90
45	21	20.92	3.90	0.81	0.91
52	21	20.84	3.93	0.82	0.92
60	21	20.86	3.92	0.82	0.92
100	21	20.48	4.07	0.85	0.96
122	21	20.40	4.10	0.86	0.96
150	21	20.40	4.10	0.86	0.96
256	21	20.36	4.12	0.86	0.97
1400	21	19.99	4.26	0.89	1.00

APPENDIX 7/5

Red#44

Zeolite 4.8Cr5A, (1.784g), 2.05 Wt%Cr_2O_3, N_{Cr} = (4.79± 0.02)x10^{-4}
V_{man} = 44.3±0.2 cm^3, V_{tot} = 72.0±0.4 cm^3, P_i = 44.79±0.01 cmHg, T_r = 20.5±0.2°C
N_i = (10.84±0.04)x10^{-4}, T_f = 550°C, $H_2/Cr(\infty)$ = 0.74±0.04.

Time/min	T/°C	P/cmHg ± 0.01	(Moles Ads ±0.05) x10^4	H_2/Cr ± 0.04	θ ± 0.08
1	20.5	19.79	3.17	0.66	0.89
2	20.5	19.27	3.38	0.70	0.95
3	20.5	19.15	3.42	0.71	0.96
5	20.5	19.03	3.47	0.72	0.97
7	20.5	18.96	3.50	0.73	0.99
10	20.5	18.90	3.52	0.73	0.99
15	20.5	18.86	3.53	0.74	1.00
47	20.5	18.83	3.54	0.74	1.00
70	20.5	18.83	3.54	0.74	1.00

APPENDIX 7/6

Red#57

Zeolite 4.8Cr5A, (0.830g), 2.05 Wt%Cr_2O_3, N_{Cr} = (2.23±0.02)x10^{-4}
V_{man} = 44.3±0.2 cm^3, V_{tot} = 70.1±0.4 cm^3, P_i = 62.23±0.01 cmHg, T_r = 21.0±0.2°C
N_i = (15.03±0.04)x10^{-4}, T_f = 450°C, $H_2/Cr(\infty)$ = 0.87±0.04.

Time/min	T/°C	P/cmHg ± 0.01	(Moles Ads ± 0.05) x10^4	H_2/Cr ± 0.04	θ ± 0.08
1	21	37.27	0.78	0.35	0.40
2	21	36.31	1.15	0.51	0.59
3	21	35.81	1.34	0.60	0.69
4	21	35.46	1.47	0.66	0.76
5	21	35.16	1.59	0.71	0.82
6	21	34.98	1.66	0.74	0.85
7	21	34.87	1.70	0.76	0.88
8	21	34.80	1.72	0.77	0.89
9	21	34.74	1.75	0.78	0.90
10	21	34.70	1.76	0.79	0.91
12	21	34.63	1.79	0.80	0.92
14	21	34.57	1.81	0.81	0.94
17	21	34.50	1.84	0.82	0.95
23	21	34.44	1.86	0.84	0.96
31	21	34.38	1.88	0.84	0.97
41	21	34.38	1.88	0.85	0.97
90	21	34.31	1.91	0.86	0.99
131	21.25	34.27	1.94	0.87	1.00
155	21.25	34.27	1.94	0.87	1.00

Appendix Eight

APPENDIX 8/1

Reox # 34

Zeolite 4.8Cr5A, (1.784g), 2.05 Wt%Cr_2O_3, N_{Cr} = (4.79±0.02)x10^{-4}
V_{man} = 44.3±0.2 cm^3, V_{tot} = 72.0±0.4 cm^3, P_i = 45.59±0.01 cmHg, T_r = 21.0±0.2°C
N_i = (11.01±0.01)x10^{-4}, T_f = 400°C, $H_2/Cr(\infty)$ = 0.50±0.04.

Time/min	T/°C	P/cmHg ± 0.01	(Moles Ads ± 0.05) x10^4	O_2/Cr ± 0.04	θ ± 0.08
1	21	27.71	0.13	0.03	0.06
2	21	27.50	0.22	0.05	0.09
3	21	27.44	0.24	0.05	0.10
4	21	27.33	0.28	0.06	0.12
6	21	27.22	0.32	0.07	0.14
8	21	27.16	0.35	0.07	0.15
10	21	27.06	0.39	0.08	0.16
13	21	26.98	0.42	0.09	0.18
16	21	26.91	0.45	0.09	0.19
20	21	26.85	0.47	0.10	0.20
25	21	26.72	0.52	0.11	0.22
30	21.5	26.64	0.57	0.12	0.24
37	21.5	26.54	0.61	0.13	0.26
45	21.5	26.42	0.66	0.14	0.27
56	21.5	26.29	0.71	0.15	0.30
66	22	26.19	0.76	0.16	0.32
77	22	26.10	0.80	0.17	0.33
86	22	25.98	0.85	0.18	0.35
98	22	25.85	0.90	0.19	0.38
111	22	25.67	0.97	0.20	0.40
122	22	25.58	1.00	0.22	0.42
135	22	25.49	1.04	0.22	0.43
151	22	25.35	1.09	0.23	0.46
163	22	25.24	1.14	0.24	0.48
180	22	25.03	1.22	0.25	0.51
225	22	24.74	1.33	0.28	0.56
240	21	24.58	1.36	0.28	0.57
1410	18	21.80	2.39	0.50	1.00

APPENDIX 8/2

Reox # 35

Zeolite 4.8Cr5A, (1.784g), 2.05 Wt%Cr_2O_3, N_{Cr} = (4.79±0.02)x10^{-4}
V_{man} = 44.3±0.2 cm^3, V_{tot} = 71.7±0.4 cm^3, P_i = 44.10±0.01 cmHg, T_r = 20.0±0.2°C
N_i = (10.69±0.04)x10^{-4}, T_f = 450°C, $H_2/Cr(\infty)$ = 0.47±0.04.

Time/min	T/°C	P/cmHg ± 0.01	(Moles Ads ± 0.05) x10^4	O_2/Cr ± 0.04	θ ± 0.08
1	20	26.92	0.13	0.03	0.06
2	20	26.76	0.19	0.04	0.09
3	20	26.68	0.23	0.05	0.10
4	20	26.60	0.26	0.05	0.11
5	20	26.52	0.29	0.06	0.13
7	20	26.43	0.33	0.07	0.14
9	20	26.33	0.36	0.08	0.16
11	20	26.25	0.39	0.08	0.17
13	20	26.21	0.41	0.09	0.18
16	20	26.13	0.44	0.09	0.19
20	20	26.06	0.47	0.10	0.21
25	20	25.98	0.51	0.11	0.22
30	20	25.87	0.54	0.11	0.240
37	20	25.73	0.60	0.13	0.26
46	20	25.57	0.66	0.14	0.29
56	20	25.44	0.71	0.15	0.31
70	20	25.30	0.77	0.16	0.34
91	20	25.05	0.87	0.18	0.38
117	20	24.85	0.94	0.20	0.42
132	20	24.67	1.02	0.21	0.45
150	20	24.52	1.07	0.22	0.47
162	20	24.41	1.12	0.23	0.49
177	20	24.28	1.17	0.24	0.52
192	20	24.14	1.22	0.26	0.54
203	19.25	24.06	1.23	0.26	0.54
1140	20	21.59	2.22	0.46	0.98
1170	20	21.55	2.24	0.47	0.99
1405	20	21.48	2.27	0.47	1.00
1553	20.75	21.52	2.27	0.47	1.00

APPENDIX 8/3

Reox # 36

Zeolite 4.8Cr5A, (1.784g), 2.05 Wt%Cr_2O_3, N_{Cr} = (4.79±0.02)x10^{-4}
V_{man} = 44.3±0.2 cm^3, V_{tot} = 70.9±0.4 cm^3, P_i = 41.88±0.01 cmHg, T_r = 21.0±0.2°C
N_i = (10.12±0.04)x10^{-4}, T_f = 500°C, $H_2/Cr(\infty)$ = 0.50±0.04.

Time/min	T/°C	P/cmHg ± 0.01	(Moles Ads ± 0.05) x10^4	O_2/Cr ± 0.04	θ ± 0.08
1	21	25.70	0.18	0.04	0.07
2	21	25.54	0.24	0.05	0.10
3	21	25.42	0.29	0.06	0.12
4	21	25.35	0.31	0.07	0.13
5	21	25.26	0.25	0.07	0.15
7	21	25.16	0.38	0.08	0.16
9	21	25.09	0.41	0.09	0.17
11	21	25.02	0.44	0.09	0.19
13	21	24.97	0.46	0.10	0.19
16	21	24.90	0.49	0.10	0.20
20	21	24.82	0.52	0.11	0.22
25	21	24.74	0.55	0.11	0.23
30	21	24.65	0.58	0.12	0.24
38	21	24.49	0.64	0.13	0.27
46	21	24.40	0.68	0.14	0.29
55	21	24.28	0.72	0.15	0.30
66	21	24.15	0.78	0.16	0.33
76	21	24.04	0.82	0.17	0.34
114	21	23.65	0.97	0.20	0.41
175	21	23.08	1.19	0.25	0.50
1320	21	20.12	2.28	0.48	0.96
2880	19	19.85	2.39	0.50	1.00

APPENDIX 8/4

Reox # 37

Zeolite 4.8Cr5A, (1.784g), 2.05 Wt%Cr_2O_3, N_{Cr} = (4.79±0.02)x10^{-4}
V_{man} = 44.3±0.2 cm^3, V_{tot} = 72.6±0.4 cm^3, P_i = 48.03±0.01 cmHg, T_r = 21.0±0.2°C
N_i = (11.60±0.04)x10^{-4}, T_f = 350°C, $H_2/Cr(\infty)$ = 0.36±0.04.

Time/min	T/°C	P/cmHg ± 0.01	(Moles Ads ± 0.05) x10^4	O_2/Cr ± 0.04	θ ± 0.08
1	21	28.97	0.14	0.03	0.08
2	21	28.81	0.20	0.04	0.12
3	21	28.70	0.24	0.05	0.14
4	21	28.62	0.28	0.06	0.16
5	21	28.55	0.30	0.06	0.18
7	21	28.41	0.36	0.07	0.21
9	21	28.31	0.40	0.08	0.23
12	21	28.23	0.43	0.09	0.25
15	21	28.13	0.47	0.20	0.27
18	21	28.06	0.50	0.10	0.29
27	21	27.87	0.57	0.12	0.33
35	21	27.73	0.63	0.13	0.37
50	21	27.54	0.70	0.15	0.41
75	21	27.22	0.83	0.17	0.49
112	21	26.86	0.97	0.20	0.57
128	21	26.66	1.05	0.22	0.62
145	21	26.57	1.09	0.23	0.64
178	21	26.33	1.18	0.25	0.69
1200	20	24.91	1.71	0.36	1.00

APPENDIX 8/5

Reox # 38

Zeolite 4.8Cr5A, (1.784g), 2.05 Wt%Cr_2O_3, N_{Cr} = (4.79± 0.02)x10^{-4}
V_{man} = 44.3±0.2 cm^3, V_{tot} = 70.3±0.4 cm^3, P_i = 48.98±0.01 cmHg, T_r = 20.5±0.2°C
N_i = (11.85±0.04)x10^{-4}, T_f = 650°C, $H_2/Cr(\infty)$ = 0.55±0.04.

Time/min	T/°C	P/cmHg ± 0.01	(Moles Ads ± 0.05) x10^4	O_2/Cr ± 0.04	θ ± 0.08
1	20.5	30.36	0.19	0.04	0.07
2	20.5	30.18	0.26	0.05	0.10
3	20.5	30.07	0.30	0.06	0.12
4	20.5	29.96	0.34	0.07	0.13
5	20.5	29.89	0.37	0.08	0.14
7	20.5	29.77	0.42	0.09	0.16
9	20.5	29.69	0.45	0.09	0.17
11	20.5	29.61	0.48	0.10	0.18
13	20.5	29.55	0.50	0.11	0.19
16	20.5	29.46	0.54	0.11	0.20
20	20.5	29.38	0.57	0.12	0.22
25	20.5	29.28	0.60	0.13	0.23
30	20.5	29.21	0.63	0.13	0.24
38	20.5	29.07	0.69	0.14	0.26
51	20.5	28.87	0.76	0.16	0.29
62	20.5	28.76	0.80	0.17	0.31
70	20.5	28.65	0.85	0.18	0.32
80	20.5	28.52	0.90	0.19	0.34
92	20.5	28.37	0.96	0.20	0.36
102	20.5	28.26	1.00	0.21	0.38
133	20.5	27.78	1.18	0.25	0.45
180	20.5	27.50	1.29	0.27	0.49
1380	19	23.89	2.63	0.55	1.00

APPENDIX 8/6

Reox # 52

Zeolite 4.8Cr5A, (0.830g), 2.05 Wt%Cr_2O_3, N_{Cr} = (2.23±0.02)x10^{-4}
V_{man} = 44.3±0.2 cm^3, V_{tot} = 70.1±0.4 cm^3, P_i = 62.83±0.01 cmHg, T_r = 20.0±0.2°C
N_i = (15.23±0.04)x10^{-4}, T_f = 450°C, $O_2/Cr(\infty)$ = 0.67±0.04.

Time/min	T/°C	P/cmHg ± 0.01	(Moles Ads ± 0.05) x10^4	O_2/Cr ± 0.04	θ ± 0.08
1	20	37.54	0.82	0.37	0.55
2	20	37.47	0.85	0.38	0.57
3	20	37.28	0.92	0.41	0.62
4	20	37.20	0.95	0.43	0.64
5	20	37.16	0.97	0.44	0.65
7	20	37.11	0.99	0.44	0.66
9	20	37.07	1.00	0.45	0.67
12	20	37.02	1.02	0.46	0.68
15	20	36.97	1.04	0.47	0.70
18	20	36.93	1.06	0.47	0.71
22	20	36.87	1.08	0.48	0.72
26	20	36.82	1.10	0.49	0.74
30	20	36.80	1.11	0.50	0.74
36	20	36.76	1.12	0.50	0.75
48	20	36.71	1.14	0.51	0.77
97	20	36.58	1.19	0.54	0.80
118	20	36.47	1.24	0.55	0.83
133	20	36.44	1.25	0.56	0.83
203	20	36.34	1.28	0.58	0.86
1200	18.25	35.58	1.50	0.67	1.00

Appendix Nine

APPENDIX 9/1

Red # 50

Zeolite 13.4CrY, (1.016g), 5.26 Wt%Cr_2O_3, N_{Cr} = (7.03±0.02)x10^{-4}
V_{man} = 44.4±0.2 cm^3, V_{tot} = 70.5±0.4 cm^3, P_i = 53.75±0.01 cmHg, T_r = 21.0±0.2°C
N_i = (13.00±0.04)x10^{-4}, T_f = 400°C, $H_2/Cr(\infty)$ = 1.16±0.04.

Time/min	T/°C	P/cmHg ± 0.01	(Moles Ads ± 0.05) x10^4	H_2/Cr ± 0.04	θ ± 0.08
1	21	32.75	0.42	0.06	0.05
2	21	31.97	0.72	0.10	0.09
3	21	31.36	0.95	0.14	0.12
4	21	30.82	1.16	0.17	0.14
5	21	30.36	1.34	0.19	0.16
6	21	29.89	1.52	0.22	0.19
7	21	29.49	1.67	0.24	0.20
8	21	29.07	1.83	0.26	0.22
9	21	27.83	2.31	0.33	0.28
11	21	27.73	2.35	0.33	0.29
15	21	27.07	2.60	0.37	0.32
18	21	26.39	2.86	0.41	0.35
21	21	25.81	3.08	0.44	0.38
24	21	25.32	3.27	0.47	0.40
27	21	24.83	3.46	0.49	0.42
31	21	24.31	3.66	0.52	0.45
35	21	23.77	3.87	0.55	0.47
40	21	23.16	4.10	0.58	0.50
45	21	22.74	4.26	0.61	0.52
50	21	22.26	4.45	0.63	0.55
55	21	21.96	4.56	0.65	0.56
60	21	21.45	4.76	0.68	0.58
66	21	21.08	4.90	0.70	0.60
72	21	20.77	5.02	0.71	0.62
80	21	20.39	5.16	0.73	0.63
88	21	19.99	5.32	0.76	0.65
95	21	19.63	5.46	0.78	0.67
107	21	19.21	5.62	0.80	0.69
119	21	18.76	5.79	0.82	0.71
137	21	18.27	5.98	0.85	0.73
146	21	18.05	6.06	0.86	0.74
154	21	17.86	6.14	0.87	0.75
171	21	17.47	6.29	0.89	0.77
180	21	17.24	6.37	0.91	0.78
194	21	16.93	6.50	0.92	0.80
213	21.5	16.73	6.58	0.94	0.81
225	21.5	16.41	6.71	0.95	0.82

Appendix 9/1 Continued Next Page

Appendix 9/1 Continued

237	21.5	16.33	6.74	0.96	0.83
258	21.5	16.06	6.84	0.97	0.84
275	21.5	15.90	6.90	0.98	0.85
300	21.5	15.63	7.00	1.00	0.86
380	21.5	15.08	7.22	1.03	0.88
440	21.5	14.59	7.40	1.05	0.91
1400	18.5	12.48	8.17	1.16	1.00

APPENDIX 9/2

Red # 51

Zeolite 13.4CrY, (1.016g), 5.26 Wt%Cr_2O_3, N_{Cr} = (7.03±0.02)x10^{-4}
V_{man} = 44.4±0.2 cm^3, V_{tot} = 69.6±0.04 cm^3, P_i = 65.884 cmHg, T_r = 20.0±0.2°C
N_i = (15.99±0.04)x10^{-4}, T_f = 450°C, $H_2/Cr(\infty)$ = 0.55±0.04.

Time/min	T/°C	P/cmHg ± 0.01	(Moles Ads ± 0.05) x10^4	H_2/Cr ± 0.04	θ ± 0.08
1	20	38.50	1.33	0.19	0.34
2	20	37.68	1.64	0.23	0.42
3	20	36.99	1.90	0.27	0.49
4	20	36.67	2.02	0.29	0.52
5	20	36.18	2.21	0.31	0.57
6	20	35.79	2.36	0.34	0.61
7	20	35.71	2.39	0.34	0.61
8	20	35.30	2.54	0.36	0.65
9	20	35.02	2.65	0.38	0.68
11	20	34.64	2.80	0.40	0.72
13	20	34.34	2.91	0.41	0.75
15	20	34.01	3.04	0.43	0.78
17	20	33.75	3.13	0.45	0.80
19	20	33.54	3.21	0.46	0.83
21	20	33.35	3.29	0.47	0.84
24	20	33.10	3.38	0.48	0.87
27	20	32.90	3.46	0.49	0.89
31	20	32.66	3.55	0.51	0.91
35	20	32.48	3.62	0.52	0.93
40	20	32.31	3.68	0.52	0.95
45	20	32.19	3.73	0.53	0.96
50	20	32.09	3.77	0.54	0.97
55	20	32.00	3.80	0.54	0.98
61	20	31.94	3.82	0.54	0.98
67	20	31.90	3.84	0.55	0.99
78	21	31.86	3.90	0.55	1.00
102	21	31.38	4.08	0.58	1.05
122	21	31.86	3.90	0.55	1.00

APPENDIX 9/3

Red # 52

Zeolite 13.4CrY, (1.016g), 5.26 Wt%Cr_2O_3, N_{Cr} = (7.03±0.02)x10^{-4}
V_{man} = 44.4±0.2 cm^3, V_{tot} = 69.6±0.4 cm^3, P_i = 54.48±0.01 cmHg, T_r = 22.0±0.2°C
N_i = (13.13±0.04)x10^{-4}, T_f = 450°C, $H_2/Cr(\infty)$ = 0.85±0.04.

Time/min	T/°C	P/cmHg ± 0.01	(Moles Ads ± 0.05) x10^4	H_2/Cr ± 0.04	θ ± 0.08
0.75	22	32.18	0.96	0.14	0.16
1.5	22	30.73	1.51	0.21	0.25
3	22	29.37	2.02	0.29	0.34
4.5	22	28.51	2.35	0.33	0.39
7	22	27.03	2.91	0.41	0.49
8	22	26.71	3.03	0.43	0.51
11.5	22	25.92	3.33	0.47	0.56
13	22	25.40	3.53	0.50	0.59
14	22	25.14	3.62	0.52	0.61
15.5	22	24.78	3.76	0.54	0.63
17	22	24.50	3.87	0.55	0.65
18	22	24.24	3.96	0.56	0.66
20	22	23.79	4.13	0.59	0.69
22	22	23.56	4.22	0.60	0.71
24	22	23.32	4.31	0.61	0.72
26.5	22	23.06	4.41	0.63	0.74
29	22	22.79	4.51	0.64	0.76
32	22	22.46	4.64	0.66	0.78
38	22	22.06	4.79	0.68	0.80
42	22	21.90	4.85	0.69	0.81
45	22	21.35	5.06	0.72	0.85
50	22	21.16	5.13	0.73	0.86
70	22	20.69	5.31	0.76	0.89
80	22	20.19	5.49	0.78	0.92
95	22	19.91	5.60	0.80	0.94
113	22	19.77	5.65	0.80	0.95
1140	18	18.69	5.97	0.85	1.00

APPENDIX 9/4

Red # 53

Zeolite 13.4CrY, (1.016g), 5.26 Wt%Cr_2O_3, N_{Cr} = (7.03±0.02)x10^{-4}
V_{man} = 44.4±0.2 cm^3, V_{tot} = 69.4±0.4 cm^3, P_i = 50.27±0.01 cmHg, T_r = 21.5±0.2°C
N_i = (12.14±0.04)x10^{-4}, T_f = 475°C, $H_2/Cr(\infty)$ = 1.05±0.04.

Time/min	T/°C	P/cmHg ± 0.01	(Moles Ads ± 0.05) x10^4	H_2/Cr ± 0.04	θ ± 0.08
1.5	21.5	27.92	1.59	0.23	0.21
3	21.5	25.88	2.36	0.34	0.32
4	21.5	24.63	2.83	0.40	0.38
6	21.5	22.60	3.60	0.51	0.49
8	21.5	21.20	4.13	0.59	0.56
10	21.5	20.12	4.54	0.65	0.61
12	21.5	19.25	4.87	0.69	0.66
14	21.5	18.50	5.15	0.73	0.70
16	21.5	17.89	5.38	0.77	0.73
19	21.5	17.18	5.65	0.80	0.76
22	21.5	16.61	5.86	0.83	0.79
25	21.5	16.09	6.06	0.86	0.82
28	21.5	15.67	6.22	0.88	0.84
31	21.5	15.32	6.35	0.90	0.86
38	21.5	14.76	6.56	0.93	0.89
45	21.5	14.28	6.74	0.96	0.91
56	21.5	13.74	6.95	0.99	0.94
70	21.5	13.46	7.05	1.00	0.95
105	21.5	13.03	7.21	1.03	0.97
118	21	12.92	7.25	1.03	0.98
1110	19.5	12.43	7.4	1.05	1.00

APPENDIX 9/5

Red # 54

Zeolite 13.4CrY, (1.016g), 5.26 Wt%Cr_2O_3, N_{Cr} = (7.03±0.02)x10^{-4}
V_{man} = 44.4±0.2 cm^3, V_{tot} = 69.2±0.4 cm^3, P_i = 62.72±0.01 cmHg, T_r = 20.3±0.2°C
N_i = (15.21±0.04)x10^{-4}, T_f = 475°C, $H_2/Cr(\infty)$ = 1.07±0.04.

Time/min	T/°C	P/cmHg ± 0.01	(Moles Ads ± 0.05)x10^4	H_2/Cr ± 0.04	θ ± 0.08
1	20.25	35.79	1.67	0.24	0.22
2	20.25	33.59	2.50	0.36	0.33
3	20.25	31.68	3.22	0.46	0.43
4	20.25	30.16	3.80	0.54	0.51
5	20.25	28.78	4.32	0.61	0.57
6	20.25	27.58	4.77	0.68	0.63
7	20.25	26.70	5.11	0.73	0.68
8	20.25	25.89	5.41	0.77	0.72
9	20.25	25.33	5.63	0.80	0.75
10	20.25	24.68	5.87	0.84	0.78
11	20.25	24.22	6.04	0.86	0.80
12	20.25	23.84	6.19	0.88	0.82
13	20.25	23.30	6.40	0.91	0.85
14	20.25	23.06	6.48	0.92	0.86
15	20.25	22.65	6.64	0.94	0.88
16	20.25	22.32	6.76	0.96	0.90
17	20.25	22.10	6.85	0.97	0.91
18	20.25	22.04	6.87	0.98	0.91
19	20.25	21.73	6.99	0.99	0.93
20	20.25	21.54	7.06	1.00	0.94
21	20.25	21.34	7.14	1.02	0.95
23	20.25	21.07	7.24	1.03	0.96
25	20.25	20.88	7.31	1.04	0.97
28	20.25	20.61	7.41	1.05	0.99
31	20.25	20.42	7.48	1.06	0.99
35	20.25	20.22	7.56	1.08	1.00
40	20.25	20.08	7.61	1.08	1.01
47	20.25	19.99	7.65	1.09	1.02
53	20.25	19.99	7.65	1.09	1.02
67	20.25	19.98	7.65	1.09	1.02
105	20	20.20	7.56	1.08	1.01
133	20	20.31	7.52	1.07	1.00
1140	18.5	20.19	7.53	1.07	1.00

APPENDIX 9/6

Red # 55

Zeolite 13.4CrY, (1.016g), 5.26 Wt%Cr_2O_3, N_{Cr} = (7.03±0.02)x10^{-4}
V_{man} = 44.4±0.2 cm^3, V_{tot} = 70.5±0.4 cm^3, P_i = 65.59±0.01 cmHg, T_r = 21.5±0.2°C
N_i = (15.84±0.04)x10^{-4}, T_f = 400°C, $H_2/Cr(\infty)$ = 1.00±0.04.

Time/min	T/°C	P/cmHg ± 0.01	(Moles Ads ± 0.05) x10^4	H_2/Cr ± 0.04	θ ± 0.08
1	21.5	39.83	0.56	0.08	0.08
2	21.5	39.11	0.83	0.12	0.12
3	21.5	38.47	1.08	0.15	0.15
4	21.5	38.07	1.23	0.18	0.18
5	21.5	37.13	1.59	0.23	0.23
6	21.5	36.94	1.67	0.24	0.24
7	21.5	36.37	1.89	0.27	0.27
8	21.5	35.96	2.04	0.29	0.29
9	21.5	35.59	2.19	0.31	0.31
10	21.5	35.23	2.32	0.33	0.33
11	21.5	34.90	2.45	0.35	0.35
12	21.5	34.53	2.59	0.37	0.37
14	21.5	33.92	2.83	0.40	0.40
16	21.5	33.40	3.03	0.43	0.43
18	21.5	32.92	3.21	0.46	0.46
21	21.5	32.34	3.43	0.49	0.49
24	21.5	31.78	3.65	0.52	0.52
27	21.5	31.26	3.85	0.55	0.55
30	21.5	30.95	3.96	0.56	0.56
33	21.5	30.50	4.14	0.59	0.59
36	21.5	30.27	4.23	0.60	0.60
39	21.5	29.87	4.38	0.62	0.62
42	21.5	29.66	4.46	0.63	0.64
45	21.5	29.39	4.56	0.65	0.65
50	21.5	28.99	4.72	0.67	0.67
55	21.5	28.72	4.82	0.69	0.69
60	21.5	28.47	4.92	0.70	0.70
158	20.75	25.78	5.92	0.84	0.84
1170	18	22.76	7.00	1.00	1.00
1290	19	22.79	7.02	1.00	1.00

APPENDIX 9/7

Red # 56

Zeolite 13.4CrY, (1.016g), 5.26 Wt%Cr_2O_3, N_{Cr} = (7.03±0.02)x10^{-4}
V_{man} = 44.4±0.2 cm^3, V_{tot} = 69.8±0.4 cm^3, P_i = 66.47±0.01 cmHg, T_r = 20.5±0.2°C
N_i = (16.11±0.02)x10^{-4}, T_f = 350°C, $H_2/Cr(\infty)$ = 0.92±0.04.

Time/min	T/°C	P/cmHg ± 0.01	(Moles Ads ± 0.05) x10^4	H_2/Cr ± 0.04	θ ± 0.08
1	21	40.20	0.79	0.11	0.12
2	21	39.83	0.93	0.13	0.15
3	21	39.68	0.99	0.14	0.15
4	21	39.31	1.14	0.16	0.18
5	21	38.98	1.26	0.18	0.20
6	21	38.87	1.30	0.19	0.20
7	21	38.70	1.37	0.19	0.21
8	21	38.54	1.43	0.20	0.22
9	21	38.37	1.49	0.21	0.23
10	21	38.21	1.55	0.22	0.24
12	21	37.98	1.64	0.23	0.25
14	21	37.73	1.74	0.25	0.27
16	21	37.47	1.83	0.26	0.29
18	21	37.23	1.92	0.27	0.30
20	21	37.04	2.00	0.28	0.31
22	21	36.85	2.07	0.29	0.32
25	21	36.57	2.18	0.31	0.34
38	21	36.30	2.28	0.32	0.35
31	21	36.08	2.36	0.34	0.37
35	21	35.76	2.49	0.35	0.39
39	21	35.47	2.60	0.37	0.40
44	21	35.12	2.73	0.39	0.42
51	21	34.69	2.89	0.41	0.45
60	21	34.22	3.07	0.44	0.48
136	21.5	31.64	4.08	0.58	0.63
148	21	31.40	4.15	0.59	0.64
212	21	30.25	4.59	0.65	0.71
287	21	29.38	4.92	0.70	0.76
352	21	28.89	5.10	0.73	0.79
388	21	28.43	5.28	0.75	0.82
1350	20.5	25.32	6.45	0.92	1.00

Appendix Ten

APPENDIX 10/1

Reox # 43

Zeolite 13.4CrY, (1.016g), 5.26 Wt%Cr_2O_3, N_{Cr} = (7.03±0.02)x10^{-4}
V_{man} = 44.4±0.2 cm^3, V_{tot} = 70.5±0.4 cm^3, P_i =46.73±0.01 cmHg, T_r = 19.0±0.2°C
N_i = (11.38±0.04)x10^{-4}, T_f = 500°C, $O_2/Cr(\infty)$ = 0.03±0.04.

Time/min	T/°C	P/cmHg ± 0.01	(Moles Ads ±0.05) x10^4	O_2/Cr ± 0.04	θ ± 0.08
1	19	29.42	0.00	0.00	0.00
2	19	29.33	0.03	0.01	0.15
5	19	29.21	0.08	0.01	0.34
9	19	29.16	0.10	0.01	0.43
15	19	29.11	0.12	0.02	0.52
19	19	29.07	0.13	0.02	0.58
25	19	29.02	0.15	0.02	0.65
40	19	28.97	0.17	0.02	0.75
60	19	28.93	0.19	0.03	0.80
90	19	28.90	0.20	0.03	0.86
195	19	28.88	0.21	0.03	0.90
256	19.5	28.87	0.23	0.03	0.99
300	19.5	28.87	0.23	0.03	1.00

APPENDIX 10/2

Reox # 44

Zeolite 13.4CrY, (1.016g), 5.26 Wt%Cr_2O_3, N_{Cr} = (7.03±0.02)x10^{-4}
V_{man} = 44.4±0.2 cm^3, V_{tot} = 70.5±0.4 cm^3, P_i = 60.50±0.01 cmHg, T_r = 19.5±0.2°C
N_i = (14.71±0.05)x10^{-4}, T_f = 400°C, $O_2/Cr(\infty)$ = 0.28±0.04.

Time/min	T/°C	P/cmHg ± 0.01	(Moles Ads ± 0.05) x10^4	O_2/Cr ± 0.04	θ ± 0.08
1	19.5	38.05	0.01	0.00	0.01
2	19.5	37.86	0.09	0.01	0.05
4	19.5	37.66	0.16	0.02	0.08
6	19.5	37.52	0.22	0.03	0.11
8	19.5	37.43	0.25	0.04	0.13
10	19.5	37.34	0.29	0.04	0.15
12	19.5	37.26	0.32	0.05	0.17
15	19.5	37.16	0.35	0.05	0.18
20	19.5	37.12	0.37	0.05	0.19
25	19.5	36.98	0.42	0.06	0.22
30	19.5	36.86	0.47	0.07	0.24
35	19.5	36.78	0.51	0.07	0.26
42	19.5	36.69	0.54	0.08	0.28
50	19.5	36.59	0.58	0.08	0.30
60	19.5	36.47	0.63	0.09	0.32
74	19.5	36.29	0.69	0.10	0.36
87	19.5	36.19	0.73	0.10	0.38
100	19.5	36.07	0.78	0.11	0.40
121	19.5	35.93	0.83	0.12	0.43
140	19.5	35.82	0.88	0.12	0.45
170	19.5	35.64	0.95	0.13	0.49
207	19.5	35.45	1.02	0.15	0.53
290	19.5	34.85	1.25	0.18	0.64
1360	19.5	33.06	1.94	0.28	1.00

APPENDIX 10/3

Reox # 45

Zeolite 13.4CrY, (1.016g), 5.26 Wt%Cr_2O_3, N_{Cr} = (7.03±0.02)x10^{-4}
V_{man} = 44.4±0.2 cm^3, V_{tot} = 70.5±0.4 cm^3, P_i = 61.05±0.01 cmHg, Tr = 20.5±0.2°C
N_i = (14.79±0.04)x10^{-4}, T_f = 450°C, $O_2/Cr(\infty)$ = 0.52±0.04.

Time/min	T/°C	P/cmHg ± 0.01	(Moles Ads ± 0.05) x10^4	O_2/Cr ± 0.04	θ ± 0.08
1	20.5	37.75	0.26	0.04	0.07
2	20.5	37.44	0.38	0.05	0.10
3	20.5	37.24	0.46	0.07	0.13
5	20.5	36.91	0.58	0.08	0.16
7	20.5	36.79	0.63	0.09	0.17
9	20.5	36.48	0.75	0.11	0.21
11	20.5	36.30	0.82	0.12	0.22
13	20.5	36.16	0.87	0.12	0.24
16	20.5	35.98	0.94	0.13	0.26
24	20.5	35.57	1.10	0.16	0.30
42	20.5	34.97	1.33	0.19	0.36
52	20.5	34.59	1.48	0.21	0.40
65	20	34.30	1.57	0.22	0.43
1320	20	28.86	3.66	0.52	1.00

APPENDIX 10/4

Reox # 46

Zeolite 13.4CrY, (1.016g), 5.26 Wt%Cr_2O_3, N_{Cr} = (7.03±0.02)x10^{-4}
V_{man} = 44.4±0.2 cm^3, V_{tot} = 69.2±0.4 cm^3, P_i = 54.61±0.01 cmHg, T_r = 20.0±0.2°C
N_i = (13.26±0.04)x10^{-4}, T_f = 500°C, $O_2/Cr(\infty)$ = 0.57±0.04.

Time/min	T/K	P/cmHg ± 0.01	(Moles Ads ± 0.05) x10^4	O_2/Cr ± 0.04	θ ± 0.08
1	20	34.01	0.38	0.05	0.09
2	20	33.53	0.56	0.08	0.14
3	20	33.13	0.71	0.10	0.18
4	20	32.86	0.81	0.12	0.20
5	20	32.64	0.89	0.13	0.22
6	20	32.43	0.97	0.14	0.24
7	20	32.35	1.00	0.14	0.25
8	20	32.12	1.09	0.16	0.27
9	20	31.91	1.17	0.17	0.29
10	20	31.80	1.21	0.17	0.30
11	20	31.70	1.25	0.18	0.31
13	20	31.48	1.34	0.19	0.33
16	29	31.11	1.48	0.21	0.37
19	20	30.85	1.57	0.22	0.39
22	20	30.62	1.66	0.24	0.41
25	20	30.42	1.74	0.25	0.43
28	20	30.24	1.80	0.26	0.45
32	20	30.08	1.86	0.27	0.46
37	20	29.86	1.95	0.28	0.48
45	20	29.65	2.03	0.29	0.50
52	20	29.37	2.13	0.30	0.53
61	20	29.14	2.22	0.32	0.55
66	20	28.90	2.31	0.33	0.57
75	20	28.72	2.38	0.34	0.59
87	20	28.47	2.48	0.35	0.61
111	20	28.10	2.61	0.37	0.65
139	20	27.70	2.77	0.39	0.69
159	20	27.57	2.82	0.40	0.70
173	20	27.44	2.87	0.41	0.71
192	20	27.24	2.94	0.42	0.73
1260	19.5	24.32	4.03	0.57	1.00

APPENDIX 10/5

Reox # 47

Zeolite 13.4CrY, (1.016g), 5.26 Wt%Cr_2O_3, N_{Cr} = (7.03±0.02)x10^{-4}
V_{man} = 44.4±0.2 cm^3, V_{tot} = 69.2±0.4 cm^3, P_i = 55.75±0.01 cmHg, T_r = 21.5±0.2°C
N_i = (13.46±0.04)x10^{-4}, T_f = 500°C, $O_2/Cr(\infty)$ = 0.57±0.04.

Time/min	T/°C	P/cmHg ± 0.01	(Moles Ads ± 0.05) x10^4	O_2/Cr ± 0.04	θ ± 0.08
1	20	34.70	0.32	0.05	0.08
2	20	34.39	0.44	0.06	0.11
3	20	34.11	0.55	0.08	0.14
4	20	33.85	0.64	0.09	0.16
5	20	33.64	0.72	0.10	0.18
6	20	33.47	0.78	0.11	0.20
8	20	33.12	0.92	0.13	0.23
10	20	32.85	1.02	0.15	0.26
12	20	32.54	1.14	0.16	0.28
14	20	32.34	1.21	0.17	0.30
17	20	32.04	1.33	0.19	0.33
20	20	31.78	1.43	0.20	0.36
23	20	31.54	1.52	0.22	0.38
27	20	31.26	1.62	0.23	0.41
32	20	31.07	1.70	0.24	0.42
37	20	30.68	1.84	0.26	0.46
42	20	30.45	1.93	0.28	0.48
56	20	29.93	2.13	0.30	0.53
65	20	29.65	2.23	0.32	0.56
75	20	29.43	2.32	0.33	0.58
90	20	29.16	2.42	0.34	0.60
105	20	28.88	2.52	0.36	0.63
125	20	28.47	2.68	0.38	0.67
150	20	28.08	2.83	0.40	0.71
162	20	27.96	2.87	0.41	0.72
1400	19	24.90	4.00	0.57	1.00

APPENDIX 10/6

Reox # 48

Zeolite 13.4CrY, (1.016g), 5.26 Wt%Cr_2O_3, N_{Cr} = (7.03±0.02)x10^{-4}
V_{man} = 44.4±0.2 cm^3, V_{tot} = 69.2±0.4 cm^3, P_i = 54.23±0.01 cmHg, T_r = 21.0±0.2°C
N_i = (13.12±0.04)x10^{-4}, T_f = 500°C, $O_2/Cr(\infty)$ = 0.56±0.04.

Time/min	T/°C	P/cmHg ± 0.01	(Moles Ads ± 0.05) x10^4	O_2/Cr ± 0.04	θ ± 0.08
1	21	34.01	0.28	0.04	0.07
2	21	33.72	0.39	0.06	0.10
3	21	33.59	0.44	0.06	0.11
4	21	33.43	0.50	0.07	0.13
5	21	33.24	0.57	0.08	0.15
6	21	33.10	0.63	0.09	0.16
7	21	32.96	0.68	0.10	0.17
8	21	32.83	0.73	0.10	0.19
10	21	32.58	0.82	0.12	0.21
12	21	32.35	0.91	0.13	0.23
15	21	32.11	1.00	0.14	0.25
18	21	31.90	1.08	0.15	0.27
21	21	31.71	1.15	0.16	0.29
24	21	31.46	1.25	0.18	0.32
28	21	31.19	1.35	0.19	0.34
32	21	30.96	1.43	0.20	0.36
36	21	30.73	1.52	0.22	0.39
40	21	30.49	1.61	0.23	0.41
45	21	30.29	1.69	0.24	0.43
56	21	29.93	1.82	0.26	0.46
65	21	29.63	1.94	0.28	0.49
80	21	29.26	2.07	0.30	0.53
1287	21	24.31	3.94	0.56	1.00

APPENDIX 10/7

Reox # 49

Zeolite 13.4CrY, (1.016g), 5.26 Wt%Cr_2O_3, N_{Cr} = (7.03±0.02)x10^{-4}
V_{man} = 44.4±0.2 cm^3, V_{tot} = 69.2±0.4 cm^3, P_i = 41.09±0.01 cmHg, T_r = 22.0±0.2°C
N_i = (9.91±0.04)x10^{-4}, T_f = 500°C, $O_2/Cr(\infty)$ = 0.02±0.04.

Time/min	T/°C	P/cmHg ± 0.01	(Moles Ads ± 0.05) x10^4	O_2/Cr ± 0.04	θ ± 0.08
1	22	26.13	0.07	0.01	0.46
2	22	26.08	0.10	0.01	0.59
4	22	26.04	0.11	0.02	0.68
7	22	25.98	0.13	0.02	0.81
10	22	25.98	0.13	0.02	0.82
23	22	25.97	0.14	0.02	0.84
30	22	25.92	0.15	0.02	0.94
52	22	25.90	0.16	0.02	0.99
64	22	25.90	0.16	0.02	1.000

APPENDIX 10/8

Reox # 50

Zeolite 13.4CrY, (1.016g), 5.26 Wt%Cr_2O_3, N_{Cr} = (7.03±0.02)x10^{-4}
V_{man} = 44.4±0.2 cm^3, V_{tot} = 69.7±0.4 cm^3, P_i = 68.18±0.01 cmHg, T_r = 22.0±0.2°C
N_i = (16.44±0.04)x10^{-4}, T_f = 400°C, $O_2/Cr(\infty)$ = 0.32±0.04.

Time/min	T/°C	P/cmHg ± 0.01	(Moles Ads ± 0.05) x10^4	O_2/Cr ± 0.04	θ ± 0.08
1	19.5	41.65	0.52	0.07	0.23
2	19.5	41.56	0.55	0.08	0.25
4	19.5	41.45	0.60	0.09	0.27
6	19.5	41.32	0.65	0.09	0.29
8	19.5	41.18	0.70	0.10	0.31
11	19.5	41.03	0.76	0.11	0.34
14	19.5	40.90	0.81	0.12	0.36
17	19.5	40.79	0.85	0.12	0.38
21	19.5	40.59	0.93	0.13	0.41
28	19.5	40.32	1.03	0.15	0.46
37	19.5	40.04	1.14	0.16	0.50
46	19.5	39.80	1.23	0.18	0.54
53	19.5	39.576	1.31	0.19	0.58
62	19.5	39.41	1.38	0.20	0.61
71	19.5	39.22	1.45	0.21	0.64
91	19.5	38.96	1.55	0.22	0.69
141	19.5	38.20	1.84	0.26	0.81
159	19.5	38.05	1.90	0.27	0.84
236	19.5	37.44	2.13	0.30	0.94
1350	17.75	36.89	2.26	0.32	1.00

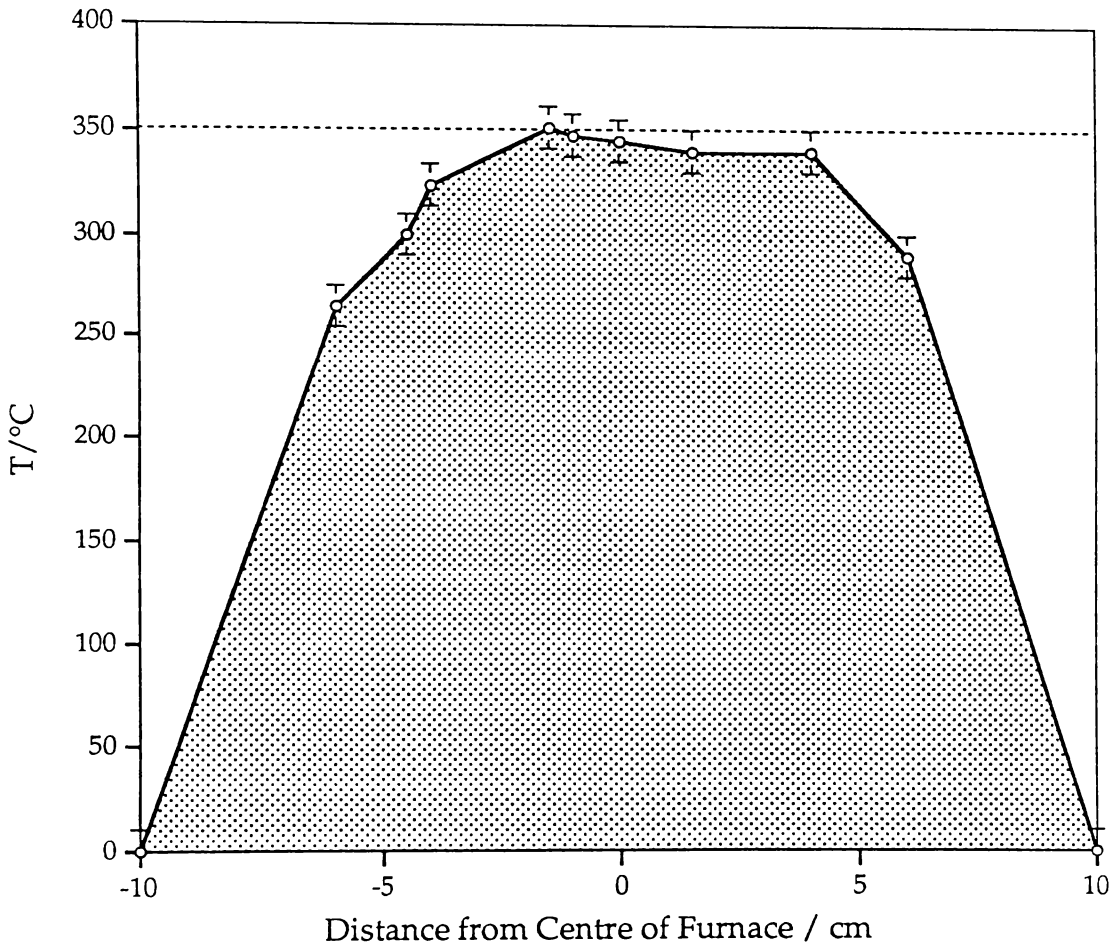
APPENDIX 10/9

Reox # 51

Zeolite 13.4CrY, (1.016g), 5.26 Wt%Cr_2O_3, N_{Cr} = (7.03≠0.020x10^{-4}
V_{man} = 44.4±0.2 cm^3, Vtot = 69.2±0.4 cm^3, P_i = 61.81±0.01 cmHg, T_r = 19.8±0.2°C
N_i = (15.01±0.04)x10^{-4}, T_f = 500°C, O_2/Cr(∞) = 0.24±0.04.

Time/min	T/°C	P/cmHg ± 0.01	(Moles Ads ± 0.05) x10^4	O_2/Cr ± 0.04	θ ± 0.08
1	19.75	39.49	0.05	0.01	0.03
2	19.75	39.39	0.08	0.01	0.05
4	19.75	39.29	0.12	0.02	0.07
7	19.75	39.19	0.16	0.02	0.09
10	19.75	39.12	0.19	0.03	0.11
15	19.75	39.03	0.22	0.03	0.13
21	19.75	38.89	0.27	0.04	0.16
31	19.75	38.71	0134	0.05	0.20
44	19.75	38.45	0.44	0.06	0.26
58	19.75	38.26	0.51	0.07	0.30
82	19.75	38.02	0.60	0.09	0.36
150	19.75	37.33	0.87	0.12	0.51
2820	20.25	35.21	1.69	0.24	1.00

Appendix Eleven



Thermal characteristics of the furnace used for the gas-solid reactions.